

I. Novikov  
THEORY  
OF HEAT  
TREAT-  
MENT  
OF  
METALS

THEORY  
OF HEAT  
TREAT-  
MENT  
OF  
METALS



Prof. I. I. Novikov, born in 1926, finished his studies at the Moscow Institute of Non-ferrous Metals and Gold in 1948, where he worked with Acad. A. A. Bochvar. He received his Cand. Sc. degree in 1951 and D. Sc. degree in 1964 for original research work in the strength and plasticity of alloys in solid-liquid state. From 1965 he heads the chair of physical metallurgy of non-ferrous and rare metals at the Moscow Institute of Steel and Alloys.

His published works (around 200) include some monographs, such as *Hot-shortness of Non-ferrous Metals and Alloys* (1966), *Coring in Alloys* (1966), *C-diagrams of Aluminium Alloys* (1973) and higher-school textbooks *The Theory of Heat Treatment of Metals* (1974) and *Imperfections in Crystal Structure of Metals* (1975).

At present, he is engaged in studies of superplasticity, substructure of cast alloys and development of high-strength casting aluminium alloys.

I. Novikov  
THEORY  
OF HEAT  
TREAT-  
MENT  
OF  
METALS



## *ABOUT THE BOOK*

The book systematizes the theoretical principles of heat treatment of metals and alloys. Its main emphasis is the study of changes in the structure and properties of metallic materials upon thermal treatment. Variations in the structure and properties (mainly mechanical) upon quenching, tempering, ageing, annealing with phase transformations, recrystallization and prerecrystallization annealing, homogenizing, stress-relief annealing, chemical heat treatment and thermo-mechanical treatment are analysed in much detail.

The book is written at a high scientific level but in a clear language comprehensible for higher-school students. The author has used his many-years' experience in lecturing at the Moscow Institute of Steel and Alloys. The book is intended as a textbook for students of metallurgical and mechanical engineering institutes and may be of use for engineers engaged in physical metallurgy, heat treatment of metals, plastic metal working, casting and welding

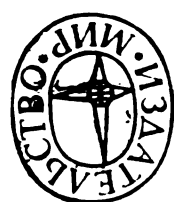




И. И. Новиков

ТЕОРИЯ ТЕРМИЧЕСКОЙ ОБРАБОТКИ МЕТАЛЛОВ

Издательство «Металлургия» Москва





**I. Novikov**

---

**THEORY  
OF HEAT  
TREAT-  
MENT  
OF  
METALS**

Translated from the Russian  
by  
V. AFANASYEV

Mir Publishers · Moscow

First published 1978  
 Revised from the 1974 (2nd) Russian edition

### The Russian Alphabet and Transliteration

Аа	a	Кк	k	Хх	kh
Бб	b	Лл	l	Цц	ts
Вв	v	Мм	m	Чч	ch
Гг	g	Нн	n	Шш	sh
Дд	d	Оо	o	Щщ	shch
Ее	e	Пп	p	Ъ	"
Ёё	ë	Рр	r	Ы	y
Жж	zh	Сс	s	Ь	'
Зз	z	Тт	t	Ээ	e
Ии	i	Уу	u	Юю	yu
Йй	y	Фф	f	Яя	ya

### The Greek Alphabet

Αα	Alpha	Ιι	Iota	Ρρ	Rho
Ββ	Beta	Κκ	Kappa	Σσ	Sigma
Γγ	Gamma	Λλ	Lambda	Ττ	Tau
Δδ	Delta	Μμ	Mu	Υυ	Upsilon
Εε	Epsilon	Νν	Nu	Φφ	Phi
Ζζ	Zeta	Ξξ	Xi	Χχ	Chi
Ηη	Eta	Οο	Omicron	Ψψ	Psi
Θθθ	Theta	Ππ	Pi	Ωω	Omega

*На английском языке*

© Издательство «Металлургия», 1974

© English translation, Mir Publishers, 1978



# CONTENTS

Preface . . . . .	7
Introduction . . . . .	9
<b>1. First-order Annealing . . . . .</b>	<b>17</b>
<i>1.1. Homogenizing Annealing . . . . .</i>	<i>17</i>
1.1.1. Non-equilibrium Crystallization of Alloys . . . . .	17
1.1.2. Structural Changes in Alloys on Homogenizing Annealing . . . . .	24
1.1.3. Variations of Properties of Alloys on Homogenizing Annealing . . . . .	33
1.1.4. Homogenizing with Heating Above the Non-equilibrium Solidus Temperature . . . . .	36
<i>1.2. Recrystallization and Prerecrystallization Annealing . . . . .</i>	<i>39</i>
1.2.1. Structural Changes in Metal on Cold Plastic Working . . . . .	39
1.2.2. Alteration of Metal Properties on Cold Plastic Working . . . . .	44
1.2.3. Structural Changes on Prerecrystallization Annealing . . . . .	47
1.2.4. Primary Recrystallization . . . . .	56
1.2.5. Grain Growth . . . . .	71
1.2.6. Textures of Primary Recrystallization and Grain Growth . . . . .	76
1.2.7. Secondary Recrystallization . . . . .	82
1.2.8. Size of Recrystallized Grains in Annealed Metal . . . . .	87
1.2.9. Changes in Metal Properties Upon Prerecrystallization and Recrystallization Annealing . . . . .	98
1.2.10. Anisotropy of Properties in Annealed Metal . . . . .	108
1.2.11. Selecting Conditions of Prerecrystallization and Recrystallization Annealing . . . . .	113
<i>1.3. Stress-relief Annealing . . . . .</i>	<i>117</i>
1.3.1. Appearance and Role of Residual Stresses . . . . .	118
1.3.2. Lowering Residual Stresses by Annealing . . . . .	121
<b>2. Second-order Annealing . . . . .</b>	<b>127</b>
<i>2.1. General Laws of Phase Transformations in the Solid State . . . . .</i>	<i>129</i>
2.1.1. Thermodynamics of Phase Transformations . . . . .	129
2.1.2. The Role of Structure of Interfaces in Phase Transformations . . . . .	139
2.1.3. Homogeneous and Heterogeneous Nucleation of Phases . . . . .	142
2.1.4. Formation of Intermediate Metastable Phases . . . . .	149
2.1.5. Kinetics of Phase Transformations . . . . .	153
<i>2.2. Annealing of Steels . . . . .</i>	<i>160</i>
2.2.1. Formation of Austenite on Heating . . . . .	160
2.2.2. Diffusion Transformations in Austenite on Cooling . . . . .	169
2.2.3. Types of Steel Annealing . . . . .	179
<i>2.3. Annealing of Cast Irons . . . . .</i>	<i>191</i>
2.3.1. Graphitizing Annealing . . . . .	192
2.3.2. Normalizing of Cast Irons . . . . .	199
<i>2.4. Annealing of Non-ferrous Metals and Alloys . . . . .</i>	<i>200</i>
2.4.1. Heterogenizing Annealing . . . . .	201
2.4.2. Annealing with Phase Transformation . . . . .	206

<b>3. Quenching</b>	208
<i>3.1. Quenching Without Polymorphic Change</i>	208
3.1.1. Variations of Properties During Quenching Without Polymorphic Change	210
3.1.2. Heating and Cooling During Quenching Without Polymorphic Change	212
<i>3.2. Quenching with Polymorphic Change</i>	220
3.2.1. Martensitic Transformation in Carbon Steels	221
3.2.2. Thermodynamics of Martensitic Transformations	223
3.2.3. Mechanism of Martensitic Transformation	232
3.2.4. Microstructure and Substructure of Martensite-hardened Alloys	244
3.2.5. Kinetics of Martensitic Transformations	252
3.2.6. Variations of Properties of Alloys on Martensitic Hardening	264
3.2.7. Bainitic Transformation	269
3.2.8. Hardenability of Steels	278
3.2.9. Heating and Cooling in Steel Hardening	286
<b>4. Ageing and Tempering</b>	298
<i>4.1. Ageing</i>	299
4.1.1. Thermodynamics of Precipitation from Solid Solution	301
4.1.2. Structural Changes on Ageing	306
4.1.3. Variations of Alloy Properties on Ageing	338
4.1.4. Effect of Alloy Composition on Ageing	347
4.1.5. Selection of Ageing Conditions	352
4.1.6. Reversion in Age-hardened Alloys	359
<i>4.2. Tempering</i>	361
4.2.1. Structural Changes in Tempered Steel	361
4.2.2. Variations of Mechanical Properties in Tempered Steels and Selection of Tempering Conditions	373
<b>5. Chemical Heat Treatment and Thermo-mechanical Treatment</b>	384
<i>5.1. Chemical Heat Treatment</i>	384
5.1.1. Changes in Composition and Structure of Metal on Chemical Heat Treatment	384
5.1.2. Kinds of Chemical Heat Treatment	397
<i>5.2. Thermo-mechanical Treatment</i>	406
5.2.1. Thermo-mechanical Treatment of Ageing Alloys	407
5.2.2. Thermo-mechanical Treatment of Martensite-hardenable Steels	418
Appendix. Compositions (mass percentage) of Steels and Non-ferrous Alloys Mentioned in the Book	426
Index	430



## PREFACE

The book covers the course in the Theory of heat treatment of metals which the author has read at the Moscow Institute of Steels and Alloys for students specializing in physical metallurgy of non-ferrous and rare metals.

The theory of heat treatment of metals is a key discipline for metallurgists and thermists. Before studying it, the student ought to gain knowledge in physical chemistry, crystallography, physical metallurgy, science of crystal lattice defects, mechanical properties and testing methods of metals. In turn, the theory of heat treatment underlies the study of heat treatment of metals and some special courses in physical metallurgy, such as Alloy steels or Alloys of non-ferrous and rare metals.

In the last two decades, the theory of heat treatment has been developing extremely extensively. Typically, in its progress it is resorting more and more to the scientific concepts and experimental methods of the physics of metals, especially the science of crystal lattice defects, with the aim at deeper understanding of the nature, mechanisms and kinetics of the structural changes and variations in the properties of metals and alloys effected through thermal actions. As a result, the processes of heat treatment of conventional and novel metals and alloys have been investigated theoretically in much detail.

It has now become impossible to cover both the general theory of heat treatment and the specifics of heat treatment of individual groups of alloys in a single textbook. Because of this, the earlier edition<sup>1</sup> has been revised to exclude some specific topics, such as heat treatment of alloy steels, aluminium, titanium and copper alloys, which are more appropriate in special courses, as is now the practice in most higher technical schools.

The main content of the book is the analysis of structural changes and variations of metal properties caused by thermal actions, with greater emphasis being laid on recrystallization, martensitic transformation, precipitation from solid solution, homogenizing, etc., i.e. the structural changes that are most common in heat treatment of various metals and alloys.

---

<sup>1</sup> Novikov I. I., Zakharov M. V., Heat Treatment of Metals and Alloys (Termicheskaya obrabotka metallov i splavov). Moscow, Metallurgizdat, 1962.

The book uses the well-known classification of types of heat treatment proposed by Acad. A. A. Bochvar and the recommendations on classification and terminology of heat treatment suggested by the CMEA Commission on Standardization.

The processes of annealing, quenching, tempering and ageing are dealt with most thoroughly. Lesser attention is paid to problems of chemical heat treatment, thermo-mechanical treatment and case hardening, since they are often studied in special courses.

The Appendix at the end of the book gives analyses of some steels and non-ferrous alloys which are mentioned in the text.

The author thanks sincerely Prof. V. A. Livanov, head of the chair of physical metallurgy and heat treatment of metals at the Moscow Institute of Aviation Technology, as also his colleagues, in particular Prof. B. A. Kolachev, who have carefully reviewed the manuscript.

The author is also deeply grateful to Prof. S. S. Gorelik, Prof. V. M. Glazov, Prof. G. N. Dubinin, E. I. Estrin, Cand. Sc., Ass. Prof. V. A. Zaimovsky, and to his colleagues at the chair — Prof. M. V. Zakharov, G. M. Kuznetsov, D. Sc., assistant professors A. M. Zakharov, V. S. Zolotorevsky, G. A. Korol'kov, and V. K. Portnoi — for revision of some chapters and valuable comments which have helped in improving the book.

## INTRODUCTION

*Heat treatment is a process in which products made of metals or alloys are acted upon thermally so as to change their structure and properties in the desired direction.*

This type of treatment can be combined with chemical action, deformation, magnetic action, etc.

Heat treatment is a process that is used most extensively in modern technology to change the properties of metals and alloys. At metallurgical and machine-building works, it is one of the principal links in the manufacturing process for making semi-products and machine elements. Heat treatment is used as an intermediate procedure for improving some engineering properties (forgeability, machinability, etc.) or as a final operation to impart to metals and alloys the desired combination of mechanical, physical and chemical properties which can ensure the specified operational characteristics of products. As a general rule, major structures and machines have more heat-treated elements.

The theory of heat treatment is a part of physical metallurgy. One of the main problems with which physical metallurgy is concerned is how the structure of metals and alloys is related with their properties of engineering importance. Heating or cooling of a metal can change its structure, which causes variations in the mechanical, physical and chemical properties and affects the behaviour of the metal in processing and operation.

*The theory of heat treatment studies thermally induced alterations in the structure and properties of metals and alloys which do not disappear upon the thermal factor stopped acting.*

As regards the depth and diversity of structural changes, heat treatment is incomparably more effective than mechanical or other methods of metal treatment.

### **Brief Historical Outline**

Man uses heat treatment from the deep antiquity. Results of archaeological excavations enabled some conclusions to be drawn on the time of appearance and nature of the ancient heat treatment procedures.

First man-made metallic articles appeared on the Earth at the turn from Stone Age to Bronze Age (in the Eneolithic epoch). They were forged by stone hammers first from native gold or copper and later, from copper smelted from ore.

When making cold forging, the primitive man came across the phenomenon of strain hardening, which was an obstacle in making thin knives and sharp arrow-heads. To make the metal plastic again, the smith had to heat cold-forged copper in a hearth. The earliest reliable evidences of the use of this method, which essentially was recrystallization annealing, are dated at the end of the fifth millennium B. C. They were obtained from investigations of forged tools (such as knives) made of smelted copper which were found in the South-Turkmenistan Eneolithic culture. Recrystallization annealing was indispensable for restoring the plasticity in thin sheets made by forging from copper and later, from bronze. In the second millennium B. C. (Bronze Age), these sheets were used in large quantities to make plates and dishes.

Thus, recrystallization annealing was the first heat-treatment procedure to be employed by the man beginning already from the fifth millennium B. C.

Quenching was discovered at much later time. Metallurgical production of iron began from the end of the second millennium B. C. Iron was then made by bloomery process directly from ore. Arms made from this iron could not be hardened by quenching, since the carbon content was too low. At the earlier period of using iron, quenching was done together with carburizing. The ancient smith found some day that the properties of iron arms and tools could be improved appreciably by heating blanks before hot forging in a charcoal-fired hearth (which produced a carburizing effect) and then quenching them in water.

The discovery of bloomery process of iron-making with subsequent carburizing and quenching was one of the greatest achievements in the history of humanity.

Metallurgical analysis of the Hallstatt forging appliances (Central Europe) showed that carburizing of iron articles (knives and spear-heads) and subsequent quenching in water were known already from the beginning of the first millennium B. C., but these methods of hardening heat treatment were relatively seldom used at that time.

Hardening heat treatment of steel was well known in Ancient Greece and Rome, as evidenced by the antique literary monuments. It may be cited from Book IX of the *Odyssey* of Homer (written in the 8th-7th century B. C.) that "Just as a smith plunges into cold water some great axe-head or adze and it hisses angrily — for that is the treatment, and the strength of iron lies in its temper . . ." <sup>1</sup>. Aristotle noted that the best steel could be made by heating iron in a hearth more than once. This treatment car-

---

<sup>1</sup> The *Odyssey* of Homer. Translated into English by T. E. Shaw. New York, Oxford University Press, 1944.

burized the iron and ensured a higher strength and higher hardness on quenching. Aristotle also mentioned oil-quenching of steel. Pliny, Sen., (1st century) wrote that thin steel articles must be quenched in oil to prevent warping and cracking.

Metallurgical analysis of archaeological findings in Europe showed that steel (carburized iron) and quenching of steel articles came into general use from the 5th-4th century B. C.

Quenching of copper alloys was also known to Man long before the Common Era. Relatively recent studies of Etruscan mirrors cast of high-tin bronze (Italy, 5th-4th century B. C.) and Sarmatian mirrors (Volga region, 4th-2nd century B. C.) showed that these articles were martensite-hardened in water, most probably to improve lustre on polishing.

In the Middle Ages, very diverse heat-treatment procedures came into use, such as liquid quenching, air-jet hardening, local hardening of cutting blades, low-, medium- and high-temperature tempering, carburizing, protection of steel against decarburizing in heating, recrystallization annealing, etc.

Microstructural studies, X-ray analysis and microhardness measurements of many hundreds of old-Russian archaeological findings from the 10th-15th centuries indicated that  $\frac{9}{10}$  of all the tools and arms analysed had been heat-treated, of them one-third had been quenched and the remaining two-thirds, quenched and tempered. Carburizing in charcoal or organic substances was used widely to harden knives, swords, spears, files, cutters and other tools.

The art of heat treatment of cutting and thrust weapon was highly developed in the Middle Ages. For instance, famous Damask steel blades had excellent cutting and elastic properties owing to the finely elaborated processes of melting, forging and heat treatment of Damask steel.

Being unaware of the essence of internal transformations in the metal, Mediaeval craftsmen explained the high properties of heat-treated metal by supernatural forces. Methods of heat treatment of steel, in particular when making weapons, were described in much detail in the Mediaeval literature. Disregarding some inessential details and invocations, most of those mediaeval recipes turn to be quite appropriate from the standpoint of a modern thermist.

Though heat treatment was being used from the most ancient times as a manufacturing procedure, its development into a science became possible only beginning from the middle of the 19th century. Up to that time, man's knowledge of heat treatment had been reduced to a collection of recipes based on many centuries of experience. These recipes, often quite valuable, were passed on from father to son, some secrets were lost in ages and re-dis-

covered, but the actual nature of the processes taking place in metal in heat treatment remained a mystery.

The engineering progress in the 19th century stimulated the transformation of heat treatment from art to science.

In the middle of the 19th century, army and navy attempted to replace bronze and cast-iron guns with stronger, and therefore, more powerful steel guns. The beginning of a wide manufacture of steel guns can be dated at 1850's. At the period, the problem of manufacturing steel gun barrels of reliably high strength was extremely urgent. Prominent metallurgists of that time, in particular General P. M. Obukhov, knew well how to melt and cast steel, but nonetheless, bursts of steel guns in firing practice were too frequent.

Many steel guns made by Krupp burst without apparent cause during the Prusso-Austrian war in 1866. Steel was distrusted as a proper material for gun barrels and return to bronze guns began.

In 1866, Dmitry K. Chernov (1839-1921) was invited to the Obukhov steelmaking works in Peterburg as a technician of the hammer-forging shop. In 1868, Chernov presented before the Russian Engineering Society his famous report "Critical Review of Mr. Lavroff's and Mr. Kalakutsky's Articles on Steel and Steel Guns and D. K. Tschernoff's <sup>1</sup> Personal Investigations on the Same Subject" <sup>2</sup>. In that report, he presented his results on establishing the causes of failure in steel forgings. When inspecting microscopically the microsections prepared from gun barrels and simultaneously studying the structure of barrel fracture in a magnifying glass, Chernov came to a conclusion that the finer is the structure, the higher is the strength of a steel. He then "started to search for a cause that formed a fine structure in steel". Comparative studies of steel as forged at various temperatures showed that "variations in the structure of steel should be attributed to the effect of temperature, rather than that of mechanical treatment proper". After that, it was essential to determine the temperatures at which each grade of steel with a definite carbon content changed its structure. Chernov made a brilliant assumption that the hardly visible surface changes that took place at two definite temperatures on the surface of a red-hot forging being cooled could be attributed to deep internal changes in the structure. Chernov estimated these temperatures by eye and designated them *a* and *b*

---

<sup>1</sup> Note the two different spellings of the name. Though the former spelling ('Tschernoff') is still used in the specialist literature, the standard version ('Chernov') seems to be more appropriate and is adhered to in the book.

<sup>2</sup> Zapiski Russkogo Tekhnicheskogo Obshchestva, 1868, issue 7, p. 399; full English translation in: Proc. Inst. Mech. Engrs., 1880, pp. 286—307.

points. "A steel, however hard, cannot be hardened when heated below point *a*, however fast it be cooled". To form a fine-grain fracture, a steel must be heated slightly above the *b* point.

Thus, in 1868 Chernov discovered internal structural transformations in steel and related them to the thermal conditions of forging and techniques of heat treatment. By doing this, the great Russian metallurgist founded the scientific principles of heat treatment.

Chernov's fundamental report was translated into many languages and his suggestions on heat treatment of steels were immediately realized practically in many countries. Chernov's work in physical metallurgy and heat treatment was generally recognized. A. Sauveur, a reputed American metallurgist wrote to Chernov: "The theory of steel heat-treatment created by You is a masterpiece, and Your followers have added but little to Your basic conceptions". A. Portevin of France wrote in the obituary notice on Chernov's activities in the words as follows: "Chernov was the herald and head of a new school; his earlier work served the basis for later amazing progress in the field of steelmaking, which has been actually revolutionized through the intrusion of science".

In 1886, F. Osmond (1849-1912), a French engineer and Chernov's prominent follower, used thermal analysis with Le-Chatelier thermo-couples to determine the critical points in steel. Osmond's work confirmed and developed Chernov's conclusions, attracted many metallurgists and chemists to the problem of structural changes in metals, and gave an additional impetus for a wide experimental research in the field.

In the physical metallurgy history the end of XIX century and the onset of this century witnessed a wide application of the thermodynamic theory of heterogeneous equilibria to metallic systems. Systematic work was started in many countries on plotting constitutional diagrams of alloys. These diagrams show that phase transformations are feasible in an alloy, and therefore, provide starting data for analysis of the main kinds of heat treatment.

First vast research work in the field of heat treatment of non-ferrous alloys was accomplished at the beginning of this century. In 1900, A. A. Baikov (1870-1946) showed on copper-antimony alloys that hardening capacity was intrinsic not only in steels, as had been considered before, but also in non-ferrous alloys. In 1903, a patent was granted in Germany for a method for improvement of aluminium alloys by heating and quenching; it was shown that the ultimate strength of cast copper-aluminium alloys could be increased 1.5 times by quenching.

In 1906, A. Wilm (1869-1937), a German engineer who had invented duralumin, discovered the phenomenon of ageing in quenched duralumin; ageing is now one of the principal methods

for hardening alloys. In 1919, P. Merica (1889-1957) of the USA explained the nature of ageing in duralumins by relating the hardening effect on ageing to the formation of disperse precipitates in a supersaturated solid solution. This was one of the most remarkable achievements in the theory of heat treatment: by using constitutional diagrams with a variable solubility of components in the solid state, it became possible to predict compositional ranges of alloys capable of precipitation hardening.

The progress of the theory of heat treatment after 1920's may be characterized by a detailed study into the nature, mechanism and kinetics of structural transformations in the solid state by means of diverse physical methods, in the first place, by X-ray structural analysis. During two or three decades, vast information was gained on the laws of thermal effects on the structure and properties of metals and alloys. At the end of 1950's, transmission (diffraction) electron microscopy came into wide use for studying substructural changes upon heat treatment.

At the modern stage, the theory of heat treatment widely employs the theory of crystal lattice defects in metals, since these defects can have a strong and sometimes decisive influence on the mechanism and laws of structural changes.

The practice of heat treatment followed the progress in the theory and improved the conventional methods and developed new ones, such as thermo-mechanical treatment; new thermally hardenable alloys have also been developed.

The numerous theoretical studies have resulted in a harmonious theory of heat treatment as a scientific basis for the development of new engineering processes and novel alloys with predetermined properties.

### **Classification of Types of Heat Treatment**

Any process of heat treatment can be described by a curve showing how the temperature varies in time. Such curves can be used to determine the temperature of heating, the time needed for heating and cooling, the average and actual rates of heating and cooling, holding time at a given heating temperature, and the total time of a production cycle. But the shape of the curve says nothing on the type of heat treatment we have to deal with. The type of heat treatment is determined by the phase and structural changes taking place in the metal, rather than by the form of the time-temperature curve. Having this in view, A. A. Bochvar has worked out a classification which covers numerous varieties of heat treatment of ferrous and non-ferrous metals and alloys.

Using Bochvar's classification as the basis, the Standardization Commission at the Council for Mutual Economic Assistance



(CMEA) has developed a new classification of the types and varieties of heat treatment and an appropriate terminology. This classification is shown schematically in Fig. 1.

Heat treatment is classed into *heat treatment proper*, *chemical heat treatment* and *thermo-mechanical treatment* (or deformation-assisted heat treatment). Heat treatment proper consists solely in a thermal action on a metal or alloy; chemical heat treatment combines a thermal and a chemical action; thermo-mechanical treatment is a combination of thermal action and plastic deformation.

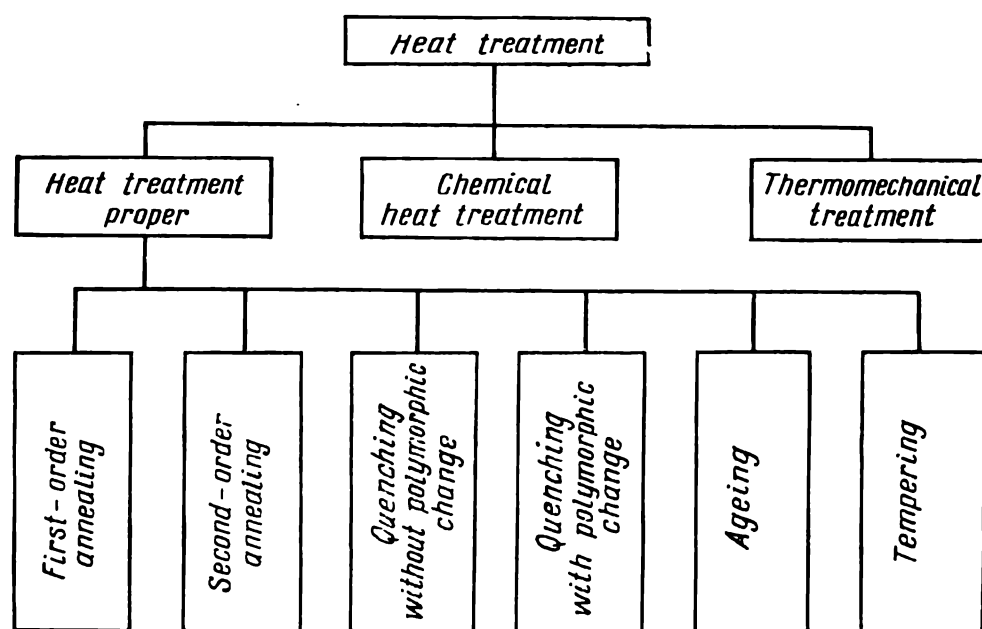


Fig. 1. Classification of principal types of heat treatment of metals and alloys

The main types of heat treatment are as follows: first- and second-order annealing, quenching with and without polymorphic change, ageing and tempering. All these procedures are applicable with steels and non-ferrous metals and alloys. Each of them can be subdivided into varieties specific for particular base alloys. The varieties of chemical heat treatment and thermo-mechanical treatment will be discussed in corresponding chapters.

Some types of heat treatment phenomena may occur as secondary processes in hot plastic working, casting, welding and other manufacturing processes. For instance, rapid cooling of castings upon solidification can cause full or partial hardening in them. In grinding, excessive heating of the surface can result in tempering of the metal. In welding, recrystallization annealing can take place in the affected zone of a weld seam. These secondary processes of heat treatment can be either useful or detrimental, i.e. cause unwanted changes in the structure and properties of metal,

The industrial names of some heat treatment procedures have been established historically so that they often reflect purely external features rather than the actual nature of transformations occurring in a metal or alloy. This is why one and the same term may be applied to heat treatment varieties differing appreciably in their physical essence. For example, annealing is commonly referred to as a procedure comprising heating, holding at the temperature of heating, and slow cooling. In cold-rolled copper, this type of heat treatment causes recrystallization and grain coarsening, while in cast carbon steel it causes phase recrystallization and grain refinement. Heating above the critical point, holding at that temperature and cooling in air is usually termed normalizing. In carbon steels, this procedure results in phase transformation processes which relate to second-order annealing; in high-alloyed steels, it can form martensite, i.e. produce hardening with polymorphic change; and in some non-ferrous alloys, the actual process is quenching without polymorphic change.

Examples of this kind may be numerous. Thus, when some or other industrial name turns to be vague as regards the physical essence of the related process, it should be replaced with or supported by an appropriate term from the approved scientific classification of heat treatment processes.

#### LITERATURE

Chernov D. K. and the Science of Metals (*D. K. Chernov i nauka o metallakh*). Ed. by N. T. Gudtsov. Moscow, Metallurgizdat, 1950, 563 pp., ill.

Bochvar A. A., Principles of Heat Treatment of Alloys (*Osnovy termicheskoi obrabotki splavov*). Moscow, Metallurgizdat, 1940, 298 pp., ill.

# FIRST-ORDER ANNEALING

Casting, plastic working, welding and other manufacturing processes may cause some non-equilibrium changes in the structure of metals and alloys. These changes can be eliminated partially or fully by first-order annealing, the process that brings the metals and alloys into a state closer to the equilibrium. First-order annealing may be classed according to the type of the change being eliminated into homogenizing, pre-recrystallizational softening, pre-recrystallizational strengthening, recrystallizational annealing, and stress-relief annealing. The processes that eliminate non-equilibrium changes occur spontaneously and heating for first-order annealing is only needed to accelerate them.

The principal parameters of first-order annealing are the temperature of heating and the time of holding at that temperature. The rates of heating and cooling are only of secondary significance.

First-order annealing differs from second-order annealing in that it involves no phase transformations in the solid state.

## 1.1. HOMOGENIZING ANNEALING

Homogenizing annealing is used to eliminate dendritic segregation in cast and, less frequently, in deformed alloys.

### 1.1.1. NON-EQUILIBRIUM CRYSTALLIZATION OF ALLOYS

If a molten alloy of the composition  $X$  (Fig. 2) is supercooled somewhat, crystals of solid solution of the composition corresponding to point  $a$  are first formed in it. These crystals grow with further cooling of the alloy within the range of crystallization temperatures. The composition of successively crystallizing layers at any temperature is determined by the corresponding point of the equilibrium solidus line, for instance point  $a$  at  $t_1$  or point  $b$  at  $t_2$ . Therefore, as the temperature is lowered, the crystal layers that are formed become ever richer in the component that lowers the liquidus point. With equilibrium conditions at any temperature

within the crystallization range, a point of the solidus line determines the composition in the whole volume of the solid solution, rather than in the surface layers of crystals only. For example, at temperature  $t_2$  crystals of the solid solution should have the composition corresponding to point  $b$  throughout the whole volume. For this to occur, equalizing diffusion should take place between the earlier crystal layers and those that form later. But this diffusion alone is insufficient to bring the solid phase into equilibrium. For instance, a crystal, whose composition in the core and at the

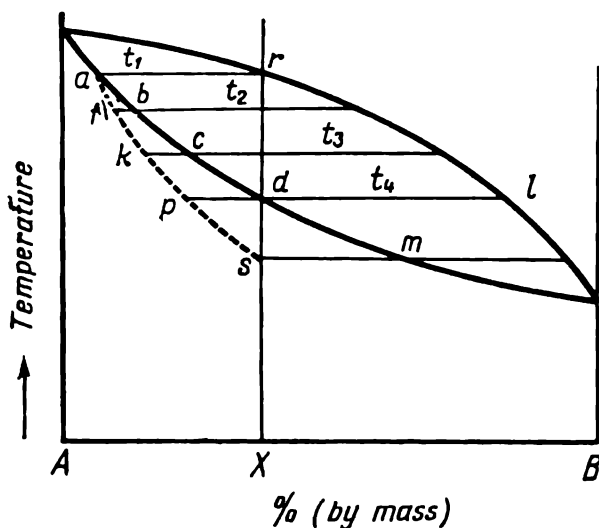


Fig. 2. Variation of average composition of solid solution on non-equilibrium crystallization (curve  $as$ )

surface is determined by points  $a$  and  $b$  respectively, will have an intermediate composition (to the left of point  $b$ ) upon the end of equalizing diffusion at temperature  $t_2$ .

Apart from equalizing diffusion, an interphase interaction between the melt and crystals should take place in the solid phase. This can enrich additionally the solid solution with the component  $B$  from the melt, so that the composition of the solid phase throughout its whole volume will correspond to point  $b$  of the solidus line.

Under real conditions of crystallization with a continuously lowering temperature, equalizing diffusion in the solid phase has no time to proceed to its end. A non-uniform composition of the solid solution may be characterized by an average concentration, which should be somewhere to the left of the solidus line (Fig. 2). For instance, the average composition of the solid phase at a temperature  $t_2$  may be determined by point  $f$ . The composition of the surface layer of a crystal at temperature  $t_3$  is determined by point  $c$ , whereas the average composition of the whole solid phase should be somewhere between points  $f$  and  $c$ . At temperature  $t_3$ , this may be determined by point  $k$ . A curve drawn through the points  $a$ ,  $f$  and  $k$  will thus describe variations in the average composition of a heterogeneous solid solution at a definite cooling rate.

Crystallization of the solid solution comes to its end when the average composition of the solution becomes the same as that of the melt. For instance, equilibrium crystallization of alloy  $X$  terminates at temperature  $t_4$  in point  $d$ . Under non-equilibrium conditions, the average composition of the solid solution at this temperature (point  $p$ ) may be other than that of the alloy. The  $pd/pl$

ratio characterizes the relative weight amount of non-equilibrium liquid phase at temperature  $t_4$ . Non-equilibrium crystallization will proceed further at temperatures below  $t_4$  until the average composition of the solid phase becomes the same as that of the alloy in point  $s$ . At this moment the surface layer of a crystal will have the composition of point  $m$ . If diffusion in the solid phase is suppressed fully, crystallization will end at the melting point of component  $B$ .

With a definite cooling rate, and therefore, a definite extent of diffusion processes, any alloy can be characterized by its own line of variation of the average composition of solid solution, and correspondingly, its intrinsic temperature of non-equilibrium solidus (Fig. 3). Line  $A'bdkB'$  which connects the end points of crystallization of all alloys of a system is called the non-equilibrium solidus of that system.

The lines of equilibrium and non-equilibrium solidus differ from each other not only quantitatively (in having different temperature points), but there is also an essential qualitative difference. The equilibrium solidus line has two functions: firstly, it is the locus of temperature points of the end of crystallization of alloys and, secondly, it at the same time is the locus of points of compositions of the solid phase at equilibrium with the liquid phase within the temperature range of crystallization. On the other hand, the non-equilibrium solidus line is merely the locus of finishing points of crystallization of alloys under particular cooling conditions. Therefore, the non-equilibrium solidus line of a system cannot be used to determine the average composition of the solid solution in coexistence with the liquid phase (this incorrect method is sometimes used in practice).

The non-equilibrium crystallization of solid solution results in the composition of crystallites varying over their cross-section. Solid-solution crystals usually grow as dendrites. The dendritic branches formed at higher temperatures are enriched in the component that raises the solidus point, whereas other branches and intermediate spaces that form at lower temperatures turn to be richer in the component that lowers the solidus point. These

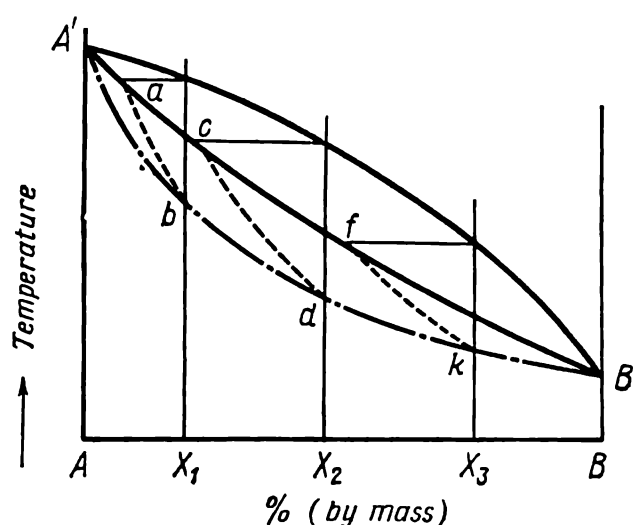


Fig. 3. Non-equilibrium solidus line of a system that forms a continuous series of solid solutions

$cb$ ,  $cd$  and  $fk$ —lines of variation of the average composition of solid solution during non-equilibrium crystallization of alloys  $X_1$ ,  $X_2$  and  $X_3$ ;  $A'bdkB'$ —non-equilibrium solidus line;  $A'acfB'$ —equilibrium solidus line

portions of a crystal have different etchability, so that an etched microsection may reveal inhomogeneous composition within a grain (Fig. 4a). The process resulting in a non-uniform composition in crystallites of solid solution is known in the course of physical metallurgy as *coring*, or *dendritic segregation*.

In eutectic and peritectic systems, dendritic segregation causes more pronounced non-equilibrium changes in the structure (Fig. 5) as compared with alloys forming a continuous series of

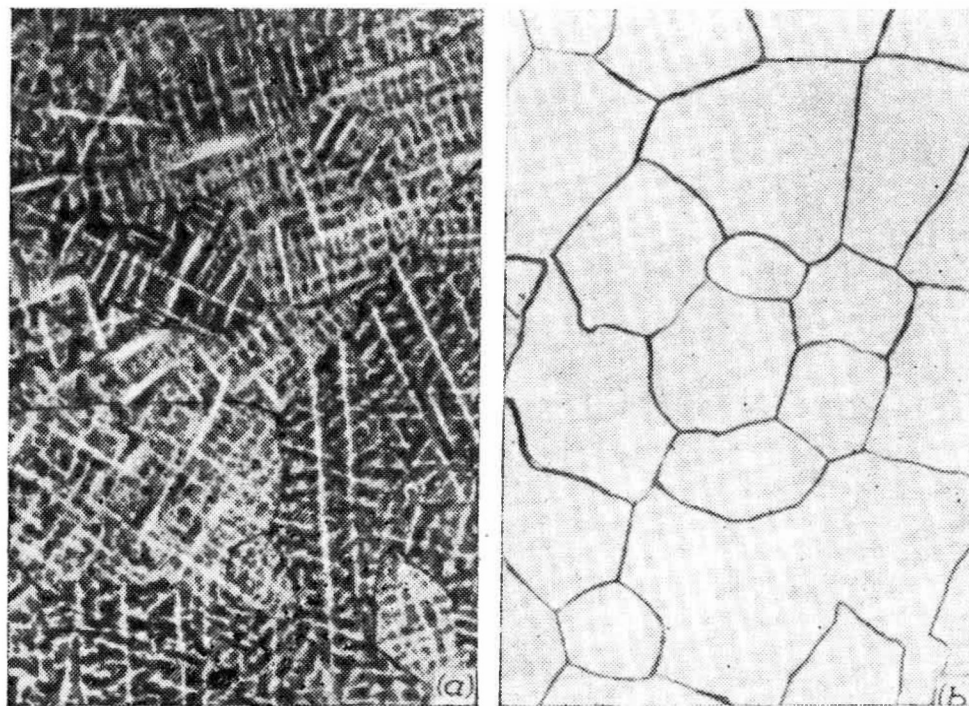


Fig. 4. Microstructure of Cu + 20% Ni alloy,  $\times 100$   
a—as cast; b—upon annealing at 1000 °C for 40 h

solid solutions. In low-alloyed melts (such as  $X_1$  in Fig. 5a and b), non-equilibrium crystallization proceeds in the same way as in a system with a continuous series of solid solutions. With restricted diffusion in the solid phase, solidification of alloy  $X_1$  completes at point  $c$ , i.e. when the average composition of the solid solution is the same as that of the alloy.

In a more heavily alloyed melt, say,  $X_2$ , the average composition of solid solution during non-equilibrium crystallization varies along the  $df$  curve. An uncommon feature here is that the average composition of the solid solution does not hit the figurative line (ordinate) of the alloy above the eutectic or peritectic point. Equilibrium crystallization of  $X_2$  alloy should come to the end at point  $m$ . Under non-equilibrium conditions, below the  $m$  point, the composition of liquid solution in  $X_2$  alloy will vary up to the eutectic ( $e$ ) or peritectic ( $p$ ) point and the composition of peripheral layer of initial  $\alpha$ -crystals, up to point  $a$ . Therefore,  $X_2$  alloy

will either crystallize into a eutectic (Fig. 5a) or form  $\beta$ -phase by peritectic reaction (Fig. 5b). Non-equilibrium crystallization of  $X_2$  alloy comes to the end at point  $n$ .

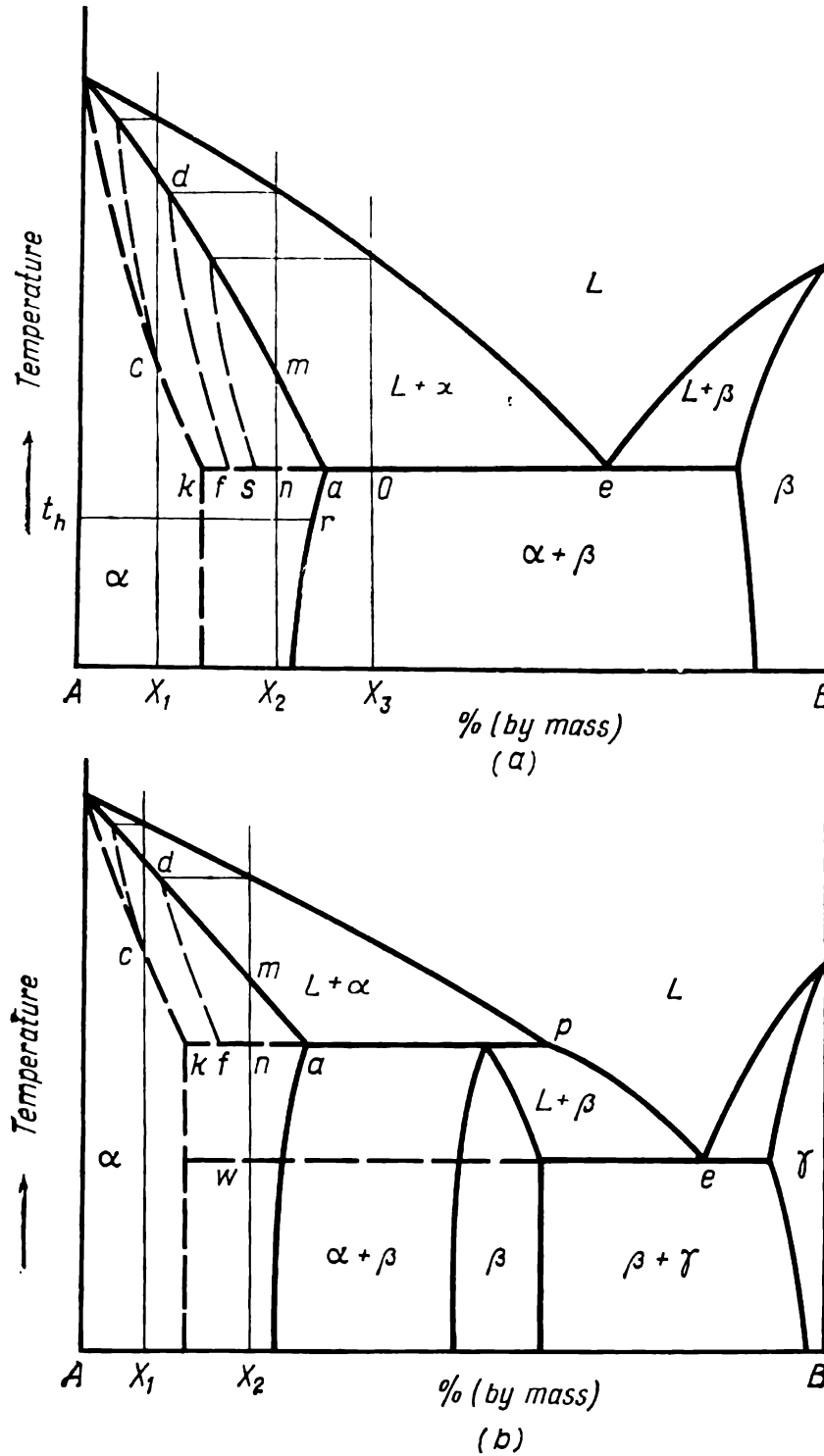


Fig. 5. Non-equilibrium solidus lines in systems of (a) eutectic and (b) peritectic type

Thus, dendritic segregation in alloys existing to the left of the point of ultimate solubility (point  $a$ ), i.e. in the region of solid solutions in constitutional diagrams, results in a non-equilibrium secondary phase formed by eutectic or peritectic reaction. The concentration corresponding to point  $k$  is a boundary. To the right

of that boundary, a secondary phase should crystallize from the melt under the given non-equilibrium conditions. The points  $k$  and  $a$  may be connected by a dotted line, which is an extension of the eutectic (peritectic) horizontal line beyond the point of ultimate solubility. In alloys of the type of  $X_2$ , non-equilibrium crystallization should end at temperatures below that dotted horizontal line, but the degree of supercooling under ordinary conditions is not high and can be neglected when determining the temperature of the end of non-equilibrium crystallization by means of constitutional diagrams.

If an alloy can form a secondary phase under equilibrium conditions, then the concentration of that phase under non-equilibrium conditions should be even larger. For instance, the relative weight concentration of eutectic in alloy  $X_3$  (Fig. 5a) under equilibrium conditions is determined by the  $ao/ae$  ratio and under non-equilibrium conditions, by  $so/se$  ratio (where point  $s$  determines the average composition of initial crystals at the eutectic point for a given cooling rate).

The position of the concentration boundary for the formation of a secondary phase in a melt (point  $k$ ) depends on cooling rate. Under equilibrium conditions, this boundary coincides with the point of ultimate solubility at eutectic or peritectic temperature (i.e. with point  $a$  in Fig. 5). As the cooling rate is increased, the concentration boundary for the appearance of a secondary phase shifts towards the main component owing to the fact that equalizing diffusion in the solid solution is suppressed ever more, so that in the extreme case (at no diffusion) it coincides with the ordinate of that component on the constitutional diagram.

As has been shown experimentally, equalizing diffusion in solid solutions is strongly suppressed within the range of cooling rates feasible under industrial conditions, so that a non-equilib-

**Table 1. Concentration Boundary for the Appearance of Secondary Phase from Melt ( $k$ ) in Die-casting of Binary Alloys, Compared with Ultimate Solubility Point ( $a$ ) at Eutectic or Peritectic Temperature (I. I. Novikov and V. S. Zolotarevsky)**

System	$k$ , %	$a$ , %	System	$k$ , %	$a$ , %
Al-Zn	2.0	82.2	Mg-Zn	0.3	8.4
Al-Cu	0.1	5.7	Cu-Sn	4.0	13.5
Al-Mg	0.5	15.35	Cu-Si	3.5	5.3
Al-Si	0.1	1.65	Cu-Al	7.0	7.5
Mg-Al	0.1	12.7			

\* Cooling rate:  $v_c \approx 1.5$  °C/s for aluminium and magnesium alloys and 5 °C/s for copper alloys.



**Fig. 6.** Diagram of distribution of an alloying element over the cross-section of a dendritic cell of  $\alpha$ -solution with  $\beta$ -phase at the boundaries during (1) initial, (2) intermediate and (3) final stage of homogenization (point  $r$  see in Fig. 5a)

### 1.1.2. STRUCTURAL CHANGES IN ALLOYS ON HOMOGENIZING ANNEALING

Non-equilibrium changes during crystallization can cause the following defects in cast alloys:

1. A reduced ductility of an alloy in the case of the appearance of a brittle excess phase as a result of dendritic segregation. The defect is quite common with cast alloys and can appreciably lower their ductility, especially when continuous layers of coarse brittle particles (intermetallics, carbides, etc.) have formed at boundaries of dendritic cells.

2. Galvanic microcouples formed owing to different composition in central portions of dendritic cells and at their boundaries. This defect, caused by dendritic segregation in the solid solution, can lower the resistance of a metal to electrochemical corrosion. The formation of an excess phase in the solid solution usually affects the corrosion resistance of the metal.

3. Lineage structure of deformed (rolled or forged) metal resulting from stretching of microportions having different composition. This structure is responsible for anisotropy of mechanical properties of products and an increased susceptibility to intercrystalline or fish-scale fracture. The defect can cause an appreciable loss in the relative elongation and contraction and impact toughness of the metal in transverse direction.

4. Lowering of the solidus point through dendritic segregation, which is usually undesirable. For instance, an article may undergo partial melting when heated quickly for hardening or plastic deformation. This melting starts in portions where a eutectic has formed through non-equilibrium conditions, as also in interdendritic spaces between crystals of solid solution which have been enriched in components that can lower the solidus point.

5. Time instability of the structure and properties of cast alloys. In articles operating at elevated temperatures, the processes of equalization of the composition of solid solution and disappearance of excess phases may occur spontaneously. These processes increase the creep of metal and may gradually change other properties beyond tolerable limits.

In order to eliminate these structural defects, ingots and castings are usually subjected to homogenizing annealing.

#### Principal Structural Changes

In single-phase alloys, such as  $X_1$  in Figs. 3 and 5, the principal process occurring during homogenizing annealing is the equalization of the composition of solid solution grains, i.e. elimination of dendritic segregation (see Fig. 4b). In alloys containing

non-equilibrium excess phases, such as alloy  $X_2$  in Fig. 5, homogenizing annealing involves two principal processes: equalization of concentration inside grains of solid solution and dissolution of non-equilibrium excess phases (Fig. 6). Both processes are based on diffusion, and homogenizing annealing may also be called diffusion annealing.

At the very beginning of homogenizing annealing of an alloy  $X_2$  or  $X_3$ , the concentration of the  $\alpha$ -solution at the boundary between a dendritic cell and excess  $\beta$ -phase is brought to an equilibrium corresponding to the point of ultimate solubility at the temperature of homogenizing (for instance, to point  $r$  at temperature  $t_h$  in Fig. 5a). This concentration of the peripheral layer of  $\alpha$ -solution is maintained constant until the excess  $\beta$ -phase exists in the metal (Fig. 6).

Equalization of the composition in dendritic cells serves to control the homogenizing process, i.e. it determines the rate and time of full dissolution of the excess phase. If the process of equalization of composition in  $\alpha$ -phase is conditionally separated from that of dissolution of excess  $\beta$ -phase, then the following picture may be drawn schematically. The equalization of composition in  $\alpha$ -solution lowers the concentration of  $\alpha$ -solution at its boundary with  $\beta$ -phase to values below the  $r$  point in Figs. 5a and 6, so that the peripheral layer of a dendritic cell becomes unsaturated relative to  $\beta$ -phase. This causes dissolution of  $\beta$ -phase, increases the concentration of  $\alpha$ -solution in the peripheral layer up to the equilibrium value, and so on. The  $\alpha/\beta$  boundary gradually moves towards the  $\beta$ -phase as this is being dissolved and the composition of  $\alpha$ -phase over the cross-section of the dendritic cell is thus equalized (see dotted lines in Fig. 6 for various moments of the homogenizing).

If an excess  $\beta$ -phase is fully soluble (in accordance with the constitutional diagram), then the equalization of concentration in  $\alpha$ -solution comes to completion some time after  $\beta$ -phase has disappeared (see  $X_2$  alloy in Fig. 5a). If, however, the composition of an alloy, for instance  $X_3$ , is such that it cannot be single-phase even under equilibrium conditions, then homogenizing will result in dissolution of the non-equilibrium excess quantity of the secondary phase (or phases), a certain equilibrium amount of these phases remaining after homogenizing (Fig. 7). Experiments with aluminium alloys have shown that the time of full elimination of dendritic segregation is only slightly greater than the time ( $\tau_d$ ) required for full dissolution of a non-equilibrium excess of phases. Noting that  $\tau_d$  can be easily determined by studying the structure of metal in the optical microscope, while the kinetics of concentration equalization in a solid solution can only be studied by the method of X-ray structural analysis, which is more expensive and

complicated, it is quite admissible in most practical problems to determine the end of homogenizing process by the time of full dissolution of non-equilibrium excess phases.

According to Fick's first law of diffusion, the amount of a substance,  $dm$ , which can diffuse during time  $d\tau$  through an area  $ds$

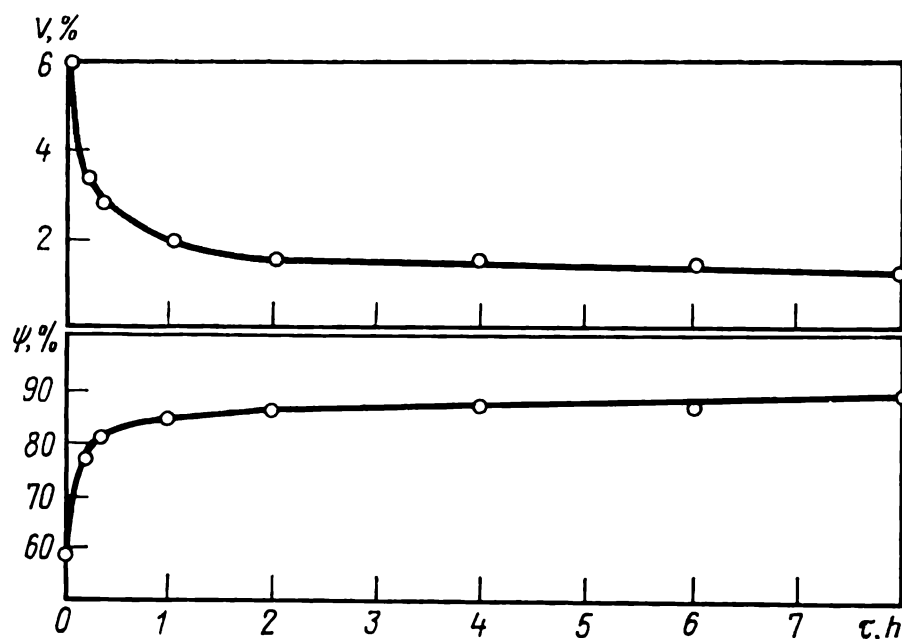


Fig. 7. Volume percentage of dissolved structural components ( $V$ ) and relative reduction at 400 °C ( $\psi$ ) versus time of homogenizing at 500 °C; ingot of duralumin Д16 150 mm in diameter (*I. I. Novikov, V. S. Zolotarevsky and T. N. Churbakova*)

normal to the diffusion line  $x$  is proportional to the time  $d\tau$ , area  $ds$ , and concentration gradient  $dC/dx$ :

$$dm = -D \frac{dC}{dx} ds d\tau \quad (1)$$

The diffusion coefficient  $D$  depends on the nature of alloy, the type and composition of the solid solution, grain size, and especially on temperature:

$$D = Ae^{-Q/RT} \quad (2)$$

where  $R$  = gas constant

$T$  = temperature

$Q$  = activation energy of diffusion

$A$  = a constant virtually independent of temperature

Temperature enters the exponent of the expression for the diffusion coefficient, and therefore, a slight increase in temperature should give an appreciable acceleration of the diffusion rate. Homogenizing annealing is usually carried out at temperatures above 0.90-0.95  $T_{m.p}$  (Kelvin scale), but below the solidus point of an alloy. In some cases the homogenizing temperature may be within a range of 0.8-0.9  $T_{m.p}$ .

The activation energy  $Q$  of diffusion ensures transition of atoms in the lattice from one position to another. An excess energy required for such transition is obtained by an atom from its neighbours, since the process of interchange of kinetic energy between atoms takes place continually. Since the activation energy also enters the exponent of the above equation, it can have an appreciable effect on the diffusion coefficient.

The activation energy of elements dissolved interstitially is lower than that of substitutionally dissolved elements, and therefore, the latter can diffuse less quickly than the former. For instance, the alloying elements which dissolve substitutionally in the austenite have an appreciably lower diffusion mobility than the carbon which is dissolved interstitially in iron. The activation energy of carbon diffusion in the austenite of medium-carbon steel is roughly 31 000 cal/g-atom, while the activation energy of diffusion of the principal alloying elements in austenite usually exceeds 60 000 cal/g-atom. The rate of carbon diffusion in austenite is several orders of magnitude greater than that of the principal alloying elements.

Some alloying elements (Cr, Mo, W, etc.) not only diffuse slowly by themselves, but also slow down the diffusion of carbon in austenite. For instance, the activation energy of carbon diffusion in steel with 0.4 per cent C is approximately 31 000 cal/g-atom; alloying this steel with 2.5 per cent Cr increases the activation energy of carbon diffusion up to 37 000 cal/g-atom.

In carbon-steel ingots, dendritic segregation usually disappears upon heating for plastic forming, owing to quick diffusion of carbon in the austenite, so that homogenizing annealing is not needed. On the contrary, alloy-steel ingots must be specially homogenized, i.e. heated at 1050-1250 °C to eliminate intercrystalline segregation and dissolve the non-equilibrium excess carbides of eutectic origin.

It follows from Fick's law that the rate of diffusion processes should diminish as the process of homogenization develops. Indeed, the rate of diffusion is  $\left| \frac{dm}{d\tau} \right| = D \frac{dC}{dx} ds$ , and the concentration gradient  $dC/dx$  diminishes during homogenizing, i.e. the process may be assumed to be self-decelerating. A conclusion of practical importance can then be made that homogenizing is most intensive at the initial stage of annealing. This may be illustrated by the graph in Fig. 7, which shows that the total amount of excess phases in duralumin Д16 diminishes after the first 30 minutes of heating much more appreciably than after 7 hours of subsequent heating. Therefore, a very long time of homogenizing is not practicable, since it causes an unnecessary consumption of electric energy (or fuel) and lowers labour productivity. Raising the

temperature of annealing can provide an incomparably better effect than increasing the time of heating.

The holding time in homogenizing annealing usually varies between a few hours and a few tens of hours (excluding the time of heating to the specified temperature). The holding time can be reduced by raising the temperature of heating.

The time of full homogenization depends not only on the temperature of annealing and the nature of alloy, which both determine the diffusion mobility of components in the solid solution, but also on the initial microstructure of the alloy as cast. The rate of homogenizing depends on the size of excess-phase particles and the size of dendritic cells of the main phase.

The relationship between the time of full dissolution of the excess phase,  $\tau_d$ , and the average size  $m$  of particles of that phase may be written as

$$\tau_d = am^b \quad (3)$$

where  $a$  and  $b$  are constants for the given alloy and given temperature of homogenizing annealing. For aluminium alloys, the exponent in the formula is within a range of 1.2-2.5. Naturally, the time of full dissolution lessens with diminishing the size of inclusions. Within the range of practical values of  $m$ , the relationship between  $\tau_d$  and  $m$  is almost linear.

As the size of dendritic cells decreases, the average concentration gradient across the cell cross-section increases (for a constant difference of concentrations of solution at the boundary and in the centre of a cell) and, in accordance with Fick's law, the diffusion should proceed quicker. The size of dendritic cells can also have an indirect effect on the rate of homogenization, since the size of excess phase particles diminishes with diminishing the size of dendritic cell.

There can be two ways of accelerating homogenization by controlling the microstructure. The first is to increase the rate of crystallization of an alloy. The higher is the rate of crystallization, the smaller is the size of dendritic cells, and therefore, the finer will be the particles of the excess phase that crystallize at their boundaries. For that reason ingots and castings that solidify at a high cooling rate are homogenized more quickly and thoroughly, since they have a finer structure. For instance, continuously cast ingots of small cross-section are homogenized more quickly than the larger ones; die castings are homogenized more quickly than sand-mould castings.

The second way to accelerate homogenizing is to refine the structure of ingots by plastic working. For instance, a prolonged homogenizing annealing of alloy steel ingots can be replaced with

increasing the time of heating of deformed articles of that steel before the last deforming stage. With aluminium alloys, annealing of ingots is sometimes replaced with homogenizing of pressed tubes or die blanks. This method can accelerate homogenizing annealing appreciably, though requires that the rate of ingot pressing be somewhat reduced.

The accelerating effect of plastic working on dissolution of excess phases is determined by the nature of the structural changes occurring during the process. The structure of various alloys may change differently during plastic deformation, depending on the nature of the excess phase and the relation between the mechanical properties of that phase and the matrix. For instance, the *T*-phase ( $\text{Al}_2\text{Mg}_3\text{Zn}_3$ ) in aluminium alloy, type B95, is refined appreciably and stretched into thin fibres on hot rolling, the distance between the fibres diminishing as the reduction ratio is increased. Thus, hot plastic working of this alloy accelerates sharply the dissolution of excess phase, the effect being greater at larger deformation ratios (Fig. 8). On the other hand, hot or cold working of an aluminium alloy with 4.5 per cent Cu has only a slight effect on the size of  $\text{CuAl}_2$  particles and distances between them. For that reason the time of dissolution of  $\text{CuAl}_2$  particles in that alloy varies only slightly even at high reduction ratios.

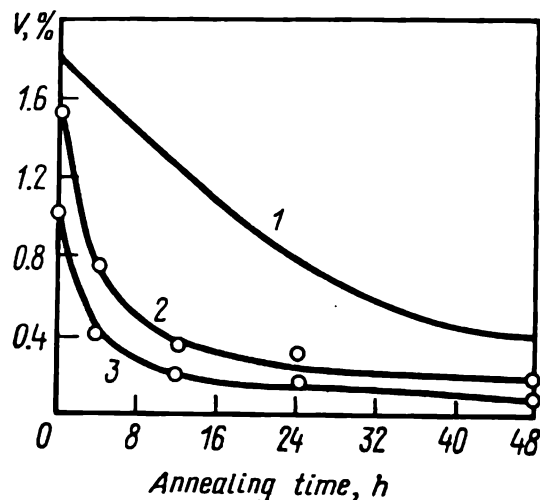


Fig. 8. Effect of time of annealing at  $460^\circ\text{C}$  on volume percentage of dissolved phase ( $V$ ) in type B95 alloy (1) as cast; (2) rolled at  $460^\circ\text{C}$  with 50% reduction; (3) ditto, 75-% reduction (after A. M. Peti and M. C. Flemings)

### Secondary Structural Changes

Along with the principal structural changes discussed above, which are the object of homogenizing annealing, secondary structural changes can also take place; these should be taken into consideration when selecting the conditions of heat treatment.

**Grain coarsening.** In alloys susceptible to polymorphic transformations, homogenizing in the region of high-temperature phase may result in grain coarsening (on the causes of grain coarsening upon passage through polymorphic change point see 2.2.1). For example, homogenizing annealing of alloy steels, which is done at high temperatures, forms coarse austenitic grain. This coarse grain can be refined in steel ingots through subsequent plastic working. Shaped castings of alloy steel must be subjected to second-order annealing or normalizing in order to refine their grain and eliminate the unwanted aftereffects of overheating (see 2.2.3).

**Grain refinement.** In cast alloys based on Al-Mg or Al-Zn-Mg system (types AЛ8, AЛ27-1, AМr6 and 1915), homogenizing

produces grain refinement (with the grain size diminishing by 33-66 per cent). This unusual phenomenon has been discovered quite recently and its practical significance is not yet established. It may be assumed that new grain boundaries are formed owing to the processes of polygonization and recrystallization.

**Particle coarsening of excess phases.** If an alloy cannot be single-phase in equilibrium, then the excess phases that are not able to dissolve fully at the temperature of homogenizing will coagulate and form rounded-off particles as the time of annealing is increased. For instance, branched crystals of  $\text{Mg}_2\text{Si}$  silicide, which cannot pass fully into the solid solution, become more compact at sufficiently high temperatures of annealing. The shape of some excess phases in alloy steels changes in a similar way.

**Heterogenization.** In order to transfer non-equilibrium excess phases into solid solution, the temperature of homogenizing annealing is chosen such as to have a sufficiently high solubility of the components of the excess phases in the base metal. In multi-component alloys, this may result in a low solubility of the components that are not included into the non-equilibrium excess phases, i.e. are present in the basic solid solution after crystallization. Two different processes will then occur simultaneously during homogenizing annealing: (a) dissolution of the non-equilibrium excess phases in the solid solution which is unsaturated relative to them, i.e. homogenization of the alloy proper, and (b) precipitation of the other phases from the solid solution, which is supersaturated relative to these phases, i.e. heterogenization of the structure, which plays an important part in homogenizing annealing of many aluminium alloys.

Most aluminium alloys contain manganese and some of them, also zirconium and chromium. With a quick crystallization, such as in continuously cast ingots or thin-walled die castings, these elements pass fully or partially into the aluminium-based solid solution. The eutectic or peritectic temperatures of the corresponding binary systems are close to the melting point of aluminium (658.5 °C in Al-Mn, 660.5 °C in Al-Zr, and 661.4 °C in Al-Cr system). The temperature of homogenizing annealing of aluminium-alloy ingots is substantially lower (450-550 °C) than these temperatures of eutectic or peritectic equilibrium at which the solubility of the elements considered is at its maximum, while their equilibrium solubility at 450-550 °C is substantially lower than the maximum value. For instance, the solubility of these elements in binary systems at the eutectic or peritectic temperature and at 500 °C is respectively: 1.4 per cent and 0.34 per cent Mn; 0.28 per cent and 0.05 per cent Zr; 0.72 per cent and 0.19 per cent Cr. For that reason, homogenizing annealing of ingots may result in pre-



precipitation of intermetallic compounds of manganese, chromium or zirconium from the solid solution which is supersaturated with a corresponding element.

Owing to coring, the amount of intermetallic precipitates in the central zone and peripheral layers of a dendritic cell may be different. For instance, if a solid solution supersaturated more with manganese is formed at the periphery of dendritic cells, then the density (i.e. the number of particles per unit volume) of manganese aluminide will be large there (Fig. 9).

Heterogenization upon homogenizing annealing may have an appreciable effect on the behaviour of an alloy in subsequent treatment and on the properties of final products. For instance, precipitation from the aluminium solution, which is supersaturated with manganese, chromium or zirconium, upon homogenizing annealing of ingots may change the extrusion effect of the metal (see 5.2.1). Disperse aluminides of these transition metals increase the temperature of the beginning of recrystallization of an alloy. If this temperature turns to be higher than the tempera-

ture of heating for hardening, then the deformed semiproduct will remain unrecrystallized after the full heat treatment and will therefore have an increased strength. The higher is the density of disperse precipitates of transition metal aluminides, the higher will be the temperature of the beginning of recrystallization. A high temperature and a long holding time in homogenizing annealing of ingots promote coagulation of the products of decomposition of supersaturated solution and thus lower the density of aluminide precipitates. As a result, the temperature of the beginning of recrystallization of deformed semiproducts diminishes and, if it turns to be lower than the temperature of heating for hardening, there will be no extrusion effect (i.e. the strength of non-recrystallized material will not rise). Thus, in order to utilize the effect of heterogenization of ingot structure, the conditions of annealing should be chosen such as to ensure the required dispersity and density of precipitates of transition metal aluminides.

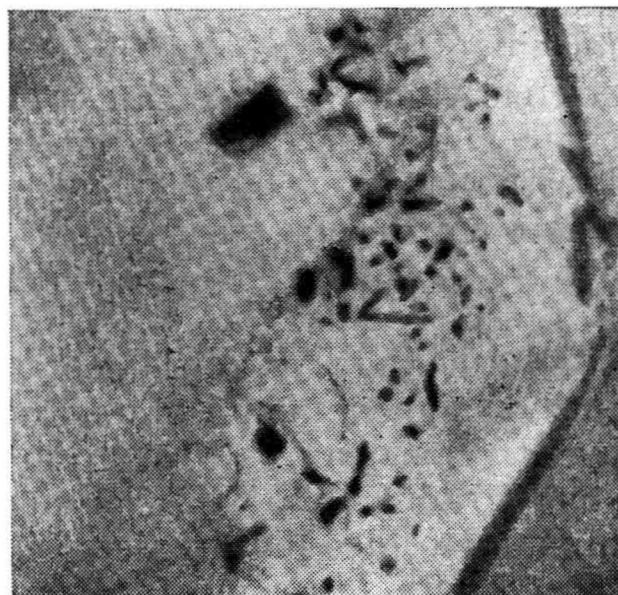


Fig. 9. Microstructure of AMr-6 alloy ingot as annealed at 450 °C for 2 h; thin-foil electron micrograph,  $\times 10\,000$  (after V. S. Zolotarevsky and V. V. Istomin)

The process of heterogenization in ingots may develop not only during isothermal holding, but also during cooling from the temperature of annealing. The cooling rate of ingots in annealing is not specified as a rule. Under industrial conditions a batch of articles is cooled in the furnace or in air. As the temperature lowers, the solubility of the principal alloying elements (copper, magnesium, etc.) in aluminium decreases. With a very slow cooling of ingots, precipitation of coarse particles of  $\text{CuAl}_2$ , S-phase and other phases is probable. With subsequent heating before forming, these coarse precipitates cannot dissolve fully, are stretched in the direction of deformation, and impair the mechanical properties, especially ductility, in lateral directions. In order to prevent this and other unwanted effects of structural heterogenization, aluminium alloy ingots should be cooled quickly (in open air) from the temperature of homogenizing annealing.

**Hardening.** Air cooling of alloy steel ingots from the temperature of homogenizing annealing may result in full or partial martensitic hardening of surface layers (for instance, in ingots of steel Grades 18X2H4BA and 40XHMA). If surface defects of the ingots (welded-on droplets, films, sandmarks, etc.) are not removed with scale and the ingots are to be subjected to roughing, then high-temperature softening is needed after homogenizing annealing.

**Secondary porosity.** A long holding time in annealing of cast aluminium alloys may sometimes result in the development of porosity. For instance, if the volume proportion of pores in a specimen of Д16 duralumin (as cast) may be 0.5 per cent it increases up to 0.8 per cent upon annealing for 3 h at 490 °C.

The porosity that develops in alloys during heating is called secondary, to distinguish it from the primary porosity which forms on crystallization. The effect of secondary porosity increases with higher temperatures of annealing.

One of probable causes of secondary porosity is precipitation of hydrogen from the supersaturated solid solution formed through rapid crystallization. Another cause is the Kirkendall effect, i.e. inequality of opposite diffusion fluxes of atoms of two different constituents. With the vacancy mechanism of diffusion, the diffusing atoms that move most quickly from the solid solution leave excess vacancies behind them and thus form what is called *diffusion porosity*.

The increase in porosity on common homogenizing annealing is quite small in the absolute magnitude and can hardly have any effect on the properties of final products, especially in cases when pores are welded up through hot plastic deformation.

### 1.1.3. VARIATIONS OF PROPERTIES OF ALLOYS ON HOMOGENIZING ANNEALING

#### Cast Alloys

The principal effect of homogenizing annealing is an increased ductility of cast alloys. When selecting the conditions of annealing of ingots, the ductility indices should be measured at the temperature of the first operation of hot working, rather than at room temperature. If, for instance, ingots of alloy Grade Д16 are intended for pressure moulding, the ductility indices should be determined at the corresponding temperature, i.e. at 400°C (see Fig. 7).

The mechanical properties of shaped castings should be checked at the operating temperature of final products, for instance, at room temperature.

As brittle phases are being dissolved, the ductility increases and, after these phases have been dissolved fully, remains at a constant value (see Fig. 7). The relative elongation and relative reduction of aluminium alloy ingots at the temperatures of hot working increases 1.5-3 times owing to homogenizing.

When homogenizing annealing is aimed at increasing the ductility, the optimum time of homogenizing may be taken as the time for full dissolution of non-equilibrium excess phases. As has been noted in 1.1.2, this time reduces, by formula (3), with refinement of excess phase particles and also with refinement of dendritic cells. Apart from dissolution of brittle excess phases, coagulation of these phases may also produce a useful effect. For instance, homogenizing annealing of heat-resistant steel Grade X25H16Г7 at 1150°C involves partial dissolution and coagulation of the excess phases, so that only rounded-off isolated inclusions of these phases remain at grain boundaries instead of continuous interlayers, and the ductility of the ingot increases.

A higher ductility in ingots of alloy steels and aluminium and other alloys diminishes the loss of metal through fissure defects after the first operation of hot working, enables higher deformation ratios and higher deformation rates to be employed, especially at the initial deforming stages, and improves the state of strip edges (diminishes the percentage of edge flaws in hot-rolled strips).

The role of homogenizing is especially important for shaped cast articles, since these are not subjected to plastic deformation which might refine their structure.

Homogenizing annealing cannot eliminate fully the effect of the initial cast structure: the smaller the size of dendritic cells in cast alloy, the higher will be the ductility index of ingots after homogenizing.

### Deformed Alloys

Though hot working causes radical changes in the structure of an alloy, these changes are still insufficient to eliminate the effect of cast structure in subsequent cold working. The "inherited" cast structure in which dendritic segregation has not been eliminated fully may manifest itself in a reduced ductility of the cold-deformed alloy. This may be explained by the fact that hot working, even though having a strong refining and "intermixing" effect on the structure, cannot eliminate fully the microscopic heterogeneity of the alloy produced through dendritic segregation. Homogenizing of ingots increases the ductility of cold-deformed alloys and thus improves the state of edges of cold-deformed strips, makes it possible to reduce the number of intermediate annealing operations and increase the reduction ratio in cold rolling, and improves the drawability of sheets in deep drawing.

The inherited cast structure may sometimes be very stable and influence the service properties of products, notwithstanding the substantial treatment (such as plastic working, hardening, tempering, etc.) during processing of ingots. For instance, in high-carbon steels alloyed with chromium and tungsten, carbide eutectic may appear owing to dendritic segregation. This phenomenon has been termed *carbide segregation*. Coarse aggregates of eutectic carbides will then remain in final products even after hot rolling and hardening. In tool edges and friction faces of ball-bearings, such places are likely to cause crumbling.

Hot or cold rolling with subsequent recrystallization annealing or hardening, which change strongly the structure, are often unable to eliminate the difference between the properties of aluminium alloy sheets produced from non-homogenized and homogenized ingots. For instance, a sufficiently deep homogenization of ingots of Avial alloy (Grade AB) increases the relative elongation of annealed sheets by one-fourth compared with that of sheets produced from non-homogenized ingots).

Homogenizing of ingots may even have an adverse, rather than improving, effect on some properties of final products. For instance, 24-h homogenizing of duralumin ingots (Grade Д16) at 490 °C increases by a few per cent the relative elongation of hardened and age-hardened sheets, but concurrently lowers the ultimate strength by 1-1.5 kgf/mm<sup>2</sup><sup>1</sup>, which may be attributed to the specific behaviour of manganese during homogenizing. As has been mentioned earlier, the solubility of manganese in aluminium at temperatures near 500 °C is relatively low, so that the

---

<sup>1</sup> A stable change of the ultimate strength of deformed light alloys by 1-1.5 kgf/mm<sup>2</sup> may be of practical value, whereas for most steels this change is too little to be considered seriously.

manganese-supersaturated solution formed on crystallization undergoes precipitation. Precipitated particles of manganese intermetallide somewhat reduce the strength of recrystallized duralumin sheets after full heat treatment (quenching and age-hardening).

Homogenizing annealing has the most marked and practically important effect on ductility, impact toughness and fatigue properties of articles (pressed strips, shaped rolled products, forgings, etc.) in directions across metal fibres, since the brittle excess phases are stretched along the direction of the main deformation during plastic working.

Homogenizing annealing is an operation that takes up relatively much time and is linked with high consumption of fuel or electric energy, since large masses of metal should be heated. For that reason the practicability of this process should be decided for each particular case.

Homogenizing annealing of iron alloys, which requires much fuel and is linked with large losses of metal to scale, is only employed for high-quality alloy steels for critical applications (the temperature of annealing is chosen within a range of 1050-1250 °C). Among carbon steels, only free-cutting steels are subjected to homogenizing annealing. They contain an increased percentage of sulphur (up to 0.2-0.3 per cent against 0.04-0.06 per cent S in common steels), which improves their machinability. Sulphur can segregate strongly at grain boundaries during crystallization and cause red shortness during rolling. This defect in free-cutting steels can be eliminated by homogenizing annealing at 1150 °C.

Most of deformable aluminium alloys are homogenized in ingots to improve their deformability and increase the mechanical properties of semiproducts. The temperature of annealing, usually within the range of 450-550 °C, is selected according to the type of alloy and kind of semiproduct.

Deformable magnesium alloys are homogenized in ingots at 390-405 °C for the same purpose as aluminium alloys. Homogenizing is often combined with the operation of heating of ingots before hot working, with increasing accordingly the time of holding in the furnace.

Homogenizing annealing as a separate operation is not employed with shaped castings of aluminium and magnesium alloys. Instead, their homogenizing is included organically into the operation of heating before quenching. The temperature and time of the heating are chosen such as to transfer into the solid solution as much of the excess phases as possible.

Homogenizing annealing of ingots and shaped castings of copper, nickel, titanium and zinc alloys gives no marked effect

and is therefore resorted to only very seldom. An exception are ingots and shaped castings of some tin bronzes for critical applications, which are homogenized at 650-700 °C to obtain a higher ductility; the process is aimed at dissolving the non-equilibrium excess of brittle  $\alpha + \text{Cu}_{31}\text{Sn}_8$  eutectoid. Homogenizing annealing at temperatures near 350 °C is also used for superplastic zinc-aluminium alloys in which the superplastic properties have been impaired by inclusions of non-equilibrium eutectic.

#### **1.1.4. HOMOGENIZING WITH HEATING ABOVE THE NON-EQUILIBRIUM SOLIDUS TEMPERATURE**

In certain cases the degree of homogenization obtained at temperatures near and below the non-equilibrium solidus may turn to be insufficient. The required completeness of homogenization is then either utterly unattainable or can only be achieved with very long holding time unsuitable for industrial conditions. In addition, it is always desirable to shorten the time of homogenizing as much as possible. In that connection the possibility of homogenizing annealing at temperatures above the non-equilibrium solidus seems very attractive. This method with heating above the non-equilibrium solidus but below the equilibrium solidus is used industrially for some aluminium alloys.

Industrial annealing of aluminium alloy ingots above the non-equilibrium solidus is usually avoided because of the risk of *burning*. The phenomenon of burning is well known from the practice of hardening of aluminium alloy sheets, where it causes various irreparable metal defects, such as hardening cracks and small blowholes in the surface of sheets, and in addition, can reduce appreciably the strength and ductility. The common cause of burning is partial melting of the metal during heating for hardening. Intercrystalline hardening cracks then easily form at molten portions under the action of hardening stresses. The molten portions have a eutectic composition, so that quick crystallization during hardening forms at grain boundaries an intermediate layer of a brittle intermetallide which is a constituent of the eutectic. Even if no visible hardening cracks were formed through burning, these brittle intercrystalline layers reduce the ductility of sheets and may be the cause of metal spoilage.

Also well known in the practice is the phenomenon of strong burning of thin articles made of steel, copper or copper alloys if held for an excessively long time or at too high a temperature in an oxidizing atmosphere. This type of burning is caused by the penetration of oxygen along grain boundaries through the whole section of articles and the formation of oxides at grain boundaries; the ductility index can then drop to zero.

The conditions of an ingot during homogenizing annealing at a temperature above the non-equilibrium, but below the equilibrium solidus differ radically from those just described. For instance, the aluminium-based solid solution at  $t_1$  (Fig. 10) is unsaturated relative to the non-equilibrium inclusions in the melt. The alloying element of the melt (copper) will diffuse into the aluminium solution and dissolve the non-equilibrium inclusions. Thus, heating above the non-equilibrium but below the equilibrium solidus causes no burning on melting, since portions of the melt disappear in the process of isothermal holding on homogenizing annealing.

Burning due to intercrystalline oxidation is not dangerous here, since, firstly, the surface of an aluminium-alloy ingot is protected by a dense oxide film, and secondly, probable intergrain oxidation in a thin surface layer of the ingot will have no effect on the properties of metal (unlike the case with sheets, wire and other thin-section articles).

The processes of homogenizing on heating above the non-equilibrium solidus point develop appreciably more quickly than with the common annealing below the solidus. For instance, the temperature of non-equilibrium solidus for duralumin Д16 is roughly 508°C, and that of equilibrium solidus, near 530°C (the solidus points may vary somewhat with variations in the metal composition within the limits specified for the given grade). The time of dissolution of non-equilibrium excess phases in an ingot 150 mm in diameter at 515°C is by 60 per cent shorter than that at 480°C.

The reason why heating to temperatures above the non-equilibrium solidus point accelerates appreciably the process of homogenizing is not the presence of a liquid phase, but the fact that the diffusion coefficients of alloying elements increase with temperature. The principal link in the process of dissolution of phases at temperatures either above or below the non-equilibrium solidus point is the removal of atoms of alloying elements through diffusion from interphase boundaries into the central zone of a dendritic cell. The passage via the solidus point is not in itself critical

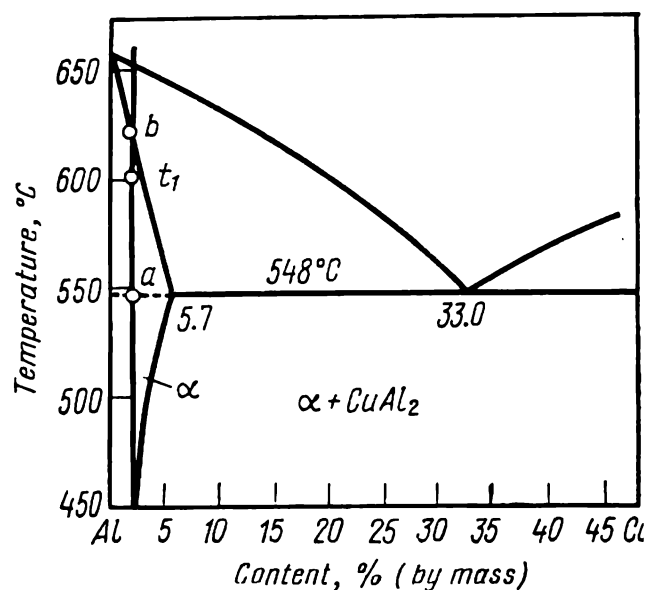


Fig. 10. Constitutional diagram of Al-Cu system

$a$ —non-equilibrium solidus point of Al + 2.3% Cu alloy;  $b$ —equilibrium solidus point of the same alloy;  $t_1$ —homogenizing temperature

for the process of homogenization, but increasing the temperature of annealing even by 20-30 degrees C can increase the diffusion coefficients significantly, for instance, two times compared with the conditions of common annealing [it should be recalled that temperature enters exponentially into the equation of diffusion coefficient (formula 2)].

Homogenizing at temperatures above the non-equilibrium solidus point shortens appreciably the time of annealing required for obtaining the specified ductility for plastic forming. For some

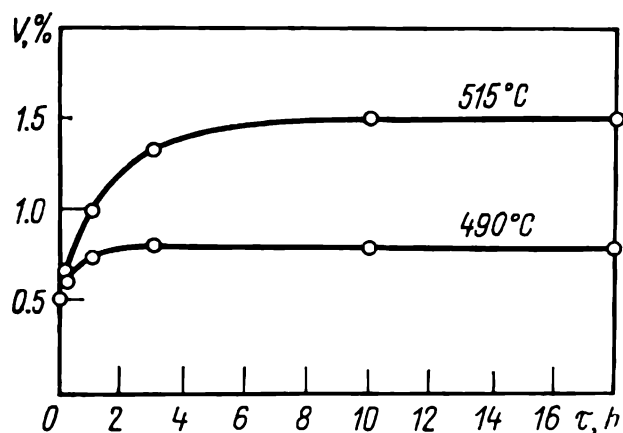


Fig. 11. Dependence of volume percentage of pores ( $V$ ) on time  $\tau$  of annealing of Al6 duralumin at temperatures above and below the non-equilibrium solidus point (508°C) (I. I. Novikov, V. S. Zolotarevsky, and A. V. Kurbatova)

types of alloy, it is possible to increase the technological ductility (compared with that obtained through common homogenizing) and correspondingly to employ higher reduction ratios and rates. Besides, the ductility indices of deformed semiproducts, especially in directions across fibres, are also improved. The strength properties of deformed semiproducts of aluminium alloys may be either slightly lower or higher than after common annealing, depending on the conditions of annealing at temperatures above the non-equilibrium solidus

point, since these conditions determine the dispersity of particles of manganese aluminide which precipitate upon decomposition of manganese-supersaturated aluminium solution.

The principal drawback of homogenizing with heating above the non-equilibrium solidus point is that porosity can develop appreciably more rapidly (Fig. 11). In addition to the causes of porosity in common annealing (see Sec. 1.1.2), a new cause may be named here (according to E. D. Zakharov). With a quick crystallization in the ingot, the aluminium-based solid solution becomes supersaturated with hydrogen. The solubility of hydrogen in melt is much more greater than that in crystals, so that the hydrogen tends to move from this supersaturated solid solution into the liquid phase that forms upon heating the ingot above the non-equilibrium solidus point. The subsequent relatively slow isothermal crystallization of non-equilibrium inclusions in the melt results in precipitation of the hydrogen, which forms gas blowholes. It is still not established definitely whether these blowholes can be welded up completely by hot forming of the ingot and also what is their effect on the operational properties of ar-



ticles. For the reasons given above, homogenizing annealing with heating above the non-equilibrium solidus point, which is called 'high-temperature' homogenizing in the processing of aluminium alloys, should be resorted to only after careful testing.

High-temperature homogenizing is quite effective with alloys in which the non-equilibrium fusible constituent is fully soluble on slow heating of ingots. For instance, the  $\beta$ -phase ( $\text{Al}_3\text{Mg}_2$ ) in magnaliums or  $T$ -phase ( $\text{Al}_2\text{Mg}_3\text{Zn}_3$ ) in Al-Zn-Mg alloys can pass very quickly into the solid aluminium solution on heating the ingots and disappear before being melted at the temperature of non-equilibrium solidus of the alloy. For that reason, for instance, ingots of magnalium Grade AMr6 are recommended to be subjected to high-temperature homogenizing at 490-510 °C (the non-equilibrium solidus point of the alloy is 450 °C). With such conditions of annealing, the dissolution of the non-equilibrium  $\beta$ -phase during heating is accompanied with another important process which takes place during high-temperature holding, i. e. coagulation of branched particles of  $\text{Mg}_2\text{Si}$ , which cannot dissolve fully; these particles then acquire a more desirable compact shape during a relatively short time.

#### LITERATURE

Golikov I. N., Dendritic Segregation in Steel (*Dendritnaya likvatsiya v stali*). Moscow, Metallurgizdat, 1958, 352 pp., ill.

Novikov I. I., Zolotarevsky V. S., Dendritic Segregation in Alloys (*Dendritnaya likvatsiya v splavakh*). Moscow, Nauka, 1966, 155 pp., ill.

Kolachev B. A., Livanov V. A., Elagin V. I., Physical Metallurgy and Heat Treatment of Non-ferrous Metals and Alloys (*Metallovedenie i termicheskaya obrabotka tsvetnykh metallov i splavov*). Moscow, Metallurgiya, 1972, 480 pp., ill.

Flemings M. F., Solidification Processing. New York, McGraw-Hill, 1974.

Martin J. W., Doherty R. D., Stability of Microstructure in Metallic Systems. Cambridge, Cambridge University Press, 1976.

## 1.2. RECRYSTALLIZATION AND PRERECRYSTALLIZATION ANNEALING

Recrystallization and prerecrystallization annealing can eliminate various non-equilibrium deviations in the structure of a metal which have formed through work hardening due to plastic deformation. These types of heat treatment are usually made after cold plastic working.

### 1.2.1. STRUCTURAL CHANGES IN METAL ON COLD PLASTIC WORKING

Plastic deformation causes certain structural changes in metal, which can be conditionally classed into three groups as follows: (a) changes in the shape and size of crystallites; (b) changes in the space orientation of crystals; and (c) changes in the internal structure of crystallites<sup>1</sup>.

<sup>1</sup> Intercrystalline voids and microfissures, which may lead to fracture of metal, are not discussed here, since these defects cannot be eliminated by annealing.

### Changes in Shape and Size of Crystallites

The shape of metal changes during plastic working owing to plastic deformation of each crystallite. As is known from the course of physical metallurgy, the shape and size of crystallites change through the processes of glide and twinning. The principal change in the shape of crystallites consists in that they are stretched in the direction of the main tensile deformation (for instance, in the direction of rolling or drawing). Besides, metal grains may widen in conformity to the pattern of principal deformations.

As the degree of cold deformation (for instance, the reduction ratio in rolling) is increased, metal grains are stretched ever more and the structure of the metal becomes fibrous.

Changes in the shape and size of crystallites are readily visible in etched microsections or under the microscope.

### Deformation Texture

On plastic deformation, crystal lattices of grains become preferably oriented in space, i.e. a deformation texture is formed in plastic-worked metal. The appearance of a texture is one of the most important consequences of glide orientation in each grain along definite planes and directions of the spatial lattice, since these directions regularly rotate relative to the deformation axes of an article. For example, the direction of glide in a tensioned monocrystal approaches the axis of tension.

The nature of deformation texture depends on the kind and conditions of plastic working (mainly on the pattern of main deformations) and on the nature of the metal (the type of crystal lattice and the stacking fault energy). Table 2 gives the textures for cold drawing and cold rolling that are most typical of each type of crystal lattice.

**Table 2. Typical Deformation Textures on Cold Plastic Working**

Plastic working	Crystal lattice	Texture	Plastic working	Crystal lattice	Texture
Drawing	f.c.c.	$\langle 111 \rangle$ and $\langle 100 \rangle$	Rolling	f.c.c.	$\{110\}$ $\langle 112 \rangle$ and $\{112\}$ $\langle 111 \rangle$
	b.c.c.	$\langle 110 \rangle$		b.c.c.	$\{100\}$ $\langle 110 \rangle$
	h.c.p.	$\langle 10\bar{1}0 \rangle$		h.c.p.	$\{0001\}$ $\langle 11\bar{2}0 \rangle$

In f.c.c. metals (Al, Cu, Ni, Au, Ag, Pb), drawing of a wire results in metal grains being preferably oriented with their  $\langle 111 \rangle$  cube diagonals along the axis of wire or some grains being orient-

ed as  $\langle 111 \rangle$  and others, with their  $\langle 100 \rangle$  cube edges along the axis; in the latter case we have what is called *double texture*.

In b.c.c. metals (Fe, W, Mo),  $\langle 110 \rangle$  cube face diagonals are oriented along the axis of wire.

The texture obtained on pressing is usually similar to that formed on drawing. A drawing texture can be characterized by space orientation of a definite crystal direction relative to which the crystal may be rotated randomly. As distinct from this, a rolling texture can be characterized by preferable orientation of both crystal direction and crystal plane.

In cold-rolled f.c.c. metals the  $\{110\}$  plane is most often oriented parallel with the rolling plane, and the  $\langle 112 \rangle$  direction is parallel with the direction of rolling. This texture, termed *brass-type texture*, is designated as  $\{110\} \langle 112 \rangle$ .

Rolling of copper with a heavy reduction yields a different texture:  $\{112\} \langle 111 \rangle$ , which has been called *copper-type texture*. This texture can appear under the conditions of cross-slip of dislocations. In copper, the stacking fault energy is higher than in brass and therefore dislocation cross-slip can occur more easily. In aluminium, which has an appreciably higher stacking fault energy, dislocations can freely cross-slip, and the texture usually formed in aluminium is  $\{112\} \langle 111 \rangle$ . Alloying with an element which can lower the stacking fault energy (for instance, adding zinc or aluminium to copper) inhibits cross-slip, so that the copper-type texture changes to brass-type texture  $\{110\} \langle 112 \rangle$ . With increasing temperature of rolling, thermal fluctuations promote constriction of stacking faults, cross-slip of dislocations is facilitated, and the brass-type texture tends to change to copper-type texture.

In cold-rolled b.c.c. metals, the  $\{100\}$  cube plane sets parallel with the plane of rolling and the  $\langle 110 \rangle$  face diagonal of the cube is oriented along the direction of rolling. In cold-rolled iron, low-carbon steel and transformer steel (3 per cent Si), superposition of three types of orientation has been found, i.e.  $\{100\} \langle 110 \rangle$ ,  $\{112\} \langle 110 \rangle$ , and  $\{111\} \langle 112 \rangle$ , the  $\{100\} \langle 110 \rangle$  orientation being the principal one and typical of most crystallites.

It may be noted in conclusion that not all crystals in deformed metal have the ideal preferable orientation. The perfection of a texture improves with increasing deformation.

### Changes in Internal Structure of Crystals

The amount of heat liberated in plastic-worked metal is less than the energy spent on deformation. Up to 10-20 per cent of the work of forming is absorbed in the metal. This portion of the work, which amounts to 0.1-1 cal/g at medium or large degrees of

deformation, is retained in the metal in the form of the energy of crystal lattice defects formed through plastic deformation.

The most important change in the fine structure of deformed metal is an increase in the density of dislocations (the ratio of the total length of dislocations to the volume of metal). In a thoroughly annealed piece of polycrystalline metal the density of dislocations is  $10^6$ - $10^8$   $\text{cm}^{-2}$ , on deforming by a few per cent it increases up to  $10^8$ - $10^9$   $\text{cm}^{-2}$ , and on a heavy deformation, up to  $10^{11}$ - $10^{12}$   $\text{cm}^{-2}$ . Therefore, the density of dislocations can be increased five or six orders of magnitude through cold plastic working.

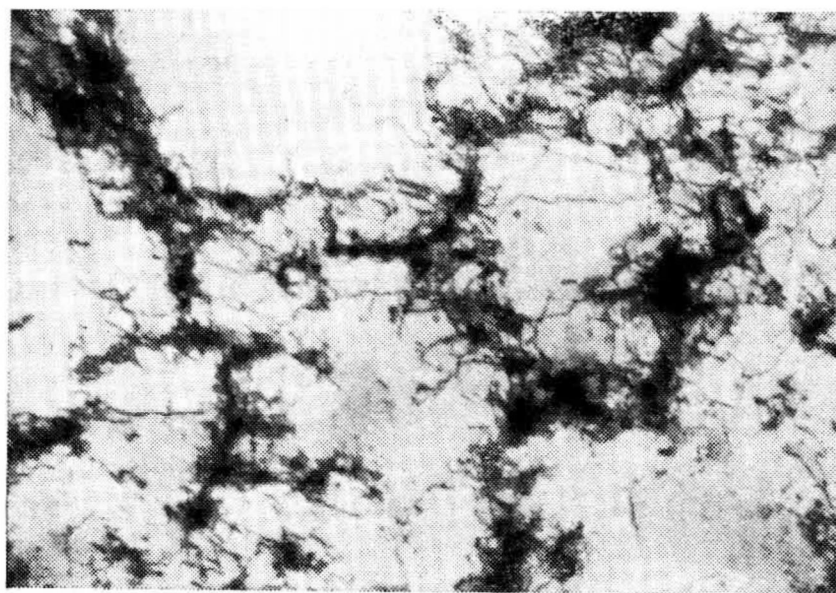


Fig. 12. Cellular structure of chrome-zirconium bronze (0.33% Cr, 0.07% Zr) after 5% extension. Thin-foil electron micrograph,  $\times 12\,000$  (after V. M. Rosenberg and A. I. Novikov)

Thin-foil electron-microscopic studies have revealed the following general tendencies in the pattern of variation of dislocation distribution with increasing deformation.

Even at low deformations, the distribution of dislocations over the volume of crystallites becomes non-uniform, with dislocation pileups being formed in some portions. In most metals and alloys, unhindered cross-slip of unextended or weakly extended screw dislocations results in the formation of spatial dislocation pileups. Typically, this forms dislocation tangles in which the dislocations are intermingled irregularly. As the deformation is increased, the number of tangles and the density of dislocations in them also increase.

At deformation ratios of around 5-10 per cent, a *cellular structure* begins to form in many metals and alloys: dislocation tangles interconnect with one another, thus forming blurred spatial boundaries of regions within which the density of dislocations is relatively low (Fig. 12). These regions are called cells. The size of

cells is of an order of  $1\text{ }\mu\text{m}$  and the thickness of their boundaries, a few tenths of a micron. With increasing deformation, cellular structure becomes more distinct. Cell boundaries become narrower and tend to change from spatial to flat. The cells are fully enclosed by boundaries and only a few dislocations remain inside them. Properly formed cells with flat walls are usually called subgrains, and the corresponding structure, *subgrain structure*.

With increasing deformation, the average density of dislocations increases owing to an increase of their density in tangles at cell boundaries, rather than inside cells.

As the deformation ratio increases, the size of cells diminishes only insignificantly; this is especially true of medium and high deformations. The size of cells is usually within a range of  $0.3\text{--}3\text{ }\mu\text{m}$ . Owing to an excess of dislocations of the same sign at cell boundaries, neighbouring cells and subgrains are disoriented through angles from a few seconds to a few degrees.

The processes of cross-slip and climb of dislocations play an important part in the formation of cellular structure. For that reason, a more perfect cellular structure with larger cells forms at higher temperatures of deforming.

With a low stacking fault energy, cross-slip of extended dislocations is impeded, i.e. cellular structure is less likely to form. Therefore, various metals and alloys, which differ in their stacking fault energy, should be disposed differently to forming cellular structure on being plastic-worked. Cellular structure has been found in cold-deformed Al, Ni, Cu, Ag, Au, Fe, Mo, and many alloys. Austenitic stainless steel,  $\alpha$ -brass, single-phase aluminium and silicon bronzes, which are characterized by a very low stacking fault energy and the tendency of strongly extended dislocations to remain in their glide planes, either show no cellular structure at all or this structure is observed in them at high deformation ratios only.

Plastic deformation increases the concentration of point defects: vacancies and interstitial atoms. Point defects can be generated by jogs on gliding screw dislocations, through annihilation of edge dislocations of opposite signs in neighbouring parallel glide planes or due to some other causes. As the temperature of deforming increases, the non-equilibrium excess of point defects diminishes owing to their accelerated migration to dislocations and grain boundaries, which takes place in the process of deforming.

As the ratio of plastic deformation increases, the number of stacking faults increases along with the increasing density of extended dislocations.

Thus, the theoretical analysis and the results of direct and indirect experiments show that *an increase in the ratio of plastic*

deformation increases the density of dislocations and the excess of dislocations of the same sign, increases the number of jogs and dipoles, can form a cellular structure in the metal, and increases the concentration of point defects and stacking faults. All these changes in the internal structure of crystallites represent the most important result of plastic deformation of metals and alloys.

### 1.2.2. ALTERATION OF METAL PROPERTIES ON COLD PLASTIC WORKING

#### Work Hardening

Plastic working changes various mechanical, physical and chemical properties of metal. The term work hardening (or strain hardening) is commonly understood as the hardening effect in a metal produced through plastic working. In a broader sense it

means the whole combination of structural changes and related changes in the properties of metal caused by plastic deformation.

As the ratio of cold deforming increases, the indices of resistance to deformation (i.e. the ultimate strength, yield strength and hardness) increase, while the ductility indices (relative elongation and relative reduction) diminish (Fig. 13). On deforming a piece of metal by 50-70 per cent, the ultimate strength and hardness usually increase by a factor of 1.5-2 or even three times, depending on the nature of the metal and the kind of plastic working.

Low deformations (up to 10 per cent) usually have more effect on

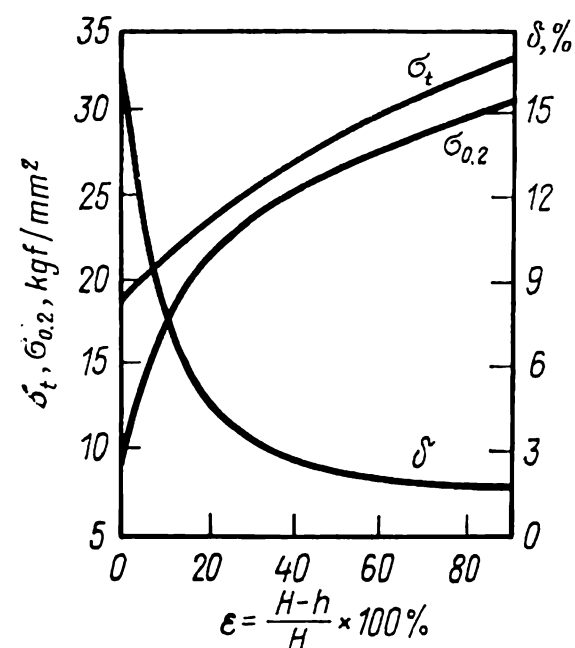


Fig. 13. Dependence of mechanical properties of D1 duralumin on reduction ratio in cold rolling (after A. V. Tretyakov and K. M. Radchenko)

the yield limit than on ultimate strength. At high deformations, the yield limit of some alloys may increase 5-8 times or even more.

The relative elongation decreases sharply even at comparatively low deformations (Fig. 13). A heavy deformation, which can increase the ultimate strength and hardness 1.5-2 times, lowers the relative elongation to 1/10-1/20, or sometimes to 1/30-1/40 of the initial value.

Strain hardening is caused by the structural changes that appear in a metal on plastic working. Putting aside the mecha-

nisms of strain hardening and the nature of dislocation structure, we may say that the rise in deformation resistance indices and the drop in ductility indices on increasing the degree of preliminary cold deformation are due to an increase in the density of dislocations. Owing to a higher density of dislocations in work-hardened metal, the glide of existing dislocations and the generation and glide of "fresh" dislocations are largely impeded.

The boundaries of cells and subgrains serve as barriers for slip dislocations. With increasing deformation, the distances between these barriers diminish (i.e. the cells become smaller), which produces strengthening effect in the metal.

Work hardening may be accompanied with noticeable and sometimes very substantial changes in the physical properties.

Conduction electrons are scattered at point defects and dislocations, because of which the electric resistivity of metal increases on increasing the number of lattice defects through plastic deformation. This change in resistivity is however not large. For instance, on high deformation the resistivity of pure metals may change by 2-6 per cent, whereas their mechanical properties are changed many times.

In alloys, cold deformation may cause changes in electric resistivity different in magnitude and even in sign. In disordered solid solutions, the electric resistivity varies on cold deformation roughly in the same way as in pure metals. If a solution is characterized by long-range order, short-range order, or short-range segregation, then plastic deformation will have a more complicated effect on electric resistivity.

Annealing, which forms a long-range order (superstructure) with a stringent periodicity in the positions of unlike atoms, can strongly lower the electric resistivity. Cold deformation destroys the long-range order and correspondingly increases appreciably the electric resistivity.

Many alloys containing transition metals, including those widely used in industry, such as Nichrome, Chromel (Ni-Cr), Alumel (Ni-Cr-Al-Mn-Si), and German silver (Cu-Ni-Zn), can be brought into what is called the *K*-state, which is characterized by an increased electric resistivity compared with that existing in a solid solution with statistically uniform distribution of atoms. The appearance of *K*-state can be explained by diffusion redistribution of atoms so that the number of bonds between unlike atoms becomes greater than that in statistically disordered solid solution. The most typical feature of the *K*-state is that the electric resistivity decreases appreciably on cold deformation (Fig. 14). Cold deformation destroys the distribution of unlike atoms typical of the *K*-state and the alloy transforms into disordered solid solution.

Dislocations pin domain boundaries in a ferromagnetic and thus impede its magnetization and demagnetization, since these processes are effected through movement of domain boundaries. A higher ratio of cold deformation increases the density of dislocations, and therefore, reduces the magnetic permeability and increases the coercive force.

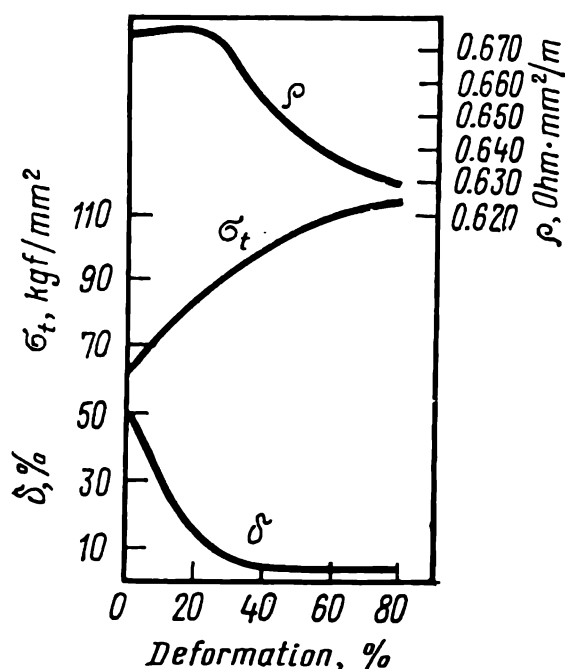


Fig. 14. Effect of deformation on electric resistivity and mechanical properties of Chromel (after I. Ya. Berkovsky, A. G. Kolokolova)

Cold deformation can change the thermoelectromotive force. In a thermocouple made of one and the same metal (work-hardened in one electrode and annealed in the other), the thermo-e.m.f. will increase on increasing the ratio of cold deformation of one of the electrodes.

Work-hardening can only insignificantly vary the modulus of elasticity, so that this effect can be virtually neglected.

Cold deformation increases the chemical activity of a metal, for instance, accelerates its dissolution in acids, and therefore, lowers the corrosion resistance. Exposed dislocations on the surface of

metal serve as centres for metal dissolution in corrosive media.

### Anisotropy of Properties

The properties of cold-deformed metal are different in various directions. This anisotropy of properties is due to two factors: fibrous structure and deformation texture.

In a tensile-test specimen cut across fibres the number of grain boundaries is appreciably greater than in a specimen cut along fibres. Grain boundaries are places where impurities and non-metallic inclusions, such as oxide films, can concentrate. Naturally, the mechanical properties of a metal along fibres will differ from those across fibres. For that reason, a distinction is made between 'longitudinal' and 'transverse' specimens and correspondingly, between 'longitudinal' and 'transverse' properties when inspecting plastic-worked semiproductions. Transverse specimens usually have lower indices of ductility and impact toughness than longitudinal ones.

Any crystallite is anisotropic, i.e. its properties are dependent on crystal orientation. In metals with chaotically oriented (i.e. dis-



oriented) crystals, the properties are averaged statistically in all directions; the metal is known to be quasi-isotropic. In textured metals with preferential orientation of crystals, these are directions along which some properties may be enhanced and others, weakened. Thus, deformation texture is the source of anisotropy of properties.

### 1.2.3. STRUCTURAL CHANGES ON PRERECRYSTALLIZATION ANNEALING

Cold plastic working brings the metal into non-equilibrium state with an increased free energy. Work-hardened metals tend spontaneously to pass into a state of greater equilibrium with a lower free energy. The restoring processes consist essentially in that the defects of the crystal lattice reduce in number and redistribute in crystallites with the formation of more balanced configurations. These processes occur through displacements of atoms and thus are largely influenced by temperature.

In most industrial metals and alloys, except for low-melting point grades, the mobility of atoms at room temperature is insufficient to ensure active development of restoration processes which might lower the free energy of work-hardened material. Thus, in order to eliminate the work-hardening effect in cold-deformed metal in a practically feasible time, the metal should be heated, i.e. annealing is required.

Depending on the temperature and time of annealing, various structural changes can take place in cold-deformed metal; these are separated into recovery and recrystallization processes.

On heating work-hardened metal at a relatively low homological temperature<sup>1</sup> (for common-purity metals below  $0.3 T_{m.p}$ ), optical microscopy fails to detect any changes in the shape and size of deformed grains or reveal new recrystallized grains. This prerecrystallization annealing can, however, produce noticeable changes in some properties of the metal. Furthermore, certain changes in the internal structure of deformed grains do take place, and can be detected by X-ray structural analysis, electron microscopy or some other direct or indirect methods.

*The combination of all spontaneous processes that change the density and distribution of defects in deformed crystals before recrystallization takes place is called recovery.* This collective term, which covers various phenomena that may differ appreciably in their mechanisms, has been generally adopted, since certain properties of work-hardened metal can be recovered fully

---

<sup>1</sup> Homological temperature is the ratio of a given temperature to the melting point (on absolute scale).

or partially through prerecrystallization annealing to the values the metal had before cold deformation.

If the process occurs without formation or migration of sub-boundaries inside deformed grains, it is called *first-order recovery*. If, however, it is linked with formation and migration of small-angle boundaries in deformed crystallites, it is termed *second-order recovery*, or *polygonization*.

### First-order Recovery

Our knowledge of the mechanism of first-order recovery is based on the results of studies of the kinetics of variation of electric resistivity, evolution of the energy stored on work-hardening, and other indirect data, rather than on direct structural observations on the behaviour of crystal defects.

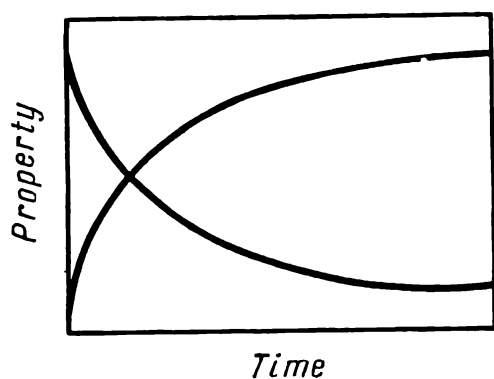


Fig. 15. Variation of physical properties on first-order recovery (schematically)

The rate of first-order recovery is at its maximum at the starting moment and then gradually diminishes with the time of isothermal holding (Fig. 15). A typical feature of first-order recovery is that it has no induction period, i.e. variations in properties occur from the very beginning of annealing.

The rate of variation ( $\Delta X$ ) of a property may be assumed to be inversely proportional to the time of recovery ( $\tau$ ):

$$\frac{d \Delta X}{d \tau} = \frac{K}{\tau} \quad (4)$$

where  $K$  is a constant for a given temperature; it depends on the activation energy  $Q$  of the process in accordance with Arrhenius' equation:

$$K = A \exp(-Q/RT) \quad (5)$$

First-order recovery is the most low-temperature variety among all the phenomena of spontaneous transition of work-hardened metal into a state of more equilibrium. Experiments with gold and copper deformed at the temperature of liquid helium have shown that the electric resistivity, for instance, begins to diminish already at a temperature near  $-190^\circ\text{C}$ . As temperature is raised, the curve of resistivity passes through number of inflexion points which mark different stages of recovery and different mechanisms of reduction of the energy stored during deformation. These processes include rearrangement of point defects and reduction of

their concentration (which has been in excess of the equilibrium concentration for the given temperature).

Interstitial atoms annihilate at edge dislocations and on meeting vacancies. Vacancies migrate to dislocations and grain boundaries and annihilate there.

Other processes involved in first-order recovery are rearrangement of dislocations and mutual annihilation of dislocations of unlike signs. In deformed grains, dislocations are distributed non-uniformly. On annealing, thermal activation produces glide, cross-slip and climb of dislocations over small distances, i.e. such a rearrangement of dislocations that the energy peaks are smoothed off. This may be interpreted as stress release in those submicro-volumes where the internal stresses have been larger than the yield limit at the temperature of annealing. During this rearrangement, dislocations of unlike signs annihilate on meeting each other, so that the total dislocation density reduces somewhat. Apart from the processes just discussed, long dislocation dipoles can spontaneously disintegrate into small closed dislocation loops, which results in a lower elastic energy.

At the stage of recovery, all displacements of dislocations are of local nature.

Direct electron-microscopic observations of deformed aluminium foils at room temperature have shown that only a slight rearrangement of dislocations takes place during recovery and that the dislocation density does not diminish substantially. In industrial metals and alloys, dislocations are pinned by impurities, which additionally impedes their migration in the temperature range of recovery.

During recovery of cold-deformed metals and alloys of industrial purity, the most important structural change is evidently the reduction of surplus concentration of point defects, in particular, vacancies.

The rate of annihilation of surplus point defects depends on the temperature and activation energy of diffusion. The activation energy  $Q$  of diffusion in metals increases linearly with the melting point. Assuming that  $Q = \alpha T_{m.p.}$ , we get

$$\exp\left(-\frac{Q}{RT}\right) = \exp\left(-\frac{\alpha T_{m.p.}}{RT}\right)$$

Hence,  $\exp(-Q/RT)$  should be approximately equal for all metals if the temperature is the same fraction of the melting point. Consequently, as follows from equations (4) and (5), the recovery rate at the same homological temperature is approximately at the same level in different metals. The higher is the melting point, the higher should be the temperature of annealing to give the same recovery effect. For instance, in cold-rolled copper and nickel, most

of the surplus vacancies formed on deformation disappear during recovery respectively at 20° and 100 °C. These temperatures correspond to a homological temperature of  $0.21 T_{m.p.}$ . For aluminium, the room temperature is a higher temperature as measured on the homological scale ( $0.31 T_{m.p.}$ ). For that reason, recovery of cold-deformed aluminium at room temperature results in disappearance of virtually all surplus vacancies.

Atoms of impurities and alloying elements may serve as traps for point defects. For instance, the energy of distortion of a lattice around an impurity atom will diminish when a vacancy enters the distortion zone. The gain in energy ensures mutual attraction of the vacancy and impurity atom. Apart from elastic attraction, a kind of electrostatic attraction can also exist between them. Atoms of impurities and alloying elements impede migration of vacancies in solid solution and thus reduce the rate of recovery.

### Polygonization

A Laue photograph of a deformed single crystal has a characteristic asterism, i.e. radial extension of X-ray spots. This asterism is due to the fact that the lattice orientation in a deformed (for instance, bent) crystal varies continuously and the corresponding X-ray reflections are blurred. Annealing under definite conditions may split a blurred spot into a number of spots, preserving the general pattern of each initial spot of asterism. This effect, which has been discovered by S. T. Konobeevsky and I. I. Mirer in 1932 in annealing of bent crystals of rock salt may be treated as spontaneous breakup of a crystal during recovery into slightly misoriented fragments (blocks), inside which the crystal planes are straightened. Each fragment then produces a clear reflection on a Laue photograph. Small distances between these reflections and preservation of the general pattern of the initial spot of asterism indicate that the fragments are misoriented through small angles only.

In order to characterize the kind of prerecrystallization annealing in which metal grains are broken into subgrains of slightly different crystal orientations, E. F. Bakhmetyev, A. A. Bochvar, G. S. Zhdanov and Ya. S. Umansky proposed in 1933 to call it "the second-order recovery", in contrast to the first-order recovery in which subgrains do not form.

In 1949, R. W. Cahn of Britain found that a bent single crystal of zinc breaks up on annealing into fragments and that the curvilinear axis of the bent crystal breaks into sections which are sides of a polygon; the phenomenon has been correspondingly named polygonization.

The mechanism of polygonization can be well explained by referring to the theory of dislocations. The residual bent of a crystal is linked with an excess of edge dislocations of like sign (Fig. 16a). The corresponding incomplete vertical atomic planes which pass out to the upper face of the crystal act as wedges, i.e. bend the crystal. Upon annealing, the dislocations of the same sign rearrange themselves into arrays which form or tilt boundaries of dislocations, (Fig. 16b). A dilatation region formed by one dislocation will then have below it a corresponding compression region of another dislocation, so that the elastic stress fields of

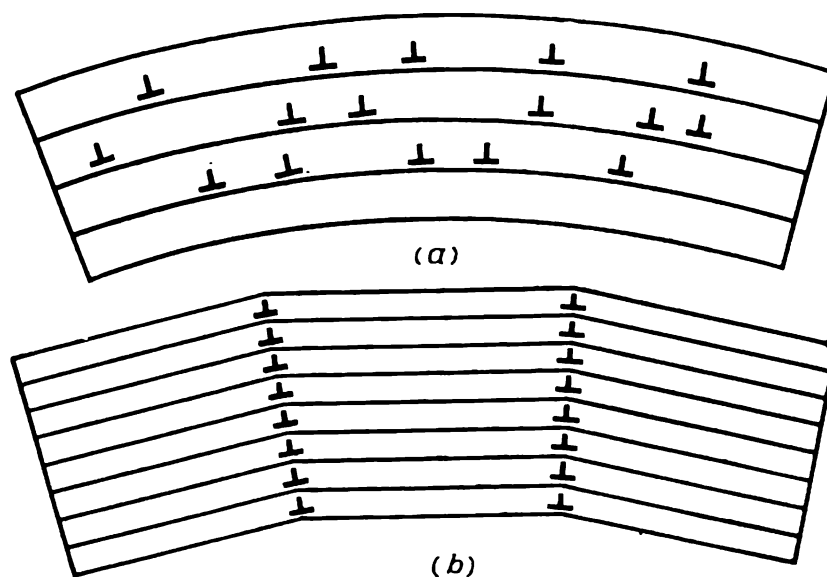


Fig. 16. A scheme of polygonization

*a*—chaotically positioned edge dislocations in a bent crystal; *b*—dislocation arrays upon polygonization

the dislocations mutually compensate one another to an appreciable extent. A dislocation array has no long-range stress field. Therefore, the formation of dislocation arrays is energetically favourable and should proceed spontaneously, but thermal activation is necessary for its development.

Dislocation arrays form in bent crystals owing to combined action of dislocation glide and climb. It may be readily seen in Fig. 16a and b, that glide in horizontal planes is in itself insufficient for rearrangement of dislocations into a vertical array. This inevitably should involve dislocation climb, which consists in completion or dissolution of the edges of partial atomic planes and can only be ensured through a slow diffusion process. The rate of climb, which is the slowest among the processes involved, determines the rate of rearrangement of dislocations into arrays.

An array of dislocations of one sign is a low-angle boundary that separates neighbouring subgrains whose lattices are slightly misoriented relative to one another. Thus, recovery of a subgrain

with polygonal boundaries results in the appearance of low-angle boundaries owing to rearrangement of dislocations into arrays. Heating is necessary here to activate the climb of a large number of dislocations. Thus the temperature of annealing for polygonization should be higher than that needed for first-order recovery.

Simple tilt boundaries, which consist of edge dislocations only, and corresponding subgrains in the form of parallel plates extending through the whole crystal, are usually observed on annealing of deformed metal when only one glide system is in action. Medium or high plastic deformations of polycrystalline metals always result in turbulent creep, in which different glide systems operate simultaneously. In that case annealing forms subgrain boundaries composed of mixed dislocations having different Burgers vectors. Such boundaries may form through glide, cross-slip and climb of dislocations, the latter process being the slowest.

Subgrains formed on annealing of cold-deformed polycrystalline metal are usually more or less equiaxial, but have curved boundaries. Angular misorientation of neighbouring subgrains is then due to an excess of dislocations of like sign in a subboundary. The body of subgrains is free or almost free of dislocations. The formation of such subgrains on annealing is also called polygonization, though there are no regular polygonal boundaries at all. Therefore, the term 'polygonization' has lost its initial meaning and, as used now, *implies the formation of subgrains separated by low-angle boundaries* produced through rearrangement of dislocations, the dislocation climb being the leading process.

If a cellular or subgranular structure has been produced through plastic deformation (see Fig. 12), then the polygonization on annealing will consist in further development of the existing cellular (or subgranular) structure, rather than in the formation of subgrains from chaotically arranged dislocations. Poorly shaped diffuse cells become fully enclosed in boundaries, curved walls of the cells become straight and thinner, the cores of cells become increasingly more free of dislocations, and the cells gradually transform into well-shaped subgrains.

Subgrain boundaries can be revealed metallographically by using an appropriate etchant. They are seen in the microscope as chains of etch pits, each pit corresponding to the exit of a dislocation within a low-angle boundary onto the surface of a microsection. More often subgrain boundaries are seen on microsections as a network of fine lines inside grains, the boundaries of the grains being revealed as thicker lines.

Subgrains formed through polygonization tend to grow larger as the time or temperature of annealing is increased. Two different mechanisms of this growth have been established experimentally: migration of subboundaries and coalescence of subgrains.

Figure 17 shows schematically a Y-shaped junction (triple point) of three subgrains separated by boundaries  $P$ ,  $P'$  and  $P''$ . The two adjacent dislocation arrays  $P'$  and  $P''$  tend to merge and extend the  $P$  wall (i.e. the triple point tends to move upwards). In the process, the two subgrains grow at the expense of the third, and the misorientation of the subgrains near the new boundary that forms is equal to the sum of misorientations at the initial subboundaries. The driving force of this process is the tendency of the crystal to minimize the energy of subboundaries per dislocation.

Arrows in Fig. 17 indicate the directions along which the dislocations should migrate to produce junction of  $P'$  and  $P''$  boundaries. Clearly, the boundaries merge owing to a combined effect of glide and climb. Glide alone cannot give a uniform distribution of dislocations upon merging of dislocation arrays. Therefore, dislocation climb, which is the slowest process, plays the leading part in coarsening the subgrains through migration of subboundaries, and also in the formation of subboundaries at the early stages of polygonization.

Coarsening of subgrains through coalescence was observed directly during annealing of a foil in the column of an electron microscope. These direct observations have shown that subboundaries, which have been sharp initially, gradually become more and more diffuse, so that the contrast between subgrains disappears. This means that the subgrains become oriented in the same direction in the crystal.

Coalescence stages of two subgrains are illustrated in Fig. 18. It is quite clear from the figure that disappearance of a subboundary should involve tilting of the lattice of one (Fig. 18*b*) or both subgrains through a definite angle, so as to form the same lattice orientation in the region where slightly misoriented subgrains have been present.

The boundary between subgrains gradually disappears, since dislocations leave the subgrains and concentrate at the subboundaries of these subgrains. The process is sometimes called "unraveling" of a boundary. Dislocation climb is supposed to play the principal part in unraveling of subboundaries.

As may be seen from the diagram in Fig. 18*b*, a tilt of a subgrain is only possible when atoms in the enclosing subgrains leave the hatched areas. Therefore, the process that controls coalescence is volume diffusion. The rate of coalescence is proportional to the

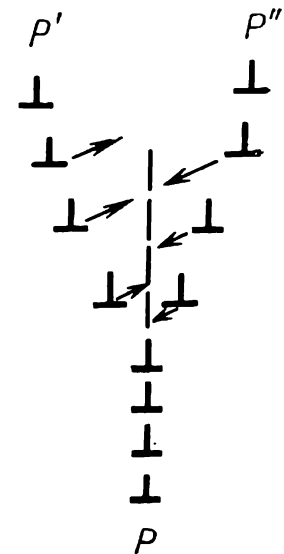


Fig. 17. A scheme showing how two neighbouring low-angle boundaries merge and coarsen subgrains

coefficient of self-diffusion and inversely proportional to the cube of subgrain diameter. In larger subgrains, atoms have to diffuse to greater distances. With very large or stretched subgrains, the mechanism of their growth through coalescence may fail to work.

The disappearance of a subboundary, which is always linked with an excess of energy, is a spontaneous process. On the other hand, it involves an increase in the angular misorientation of the boundaries enclosing the merging subgrains, and therefore, an

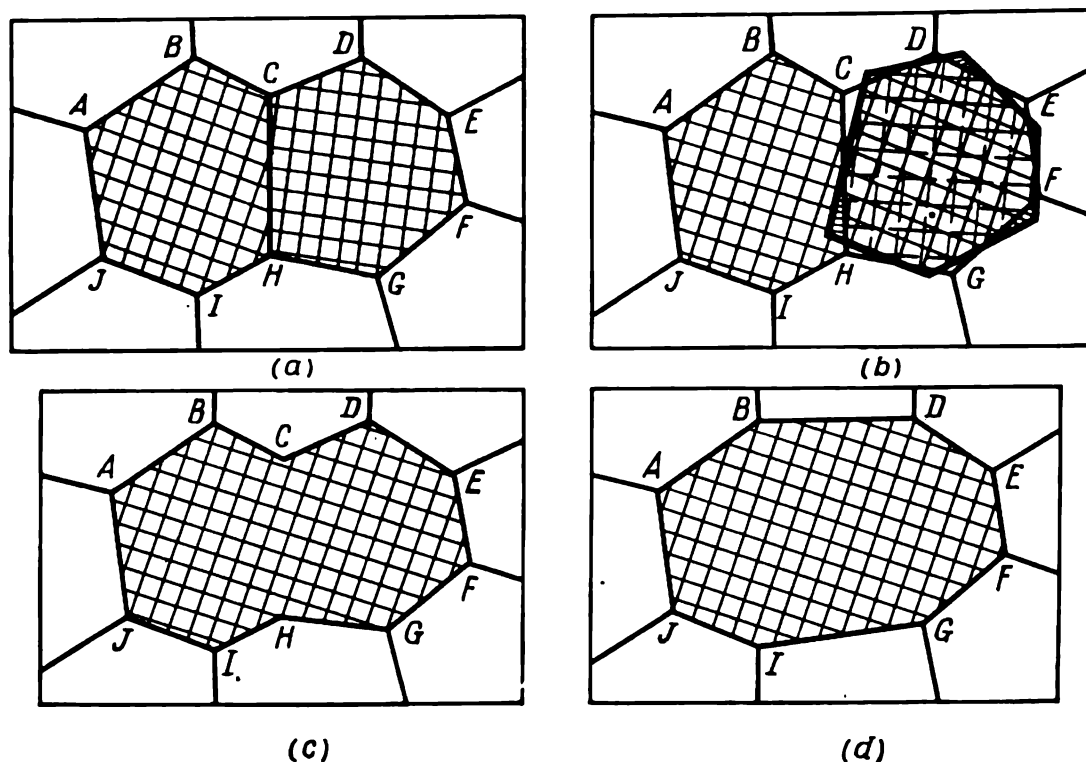


Fig. 18. Coalescence stages of two subgrains (after J. C. M. Li)  
*a*—structure before coalescence; *b*—one of grains has tilted; *c*—structure immediately after coalescence; *d*—final structure after straightening of sub-boundaries through migration

increase in the energy of these boundaries. If the angular misorientation of these boundaries is greater than that of the disappearing boundary, this will retain the thermodynamic stimulus of coalescence. The point is that as the angle of misorientation  $\varphi$  increases, the boundary energy  $E$  increases by an attenuating pattern, so that, for the same  $\Delta\varphi$ , the increment  $\Delta E$  in the high-angle region will be lesser than that in the low-angle region. For that reason, the loss of energy of a disappearing low-angle boundary in the low-angle region will outweigh the increase in the energy of the boundaries having high angles of misorientation.

Electron-microscopic observations of the structures of foils during annealing have revealed that a number of boundaries enclosing adjacent subgrains can unravel simultaneously, i.e. apart from pairwise coalescence discussed just above, *group coalescence* is also possible.



Coalescence of subgrains and migration of their boundaries in a moving triple point are only possible when atoms possess a definite mobility.

On increasing the time and temperature of polygonization, subgrains may grow to an appreciable size (around 10  $\mu\text{m}$ ). Their growth occurs, however, within the limit of crystal orientation of the original deformed grains, i.e. typical asterism spots remain on Laue photographs. This far-going polygonization has been termed *in-situ recrystallization*. In-situ recrystallization is not a variety of common primary recrystallization which may be characterized by the formation of new grains separated by high-angle boundaries from the matrix. In contrast, it is a polygonization process, rather than a recrystallization process, in its nature.

As has been mentioned earlier, the growth of subgrains during polygonization, which is linked with the formation of an excess of dislocations of one sign at subboundaries, results in increased misorientation angles of neighbouring subgrains. However, these remain low-angle boundaries all the time of the polygonization stage, including the process of in-situ recrystallization, i.e. their structure may be described by a dislocation diagram, such as that in Fig. 16b, and the misorientation angle of neighbouring subgrains does not exceed 10-15° (most often not more than 1°).

Since polygonization consists essentially in gradual formation of subgrains from separate dislocations rearranged into dislocation arrays, and also in growth of the subgrains formed, or else (with a cellular structure of deformed metal) in the development of the existing cells (these being gradually transformed into subgrains), the temperature of the beginning of polygonization is not a clearly defined physical constant such as is, for instance, the melting point. We can however speak definitely of the temperature of beginning of all or any one of the processes discussed.

The rate of polygonization depends on the nature of metal, the degree of preceding deformation, prehistory of heat treatment, the content of impurities, and other factors.

The stacking fault energy, which is the most important characteristic of a metal, may have an appreciable effect on the susceptibility of the metal to polygonization. With a low stacking fault energy, extended dislocations have an appreciable width, which hampers the processes of dislocation climb and cross-slip needed for polygonization to occur. For instance, polygonization is difficult to be induced in copper and is not usually observed in  $\alpha$ -brass, which has a low stacking fault energy. In contrast, the process can be provoked comparatively easily in aluminium, which has a high stacking fault energy, and therefore, only weakly extended dislocations,

As will be shown in 1.2.4, at high deformation ratios recrystallization prevents development of polygonization. For that reason, polygonization on annealing is observed only after slight deformations.

Impurity atoms can decelerate polygonization owing to the formation of what is called Cottrell atmospheres, which impede redistribution of dislocations through glide and climb, and also to the formation of Suzuki atmospheres, which lower the stacking fault energy and also impede dislocation redistribution. With the same temperature of annealing, a pure metal can be polygonized in a shorter time than that contaminated with impurities.

#### 1.2.4. PRIMARY RECRYSTALLIZATION

Beginning from a definite temperature, annealing of deformed metal produces strong changes in the microstructure which may be attributed to a process called recrystallization. Optical microscopy, even at low magnifications, then reveals more or less equiaxed recrystallized grains along with the original stretched deformed grains (Fig. 19*b*). As the time or temperature of annealing increases, the area occupied by new grains in a microsection increases, and the original deformed grains gradually disappear (Fig. 19*c*). X-ray structural analysis, and later thin-foil electron microscopy have shown that the new equiaxed grains differ from the original stretched grains of the deformed matrix not only in their shape, but, what is much more important, in having a more perfect internal structure with a sharply reduced dislocation density. For instance, the dislocation density in a strongly deformed metal may be  $10^{11}$ - $10^{12}$  cm<sup>-2</sup> but drop to  $10^6$ - $10^8$  cm<sup>-2</sup> upon recrystallization.

As distinct from a polygonized structure (which is also more perfect than the deformed matrix), whose subgrains are separated from the matrix by low-angle boundaries, the recrystallized grains have high-angle boundaries. This difference is of principal importance. High-angle boundaries, which represent a transition zone with disordered atoms, are capable of migrating quickly, since atoms in such a zone can easily leave the parent crystal and pass to an adjacent one. Owing to the quick migration of high-angle boundaries, recrystallized grains intensively consume the deformed matrix, as it were. At the polygonization stage, subgrains grow within the limits of the original orientation of deformed crystallite, whereas the growth of a recrystallized grain, which is enclosed in a high-angle boundary, may be linked with an appreciable re-orientation of the crystal lattice.

*The formation and growth of grains of a more perfect structure and surrounded by high-angle boundaries at the expense of the*

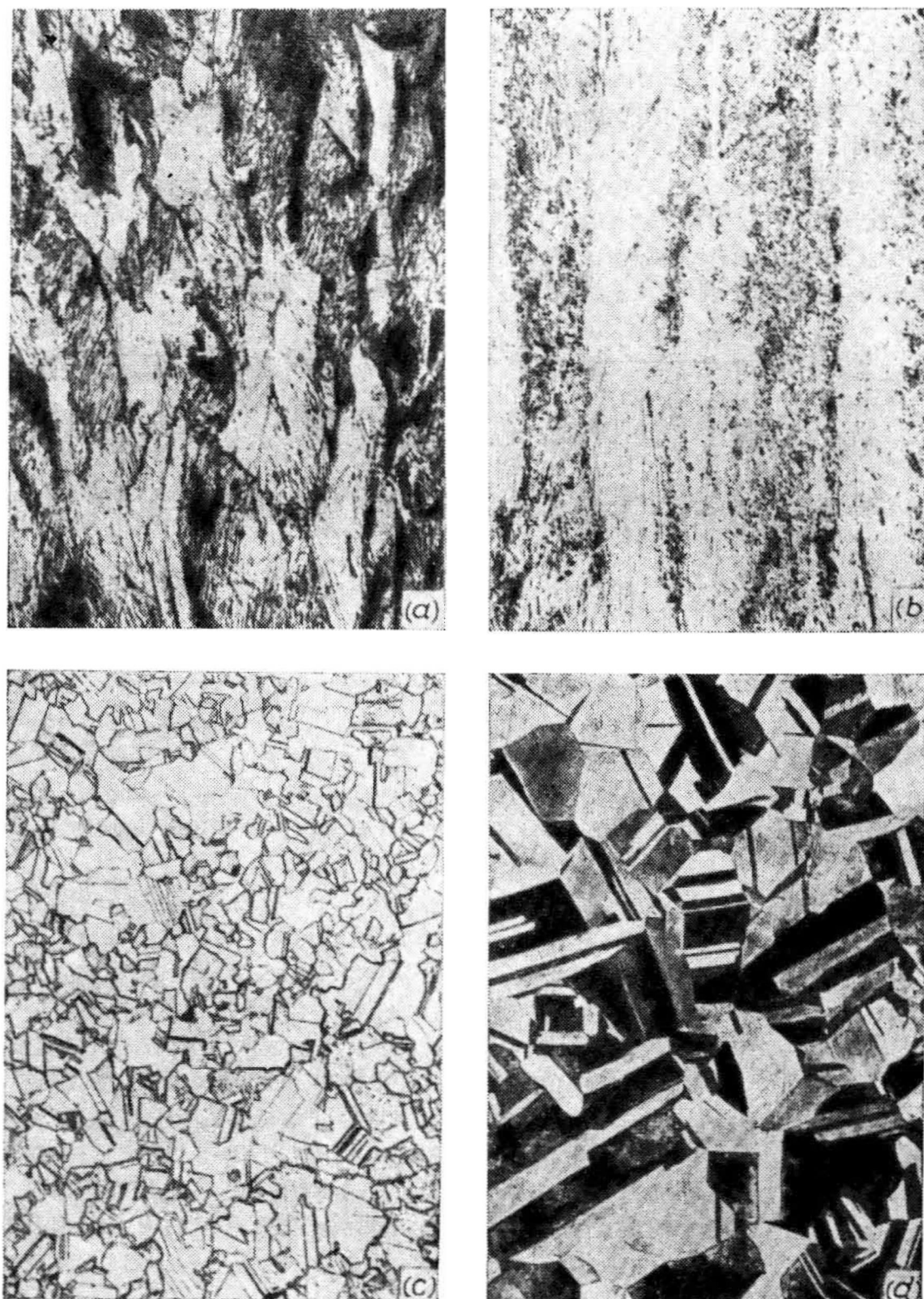


Fig. 19. Changes in microstructure of Л68 brass upon recrystallization annealing for 2 h,  $\times 100$

*a*—initial cold-rolled structure (40-per cent reduction); *b*—at 350 °C, incomplete primary recrystallization; *c*—at 450 °C, full primary recrystallization; *d*—at 650 °C, grain growth

original deformed grains of the same phase is called *primary recrystallization*.

Figure 20 shows the course of primary recrystallization during isothermal holding of aluminium. The kinetics of recrystallization resembles that of a phase transformation: for isothermal conditions, both processes can be depicted by a sigmoid line (see Fig. 79). For some time, new grains cannot be revealed. This is called the induction period. The induction period of recrystallization reduces on increasing the deformation ratio and annealing temperature or on improving the purity of metal.

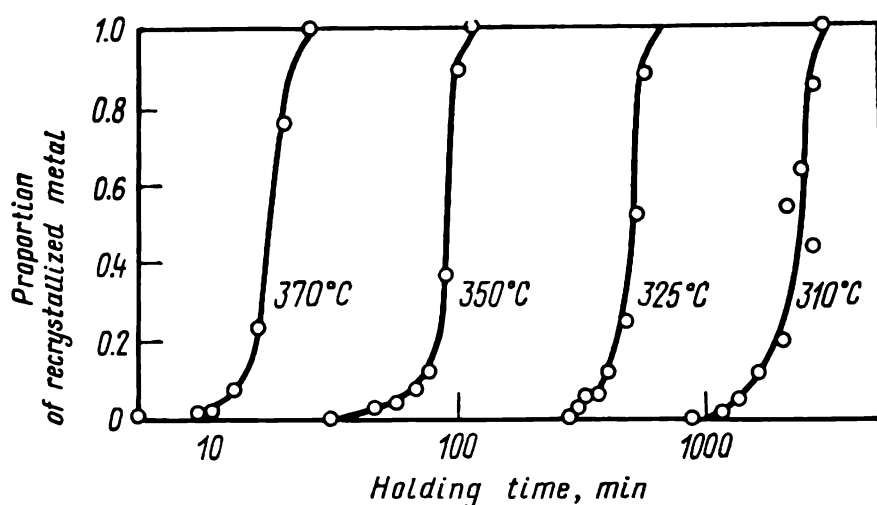


Fig. 20. Development of primary recrystallization in 99.96-per cent pure aluminium at various temperatures upon 10-per cent tension (after M. A. Anderson and R. F. Mehl)

The kinetics of primary recrystallization differs appreciably from that of recovery. Whereas recovery has no induction period and may be characterized by its rate being at the maximum in the initial period and then reducing continuously during isothermal holding (see Fig. 15), the process of recrystallization starts only after a definite induction period and the rate of the process (i.e. the increment of recrystallized volume per unit time) increases first from zero to a maximum and then lowers again. The attenuation of recrystallization may be attributed to the interference of grains as their number is being increased, which ceases the growth of grains.

The thermodynamic stimulus of primary recrystallization is the energy stored during plastic deformation, which is mainly due to dislocations. Reduction in the density of dislocations on primary recrystallization results in liberation of an appreciable part of that energy, which may be revealed by calorimetric measurements.

As the structure of crystals is being perfected, their volume energy decreases, this decrease outweighing the rise in the surface energy for any, even the smallest, size of grains. It is far from

being always true that recrystallized metal should have coarser grains than as deformed. At the end of primary recrystallization the total surface area of equiaxed grains that have grown from a plurality of nuclei can be greater than the total surface area of stretched deformed grains. Despite this, recrystallized metal has a lower free energy than as deformed, owing to the lower dislocation density inside grains.

### Mechanism of Formation of Recrystallization Nuclei

To control effectively the processes of recrystallization, we have to know the mechanism of nucleation of recrystallized grains. Much knowledge have been gained on that mechanism, though some of its details are still being debated.

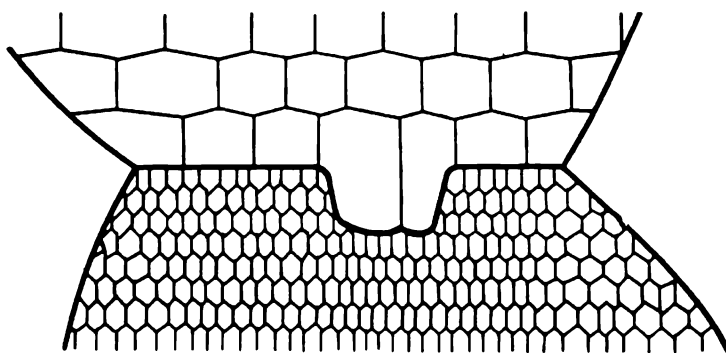


Fig. 21. A tongue formed through migration of a boundary due to work-hardening (after P. A. Beck)

The principal feature of the mechanism of nucleation of recrystallized grains in all materials and for any conditions is the formation of a portion of high structural perfection which is enclosed in high-angle boundaries. The formation of a recrystallization nucleus in deformed matrix may follow different ways, depending on the nature of metal, temperature, rate, degree and type of plastic deformation, rate of heating during annealing, and other factors.

This formation is likely to occur in portions of deformed grains where conditions are favourable for the appearance of a high-angle boundary. It has been established long ago by metallographic examination that recrystallized grains form preferably at boundaries of deformed grains and twins, in deformation and kink bands and near inclusions. Direct electron-microscopic observations of structural changes in thin foils during annealing have shown that recrystallization nuclei can form from subgrains.

Recrystallization nuclei can form directly at boundaries of deformed grains as a portion of a high-angle boundary migrates towards one of the grains and thus forms a protrusion, or 'tongue' (Fig. 21). The driving force of this migration is the difference in

energies of work-hardened portions on the two sides of the boundary, so that the latter moves into the grain having a higher density of dislocations (in the scheme of Fig. 21, the difference in

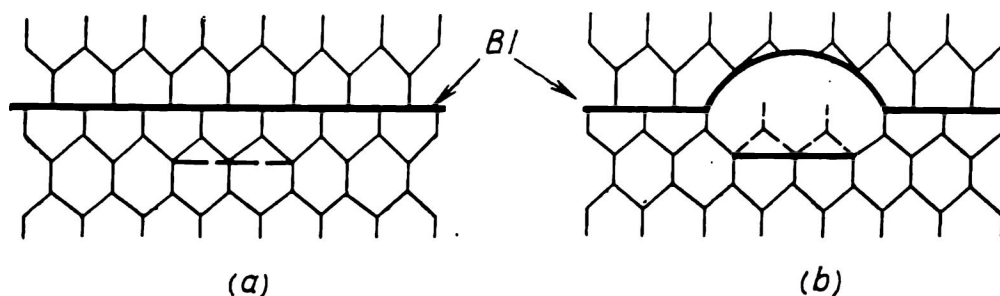


Fig. 22. A tongue formed through coalescence of subgrains at a high-angle boundary (after S. S. Gorelik)

*a*—before coalescence; *b*—after coalescence of subgrains and migration of a portion of high-angle boundary

dislocation density on the two sides of the boundary is depicted by the different size of cells). The moving boundary “sweeps out”

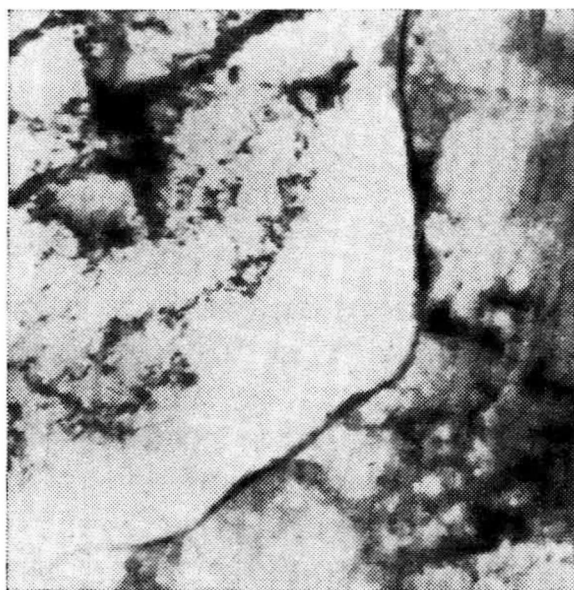


Fig. 23. A tongue formed on migration of a portion of high-angle boundary in annealed nickel (425 °C, 10 min) upon tensioning by 16 per cent. Thin-foil electron micrograph,  $\times 10\,000$  (after J. E. Bailey and P. B. Hirsch)

lattice defects from the deformed grain. An increase in the surface energy on the formation of a ‘tongue’ is outweighed by the reduction in the energy stored on deformation.

Bending of a high-angle boundary may start near a perfect relatively large subgrain. The formation of a protrusion may also be preceded by the coalescence of subgrains in a grain near the grain boundary (Fig. 22). This coalescence can form a large portion of a rather perfect structure which is capable of consuming its neighbours.

The photograph in Fig. 23 shows a bright protrusion of the left-hand grain, which is almost free of dislocations. The right-hand grain has dark dis-

location tangles of a high density. The migrating boundary of the protrusion ‘sweeps out’ these dislocations. The protrusion is separated from its own grain by a rather clear boundary to the left of which the dislocation density is high. The growth of the large subgrain, which is almost free of dislocations, into

an adjacent grain having an increased density of dislocations forms a recrystallization nucleus in the latter. The mechanism of nucleation of recrystallized grains by strain-induced migration of individual portions (of a size of an order of  $1\ \mu\text{m}$ ) of an existing high-angle boundary was observed in aluminium, copper, silver, nickel and iron upon low and medium deformations. Upon high deformations, a different mechanism of nucleation of recrystallized grains becomes predominant; this is linked with the formation of new high-angle boundaries, rather than with bending of existing boundaries.

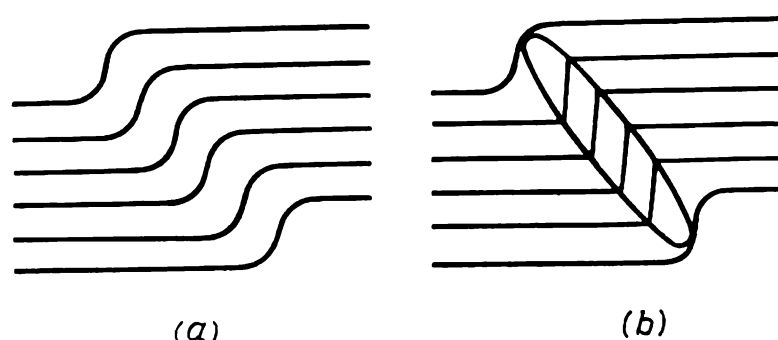


Fig. 24. Formation of a recrystallization nucleus in a kink band (after P. G. Shewmon)

*a*—lattice bent in a kink band prior to formation of recrystallized portion; *b*—recrystallization nucleus

In portions of a deformed grain where the lattice has an increased curvature (for instance, in a kink band) and the local orientation of the lattice differs substantially from that of the surrounding material, the formation of high-angle boundaries which separate these portions of different orientation is facilitated (Fig. 24). The process of formation of a nucleus may be reduced to that a comparatively smooth, though strong, variation in the crystal orientation (Fig. 24*a*) becomes thicker, as it were, and concentrates in the form of high-angle boundaries (Fig. 24*b*). Inside the nucleus, however, the orientation of the perfect lattice is close to the mean orientation in the initial portion of curved lattice. This very fact results in the nucleation of a recrystallized grain having a different orientation than the initial deformed grain.

The scheme just discussed, though largely formal, describes quite correctly the appearance of a nucleus in places having a strong local curvature of the lattice of deformed grains.

Dislocation mechanisms of formation of a recrystallization nucleus in portions of a strong curvature of the lattice may be reduced to polygonization as the initial stage of nucleation. This stage constitutes the essence of the induction period.

A portion having an increased curvature of the lattice, i.e. an excess of dislocations of one sign, is more likely to form sub-



grains, for instance, by means of the simplest mechanism depicted in Fig. 16. The higher the excess of dislocations of one sign, the greater will be the misorientation angle at the subboundary. As a subgrain grows, penetration of ever greater number of dislocations of one sign into its boundary results in an increased misorientation angle and gradual transformation of the subgrain into recrystallization nucleus proper, which is enclosed by a high-angle boundary.

The nuclei from which recrystallization centres are gradually formed can be individual most perfect and well-shaped large cells and subgrains in the deformed metal; these grow at the expense of the surrounding cells and subgrains. When, with such slow growth of a subgrain, a low-angle boundary changes to a high-angle one, the rate of its migration increases appreciably. This moment corresponds to the end of formation of a crystallization nucleus.

As has been noted in 1.2.1, at higher degrees of deformation the cellular and subgranular structures are perfected and, therefore, the number of recrystallization nuclei increases.

In metals having a high stacking fault energy, the mechanism of coalescence seems to play an important part in the formation of recrystallization nuclei. This follows, in particular, from the results of direct observations of nucleation of recrystallized grains in thin foils annealed in a high-voltage electron microscope. With group coalescence, the disappearance of individual low-angle boundaries results in a gradual formation of a high-angle boundary that encloses a portion of coalesced subgrains, which is the recrystallization nucleus proper. As has been shown in a work, in aluminium such a centre first grows through coalescence of adjacent subgrains, then through coalescence and migration of its boundaries, and finally the mechanism of subgrain coalescence changes fully to that of migration of the high-angle boundary towards the deformed matrix.

In any of the mechanisms discussed, the leading part is played by diffusion processes, in particular, dislocation climb, volume diffusion which is needed for tilting of subgrains (see 1.2.3), etc. For these reasons, the formation of recrystallization nuclei is a thermally activated process, i.e. it occurs quicker at higher temperatures.

Recovery prior to recrystallization may have a dual effect on nucleation.

First-order recovery always inhibits to some or other extent the formation of recrystallization nuclei, since a lower concentration of vacancies on recovery slows down the diffusion processes which control the rate of formation of recrystallization nuclei.



The effect of second-order recovery (polygonization) is more complex. If subgrains form and grow with the same rate simultaneously over the whole volume of a slightly deformed metal, then they can reach a large size and high perfection, while the boundaries between them will remain low-angle. This type of polygonization impedes recrystallization. On annealing after a deformation that has been characterized by a more uniform distribution of dislocations and a small excess of dislocations of one sign, the far-going polygonization (in-situ recrystallization) results in the formation of a very perfect substructure with a stable network of low-angle boundaries surrounding large subgrains, so that primary recrystallization will not be observed up to the melting point. In that case we may say that recovery is a process competing with recrystallization.

If, however, the deformed metal has a non-uniform distribution of dislocations with some portions having a large excess of dislocations of one sign, then accelerated polygonization in the preferable portions will lead to the formation of large subgrains which grow at the expense of their neighbours, become rapidly misoriented at their boundary and turn into recrystallization nuclei. This type of polygonization is actually the starting stage of recrystallization. As soon as recrystallization has begun, it affects the whole volume of the metal (due to the high mobility of high-angle boundaries) and leaves no 'field of action' for the slower polygonization. This is true of annealing of polycrystals after medium and large deformations.

### **The Temperature of Beginning of Recrystallization**

When choosing heat treatment conditions or for other purposes, a simple method is essential which might fix experimentally the moment of appearance of recrystallized grains. In many applied problems, the beginning of recrystallization is determined conditionally by optical microscopy as the appearance of the first, usually brighter, equiaxed grains at the background of a more etchable deformed matrix, or by X-ray analysis, by the appearance of dotted pits ('stitches') in blurred interference lines of an X-ray photograph. Each pit corresponds to the reflection of X-rays by a recrystallized grain 2-5  $\mu\text{m}$  in diameter. Optical microscopy can reliably reveal recrystallized grains upon their growth up to 10-50  $\mu\text{m}$ . The beginning of recrystallization is sometimes determined by the onset of an intense drop of the hardness or ultimate strength, but, as will be shown in 1.2.9, this method does not work with some materials.

The temperature at which recrystallized grains appear, i.e. the temperature of beginning of recrystallization ( $t_r^s$ ) is not a physical

constant, unlike the melting point or modulus of elasticity. As distinct from the temperature of phase equilibrium, it depends on the time of annealing, as follows from an analysis of the curves in Fig. 20. For an annealing time of 1000 minutes, primary recrystallization has enough time to proceed fully at temperatures of 325°, 350° and 370°C, but just only starts at 310°C. For an annealing time of 10 minutes, the beginning of recrystallization is fixed at 370°C, with no new grains being found at lower temperatures. Therefore,  $t_r^s = 310^\circ\text{C}$  for an annealing time of 1000 minutes and for that of 10 minutes  $t_r^s = 370^\circ\text{C}$ .

Another factor that can affect appreciably the temperature of beginning of recrystallization is the degree of deformation on plastic working.

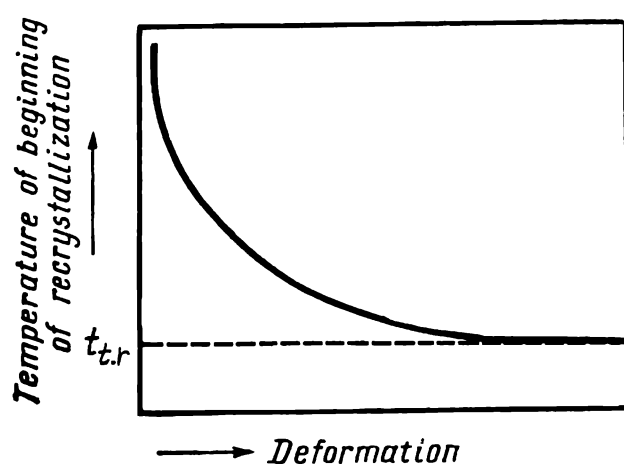


Fig. 25. Effect of deformation on the temperature of beginning of recrystallization

On increasing the degree of deformation, the temperature of beginning of recrystallization drops (Fig. 25). An explanation to this may be that this increases the density of dislocations and the energy stored during deformation, i.e. the thermodynamic stimulus of recrystallization. Besides, an increased degree of deformation gives a higher concentration of vacancies, which also promotes the formation of recrystallization centres at lower

temperatures. Since the density of dislocations and the stored energy of deformation increase by an attenuating curve with an increase in the degree of deformation, the temperature of beginning of recrystallization also drops with an attenuation, approaching a definite limit for a given annealing time (Fig. 25).

As the time of annealing of a strongly deformed metal increases, the temperature of beginning of recrystallization drops with an attenuation and becomes approximately constant for an annealing time of 1-2 h. The lowest temperature of the beginning of recrystallization of a metal or alloy that corresponds to large deformations (over 60-70 per cent) and an annealing time of 1-2 h, may serve a definite characteristic of that metal and will further be called the *temperature threshold of recrystallization* ( $t_{t,r}$  in Fig. 25), to distinguish it from other, higher, values of  $t_r^s$ .

The temperature threshold of recrystallization diminishes as the purity of a metal increases, as may be seen from the following data for aluminium:

Purity, %:	99.7	99.9	99.99	99.9992
$t_{t,r}$ , °C:	240	200	100	—45

A. A. Bochvar has shown that the temperature threshold of recrystallization is linked by a simple relationship with the melting point, namely that recrystallization starts at a temperature that is a constant fraction of the melting point on the absolute scale for all metals:

$$T_{t.r} = (0.3-0.4) T_{m.p} \quad (6)$$

The coefficient 0.3-0.4 in the formula refers to metals of relatively high commercial purity (roughly 99.99 per cent). For very pure metals:  $T_{t.r} = (0.25-0.3) T_{m.p}$ .

The correctness of formula (6) may be verified by the data in Table 3.

**Table 3. Temperature Threshold of Recrystallization of Metals ( $t_{t.r}$ )**

Metal	$t_{m.p}, ^\circ\text{C}$	$t_{t.r}, ^\circ\text{C}$	$\frac{T_{t.r}}{T_{m.p}}$	Metal	$t_{m.p}, ^\circ\text{C}$	$t_{t.r}, ^\circ\text{C}$	$\frac{T_{t.r}}{T_{m.p}}$
W	3400	1200	0.4	Cu	1084	200	0.35
Ti	1668	450	0.37	Al	660	100	0.4
Fe	1539	450	0.4	Zn	419.5	20	0.4
Ni	1455	350	0.36				

Using Bochvar's rule, we can find the temperature threshold of recrystallization for the given melting point of a metal; this may be needed when the corresponding reference data are not available. For instance, we may find for lead that its temperature threshold of recrystallization is:  $(327 + 273) 0.4 - 273 = -33^\circ\text{C}$ .

In addition to the degree of deformation, time of annealing, and the content of impurities, the temperature and rate of deformation and the size of grains prior to deformation may also affect the temperature of beginning of recrystallization.

A higher temperature of deforming increases the temperature of beginning of recrystallization. This can be explained by the fact that a higher temperature of plastic working allows the recovery processes to pass to a more advanced degree, which lowers the energy stored on deformation, and therefore, the thermodynamic stimulus of recrystallization. With a high stacking fault energy, polygonization on hot deforming can produce a rather perfect subgranular structure with a stable network of low-angle boundaries, so that recrystallization on subsequent annealing will be drastically impeded.

With a higher rate of deformation, the temperature of beginning of recrystallization becomes lower, since high-speed deformation, for instance, of explosion type, produces a higher general

density of dislocations and a greater excess of dislocations of one sign.

Refinement of the initial grain (prior to deformation) yields a lower temperature of beginning of recrystallization, since a finer grain has a larger total area of high-angle boundaries where recrystallization nuclei can form, and possesses a higher energy stored on deformation.

### Effect of Alloy Composition on the Temperature of Beginning of Recrystallization

The nature and concentration of an alloying element may have an appreciable effect on the temperature of beginning of recrystallization in an alloy. A detailed analysis of this relationship has been made by S. S. Gorelik.

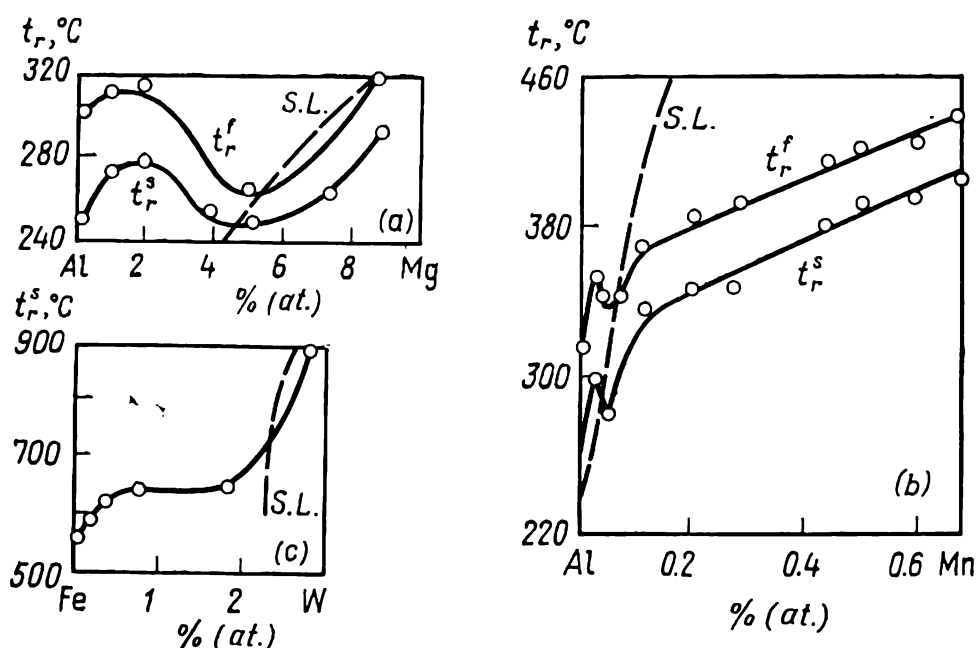


Fig. 26. Temperatures of beginning and end of recrystallization in binary systems of various composition

a—Al-Mg (after V. I. Iveronova); b—Al-Mn (after S. S. Gorelik); c—Fe-W (after S. S. Gorelik); S. L.—solubility limit in constitutional diagram

Even in the single-phase region of solid solutions in binary systems, the dependence of the temperature of beginning of recrystallization on composition has a varying pattern (Fig. 26). Only at low concentrations, a simple relationship is observed: small additions and impurities almost invariably raise the temperature of beginning of recrystallization; on increasing further their concentration, the temperature of beginning of recrystallization increases by an attenuating pattern.

Addition or impurity atoms are elastically attracted to dislocations and form Cottrell atmospheres. These impurity atmospheres inhibit the redistribution of dislocations which is needed for the

formation of recrystallization nuclei. The impurities are attracted to the boundary of a nucleus and thus retard both nucleation and growth of recrystallization nuclei. On heating the metal to a higher temperature, impurity atmospheres disappear owing to an increased thermal motion, which enables the formation of recrystallization nuclei and facilitates their growth. As the concentration of foreign atoms increases, they saturate portions near dislocations, because of which the temperature of beginning of recrystallization rises with deceleration.

The energy of elastic attraction of an impurity atom of radius  $R_i$  to an edge dislocation is proportional to the 'misfit parameter'  $\epsilon = \frac{R_i - R_0}{R_0}$ , where  $R_0$  is the radius of a base atom in a substitutional solution; in an interstitial solution,  $R_0$  is the radius of a rigid sphere which will cause no volume distortions when placed in the lattice instead of the impurity atom. Thus, the greater is the misfit parameter, the higher will be the temperature of beginning of recrystallization.

The greatest effect on increasing the temperature of beginning of recrystallization have the elements which are poorly soluble in solid state in the base metal. This is firstly linked with the fact that a low solubility in solid state is usually due to a large difference in atomic radii of elements and, secondly, with a large difference between the valency of the base and that of the alloying element. Recall that the energy of electric interaction of an edge dislocation and impurity atoms is proportional to the difference between the valencies of base and alloying element.

The effect of an impurity element is stronger in pure metals. In more contaminated metals, recrystallization can be impeded by impurity atmospheres that have formed at dislocations.

In some rare cases when a small addition lowers the temperature of beginning of recrystallization, this may result from the initial metal being contaminated with impurities which have raised the temperature of beginning of recrystallization. The alloying element added then combines these impurities and removes them from the solid solution.

In many systems, the temperature of beginning of recrystallization may drop on attaining its maximum in the region of relatively low concentrations (fractions of a per cent or a few per cent), see Fig. 26*a* and *b*. S. S. Gorelik explains this fact by the effect of the alloying element on the structure of deformed alloy. If an addition can lower the stacking fault energy of the solid solution, then dislocations will be strongly extended, their cross-slip will be impeded, and portions with a large excess of dislocations of one sign will form on plastic deformation. The temperature of beginning of recrystallization in such a solid solution

should then be lower than in a less alloyed solution having a higher stacking fault energy.

A heavier alloying of a solid solution (a few per cent or tens per cent) may either raise or lower the temperature of beginning of recrystallization. The effect of composition on  $t_r^s$  in the region of large concentrations is mainly due to a change in forces of interatomic bond and diffusion mobility of atoms. For instance, if alloying lowers the melting point and interatomic forces (such as, for instance, in Al-Mg system, see Fig. 26a), then the temperature of beginning of recrystallization in the region of high concentrations of solid solution will diminish continuously.

In contrast to metals of highest purity, where additions of a few hundredths or tenths of a per cent can raise the temperature of beginning of recrystallization by 100 degrees C or even more, at high concentrations of alloying elements in the metal, additions of a few per cent or a few tens per cent can only slightly change this temperature (usually by a few degrees C or, at maximum, a few tens of degrees). The ratio of the temperature of beginning of crystallization to the melting point is higher in solid solutions than in pure metals; in single-phase solutions,  $T_r^s/T_{m.p}$  is not more than 0.6 (against 0.25-0.4 in pure metals).

As the solubility limit is surpassed and the process enters the two-phase region, the temperature of beginning of recrystallization increases intensively with the content of a second phase (Fig. 26).

The effect of an excess phase on  $t_r^s$  depends on the amount, dispersity and structure of particles of that phase. With a small amount of an excess phase and low dispersity of its particles prior to plastic deformation, the latter will be more turbulent than in the case of a single-phase alloy, with dislocation tangles being formed around particles of that phase, which will lower the temperature of beginning of recrystallization in subsequent annealing (the minimum of  $t_r^s$  in Fig. 26b is to the right of the solubility limit).

With a higher amount of an excess phase, its particles serve as barriers to migrating boundaries of recrystallization nuclei and, though the temperature of formation of recrystallization nuclei may remain at the same level, the growth of these nuclei is only possible at higher temperatures. Thus, in two-phase alloys there may be an appreciable temperature or time interval between the formation of recrystallization nuclei and the beginning of their growth. Conventional experimental methods (optical microscopy and X-ray structural analysis) can detect recrystallization nuclei only after these have grown to an appreciable size. For that reason, these methods show a rise of  $t_r^s$  on increasing the content of

an excess phase, though the actual temperature of nucleation may practically remain unchanged. But the temperature at which intense growth of recrystallization nuclei begins is of more interest for the practice, since it is linked with large variations in the properties of the metal. With an excess phase present in an amount of more than 6-10 per cent (by volume), it can retard both the growth and formation of recrystallization nuclei.

If a supersaturated solution is deformed, the processes of recrystallization and precipitation in it will overlap in subsequent annealing. Segregations of atoms of the dissolved element and precipitates of intermediate and stable phases at dislocations, low-angle and high-angle boundaries (see 4.1.2) impede the redistribution of dislocations and migration of boundaries and thus interfere with the nucleation and growth of recrystallization nuclei. At higher temperatures, when precipitated particles grow coarser or are dissolved (in accordance with the solvus line<sup>1</sup> in the constitutional diagram), dislocations and boundaries are unpinned, thus enabling the formation and growth of recrystallization nuclei. Therefore, recrystallization in age-hardening alloy may be impeded appreciably by precipitation from the solid solution.

### Temperature of End of Recrystallization

The temperature at which a deformed matrix disappears fully in a given time of annealing is called the temperature of the end of recrystallization,  $t_r^f$ . It can be determined experimentally with optical microscopy, by disappearance of deep-etchable remnants of a deformed matrix, or through X-ray analysis, by disappearance of diffused Debye rings in X-ray photographs. Besides, it is possible to count on an X-ray photograph the number of reflection spots produced by recrystallized grains. The maximum number of such reflections determines the end of primary recrystallization, since grain growth that follows diminishes the number of recrystallized grains.

The temperature of the end of recrystallization is affected by all the factors which vary the temperature of the beginning of recrystallization. A higher  $t_r^s$  most often (but not always) has a correspondingly higher  $t_r^f$  (see Fig. 26a and b). There can be no direct proportional relation between  $t_r^f$  and  $t_r^s$ , since  $t_r^s$  is determined by the formation of recrystallization centres, while  $t_r^f$  is additionally determined by the rate of growth of recrystallized grains at the expense of deformed matrix. This difference is par-

---

<sup>1</sup> Solvus line is the curve of limited solubility in the solid state.

tially smoothed by the fact that recrystallization nuclei are usually detected only after they have grown for some time at the expense of the deformed matrix.

### Grain Coarsening in Primary Recrystallization

Recrystallized grains grow through quick migration of their boundaries into the deformed matrix. The driving force of the migration is the difference in elastic energies of crystals on the two sides of a boundary, owing to different dislocation density. In contrast to grain growth (see 1.2.5), grain boundaries in primary recrystallization migrate away from the centre of curvature.

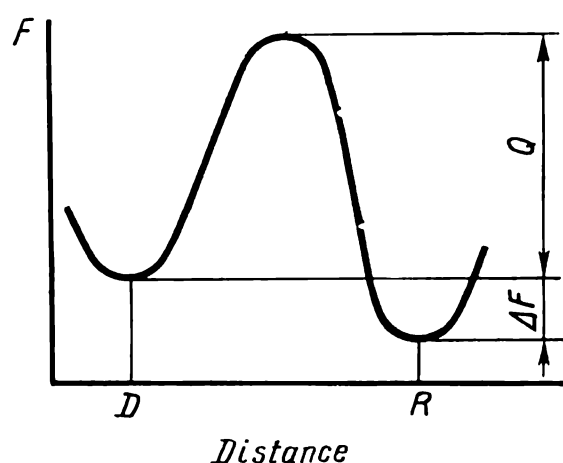


Fig. 27. Free energy variation on passage of an atom through a boundary between deformed (*D*) and recrystallized (*R*) grains

A migrating high-angle boundary "sweeps out" all lattice defects of the deformed matrix, thus increasing the volume of more perfect structure with appreciably lower dislocation density.

The average rate of migration of grain boundaries in primary recrystallization is dependent on temperature:

$$v = v_0 e^{-Q/RT} \quad (7)$$

where  $Q$  is the activation energy of migration.

It is still unclear what are the elementary actions that are responsible for boundary migration, and therefore, the physical essence of the activation energy of migration is also unclear. Direct experimental data on the structure of high-angle boundaries are still too scarce.

The migration of a high-angle boundary in recrystallization may be regarded as a result of alternate individual or groupwise passage of atoms from a deformed grain to a recrystallized one. Fluctuating atoms on both sides of a boundary may sometimes detach from one grain and attach to another. Single jumps of atoms may occur by a mechanism in which a boundary atom changes places with a vacancy located at the very boundary. This mechanism is diffusional in its nature (i.e. there occurs a directed self-diffusion of atoms normal to a boundary).

Figure 27 shows how the free energy varies when an atom passes across the boundary between grains. As may be seen, there is a certain difference of free energy  $\Delta F$  linked with different dislocation densities on the two sides of a boundary, because of which an atom passing from a recrystallized to a deformed grain



should overcome a larger potential barrier ( $Q + \Delta F$ ) than on a reverse passage ( $Q$ ). Accordingly, atoms should pass from deformed to recrystallized grains more frequently than in the opposite direction, which fact determines why recrystallized grains 'consume' deformed ones.

Atoms of dissolved impurities segregate at boundaries and retard their migration. One of the causes of this retardation is the necessity for a boundary to drag along the impurity atoms attracted to it. An impurity can have a strong retarding effect even in a very low content, since its atoms concentrate at a boundary. With only 0.0001 per cent of an impurity introduced into a zone-refined metal, the rate of boundary migration can be lowered by two orders of magnitude.

The effect of holding time on average size of grains at various temperatures may be presented schematically in the form of curves, such as those in Fig. 28. It is assumed here that the rate of grain coarsening in primary recrystallization is constant. The slope of corresponding linear portions of curves increases with temperature.

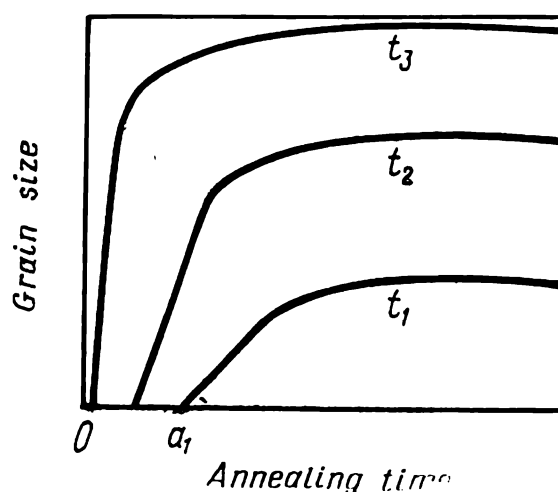


Fig. 28. Size of recrystallized grains versus annealing time at various temperatures (schematically);  $oa_1$ —induction period at  $t_1$ ;  $t_3 > t_2 > t_1$

### 1.2.5. GRAIN GROWTH

When primary recrystallization is complete, i.e. when deformed grains disappear, the free energy lowers appreciably, but the structure remains unstable owing to the high free energy of the extended surface of boundaries of recrystallized grains and uneven surface tension at these boundaries.

Consider the granular structure of a metal by using a two-dimensional model. At the junction of three grains (Fig. 29a), surface tension forces should be balanced. The surface tension in a metal or single-phase alloy can be taken approximately the same for all high-angle boundaries. The surface tension forces  $\gamma$  applied along the grain boundaries will then be balanced, provided that  $\gamma = 2\gamma \cos \theta/2$ , or  $\cos \theta/2 = 1/2$  and  $\theta/2 = 60^\circ$ .

Therefore, an equilibrium configuration is the one in which three grains meet at angles of  $120^\circ$  at the apex.

In a two-dimensional model of a grain, regular straight-side hexagons forming a hexagonal network of boundaries correspond

to an equilibrium of surface tension forces. Such a network is mechanically stable.

With primary recrystallization in an actual metal, grains meet one another at different moments of time and in different points of their surface, so that upon the end of recrystallization they have an irregular form with different size and different number of faces.

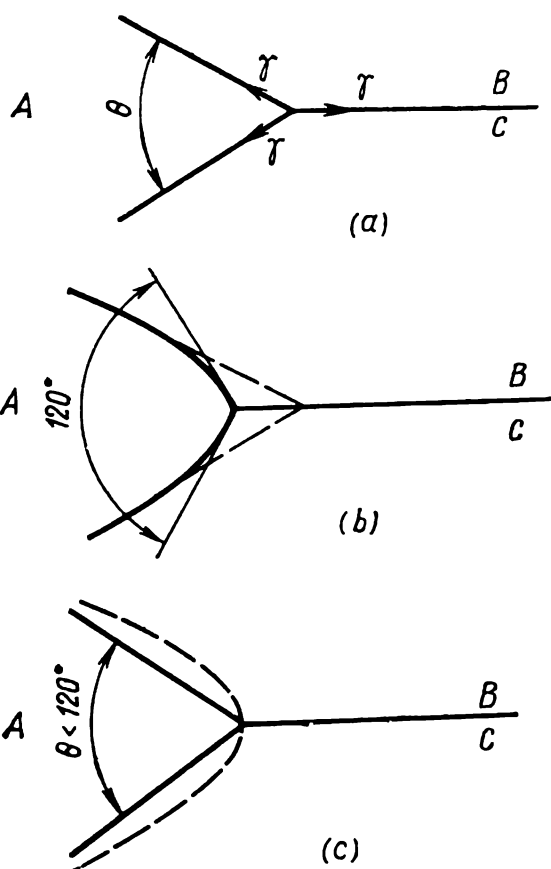


Fig. 29. Boundaries of a triple joint at various moments of annealing

*a*—before annealing; *b*—after surface tension forces in the triple joint have come to equilibrium through boundary bending; *c*—upon straightening of boundaries that disturbs the equilibrium

In a planar model, such grains are depicted by polygons with a different number of sides: 3, 4, 6, 10, 50, etc. (see Fig. 30).

From the above condition of equilibrium of surface tension forces in triple points, grains with less than six sides should have their boundaries convex outwards and those with more than six sides, convex inwards.

Bending of boundaries occurs through their migration with simultaneous displacement of triple points. In Fig. 29*b*, solid lines show curved boundaries of a balanced triple joint upon migration and dotted lines, the initial position of the boundaries in an unbalanced triple joint. Curved boundaries are, however unstable, and tend to shorten themselves under the action of surface tension. Each boundary straightens during migration in the direction of its

centre of curvature. These directions are indicated by arrows in Fig. 30. The solid lines in Fig. 29*c* show straightened boundaries and dotted ones, their initial position in a balanced joint.

A boundary migrates towards its centre of curvature, since atoms on a concave surface have more bonds with their neighbours in the same grains than those on a convex surface. Uncompensated passage of atoms through a boundary ensures that grains with concave boundaries grow at the expense of those with convex boundaries, which vanish.

The straightening of boundaries disturbs the equilibrium that has been attained in triple joints (the apex angle of grain *A* in Fig. 29*c* has become less than  $120^\circ$ ). To restore equilibrium in a triple joint, its boundaries curve again through migration, and

so on. Thus, grains *B* and *C* in Fig. 29 gradually grow at the expense of grain *A*.

In a planar model of granular structure of a polycrystal, grains with more than six sides should grow and become larger, while those with less than six sides, should be consumed by their neighbours. In real metals, a grain may have a concave boundary on one side and grow here at the expense of its neighbour and a convex boundary on another side and will be here consumed by the neighbour. On the whole, the average size of grains increases.

With isothermal annealing, grain growth proceeds with attenuation, since the network of boundaries approaches the equilibrium state and the driving force of boundary migration gradually diminishes. When analysing the structure on microsections, one should keep in mind that the configuration of a three-dimensional balanced network of boundaries is more complex than that of a two-dimensional system.

In a three-dimensional space, surface tension forces are brought into equilibrium in a packed array of grains in the form of 14-hedrons with slightly curved boundaries. Even if such an idealized grain configuration might be obtained by annealing, sections of various grains by the microsection plane would be different in size and the meeting angles of boundaries in triple points would be other than  $120^\circ$ .

*The growth of some recrystallized grains at the expense of neighbouring recrystallized grains through migration of high-angle boundaries is called grain growth.*

The thermodynamic stimulus of grain growth is the free energy of grain boundaries. An indispensable condition for the process to occur is that the surface tension forces are unbalanced and tend to straighten curved boundaries and form an equilibrium configuration of boundaries at triple joints. Even with relatively fine grains and an almost equilibrium boundary network, no grain growth can take place (the state of mechanical equilibrium), notwithstanding the high grain-boundary energy per unit volume. Consequently, an excess of the grain-boundary energy (compared with the energy of a monocrystalline specimen of the same volume) cannot in itself induce grain growth if disbalance of surface tension is not present.

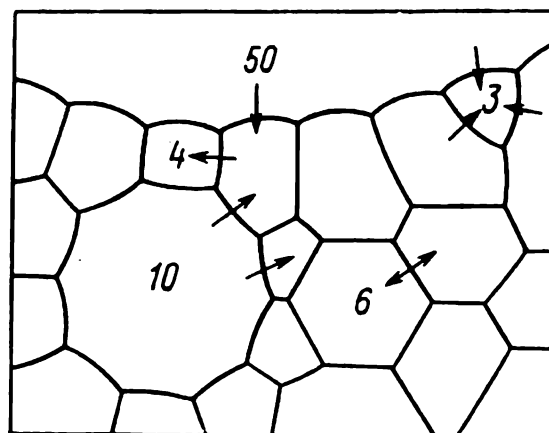


Fig. 30. Plane model of metal structure with grains having different number of sides (arrows indicate the directions of boundary migration)

The atomic mechanism of boundary migration in grain growth may be the same as in primary recrystallization (see 1.2.4).

The beginning of grain growth need not coincide exactly with the moment of full completion of primary recrystallization. In some portions of the metal where recrystallized grains have already come into interference with one another, grain growth may start before primary recrystallization is completed in other portions.

The rate of boundary migration should be the higher, the more curved the boundary is, i.e. the smaller is its radius of curvature. Assuming that the radius of curvature of boundaries of an equiaxed grain is proportional to grain diameter, the rate of grain growth should be inversely proportional to grain diameter  $D$  and directly proportional to surface tension  $\gamma$ , i.e.:

$$\frac{dD}{d\tau} = K \frac{\gamma}{D} \quad (8)$$

where  $K$  is a constant exponentially dependent on temperature ( $K = Ae^{-Q/RT}$ ).

Integration gives

$$D^2 = D_0^2 + K'\gamma\tau \quad (9)$$

where  $D_0$  = initial diameter of recrystallized grains and  $\tau$  = annealing time.

If the initial diameter of grains is much smaller than the current diameter ( $D_0^2 \ll D^2$ ), then

$$D = B\tau^{1/2} \quad (10)$$

As has been shown experimentally, the effect of annealing time on the average grain size in metals and single-phase alloys is governed by the expression

$$D = B\tau^n \quad (11)$$

where  $n$  may be from 0.1 to 0.5 and  $B$  is a temperature-dependent constant. Deviation of  $n$  from the theoretical value of  $1/2$  towards smaller value, i.e. a less intensive growth of grains, may be caused by boundary drag through dissolved impurities, inclusions, etc.

As has been indicated earlier, atoms of dissolved impurities are elastically attracted to a boundary and the latter drags them along during migration. A migrating boundary meets impurity atoms distributed in the body of a grain that is being consumed, the concentration of impurities at the boundary increases, and the boundary drag becomes stronger.

If a migrating boundary meets inclusions of a second phase on its way, it should circumvent them and then detach from them. But since the driving force of grain growth diminishes in the process, inclusions can fully inhibit grain growth in a certain time. The greater is the volumetric proportion  $f$  of inclusions and the smaller the size  $d$  of inclusion particles, the smaller will be the final grain size  $D_f$  attainable at a given annealing temperature, i.e.

$$D_f = \frac{d}{f} \quad (12)$$

Consequently, highly dispersed inclusions with a high volumetric concentration in an alloy present the greatest obstacle to grain growth, whereas the barrier effect from individual large inclusions is relatively small.

When annealing thin sheets, where the size of grains may become equal to the thickness of a sheet, grain growth slows down but grains continue to grow in the plane of sheet. After the size of grains in the plane of sheet becomes 2-3 times the sheet thickness, grain growth fully ceases to continue. One of the causes of retarding effect of free surfaces, which is called 'the thickness effect', is the formation of thermal etch pits in places where grain boundaries pass out onto the surface. In annealing, such pits are formed owing to rapid evaporation of atoms from grain boundaries, which pins up the boundaries to corresponding portions of the surface.

Grain growth may be strongly retarded by the textures formed on primary recrystallization. 'Texture-induced retardation' is due to the fact that grain boundaries having only a slight angular misorientation (which is typical of a perfect texture) have a lower surface energy and, in accordance with formula (8), the rate of grain growth should also be lower.

The growth of some grains at the expense of similar grains of the same phase need not be preceded with primary recrystallization. This growth is a rather common process, for which it is only needed that the surface tension at grain boundaries be unbalanced owing, for instance, to curvature of the boundaries.

It is often assumed that grain coarsening in cast (undeformed) metals through the growth of some crystallites at the expense of adjacent ones does not take place. This is only true of metals of relatively low purity, in which impurities concentrate at grain boundaries in the course of crystallization and thus impede boundary migration in annealing. In cast pure metals and single-phase alloys, grain growth can proceed readily without any preliminary deformation.

### 1.2.6. TEXTURES OF PRIMARY RECRYSTALLIZATION AND GRAIN GROWTH

#### Principal Laws of Formation of Recrystallization Textures

As has been found experimentally, there are three types of relationship between crystal orientation in deformed and recrystallized metals. Firstly, a deformation texture may change into an identical recrystallization texture, i.e. recrystallized grains have the same preferable orientation as the initial deformed grains. Secondly, a deformation texture may transform into a different recrystallization texture (the most common case). Thirdly, recrystallized grains may have a chaotic crystal orientation, whereas the initial deformed metal had been textured.

The nature and degree of perfection of a recrystallization texture depend on the type of plastic working, the degree and temperature of the last deformation stage, the temperature and time of the last annealing stage, the degree of intermediate deformation, the temperature of intermediate annealing, the content in alloying elements and impurities, and other factors. Therefore, the factors affecting recrystallization textures are more numerous than those affecting deformation textures.

When annealing is done below a definite temperature limit, the recrystallization texture that is formed is qualitatively identical with the deformation texture, the only difference being that some texture components may be enhanced or weakened. For instance, if cold-drawn copper wire has had a double axial  $\langle 111 \rangle$   $\langle 100 \rangle$  texture, then upon primary recrystallization its texture will be identical, but the number of grains having the  $\langle 100 \rangle$  orientation will diminish with increasing temperature of annealing.

Recrystallization textures of f.c.c. metals and solid solutions have been studied in much detail. In many cases the deformation texture of the copper type,  $\{112\}$   $\langle 111 \rangle$ , changes to a *cubic recrystallization texture*  $\{100\}$   $\langle 100 \rangle$ : the  $\{100\}$  cube face in recrystallized grains turns to be parallel with the plane of rolled strip, whereas  $\langle 100 \rangle$  edges of cubes are oriented quite accurately either along or across the direction of rolling. A cubic texture forms on recrystallization annealing of copper, nickel, aluminium, gold, and some alloys, such as cupronickel.

If a brass-type  $\{110\}$   $\langle 112 \rangle$  texture has formed on rolling, it may often change upon annealing to a  $\{113\}$   $\langle 112 \rangle$  recrystallization texture. For that reason, when the content of zinc in Cu-Zn alloys is increased, i.e. the stacking fault energy is lowered, the copper-type rolling texture gradually changes to brass-type texture, and accordingly, recrystallization texture changes from cubic to  $\{113\}$   $\langle 112 \rangle$ . A higher temperature of rolling, which causes the brass-type deformation texture to change to copper-type texture,

also causes a corresponding change in recrystallization textures from  $\{113\} \langle 112 \rangle$  to  $\{100\} \langle 100 \rangle$ . It may be taken as a rule that a more perfect deformation texture produces a clearer recrystallization texture.

Small additions and impurities present in the solid solution may have an extremely strong effect on the nature and perfection of recrystallization texture. They may preclude the formation of some or other recrystallization texture or, on the contrary, improve the perfection of a texture. Important is that, firstly, small additions and impurities, though affecting appreciably the recrystallization texture, have usually no effect on deformation texture, and secondly, their effect on recrystallization texture depends on the degree of deformation, annealing temperature and other engineering factors, as well as on the concentration of an impurity, so that the total effect cannot be described by simple relationships. The controversial results obtained by various researchers on the effect of deformation and temperature and time of intermediate and final annealing on the nature and perfection of recrystallization textures in the same metals and alloys, especially in commercially pure metals, can be attributed to different contents of impurities, including of uncontrollable ones, in the tested specimens.

The most important feature of recrystallization textures is that they are often crystallographically related to the initial deformation textures. For instance, the lattice of recrystallized grains of f.c.c. metals is tilted through an angle of approximately  $30\text{--}40^\circ$  around the common  $\langle 111 \rangle$  axis relative to the lattice of deformed grains. The texture of primary recrystallization in b.c.c. metals may be assumed to be obtained by tilting the lattice through an angle of roughly  $25\text{--}30^\circ$  on the  $\langle 110 \rangle$  axis. In recrystallized h.c.p. metals, the lattice is tilted through  $30^\circ$  around the  $\langle 0001 \rangle$  direction, which is common for both deformed and recrystallized grains.

### The Nature of Recrystallization Textures

Recrystallization textures are now explained by using the hypotheses of oriented nucleation and oriented growth of recrystallized grains.

It is assumed that all recrystallization nuclei are already present in a deformed matrix in the form of subgrains. For instance, it has been found for heavily deformed cold-rolled copper that its deformation texture contains not only the well-known main orientation  $\{112\} \langle 111 \rangle$ , but also traces of the  $\{100\} \langle 100 \rangle$  orientation, which may be regarded as nuclei of cubical texture of recrystallized metal. This explains well why the degree of deformation, temperature and other conditions of plastic working can effect the recrystallization texture.

The hypothesis of oriented nucleation proceeds from the assumption that some or other orientation is being determined directly at the stage of formation of recrystallization nuclei. Subgrains of a definite orientation grow larger and more perfect and thus serve as recrystallization nuclei. The hypothesis of oriented nucleation is helpful in cases where a deformation texture changes to a qualitatively identical recrystallization texture.

The principal role in the formation of recrystallization texture is taken by oriented growth of nuclei. According to the hypothesis of oriented growth, a texture of recrystallization is determined by the original orientation of the nuclei which have the highest rate of growth in the deformed matrix. In heavily deformed cold-rolled copper, such nuclei are subgrains with the  $\{100\} \langle 100 \rangle$  orientation. Though these cubically oriented nuclei are incomparably less numerous than the nuclei with the principal  $\{112\} \langle 111 \rangle$  orientation, they can grow much more rapidly under definite conditions and thus determine the formation of a cubic texture in recrystallized metal, which replaces all other orientations.

When cold-rolled copper is being annealed at  $600^\circ\text{C}$ , the recrystallized grains formed at the early stages of primary recrystallization may have the  $\{112\} \langle 111 \rangle$  and  $\{110\} \langle 112 \rangle$  orientation, which are typical of rolled texture, and also new orientations:  $\{100\} \langle 100 \rangle$  and  $\{110\} \langle 111 \rangle$ . As the time of annealing is increased from 1 s to 10 minutes, all the orientations, except for  $\{100\} \langle 100 \rangle$ , gradually become less pronounced and after annealing for an hour at  $600^\circ\text{C}$ , i.e. after grain growth has taken place, only the cubic  $\{100\} \langle 100 \rangle$  texture remains in the metal. Therefore, as primary recrystallization and grain growth proceed in copper, grains of a definite orientation grow preferably, this orientation gradually replacing all other orientations.

The hypothesis of oriented grain growth agrees well with the fact that the lattice of recrystallized grains is rotated relative to that of deformed grains on a common axis through an angle within an interval of  $25\text{--}40^\circ$ . High-angle boundaries of the greatest mobility are found in this very interval of misorientation angles of crystals on both sides of a boundary.

In f.c.c. metals, the most mobile boundaries are those with a misorientation angle of approximately  $38^\circ$  relative to the common  $\langle 111 \rangle$  axis of two neighbouring grains. As has been shown by M. L. Kronberg and H. F. Wilson, with such mutual orientation of two crystals, a plurality of atoms may belong simultaneously to lattice nodes of both crystals. Figure 31 shows two closely packed atomic layers  $\{111\}$  (dark and bright circles) which belong to two lattices mutually rotated in the plane of drawing on the common  $\langle 111 \rangle$  axis normal to that plane. In the interface between the two crystals, every seventh atom is in a coincidence site. These



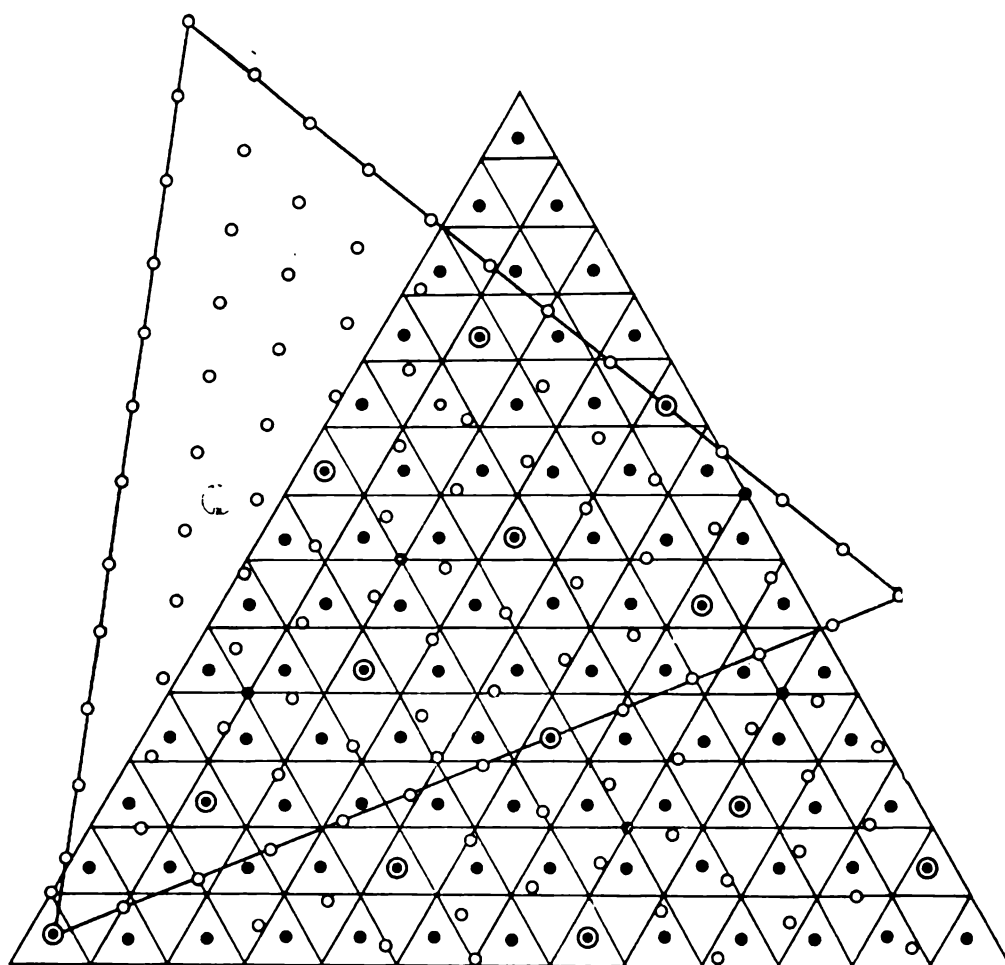


Fig. 31. A scheme to explain the appearance of coincidence sites at a partially matched boundary on tilting two f.c.c. lattices in the  $\{111\}$  plane through an angle of  $38.2^\circ$  on the common  $\langle 111 \rangle$  axis

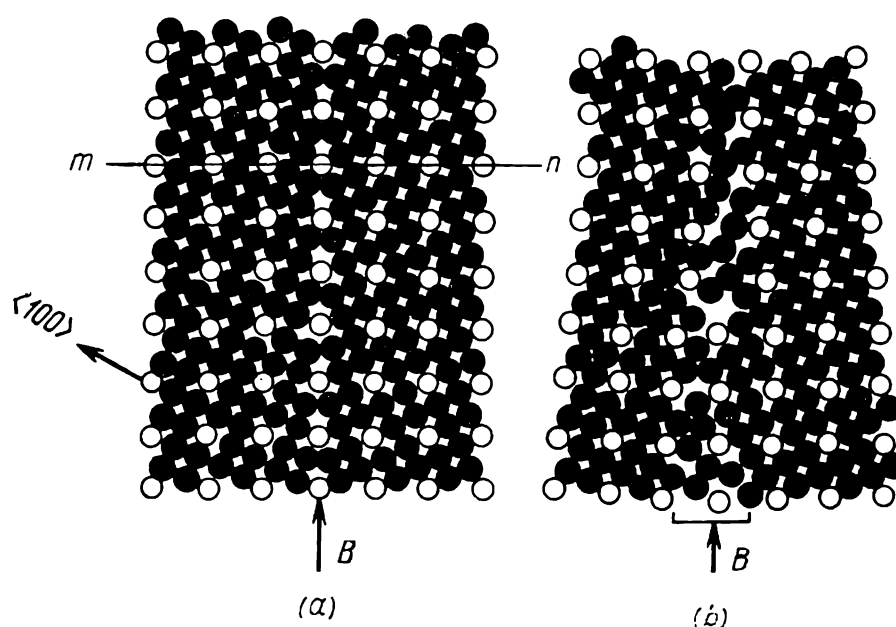


Fig. 32. The structure of Kronberg-Wilson boundary between crystals having simple cubic lattices. Lattice tilting on the common  $\langle 001 \rangle$  axis (after *P. Gordon* and *R. A. Vandermeer*)

*a*—tilting angle  $37^\circ$ ; *b*—a smaller angle; *B*—boundary

'coincidence sites' form a 'superlattice' in the space whose period is greater than that of the common lattice of the metal. A superlattice formed by coincidence sites (bright circles) is shown in Fig. 32*a* and *b* for two adjacent grains each having a primitive cubic lattice. The grain lattices are mutually so oriented that form a superlattice of a high density of coincidence sites. Dark circles are rows of atoms which meet at different angles at the boundary

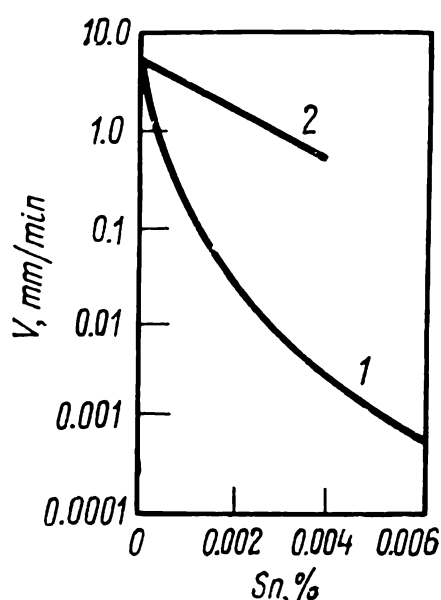


Fig. 33. Migration rate,  $v$ , at 300 °C of (1) arbitrary and (2) partially matched high-angle boundaries with various amounts of tin in zone-refined lead (after K. T. Aust and J. W. Rutter)

between the grains and bright circles (every fifth atom in the  $\langle 100 \rangle$  direction) are atoms in the coincidence sites located on straight lines, such as  $mn$ , which pass through both grains and belong to the superlattice.

The boundaries of grains whose mutual orientation obeys the Kronberg-Wilson relation are called *Kronberg-Wilson boundaries*, alternative terms being *coincidence-site boundaries* and *partially conjugated boundaries*. In b.c.c. metals, such boundaries are observed on rotation of two lattices through an angle of 26.5° on the common  $\langle 100 \rangle$  axis.

The most important feature of Kronberg-Wilson boundaries is that their structure is highly perfect (owing to coincidence of many nodes in two lattices), as may be readily seen in Fig. 32*a*. A slight deviation in the orientation

from the Kronberg-Wilson relation results in the boundary becoming wider and less sharp (Fig. 32*b*).

The mobility of Kronberg-Wilson boundaries differs appreciably from that of high-angle boundaries having an arbitrary grain orientation (Fig. 33). In very pure metals, the mobilities of high-angle boundaries of different type differ only slightly. According to some estimates, the mobility of Kronberg-Wilson boundaries in pure metal should even be lower than that of arbitrary boundaries, if we assume that boundary migration occurs through alternate passage of atoms from a grain being 'consumed' to a growing grain. The passage of atoms through a less sharp arbitrary boundary is facilitated owing to that the atoms may change places with vacancies in the boundary proper.

As has been shown experimentally, impurities can retard the migration of arbitrarily oriented boundaries much more appreciably than that of Kronberg-Wilson boundaries, the difference in boundary mobilities increasing with an increase in the content of

an impurity (Fig. 33). For instance, with 0.003 per cent Sn contained in lead, the rate of migration of Kronberg-Wilson boundary at 300° C is two orders of magnitude greater than that of an arbitrarily oriented boundary. An explanation to this may be that a Kronberg-Wilson boundary, as being more perfect in its structure, attracts impurity atoms less efficiently than an arbitrary boundary (an equilibrium segregation of impurity atoms on a high-angle boundary is due to the difference in the crystal structure at the boundary and in the body of a grain, see 2.1.2). An arbitrarily oriented boundary should drag along an atmosphere of impurity atoms and thus can migrate only with an appreciably slower rate than the more perfect Kronberg-Wilson boundary.

Thus, the recrystallization nuclei whose orientation relative to the lattice of deformed matrix obeys the Kronberg-Wilson relation possess the highest rate of growth. For that reason the recrystallization textures that may be produced geometrically from deformation textures by rotating their crystals on a common axis through an angle typical of the given type of lattice are so often found in metals.

Experimental studies of recrystallization textures show that the angle of rotation may deviate by a few degrees from the ideal Kronberg-Wilson relation. A probable explanation is that such small deviations of a Kronberg-Wilson boundary from the ideal structure still cause no appreciable segregation of impurity atoms on it, but are sufficient to make the boundary less pronounced (see Fig. 32*b*), which facilitates passage of atoms of the base metal from grain to grain.

It should be clear from the above what is the role of impurities, including uncontrollable ones, in the formation of recrystallization textures and also why the temperature of annealing can have an appreciable effect on the texture (as the temperature increases, segregations of impurity atoms at boundaries are dissolved, as it were, by thermal motion and the difference in the mobilities of singular and arbitrary boundaries becomes less marked).

Various impurities segregate in different ways on arbitrary boundaries and may have different retarding effect on boundary migration, thus producing different recrystallization textures.

The hypotheses of oriented nucleation and oriented grain growth, with due regard to the high mobility of singular boundaries and retarding effect of impurities, help us in understanding why the nature and perfection of recrystallization textures are so diverse and depend on a great number of factors — much more numerous than the factors affecting deformation textures. Whereas the formation of deformation textures is mainly affected by the peculiarities of dislocation glide, the formation of recrystallization

textures is dependent on the initial structure of deformed metal and the ratio of migration rates of various high-angle boundaries, which in turn may be affected by many factors.

### 1.2.7. SECONDARY RECRYSTALLIZATION

#### Patterns of Secondary Recrystallization

In grain growth, all grains grow larger more or less uniformly and the metal may be characterized by an average grain size index. Such uniform growth of grains, which may be called *continuous*, has been discussed in 1.2.5.

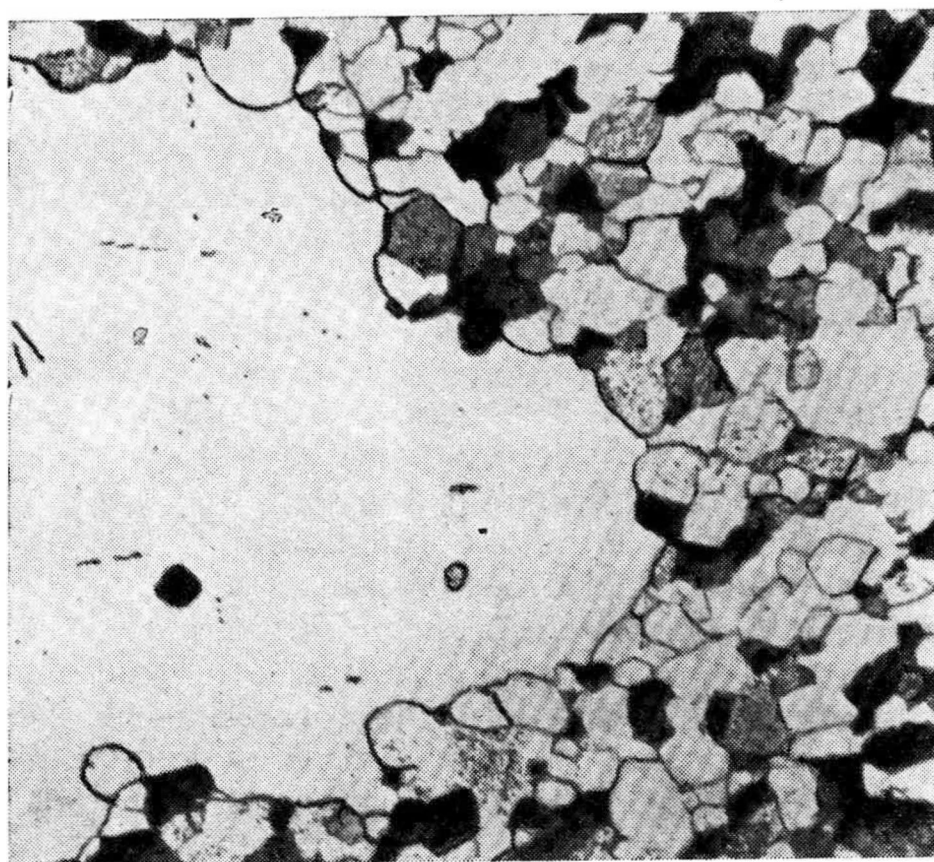


Fig. 34. The boundary between a large and fine grains that formed in zinc through secondary recrystallization during annealing at 200 °C, X60 (after J. E. Burke)

Certain conditions of annealing may produce a structure composed of a multitude of relatively small grains of approximately the same size and an appreciably smaller number of very large, sometimes gigantic, grains attaining a few centimeters in diameter (Fig. 34). Such a structure may form owing to *discontinuous grain growth* in which most grains grow in size very slowly or virtually do not grow at all, whereas some individual grains grow to a large size by 'consuming' their smaller neighbours. The process

is called *secondary recrystallization*. Its kinetics is very similar to that of primary recrystallization.

The growth of individual grains begins after a certain induction period (Fig. 35). The size of grains in secondary recrystallization increases linearly with the time of annealing, i.e. their rate of growth is constant at a given temperature. With increasing temperature of annealing, the rate of growth in secondary recrystallization increases exponentially according to equation (7) and the induction period becomes shorter.

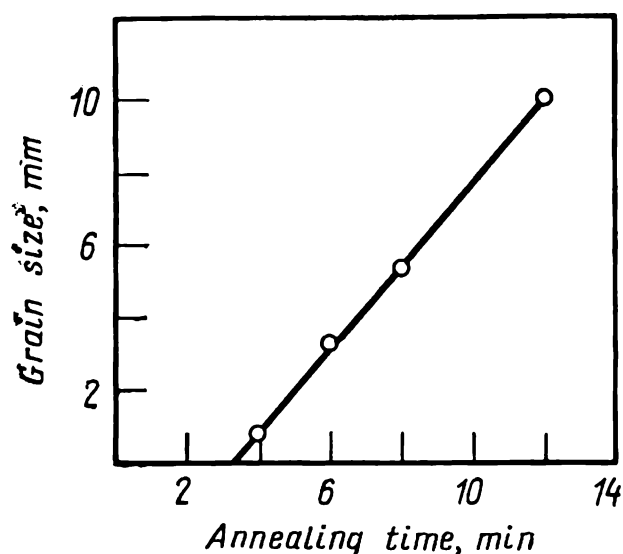


Fig. 35. Size variations of {110}-oriented grains in secondary recrystallization of Fe + 3% Si alloy strip 0.025 mm thick at 1200 °C (after C. G. Dunn and J. L. Walter)

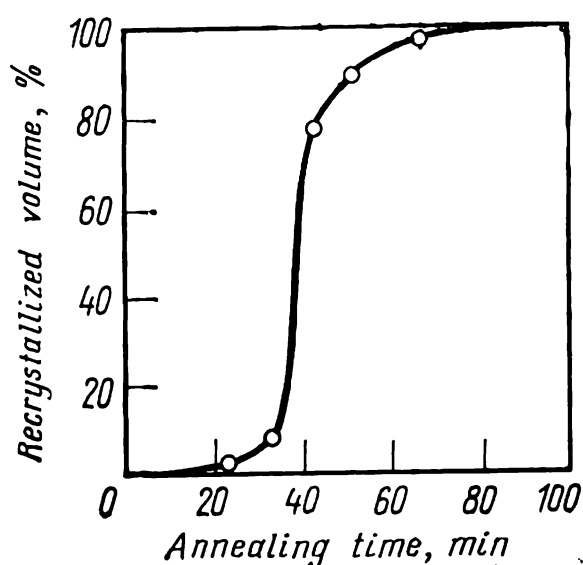


Fig. 36. Development of secondary recrystallization at 1050 °C in a strip of Fe + 3% Si alloy 0.04 mm thick (after F. Assmus, K. Detert, and G. Ibe)

As in primary recrystallization, the growth of recrystallized volume in secondary recrystallization on increasing the time of annealing is described by a sigmoid curve (cf. Figs. 36 and 20). The process gradually fades as ever greater number of grains interfere with their neighbours and thus stop growing.

Secondary recrystallization begins at a definite temperature ( $t_{s.r} = 925^\circ\text{C}$  in Fig. 37), below which only very slow grain growth is possible. On heating at 925 °C for one hour, i.e. for a longer time than the induction period of secondary recrystallization, some grains may increase their size roughly 50 times, i.e. up to 10 mm, whereas the main mass of grains remains small (around 0.02 mm).

The maximum growth of grains is obtained at  $t_{s.r}$ . At higher temperatures, the growth of individual grains is less intensive, since more centres of secondary recrystallization form in the metal. At temperatures above  $t_{s.r}$ , continuous grain growth in the matrix is accelerated, so that at a sufficiently high temperature

grain growth and secondary recrystallization begin to compete with each other (curves 1 and 2 in Fig. 37 converge). At a temperature of 1200 °C, only continuous grain growth occurs in the metal. Thus, secondary recrystallization can develop within a definite temperature range in which continuous grain growth proceeds relatively slowly.

Grains grown through secondary recrystallization often have a preferable crystal orientation, their texture being always unlike

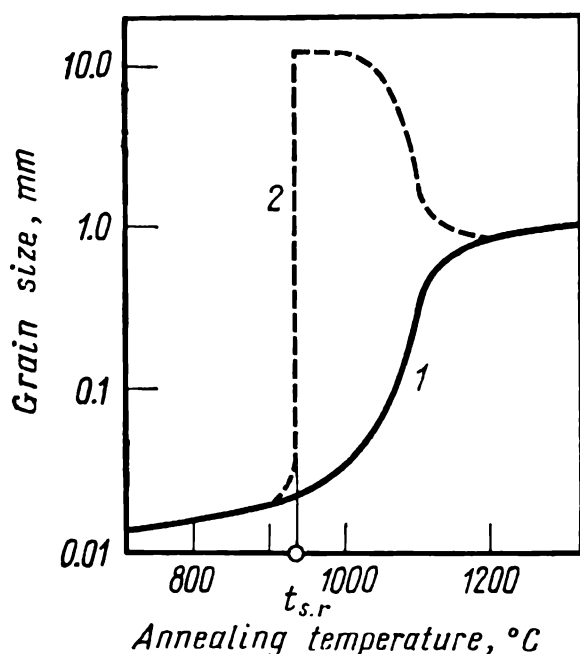


Fig. 37. Effect of annealing temperature (for 1 h) on grain size in Fe + 3% Si alloy sheets 0.35 mm thick

1—size of normally grown grains in stabilized matrix; 2—size of grains grown in secondary recrystallization

that on primary recrystallization or grain growth (being more sharp, i.e. more perfect). If a cubic texture has been formed in copper or aluminium upon primary recrystallization, then the texture of secondary recrystallization will form in them by the Kronberg-Wilson relation, i.e. the lattice of recrystallized grains will be rotated relative to the lattice of grains of stabilized matrix through an angle of 38° on the common  $\langle 111 \rangle$  axis. It should be noted in passing that coincidence boundaries proper were discovered by Kronberg and Wilson in their studies of textures of secondary recrystallization in copper.

The nature and perfection of secondary recrystallization textures depend on the conditions of plastic working, intermediate and

final annealing stages, including annealing atmosphere, the thickness of annealed sheets, and other factors.

Secondary recrystallization is by no means a rare special case of grain growth (i.e. discontinuous growth), as was assumed earlier, but a phenomenon inherent in many metals and alloys. It has been found in zone-refined metals and commercially pure metals, such as Fe, Cu, Ag, Zn, Ni, Pt, Ti, Al, W and Ta, and in various alloys, for instance, transformer and austenitic steels, alloys of aluminium with manganese and copper, and many others.

### The Nature of Secondary Recrystallization

Experiments show that discontinuous grain growth in various metals and alloys, under different conditions of heat treatment or even with a non-uniform thickness of metal sheets, may be caused

by different factors. In all cases, however, an indispensable condition for the development of secondary recrystallization is what is called the *stabilization of matrix*, i.e. strong retardation of the growth of most grains formed on primary recrystallization. If the matrix is stabilized on the whole, then the discontinuous growth of some grains, which for some or other reasons is not retarded, constitutes the essence of secondary recrystallization. Consequently, when analysing the causes of secondary recrystallization in each particular case, we should establish, firstly, why the matrix has been stabilized and, secondly, why individual grains could grow unobstructedly and consume the stabilized matrix.

The causes of stabilization of recrystallized matrix may be as follows:

- (a) disperse particles or segregated impurities at boundaries;
- (b) 'textural retardation'; and
- (c) 'thickness effect'.

All these causes have been considered in 1.2.5 when discussing the causes of retardation of grain growth. The role of the retardation by disperse particles, 'textural retardation', and 'thickness effect' was proved experimentally in various particular cases of secondary recrystallization.

It is more difficult to find out which ones of recrystallized grains in the stabilized matrix can grow rapidly, i.e. serve as nuclei of secondary recrystallization. In doing this, it is most important to understand why these grains are capable of outgrowing their neighbours at the initial stage of secondary recrystallization. Their subsequent growth is quite explainable: the boundaries of a large grain are concave outwards (i.e. towards smaller grains, as in Fig. 34 and grains 10 and 50 in Fig. 30) and thus should migrate towards their centre of curvature. Upon straightening of these curved boundaries in triple joints with smaller grains, the equilibrium of surface tension forces is disturbed and the triple joints displace towards the smaller grains and approach the junction angles to  $120^\circ$ . In this process, the boundaries of the large grain again become concave towards smaller grains, are again straightened through migration, and so on (see Fig. 29). In this way, a large grain grows continuously and consumes smaller grains until the latter vanish. The process is analogous with the process of grain growth discussed in 1.2.5, except for the fact that here only a few grains grow and they are surrounded by smaller grains whose growth is retarded.

Let us return to the question of which particular grains in the stabilized matrix at the initial stage of secondary recrystallization are capable of outgrowing their neighbours, i.e. serve potential nuclei of secondary recrystallization.

If the matrix is stabilized by disperse particles of a second phase, then, owing to non-uniform distribution of these particles or some other casual circumstances, the boundaries of some individual grains may turn to be locked appreciably less firmly than those of the majority of grains. Such grains will be capable of growing selectively. The retarding effect of disperse particles depends on their dispersity, volumetric proportion [see formula (12)], pattern of distribution, coagulating ability and solubility. If the retarding effect is not high, the matrix will be insufficiently stabilized, so that continuous grain growth will take place in the metal. If, on the other hand, the retarding effect is excessively strong, for instance, if the volumetric proportion of disperse particles is very high, the matrix is overstabilized, i.e. has no grains capable of growing discontinuously, and secondary recrystallization will not take place.

When secondary recrystallization is favourable (see 1.2.10), the optimum amount, size and distribution of disperse particles for its development are obtained by introducing special additions and by properly selecting the conditions of plastic working and heat treatment.

If the matrix has been stabilized owing to the perfect texture formed on primary recrystallization, then most grains are separated by boundaries having only slight angles of misorientation, and therefore, a low boundary energy, because of which these boundaries will be low-mobile. Under conditions of 'texture-induced' retardation, only a few grains whose orientation differs appreciably from the main orientation of the stabilized matrix are capable of growing selectively. The maximum mobility is possessed by the grain boundaries obeying the Kronberg-Wilson relation or having a structure close to that relation. Thus, if upon primary recrystallization there are a few grains separated from other grains by Kronberg-Wilson boundaries, these grains will grow rapidly during secondary recrystallization and determine the main orientation of the whole metal. It is this nature of secondary recrystallization that is inherent in copper. It should then also be clear that a more perfect texture of primary recrystallization gives a sharper picture of secondary recrystallization.

If the matrix has been stabilized owing to the 'effect of thickness', i.e. through locking of grain boundaries in thin sheets by thermal etch pits in places where the boundaries pass out onto the sheet surface, the free surface energy of grains will have the decisive effect on the rate of grain growth. In crystals of transformer steel ( $\text{Fe} + 3\% \text{ Si}$ ), the  $\{110\}$  faces possess the least surface energy (as those having the maximum density of atom stacking in the b.c.c. lattice). For that reason, the growth of crystals whose  $\{110\}$  faces coincide with the plane of sheet will be energetically



favourable and these crystals will outgrow all other crystals in the sheet.

The surface energy of crystal faces in Fe + 3% Si has turned to be very sensitive to the composition of the surrounding atmosphere (owing to adsorption). If the atmosphere of the annealing furnace contains oxygen, the {100} faces have a lower surface energy than {110} faces. Thus, if thin sheets of transformer steel are annealed in vacuum or dry hydrogen, secondary recrystallization forms the {110}  $\langle$ 100 $\rangle$  *rib texture* in them, whereas annealing in an oxygen-containing atmosphere can produce the {100}  $\langle$ 100 $\rangle$  *cubic texture*. By controlling furnace atmosphere (and also the composition of alloy), we can change the free surface energy and thus control the texture of secondary recrystallization by causing the grains having the lowest energy on the faces passing out onto the sheet surface to grow selectively. Naturally, this control of secondary recrystallization texture is only possible in sheets whose thickness is commensurable with the size of grains formed on primary recrystallization or grain growth.

Knowing the effect of disperse particles of excess phases, the texture of primary recrystallization, annealing atmosphere, thickness of articles and other factors on matrix stabilization and selective grain growth, we can control the process of secondary recrystallization (i.e. either suppress or promote it) by changing the composition of alloy and the conditions of plastic working and heat treatment.

#### 1.2.8. SIZE OF RECRYSTALLIZED GRAINS IN ANNEALED METAL

The size of recrystallized grains is one of the principal characteristics of annealed metal. The time of annealing is usually longer than the time needed for recrystallization. Therefore, the size of grains of annealed metal may be influenced by all the factors active in primary recrystallization and grain growth. When analysing the factors affecting grain size in primary recrystallization, use may be conveniently made of the parameters widely employed in the theory of phase transformations: *the rate of nucleation of recrystallization centres* ( $N$ ), measured as the number of new crystals formed in unit volume per unit time, and the *linear rate of growth of new crystals* ( $G$ ), which actually is the rate of migration of a grain boundary.

At the final moment of recrystallization, the size of grains depends on the  $N/G$  ratio. The greater this ratio (i.e. the greater its numerator or smaller the denominator), the finer is the grain formed at the end of primary recrystallization, and *vice versa*. Upon primary recrystallization, grains may increase further in

size owing to grain growth. For that reason, the final size of grains may also depend on the linear rate of growth of crystallites in grain growth (secondary recrystallization is not yet considered).

Numerous experiments show that the main factors affecting the final size of grains in annealed metal are as follows: the temperature and time of annealing, degree of deformation, size of

initial grains (prior to deformation), heating rate, and naturally, the composition of the metal.

At higher temperatures of annealing, both  $N$  and  $G$  increase. If both parameters change similarly with temperature, then the size of grains upon primary recrystallization should be independent of the temperature of annealing. If however,  $N$  varies with temperature more appreciably than  $G$ , the size of grains at the end of primary recrystallization should be the smaller, the higher is the temperature of annealing. Both cases were observed more than once during annealing of aluminium, aluminium alloys, brass and other alloys. It may seem, on the face of it, that these facts contradict the common concept that higher temperatures of annealing cause grain coarsening. Actually, however, the size of grains we spoke of above is that

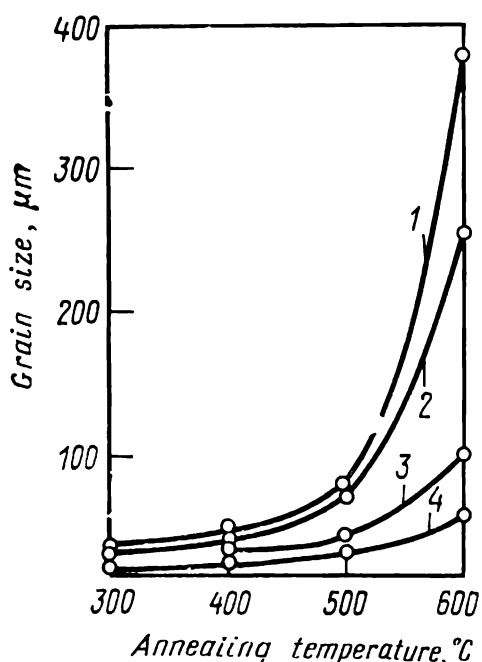


Fig. 38. Effect of annealing temperature (1-h annealing) on size of recrystallized grains in aluminium and some aluminium alloys (I. I. Novikov)

1—99.7-% pure aluminium; 2—Al + 1.2% Zn; 3—Al + 0.6% Mn; 4—Al + 0.55% Fe

formed at the end of primary recrystallization, whereas the time of annealing is usually much longer than the time needed for primary recrystallization. Thus, in the latter case, grain coarsening at higher temperatures of annealing should be explained by a higher intensity of grain growth. Figure 38 shows the most typical curve of the effect of annealing temperature on grain size at a constant time of annealing. In the region of high temperatures, grain growth may sometimes slow down or even cease completely at an increase of temperature. This can happen when for instance, the boundaries of crystallites become partially molten or when the size of the grains formed approaches the thickness of the article.

On increasing the time of annealing, grain growth decelerates, since its rate gradually diminishes and the size of grains being formed approaches the limit at the given temperature (Fig. 39).

If annealing has produced grains that have the maximum size at a given temperature, further coarsening of grains is possible through a new annealing operation at a higher temperature. A higher temperature facilitates the passage of atoms from one grain to another. Besides, a higher temperature of annealing can

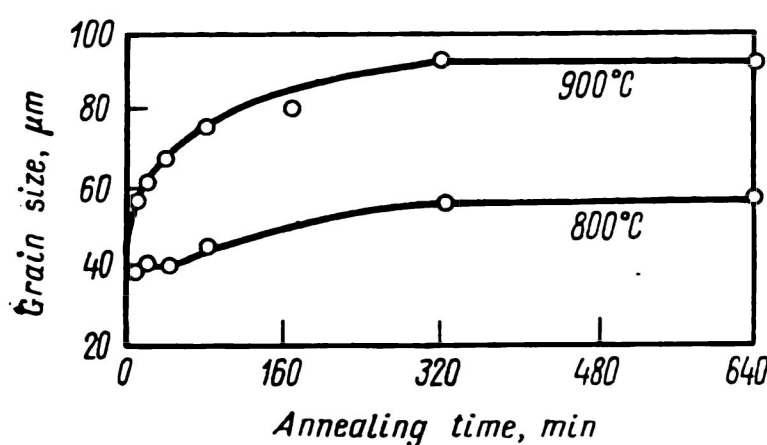


Fig. 39. Effect of holding time on grain size in nickel at two annealing temperatures (*I. I. Novikov and I. L. Rogelberg*)

eliminate segregations of impurity atoms at grain boundaries and partially dissolve the excess phases that might retard boundary migration during grain growth.

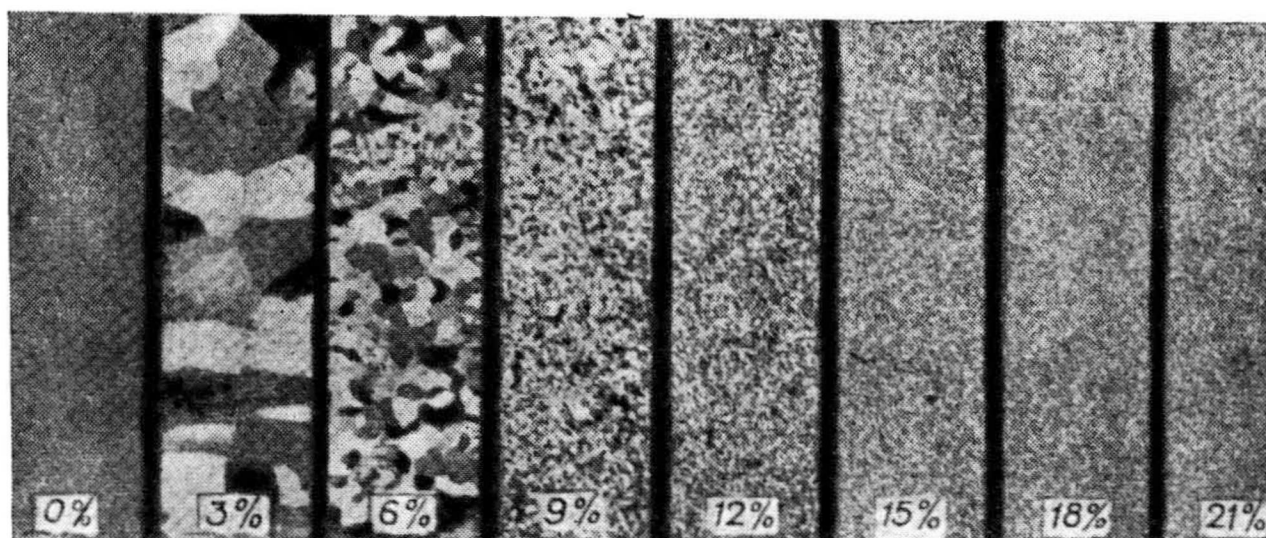


Fig. 40. Microstructure of pure aluminium plates annealed at 500°C and tensioned with different deformations (as shown in figure). Full size

The degree of deformation may have an extremely strong effect on the size of grains at the end of primary recrystallization (Figs. 40 and 41). Since the time of annealing is usually longer than the period of primary recrystallization, curves of the type shown in Fig. 41 actually describe the effect of deformation on the final size of grains obtained upon grain growth. The latter

only increases the size of grains, but does not change the nature of the effect of deformation on the size of crystallites at the end of primary recrystallization.

A higher deformation gives a higher density of dislocations and produces an excess of dislocations of one sign, which naturally increases both  $N$  and  $G$ . If both increased similarly on increasing the degree of deformation, the latter would have no effect on the size of recrystallized grains. But since the size of recrystallized grains diminishes on increasing the degree of de-

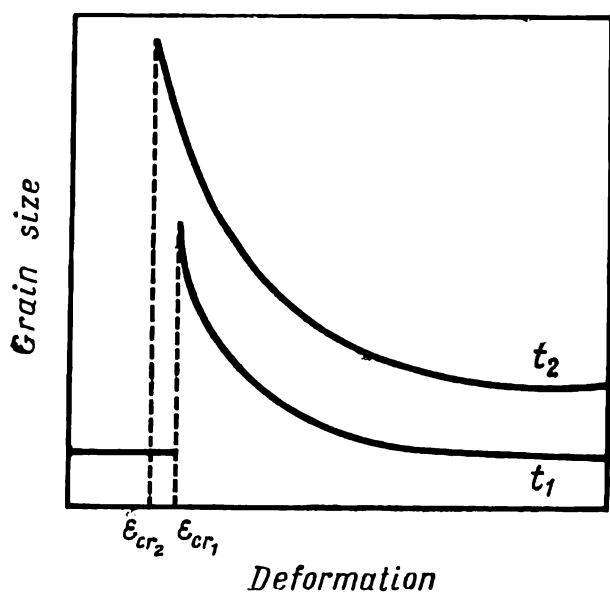


Fig. 41. Effect of preliminary deformation on grain size of metal annealed at two different temperatures  $\epsilon_{cr}$ —critical deformation;  $t_2 > t_1$

formation, we can conclude that  $N$  increases more rapidly than  $G$ . This conclusion has been confirmed by direct measurements of these rates.

With a relatively low *critical deformation* (usually from 1 to 15 per cent), grains can grow on annealing to a very large size, sometimes up to a few centimeters. The mechanism of formation of large grains at a critical deformation differs qualitatively from the mechanism of recrystallization in the supercritical region, i.e. at higher degrees of deformation.

The structural changes upon annealing of deformed metal with critical or almost critical deformations have been studied experimentally in much detail and analysed by S. S. Gorelik. These changes are essentially as follows.

Annealing after a deformation below critical causes polygonization and displacement of high-angle boundaries of deformed grains over relatively small distances, only a few hundredths or tenths of the size of grains.

On increasing the degree of deformation in the below-critical region, the non-uniformity of strain-hardening of various grains increases. The critical degree of deformation corresponds to a state where this non-uniformity becomes so great that, owing to a difference in the stored volume energy of neighbouring grains, some individual boundaries can rapidly migrate on heating over distances that are commensurable with the size of grains, i.e. individual initial grains can grow at the expense of their neighbours.

The total density of dislocations and an excess of dislocations of one sign at the critical deformation are still insufficient for the

formation of new high-angle boundaries and nuclei of primary recrystallization on heating. Therefore, annealing after the critical deformation causes no primary recrystallization; instead, some slightly deformed grains grow larger at the expense of other deformed grains, the driving force of this recrystallization being the difference between the volume energies of non-uniformly deformed adjacent grains.

In the region of deformations appreciably above the critical, the total density of dislocations and an excess of dislocations of one sign are so great that a large number of centres of primary recrystallization forms on annealing and the process spreads rapidly over the whole volume of the metal.

The slower growth of deformed grains at the expense of their neighbours through migration of the initial boundaries cannot compete with this process, since the difference in the stored energy of adjacent deformed grains is incomparably lower than the difference in the volume energy between deformed grains and new recrystallized grains.

On annealing after deformations which are only slightly above the critical, i.e. when the number of nuclei of primary recrystallization is still very low, two processes may compete with each other, i.e. the grain growth through migration of the initial boundaries and the growth of new grains in nuclei of primary recrystallization. Owing to the latter process, the average size of grains is smaller than that obtained on annealing after the critical deformation.

The magnitude of critical deformation may depend on annealing temperature, temperature of deforming, composition of alloy (purity of metal), and the initial structure.

A higher temperature of annealing corresponds to a lower critical deformation (Fig. 41). This is quite understandable, since the higher is the temperature of annealing, the smaller is the difference in the stored energy of adjacent grains that is needed to initiate grain growth (owing to the higher mobility of atoms).

An increase in the temperature of deforming increases the critical deformation in subsequent annealing (Fig. 42). At higher temperatures of deforming, a greater degree of deformation is needed to produce the required non-uniform strain-hardening of

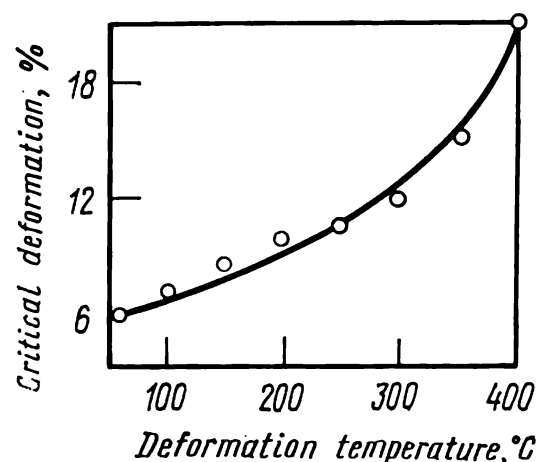


Fig. 42. Effect of deformation temperature on critical degree of deformation of aluminium. Annealing for 30 min at 450 °C (after V. Z. Zakharov, I. I. Novikov, I. L. Rogelberg, and Yao Ming-chi)

adjacent grains, since the process of recovery occurring during the deformation proper can partially eliminate the effect of strain-hardening.

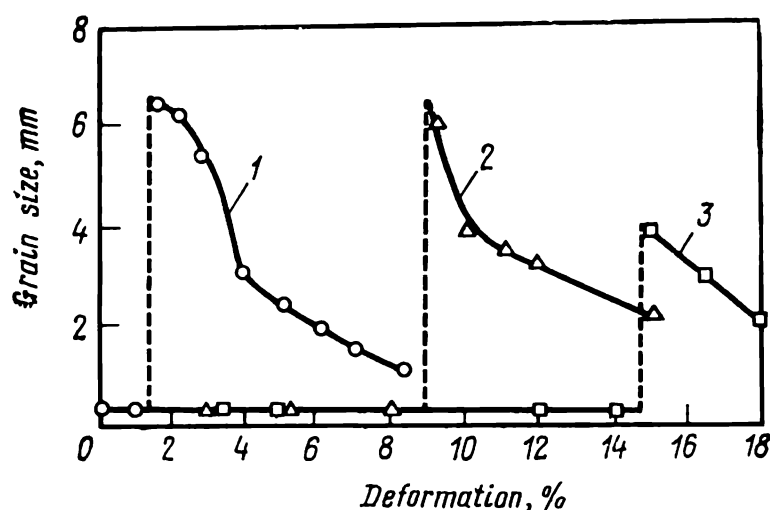


Fig. 43. Effect of deformation on size of recrystallized grains in manganese-doped aluminium. Annealing at 500 °C for 30 min (after V. Z. Zakharov, I. I. Novikov, I. L. Rogelberg, and Yao Ming-chi)  
1—99.7% pure aluminium; 2—Al + 0.3% Mn; 3—Al + 0.6% Mn

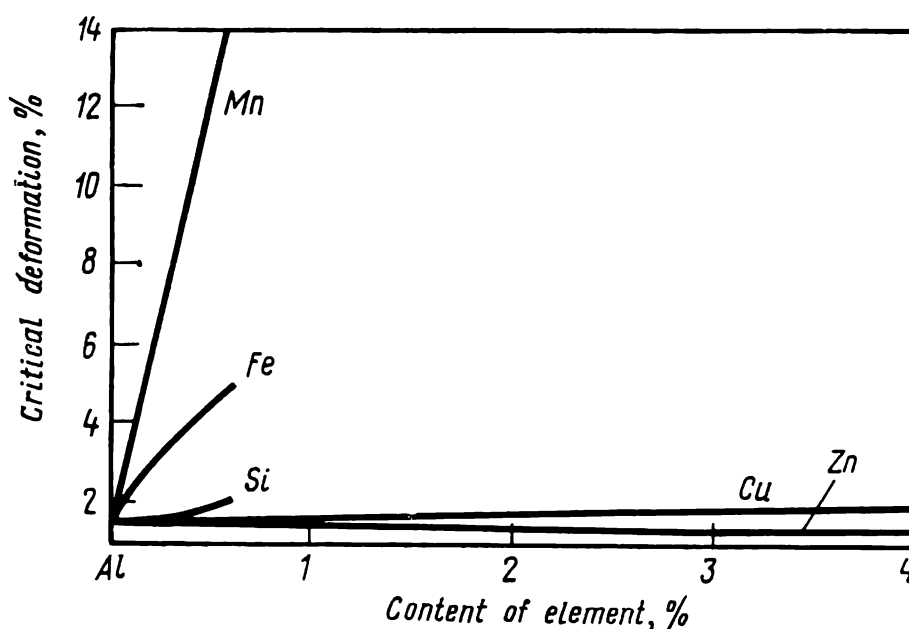


Fig. 44 Effect of various elements on critical degree of deformation of aluminium. Annealing at 500 °C for 30 min (after V. Z. Zakharov, I. I. Novikov, I. L. Rogelberg, and Yao Ming-chi)

The critical deformation diminishes on improving the purity of metal. Alloying elements and impurities may have different effect on the critical degree of deformation. Some elements (such as Mn and Fe in aluminium) can appreciably increase the critical deformation even when added in small amounts, while others (for instance, Zn and Cu in aluminium) produce only a slight effect even in large quantities (Figs. 43 and 44). The strong effect of

small amounts of manganese and iron is due to the fact that, unlike zinc and copper, they are only poorly soluble in solid aluminium and form disperse particles of excess phases which retard boundary migration of initial deformed grains.

A second maximum of grain size has been discovered in aluminium, copper and some alloys at large deformations and very high temperatures of annealing (Fig. 45). In some cases, for instance, in electrolytic copper at a deformation of 80 per cent and annealing temperature over  $1000^{\circ}\text{C}$ , the size of grains is larger than at the critical deformation of the first maximum. It may be assumed that large grains form in high-temperature annealing by the mechanism of secondary recrystallization, owing to the perfect texture appearing at high degrees of deformation.

In some commercial alloys based on nickel and iron, such as Grades XH77T10P and X12H20T3P, a second maximum of grain size appears in the region of medium and low deformations (from 5 to 60 per cent). In that case, large grains grow in secondary recrystallization under the conditions promoting partial dissolution of disperse phases which might retard boundary migration in grain growth. The size of recrystallized grains upon grain growth is usually the larger, the larger are the initial grains. This is quite understandable if we recall that nuclei of primary recrystallization form preferably at grain boundaries. The difference in the size of recrystallized grains is appreciably lower than that of the initial grains and the effect of initial grains diminishes on increasing the degree of deformation.

As may be seen from Table 4, when the difference in the size of initial grains is almost 20 times, recrystallized grains will differ in their size by approximately 4 times at low deformations and only by 20 per cent at high deformations.

As the rate of heating to the temperature of annealing is increased, the size of recrystallized grains that form diminishes in the general case. This may be explained by the process of recovery which is possible in the metal at slow heating; this can partially eliminate strain-hardening and thus diminish the number of recrystallization nuclei. Besides, slow heating can result in a coarser grain, owing to a low number of nuclei of primary recrystallization.

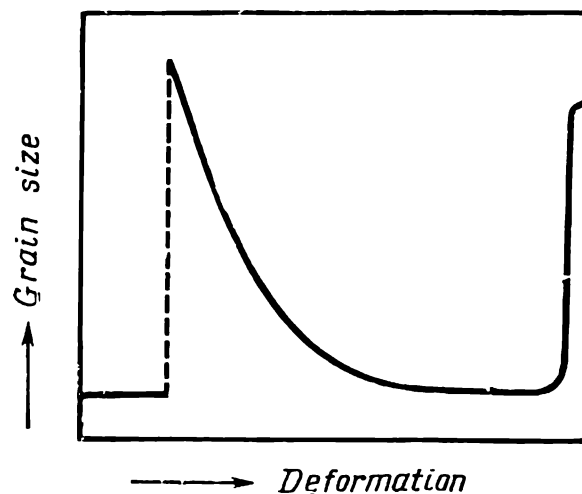


Fig. 45. Effect of preliminary deformation on grain size in annealed metal

**Table 4. Size of Recrystallized Grains  
in 99.7-per cent Pure Aluminium upon Annealing  
at 600 °C for 40 min (after I. I. Novikov  
and I. L. Rogelberg)**

Deformation, %	Size of recrystallized grains, mm, against the initial grain size, mm	
	1.13 mm	0.06 mm
5	2.64	0.75
10	2.05	0.51
50	0.54	0.44

With pure metals and single-phase alloys, the effect of heating rate on grain size in the range of practicable heating rates often remains unnoticed. With heterogeneous alloys, though with a low amount of a second phase, quick heating in a salt bath can form appreciably finer recrystallized grains than slow heating in the furnace.

This may be well illustrated by the following data on the number of grains per 1 mm<sup>2</sup> upon cold rolling with 30-per cent reduction and subsequent annealing at 420 °C.

	99.95%-pure Al	Al+4% Cu	Al+0.5% Si	Al+1% Mg <sub>2</sub> Si
Slow heating in the furnace . . . . .	36	225	49	30
Quick heating in molten salt . . . . .	36	1150	64	145

The composition of metal can have an appreciable effect on the size of recrystallized grains. It may be taken as the general rule that the size of recrystallized grains in the metal diminishes on increasing the content of impurities, the main cause for this being impediment of grain growth.

Elements which form poorly soluble second phases in the base metal have an appreciable effect on grain size. As may be seen from Fig. 38, zinc has only a slight effect on grain size in aluminium, even when it is present in a relatively large amount in the solution. On the other hand, manganese, which forms with aluminium a poorly soluble MnAl<sub>6</sub> compound, and especially iron, which forms insoluble FeAl<sub>3</sub>, can strongly retard grain growth.

### *Recrystallization Diagrams*

The dependence of grain size on all the factors discussed above cannot be shown graphically on a single diagram. In practice, *recrystallization diagrams* have found a rather wide application;



they give the dependence of the grain size in metal or alloy on deformation and annealing temperature for a given time of annealing (Fig. 46). These diagrams enable us, in the first approximation, to select annealing conditions to form the desired structure in the metal.

Vertical sections through a three-dimensional recrystallization diagram at a constant degree of deformation and constant temperature of annealing give curves of the types shown respectively

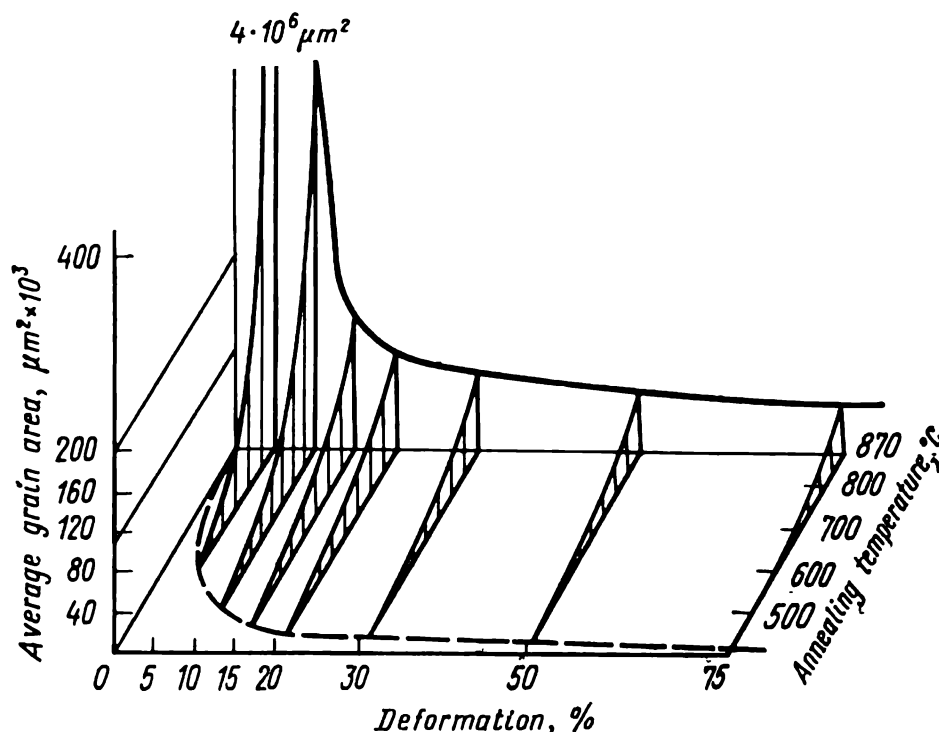


Fig. 46. Recrystallization diagram for electrolytically refined iron. Preliminary treatment: forging and annealing at 930°C; final treatment: cold upsetting and annealing for 1 h (after P. Oberhoffer and W. Ortel)

in Figs. 38 and 41. A curve representing the dependence of the temperature of beginning of recrystallization on degree of deformation is often drawn in the lower horizontal plane of a recrystallization diagram (see the dotted line in Fig. 46).

When using recrystallization diagrams, one has to consider accurately the conditions under which they have been obtained, namely: the time of annealing, content of impurities, initial grain size, rate of heating in annealing, type of plastic working, etc. For that matter, each recrystallization diagram should be supplied with detailed data on the initial state and final treatment of the metal. Since even slight variations in the content of impurities, as also some uncontrollable factors, may have an appreciable effect on grain size, this substantially lowers the value of recrystallization diagrams as means for quantitative characterization of metals. Actually they rather serve as semi-quantitative tools orienting us in how the degree of deformation and temperature of annealing can affect the size of grains in metals and alloys.

### *Inequigranular Structures*

Various portions of metal upon recrystallization annealing may have either roughly the same grain size (only fine or only large grains) or undesirable inequigranularity. This may be in the principal forms as follows:

- (1) uniform inequigranularity, i.e. regular alternation of large and fine grains throughout the volume of the metal;
- (2) zonal inequigranularity, with large grains concentrated in certain portions or zones;
- (3) line inequigranularity, with large grains usually stretched along the direction of main deformation;
- (4) island inequigranularity, with groups of very large or very fine grains distributed non-uniformly throughout the volume.

The causes and conditions for the appearance of inequigranularity may be very diverse and differ substantially in various metals and alloys even with the same type of inequigranularity.

Uniform inequigranularity may appear at the stage of incomplete secondary recrystallization. It can be prevented by annealing the metal at a temperature below that of the beginning of secondary recrystallization, which gives fine-grained recrystallized structure throughout the volume of metal. Another way is to raise the temperature or increase the time of annealing at a temperature above  $t_{s.r.}$ , but this produces coarse-grained structure all over the metal. On raising the temperature of annealing well above  $t_{s.r.}$ , the structure will be more fine-grained than after annealing at temperature near  $t_{s.r.}$  (see Fig. 37).

The simplest case of zonal inequigranularity is when it forms in definite zones of a product at the critical deformation of the metal. With a strong local deformation, the degree of deformation may diminish from a high value above critical, for instance at the edge of a pierced hole, down to zero (far away from that edge). In that case, a certain portion of the product always turns to be deformed to the critical degree, with large grains forming here upon annealing. Since the critical deformation cannot be avoided technologically, a method to prevent inequigranularity is to abandon recrystallization annealing and use only prerecrystallization annealing.

Zonal inequigranularity may appear in individual zones of articles where the deformed matrix has been made stable against primary recrystallization. This stabilization may be caused, in the first place, by disperse particles of excess phases. These particles can retard appreciably the migration of low-angle boundaries and prevent subgrains from becoming recrystallization nuclei. As a result, the number of nuclei of primary recrystallization diminishes appreciably. However, grains grow from these nuclei com-

paratively easily, since high-angle boundaries are retarded by disperse particles much more feebly than are low-angle boundaries. Disperse particles may form on precipitation of excess phases from a supersaturated solid solution during hot working or in some other way. Disperse particles can be effective in this respect only when they remain undissolved on heating to the temperature of annealing.

Another cause of stabilization of deformed matrix may be the process of recovery during hot working, if the hot plastic working proper has involved no recrystallization and the structure of hot-worked alloy has only been polygonized. Still another cause of stabilization of deformed matrix may be a textured pattern of that matrix: with a very close orientation of most subgrains, recrystallization nuclei appear only in some few subgrains whose orientation differs appreciably from that of their neighbours.

When the factors considered stabilize the deformed matrix uniformly over the whole volume of an article, annealing produces a coarse-grained structure (owing to the low number of recrystallization nuclei), but without any noticeable inequigranularity. When, however, the degree of stabilization is different in various zones of an article, annealing will result in inequigranularity. Non-uniform stabilization of the deformed matrix may be due to different degree and nature of deformation (for instance, laminar deformation in the centre and turbulent at the periphery of a formed rod).

Line arrangement of disperse particles in a deformed article can cause line inequigranularity upon recrystallization annealing.

Zonal segregation in an ingot can produce macroheterogeneity in the composition of a deformed product, so that primary and secondary recrystallization and grain growth will occur with different rates in various portions of the metal and thus cause zonal or island-type inequigranularity.

The phenomenon of inequigranularity can be prevented by properly controlling the conditions of crystallization in ingots, conditions of homogenizing annealing, conditions of plastic working, and also the composition of alloys. Because of the diverse causes and forms of inequigranularity, particular engineering conditions must be developed for each type of product in order to ensure the most uniform granular structure.

In most cases it is desirable that the structure upon annealing be both homogeneous and fine-grained. If the metal (alloy) undergoes no polymorphic transformations, then no subsequent heat treatment is capable of eliminating the inequigranularity formed on recrystallization annealing, since this inequigranularity corresponds to the state of the least free energy.

Recrystallization annealing is sometimes used intentionally to form coarse-grained structure in the metal or to produce bi- and

monocrystals which are needed for research work and specific engineering applications. Bi- and monocrystals are made by the deformation-annealing method, which uses the critical deformation and special conditions of annealing.

### 1.2.9. CHANGES IN METAL PROPERTIES UPON PRERECRYSTALLIZATION AND RECRYSTALLIZATION ANNEALING

During annealing of work-hardened metal, all its properties vary reversely to what occurs in cold deformation, i.e. the indices of resistance to deformation (ultimate and yield strength and hardness) diminish, ductility indices (relative elongation and reduction) increase, and the physical and chemical properties approach the values they had before the deformation.

#### Softening on Annealing

Depending on the temperature and time of annealing, various structural changes may develop to some or other extent in the metal and accordingly the process of softening may follow different paths.

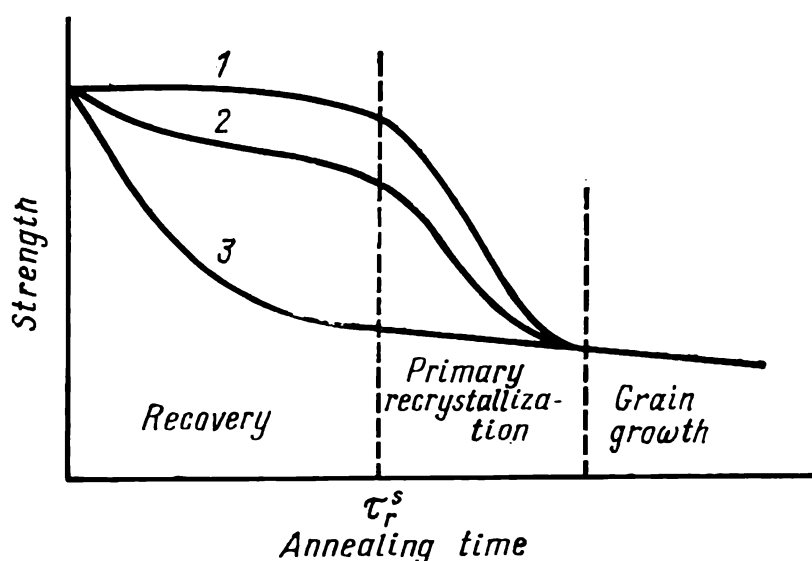


Fig. 47. Effect of isothermal annealing time on strength properties of strain-hardened metal

Figure 47 shows schematically three typical cases of variation of strength properties on increasing the time of annealing at constant temperature. During the induction period before primary recrystallization, i.e. when only recovery takes place, the effect of work hardening may virtually remain unchanged (curve 1), diminish partially (curve 2) or vanish completely (curve 3).

The nature of variation of strength properties before recrystallization completely conforms to the kinetics of recovery (see

Fig. 15): the rate of reduction of strength properties diminishes as the time of recovery increases. If the strength properties have not restored upon recovery, the subsequent primary recrystallization fully eliminates the effect of work hardening. As the time of

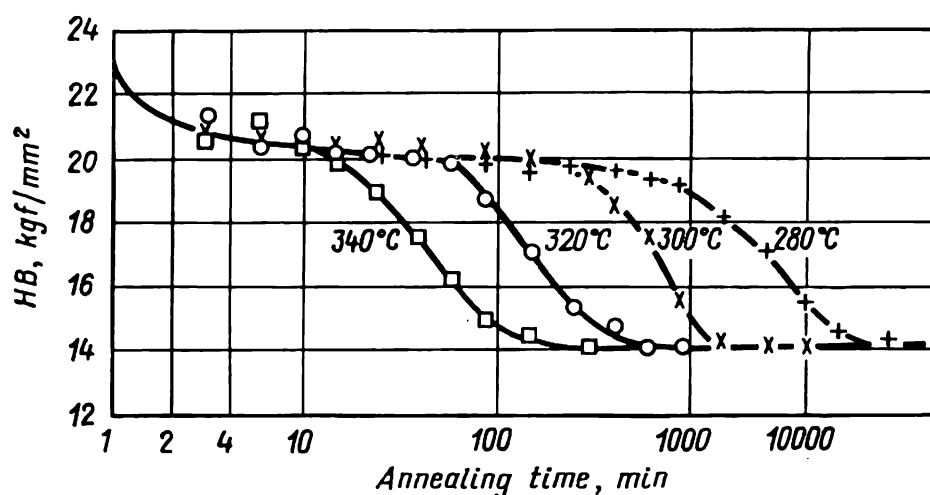


Fig 48. Curves showing how the hardness of strain-hardened pure aluminium lowers with increasing time of annealing at various temperatures. Initial state: cold tension, 20% (after *P. Laurent and M. Batisse*)

annealing is increased in this process, the rate of reduction of strength properties first increases, then remains constant for a certain time, and finally drops down in full accordance with the sigmoid curve of growth of recrystallized volume (see Fig. 20).

As may be seen from Fig. 48, the hardness of work-hardened aluminium during isothermal annealing first diminishes deceleratedly (as long as recovery takes place), after which the metal softens intensively due to primary recrystallization, the rate of this softening first increasing and finally decreasing.

Copper, nickel and silver are intrinsically capable of retaining work-hardening on recovery. A noticeable, or sometimes very substantial drop in work-hardening can occur before primary recrystallization in aluminium and titanium during annealing. Full elimination of work-hardening during the period of recovery takes place in deformed single crystals of refractory b.c.c. metals (tungsten and molybdenum) and in polycrystalline alloys of aluminium and magnesium (Fig. 49). It is important for practical purposes

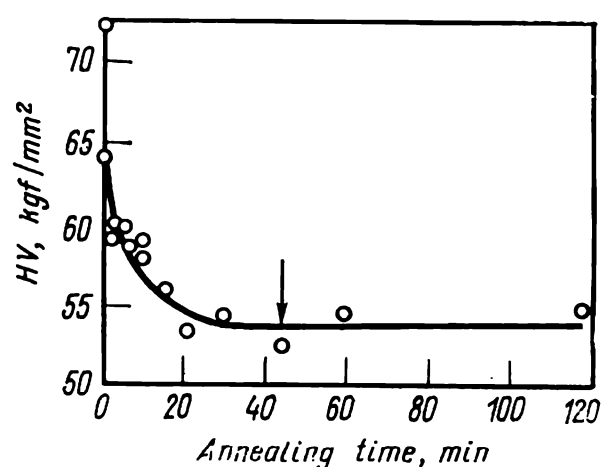


Fig. 49. Effect of time of annealing at 250°C on hardness of cold-rolled Al + 2.87% Mg alloy. Arrow shows the appearance of first recrystallized grains 2  $\mu$ m in diameter (after *E. C. W. Perryman*)

that work-hardened aluminium-magnesium alloys can soften appreciably even at room temperature, as may be seen from the following data for cold-rolled magnalium with 6 per cent Mg:

Time . . . . .	0	10 days	4 months	2 years	12.5 years
$\sigma_t$ , kgf/mm <sup>2</sup> . . . .	50	48	45.5	44	43.5

Typical cases of dependence of strength properties on annealing temperature (for a constant time of annealing) are shown diagrammatically in Fig. 50. At temperatures above that of the

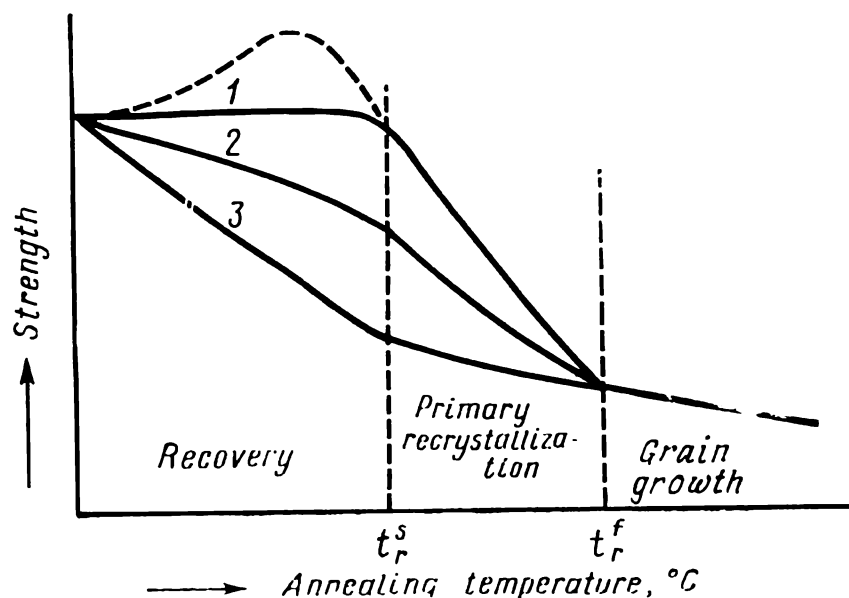


Fig. 50. Effect of annealing temperature on strength properties of strain-hardened metal

beginning of recrystallization, the work-hardening effect can remain fully (curve 1), or partially (curve 2) or disappear (curve 3). In the first case, intensive softening begins at the temperature of the beginning of primary recrystallization, while in the second and third cases the onset of softening cannot be used to determine  $t_r^s$ . Therefore, the well-known method for determining by measuring the strength properties of a metal is not universally applicable.

Whereas the loss in strength properties within the region of primary recrystallization is appreciable, these properties drop in the region of grain growth only feebly.

At temperatures below  $t_r^s$ , work hardening is observed to remain almost fully in copper, nickel and silver, diminish noticeably in aluminium and iron, and drop strongly in many refractory b.c.c. metals. For instance, work-hardened tungsten, when being annealed at the temperature of beginning of recrystallization (1200 °C), softens almost to the same extent as on primary recrystallization (Fig. 51).

The strength properties of metals may depend on dislocation structure and grain size. If only low-temperature recovery takes place during prerecrystallization annealing, and therefore, the main structural changes consist in diminished concentration of point defects, while the density of dislocations lowers insignificantly, then the effect of strain hardening will essentially remain in the metal. If, however, prerecrystallization annealing results in the development of polygonization, which is linked with the formation and growth of subgrains and removal of dislocations from them, then the strength properties can drop substantially.

The yield limit  $\sigma_y$  is linked with subgrain diameter  $d$  by the Petch-Hall relation:

$$\sigma_y = \sigma_0 + kd^{-1/2} \quad (13)$$

In accordance with this relation, the growth of subgrains during polygonization causes a loss in the yield limit on prerecrystallization annealing.

Primary recrystallization, which can lower strongly the dislocations density (from  $10^{11}$ - $10^{12}$  to  $10^6$ - $10^8$   $\text{cm}^{-2}$ ) and "sweep out" the arrays of subgrains, can cause strong softening proportional to the fraction of recrystallized volume. As the temperature of annealing is raised between  $t_r^s$  and  $t_r^f$  (Fig. 50) or the time of annealing is increased at a constant temperature (to the right of  $\tau_r^s$  in Fig. 47), the strength properties diminish appreciably due to primary recrystallization. Besides, the process of recovery that continues in those deformed grains which are still not consumed by recrystallized ones, also contributes much to the softening effect. An indication to this is a lower microhardness in unrecrystallized grains.

As soon as all work-hardened grains have been replaced by much more perfect recrystallized grains, grain growth can only slightly lower the strength properties. In particular, the yield limit diminishes owing to grain growth in accordance with the Petch-Hall relation [in that case,  $d$  is the diameter of grains in formula (13)].

Different capacity of metals for softening in prerecrystallization annealing may be attributed to their different polygonizing

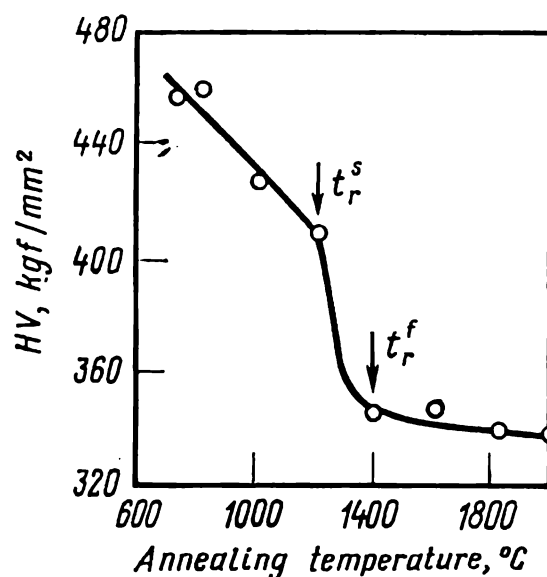


Fig. 51. Effect of temperature of annealing (1 h) on hardness of electron-beam melted tungsten deformed with 50-per cent reduction at 800 °C (after B. C. Allen)

capability. In metals of the same type of lattice, the ease with which polygonization can proceed depends on the stacking fault energy (see 1.2.3). For instance, aluminium has a higher stacking

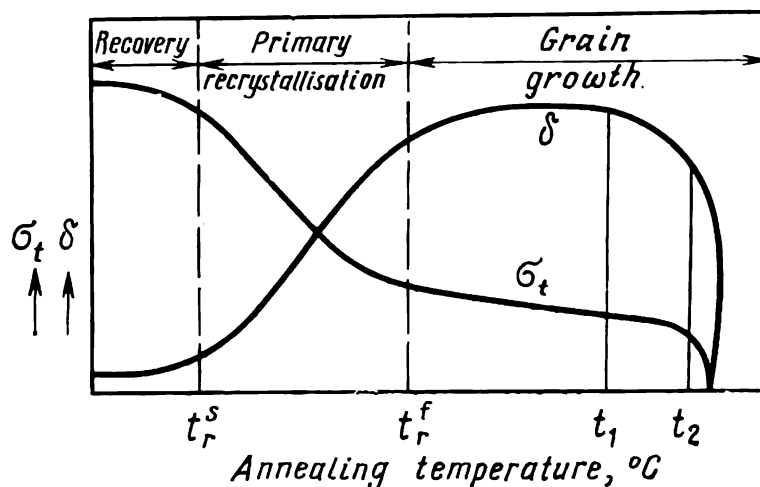


Fig. 52. Effect of annealing temperature on mechanical properties of deformed metal (one of the most common cases);  $t_r^s$ ,  $t_r^f$ ,  $t_1$  and  $t_2$  are respectively temperatures of the beginning and end of recrystallization, temperature of overheating, and that of burning

fault energy than copper, so that polygonization in it proceeds more intensively and results in a strong softening on prerecrystallization annealing. In some refractory b.c.c. metals, such as

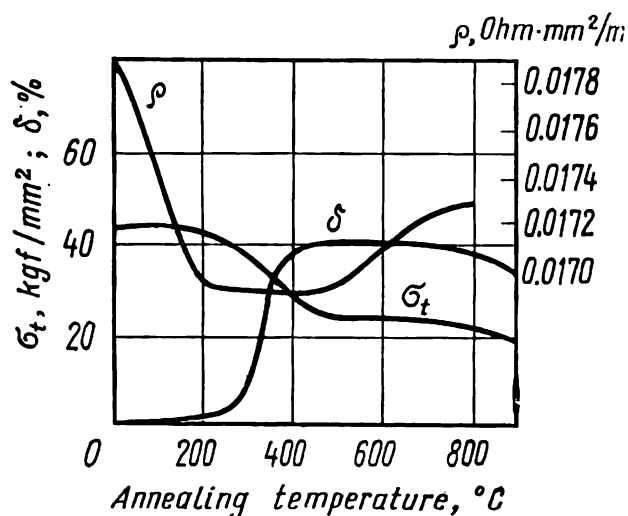


Fig. 53. Effect of temperature of annealing (1 h) on electric resistivity and mechanical properties of Grade M1 copper (after A. P. Smiryagin)

molybdenum or tungsten, polygonization develops especially actively, because of which a greater deal of softening in these metals occurs during prerecrystallization annealing.

Softening in prerecrystallization annealing can be accelerated or enhanced by applying light stresses to the product during annealing. These stresses are insufficient for forming an appreciable work-hardening effect, but accelerate the climb of dislocations which is essential for the development of recovery.

The ductility indices vary during annealing of cold-deformed metal generally in the opposite sense to what happens to the strength properties: they increase relatively feebly in the recovery region, rise appreciably in primary recrystallization, when the work-hardening effect is essentially removed, and vary only slightly in grain growth (Figs. 52 and 53). The maximum ducti-



lity is obtained within a definite temperature range in grain growth. Beginning from a definite temperature ( $t_1$  in Fig. 52 and approximately 800°C in Fig. 53), ductility decreases smoothly, since the far-developed grain growth results in the formation of excessively large grains. This phenomenon is called *overheating in recrystallization annealing*.

At very high temperatures of annealing (above  $t_2$  in Fig. 52), both ductility and strength can drop appreciably owing to *burning*, i.e. strong intercrystalline oxidation and sometimes partial melting of impurities at grain boundaries. For instance, annealing of copper wire at 1000°C in air can cause intercrystalline oxidation over the whole cross-section, so that the wire becomes very brittle and breaks at the first bend.

Secondary recrystallization, which gives very coarse grain and causes inequigranularity, lowers the ductility indices.

In the region of nearly critical deformations, the relative elongation of annealed metals and alloys first decrease with increasing degree of preliminary deformation (prior to annealing), drops to a minimum at the critical deformation, and finally increases (Fig. 54). The loss in ductility on increasing the degree of deformation (before the critical value is reached) is due to an increasing effect of work-hardening, which remains after the annealing. In the post-critical region, the ductility increases owing to the formation of finer grains upon recrystallization annealing (see Fig. 41). The minimum of ductility at the critical deformation is due, firstly, to the large grain and, secondly, to the maximum degree of work-hardening. In the post-critical region, work-hardening is eliminated through primary recrystallization, whereas at the critical deformation it partially remains upon annealing (which has been verified directly by hardness measurements), since grain coarsening is mainly due to the growth of some work-hardened grains at the expense of others, rather than to full replacement of deformed grains with new recrystallized grains.

A different pattern of ductility variation on recrystallization annealing is found in refractory metals of group VIA (Cr, Mo, and W). These metals are known to be brittle below a definite temperature which depends on their purity, structure, deformation rate in tests, and other factors. The plastic-to-brittle transition is

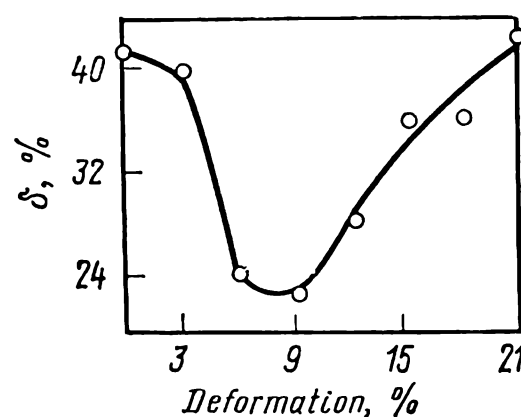


Fig. 54. Effect of preliminary deformation at 20° C on relative elongation in 99.7-% pure aluminium annealed at 450° C (after A. Yu. Zolotarevskaya, V. Z. Zakharov, I. I. Novikov and I. L. Rogelberg)

attributed to the fact that atoms of interstitial impurities (carbon, oxygen and nitrogen), which are present in the solid solution, segregate at intercrystalline boundaries and also that carbides, oxides and nitrides precipitate here (in commercially pure metals of group VIA, the content of interstitial impurities always exceeds their solubility in the solid state, which is very low). The segregation of impurities and precipitation of excess phases are most marked at high-angle boundaries which form on primary recrystallization. This initiates brittle cracks which develop along boun-

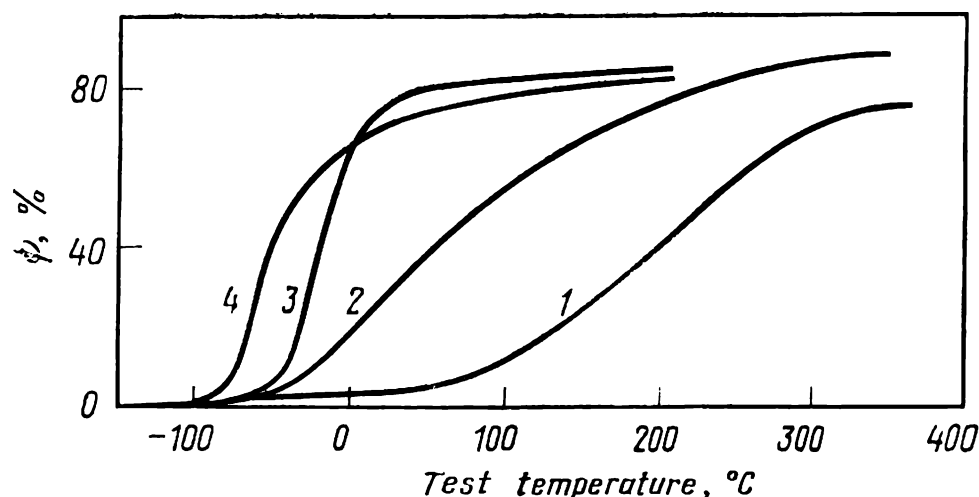


Fig. 55. Effect of temperature on relative contraction of molybdenum (1) in recrystallized state, (2) after cold deformation, 25%; (3) ditto, 68%, and (4) after prerecrystallization annealing of cold-deformed metal at 870°C for 30 min (after A. G. Imgram)

daries or inside grains. For that matter, recrystallization annealing can drastically (by 200-300 degrees C) raise the temperature limit of cold brittleness of chromium, molybdenum and tungsten above the value they have in deformed state (Fig. 55). These metals are an unusual and important example of how strain hardening can increase ductility (curves 2 and 3), whereas recrystallization, which usually removes the effect of strain hardening, can produce strong embrittlement (curve 1). In that respect, low-angle boundaries behave in a different way: polygonization usually lowers the temperature limit of brittleness of the metals considered (curve 4 in Fig. 55).

### Strengthening on Prerecrystallization Annealing

It has been established long ago that in low-temperature annealing of some metals and alloys their hardness, ultimate strength and especially yield and elastic limits increase appreciably before the onset of recrystallization (see the dotted line in Fig. 50). Each of these materials has its own optimum annealing temperature at which the strengthening effect is at the maximum (Table 5).

The strengthening in the temperature region of recovery contradicts, on the face of it, the concept of recovery proper, which implies partial removal of work-hardening and restoration of the properties the metal had before deformation. Attempts were made in that connection to explain the strengthening effect on prerecrystallization annealing by some errors in experiments. However, the absolute gain in elastic limit may in some cases exceed 10-30 kgf/mm<sup>2</sup>, which not only is far beyond any experimental error, but also makes it possible to use low-temperature annealing upon cold deformation for increasing additionally the elastic limit of springs and membranes (by 100-170 per cent, see Table 5).

**Table 5. Maximum Gain in Elastic Limit ( $\Delta\sigma/\sigma$ ) upon Prerecrystallization Annealing for  $\frac{1}{2}$  h at the Optimum Temperature ( $t_{opt}$ ) (after E. N. Spektor, S. S. Gorelik, and A. G. Rachstadt)**

Material	$\varepsilon^*$ , %	$\frac{\Delta\sigma}{\sigma} \cdot 100$ , %	$t_{opt}$ , °C	$t_r^s$ , °C
Cu (99.98-% pure)	75	10	150	200
Cu + 7% Al	7	35	280	450
	90	170	280	350
Cu + 32% Zn	60	100	200	250
Ni (99.99% pure)	60	40	200	350
Ni + 20% Cr	10	40	400	800
	65	170	400	600
Nb (electron-beam melting, < 0.01% C, N, O)	90	40	950	1100
Nb (0.02% C; 0.03% O; 0.02% N)	80	120	1000	1200

\*  $\varepsilon$  = reduction in cold rolling before annealing.

The effect of strengthening on prerecrystallization annealing is inherent in most copper and nickel alloys in which it has been studied in detail. The degree of strengthening depends on the composition of solid solution. In many alloys this effect increases on increasing the degree of alloying of the solid solution (Fig. 56). The effect of strengthening on annealing usually increases at larger degrees of cold deformation (Table 5), though an inverse relationship is sometimes observed. Strengthening is sometimes preceded with slight 'normal' softening on recovery (Fig. 56).

Of interest is the fact that strengthening on low-temperature annealing is often intrinsically reversible: cold deformation on annealing causes softening, the subsequent annealing again strengthens the metal, and so on. Softening can take place at low deformation: only 1-5 per cent. For instance; the elastic limit of cold-

rolled pure nickel is  $\sigma_{0.005} = 40$  kgf/mm<sup>2</sup>, annealing at 200 °C raises it to 48 kgf/mm<sup>2</sup>, while further cold rolling with 3-per cent reduction can again lower it to the initial level, i.e. 40 kgf/mm<sup>2</sup>. The phenomenon of softening on repeated cold deformation is in itself rather peculiar.

The nature of strengthening upon prerecrystallization annealing is different in various alloys. The most common cause of strengthening is pinning of mobile dislocations in the initial cold-

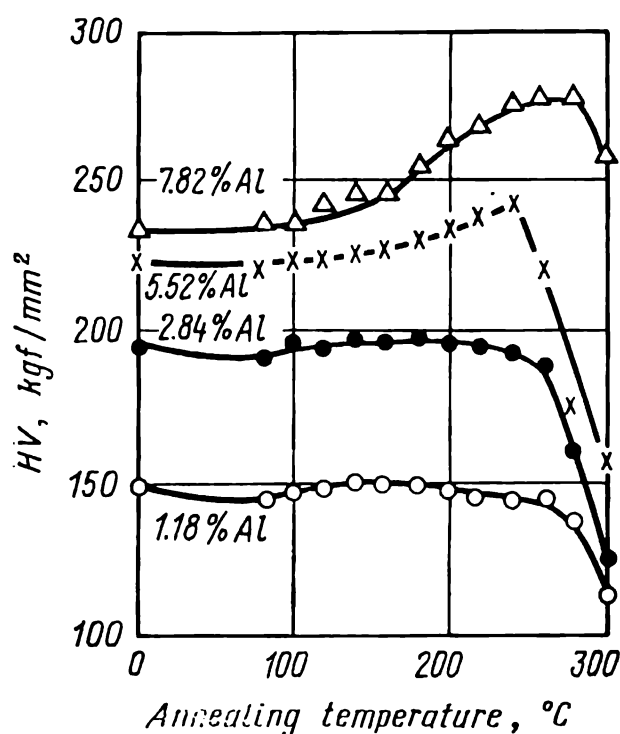


Fig. 56. Effect of annealing temperature on hardness of cold-rolled aluminium bronzes (after I. L. Rogelberg)

deformed metal and in the dislocation arrays formed through polygonization during annealing. A lower strengthening effect in prerecrystallization annealing of high-purity metals and a higher effect at higher concentrations of impurities and some alloying elements are indicative of the fact that dislocations are pinned by atoms of impurities and alloying elements during annealing.

The strong rise in the elastic limit on prerecrystallization annealing of f.c.c. solid solutions based on copper or nickel (sometimes 2-2.5 times or even more, see Table 5) may be attributed to the formation of Suzuki atmospheres at stacking faults of extended dislocations and the formation of short-

range order regions in the solution. The effect of softening on cold deformation after prerecrystallization annealing may be explained by destruction of these regions and detachment of dislocations from Suzuki atmospheres.

In b.c.c. metals, such as niobium (see Table 5), the growth of the elastic limit on prerecrystallization annealing can be most probably explained by pinning of dislocations by Cottrell atmospheres which have formed from interstitial impurity atoms.

In metals and single-phase alloys of commercial purity, a probable cause of strengthening on prerecrystallization annealing is age-hardening (precipitation hardening) due to the precipitation of disperse particles of impurity phases at dislocations.

The elastic limit increases on prerecrystallization annealing much more appreciably than do the hardness and ultimate strength. This is quite understandable, since the elastic limit,

which characterizes the resistance of a material to low plastic deformations, can be strongly affected by the initial (prior to mechanical tests) dislocation structure, which varies only slightly in the course of tests. On the other hand, in determinations of hardness and ultimate strength, which characterize the resistance of material to high plastic deformations, the initial dislocation structure can change appreciably during the mechanical tests proper: dislocations increase in density and rearrange to form a new dislocation structure. For that reason pinning of dislocations in the initial structure upon prerecrystallization annealing affects more the elastic limit and less the ultimate strength.

It is now generally accepted that the rise in elastic limit on prerecrystallization annealing is a rather common phenomenon inherent in metals and alloys of any type of lattice, either of common or high purity.

On the whole, the dependence of strength properties on the temperature of annealing, shown by dotted line in Fig. 50, is one of the most typical and most often encountered phenomena in metals.

### Changes of Physical Properties on Annealing

Electric resistivity changes on annealing follow an intricate pattern. In many deformed metals and disordered solid solutions, the electric resistivity restores to an appreciable extent upon prerecrystallization annealing. Primary recrystallization completely eliminates the increase in electric resistivity induced by deformation.

It is commonly assumed that an increased temperature of recrystallization annealing lowers the electric resistivity (provided that this has been raised through work-hardening). This view, however, contradicts the available reference data. In copper, nickel, silver, aluminium, iron and many alloys, as the temperature of recrystallization annealing increases, the electric resistivity, upon lowering in the common way, then begins to rise anomalously due to reasons which are not yet established (see Fig. 53).

If the electric resistivity lowers on cold deformation, as in Chromel, Alumel and German silver (see Fig. 14), annealing should naturally increase it (Fig. 57), since this restores the  $K$ -state that has been disturbed through the preliminary deformation.

Annealing lowers the density of dislocations and thus facilitates the displacement of domain boundaries and the processes of magnetization and demagnetization, and therefore, should increase the magnetic permeability and lower the coercive force and remagnetization losses.

Strain-relief annealing restores the thermo-e.m.f. to its initial value.

It should be noted in conclusion that various properties begin to change intensively at different temperatures of annealing. For instance, the electric resistivity begins to drop in annealing be-

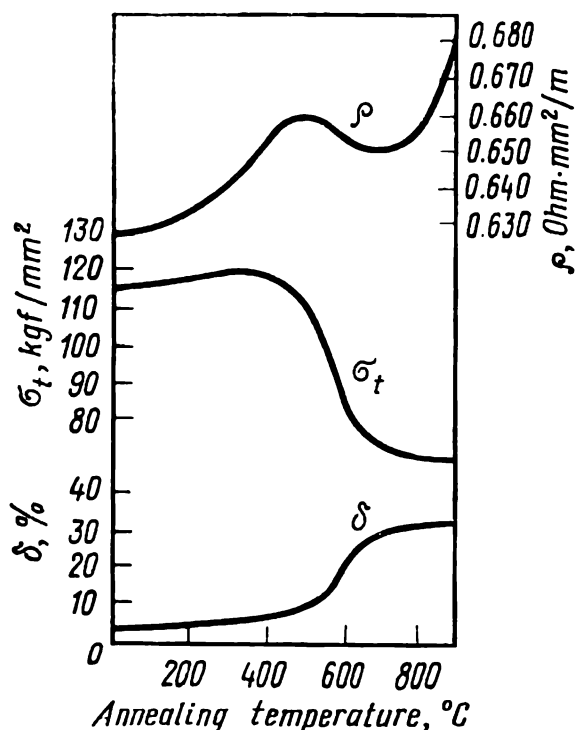


Fig. 57. Effect of annealing temperature on electric resistivity and mechanical properties of Chromel (after I. Ya. Berkovsky and A. G. Kolokolova)

fore the ultimate strength has lowered appreciably (Fig. 53), since it can diminish appreciably owing to a lower concentration of point defects caused by recovery, while an intensive drop in ultimate strength becomes only possible when the density of dislocations lowers appreciably.

#### 1.2.10. ANISOTROPY OF PROPERTIES IN ANNEALED METAL

In recrystallized metal with chaotically oriented crystallites, the vector properties of individual single crystals are statistically averaged in all possible directions in the macrovolume of the polycrystal. With recrystallization texture formed in annealed metal, its properties become anisotropic, the effect of anisotropy being the

greater, the more perfect is the texture. Anisotropy is most often troublesome, though in certain products it is desirable to enhance some or other property in a definite direction. Production of metals with isotropic properties or, on the contrary, with markedly anisotropic properties is an issue of great scientific and technical significance.

#### Earing

Recrystallization texture is most detrimental in sheets or strips intended for deep drawing. Cold-rolled sheets and strips are annealed before stamping. If a sufficiently perfect recrystallization texture has formed on annealing, the metal in sheets becomes anisotropic. This can be easily verified by cutting plane tensile specimens from a sheet at different angles to the direction of rolling (Fig. 58). The anisotropy of mechanical properties is especially marked in annealed f.c.c. metals and alloys possessing the  $\{001\}$   $\langle 001 \rangle$  cube texture, since this texture is intrinsically very perfect. For instance, the relative elongation of a copper strip hav-

ing the perfect cube texture is only 16 per cent along and across the direction of rolling and as high as 73 per cent at an angle of

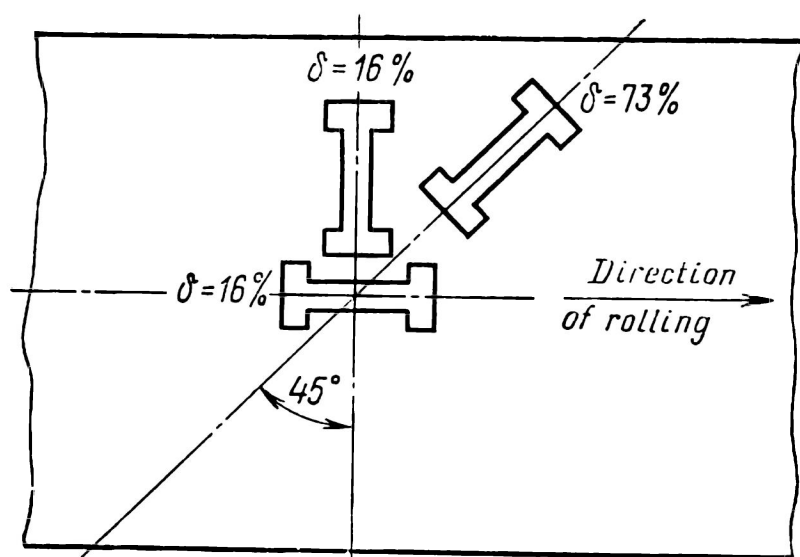


Fig. 58. Diagram of cutting tensile specimens from annealed copper sheet to determine the anisotropy of mechanical properties of metal

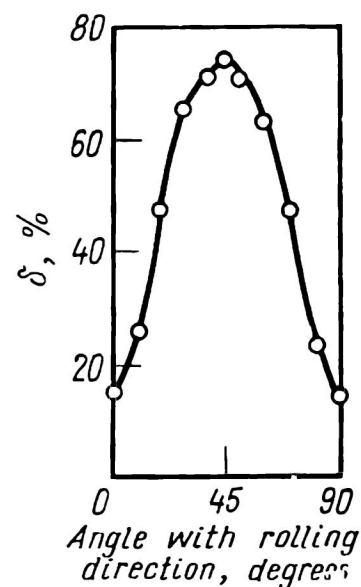


Fig. 59. Anisotropy of relative elongation in annealed copper strip possessing cubic texture (after W. M. Baldwin)

45°. This large difference is quite understandable if we recall that tension of single crystals of copper gives a low relative elongation in the direction perpendicular to the {100} cube face and a high elongation, perpendicular to the {110} face of rhombic dodecahedron. With a cube texture, the axis of a tensile specimen cut along or across the direction of rolling turns to be perpendicular to the {100} plane, while the axis of a tensile specimen cut at an angle of 45° is perpendicular to the {110} plane.

Anisotropy of properties can be expressed graphically in coordinates: property-angle to the direction of rolling (Fig. 59).

A sleeve stamped from an anisotropic sheet has wavy edges, or 'ears' (Fig. 60). The height of 'ears' may be substantial, for instance, 15-25 per cent of the height of an aluminium can. The phenomenon of 'earing' results from

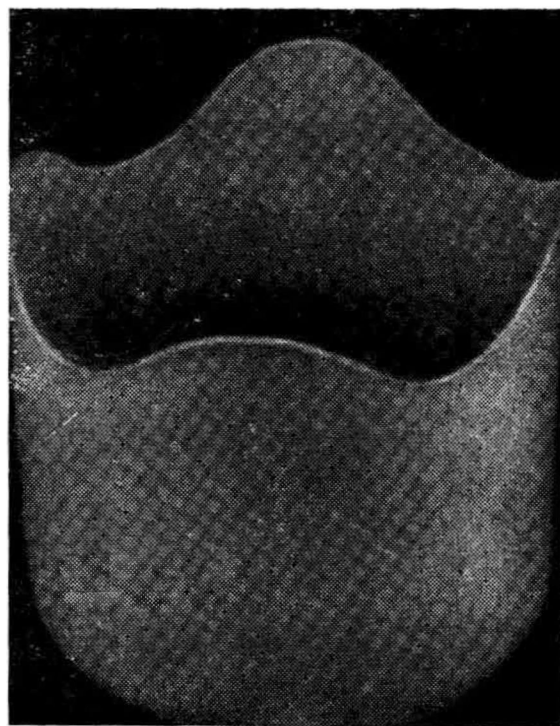


Fig. 60. Earing of a stamped aluminium sleeve

a different degree of drawing of the metal in different directions and accordingly, from different thinning of the walls. A drawn sleeve may have four or six symmetrical 'ears' at the edge, depending on the type of texture. Earing is a serious problem in mass production of stamped sleeves; wavy edges must be cut off and returned to remelting, which increases the expenditure of rolled blanks and production cost.

The size of 'ears' is the greater, the more grains have the same crystal orientation. It is then understandable why the size of 'ears'

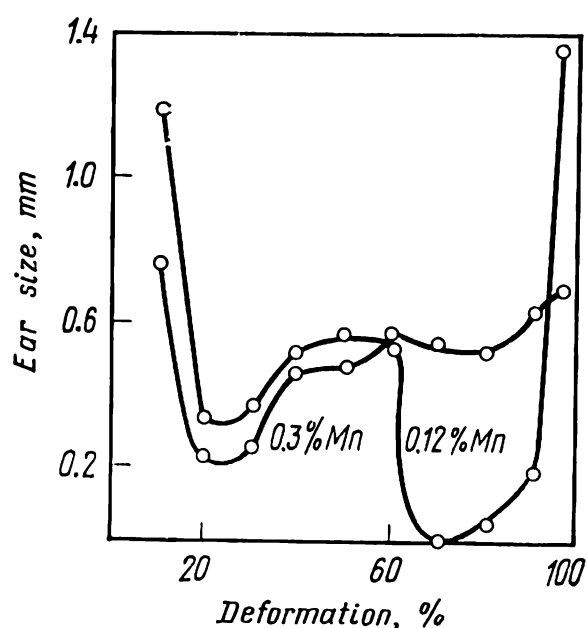


Fig. 61. Effect of reduction in cold rolling of Grade 80/20 cupronickel (with 0.12 or 0.3 per cent Mn) on the size of ears in sleeves stamped from it. The metal after rolling was annealed at 700°C for 2 h (after D. I. Lainer)

depends on the conditions of heat treatment. Earing can be fully prevented by properly selecting the conditions of rolling and annealing. For instance, a method often recommended for making isotropic copper and brass is to use a low reduction in the last rolling operation and a low temperature in the final annealing.

Recommendations of various researchers on combatting earing are sometimes contradictory. D. I. Lainer has carried out systematic studies into the effect of impurities and additions on recrystallization texture and anisotropy of mechanical properties in nickel, copper, aluminium and cupronickel, which have enabled him to conclude that the composition of metal is one of the principal factors of earing. The optimum conditions of rolling and annealing to produce 'earless' sleeves can change appreciably

even at slight and often disregarded changes in the composition. For instance, as follows from Fig. 61, the least size of 'ears' in cupronickel with 0.3 per cent Mn is obtained on rolling with 20-30-% reduction, whereas for cupronickel with 0.12 per cent Mn the optimum total reduction is 70-80 per cent. Manganese-free cupronickel can be drawn into sleeves without the formation of 'ears' at any deformation up to 90 per cent and any temperature of annealing up to 900°C. As is known, manganese is used as deoxidant in smelting of cupronickel. Replacing manganese with silicon for deoxidation of cupronickel thus can fully prevent the earing effect in drawn articles.

In some cases, well proportioned small additions can be used to prevent earing or anisotropy of properties in the general. For instance, addition of 0.05 per cent Si to copper Grade B4 lowers the rate of development of cubic texture in annealing and thus strongly diminishes the anisotropy of relative elongation.

With a properly selected composition of a metal, it can be deep-drawn without the earing effect within a wide range of deformations and annealing temperatures. This selection of the composition and heat treatment is still being made purely empirically.



### Textured Transformer Steel

An important example of industrial materials in which recrystallization texture is desirable is transformer steel. Steel sheets in a transformer core are continuously remagnetized. Nearly 0.4 per cent of the total electric energy is lost for heating transformer cores.

A high efficiency of transformers can be ensured by minimizing the remagnetization loss along the direction of the magnetic circuit.

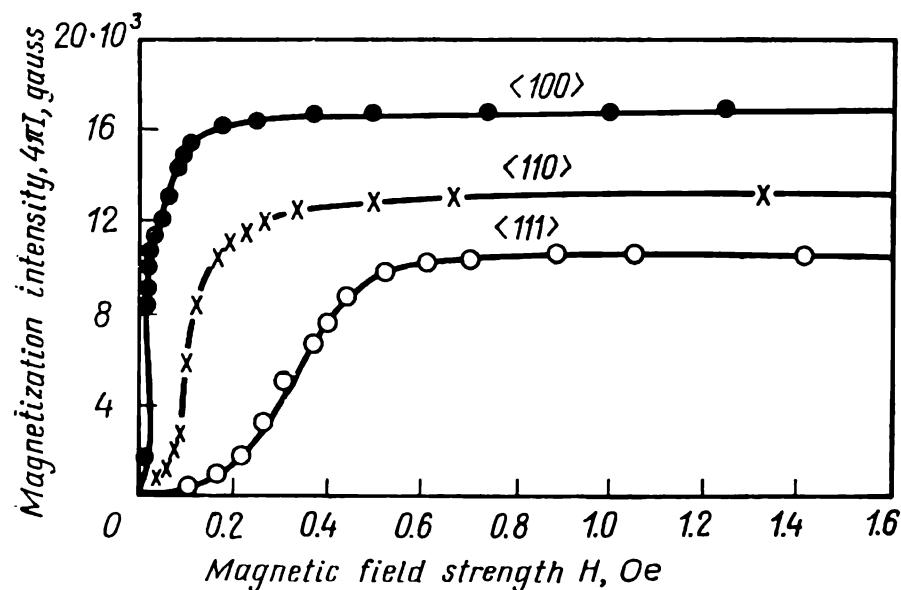


Fig. 62. Magnetization curves for different crystal orientations of a single crystal of transformer steel (after H. J. Williams)

Transformer steel should contain 2.8-3.5 per cent Si and as little carbon as practicable. The magnetic properties of a single crystal of iron silicide are strongly anisotropic. Like in pure iron, the  $\langle 100 \rangle$  cube edge in it is the direction of the easiest magnetization, while the spatial  $\langle 111 \rangle$  cube diagonal is the direction along which magnetization is impeded at most (Fig. 62). In a single crystal of siliceous ferrite the maximum magnetic permeability  $\mu_{\max}$  along the  $\langle 100 \rangle$  direction is 30 times that along the  $\langle 111 \rangle$  direction.

Beginning from the middle of 1930's, a lot of research has been done on manufacturing transformer steels with a marked recrystallization texture which ensures the highest magnetic permeability in the direction of rolling and the lowest hysteresis loss, with the magnetic properties in other directions being largely suppressed. A magnetic circuit is made of transformer steel in such a way that the direction of sheet rolling coincides with the direction of magnetic flux.

At present, cold-rolled transformer steel with the  $\{110\} \langle 100 \rangle$  rib texture, which is called the *Goss texture*, is produced in ever increasing quantities. In the USSR, the respective steel grades are Э310, Э320, etc.

In a rib texture, the  $\langle 100 \rangle$  cube edge, i.e. the direction of the easiest magnetization, is parallel with the direction of rolling, while the  $\{110\}$  face of the rhombic dodecahedron is parallel with the rolling plane (Fig. 63). The direction of the hardest magneti-

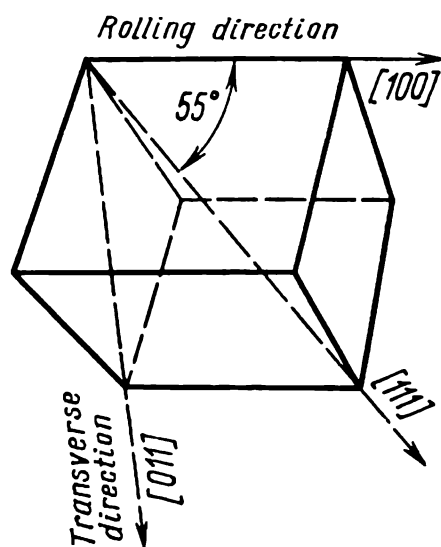


Fig. 63. Orientation of crystal axes relative to the direction of rolling in Goss-texture transformer steel (after R. M. Bozorth)

zation,  $\langle 111 \rangle$ , is at an angle of  $54.7^\circ$  to the rolling direction, and the direction of intermediate magnetization,  $\langle 110 \rangle$ , is across the rolling direction.

Industrial production of sheets 0.2-0.5 mm thick with a rib texture is a complicated manufacturing process, which includes hot rolling, two cold rolling operations with intermediate annealing, annealing (at approximately  $800^\circ\text{C}$ ) after the second cold rolling operation, and finally, long high-temperature annealing (at roughly  $1100^\circ\text{C}$ ) in dry hydrogen.

The first annealing stage induces primary recrystallization which gives a texture having  $\{110\} \langle 110 \rangle$  as one of its components. The recrystallized matrix is stabilized by disperse particles of silicon nitride, manganese sulphide and other compounds formed from the impurities. During the final high-temperature annealing, secondary recrystallization develops in the stabilized matrix, with the preferable growth of grains having the  $\{110\} \langle 100 \rangle$  orientation. In a very pure alloy of iron and silicon, the recrystallized matrix is not stabilized and thus no rib texture is formed.

Cold-rolled transformer steels with rib texture gradually replace isotropic hot-rolled steels. Their use makes it possible to lower the mass and dimensions of powerful transformers by 20-25 per cent and reduce energy losses in national economy.

Still better magnetic properties are inherent in magnetic circuits made of steel with the  $\{100\} \langle 001 \rangle$  cube texture where recrystallized grains are arranged with their  $\{100\}$  planes parallel to the rolling plane and their  $\langle 001 \rangle$  directions, parallel to or across the direction of rolling. As distinct from rib-texture steel, the direction of easy magnetization in such steel lies in the rolling plane along or across the rolled strip. Cube texture in transformer steel can be produced in strips nearly 0.04 mm thick, i.e. an order of magnitude thinner than with the rib texture. The cube texture

forms on secondary recrystallization: in the matrix stabilized through the 'thickness effect' (see 1.2.5), grains which pass out onto the rolling surface grow preferably, with their {100} faces having the least surface energy (in the presence of oxygen in furnace atmosphere).

#### 1.2.11. SELECTING CONDITIONS OF PRERECRYSTALLIZATION AND RECRYSTALLIZATION ANNEALING

The principal parameters of annealing of work-hardened metals and alloys are temperature and time. They determine the nature and extent of structural changes on annealing, and also the properties the metal or alloy will have upon annealing. In some cases, which will be discussed below, the rate of heating to the temperature of annealing and the rate of cooling from that temperature may also be essential.

For each metal or alloy, the conditions of annealing are selected considering the structure and properties required of that metal, its specific behaviour in annealing, and the initial deformed state. Proper selection of the temperature and time of annealing is facilitated by using diagrams of the type shown in Figs. 47-53.

#### Prerecrystallization Annealing

Prerecrystallization annealing can have either softening or strengthening effect on the metal.

*Prerecrystallization softening* is used to increase the ductility of a metal and retain partially the strain-hardening effect. It is resorted to when full softening provided by recrystallization annealing is unnecessary or undesirable. Prerecrystallization softening is most often employed as the final operation which forms the desired combination of strength and ductility in products and less frequently, as an intermediate operation to eliminate partially strain-hardening between two operations of plastic working. Prerecrystallization softening is, for instance, used as the final operation in mass manufacture of aluminium sheets grades АД, АД1, etc., the temperature of softening being selected within the range of 150-300 °C, depending on the content of impurities in aluminium. It is widely used with magnaliums to ensure subsequent operations of bending, flanging, etc. For instance, the ultimate strength and relative elongation of АМr2 alloy are respectively  $\sigma_t = 30 \text{ kgf/mm}^2$  and  $\delta = 7$  per cent in strain-hardened sheets and 27 kgf/mm<sup>2</sup> and 11 per cent upon annealing at 150-180 °C (in recrystallized state,  $\sigma_t = 20 \text{ kgf/mm}^2$  and  $\delta = 18$  per cent). As has been noted in 1.2.9, aluminium alloys are prone to polygonization, which ensures softening upon prerecrystallization annealing. Alu-

minium alloys grades AMr1 and AMr2, when annealed in this way at 150-180°C, show an elevated strength (as compared with recrystallized state) and a ductility sufficient to make subsequent operations, including plastic deformation. Since aluminium and magnalium sheets make up a large percentage of the total production of light-metal works, it is then clear that prerecrystallization softening is used widely and effectively in the industry.

For refractory metals of group VIA (Mo and W), prerecrystallization annealing is the sole method of softening upon plastic working, since these metals become very brittle upon recrystallization. Prerecrystallization annealing of these metals and their alloys can lower the temperature of plastic-to-brittle transition (see Fig. 55), as well as eliminate partially strain-hardening.

Apart from the aim of increasing the ductility, prerecrystallization annealing is often used to reduce residual stresses, stabilize the properties and increase the corrosion resistance of metal.

When selecting the conditions of prerecrystallization annealing, knowledge of  $t_r^s$  (at the given degree of deformation) is required. The closer the temperature selected to  $t_r^s$ , the deeper will be the softening effect.

*Prerecrystallization strengthening* is used to increase the elastic properties of springs and membranes. The optimum temperature (see 1.2.9) is chosen experimentally.

Prerecrystallization annealing of cold-worked copper alloys (aluminium and chromium bronzes and copper-nickel alloys) can sometimes result in what is called fire brittleness, owing to the formation of pores at grain boundaries. These pores appear on annealing under the action of residual stresses and, similar to creep pores, grow due to the condensation of vacancies. To prevent fire brittleness, the time of annealing within the corresponding range of critical temperatures should be as short as possible.

### Recrystallization Annealing

A distinction may be made between complete, incomplete and texturizing recrystallization annealing.

*Complete recrystallization annealing*, usually called simply recrystallization annealing, is one of the most widely used operations of heat treatment.

Recrystallization annealing is employed in the industry as the starting operation before cold plastic working (in order to make the material more ductile), as an intermediate operation between two operations of cold working (to eliminate strain hardening), or as the final operation of heat treatment (to impart the required properties to products). Recrystallization annealing of steels, non-ferrous metals and alloys is made upon cold rolling of sheets,

strips and foil, cold drawing of tubes, rods and wire, cold stamping, and other types of cold working as also after low-temperature hot working (in the latter case, the metal is strain-hardened appreciably, though less strongly than in cold working).

In certain cases, recrystallization annealing is done immediately after hot plastic working. For instance, hot-rolled rolls of some aluminium alloys are annealed before cold rolling to eliminate fully work hardening, since the slow process of recrystallization at the end of hot working, when sheets were chilled down to 280-330°C, has had no time to come to the end and eliminate work hardening.

In non-ferrous metallurgy, recrystallization annealing as a separate operation of heat treatment is used much more widely than in steelmaking. This can be explained by the fact that cold plastic working is much more popular with non-ferrous metals and alloys than with steels.

The temperature of complete recrystallization annealing should be above  $t_r^f$ . If a metal or alloy has critical points in the solid state, the temperature of recrystallization annealing should be below the critical point, for instance, below  $A_{c1}$  for steels or below the temperature of polymorphic transformation for titanium alloys. Titanium alloys form a very coarse grain when heated above the point of  $\alpha + \beta \rightarrow \beta$ -transformation.

Approximate temperatures (°C) for complete recrystallization annealing of various materials are as follows:

Carbon steel . . . . .	650-710
Copper . . . . .	500-700
Brasses and bronzes . . . . .	600-700
Copper-nickel alloys . . . . .	700-850
Nickel . . . . .	700-800
Nickel alloys . . . . .	800-1150
Titanium . . . . .	670-690
Aluminium . . . . .	300-500
Aluminium alloys . . . . .	350-430
Magnesium alloys . . . . .	300-400

The holding time is usually 10-60 minutes.

Secondary processes should sometimes be considered when selecting the time of holding. For instance, the principal process in annealing of cold-worked steels below  $A_{c1}$  is the recrystallization of ferrite, but this may be accompanied with cementite spheroidizing. The time needed for complete recrystallization does not exceed 60 minutes, but should be increased up to a few hours if it is required to transform the cementite into granular form (this form is most favourable for subsequent cold working).

The optimum conditions for annealing can be selected by using temperature curves of properties, such as those shown in Figs. 52

and 53. For instance, 1-hour annealing at 500-700 °C may be recommended for copper to restore its ductility (see Fig. 53). The upper temperature limit of the annealing is taken below the temperature of overheating (roughly 800 °C) and the lower limit, slightly above  $t_r^f$  (near 400 °C), since individual portions of an article may be deformed non-uniformly at a definite 'geometrical' degree of deformation, so that in less deformed portions recrystallization comes to its end at higher temperatures.

When selecting the conditions of annealing, use may be made of recrystallization diagrams (of the type shown in Fig. 46) in order to avoid coarse grain and inequigranularity in the metal. When doing so, one should be fully aware of the limitations linked with the use of recrystallization diagrams.

Mechanical properties alone are not always fully indicative of the quality of annealed metal. Another criterion is sometimes the size of recrystallized grains. For instance, coarse grain can cause "orange peel", i.e. typical rough pattern on the surface of articles upon deep drawing, tensioning, etc.

In a coarse-grained material, the inequality of plastic deformation in various grains and even in a single grain is expressed especially markedly. For instance, the relative elongation of various grains in a coarse-grained aluminium specimen can differ by a factor of 10. This unequal deformation of large grains then appears as "orange peel" on the free surface of product. Fine grains cannot cause "orange peel".

Inequigranularity can cause strongly non-uniform deformations and even fracture in deep drawing.

The size of grains in sheets and strips of single-phase copper alloys, when intended for deep drawing, should not exceed 0.05 mm. Grain size in  $\alpha$ -brasses and bronzes is checked by using standard structural charts.

Apart from the requirements to the properties and grain size, selection of annealing conditions should sometimes take into consideration the allowable degree of anisotropy, which is linked with recrystallization texture (see 1.2.10 on the phenomenon of earing).

The rate of heating to the temperature of annealing is most often insignificant. In some cases quick heating may be desired. For instance, slow heating of cold-deformed semiproducts of aluminium alloy Grade AM $\pi$  can produce very coarse grain, which results in a rough surface on straightening and lowers the relative elongation. With slow heating, large grains can also grow due to the fact that primary recrystallization begins at relatively low temperatures and starts in a small number of centres. With fast heating to a high temperature (for instance, to 500 °C in saltpetre

bath), primary recrystallization proceeds intensively at once from many nuclei and produces fine grain.

The rate of cooling from the temperature of recrystallization annealing has no effect on the properties of metals and alloys. Copper-alloy semiproducts are sometimes cooled in water for better removal of scale. The rate of cooling from the temperature of recrystallization annealing should sometimes be specified for alloys capable of strengthening on quenching or age-hardening. For instance, annealing of heat-hardenable aluminium alloy Grade B95 upon cold working may result in a secondary process — partial quenching with subsequent ageing — taking place in the metal along with the main process of recrystallization, which produces only an insufficient softening effect in the final result. For that reason B95 alloy must be cooled slowly in the furnace from the temperature of recrystallization annealing (380-430 °C) down to 150 °C (at a rate of not more than 30 °C/h).

*Incomplete recrystallization annealing* is carried out at temperatures above  $t_r^s$  but below  $t_r^f$  so as to eliminate partially the strain-hardening effect. It makes possible, for instance, to produce semi-workhardened sheets from thermally unhardenable aluminium alloys. The structure thus formed is partially recrystallized and partially polygonized.

*Texturizing annealing* is employed for obtaining the desirable anisotropy of properties in transformer steels, iron-nickel alloys with a constant magnetic permeability (of the Isoperm type) and some other texturized materials. The selection of optimum conditions for annealing is a highly complicated issue in this case (see 1.2.10).

#### LITERATURE

Gorelik S. S., Recrystallization in Metals and Alloys (*Rekristallizatsiya metallov i splavov*). Moscow, Metallurgiya Publishers, 1978, 565 pp., ill.

Physical Metallurgy. Ed. by R. W. Cahn. Amsterdam, North-Holland Publishing Co., 1965.

Honeycombe R. W. K., The Plastic Deformation of Metals. London, Edward Arnold, 1968.

Shewmon P. G., Transformations in Metals. New York, McGraw-Hill, 1969.

Martin J. W., Doherty R. D., Stability of Microstructure in Metallic Systems. Cambridge, Cambridge University Press, 1976.

### 1.3. STRESS-RELIEF ANNEALING

Plastic working, casting, welding, heat treatment, grinding, machining, electrodepositing of metals and other technological processes can produce internal stresses which are mutually balanced in articles without any external load being applied. In

most cases internal stresses remain fully or partially in the metal upon processing and thus are called residual stresses.

This chapter will consider only macrostresses that are balanced in the volume of a whole article or of its macroportions. Such stresses are also called zonal, or first-order, stresses.

### 1.3.1. APPEARANCE AND ROLE OF RESIDUAL STRESSES

Macro stresses can appear owing to unequal deformation or different change of the specific volume in various portions of a body.

The appearance of residual stresses due to unequal deformation in various portions of a body may be explained by a simple example as follows (Fig. 64). Suppose a strip of metal being rolled

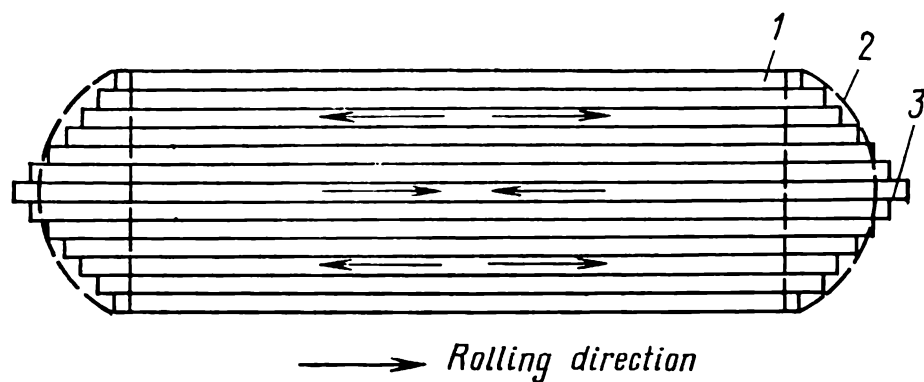


Fig. 64. Appearance of residual stresses in a metal strip due to different reduction of central and peripheral layers when rolled in barrel-shaped rolls 1—strip before rolling; 2—after rolling; 3—the central layer upon free drawing (without interaction with adjacent layers)

in barrel-shaped rolls whose diameter in the middle is appreciably greater than at the ends. The central portions of the strip will then be rolled with a greater reduction than the extreme ones. If the strip were composed, say, glued together, of a number of rods, then each of the rods would be rolled with a different reduction and the central rods would be drawn more than those at the edges of the strip. Actually, the strip is a monolithic body in which central and peripheral layers cannot be drawn isolatedly to a different length. The central layers, which are tensioned more, will be restrained by the edge layers and thus turn to be understretched. In other words, compressive internal stresses will form in the central layers. On the contrary, the extreme layers will be stretched through the action of the central layers by a greater extent than that corresponding to their reduction. Thus, tensile stresses will form in them (Fig. 64). Compressive and tensile internal stresses are mutually balanced in the strip and remain in the metal upon finishing the rolling process.

The specific volume of metal may change through thermal compression or expansion, crystallization of the melt, phase trans-



formations in the solid state or variations of the composition of surface layers. If thermal expansion and compression, melt crystallization and solid-state phase transformations occurred simultaneously and to the same extent throughout the whole volume of metal, no internal stresses would appear. But heating or cooling always forms a temperature gradient over the cross-section of a body, so that the above variations in the specific volume are different in various points of the metal, resulting in the appearance of internal stresses.

A distinction is made between *thermal* and *structural internal stresses*; the former appear owing to thermal compression or expansion and the latter, owing to phase transformations in the solid state with a temperature gradient present in the body. Internal stresses can appear practically on any type of treatment. A single processing operation may give birth to different residual stresses: thermal, structural or stresses due to non-uniform plastic deformation. For instance, hot plastic working may cause stresses due to non-uniform plastic deformation, and additionally thermal stresses or structural stresses, if the hot-formed alloy is cooled quickly and undergoes a phase transformation. Both thermal and structural stresses may form on casting, welding and quenching. Residual stresses of different origin are algebraically added together and often form complicated stress patterns.

According to the technological process that causes them, residual stresses may be classed as *casting*, *welding*, *quenching*, *grinding*, etc.

Residual stresses can affect the behaviour of articles on treatment, operation and even during storage.

Residual stresses are algebraically summed up with the external working stresses and thus can either enhance or weaken the latter. As a general rule, tensile residual stresses are most dangerous, since, when being summed up with external tensile stresses, they can cause fracture even at low external stresses.

Tensile stresses are especially dangerous in three-dimensional tension. As is well known, three-dimensional tension produces the most 'rigid' type of stressed state, since the shear stresses which cause plastic flow are extremely small or equal to zero, because of which brittle fracture becomes very probable. Residual stresses are also very dangerous in articles made of low-plastic alloys or of alloys which embrittle at lower temperatures.

With high residual stresses, fracture can often occur even from a low external load (especially if this is of the impact type). For instance, cracks in steel castings can form during cleaning with pneumatic hammers or even from draught in winter time (since thermal stresses are added to residual stresses). Large ingots produced of low-plastic aluminium alloys by semi-continuous casting can break into pieces after a certain while upon being cast owing to occasional shaking or impact; the elastic energy liberated on the breakage is

so large that a piece weighing a few hundred kilograms can detach from the ingot with a loud crash and fly a few metres away.

Residual tensile stresses in welded structures can sometimes cause serious damage. Catastrophic failures of welded bridges and all-welded ships are often attributed to the appearance of large, nearly destructive, residual stresses in them. They were the actual cause of failure in cases where all-welded ships broke from a seemingly low external load applied, such as a stroke with a crow when removing ice from the deck. The problem of residual stresses in welded structures has attracted great attention after a number of all-welded ships broke into halves during cruising or anchorage.

Residual tensile stresses in surface layers are especially dangerous in articles subjected to alternating stresses, since such stresses promote fatigue fracture (recall that fatigue cracks initiate in the surface of articles).

Residual stresses can also be detrimental by increasing the total chemical activity of a metal. In this respect, tensile residual stresses are especially dangerous, since they promote intersrystalline corrosion (season cracking in brasses).

In a piece of metal with residual stresses there are regions of elastic deformations of different sign. The elastic, i.e. reversible, removal of macrostresses is impeded by interatomic forces which combine differently strained portions of metal into a monolithic solid. If an article is cut to pieces or its surface layer is cut off (or etched off), then elastic removal of macrostresses becomes possible. For instance, if a surface layer with compressive residual stresses is cut off or etched, this will eliminate the retaining effect on the inner portion of metal and the latter will contract elastically under the action of the tensile residual stresses existing in it. Measuring the elastic deformations appearing on cutting a specimen or removing (etching off) its surface layer underlies the mechanical methods for determining the magnitude and sign of residual stresses (stresses are calculated in terms of strain).

Residual stresses may cause distortion (warping etc.) of the shape and dimensional changes in articles during treatment, operation and storage.

Warping is most often encountered in machining, since removal of a metal layer disturbs the equilibrium of residual stresses. For instance, if a layer of metal is cut off at one edge of the strip shown in Fig. 64, this will bend in the plane of the figure, since the tensile and compressive stresses existing in it will be brought out of equilibrium.

Spontaneous changes in the dimensions and shape of articles (warping) during their storage may occur owing to gradual redistribution of residual stresses through relaxation. This is why inadmissible gaps often appear between matched components of assembled machine tools and other machines, though the components have been fitted quite accurately to each other during assembly.

In some articles the operating properties of the metal can be increased by forming controllable residual stresses opposing the

working stresses. Most often, compressive residual stresses are intentionally produced in the surface layer so as to lower the dangerous tensile working stresses. Shot-blasting, nitriding and other methods of surface treatment can be used for the purpose.

In the overwhelming majority of cases, the magnitude, sign and distribution of residual stresses in the volume of article remain unknown and can only be found by destructive methods.

X-ray structural analysis makes it possible to evaluate residual macrostresses in the surface layer only, by determining the relative variation in the lattice spacing. Therefore, one should be always aware that uncontrollable residual stresses formed through plastic working, casting, welding, quenching, etc. can impair the properties of the metal and become dangerous in subsequent treatment or operation. In the general case it is desirable to eliminate uncontrollable residual stresses fully or at least partially.

### 1.3.2. LOWERING RESIDUAL STRESSES BY ANNEALING

The excessive energy in elastically strained portions of metal may be lowered without disturbing the integrity of the body if removal of residual stresses takes place through plastic deformation. Therefore, plastic flow should be initiated in an article in order to relieve fully or partially the residual macrostresses existing in it.

In annealing, residual stresses may diminish in two different ways: (1) through plastic deformation under the conditions when these stresses exceed the yield limit or (2) through creep, when the stresses are lower than the yield limit.

Consider the first way. By Hooke's law, residual stresses, as being elastic, are proportional to the modulus of elasticity and elastic strain. The modulus of elasticity diminishes only slight with increasing temperature, and therefore, residual stresses also diminish only insignificantly. The yield limit also lowers with increasing temperature, but appreciably more intensively than do residual stresses (Fig. 65).

Above a definite temperature ( $t_1$ ), the yield limit becomes lower than the residual stresses and plastic shear deformation takes place, resulting in that the residual stresses drop to the value of yield limit.

The lower temperature limit of reduction of residual stresses through shear deformation is not quite distinct, since residual

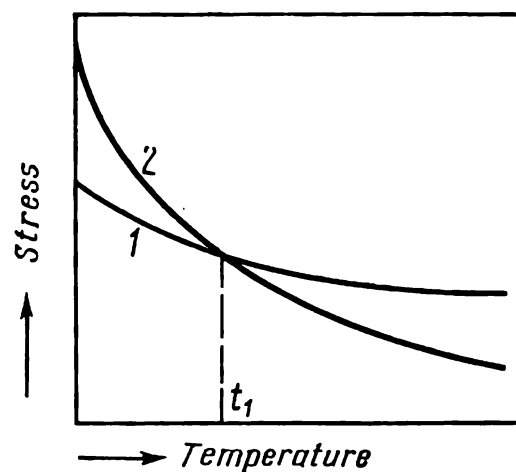


Fig. 65. Effect of temperature on (1) residual stresses and (2) yield limit

shear stresses of different magnitude act in various portions of a body.

With stresses above the yield limit, a multitude of dislocations generate in the metal, whose glide results in a very quick plastic deformation. It may be assumed that the degree of removal of residual stresses by this mechanism is determined by the temperature of annealing, rather than by the time.

Let us now consider the second way for removing residual stresses when these are lower than the yield limit. If at a certain moment a tensile specimen is left under load in the clamps of the testing machine without increasing further the deformation, then, as is well known, relaxation will take place in the specimen. In such a test, the stresses first diminish quickly and then more and more slowly until finally a practically constant stress level is established. The total deformation of a specimen is the sum of elastic and plastic deformation:

$$\varepsilon_{tot} = \varepsilon_{el} + \varepsilon_{pl} \quad (14)$$

The length of the specimen clamped in the machine remains constant. The stresses in it diminish owing to the reduction of elastic deformation with subsequent equal increase in the plastic deformation which develops under the conditions of creep. For a given total deformation, relaxation develops by creep with the stress being gradually decreased.

In articles where the residual stresses are lower than the yield limit, elastic deformation may change to plastic deformation with time.

In the temperature range where the residual stresses are lower than the yield limit (below  $t_1$  in Fig. 65), creep is the sole possible mechanism for their reduction. With stresses below the yield limit, neither mass multiplication nor mass glide of dislocation is possible. Slow plastic flow is effected through displacement of a limited number of mobile dislocations. These gliding dislocations are trapped on meeting some obstacles, such as individual sessile dislocations, dislocation tangles, disperse particles or grain boundaries. The exhaustion of mobile dislocations attenuates the creep, while the reduction of residual stresses enhances this attenuation even more.

Dislocation glide is activated by fluctuations in thermal energy. As the time of annealing increases, these fluctuations involve less favourably positioned dislocations in the creep process and help the dislocations in circumventing obstacles by crossing forest dislocations and by cross-slip. At temperatures above  $0.5 T_{m.p.}$ , dislocations can circumvent obstacles also by climb, as in the common high-temperature creep.

Even at room temperature, residual stresses in articles can diminish somewhat owing to creep. At higher temperatures, i.e. at greater thermal energy fluctuations, residual stresses are relieved more quickly and to a greater extent (Fig. 66).

The old practice of stress relieving in iron casting of intricate shape consisted essentially in keeping them for a long time (from three months to one year) at room temperature before machining. It has been found later, however, that this method could reduce residual stresses by only 15 per cent at the maximum. A more practicable technique of stress relieving is to anneal iron castings at 450-600 °C for a few hours.

If an article is heated to a definite temperature (above  $t_1$  in Fig. 65) at which the yield limit becomes smaller than the existing residual stresses, then the stresses first diminish quickly to the value of the yield limit, owing to mass multiplication and glide of dislocations, after which this mechanism of plastic deformation changes to creep, resulting in a gradual stress relaxation which attenuates in time.

Quick release of residual stresses at elevated temperatures may sometimes be dangerous, in particular, disturb the equilibrium of internal forces and momenta owing to a non-uniform distribution of stresses over the cross-section and length of an article, and thus produce warpage. The classical form of stress relaxation is ideal for annealing, where a slow plastic deformation increases gradually with simultaneous equal reduction of the elastic deformation so that the linear dimensions of an article in the direction of action of the forces do not change.

The higher the level of the initial stresses, the more quickly they are relieved in the initial period and therefore, the lower is the risk of warpage.

The time of annealing to diminish residual stresses is determined experimentally. For each particular article, a definite temperature of annealing has a corresponding final level of residual stresses, so that it is practically useless to increase the time of annealing further on reaching this level (Fig. 66).

When comparing alloys of different composition, the kinetics of residual stresses can be conveniently studied in relaxation tests with specimens tensioned to a given strain in the testing machine. However, when selecting the industrial conditions of annealing,

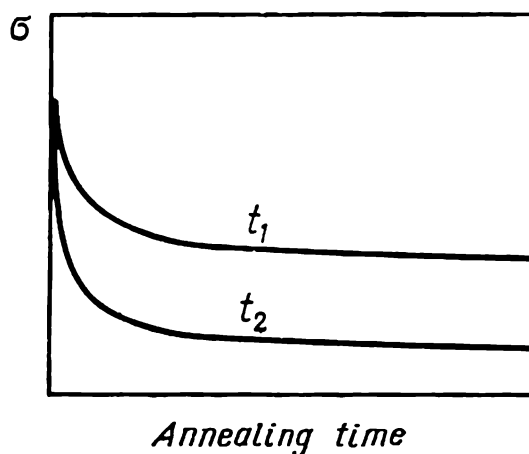


Fig. 66. Reduction of residual stresses with increasing time of annealing at two different temperatures ( $t_2 > t_1$ )

full-scale tests of articles are essential, since every particular article has its own characteristic distribution of residual stresses before and after annealing.

For alloys which contain phases with sharply differing thermal coefficients of linear expansion (silumins, cermets), *thermocycling* (*cyclic annealing with alternate freezing*) turns to be more effective than common annealing. This combined method of heat treatment is employed for elements of precision instruments in which a high stability of dimensions during storage and operation is essential. Articles made of silumins type AJ12 or AJ19 are cooled down to a temperature from  $-40^{\circ}$  to  $-196^{\circ}\text{C}$ , heated to room temperature, and placed into a furnace heated up to  $150^{\circ}\text{C}$  (or immediately transferred into the furnace). Upon heating, the articles are cooled to room temperature and again subjected to sub-zero treatment. Three cycles of such combined treatment (the final operation is always heating) can lower residual stresses by 30-70 per cent (the first cycle giving the highest effect). A common long-term annealing at the upper temperature of the thermal cycle ( $150^{\circ}\text{C}$ ) is incomparably less effective in diminishing residual stresses. The rates of cooling and heating have no effect on the results of thermocycling.

As has been shown by M. L. Khenkin, the mechanism of effective reduction of residual stresses in silumin on thermocycling is essentially as follows. The large difference between the thermal coefficients of linear expansion of the aluminium and silicon phase (approximately by a factor of 6.5) causes the formation of microstresses at phase boundaries. These stresses are enhanced through sub-zero treatment and, being added together with the residual stresses, produce appreciable plastic deformations on heating. Thus, alternating chilling to sub-zero temperatures and heating can increase plastic flow in microportions of the metal and therefore, produce a deeper stress-relieving effect.

In many cases stress relief is a secondary process occurring along with the principal structural and phase transformations during various operations of heat treatment. For instance, annealing, whose main aim is to produce recrystallization of phases, can also release casting or welding stresses (see 2.2.3). Homogenizing annealing can diminish casting stresses. High-temperature, tempering of steel, in which the main process is martensite-to-sorbite transformation, also diminishes hardening stresses. Recrystallization annealing, which is mainly resorted to for eliminating the work-hardening effect, also diminishes the residual stresses formed by cold working of the metal.

Heating to eliminate residual stresses is quite often employed as a separate operation of heat treatment, and is then respectively called stress-relief annealing.

The factors that limit the use of stress-relief annealing are the undesirable structural and phase changes possible on heating. For instance, heat-hardenable aluminium alloys must be heated to a temperature of around  $230-260^{\circ}\text{C}$  in order to relieve sufficiently fully the residual stresses in articles. These temperatures can however cause overageing, which results in a lower strength and, besides, in some alloys, in a lower corrosion resistance. For full elimination of the residual macrostresses left on cold plastic work-

**Table 6. Conditions of Stress-relief Annealing for Various Metals**

Meta	Annealing temperature, °C	Holding time, h
Carbon steel	550-680	*
Grey iron	430-600	0.5-5
Copper	150	0.5
Two-component brasses	200-260	1
Special brasses	350	1
Nickel and Monel	300	1-3
Titanium	450-480	0.5-4
Titanium alloys	500-650	0.5-4
Aluminium	150	0.5
Aluminium alloys	230-370	1-5
Magnesium alloys	150-260	1-5

\* 2.5 min per each mm of thickness.

ing, annealing should be preferably done at a temperature that causes recrystallization in the metal. But this can destroy the strengthening effect produced through the cold working, which is inadmissible in many cases. Therefore, we have always to decide whether to use a lower temperature at which only incomplete stress relief is possible or to aim at full relieving of stresses at a higher temperature at which, however, some mechanical and other properties of the metal might be impaired.

Table 6 gives conditions of stress-relief annealing for various materials. The rates of heating and especially of cooling in the annealing must be low, otherwise new internal thermal stresses can form.

The upper limit of the temperature range of stress-relief annealing is determined experimentally with due regard to the undesirable structural changes that might impair the mechanical and other properties of the metal.

Stress-relief annealing of steels is usually done at temperatures slightly below the critical point  $A_{c1}$ . As may be seen from Fig. 67, casting stresses in steel can be eliminated sufficiently fully by annealing at a temperature near 600°C. For grey iron castings, conditions of stress-relief annealing should be such as

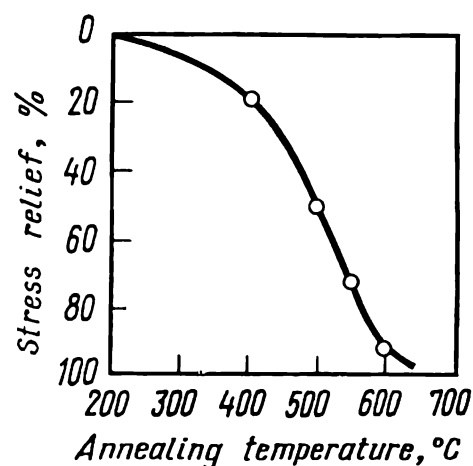


Fig. 67. Effect of annealing temperature on casting stresses in cast steel with 0.3% C. Annealing for 6 h. Initial stress 7.85 kgf/mm<sup>2</sup> (after L. Benson and H. Allison)

to prohibit strong development of graphitization and therefore, an appreciable loss of hardness.

Residual stresses in cold-rolled sheets and stampings made of copper, nickel, titanium or deformable alloys on their basis are eliminated by annealing at temperatures not above the point of the beginning of recrystallization, so as to preserve the high strength characteristics of the work-hardened metal. Stress-relief annealing is widely used with brasses containing more than 20 per cent Zn, since these are strongly susceptible to stress corrosion (season cracking).

As has been indicated earlier, the temperature of stress-relief annealing of aluminium alloys is an intermediate one between the temperature of age-hardening and that of quenching. The strength properties of thermally hardened articles fall off appreciably within this temperature range, because of which stress-relief annealing is only seldom used with deformable aluminium alloys. Annealing at 350-370 °C is sometimes made before the final (finish) machining, since otherwise the removal of a layer of metal might cause warpage. Continuously cast ingots of deformable aluminium alloys, when not homogenized, should be annealed at 300-350 °C before cutting them into sized blanks; this releases the residual stresses and eliminates the risk of ingot cracking during cutting. Cast articles of some aluminium alloys, such as elements of precision instruments, are annealed at 230-300 °C to release casting stresses and stabilize their dimensions.

Quenching stresses in plates, die-formed elements and other articles made of aluminium alloys, in which annealing might cause an inadmissible softening effect, can be reduced by a combination of sub-zero treatment and thermal shock. A hardened article is placed in liquid nitrogen (−196 °C) and the heated up quickly to a low temperature in boiling water or jet of steam. The temperature gradient in the quick heating opposes that produced in the quenching, so that the thermal stresses formed in the heating diminish those left on quenching. This treatment may be followed with conventional age-hardening. This unique method for releasing quenching stresses has still found no wide application.

Large-size articles, such as welded structures, which cannot be placed into common furnaces, are sometimes annealed locally with heating by a gas flame or other methods. It should then be kept in mind that local annealing can cause new strong stresses owing to an unavoidable difference in temperatures. Welding stresses in critical large structures can be eliminated by building a large furnace in which the whole structure is placed for annealing.

Stress-relief annealing is widely used in the industry. It can release harmful residual tensile stresses, which are especially dangerous in a three-dimensional stressed state, allows higher external loads to be applied, increases fatigue resistance and impact strength, lowers the susceptibility to brittle fracture, intercrystalline corrosion and corrosion fatigue, stabilizes the dimensions of articles, and prevents warpage.



## SECOND-ORDER ANNEALING

In second-order annealing, a metal or alloy undergoes qualitative or quantitative changes in the phase composition during heating and reverse changes during cooling.

The problem of whether second-order annealing is principally applicable with a given alloy can be decided by referring to the constitutional diagram of that alloy. The phase transformations possible in alloys in the solid state may be very diverse, for instance, polymorphic transformations (Fig. 68*a*), eutectoid transformations (Fig. 68*b* and *c*), peritectoid transformations (Fig. 68*d*), dissolution of one phase in another on heating and the reverse process of precipitation on cooling (Fig. 68*e*), etc.

Second-order annealing may be carried out with the phase composition being changed completely, i.e. with the phases existed at room temperature disappearing on heating and those which were stable at elevated temperatures disappearing on cooling. To do this, a metal or alloy must be heated up above its critical point, for instance,  $X_1$  alloys in Fig. 68 must be heated to a temperature  $t_1$  above  $t_0$ . If  $X_1$  alloys in Fig. 68*a-c* are heated to a temperature  $t_2$ , which is lower than  $t_0$ , their phase composition will change only partially, with a portion of the low-temperature  $\alpha$ -phase retained at the temperature of annealing.

If a change in the phase composition is only due to a variable solubility of the components in the solid state (such as  $X_2$  alloy in Fig. 68*e*), then complete phase on heat treatment is impossible altogether, since the main  $\alpha$ -phase in which the excess  $\beta$ -phase is being dissolved is stable both at low and high temperatures. In alloys of this type, only the quantitative proportion of the phases changes on heating or cooling (including cases where one of these phases disappears completely on heating above  $t_0$ ). A partial change of phase composition is also characteristic of the  $X_3$  alloy in Fig. 68*a*, since its high-temperature phase is stable at room temperature.

Second-order annealing is principally applicable to all metals and alloys whose phase composition in the solid state varies qualitatively or quantitatively with temperature. The practicability of the process depends on how strongly the properties of a metal

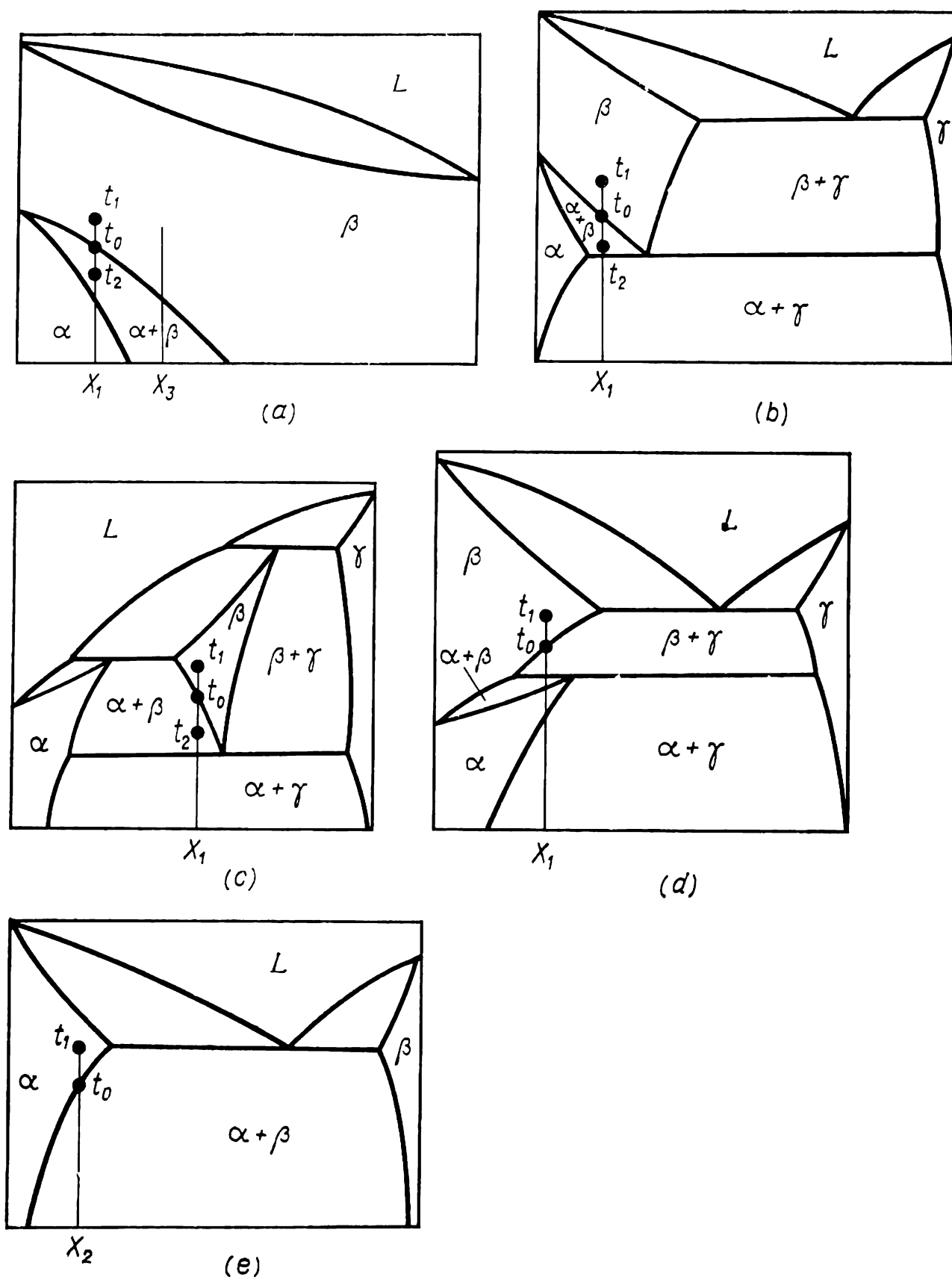


Fig. 68. Systems with various solid-state phase transformations

or alloy are affected by the structural changes caused by annealing.

The principal parameters of second-order annealing are the temperature of heating, the time of holding at that temperature, and the rate of cooling. The temperature and time of heating should ensure the desired structural changes, for instance, complete dissolution of an excess phase. The rate of cooling should be slow enough to allow reverse phase transformations based on diffusion (or self-diffusion). Annealed articles are usually cooled in the furnace or outside it in air.

Since second-order annealing is based on the use of phase transformations in the solid state, we should first discuss the general laws governing these transformations, which may also be of use in the analysis of other types of heat treatment.

## 2.1. GENERAL LAWS OF PHASE TRANSFORMATIONS IN THE SOLID STATE

### 2.1.1. THERMODYNAMICS OF PHASE TRANSFORMATIONS

As is well known, if a system of a constant volume is at a constant temperature, all spontaneous processes in it occur towards minimizing its free energy, i.e. the system tends to an equilibrium state in which the free energy is at the minimum. The free energy (or work function), which is a characteristic function of a system, is determined by the equation:

$$F = U - TS \quad (15)$$

where  $U$  = internal energy

$S$  = entropy

$T$  = absolute temperature

Phase transformations in solid alloys cause only insignificant changes of the volume. Neglecting these small volume changes, we may use the free energy as a tool for analyzing the laws of phase transformation in the bulk.

The free energy of any phase depends on temperature. To establish the nature of this relationship, we take the first and second derivatives of  $F$  with respect to  $T$ .

The total differential is:

$$dF = dU - TdS - SdT$$

For reversible processes, the generalized equation of the first and second law of thermodynamics can be written as follows:

$$TdS = dU + dA \quad (16)$$

If  $A$  is the work of expansion ( $pdV$ ), then it follows for isochoric processes with  $V = \text{const}$  and  $dA = 0$  that  $TdS = dU$ .

Substituting  $dU = TdS$  into the total differential  $dF$ , we get that  $dF = -SdT$ , whence

$$\left(\frac{\partial F}{\partial T}\right)_V = -S \quad (17)$$

Since the entropy is always positive,  $\left(\frac{\partial F}{\partial T}\right)_V$  should be always negative, i.e. the free energy always decreases with increasing temperature (Fig. 69). The second derivative is

$$\left(\frac{\partial^2 F}{\partial T^2}\right)_V = -\left(\frac{\partial S}{\partial T}\right)_V \quad (18)$$

The entropy always increases with temperature; therefore,  $\left(\frac{\partial S}{\partial T}\right)_V$  is positive and  $\left(\frac{\partial^2 F}{\partial T^2}\right)_V$ , negative. This implies that free energy-*vs*-temperature curves should always be concave downwards, but not the other way, as they are often depicted erroneously.

Let us consider the process of phase transformation in a single-component system, more particularly, a polymorphic transformation in a metal.

If two phases of a single-component system can be in equilibrium, the free-energy curves of these phases should intersect each other at the given temperature (Fig. 69).

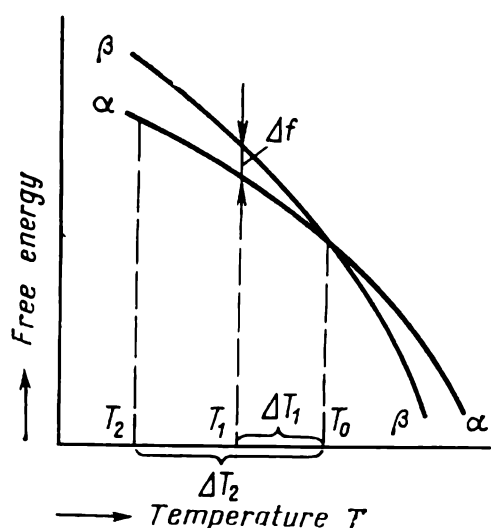


Fig. 69. Effect of temperature on free energy of two phases

The intersection of the curves determines that the free energies of the two phases are equal to each other and correspond to the temperature ( $T_0$ ) of stable equilibrium of the phases.

As may be seen from Fig. 69, at temperatures below  $T_0$  the free energy of  $\alpha$ -phase is lower than that of  $\beta$ -phase. Since the system tends to minimize its free energy,  $\beta$ -phase should transform into  $\alpha$ -phase on being cooled below  $T_0$ .

Crystallization in a molten metal occurs not at the temperature at which the solid and the liquid phase are in equilibrium, but at lower temperatures. This is also true of solid-state transformations. The temperature of transformation on cooling is always lower than the temperature of the reverse phase transformation on heating, the phenomenon being respectively called the *thermal hysteresis of transformation*. For instance, white tin transforms into the grey modification only at temperatures substantially below zero, though the equilibrium temperature is

+13 °C. The difference between the temperature of stable equilibrium of two phases ( $T_0$ ) and the actual temperature at which the transformation occurs on cooling is termed the *degree of undercooling* ( $\Delta T$ ).

The degree of undercooling increases with increasing cooling rate. Therefore, undercooling should be thought to have an impeding effect on phase transformations.

D. K. Chernov, a founder of theoretical metallurgy, noted in the second half of the last century that the process of solidification of steel consisted of two stages: the formation of crystallization nuclei and the growth of crystals from these nuclei. Later, G. Tammann, a well-known German metallurgist, determined quantitative characteristics for the two stages of crystallization: the number of nuclei appearing in unit volume per unit time, i.e. the rate of nucleation of ( $N$ ) and the linear rate of growth of crystals from these nuclei ( $G$ ). Tammann cooled transparent organic liquids to different temperatures and determined the rate of nucleation and the linear rate of crystal growth at various degrees of undercooling. He found these characteristics to be dependent on the degree of undercooling. At the temperature of equilibrium between liquid and solid phase, both  $N$  and  $G$  are equal to zero<sup>1</sup>. On increasing the degree of undercooling, both characteristics increase to a maximum and then drop down to zero on greater undercooling. Curves relating the rate of nucleation and the linear rate of crystal growth with undercooling have been called *Tammann's curves*.

It has been found later that the processes of phase crystallization in the solid state obey the same general laws as crystallization processes in liquids. Figures 70 and 71 show Tammann curves for polymorphic transformation in tin and eutectoid decomposition in steel.

The relationships that have been established experimentally may be explained by using the concepts of thermodynamics and statistical physics.

It may seem, on the face of it, that a crystallization nucleus may be an arbitrarily small combination of atoms, for instance, an elementary cell of a new phase that grows gradually due to attachment of atoms from the mother phase. A more detailed analysis shows however that this is far from being so.

Consider the isothermal process of crystallization of  $\alpha$ -phase in the mother  $\beta$ -phase at a definite temperature  $T_1$  which is lower than  $T_0$  (see Fig. 69).

---

<sup>1</sup> Since crystals in a solid system are not practically overheated during heating above the melting point, this point is usually taken as the temperature of equilibrium between the liquid and solid phase.

As soon as particles of  $\alpha$ -phase are formed, the free energy of the system should diminish, since the new phase is stabler and has a lower free energy at  $T_1$  than the initial  $\beta$ -phase. Upon the formation of a crystal of  $\alpha$ -phase the free energy decreases by  $\Delta F_v = V\Delta f$ , where  $V$  is the volume of the crystal and  $\Delta f$  is the difference of specific free energies of the two phases at  $T_1$  (see Fig. 69)<sup>1</sup>.

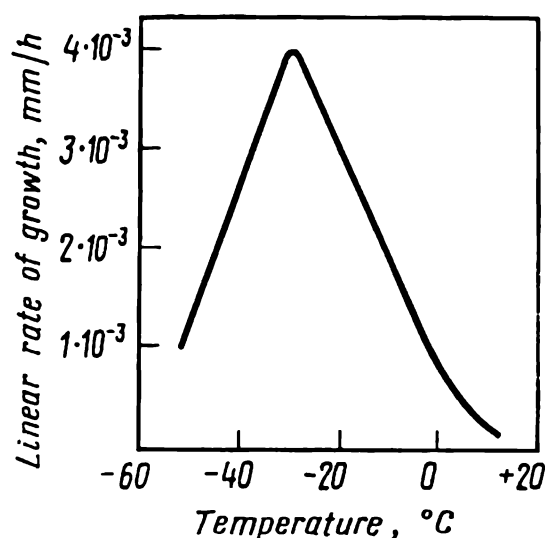


Fig. 70. Effect of temperature on linear rate of growth ( $G$ ) of grey tin crystals at the surface of white tin (after G. Tammann)

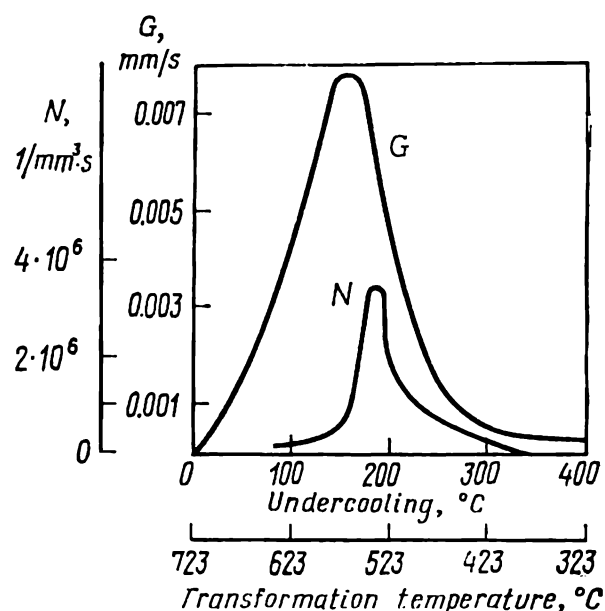


Fig. 71. Effect of undercooling on nucleation rate  $N$  and linear rate of growth  $G$  of pearlitic nodules in steel with 0.8% C (after I. L. Mirkin)

The formation of a new crystal is linked with the appearance of an interface between the new and initial phase, which requires a certain amount of work to be spent. The surface (more exactly—interface) energy of a crystal is  $\Delta F_s = s\gamma$ , where  $s$  is the surface area of the crystal and  $\gamma$  is the free energy per unit area (surface tension).

Thus, when a particle of a new phase is formed in the mother phase, the free energy of the system should, on the one hand, diminish owing to the transition of a certain volume of  $\beta$ -phase into a stabler  $\alpha$ -phase and, on the other, it should increase due to the formation of the interface possessing an excess surface energy. As a result, the actual change of the free energy on the formation of a single crystal is an algebraic sum:

$$\Delta F = -\Delta F_v + \Delta F_s \quad (19)$$

or

$$\Delta F = -V\Delta f + s\gamma$$

<sup>1</sup> In the case considered, the specific free energy is thought to be the free energy per unit volume. It is also called the 'chemical' free energy in contrast to the surface and elastic energy.

For a cubic crystal,  $\Delta F = -a^3\Delta f + 6a^2\gamma$ , where  $a$  is the length of cube edge. Similar formulae can be derived for crystals of any other shape. Since  $\Delta f$  and  $\gamma$  are constant at a given temperature  $T_1$ ,  $\Delta F$  is a function of the size of crystal (Fig. 72). Physically, this means that smaller particles have a larger area-to-volume ratio. For instance, for a cube with  $a = 10$ ,  $s/V = 6 \times 10^2/10^3 = 0.6$ , whereas for a one with  $a = 1$ ,  $s/V = 6 \times 1^2/1^3 = 6$ .

Therefore, for smaller particles, their surface energy makes up a greater proportion of the total energy. For particles smaller than a definite size  $a_0$ , the increment of free energy due to the formation of new surface ( $+\Delta F_s$ ) exceeds the loss of free energy owing to that part of the volume of the mother phase which transforms into a stabler modification ( $-\Delta F_v$ ), so that the free energy of the system increases in the whole ( $+\Delta F$ ). The larger is the size of particles compared with a definite critical size  $a_{cr}$ , the lower is the effect of surface energy, resulting in a reduction of the free energy of the system ( $-\Delta F$ , see Fig. 72) when the size of the crystals formed is greater than  $a_0$ .

When a subcritical crystal of a new phase has formed, its further growth should involve an increase in the free energy. Such a crystal is thermodynamically unstable and is readily dissolved by the initial phase. If however, a crystal of a size above  $a_{cr}$  forms in some or other way, it can grow spontaneously, since its growth will be accompanied with a reduction in surface energy. Consequently, *only nuclei of the new phase having the size at least the critical size  $a_{cr}$  and capable of growing spontaneously can serve as crystallization nuclei.*

The critical size of a nucleus can be determined by equating to zero the first derivative of  $\Delta F$  with respect to  $a$ , since the function passes through its maximum at  $a = a_{cr}$ :

$$\frac{d\Delta F}{da} = -3a_{cr}^2\Delta f + 12a_{cr}\gamma = 0$$

whence

$$a_{cr} = \frac{4\gamma}{\Delta f} \quad (20)$$

Since an increase in the degree of undercooling leaves the surface tension  $\gamma$  practically unchanged, while  $\Delta f$  rises continuously

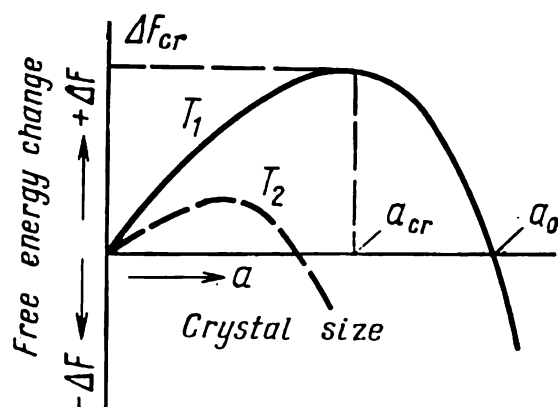


Fig. 72. Effect of the size of crystal on the free energy at its formation ( $T_2 < T_1$ , see Fig. 69)

(see Fig. 69), the critical size of a nucleus should decrease which is clearly shown in Fig. 72 where the dotted curve relates to a deeper undercooling.

Finally, we have to explain how a particle of a size above a definite critical value can form instantaneously in the mother phase.

A *critical nucleus* requires a certain amount of work to be spent on its formation ( $+\Delta F_{cr}$ ), since an interface is formed in the process (Fig. 72). This work can be expressed in terms of  $\Delta f$  and  $\gamma$ :

$$\Delta F_{cr} = -a_{cr}^3 \Delta f + 6a_{cr}^2 \gamma \quad (21)$$

Substituting  $a_{cr}$  from formula (20), we get:

$$\Delta F_{cr} = -\left(\frac{4\gamma}{\Delta f}\right)^3 \Delta f + 6\left(\frac{4\gamma}{\Delta f}\right)^2 \gamma$$

or

$$\Delta F_{cr} = \frac{32\gamma^3}{(\Delta f)^2} \quad (22)$$

Since, on increasing the degree of undercooling,  $\gamma$  remains virtually constant, while  $\Delta f$  increases (see Fig. 69), the work for the formation of a critical nucleus decreases rapidly (inversely proportional to the square of  $\Delta f$ ).

The work for the formation of a critical nucleus at a given degree of undercooling can be expressed in terms of surface energy. It follows from formula (20) that  $\Delta f = 4\gamma/a_{cr}$ . Substitution in (21) gives:

$$\Delta F_{cr} = -a_{cr}^3 \frac{4\gamma}{a_{cr}} + 6a_{cr}^2 \gamma = \frac{6a_{cr}^2 \gamma}{3}$$

Since  $6a_{cr}^2 = s$  (the surface area of the nucleus),

$$\Delta F_{cr} = \frac{1}{3} s \gamma \quad (23)$$

Thus, the work for the formation of a critical nucleus is equal to one-third of its surface energy<sup>1</sup>, the remaining two-thirds being compensated for by the loss in the volume free energy.

A question then arises: where a closed system can find the energy required to form a critical nucleus?

In a crystal, an interchange of kinetic energy between oscillating atoms takes place continually. This energy is distributed

<sup>1</sup> Since surface tension is different at different faces of a crystal, the term  $s\gamma$  in the formula for the work of formation of a critical nucleus should, strictly speaking, be replaced with a sum  $s_1\gamma_1 + s_2\gamma_2 + \dots + s_n\gamma_n$ , where  $n$  is the number of faces.



non-uniformly between the atoms, owing to the chaotic nature of thermal motion. At a given instant of time, the energy of various atoms is different, whereas the energy of a given atom varies with time. There are always atoms or groups of atoms whose kinetic energy is greater or lower than the mean value.

Deviations of energy from the mean value are termed energy fluctuations. A fluctuation-induced increase in the energy of a group of atoms in the mother phase can provide the work for the formation of a nucleus. *A critical nucleus can form where a portion of the mother phase of a size not less than the critical possesses an increased energy above a definite level.*

Thus, though the lattice of the new phase has a lower reserve of free energy than that of the mother phase, the transition from one phase to another on the formation of a crystallization nucleus passes through an intermediate state having a higher free energy than that of the initial phase.

The number of atoms whose energy is above a definite level  $E$  is proportional to the Boltzmann factor  $e^{E/kT}$ . It is clear that the greater the fluctuations in the energy and size in a crystal formed in a portion of increased energy, the lower is the probability of fluctuations within the initial phase.

We are now able to explain why the rate of nucleation of a new phase depends on the degree of undercooling. As the degree of undercooling increases, the size of critical nucleus and the work required for its formation decrease. Therefore, the greater is the degree of undercooling, the smaller are the energy level and geometrical parameter of a fluctuation required to form a critical nucleus and the greater will be the number of such fluctuations. Thus, as the degree of undercooling increases, the number of critical nuclei formed in a unit volume per unit time owing to energy fluctuations also increases. Their number should be proportional to the factor  $e^{-\Delta F_{cr}/kT}$ .

A critical nucleus becomes a centre of crystallization only when it has attracted one or a few atoms of the mother phase. The frequency with which atoms are attached to a nucleus is proportional to the factor  $e^{-Q/kT}$ , where  $Q$  is the activation energy of passage of an atom through an interface.

Consequently, the rate of nucleation, which is dependent on the probability of appearance of certain energy fluctuations and on the probability of attachment of atoms to critical nuclei, may be expressed as follows:

$$J = Ae^{\frac{-\Delta F_{cr}}{kT}} e^{\frac{-Q}{kT}} \quad (24)$$

At the temperature of equilibrium between two phases,  $T_0$ , when undercooling is zero ( $\Delta T = 0$ ) and the driving force of

transformation is also zero ( $\Delta f = 0$ , see Fig. 69), it follows from expression (20) that  $a_{cr} = \infty$ , i.e. the transformation cannot proceed [since the multiplier  $e^{-\Delta F_{cr}/kT}$  in equation (24) is zero].

As undercooling is increased, the work of formation of a critical nucleus,  $\Delta F_{cr}$ , rapidly decreases, and respectively, the number of critical fluctuations to form critical nuclei increases rapidly.

But as the temperature decreases, this at the same time diminishes the probability of attachment of atoms to a critical nucleus. The activation energy  $Q$  is independent of temperature and the multiplier  $e^{-Q/kT}$  in formula (24) quickly decreases with decreasing temperature and approaches zero as the temperature tends to the absolute zero.

Thus, on one hand, a greater degree of undercooling increases the difference of volume free energies (the driving force of transformation) and decreases the critical size of nucleus and the work required for its formation, which results in an increase of the rate of nucleation. On the other hand, a higher degree of undercooling results in a lower mobility of atoms, which impedes the formation of crystallization nuclei.

As a result of combined actions of the two opposing factors, a Tammann curve passes through a maximum. Important is that the rate of nucleation can become negligibly small at temperatures well above the absolute zero (see Fig. 71). By providing a sufficiently high degree of undercooling, we can suppress the diffusion transformation in the solid state; this is the principle that underlies quenching of alloys.

During a solid-state transformation, still another factor may act in inhibiting the nucleation of transformation nuclei. A new phase always differs from the initial one in its structure and specific volume. Since the transformation develops in an elastic crystalline medium, a change in the specific volume should cause the appearance of elastic strain energy in one or both phases; this inhibits the transformation and increases the free energy. Therefore, a certain elastic component  $\Delta F_{el}$  makes a positive contribution to the free energy change in a solid-state transformation and this component should be taken into consideration in equation (19):

$$\Delta F = -\Delta F_v + \Delta F_s + \Delta F_{el} \quad (25)$$

The term  $\Delta F_{el}$ , which has been neglected in the derivation of formulae (20), (22), (23) and (24), does not change qualitatively the conclusions on the nature of the effect of the size of nucleus on the variations of free energy  $\Delta F$  in an isothermal transformation (see Fig. 72) and on the effect of undercooling on the rate of nucleation. It only affects the magnitude of  $a_{cr}$ ,  $\Delta F_{cr}$  and  $J$ , but this effect may sometimes be very strong. For instance, the white-

to-grey tin transformation is linked with a change in the specific volume by 25 per cent and is characterized by a very high magnitude of  $\Delta F_{el}$ , so that the transformation can proceed spontaneously only upon freezing below  $-20^{\circ}\text{C}$  (and then only seldom), though the equilibrium temperature for the two modifications of tin is  $+13^{\circ}\text{C}$ .

An analysis similar to what has been done for the rate of nucleation can show how the linear rate of crystal growth depends on the degree of undercooling.

The maxima of nucleation rate and linear rate of growth correspond to different degrees of undercooling, the ascending branch of the curve of nucleation rate being shifted towards greater degrees of undercooling (see Fig. 71).

The rate of nucleation and the linear rate of crystal growth determine the total rate of a phase transformation. The average rate of an isothermal phase transformation first increases with the degree of undercooling, reaches a maximum, and then decreases again (Fig. 73)<sup>1</sup>. The average rate of a phase transformation is found experimentally as an inverse of the time of full isothermal transformation.

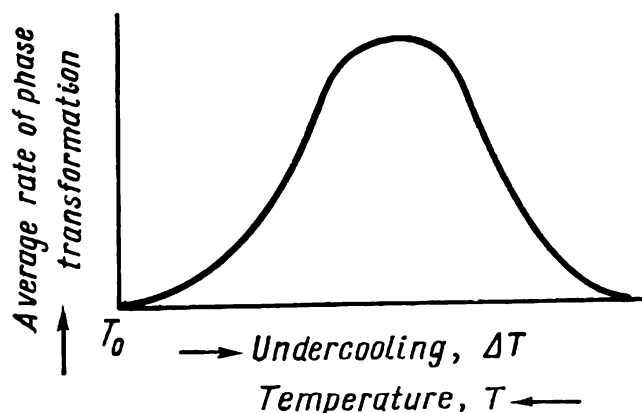


Fig. 73. Effect of undercooling on average rate of phase transformation

The thermodynamic analysis of the formation of nuclei of a new phase which has been made herein relates to isothermal conditions. The rates of nucleation and linear growth of portions of new phase can also be measured experimentally at definite degrees of undercooling. In practical processes of heat treatment, however, the processes occurring with continuous cooling are of the greatest importance. This by no means depreciates our conclusions obtained for isothermal phase transformations, since a continuously cooled metal may be thought to pass through an infinite number of degrees of undercooling. The more quickly a metal is cooled, the smaller will be the number of crystallization nuclei of the new phase that have time to form at each degree of undercooling, and therefore, the greater will be the degree of undercooling of the mother phase.

Up to this point, we have dealt with phase transformations on cooling. The principal conclusions of the fluctuational theory of

<sup>1</sup> As will be shown later in 2.1.5, the actual volume rate of isothermal transformation changes by a definite law in the process; this is why use is made of an average rate in the discussion above.

nucleation of phases are also true of processes of phase transformation on heating. As the degree of overheating above  $T_0$  increases, the difference of free energies between the initial and new phase increases (see Fig. 69), while the size of a critical nucleus and the work for its formation decrease.

The principal factor in which phase transformation on heating differs from transformation on cooling is that the mobility of atoms gradually increases as the temperature deviates from the point of equilibrium between the two phases. For that reason, *as the degree of overheating increases*, the rate of transformation

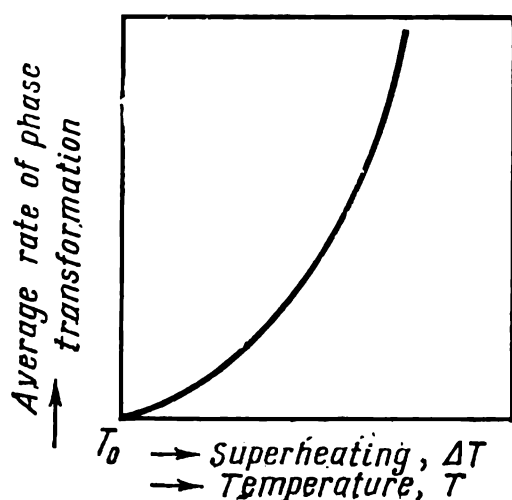


Fig. 74. Effect of overheating on average rate of phase transformation

increases intensively owing to a lesser size of the critical nucleus and lower work required for its formation, as also owing to a higher mobility of atoms (Fig. 74). This explains why the degree of overheating attainable in solid-state transformations is usually much lower than the degree of undercooling.

In phase transformations in alloys, the phase that is formed very often differs in its composition from the initial phase (see Fig. 68). In that case, energy fluctuation is insufficient for the formation of a critical nucleus and must be supplemented

with a *concentration fluctuation*. In a solid solution of a definite average composition there always are portions with a higher or lower concentration of some or other component. Naturally, the greater is the deviation from the average composition and the greater is the size of the portion having such a deviation, the lower will be the probability of concentration fluctuation within the limits of the initial phase. For instance, in order to form a nucleus of cementite with 6.67 per cent C in austenite of eutectoid composition (0.8 per cent C), the local concentration of carbon must be increased approximately by a factor of eight. Austenite may have portions high in carbon and others low in it. A probability calculation shows that  $1 \text{ cm}^3$  of eutectoid austenite may contain  $3.3 \times 10^{16}$  high-carbon portions of a size of 6 elementary cells in which the concentration of carbon is 6.67 per cent and only 1000 high-carbon portions of the same carbon concentration but of a size of 24 elementary cells ( $1 \text{ cm}^3$  of austenite contains in the whole  $2.14 \times 10^{22}$  elementary cells).

A distinction should be made between composition fluctuations in a single phase and in a disperse mixture of two phases. Concentration fluctuations appear and disappear all the time. A dif-

ferent time-independent distribution of concentration fluctuations corresponds to each temperature and each average composition of a solution. Such a distribution can also exist in a metastable, for instance, undercooled, phase before the onset of transformation. In contrast, a two-phase system cannot be characterized by an equilibrium distribution of particles of the phases according to their size, since these particles unlimitedly tend to coarsening; they first grow at the expense of the initial phase and then neighbouring particles of the same phase coagulate.

Since concentration fluctuations should necessarily be added to energy fluctuations, the formation of nuclei of a new phase in two-phase systems is not so easy as in single-phase systems, especially in cases where the composition of the new phase differs appreciably from that of the initial phase.

The difference in the compositions of initial and new phases has its effect not only on the mechanism of nucleation, but also on the mechanism of crystal growth. The growth of a new phase is ensured by diffusion inflow of atoms of one kind to the crystallization front and removal of atoms of other kind from that front. Since the rate of diffusion is largely dependent on temperature and also on the composition of solid solution, the processes of diffusion crystallization are extremely dependent on undercooling (or overheating) and on the content of alloying elements. The thermodynamics of the formation of a phase that differs in its composition from the initial phase is discussed in more detail in 4.1.1.

### 2.1.2. THE ROLE OF STRUCTURE OF INTERFACES IN PHASE TRANSFORMATIONS

The surface energy at the interface between a nucleus and initial phase depends on the structure of that interface. Three types of interface are distinguished, i.e. *coherent*, *semicoherent* and *incoherent*.

At a coherent interface, the lattice of one phase passes smoothly into the lattice of another phase (Fig. 75a): the atomic planes are not interrupted, but only bend somewhat and are continued, as it were, in the other phase. This elastic deformation, which is called coherent, ensures a smooth matching of the lattices of the two phases whose interatomic spacings are always different. If the new phase is more rigid than the initial one, the coherent deformation concentrates mainly in the initial phase, and vice versa.

If a coherent interface, or shortly, *coherence*, exists between crystals of two phases, these two phases (and their crystals) are also called coherent. If a phase transformation ensures phase

coherence, this means that the neighbours of any atom in the initial phase remain such in the new phase (see 3.2.3).

The surface energy of an interface may be thought to be composed of two components: a 'chemical' component, which appears due to short-range forces of interaction between unlike atoms in adjacent positions at both sides of the interface and a 'structural' component due to elastic deformation of the lattice.

A misfit between two lattices can be compensated through coherent deformations only when the difference in interatomic spacings of the two phases is sufficiently small.

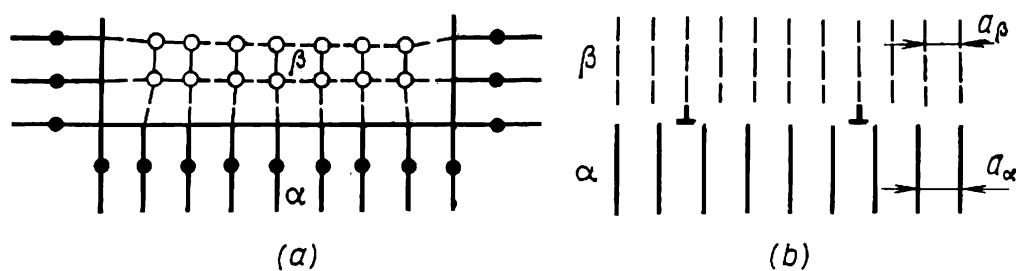


Fig. 75. The structure of (a) coherent and (b) semicoherent boundary between crystals of phases  $\alpha$  and  $\beta$

As may be seen from Fig. 75a, the vertical atomic planes become more and more bent on moving from the centre of the figure to its edges. It is then quite natural that the elastic deformation should increase with increasing area of a coherent interface. Thus, a purely coherent interface is only feasible on a relatively small surface, this surface being the smaller, the larger is the lattice misfit.

As the size of a nucleus increases, a moment may be reached when the compensation of the lattice misfit of two phases partially through dislocations becomes energetically more favourable than that resulting from coherent deformation over the whole surface of the interface (see Fig. 75b). Such dislocations are called structural, or misfit, dislocations. In the spaces between them, the lattices of two phases remain coherent. An interface having such a structure is called semicoherent. If, for instance, the misfit between two lattices is  $\varepsilon = (a_\alpha - a_\beta)/a_\beta = 0.01$  and the Burgers vector of structural dislocations is equal to one interatomic spacing in the matching plane, then the dislocations must be spaced  $1/0.01 = 100$  interatomic spacings from one another in order to compensate this lattice misfit on a semicoherent interface. The greater the lattice misfit, the greater the density of dislocations on a semicoherent interface. With a large lattice misfit between two phases, the distance between structural dislocations diminishes to such an extent that the dislocations lose their individuality (their cores merge together). Such an interface has a disordered

structure over the whole surface and is called incoherent, as also are called the phases separated by this interface. It follows from what has been said above that the prototype of incoherent interface is a high-angle boundary of grains of one phase, while the prototype of semicoherent interface is a low-angle boundary.

By rough estimation, the surface energy of a coherent interface does not exceed 200 erg/cm<sup>2</sup>, that of a semicoherent interface is equal to 200-500 erg/cm<sup>2</sup>, and that of an incoherent one, 500-1000 erg/cm<sup>2</sup>. Therefore, all other things being equal, the work of formation of a critical nucleus having coherent boundaries should be the lowest one, and the rate of formation of such nuclei, the highest.

As may be seen from Fig. 75, the lattice of nuclei that are separated from the initial phase by a coherent or semicoherent boundary is always oriented in a definite way relative to the lattice of initial phase. This by no means suggests a reverse conclusion that two phases whose lattices are mutually oriented should always be coherent. This is not so, firstly, because the lattice of an incoherent phase may have a definite orientation relative to that of the initial phase, since a nucleus of the new phase has had initially a semicoherent boundary which later has become incoherent during the growth of the crystal but retained the original orientation. Secondly, if a nucleus has an incoherent boundary from the very beginning, even then its lattice may be oriented regularly relative to the lattice of the initial phase. An oriented transformation obeys a general relationship whose essence has been most comprehensively formulated by P.D. Dankov as the *principle of orientational and dimensional correspondence*: "A chemical transformation on the surface of a solid develops in such a way that the configuration of the atoms of the initial solid phase remains the same (or almost the same) in the new solid phase. The crystal lattice of the new phase formed in the process is matched with the crystal lattice of the initial phase by similar crystal planes whose parameters only minimally differ from each other". From the standpoint of thermodynamics, the reason why two phases are mutually oriented in a regular manner consists in that, when crystallization takes place in an anisotropic medium, "the minimum of surface energy is ensured at the maximum similarity in the positions of atoms on contacting faces of the old and new phase" (S.T. Konobeevsky).

The *principle of orientational and dimensional correspondence*, or shortly, *structural correspondence*, which is also termed *Dankov-Konobeevsky's principle*, manifests itself most strikingly in the formation of a coherent phase, but it can also determine the orientation of an incoherent nucleus, since in that case the regular orientation can lower the energy of an incoherent boundary.

The principle of structural correspondence provides one of possible explanations for the appearance of stretched regularly oriented crystals of a new phase. In a polished microsection, such crystals are parallel to one another or make a definite angle. The structure is called *Widmanstätten structure*, after A. Widmanstätten of Austria, who was one of the first, in 1808, to observe a typical pattern of tangled streaks in iron-nickel meteorite.

### 2.1.3. HOMOGENEOUS AND HETEROGENEOUS NUCLEATION OF PHASES

When a new phase nucleates purely randomly in various portions of the initial phase, the process is called homogeneous nucleation.

One of the mechanisms of *homogeneous nucleation* is fluctuational formation of critical nuclei (see 2.1.1). The energy and concentration fluctuations themselves are the result of the chaotic thermal motion and their appearance in various portions of the initial phase has a probability nature. Because of this the nuclei formed on the basis of such fluctuations are also distributed at random in the volume of the initial phase.

The classical theory of homogeneous nucleation was developed originally for the condensation of vapours and crystallization of liquids. But it was well known from the very beginning that these processes took place preferably on the walls of a vessel or mould and on suspended particles, i.e. on existing interfaces.

A melt usually contains very fine inclusions — oxides, nitrides, carbides, sulphides, etc., which cannot be detected by chemical analysis. Numerous 'foreign' inclusions serve as nucleators and under common conditions we therefore usually have to deal with the nucleation on existing interfaces between phases, rather than with spontaneous homogeneous nucleation in a pure liquid. For that reason the process has been called heterogeneous nucleation.

*Heterogeneous nucleation* does not contradict the classical fluctuational theory of formation of critical nuclei. If the surface energy on the boundary between a nucleus and inclusion is lower than that on the boundary with the melt, the work of formation of a critical nucleus will also be lower<sup>1</sup>. A higher rate of nucleation on existing interfaces, which is found on increasing the degree of undercooling, can be explained, as in the case of homogeneous nucleation, by a smaller size of critical nuclei and a lower work of their formation.

---

<sup>1</sup> Owing to a lower numerator in formula (22).



In the solid state, the conditions for preferable nucleation in definite places are still more favourable, since the initial phase has numerous places of increased free energy which promote the transformation. Such places are grain and subgrain boundaries in the initial phase, disperse inclusions of other phases, dislocations, and stacking faults.

The term 'heterogeneous nucleation' has been later given a broader meaning to include all cases of preferable nucleation in solid phases, regardless of the nature of the places where nuclei are formed.

With heterogeneous nucleation in the solid state, the work of formation of critical nuclei may become lower owing to (a) a reduced surface energy on an existing interface between a nucleus and matrix and (b) full or partial disappearance of a lattice defect in the initial phase and corresponding disappearance of the free energy.

The typical cases of preferable heterogeneous nucleation will be discussed separately below.

### Nucleation at Grain Boundaries

The fact that nucleation is facilitated at grain boundaries in the initial phase may be explained in the same way as the preferable nucleation of crystals at inclusions in a melt. The phenomenon may however be treated in a somewhat different manner: when a nucleus of a new phase has formed, a certain portion of the intergranular boundary disappears and the excess energy  $\Delta F_b$  of the intergranular boundary in the initial phase that is liberated in the process is used to form a nucleus of a new phase, i.e. to construct an interface and compensate the elastic energy that has appeared. The expression (25) may be rewritten as follows:

$$\Delta F = -\Delta F_v + \Delta F_s + \Delta F_{el} - \Delta F_b \quad (26)$$

Therefore, the work for the formation of a critical nucleus will be lowered owing to the negative contribution of  $\Delta F_b$  to the total variation of free energy.

There may be other causes for the preferable nucleation at grain boundaries. As is known from the course of physical chemistry, some or other components in a liquid solution may have different effect on surface tension. Surface-active elements, which diminish the surface tension in solutions, should concentrate spontaneously at the surface, since this lowers the free energy of the system. Surface activity can be observed in solid, as well as in liquid solutions. The dissolved elements which can lower the free energy of an intercrystalline boundary and concentrate in the zone near it are called *horophile*. Spontaneous enrichment of grain

boundaries in a dissolved element is termed *equilibrium segregation*, in contrast to dendritic segregation, in which the concentration of solid solution near grain boundaries undergoes a non-equilibrium change. Whereas dendritic segregation can disappear gradually on annealing, equilibrium segregation, on the contrary, increases as the time of isothermal holding is increased.

One of probable causes of equilibrium segregation is elastic interaction between atoms of a dissolved element and an intergranular boundary. In substitutional solutions, the lattice is distorted owing to the dimensional misfit between atoms of a dissolved element and the surrounding atoms of other components. The nearest neighbours are displaced in directions away from a lattice site if the latter contains an atom of dissolved element with a larger diameter than that in the base metal. If, however, the atom of dissolved element is smaller in diameter than that of the solvent, then the nearest neighbours will be displaced towards the lattice site in which the atom of dissolved element is positioned.

Atoms on an intergranular boundary are positioned irregularly, i.e. thicker in some portions and less closely in others. When the atomic diameter of a dissolved element is larger than that of the base metal, its atoms will tend to occupy less concentrated places on the grain boundary, and in an opposite case they will occupy the thicker portions. In any case, the energy of lattice distortion around the atoms of a dissolved element decreases.

In interstitial solutions, atoms of dissolved elements also distort the volume of a crystal if their diameter is greater than the size of lattice voids they occupy. For these atoms too, it is energetically more favourable to occupy less concentrated places of an intergranular boundary.

Thus, the driving force of equilibrium segregation is the difference between the energies of lattice distortion around an atom of dissolved element in the volume of a crystal and at an intergranular boundary. This difference is the energy  $E$  of elastic bond between that atom and grain boundary. The concentration of the element at a boundary is thus determined by  $E$  and the concentration of the dissolved element  $C_0$  in the volume of a grain:

$$C_b = \frac{C_0 e^{E/kT}}{1 + C_0 e^{E/kT}} \quad (27)$$

The greater is the dimensional misfit of atoms, the larger will be the energy of elastic interaction  $E$ , and therefore, the concentration  $C_b$ . In a body-centred cubic lattice, the volume of voids that can be occupied by interstitial atoms is substantially smaller than that in a face-centred cubic or hexagonal close-packed lattice. For that reason, interstitial elements in a body-centred lattice

should segregate more strongly towards an intergranular boundary (for example, the segregation of carbon in  $\alpha$ -iron should be stronger than in  $\gamma$ -iron). In multi-component solid solutions, atoms of an element possessing the greatest dimensional misfit tend to displace all other atoms from the boundary zone.

With increasing temperature, the equilibrium segregation interferes with thermal motion of atoms and fully disappears when the temperature is sufficiently high.

Since the lattice in the volume of a crystal is always distorted around atoms of a dissolved element, it follows that these atoms always interact elastically with the intergranular boundary. This suggests that all dissolved element should be *horophilic* to some or other extent. There is some experimental evidence, however, that some elements can be *horophobic*, i.e. they concentrate more in the bulk of a crystal than at grain boundaries. This implies that, apart from elastic interaction, there should exist chemical interaction between atoms of dissolved element and an intergranular boundary. Depending on the electronic structure of atoms, this chemical interaction can either facilitate the equilibrium segregation at a boundary or, on the contrary, counteract the elastic attraction and thus purify the boundary zone from atoms of the dissolved element.

Direct experiential determination of  $C_b$  is linked with extremely large difficulties, since the boundary zone enriched in or depleted of a dissolved element is usually very thin. A suitable method for direct examination of equilibrium segregation is field-ion microscopy with a resolution of up to 2 angstroem, since it allows direct observation of atomic structures at intergranular boundaries. For instance, an ionic projector was used to observe the segregation of interstitial oxygen at boundaries of iridium grains and determine the concentration of oxygen in the boundary zone.

Whether a given element is horophilic or horophobic in a given solvent can be decided quite reliably by using the concept of an analogy between the structure of a melt and disordered structure at a grain boundary. It follows from that analogy that the ratio of the concentration of a dissolved element in the bulk of a grain and at a grain boundary should be equal to the ratio of concentrations of that element in the solid ( $C_s$ ) and liquid ( $C_l$ ) solution, i.e. to the distribution coefficient:

$$\frac{C_0}{C_b} = \frac{C_s}{C_l} = k \quad (28)$$

The coefficient  $k$  can be easily found on the constitutional diagram near the melting point of the main component. If an addition lowers the solidus point, then  $k < 1$ , and therefore, the dissolved element should be horophilic, i.e. its concentration in the

melt is greater than in the solid solution and its concentration at the grain boundary is greater than in the bulk of grain. If, however, an addition raises the solidus point of solid solution, then  $k > 1$  and the dissolved element is horophobic, i.e. its concentration in the melt is lower than in the solid solution and the concentration at the grain boundary is lower than in the bulk of grain. From this we may predict, for instance, for a Cu-Ni system, which forms a continuous series of solid solutions, that copper will be horophilic in nickel-base alloys and nickel will be horophobic in copper-base alloys. The method indicated, however, fails to provide reliable quantitative estimation of horophilic and horophobic effects, merely because the structure of grain boundaries is not identical with that of a liquid solution.

Equilibrium segregation of a horophilic element or, on the contrary, depletion of the boundary zone in a horophobic element can strongly affect the nucleation of a new phase at grain boundaries, with both processes being principally capable of either facilitating or impeding locally the phase transformation. Of special importance is that, even with an insignificant total content of a horophilic element in an alloy, its concentration at an intergranular boundary in the solution can be sufficiently high to affect the phase transformation. Various melts of the same alloy may, for some or other occasional reasons, contain different amounts of horophilic impurities which are undetectable by common methods and, therefore, will differ substantially in the rate of nucleation of a new phase at grain boundaries. Owing to equilibrium segregation, special small, or 'homeopathic', additions of elements can have a strong effect on phase transformations. For instance, boron, when added in a few thousandths of a per cent, can impede austenitic decomposition at grain boundaries.

Grain boundaries can affect the rate of growth of nuclei of a new phase, as well as their nucleation proper. If a new phase differs from the initial phase in its composition, the diffusion growth of its nuclei will proceed faster at grain boundaries than in the bulk of grains. To explain this, we should recall that the rate of diffusion at grain boundaries, where the metal structure is more 'loose', is higher than in the bulk of grains. The activation energy of grain-boundary diffusion is roughly one-half of that of volume diffusion. Since the activation energy enters the exponent in the formula for dependence of the diffusion coefficient on temperature ( $D = Ae^{-Q/RT}$ ), the indicated difference in activation energies gives a large difference in the coefficients of boundary and volume diffusion. For instance,  $Q_v$  and  $Q_b$  for silver are respectively 45 900 cal/g-atom and 20 200 cal/g-atom. The coefficients of volume and boundary self-diffusion of silver at 700 °C ( $D_v$  and  $D_b$ ) are respectively  $63 \times 10^{-12}$  cm<sup>2</sup>/s and  $87 \times 10^{-8}$  cm<sup>2</sup>/s,

i.e. differ by four orders of magnitude from one another. For  $\gamma$ -iron at 1000 °C, the coefficient of self-diffusion along grain boundaries is  $10^3$  times that within grains.

The role of grain boundaries in diffusion transformations increases at lower temperatures, since the diffusion mobility in the bulk of grains becomes quite low. Grain boundaries begin to affect noticeably the rate of diffusion phase transformations at temperatures below  $0.75 T_{m.p.}$

### Nucleation at Dislocations

An elastic stress field always exists around a dislocation. With an edge dislocation, for instance, a tensioned region forms below the edge of an incomplete atomic plane and a compressed region, above that edge. Because of this, a dislocation can compensate fully or partially the structural misfit existing between a nucleus and the initial phase, which is one of the reasons why nuclei with semi-coherent or incoherent boundaries preferably form at dislocations. Upon the formation of such a nucleus, the elastic energy of the lattice in a certain region near the dislocation line disappears. This implies that the term  $\Delta F_{el}$  in formula (25) has a 'minus' sign, i.e. the elastic energy of the dislocation is added to the driving force of transformation  $\Delta F_v$  and thus enhances nucleation. By an estimate, the resulting rate of nucleation at dislocations can be  $10^{78}$  times that of homogeneous nucleation.

Another reason for the preferable nucleation at dislocations is the formation of Cottrell atmospheres from atoms of the dissolved element along the dislocation line. If a nucleus differs from the initial phase in a higher content of an alloying element, then, naturally, it will form more easily in places where that element has already segregated. Finally, the activation energy of diffusion along edge dislocations is only about one-half of that in grain volume far from the dislocation. The faster diffusion along dislocation 'tubes' enhances the diffusion growth of nuclei of a new phase, especially at low temperatures when the diffusion in the grain bulk of the initial phase becomes very slow.

### Nucleation at Stacking Faults

A stacking fault, for instance, in a face-centred cubic lattice, is an interlayer of a hexagonal close-packed lattice, and vice versa. If the new phase has the lattice of the same type as that of a stacking fault, the latter can serve as a nucleus for that phase. Since the solubility of an alloying element should in the general case be different in lattices of different types, atoms are redistributed between the stacking fault and the remaining lattice

of the initial phase into Suzuki atmospheres which facilitate the nucleation of a phase that differs from the initial phase in composition. Because of the two reasons mentioned, extended dislocations, in which stacking faults join partial dislocations, are places of preferable nucleation of new phases.

### Nucleation at Inclusions

The initial phase may contain inclusions of oxides, carbides, nitrides, intermetallics, and other phases. Inclusions can facilitate nucleation of a new phase for the same reason as in heterogeneous nucleation in melts: the work of formation of a critical nucleus decreases if the surface energy at the boundary between the nucleus and inclusion is lower than that at the boundary with the mother phase. This is more probable in the cases where the lattice of an inclusion is isomorphic with that of the nucleus.

Inclusions can accelerate nucleation either directly or indirectly, through the formation of dislocations. Owing to a difference in the coefficients of thermal expansion of inclusions and matrix, a heat treatment process can produce such stresses around inclusions that the mother phase will form dislocations at which a new phase preferably nucleates.

The formation of crystallization nuclei at more high-melting inclusions during solidification of melts is the principal mechanism of heterogeneous nucleation. In solid-state transformations, however, direct nucleation at inclusions is of secondary importance compared with the nucleation at various lattice defects (grain boundaries, sub-boundaries, dislocations) whose number and extension are usually much greater.

### Nucleation at Microdiscontinuities

The nucleation of new phases can be largely facilitated at the surface of shrinkage microvoids, gas blowholes, microfissures and other discontinuities formed at grain boundaries or inside grains during crystallization, plastic deformation and heat treatment, as also at the open surface of articles, since these places, unlike the continuous medium, offer no elastic resistance to the formation of crystals of different specific volume. These places of preferable nucleation are especially effective when the value of  $\Delta F_{el}$  in formula (25) is large. Examples may be the nucleation of graphite at microdiscontinuities formed in austenite or the transformation of white tin into its grey modification, which always begins from the open surface of specimens.

If a new phase differs from the initial in composition, the growth of its nuclei at the free surface is enhanced by surface dif-

fusion, which proceeds much faster than boundary diffusion and especially than volume diffusion. For instance, for silver the activation energy of surface diffusion is  $Q_s = 10,300$  cal/g-atom, whereas that of boundary diffusion is  $Q_b = 20,200$  cal/g-atom. At  $700^\circ\text{C}$ , the coefficient of diffusion of silver at grain boundaries is  $D_b = 87 \times 10^{-8}$  cm<sup>2</sup>/s, while the coefficient of surface diffusion  $D_s = 83 \times 10^{-5}$  cm<sup>2</sup>/s, i.e.  $10^3$  times higher.

With heterogeneous nucleation, the dispersity and nature of distribution of particles of a new phase in an alloy are determined by the number and position of places of preferable nucleation. In contrast to homogeneous nucleation, centres of phase transformation in heterogeneous nucleation may be distributed very unevenly in the volume of alloy, for instance, they may concentrate predominantly at grain boundaries. Crystals of a new phase located at grain boundaries of the mother phase very often outline clearly these boundaries (Fig. 76). In other cases, their distribution in the volume of alloy can be rather even when the sites of preferable nucleation are themselves distributed uniformly in the initial phase; this is possible, for instance, with nucleation at dislocations, stacking faults and inclusions. Changing the number and nature of position of the sites of heterogeneous nucleation through heat treatment, plastic deformation or some other methods is one of the most effective ways of controlling the structure of metal on phase transformations. For example, refining the grain of the initial phase (and therefore, increasing the total area of grain boundaries) or increasing the density of dislocations through plastic deformation results in an increased number of nuclei of phase transformation. Particular examples of this type of structure control will be discussed in corresponding chapters.

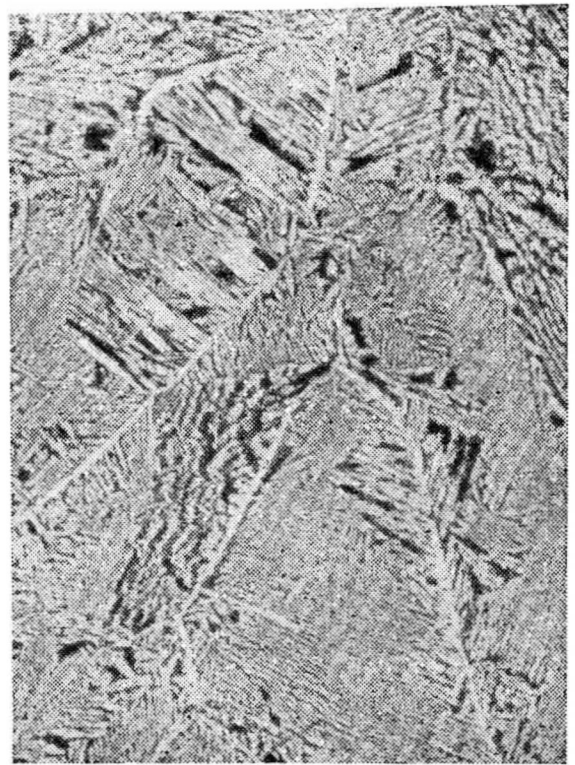


Fig. 76. Microstructure of  $(\alpha + \beta)$ -brass,  $\times 100$ . Bright chains of  $\alpha$ -phase crystals enclose the boundaries of initial  $\beta$ -phase grains

#### 2.1.4. FORMATION OF INTERMEDIATE METASTABLE PHASES

The formation of a stable phase brings the system into a state in which the free energy is at its absolute minimum. Under certain conditions, however, a metastable phase can nucleate and

grow instead of an absolutely stable phase, so that the system is brought into a state of a relative minimum of free energy.

Consider the conditions of equilibrium between the initial phase  $\alpha$  and a new stable phase  $\beta$ , which differs from the initial in structure and composition. For this, use may be made of the method of geometrical thermodynamics with plotting of 'free energy-composition' graphs.

As is known from the courses of physical chemistry and metallography, any phase is characterized at a constant temperature

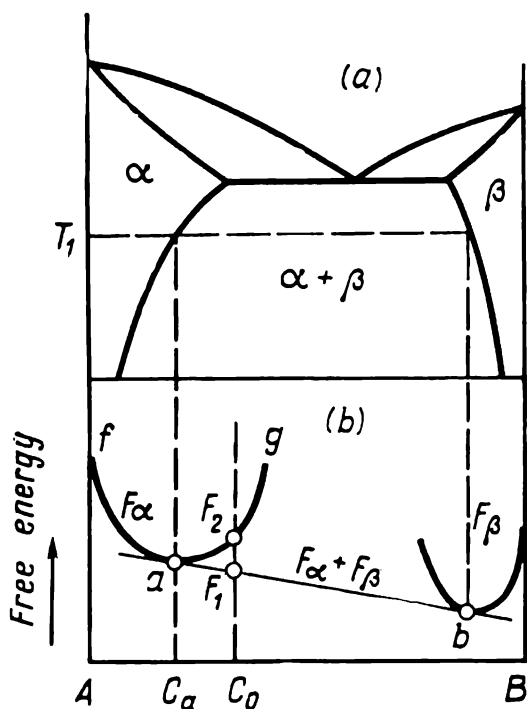


Fig. 77. Constitutional diagram (a) and effect of composition on free energy at temperature  $T_1$  (b)

by its own curve relating the composition of that phase with its free energy (Fig. 77). If a common tangent is drawn to the free-energy curves of two phases in equilibrium, then the points of contact ( $a$  and  $b$ ) will determine the compositions of the phases at a given temperature. In the general case these compositions do not correspond exactly to the minimum points of the curves in question, since the condition for heterogeneous equilibrium in a system composed of more than one component is the equality of chemical potentials of the components in the co-existing phases, rather than the minimum of free energy of each of them.

The free energy of a mixture of phases is always an additive quantity and is depicted by points on a straight line connecting the free energies of the equilibrium phases. Therefore, any point of section  $ab$ , such as  $F_1$  (Fig. 77b) determines the free energy of the mixture of equilibrium phases with the compositions corresponding to points  $a$  and  $b$  (the interface energy is neglected here).

The section  $fa$  of the free energy curve of  $\alpha$ -phase relates to the region of compositions of that phase (from  $A$  to  $C_a$ ) in which the phase is stable at a given temperature, and the section  $ag$ , to a region where the phase is metastable. In the latter case the free energy of  $\alpha$ -phase is greater than that of the mixture of  $\alpha + \beta$  of the same composition (for instance, in  $C_0$  alloy,  $F_2 > F_1$ ). If the composition of  $\alpha$ -phase is to the right of point  $C_a$ , then  $\beta$ -phase will form from it until the composition of the initial phase will reach an equilibrium ( $C_a$ ). If, however, the composition of  $\alpha$ -phase is to the left of point  $C_a$  and the phase is in contact with  $\beta$ -phase,



then the latter will dissolve in the  $\alpha$ -phase until an equilibrium composition  $C_a$  will be attained.

Imagine a system in which not only a stable  $\beta$ -phase exists, but also metastable phases  $\beta'$  and  $\beta''$  can form under definite conditions, the free energy of these phases being greater than that of  $\beta$ -phase (Fig. 78). The metastable  $\beta'$ -phase differs from the stable phase in the structure only, while the  $\beta''$ -phase differs in both the structure and composition. Imagine further that an  $\alpha$ -phase of composition  $C_a$  is in stable equilibrium with the  $\beta$ -phase and that  $\alpha$ -phases of composition  $C'$  or  $C''$ , respectively, are in metastable

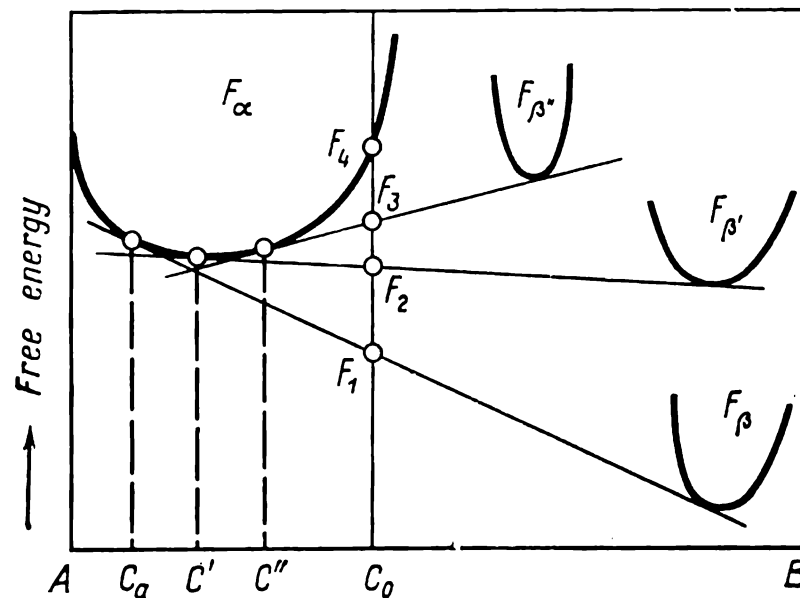


Fig. 78. Diagram for the analysis of equilibrium of  $\alpha$ -phase with stable  $\beta$ -phase or with metastable  $\beta'$ - and  $\beta''$ -phases

equilibrium with the phases  $\beta'$  and  $\beta''$ . A general conclusion can then be drawn, namely that the *solubility of a metastable phase in other phase is always higher than that of a stable phase*.

In an alloy of composition  $C_0$ , the free energy of a mixture of phases  $\alpha + \beta$  is lower than that of a mixture  $\alpha + \beta'$  or  $\alpha + \beta''$  ( $F_1 < F_2 < F_3$ ). Whence it follows that the free energy lowers more on the formation of a stable phase than on the formation of a metastable phase, since  $(F_4 - F_1) > (F_4 - F_2)$  and  $(F_4 - F_1) > > (F_4 - F_3)$ . This analysis, however, disregards the role of surface energy (the graph in Fig. 78 relates the volume free energy with composition). On the other hand, as has been shown in 2.1.1, the surface energy may be decisive at the first stages of formation of crystals of a new phase, i.e. when their surface area-to-volume ratio is large, and therefore, the surface energy contributes much to the total free energy of crystals.

The values of surface energy at boundaries between the  $\alpha$ -phase and phases  $\beta$ ,  $\beta'$  and  $\beta''$  may differ appreciably. Suppose that the crystal lattice of the stable  $\beta$ -phase differs strongly from that of

the initial  $\alpha$ -phase, so that the formation of a coherent boundary between them is impossible. At the same time the structure of the metastable phases  $\beta'$  and  $\beta''$  is closer to that of the initial  $\alpha$ -phase, so that interfaces  $\alpha/\beta'$  and  $\alpha/\beta''$  can be either coherent or semi-coherent. The surface energy at such interfaces is substantially lower than at the incoherent  $\alpha/\beta$  interface. In the cases where the  $\alpha/\beta'$  or  $\alpha/\beta''$  interface is also incoherent, its surface energy is nevertheless lower than at the  $\alpha/\beta$  interface, since crystals of the phases  $\alpha$  and  $\beta'$  (or  $\beta''$ ) can have boundaries of more similar structure than crystals of  $\alpha$ - and  $\beta$ -phase.

If the gain in surface energy exceeds appreciably the loss in volume free energy, then, according to formula (25), the work of formation of critical nucleus  $\Delta F_{cr}$  of a metastable phase is lower than for the stable phase, and, in accordance with formula (24), the rate of nucleation of the metastable phase will be higher. In the case of a coherent or semicoherent boundary between metastable phases, the gain in surface energy should also exceed the rise in elastic energy linked with these boundaries, in order to diminish  $\Delta F_{cr}$ .

If various metastable phases can exist in a system, then, with a given degree of undercooling, the first to form will be the metastable phase having the highest rate of nucleation and the least work of formation of critical nuclei. After that, on increasing the holding time, other metastable phases having higher activation energies of formation of critical nuclei will form in succession and finally the stable phase will appear, since it has the highest activation energy, and therefore, the lowest rate of nucleation.

Thus, the *sequence of phase formation is controlled by the energy barrier on nucleation of a new phase, rather than by the attained level of volume free energy*. This barrier is strongly dependent on the surface energy at the interface. The greater it is, i.e. the greater is the activation energy for the formation of critical nuclei, the later a corresponding phase will form. This relationship is called the '*step rule*'.

If a more stable  $\beta'$ -phase appears upon the formation of the  $\beta''$ -phase, then an equilibrium concentration  $C'$  of the initial phase establishes around its crystals in the initial  $\alpha$ -phase. This concentration is lower than the solubility limit  $C''$  of the  $\beta''$ -phase that has formed earlier, so that the  $\beta''$ -phase should be dissolved. Similarly, the  $\beta'$ -phase should be dissolved on the appearance of the stable  $\beta$ -phase. All this corresponds to the general rule that *the formation of a more stable phase causes the dissolution of a less stable phase that has formed earlier* and that is termed intermediate phase. In the final result the system may come to a state at which its free energy is at the absolute minimum.

The formation of an intermediate phase can also be promoted by the concentration factor. If a stable phase differs substantially from the initial phase in composition, then high concentration fluctuations will be necessary for its nucleation and a relatively high diffusion mass transfer, for its growth. If a metastable phase can exist in the system with the composition much closer to that of the initial phase, then the formation of this phase will be kinetically more favourable, especially at large degrees of undercooling, i.e. when diffusion processes are slowed down.

A classical example is the formation of metastable cementite, instead of graphite, from austenite. The composition of austenite (not more than 2.14 per cent C) is much closer to that of cementite (6.67 per cent C) as compared with that of graphite (100 per cent C). It is then quite evident that the probability of concentration fluctuations required for nucleation of cementite is incomparably greater than that required for nucleation of graphite. The rate of diffusion growth of cementite crystals is also higher than that of graphite. In addition to the concentration factor, the structural factor can also promote cementite nucleation: cementite is structurally more similar to austenite than graphite, so that the surface energy at its boundaries with austenite should be lower.

### 2.1.5. KINETICS OF PHASE TRANSFORMATIONS

The kinetics of crystallization in the solid state is determined by two factors: the rate of nucleation of transformation nuclei and the linear rate of growth from these nuclei. As has been shown earlier in the book, both factors depend on the degree of undercooling (or overheating).

The kinetics of phase transformation at a definite degree of undercooling (or overheating) is depicted by a *kinetic curve* which shows how the amount of a new structural component increases with time (Fig. 79).

The kinetic curve of a transformation during cooling is constructed as follows. A specimen is heated to a temperature above the point of phase equilibrium. At that temperature it can remain in the initial phase state for an arbitrarily long time. The specimen is then transferred quickly into a thermostat maintained at a temperature below the point of phase equilibrium, i.e. at a temperature corresponding to a definite degree of undercooling. The thermostat may be a salt or oil bath or a bath of molten metal.

The specimen should be sufficiently thin to be heated quickly to the thermostatic temperature. The degree of transformation in the specimens placed in the thermostat is determined by variations in their properties, such as magnetic or electric. It is also possible to take specimens from the thermostat in regular intervals, quench

them, and then to measure their properties or study the microstructure at room temperature.

Kinetic curves for transformations during heating are constructed in a similar manner. In that case, a specimen at an initial temperature below the phase equilibrium point is quickly transferred into the thermostat at a temperature corresponding to a given degree of overheating.

All isothermal crystallization processes can be characterized by the kinetics as follows (Fig. 79). The volume that has undergone a transformation increases

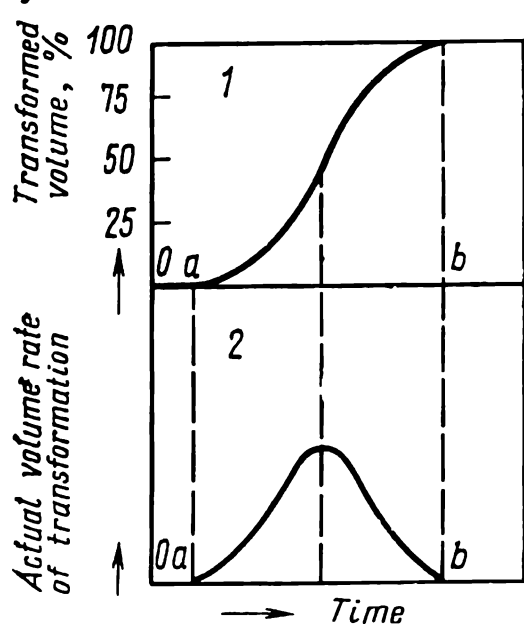


Fig. 79. Kinetics of phase transformation at constant temperature

1—kinetic curve; 2—effect of time of isothermal holding on actual volume rate of transformation;  $oa$ —induction period;  $ob$ —period of full transformation

acceleratedly, though the process is slowed down sharply by the end of transformation. Thus, the actual volume rate of transformation at constant temperature varies in the process of the transformation proper. At any time the actual volume rate of transformation can be determined graphically by slope of the angle made by a tangent to the kinetic curve.

The low volume rate in the starting period of transformation can be explained by a small number of transformation nuclei that have formed and still low surface area of the new structural component. The number of nuclei gradually increases, as also do the surface area of the new component and the total surface area

of the crystallization front, so that the volume rate of transformation, being proportional to the latter, also increases.

This rate cannot, however, increase continuously as the time of isothermal holding increases. The process inevitably slows down, especially markedly by the end of the transformation, which can be explained by the fact that growing crystals being to interfere with one another and their growth comes to an end in points of contact, i.e. the surface area of the transformation front  $s_r$  gradually decreases. The actual volume rate attains its maximum at the inflection point of the kinetic curve, i.e. when roughly half of the volume has undergone transformation. Then it should be clear why each degree of undercooling in the discussion above has been characterized by an average rate of transformation (see Fig. 73).

A mathematical analysis of the kinetics of phase transformations, which has been made by A. N. Kolmogorov and I. L. Mirkin,

gives the following relationship of the transformed volume and transformation time  $\tau$  at constant values of  $N$  and  $G$ :

$$V(\tau) = V_0 \left[ 1 - \exp \left( - \frac{\pi N G^3 \tau^4}{3} \right) \right] \quad (29)$$

where  $V_0$  is the starting volume of the initial phase.

Graphically, the formula can be expressed by a curve, such as curve 1 in Fig. 79. It has been derived under an assumption that crystals of the new phase are spherical as long as they grow freely (i.e. before contacting one another).

At the very beginning of isothermal holding, no transformation is observed (section *oa* in Fig. 79). This period is called the *induction period*. It was thought formerly that no transformation actually occurred during the induction period, except that the initial phase was being prepared internally to form crystallization nuclei. As has been shown later by mathematical analysis of transformation kinetics and by careful experiments, the transformation starts from the very instant as the isothermal holding begins, but the number of new crystals that form during the induction period is so small that the common methods of investigation fail to detect any transformation whatsoever. The end of the induction period (point *a* in Fig. 79) is conditionally taken as the onset of the transformation as detected by a given method. Thus, more sensitive methods of investigation can reveal the appearance of a new structural component at an earlier time.

The degree of transformation during the induction period is so low that it is usually disregarded in practice. In that connection we may implicate, when speaking about the end of the induction period as of the moment when the transformation starts practically, that a certain amount of the new structural component has already formed by that moment. For instance, the beginning of eutectoid transformation in steel is conditionally fixed at the moment when 0.5 to 1.0 per cent of the pearlite has already formed.

Kinetic curves for various degrees of undercooling and overheating are shown in Figs. 80 and 81. In accordance with the relationships shown graphically in Figs. 71 and 73, an increase in the degree of undercooling causes initially a decrease of both the induction period ( $oa_1 > oa_2 > oa_3$  in Fig. 80) and the time of full transformation ( $ob_1 > ob_2 > ob_3$ ). An explanation is that the initial phase state becomes less stable. At a definite degree of undercooling, the induction period decreases to its minimum ( $oa_3$ ). A further increase in the degree of undercooling increases both the induction period ( $oa_3 < oa_4 < oa_5$ ) and the time of full transformation ( $ob_3 < ob_4 < ob_5$ ), owing to a lower mobility of atoms.

With increasing degree of overheating (Fig. 81), both the induction period and the time of full transformation diminish pro-

gressively ( $oa_1 > oa_2 > oa_3 > oa_4 > oa_5$  and  $ob_1 > ob_2 > ob_3 > ob_4 > ob_5$ ), since the mobility of atoms increases along with a reduction of the thermodynamic stability of the initial phase state (see also Fig. 74).

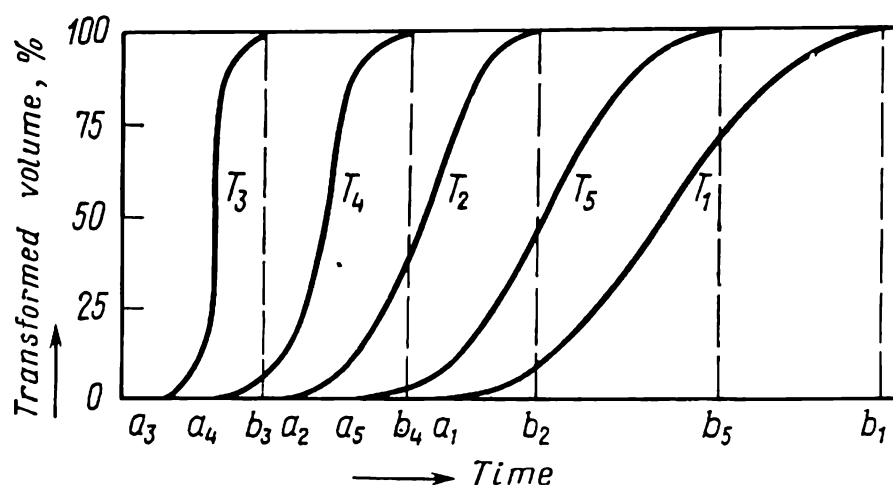


Fig. 80. Kinetic curves for various degrees of undercooling:  $T_1 > T_2 > T_3 > T_4 > T_5$

Many practical problems of heat treatment can well be solved without constructing kinetic curves. It suffices to know the induction period and the time of full transformation at various temperatures. These parameters serve as coordinates for a *diagram*

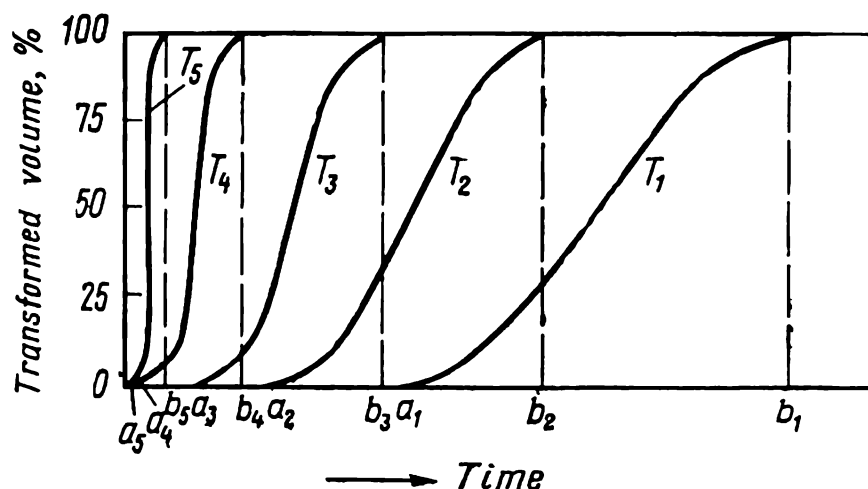


Fig. 81. Kinetic curves for various degrees of overheating:  $T_1 < T_2 < T_3 < T_4 < T_5$

of isothermal transformation. An example is the diagram in Fig. 82a, which has been plotted for undercooling of the metal on the basis of the kinetic curves in Fig. 80. The horizontal sections drawn from the axis of ordinates to points  $a_1, b_1, a_2, b_2$ , etc. in Fig. 82a are proportional to the sections  $oa_1, ob_1, oa_2, ob_2$ , etc. in Fig. 80.

To construct a diagram of isothermal transformation, we have to determine experimentally the induction period and the time of full transformation for an array of temperatures. To do this, a specimen heated to a temperature above  $T_0$  is quickly transferred

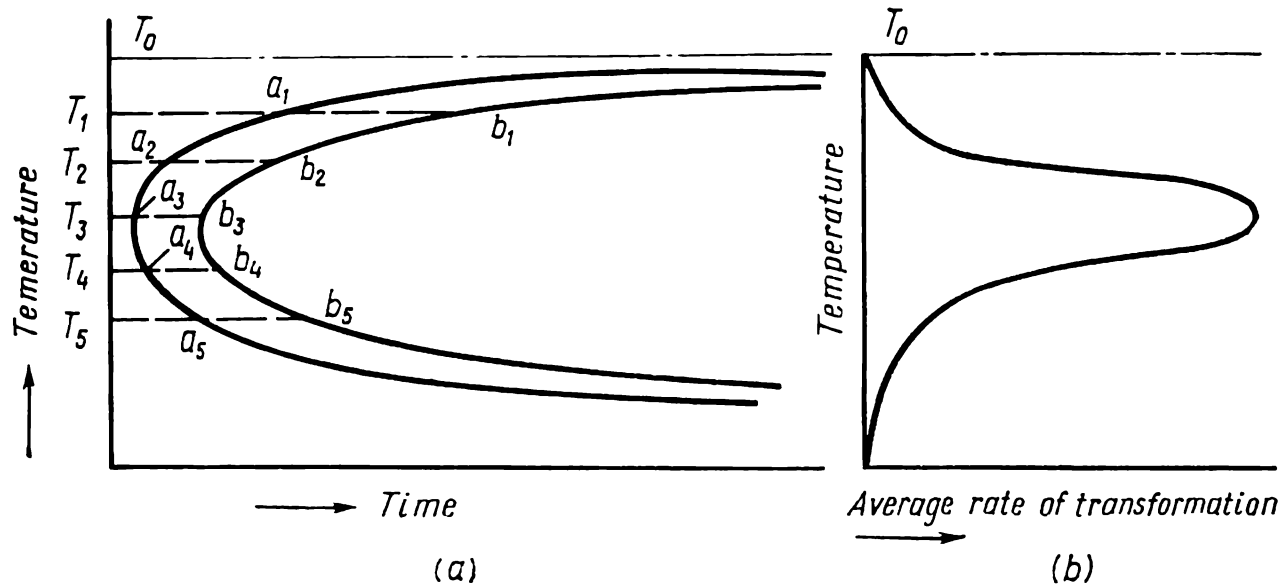


Fig. 82. Diagram of isothermal transformation on undercooling (a) and effect of undercooling on average rate of transformation (b).  $T_0$  — phase equilibrium temperature

to a thermostat kept at a temperature below  $T_0$ ; we then have to fix the time when a new structural component just appears in the metal and the time when the rest of the initial structure fully disappears.

The left-hand curve ( $a_1a_2a_3a_4a_5$ ) in Fig. 82a is the curve of the beginning of the transformation; it shows how the induction period depends on the degree of undercooling. The right-hand curve ( $b_1b_2b_3b_4b_5$ ) represents the end of the transformation and gives the dependence of the time of full transformation on the degree of undercooling. The two curves are called *C-curves*. The bend of a C-curve corresponds to the maximum of the transformation rate (Fig. 82b).

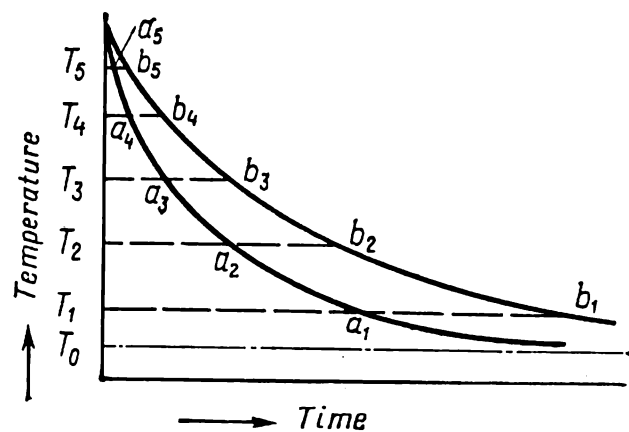


Fig. 83. TTT-diagram on overheating  
 $T_0$ —phase equilibrium temperature

A diagram of isothermal transformation on overheating is shown in Fig. 83 (compare with the kinetic curves in Fig. 81). The curves  $a_1a_2a_3a_4a_5$  and  $b_1b_2b_3b_4b_5$  show the beginning and the end of the transformation as detected by a given method. At suf-

ficiently high temperatures, transformations occur practically instantaneously, so that both curves merge with each other and with the axis of ordinates.

The first diagram of this kind was constructed by E. C. Bain and E. S. Davenport in 1930 for the isothermal decomposition of austenite in steel. Diagrams of isothermal transformation, also called *TTT-diagrams* or C-curves, proved exceptionally meaningful in the theory of heat treatment for studying the kinetics of phase transformation. The number of published TTT-diagrams for the undercooled phase in steels amounts to  $10^3$ , that for titanium

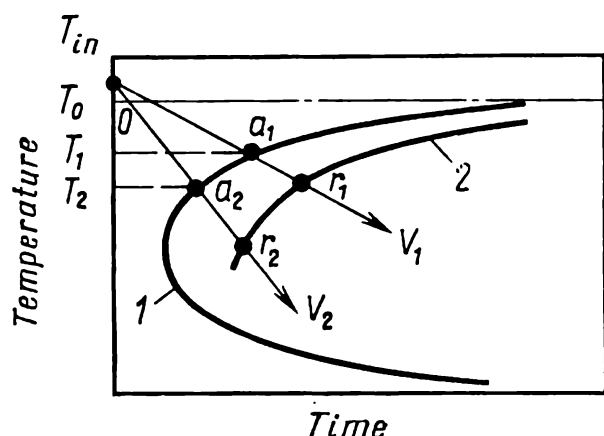


Fig. 84. Curves of the beginning of transformation in an undercooled phase (1) under isothermal conditions and (2) on continuous cooling

alloys, to  $10^2$ , and that for aluminium alloys, to  $10^2$ . TTT-diagrams are also available for cast irons and some copper, uranium and other alloys.

The wide application of TTT-diagrams is bolstered by the fact that they are plotted in the same time-temperature coordinates as the conditions of heating and cooling in heat treatment.

TTT-diagrams are especially suitable for analysing various kinds of isothermal treatment, including rapid cooling

and holding at a constant temperature, for instance, isothermal annealing or isothermal quenching (see 2.2.3 and 3.2.9). A TTT-diagram can be used to determine the time of the beginning and end of transformation of an undercooled phase at a given temperature and to select accordingly the conditions of isothermal treatment.

For analysis of phase transformations occurring under conditions of continuous cooling (such processes prevail in the practice of heat treatment), TTT-diagrams turn to be less convenient and provide only certain qualitative conclusions. For example, curve 1 in Fig. 84 indicates the onset of the transformation of undercooled  $\beta$ -phase under isothermal conditions, and curves  $v_1$  and  $v_2$  relate to two different modes of continuous cooling. If we assume that points  $a_1$  and  $a_2$  determine the onset of the transformation on continuous cooling, then, as can be clearly seen from the figure, a higher cooling rate ( $v_2$ ) implies that the transformation begins at a higher degree of undercooling ( $T_0 - T_2 > T_0 - T_1$ ).

This conclusion is true only qualitatively. In quantitative terms, however, it is impossible to determine the transformation onset



on continuous cooling by the intersection of the cooling curve with a *C*-curve plotted for isothermal conditions. The point is that the induction period  $oa_1$  has been found for a specimen held isothermally at  $T_1$ . However, we are now interested in a specimen cooled continuously by mode  $v_1$ . During the induction period this specimen was held at varying temperatures above  $T_1$ . However, at higher temperatures the transformation during the induction period proceeds more slowly than at  $T_1$ . Consequently, on attaining  $T_1$ , the degree of undercooling for a continuously cooled specimen must be lower than for the one held at  $T_1$  under isothermal conditions. For that reason, the temperature of the fixed onset of transformation for the specimen cooled continuously along  $v_1$  must be below the temperature  $T_1$ , which is determined by the intersection of the cooling curve with the *C*-curve constructed for isothermal conditions.

Quantitative analysis of transformation on continuous cooling should be made by using another type of diagram, called the continuous cooling transformation (CCT) diagram.

*CCT-diagrams* are obtained by recording the temperature during continuous cooling of a specimen. The record may be made, for instance, by means of an oscillograph. It is also possible to measure some or other characteristic of a specimen during cooling (for instance, its length by dilatometric method) and determine the onset of transformation by an abrupt deviation of the characteristic from a smooth variation.

By another method, a group of specimens are cooled under similar conditions and then quenched in water at different instants of time, after which their structure and properties are studied to determine the beginning and end of the transformation (or a given degree of transformation) under the same conditions of continuous cooling. For instance, points  $r_1$  and  $r_2$  determine the beginning of the transformation respectively at a cooling rate  $v_1$  and  $v_2$  (Fig. 84). The corresponding curve 2 in Fig. 84 gives the beginning of the transformation on continuous cooling at different cooling rates. This curve is a variety of CCT-diagram. Similarly, we can construct in the same diagram the curves of the end of transformation and the curves corresponding to a definite degree of transformation for different rates of continuous cooling.

The difference in the positions of the lines on a CCT-diagram and on a TTT-diagram (though the lines have the same sense), may be either appreciable, as is the case with steels, or insignificant, as is the case with duralumins. One cannot predict how large this difference will be. The methods that have been proposed for recalculating from TTT- to CCT-diagrams are suitable only for rough estimations. Thus, it is only advisable that both

types of diagrams should be constructed for industrial alloys, though the construction of CCT-diagrams encounters certain difficulties. The experience of using TTT-diagrams alone shows, however, that these enable a more substantiated selection of the conditions of heat treatment and can be used successfully for analysing the causes of rejects. Needless to say that their scientific value can hardly be overestimated.

#### LITERATURE

Physical Metallurgy. Ed. by R. W. Cahn. Amsterdam, North-Holland, 1965, 1100 pp.

Blanter M. E. Phase Transformations in Heat Treatment of Steels (*Fazovye prevrashcheniya pri termicheskoi obrabotke stali*). Moscow, Metallurgizdat, 1962, 268 pp.

Christian J. W., The Theory of Transformations in Metals and Alloys. 2nd ed., part I. Oxford, Pergamon Press, 1975.

## 2.2. ANNEALING OF STEELS

### 2.2.1. FORMATION OF AUSTENITE ON HEATING

#### The Mechanism and Kinetics of Austenitization

The initial structure in carbon steel prior to annealing is most often a ferrite-carbide mixture. As may be seen from the Fe-C constitutional diagram (Fig. 85), the principal transformation that can take place on heating is the transformation of pearlite into austenite at temperatures above the  $A_1$  point (727°C).

The passage of pearlite into austenite and its kinetics follow the principal laws governing phase transformations on heating.

As was found experimentally, austenitic nuclei form at boundaries between ferrite and cementite. The initial stages of their nucleation have not been studied experimentally and there only are some theoretical suppositions. The  $\alpha_{b.c.c.}$  to  $\gamma_{f.c.c.}$  transformation in pure iron is only possible at temperatures not below 911°C. If ferrite is in contact with cementite, then, as follows from the constitutional diagram, the  $\alpha \rightarrow \gamma$ -transformation must proceed at temperatures starting from 727°C. At a temperature slightly above  $A_1$ , austenite contains around 0.8 per cent C, while ferrite in steel contains only a few hundredths of a per cent of carbon. A question then arises: how a portion of the f.c.c. phase and a relatively high content in carbon can form in the metal?

Most of the hypotheses of austenitic nucleation proceed from fluctuational concepts, with two extreme cases being formally considered. In the first case, one may assume that concentration fluctuations are the basis for the nucleation of austenite. The probability of the formation of an appreciable number of fluctuation

portions of the critical size in ferrite is negligible, since there are very few carbon atoms. At a boundary between ferrite and cementite, the two phases continuously interchange atoms (a dynamic equilibrium exists), and the boundary layer of ferrite has a much greater probability for the appearance of a portion of the critical size with a concentration of around 0.8 per cent C by fluctuation.

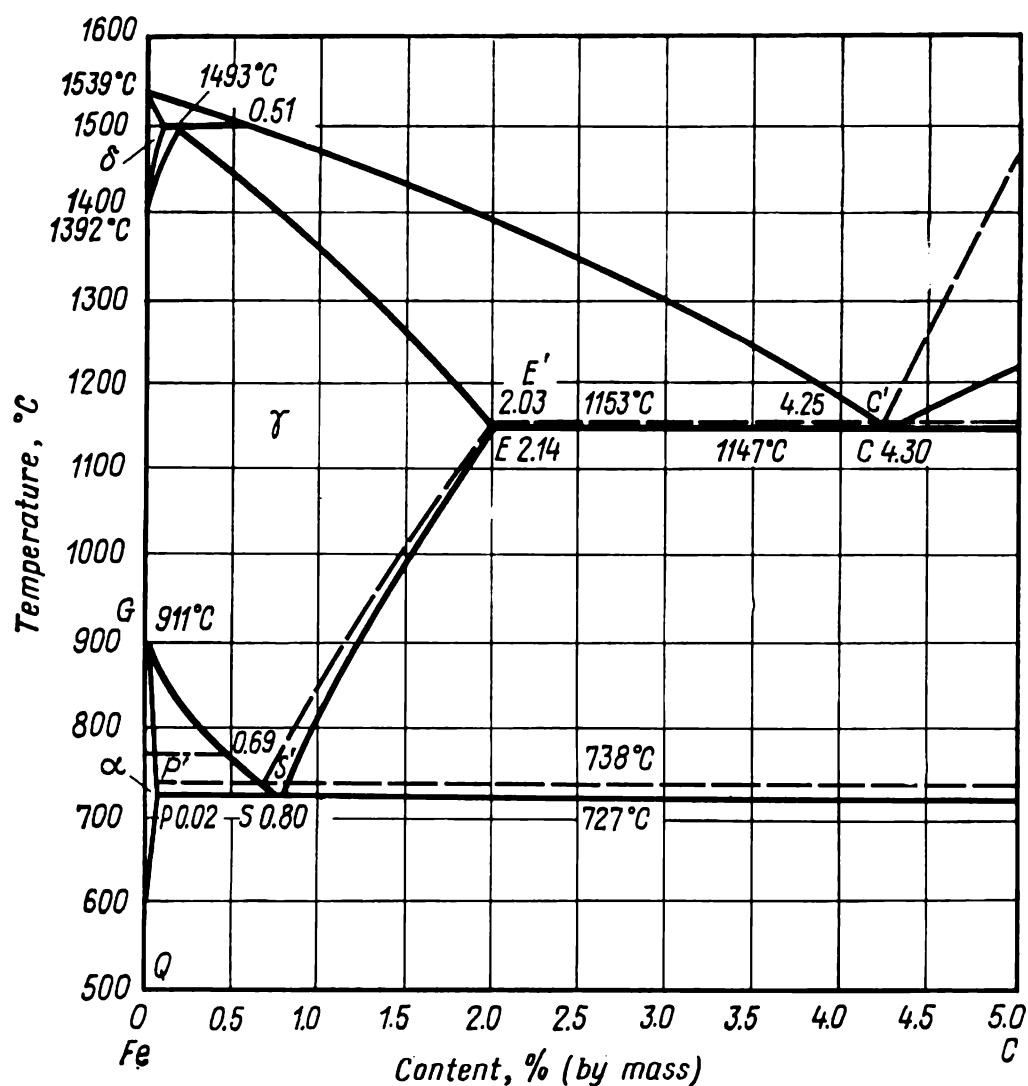


Fig. 85. Fe-C constitutional diagram

With any overheating above  $A_1$ , be it however small, these portions undergo the polymorphic  $\alpha \rightarrow \gamma$ -transformation in the solid solution and become stable nuclei for growth of austenitic grains. Such portions can also form in ferrite below  $A_1$ , but they cannot be stable nuclei for growth of austenite, since the  $\gamma$ -lattice is thermodynamically unstable.

Another hypothesis states that fluctuational rearrangement of the lattice, rather than concentration fluctuations, is of primary importance in austenitic nucleation. Portions of  $\gamma$ -lattice of fluctuational origin continuously appear and disappear in ferrite. At a boundary with cementite and at temperatures above  $A_1$ , these

portions absorb the carbon from carbides and, if their size is not less than the critical, become stable nuclei for growth of austenite.

The formation of austenite at an interface between ferrite and cementite can also be favoured by an established fact that the critical size of nuclei of the new phase is smaller here (see 2.1.3).

The picture of growth of austenitic nuclei is more clear. Consider an isothermal pearlite-to-austenite transformation at a temperature  $T_1$  (Fig. 86). As follows from the constitutional diagram,

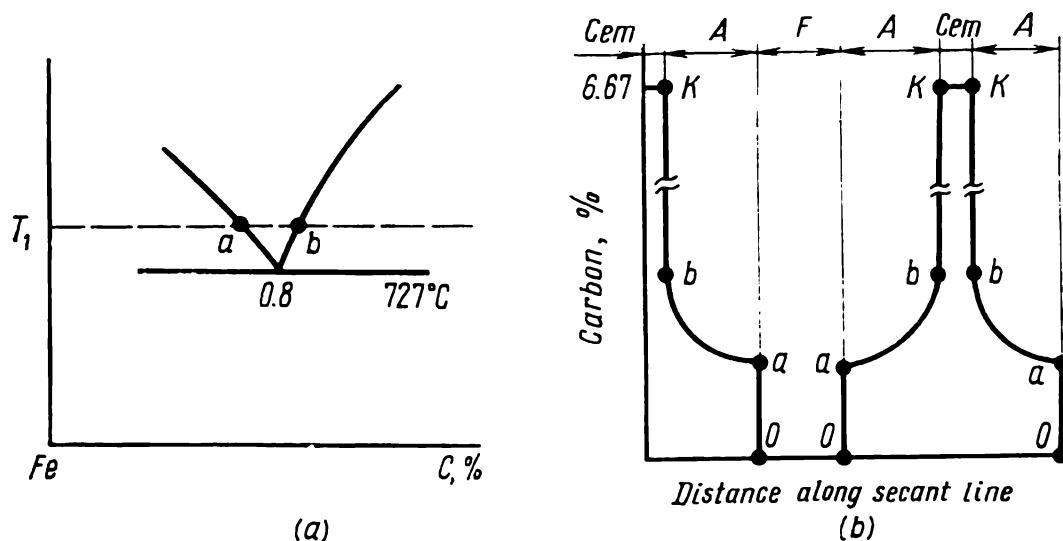


Fig. 86. A portion of Fe-C constitutional diagram (a) and diagram of carbon distribution in austenite during pearlite-to-austenite transformation at temperature  $T_1$  (b)

the equilibrium concentration of austenite at that temperature at a boundary with ferrite can be depicted by point  $a$  and that at the boundary with cementite, by point  $b$ . A concentration gradient  $ab$  then establishes inside an austenitic grain (Fig. 86b). There is a large jump of carbon concentration  $bK$  at the austenite-cementite boundary and a lower jump  $oa$ , at the boundary with ferrite (the carbon concentration in ferrite is taken equal to zero in our diagram).

The rate of isothermal growth of austenitic grains is controlled by diffusion of carbon from an austenite/cementite to austenite/ferrite boundary. The equalizing diffusion lowers the carbon concentration in the austenite at the austenite/cementite boundary by shifting the composition of austenite to the left of point  $b$  in Fig. 86a. This makes the austenite undersaturated relative to cementite; the latter dissolves and restores the equilibrium concentration of point  $b$ . At the boundary with ferrite, the equalizing diffusion increases the carbon concentration in the austenite by shifting the concentration line to the right of point  $a$  in Fig. 86a. The austenite then becomes undersaturated relative to ferrite, dissolves the latter and increases its iron concentration to the equi-

librium composition of point *a*. Thus, an austenitic grain can grow towards both ferrite and cementite.

The rate of motion of a boundary between two phases when one of the phases grows at the expense of the other is inversely proportional to the concentration jump at the boundary (the concentration of the element in the increased volume must change exactly by the magnitude of that jump). Since the concentration jump at the austenite-ferrite boundary is roughly an order of magnitude smaller than that at the austenite-cementite boundary ( $oa \ll bK$ ), the rate of growth of austenitic grain towards ferrite is much greater than that towards cementite. As a result, undissolved cementite always remains in the metal to the moment when ferrite interlayers in pearlite disappear. The pearlite-to-austenite transformation proper comes to its end just when these ferrite interlayers vanish and after that only the dissolution of the remaining cementite takes place. Upon the dissolution, the austenite will have a non-uniform concentration of carbon, with a higher concentration in the sites formerly occupied by cementite. Thus, an additional time is required after the transformation in order to equalize the composition of the austenite.

If free excess ferrite is present in the initial structure, the boundaries of austenitic grains will move towards it. But the size of grains of free ferrite is one or two orders of magnitude greater than the thickness of ferritic interlayers in pearlite. Owing to this, the time for full disappearance of free ferrite exceeds that required for removal of the rests of pearlite. When the free ferrite has disappeared, the austenite has a lowered carbon concentration in sites where its grains were present, and the composition of austenite in its grains gradually equalizes.

The kinetics of formation of austenite can be represented by a TTT-diagram (Fig. 87) similar to the diagram in Fig. 83. A difference between the two diagrams is in that, as has been shown experimentally, the pearlite-to-austenite transformation begins just at the passage through the temperature of phase equilibrium, i.e. the line of the beginning of the transformation actually merges with the horizontal line at the temperature of three-phase equilibrium (727 °C). This may be attributed to the fact that austenite can form easily at ferrite-carbide boundaries in the  $\alpha \rightarrow \gamma$ -rearrangement discussed above. This does not contradict the general theory of phase transformations, since a phase transformation can principally proceed at any, however small, degree of overheating above the equilibrium temperature. Melting of crystals is a well-known example of a phase transformation in which the degree of overheating is practically zero.

Various stages of austenitic nucleation come to the end earlier with rising temperature (see curves 1-5 in Fig. 87).

The rate of all diffusion-induced processes of austenitization is proportional to the coefficient of diffusion of carbon in austenite and the concentration gradient,  $\frac{C_b - C_a}{X}$  where  $X$  is the cross-sectional area of a growing austenitic grain and  $C_a$  and  $C_b$  are carbon concentrations in points  $a$  and  $b$  in Fig. 86. As the temperature increases the diffusion coefficient increases exponentially and the concentration gradient  $C_b - C_a$  increases too, following the divergence of lines  $GS$  and  $SE$  in the Fe-C constitutional dia-

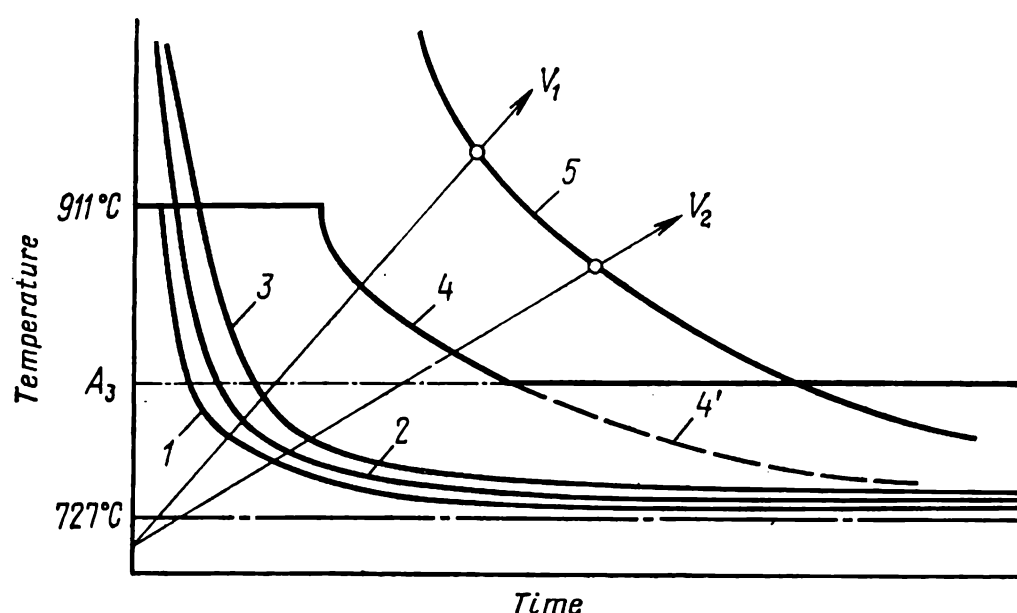


Fig. 87. TTT-diagram for austenite in hypoeutectoid steel (after I.N. Kidin and M. A. Stremel):

1—disappearance of ferritic interlayers in pearlite; 2—disappearance of cementite; 3—end of homogenization of austenite in sites of former pearlite nodules; 4—disappearance of free ferrite; 4'—end of passage of free ferrite into austenite at temperatures below  $A_3$ ; 5—end of homogenization of austenite

gram. Besides, at higher temperatures the concentration jump at austenite-ferrite boundaries decreases (since the conodes connecting  $GP$  and  $GS$  lines becomes shorter), which also accelerates the growth of austenite at the expense of ferrite.

In continuous heating, a higher heating rate increases the temperature of the end of formation of austenite and the temperature of homogenization in the austenite (see the points of intersection of the heating curves  $v_1$  and  $v_2$  with the lines of the diagram in Fig. 87;  $v_1 > v_2$ ). Quantitative data for continuous heating can be obtained by constructing a corresponding CCT-diagram.

With higher dispersity of the initial structure, the time of the end of all stages of austenitization becomes shorter. This is due to shorter paths that the growing austenitic grains have to travel and also to a higher gradient of carbon concentrations in the

austenite, since the same maximum difference of concentrations, say,  $C_b - C_a$ , relates to a shorter length of travel.

In carbon steels, the processes of formation and homogenization of austenite occur quite quickly. With furnace heating, the time of holding is usually greater than the time required for homogenization, which is at most a few minutes (including all the stages of austenitization) at common temperatures of heating.

In alloy steels, homogenization of austenite requires appreciably more time. Alloying elements are distributed non-uniformly between ferrite and carbides. Non-carbide-forming elements are present in ferrite, while those that form carbide, predominantly in carbides. The austenite formed upon pearlite-to-austenite transformation has non-uniform concentrations of carbon and alloying elements, in particular in places formerly occupied by particles of ferrite and carbides.

The rate of diffusion of most alloying elements is a few orders of magnitude less than that of carbon diffusion. That is why the austenite remains non-uniform for an appreciably long time upon pearlite-to-austenite transformation; the difference in concentrations of an alloying element then preserves a difference in carbon concentration.

The austenitization processes just discussed play an important part in high-speed induction heating of steel, where the time the metal is held within the austenitization temperature range is very short.

### The Size of Austenitic Grains

The boundaries between ferrite and carbides have an extended surface, because of which a large number of austenitic nuclei form at them and the austenite formed through transformation is quite fine-grained. The more disperse is the initial structure, the finer will be the austenitic grain.

With increasing temperature, the rate of nucleation of austenitic grains increases more intensively than the linear rate of their growth, resulting in a finer grain formed upon austenitization. Therefore, by heating quickly to a high temperature and holding for only a short time at that temperature, it is possible to obtain fine-grained austenite, which is of high importance for methods of heat treatment involving accelerated heating.

Austenitic grains formed upon austenitization are capable of further growing, the driving force of this process being the free energy of grain boundaries. An increase of temperature accelerates the growth of austenitic grains. They may grow either continuously, as in grain growth, or discontinuously, with a small

number of large grains growing at the expense of many fine grains until the latter disappear. The process is essentially secondary recrystallization (see 1.2.7). Fine austenitic grains cannot grow, since they are stabilized by disperse particles, in particular, of aluminium nitride.

The specific volume of the metal diminishes upon pearlite-to-austenite transformation roughly by 1 per cent, which causes a slight plastic deformation, or *structural strain hardening*, of the austenite. A. A. Bochvar assumed that structural strain hardening must cause primary recrystallization in austenite. As has been shown by V. D. Sadovsky, the temperature range of primary recrystallization in austenite under the action of structural strain hardening can either overlap the temperature range of austenitization or be shifted above the latter a few tens or hundreds of degrees C.

Primary recrystallization in austenite is of large practical interest when the steel has an ordered initial crystal structure, such as Widmanstätten structure (see 2.2.2) and especially when its structure is martensite or bainite (see 3.2). Air chilling of an alloy steel during casting, welding or hot plastic working can cause the formation of martensite or bainite. In such cases annealing can sometimes involve what is called structural heredity: the austenite that forms inherits the orientation of the initial structure and, if the initial grain has been coarse, the newly formed austenite is also coarse-grained. The austenite, however, has an increased density of stacking faults (owing to structural strain hardening) and possesses a thermodynamic stimulus to primary recrystallization; the latter then starts from many nuclei, refines the austenitic grains and destroys their orientational links with the initial structure.

D. K. Chernov found in 1868 that a coarse-grained steel could be ameliorated by heating it above the *b* point. Chernov's *b* point is usually identified with the  $A_{c3}$  point. However, as follows from the work of V. D. Sadovsky, the famous *b* point, which always corresponds to the temperature of recrystallization and refinement of coarse-grained structure, may either coincide with  $A_{c3}$  or be substantially (sometimes by 200 degrees C) above it, depending on the composition and initial structure of steel. In the latter case, the *b* point corresponds to the temperature of the beginning or primary recrystallization of austenite and the recrystallization proper is naturally the result of  $\alpha \rightarrow \gamma$ -transformation.

The size of austenitic grains is the most important structural characteristic of heated steel. It determines the behaviour of the steel in various operations of heat treatment and mechanical treatment and the mechanical properties of articles made of that steel.



The impact toughness of steel is most sensitive to the size of austenitic grains and falls off as the grain coarsens. The impact toughness of a fine-grained steel can exceed several times that of a coarse-grained steel of the same grade, though the hardness is the same in both.

Fine grain is not always the optimum choice. For instance, a coarser grain of austenite can be advantageous in improving the machinability of steel or reducing the resistance to deformation in cold heading.

As mentioned earlier, the size of austenitic grains depends on the temperature and time of heating, and also on the content of carbon and alloying elements in the steel. Grain growth is facilitated at higher concentrations of carbon in the  $\gamma$ -solution, which can be explained by a lower position of the solidus line of the alloy and a corresponding rise in the homologous temperature at a constant temperature of annealing. Increasing the content of carbon in austenite above the limit concentration ( $ES$  line in the  $Fe-Fe_3C$  constitutional diagram) inhibits the growth of austenitic grains, probably owing to the retarding effect of cementite particles.

Almost all alloying elements act in retarding the growth of austenitic grains, the most effective being V, Ti, Al and Zr, fairly effective, W, Mo and Cr, and only weakly effective, Ni and Si. The sole exception is manganese, which promotes grain growth.

This effect of alloying elements is mainly attributed to the formation of carbides and oxides which are hardly soluble in austenite and serve as barriers to growing grains. Ti, Zr and V, being active carbide-formers, are more effective than Cr, W or Mo in inhibiting grain growth, since their carbides are more stable and less soluble in austenite.

Various melts of the same grade of steel may differ appreciably in their liability to grain coarsening, since they may contain different amounts of microimpurities, carbides oxides, sulphides and nitrides which can inhibit grain growth. Therefore, the susceptibility of a steel to grain coarsening on heating depends not only on the contents of the main components, but also on the metallurgical quality, method of manufacture, etc., that is to say, the prehistory of heat treatment. In that connection a distinction is made between *intrinsically coarse-grained* and *intrinsically fine-grained steels*.

An intrinsically coarse-grained steel shows an intensive grain growth even when heating is done at a temperature only slightly above  $A_{c3}$ . In contrast to it, an intrinsically fine-grained steel can form fine austenitic grain within a wide range of temperatures, from  $A_{c3}$  to 950-1100°C, and becomes overheated upon passage

beyond this temperature threshold. The *overheating*<sup>1</sup> is understood here as an intensive grain coarsening and corresponding loss of impact toughness.

The susceptibility of a steel to grain coarsening is determined by a standard technological test as follows. A specimen of hypoeutectoid steel is cemented at 930 °C for 8 hours and cooled slowly. The size of grains is determined by the carbide network around austenitic grains. With hypereutectoid steels, a specimen is heated at 930 °C for 3 hours and cooled slowly. The size of grains is determined by the network of secondary carbides precipitated at boundaries of austenitic crystals. Another method consists in that a polished microsection is heated at 930 °C for 3 hours in an oxidizing medium. The boundaries of austenitic grains are revealed as a network of oxides. In medium-carbon steels (0.3-0.5 per cent C), the size of austenitic grains can be determined by a network of excess ferrite which forms at grain boundaries upon air cooling of specimen.

Industrial control employs standard grain-size charts; these are compared with microstructures as seen in the microscope at a 100-fold magnification.

In the tests described, the temperature of 930 °C has been chosen on the following basis. For most steels, the temperature of heating in various operations of heat treatment does not exceed 930 °C. On the other hand, an intrinsically fine-grained steel can resist intensive grain growth at that temperature, while an intrinsically coarse-grained steel cannot and becomes really coarse-grained.

Thus, we may distinguish between *intrinsic and actual grain in austenite*. Intrinsic grain forms under the standard conditions of a technological test and characterizes the susceptibility of a steel to grain coarsening. Actual grain is that formed on a particular operation of heat treatment. It may be either larger or smaller than the intrinsic grain, depending on whether the heating temperature in the heat treatment operation was above or below 930 °C.

Aluminium is especially effective in inhibiting grain growth of austenite in steel. An intrinsically fine-grained steel is obtained by adding roughly 0.05 per cent aluminium into the ladle before teeming. Tiniest particles of aluminium nitrides and oxides serve as barriers impeding grain coarsening. An intensive growth of grain in an intrinsically fine-grained steel at temperatures above 950-1100 °C can be explained by dissolution and probably by coagulation of barrier particles.

---

<sup>1</sup> The term should not be confused with the overheating in the theory of phase transformation.

### 2.2.2. DIFFUSION TRANSFORMATIONS IN AUSTENITE ON COOLING

#### Pearlitic Transformation

The principal transformation during cooling of annealed steel is the eutectoid decomposition of the austenite into a ferrite-carbide mixture. The kinetics of eutectoid transformation is depicted by C-shaped curves in a diagram of isothermal transformation of austenite (Fig. 88).

A C-curve can be obtained as follows. Thin specimens of a steel with 0.8 per cent C are heated at a temperature above the  $A_1$  point until full austenitization takes place and then placed quickly into a thermostat (salt bath) kept at a temperature below that point. The beginning and the end of decomposition of austenite at a given temperature can be determined by various methods. The most simple and reliable among them is microstructural analysis, though it is rather laborious. The specimens are taken from the thermostat at different time intervals and quenched in water. The part of the austenite that has not decomposed isothermally then transforms into martensite, which is readily discernible in the microscope from the products of decomposition of austenite.

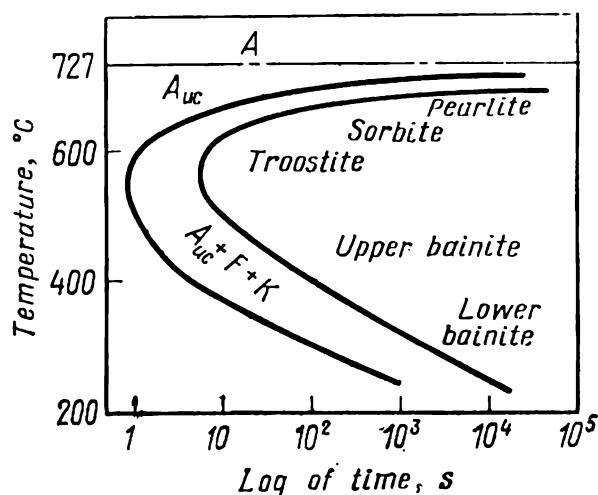


Fig. 88. TTT-diagram for austenite in eutectoid steel

$A$ —stable austenite;  $A_{uc}$ —undercooled austenite;  $F$ —ferrite;  $K$ —carbide

The eutectoid decomposition of austenite increases the specific volume and reduces the electric resistivity of steel and transforms the latter from paramagnetic into ferromagnetic state. Correspondingly, the time of the beginning and end of transformation can be determined by measuring the variations in these properties by dilatometric, electric or magnetic methods. The magnetometric method determines quantitatively the degree of austenitic transformation at any moment of isothermal holding, since the magnetization intensity of a specimen is proportional to the amount of ferromagnetic  $\alpha$ -phase in it (austenite is paramagnetic).

At 727°C ( $A_1$  point), austenite is in a thermodynamically stable equilibrium with ferrite-cementite mixture. To initiate its decomposition, it must be supercooled below that temperature.

The stability of undercooled austenite can be characterized by an induction period, i.e. an interval of time (from the axis of ordinates to the left-hand C-curve in Fig. 88) during which no

products of decomposition can be detected by conventional methods.

In eutectoid steels, undercooled austenite is most unstable at temperatures near 550 °C. These are exactly the temperatures at which the maxima of the nucleation rate and of the rate of growth of eutectoid have been established (see Fig. 71).

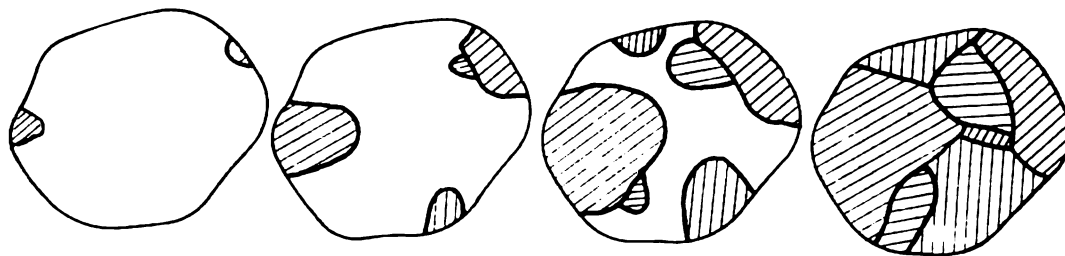


Fig. 89. Formation of eutectoid nodules in an austenitic grain (schematically)

In a eutectoid ferrite-cementite mixture, pearlite grows from individual nuclei and forms nodules (Fig. 89). A *pearlitic nodule* can nucleate at either a cementite or a ferrite particle, cementite

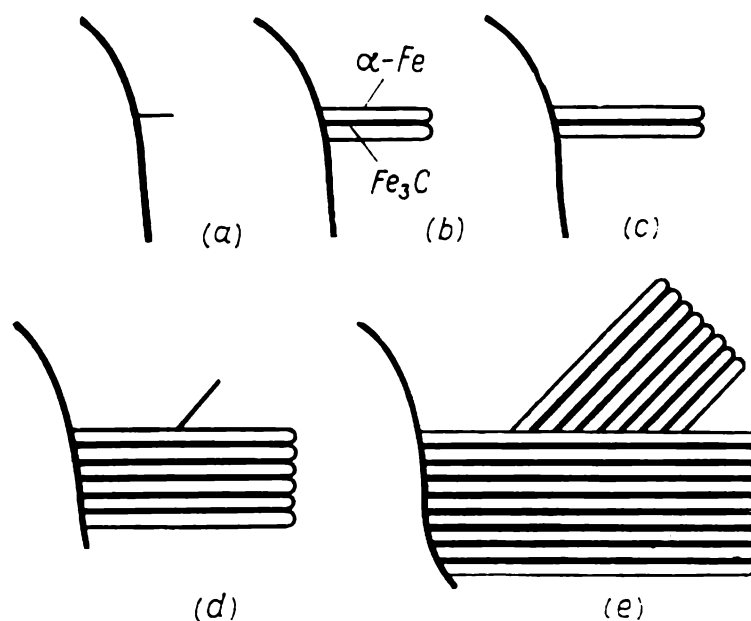


Fig. 90. Nucleation and growth of two pearlitic nodules (after R. F. Mehl and W. C. Hagel)

being more often considered the probable centre of this nucleation. In homogeneous austenite, a cementite nucleus can appear in a portion of fluctuational origin which is rich in carbon. Nucleation is more likely to occur at boundaries of austenitic grains, since the work of formation of critical nucleus is less there (Fig. 90a). When a cementite platelet becomes thicker, the austenite near it is depleted of carbon and the conditions are formed that favour the nucleation of ferrite platelets near that cementite platelet by

means of polymorphic  $\gamma \rightarrow \alpha$ -transformation (Fig. 90b). When, however, a platelet of ferrite (which contains almost no carbon) becomes thicker, the carbon is displaced into the austenite and thus the conditions are favourable for the appearance of more and more cementite platelets, and so on (Fig. 90d).

With a pearlitic nodule growing sideways, it is principally possible that ferrite and cementite platelets will alternately form repeatedly on the substrate, and also that freshly formed platelets will branch off from the earlier ones of the same phase. In micro-

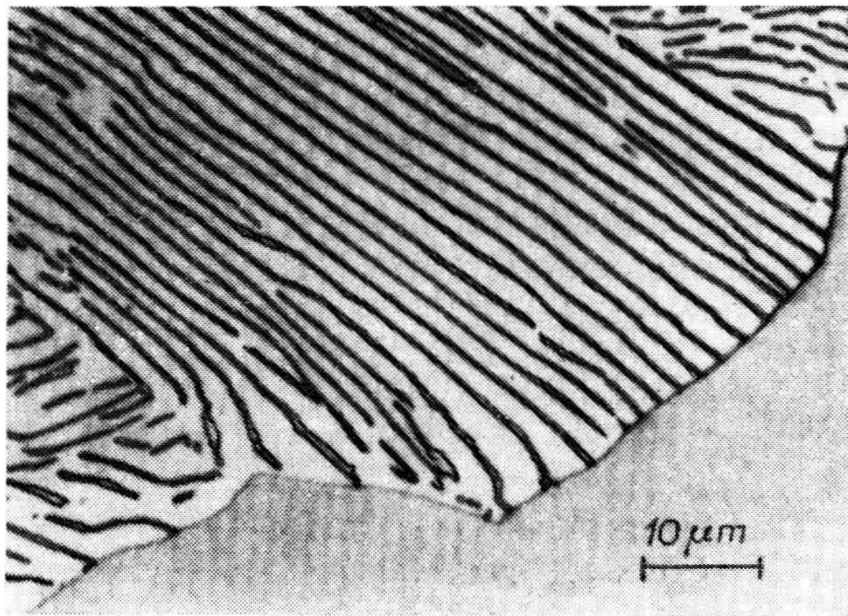


Fig. 91. Structure of pearlite at a nodule boundary (after L. S. Darken)

sections, cementite in pearlitic nodules is seen as an array of isolated plates without lateral ties (Fig. 91), but this plane picture does not necessarily imply that cementite has no spatial structure. There is reliable experimental evidence that a eutectic nodule is most often a bicrystal of mutually tangled dendrites of two phases, though one of the phases of the eutectic may be seen in microsections as isolated inclusions in the matrix. According to some data, each of the two phases in a eutectic nodule (pearlite) is also continuous, and therefore, as a nodule is growing sideways, its phases branch off rather than nucleate repeatedly.

If a platelet of a different orientation branches off from a nodule (or nucleates at the surface of that nodule), it can serve as a nucleus for a new pearlitic nodule (see Fig. 90d and e).

Ferrite and cementite platelets can grow at their ends (see Fig. 90b and c), as well as sideways. The concentration of carbon in the austenite at the ends of growing ferrite and cementite platelets is respectively increased or reduced from its mean value,

i.e. there are concentration gradients parallel and perpendicular to the transformation front (when only one phase is growing, there only is a concentration gradient perpendicular to the transformation front). The growth of pearlitic nodules is controlled by diffusion redistribution of carbon parallel to the transformation front in the volume of austenite and directly at boundaries of pearlitic nodules. The cooperative growth of a two-phase nodule by diffusion redistribution of the components is the most specific feature of pearlitic transformation.

The rate of growth of a nodule and the *interplate spacing* (the total thickness of a ferrite and a cementite platelet, or the distance between centres of two closest like platelets) are constant at a given degree of undercooling of austenite.

By an assumption, the thickness of platelets is controlled by the factors as follows:

(a) with thinner platelets of both phases, the paths of carbon diffusion at the transformation front are shorter, and therefore, redistribution of carbon, which is needed for cooperative growth of a nodule, can occur in a shorter time;

(b) with thinner platelets, the total surface area of their interfaces is greater, which diminishes the difference  $\Delta F_v - \Delta F_s$ , i.e. the resulting driving force of the transformation. The interplate spacing that establishes at a given degree of undercooling, i.e. at a given difference in free energies of austenite and pearlite ( $\Delta F_v$ ), is such that the rate of growth, which is controlled by the above factors, is at its maximum.

As the degree of undercooling,  $\Delta T$ , is increased,  $\Delta F_v$  also increases; this results in a greater extension of ferrite-cementite interfaces and consequently, in smaller interplate spacings in pearlite.

Pearlitic nodules can grow with relatively high rates at any degree of undercooling, which is favoured by the low interface energy at boundaries between ferrite and cementite platelets, since the principle of structural correspondence is observed here. The platelets are matched with one another with their  $(101)_{cem}$  and  $\{112\}_f$  or  $(001)_{cem}$  and  $\{125\}_f$  faces. The corresponding crystal planes in the lattices of ferrite and cementite are very similar in structure. This mutual orientation, which is favourable for cooperative growth, can probably form already during epitaxial nucleation of one phase at the other (see Fig. 90a).

There is a different view on the initial stage of nucleation of pearlitic nodules, which denies successive formation first of one and then of the other phase in nucleation, but states that the two phases simultaneously develop into a regular structure of alternate platelets whose cooperative growth is essentially the pearlitic transformation proper.

The interplate spacing in pearlite is the most important structural characteristic. When it diminishes, the strength properties of a steel increase.

If austenite decomposes in eutectoid steel within a temperature range from  $A_1$  down to approximately 650 °C, it forms pearlitic nodules with an interplate spacing of 0.5-1  $\mu\text{m}$ , the two-phase structure of these nodules being readily visible at moderate magnifications of the optical microscope. The eutectoid formed is called

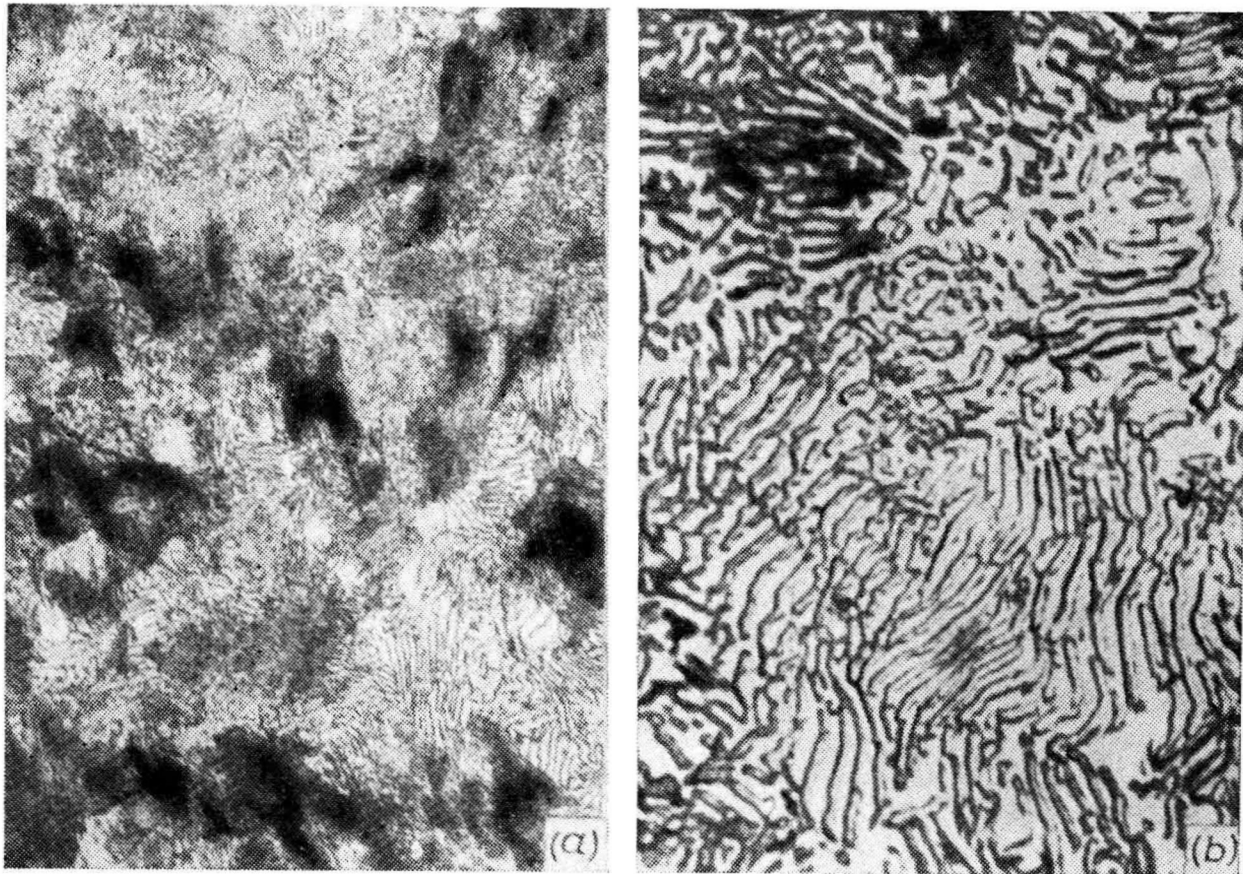


Fig. 92. Lamellar pearlite in eutectoid steel  
 $a - \times 200$ ;  $b - \times 1200$

*pearlite* (Fig. 92). With decomposition taking place within a range of 650-600 °C, the nodules formed have an interplate spacing of only 0.4-0.2  $\mu\text{m}$  and their two-phase structure can be resolved only at very large magnifications (recall that the maximum resolution of the optical microscope is roughly 0.2  $\mu\text{m}$ ). This eutectoid has been named *sorbite*. Finally, if decomposition occurs at 600-500 °C, it gives a very fine eutectoid mixture with the interplate spacing of roughly 0.1  $\mu\text{m}$ ; this is called *troostite*. The two-phase structure of troostite can only be revealed by electron microscopy.

These structures can form in a continuously cooled eutectoid carbon steel under the following conditions: (a) pearlite — on



cooling from the austenitic state in the furnace at a rate of a few degrees C per minute; (b) sorbite — on air cooling at a rate of a few ten degrees C per minute and (c) troostite — on oil cooling at a rate of a few ten degrees per second.

The hardness of pearlite, sorbite and troostite in steel with 0.8 per cent S is respectively 170-230 HB, 230-330 HB and 330-400 HB.

The division of pearlitic structures into pearlite proper, sorbite and troostite, though being out of date and rather conditional, is still used extensively, especially in the practice of heat treatment of steels.

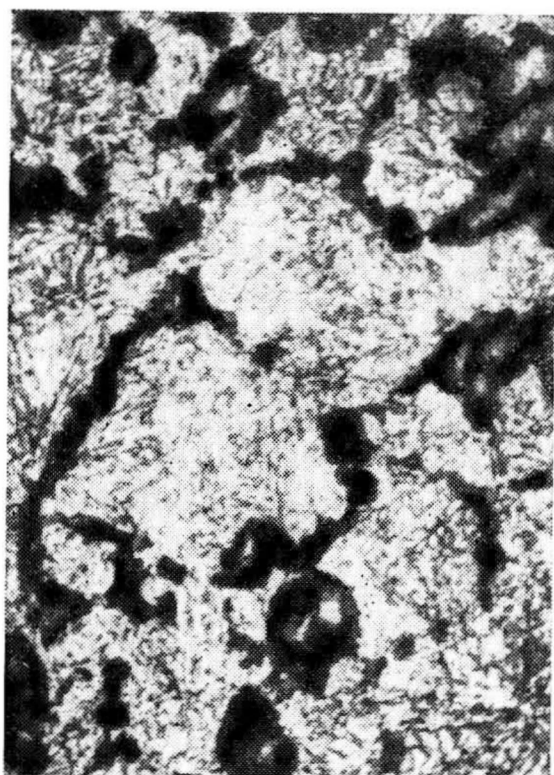


Fig. 93. Troostitic spherulites (dark) in martensite,  $\times 300$

The pearlitic transformation in eutectoid steel in the range from  $A_1$  to temperatures near the bend ('nose') of the C-curve (see Fig. 88) involves diffusion decomposition of austenite. Below the bend of C-curve, within temperatures of roughly 500-250 °C, another type of transformation, namely bainitic transformation, takes place, which is an intermediate type between pearlitic and martensite and accordingly will be discussed after martensitic transformation (see 3.2.7).

Apart from the interplate distance in pearlitic nodules, another structural characteristic of importance is the size of nodules. In fracture of steel, these nodules behave as individual grains. The size of facets in a fracture is approximately equal to the size of pearlitic nodules. Diminishing the size of pearlitic nodules (which are also called *eutectoid grains*) increases the impact toughness of steel.

The size of nodules depends on G/N ratio. With greater undercooling of austenite, the rate of nucleation of pearlitic nodules increases more than the linear rate of their growth and the size of nodules decreases.

The rate of nucleation of centres of eutectoid decomposition is a structurally sensitive characteristic, while the linear rate of growth is only weakly sensitive to structural inhomogeneities. As has been given earlier, pearlitic nodules nucleate predominantly at boundaries of austenitic grains. The shape of nodules growing



at one or both sides of a boundary between austenitic grains is nearly hemispherical or spherical (Fig. 93). The smaller is the size of austenitic grains, the greater is the total area of interface and therefore, the greater is the total number of nuclei of pearlitic transformation.

Pearlitic nodules can also nucleate inside austenitic grains: at carbide particles and in sites of uneven carbon concentration formed through incomplete homogenization of the austenite in the pearlite-to-austenite transformation. An increase of temperature in the austenitic range increases the size of grains and makes the austenite more homogeneous, which results in a smaller number of nuclei of pearlitic transformation and the formation of larger pearlitic nodules. This produces a smaller interplate spacing in the pearlite, since homogeneous and coarse-grained austenite is undercooled to a greater extent.

### Austenitic Transformation in Hypoeutectoid and Hypereutectoid Steels

In the preceding section we have discussed the austenitic transformation in steels of eutectoid composition. In hypo- and hypereutectoid steels, the pearlitic transformation should be preceded with precipitation of excess phases: ferrite and secondary cementite (see Fig. 85). Thus, the diagrams of isothermal transformations of austenite in hypo- and hypereutectoid steels must be complemented with lines at which the excess phases start to form (Fig. 94).

With continuous cooling, excess ferrite begins to form on undercooling the austenite below the  $A_3$  point and continuous to nucleate and grow to a temperature below the  $A_1$  point. During the growth of ferrite, carbon is accumulated in the austenite before the transformation front, since ferrite is almost free of carbon. At temperatures below  $A_1$ , cementite crystals can nucleate in these carbon-rich portions of the austenite, and therefore, pearlitic nodules can form. For this to occur, the composition of the austenite need not reach the concentration of 0.8 per cent C. Pearlite (sorbite or troostite) formed from austenite with less than 0.8 per cent C has a larger proportion of ferritic interlayers. This eutectoid, in which the content of iron is above the equilibrium concentration of the eutectic point, has been called *quasi-eutectoid* by A. A. Bochvar. Quasi-eutectoid in hypereutectoid steels is richer in carbon compared with the composition of point S.

The rate of cooperative growth of a two-phase nodule, which is due to short-range diffusion parallel to the transformation front (in contrast to long-range diffusion perpendicular to the transformation front in the growth of excess ferrite) is rather

high, so that the pearlitic transformation spreads quickly over the whole volume of austenite. The excess ferrite practically stops to form as soon as the pearlitic transformation has begun.

The relative amount of a structurally free excess phase depends on the degree of undercooling of austenite. Figure 95 shows the structures of steel with 0.6 per cent C obtained at different degrees of undercooling. As the cooling rate increases, the amount of excess ferrite that has time to grow separately decreases. With a sufficiently high degree of undercooling, the formation of an excess phase in the form of a separate structural component is

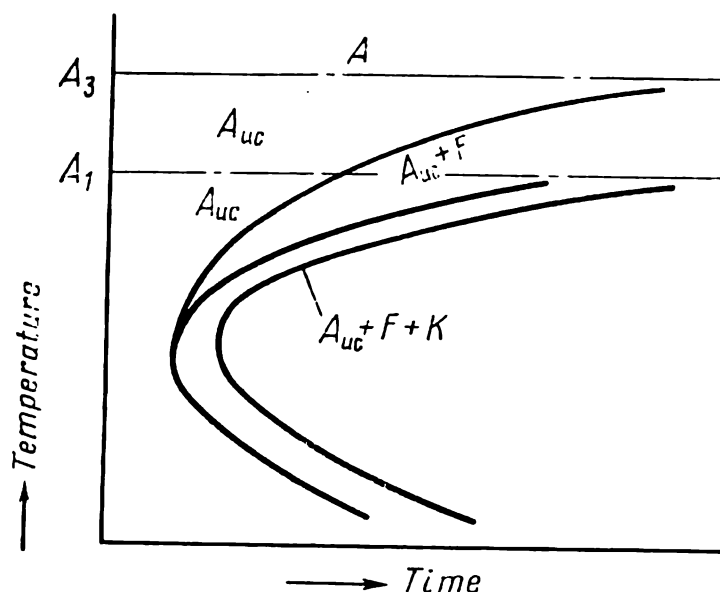


Fig. 94. TTT-diagram for austenite in hypoeutectoid steel (schematically)  
 $A$ —stable austenite;  $A_{uc}$ —undercooled austenite;  $F$ —ferrite;  $K$ —carbide

fully precluded, so that a steel that has had a non-eutectoid composition becomes purely quasieutectoid.

The shape of excess phases is decided by the undercooling of austenite and the size of austenitic grains. With a low degree of undercooling, excess ferrite precipitates as chunky crystals predominantly at boundaries of austenitic grains and forms what is called *ferrite network* (Fig. 95). Beginning from a definite degree of supercooling, ferritic platelets begin to grow from these compact crystals or directly from boundaries of austenitic grains parallel to the  $\{111\}_A$  plane, i.e. a Widmanstätten structure is formed (see Fig. 99a).

This orientation of excess ferrite platelets is due to the principle of structural correspondence:  $\{111\}_A \parallel \{110\}_F$ . These planes of closest packing in the f.c.c. and b.c.c. lattices are very similar in structure to each other.

With larger austenitic grains, the temperature at which the Widmanstätten structure starts to form increases. This is why

Widmanstätten structure is more marked in coarse-grained steels, such as cast steels or those overheated in heat treatment.

At low degrees of undercooling, secondary cementite precipitates in the form of streaks (network) at boundaries of austenitic

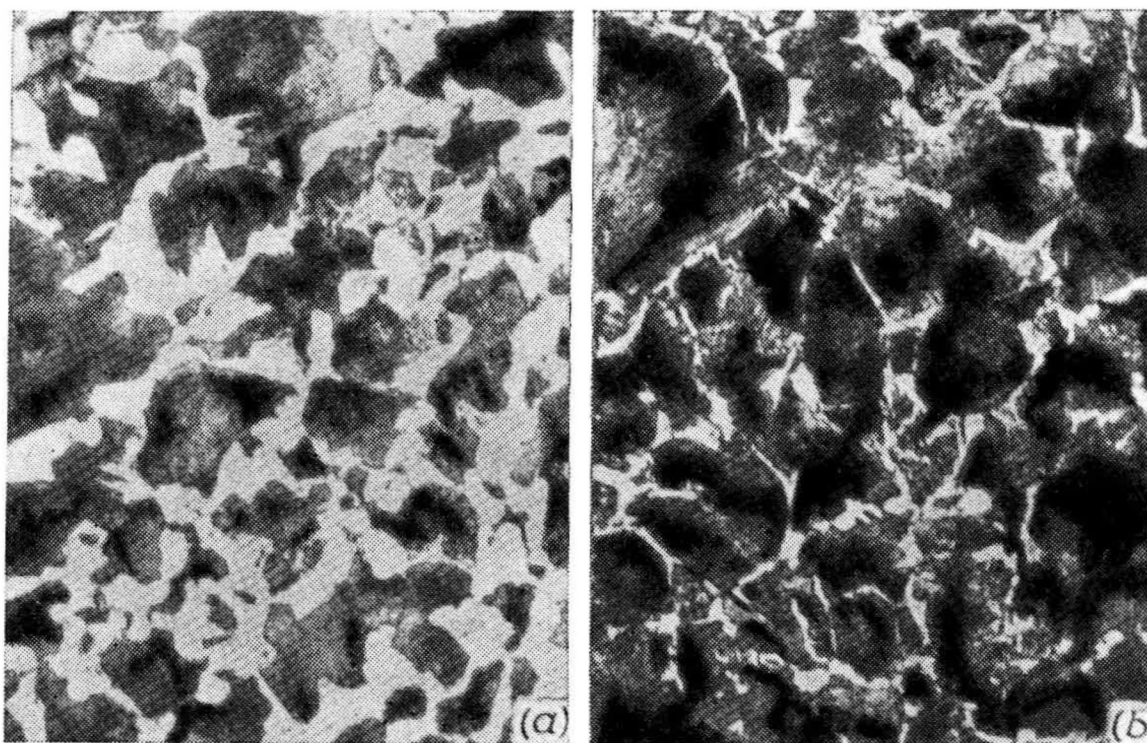


Fig. 95. Microstructure of Grade 60 steel,  $\times 200$   
*a*—furnace cooled; *b*—air cooled

grains (see Fig. 101*a*), but forms platelets (or needles) inside austenitic grains at higher degrees of supercooling.

### Effect of Alloying Elements on Pearlitic Transformation

The effect of alloying elements on the kinetics of austenitic decomposition is of extreme practical importance. All widely used alloying elements dissolved in austenite (Cr, Ni, Mn, W, Mo, V, etc.), except for cobalt, slow down the pearlitic transformation by shifting the upper portion of the *C*-curve to the right.

The stabilizing effect of alloying elements on undercooled austenite is of a rather complicated nature. In carbon steels, the pearlitic transformation is linked with  $\gamma \rightarrow \alpha$ -rearrangement of the lattice and diffusion redistribution of carbon. In alloy steels, these processes may be complemented with the formation of special carbides and diffusion redistribution of the alloying elements proper, which may have different solubilities in ferrite and carbides.

If a steel contains a special carbide in the equilibrium state, the formation of carbides in pearlitic transformation may follow different ways. Firstly, at low degrees of undercooling, a stable special carbide can form directly from the austenite. At larger degrees of undercooling, an intermediate metastable carbide can form instead, whose composition (and/or structure) is more similar to austenite than that of a stable carbide. For instance, steel with 0.47 per cent C and 16.2 per cent Cr forms a stable  $(\text{Cr, Fe})_{23}\text{C}_6$  carbide within a temperature range of 770-700 °C and both  $(\text{Cr, Fe})_{23}\text{C}_6$  and metastable  $(\text{Fe, Cr})_7\text{C}_3$  carbide at 650-600 °C.

The formation of a special carbide, which is rich in carbon and a carbide-forming alloying element, requires that both its components be diffusionaly redistributed in the austenite. The alloying elements may have a low mobility, so that this redistribution will not reach the stage at which a special (or an intermediate) carbide is formed, but will be sufficient to form alloyed cementite  $(\text{Fe, Me})_3\text{C}$ , in whose lattice the alloying element (*Me*) partially substitutes iron atoms and is contained in an appreciably lower amount than in the special carbide. The concentration of an alloying element in cementite may even be the same as that in austenite. At higher degrees of undercooling of austenite, the probability of formation of alloyed cementite instead of special carbides increases.

If a metastable carbide phase (intermediate carbide or alloyed cementite) has formed directly from austenite in pearlitic transformation, the subsequent isothermal holding within pearlitic temperatures can result in this phase being gradually replaced by a stable special carbide through redistribution of the alloying element between the ferrite and carbide. The process may sometimes take as much as a few hundred hours.

The alloying elements dissolved in austenite not only have a low coefficient of diffusion by themselves (sometimes only 0.0001 or even 0.00001 of that of carbon), but some of them (Mo and W) can slow down carbon diffusion in the  $\gamma$ -lattice. Besides, some elements (Cr, Ni) can slow down  $\gamma \rightarrow \alpha$ -rearrangement in pearlitic transformation.

Thus, pearlitic transformation can be slowed down by alloying elements:

- (a) through the formation of special carbides; this necessitates diffusion redistribution in austenite of the alloying elements, whose atoms are incomparably less mobile than carbon atoms;
- (b) owing to a slower diffusion of carbon; and
- (c) owing to a lower rate of polymorphic  $\gamma \rightarrow \alpha$ -transformation. Which of these factors will be decisive depends on steel composition and degree of undercooling of austenite. For instance,

with eutectoid carbon steel being additionally alloyed with 0.8 per cent Mo, the time for full decomposition of austenite at a temperature near the bend of C-curve increases by four orders of magnitude (!), since the formation of  $(\text{Fe, Mo})_{23}\text{C}_6$  carbide requires that the components of the austenite be diffusively re-distributed.

A stronger effect may be obtained by simultaneously alloying with several elements. The retarding effect of alloying elements on austenitic decomposition is widely used for increasing the hardenability of steels (see 3.2.9).

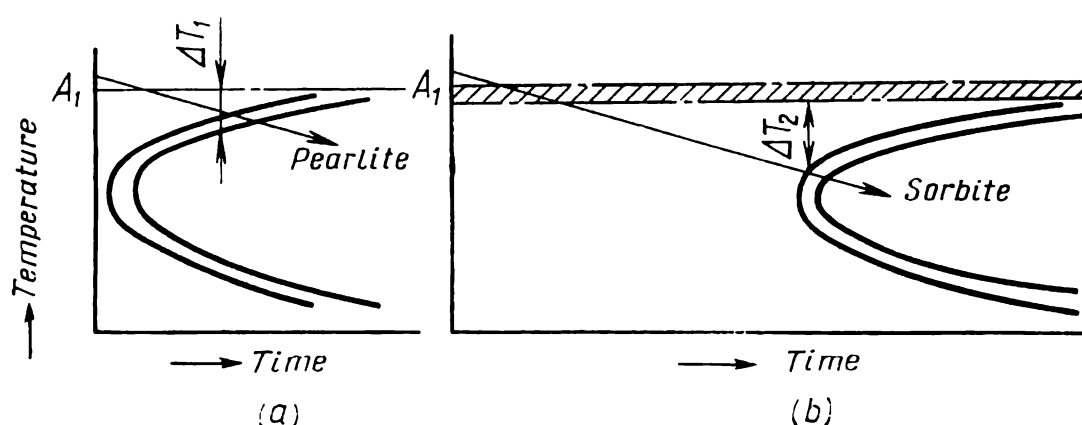


Fig. 96. TTT-diagrams for austenite in (a) carbon steel and (b) alloy steel. For the same cooling rate, the degrees of undercooling are different,  $\Delta T_2 > \Delta T_1$

Here, it is only important to note that alloying causes a deeper undercooling of austenite at the same cooling rate (Fig. 96)<sup>1</sup>. Since undercooling diminishes the interplate spacing, an alloy steel upon pearlitic transformation has a higher strength than carbon steel cooled at the same rate.

### 2.2.3. TYPES OF STEEL ANNEALING

Undercooling of austenite is the principal factor determining the microstructure of steel upon second-order annealing. The types of second-order annealing differ from one another mainly in the method of cooling and the degree of undercooling of austenite, as also by the position of heating temperatures relative to the critical points.

The required degree of undercooling can be attained by either continuous cooling or isothermal heat treatment. The cooling conditions for the various types of second-order annealing are shown

<sup>1</sup> Alloy steel is a multi-component system which, in accordance with the phase rule, has a eutectoid temperature range instead of a fixed eutectoid temperature, as shown hatched in Fig. 96.

in Fig. 97 for hypoeutectoid steel, where (1) is *full annealing*, (2)—*isothermal annealing*, (3)—*normalizing*, and (4)—*patenting*.

With hypereutectoid steels, spheroidizing annealing and normalizing are commonly used.

### Full Annealing

In this type of annealing, a steel heated above the critical point is left to cool in the furnace. Second-order annealing is based on phase transformation, unlike first-order annealing, which is based

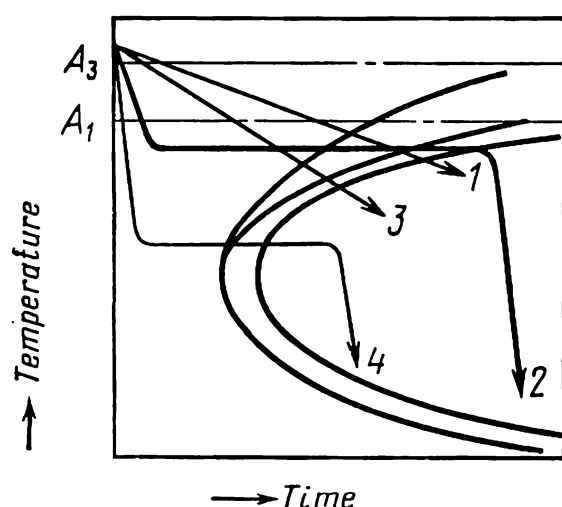


Fig. 97. Principal types of second-order annealing of hypoeutectoid steels

on recrystallization, removal of macrostresses and other structural changes not necessarily linked with phase transformations.

To make full annealing, hypoeutectoid steel is heated to a temperature 20-40 degrees C above the  $A_{c3}$  point (Fig. 98).

Cooling is effected at a slow rate so that the austenite could decompose at a small undercooling. Alloy steels must be cooled slower than carbon steels, since the austenite in them is more prone to undercooling (see Fig. 96).

The recommended cooling rates are 200 °C/h for carbon steels and 100-30 °C/h, for alloy steels. The cooling rate can be adjusted by opening or closing furnace doors, controlling the heating of the furnace, or placing the batch of annealed metal into a special slow-cooling chamber.

Since austenitic transformation on annealing comes to its end at temperatures well above the bend of C-curves, the annealed articles can be removed from the furnace into open air at temperatures of 500-600 °C, provided that the risk of thermal stresses is not high. The cooling in furnace must be continued almost to the room temperature, if annealing is aimed at reducing stresses in articles of intricate shape.

The structure of fully annealed hypoeutectoid steel is excess ferrite plus pearlite.

Full annealing is resorted to when it is needed to eliminate structural defects formed in preceding processing of the metal (casting, hot working, welding or heat treatment), soften the metal before machining or release internal stresses.

In cast metal, large grains of austenite may form on crystallization; these form coarse grains of ferrite and pearlite on cooling.

Ferrite can often form Widmanstätten structure (stretched crystals of a preferable orientation) and thus reduce the impact toughness of the metal (Fig. 99a).

If the temperature at which the plastic working (forging or rolling) is finished is excessively high, austenitic grains have enough time to grow to an appreciable size; with an excessively low temperature, a lineage structure can appear (Fig. 100).

Welded seams may have the same structural defects as cast steel, with a zone of cast structure being adjacent with a zone in which the steel is overheated in the solid state.

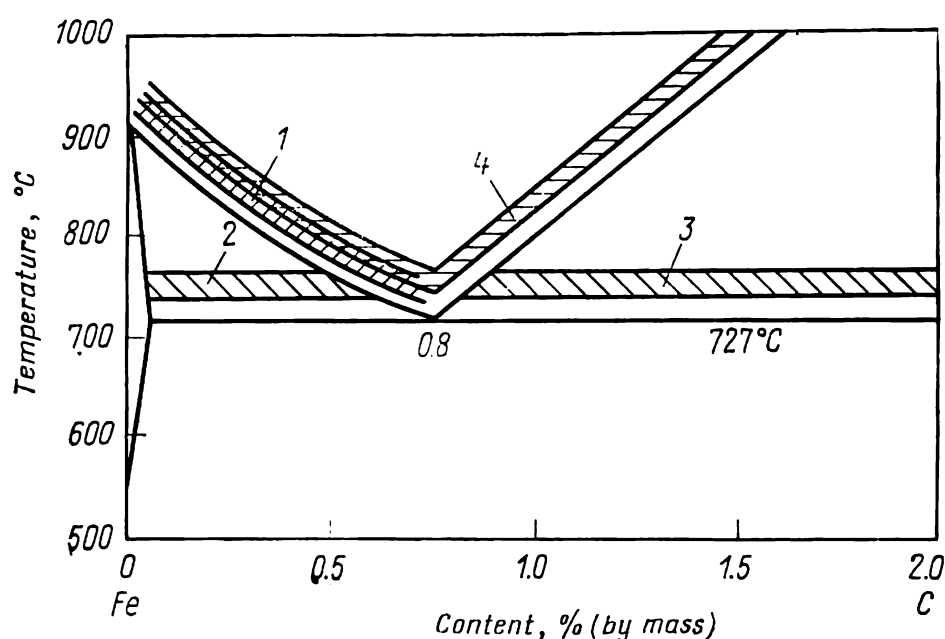


Fig. 98. Heating temperature for second-order annealing of steels  
1—full annealing; 2—partial annealing; 3—spheroidizing annealing; 4—normalizing

Overheating of steel is likely to occur during heat treatment operations. For instance, homogenizing annealing requires a heating temperature of 1100-1200°C at which austenitic grains can grow large.

In order to eliminate the above-mentioned structural defects appeared on casting, hot plastic working, welding or heat treatment, full phase transformation of the metal is required. Heating to a temperature of  $A_{c3} + (20-40 \text{ degrees C})$  refines the austenitic grain, so that a fine homogeneous structure of ferrite and pearlite forms on cooling (Fig. 99b).

A single annealing operation may sometimes be insufficient for amending the structure of steel. This may be explained, in the first place, by the fact that austenitic grains formed on heating are orientationally related to the initial Widmanstätten structure or bainite-martensite structure which has formed through air chilling of castings, weld seams or hot-rolled stock made of alloy



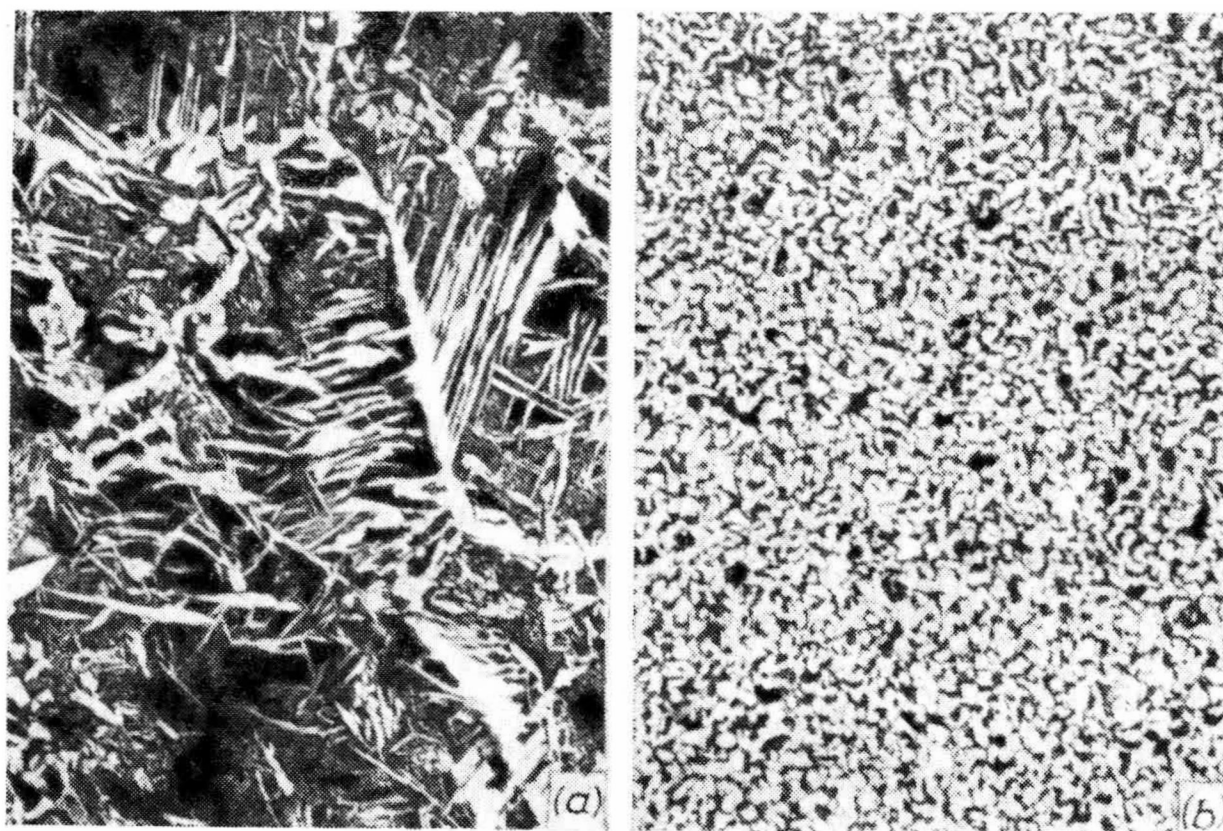


Fig. 99. Microstructures of hypoeutectoid steel,  $\times 100$   
*a*—Widmanstätten structure in cast steel; *b*—ditto, after full annealing

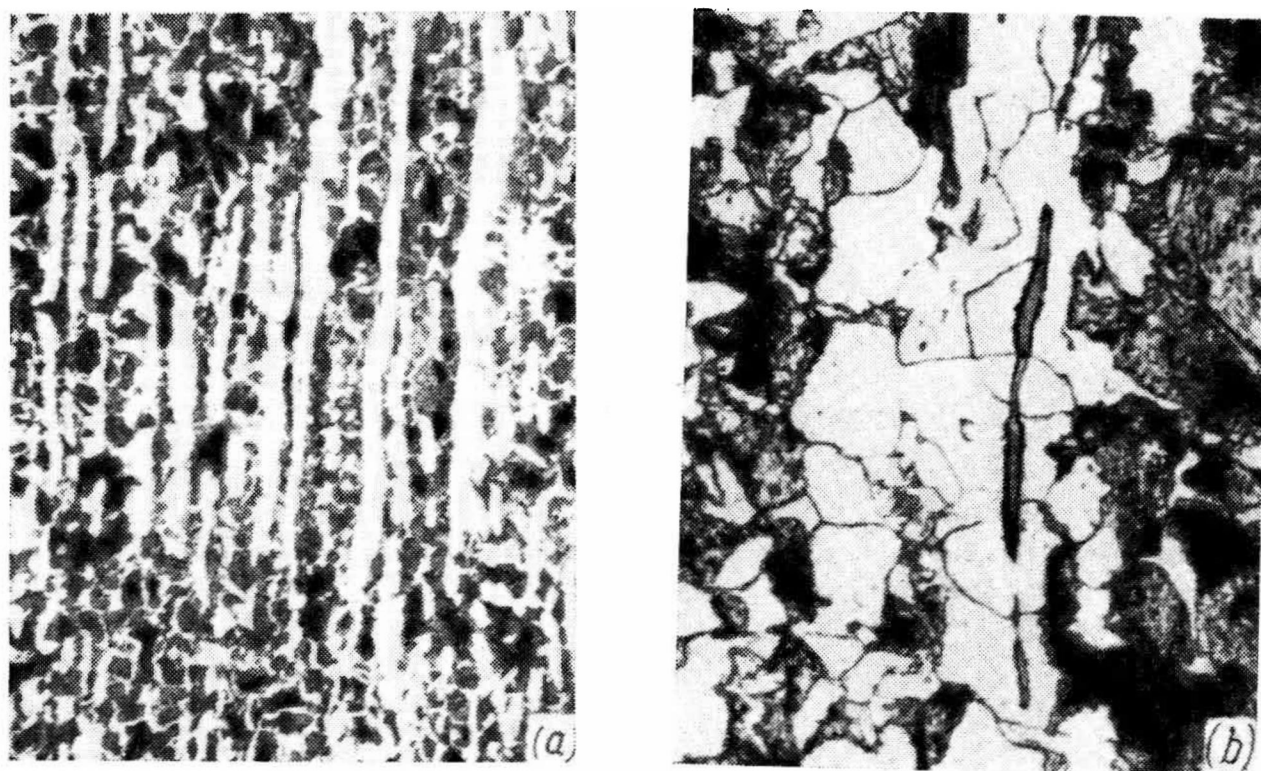


Fig. 100. Lineage structure in hypoeutectoid steel  
*a*— $\times 70$ ; *b*— $\times 300$



steel. Such a coarse-grained structure cannot be remedied by common annealing (see 2.2.1). On the second hand, slag and sulphide inclusions are stretched in hot-deformed metal along ferritic bands (Fig. 100b). With common heating at a temperature of up to  $A_{c3} + (20-40 \text{ degrees C})$ , these inclusions cannot be dissolved in the austenite and their orientation is inherited by the ferrite that precipitates on subsequent cooling, i.e. common annealing is incapable of eliminating lineage structure. In cases just considered, *double annealing* may be useful, the first annealing operation being done at an elevated temperature, and the second, at a normal temperature.

The first high-temperature annealing operation (above the Chernov  $b$  point) is needed to induce primary recrystallization of austenite eliminating its orientational links with the initial ordered structure (see 2.2.1), as also to dissolve stretched slag and sulphide inclusions. The second annealing operation, which is performed at conventional temperature, eliminates the overheated structure left after the first operation.

Common full annealing may also have an opposite aim, i.e. grain coarsening instead of grain refinement, as in the preceding cases. *Grain coarsening annealing* is applied for soft low-carbon steels. These steels are poorly machinable, form tough continuous chip, can weld on to cutting tools, and thus feature rough surface on machining. Their machinability can be improved by coarse-grain annealing at  $950-1100^\circ\text{C}$ , which yields a structure with large nodules of lamellar pearlite.

### Partial Annealing

Partial annealing of hypoeutectoid steels has only a limited application. It is carried out at a temperature above  $A_{c1}$  but below  $A_{c3}$  (see Fig. 98), which is insufficient for full disappearance of excess ferrite. Therefore, partial annealing cannot eliminate the above-mentioned steel defects which are linked with undesirable size and shape of excess ferrite particles.

With hypoeutectoid steels, partial annealing is employed to soften the metal before machining, since the eutectoid transformation that takes place forms soft pearlite. Partial softening annealing makes it possible to reduce the time and cost of metal processing.

### Spheroidizing Annealing

Full annealing with heating above  $A_{cm}$  (line  $ES$ ) is inapplicable with hypereutectoid steels, since following slow cooling results in the formation of a coarse network of secondary cementite (Fig. 101a), which impairs the mechanical and other properties

of the metal. A method that is widely used with hypereutectoid carbon steels is heating up to 740-780°C, followed with slow cooling. Upon being heated in this way, austenite retains a large number of undissolved cementite inclusions, which serve as crystallization nuclei during austenitic decomposition on cooling.

The resulting structure is granular pearlite, or *spheroidite*, and the method is accordingly called spheroidizing annealing.

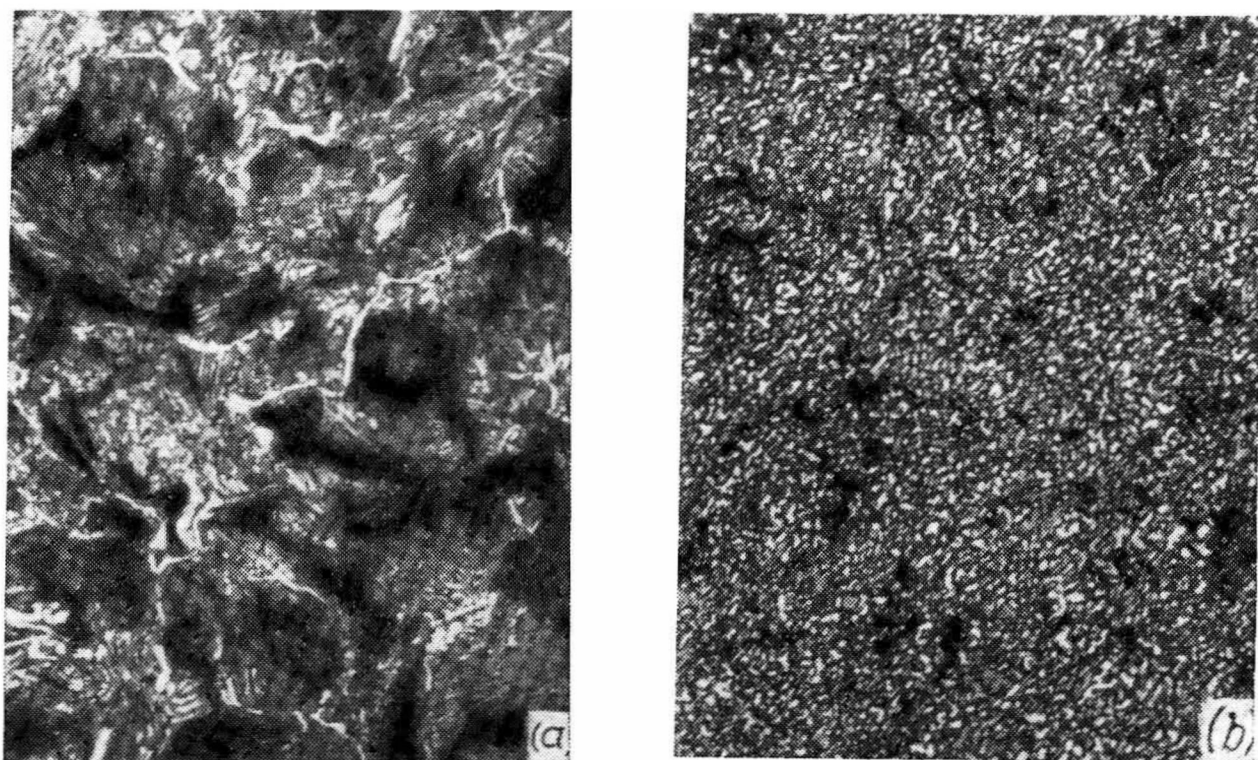


Fig. 101. Microstructure of Grade Y12 hypereutectoid steel,  $\times 300$   
*a* — after full annealing (cementite network); *b* — after cyclic annealing (granular cementite)

At annealing temperatures within a range of  $A_1 - A_{cm}$ , fine cementite particles form owing to disintegration of cementite platelets.

This phenomenon was discovered at the beginning of this century by a prominent metallurgist N. I. Belyaev. During disintegration, cementite platelets are dissolved in the thinnest portions, and also in sites of passage of subboundaries out onto cementite/austenite interface in cementite or austenite.

In a place where a subboundary in a cementite platelet passes out onto an interface, the disbalance of surface tension forces is a stimulus for local dissolution of the cementite until the shape of the surface is such that the forces are balanced (Fig. 102). Dissolution pits with their walls being convex towards austenite pass along the lines of passage of subboundaries onto the surface of a platelet.

As is known, the solubility of a particle depends on the radius of curvature of its surface and is described by Thompson-Freundlich equation:

$$\log_e \frac{C_r}{C_\infty} = \frac{2\gamma V}{kTr} \quad (30)$$

where  $C_r$  = solution concentration near an interface of radius  $r$   
 $C_\infty$  = ditto, near a flat interface  
 $\gamma$  = surface energy at interface  
 $V$  = atomic volume

The smaller the radius of curvature, the greater is the equilibrium concentration of a solution near an interface. Consequently, the carbon concentration in the austenite near convex walls of dissolution pits in cementite (Fig. 102) is greater than near the remaining flat surface of a platelet. Equalization of composition in austenite will then lower the carbon concentration near the convex walls of a pit and, since the austenite will thus be unsaturated relative to cementite, the latter will be dissolved and its boundaries will straighten. This in turn disturbs the equilibrium of surface tension forces near the passage of subboundaries onto the surface, the pit deepens and thus restores the equilibrium, and so on. As a result, the cementite platelet will be divided due to dissolution along its subboundary.

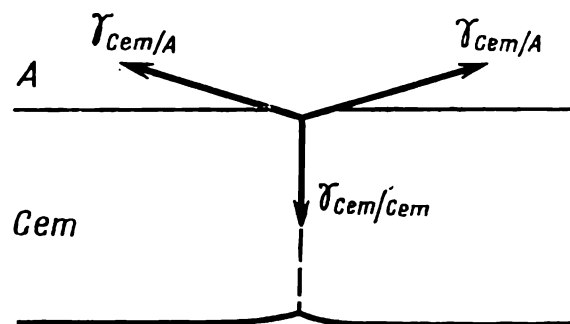


Fig. 102. Dissolution pits in sites of passage of a subboundary in cementite (shown dotted) onto cementite-austenite interface

A similar process develops in sites where an austenite/cementite subboundary in austenite passes out onto the surface. In that case, however, the surface tension forces will be equalized provided that on a cementite platelet a protrusion forms with two recesses at its sides. A platelet will be locally thinned near cementite portions with different curvature owing to different carbon concentration in the austenite, since the carbon will be transferred through the austenite.

Division of cementite platelets can be accelerated by hot or cold plastic deformation at temperatures below  $A_1$ . Cementite platelets are not destroyed in the process, as has been assumed formerly, but are only deformed plastically. The heating after cold deformation or during hot deformation causes the formation of subboundaries through polygonization, which promotes division of cementite platelets. As has been shown by thin-foil electron-microscopic studies, cementite platelets can divide not only

owing to accelerated dissolution in sites where subboundaries pass out onto the surface, but also in sites having an increased dislocation density in cementite.

Upon division of cementite platelets, smaller particles are spheroidized. According to equation (30), the concentration of carbon in austenite increases near the edges and corners of cementite particles, i.e. where the radius of curvature is small. Equalization of the composition in austenite increases the carbon concentration near portions of a boundary having a large radius of curvature, where the austenite is supersaturated, so that cementite precipitates from it. The simultaneous reduction of carbon concentration in the austenite near the edges and corners causes the latter to dissolve. As a result, the concentration gradient in the austenite is restored to the initial value, so that the process of dissolution of cementite in sites of a lower radius of curvature of a boundary and the process of cementite precipitation in sites of a greater radius of curvature cause rounding-off of cementite particles.

Thus, cementite particles are spheroidized owing to the transfer of carbon through the solid solution.

Division and spheroidization of platelets of a phase in equilibrium with solid solution are the general mechanisms active in many alloys with various bases.

The spheroidizing annealing of hypereutectoid steels is characterized by a narrow '*annealing range*'. The lower limit should be somewhat above  $A_1$  in order to allow a great number of carbide precipitation nuclei to form on subsequent cooling. The upper limit should not be too high, otherwise carbide precipitation nuclei will dissolve in the austenite on cooling and form lamellar pearlite. Since the  $A_{cm}$  and  $A_1$  points merge in the case of eutectoid concentration, the '*annealing range*' is especially narrow in steels having nearly eutectoid composition. For instance, this temperature range is only from 740° to 750 °C for steels Y9A and Y10A and appreciably wider, from 750° to 780 °C for steels Y11A, Y12A and Y13A.

The resultant structure depends on the rate of cooling and the temperature of spheroidizing annealing. A lower cooling rate produces larger carbide globules upon decomposition of the austenite. Various structures of *globular pearlite*, from dotted type to coarse-grained, can be obtained by controlling the cooling rate. Fine-grained pearlite has a higher hardness.

Figure 103 shows how the conditions of spheroidizing annealing can affect the hardness of the metal. As the temperature is increased up to 800-820 °C, the hardness lowers owing to development of spheroidization, whereas upon further increase of temperature the hardness increases since lamellar pearlite forms in ever greater amount.

Spheroidizing annealing is employed with carbon and alloy tool and ball-bearing steels. A steel having the structure of granular pearlite has the lowest hardness and is readily machinable, which is highly essential in some cases, for instance, for mass production of ball bearings in automatic flow lines. In addition, the structure of granular pearlite is the optimum structure before hardening, since it is less liable to coarsening of austenitic grains, allows a wider range of hardening temperatures, makes the metal less prone to cracking on hardening and gives higher values of strength and toughness in hardened steel (since small globuli are distributed quite uniformly in the martensite of hardened hypereutectoid steel).

This is why annealed tool steels as delivered usually have the structure of granular pearlite. Ball-bearing steel forgings are also annealed to granular pearlite.

When single annealing operation is insufficient for full spheroidization of cementite, *cyclic annealing* can be resorted to. For example, carbon steel is repeatedly heated to 740 °C and cooled down to 680 °C. Each heating operation causes cementite platelets to dissolve partially in the austenite, the process of dissolution taking place mostly at edges and corners of platelets. Each cooling then causes the cementite to precipitate from the austenite at the remnants of undissolved cementite platelets, this precipitation occurring mostly far from edges and corners. Thus, owing to alternate growth and dissolution, a cementite platelet is gradually rounded off (Fig. 101b). Unfortunately, the method is not quite suitable for industrial applications, since the temperature of a large batch of metal must be controlled within a narrow (roughly 40 degrees C) specified range.

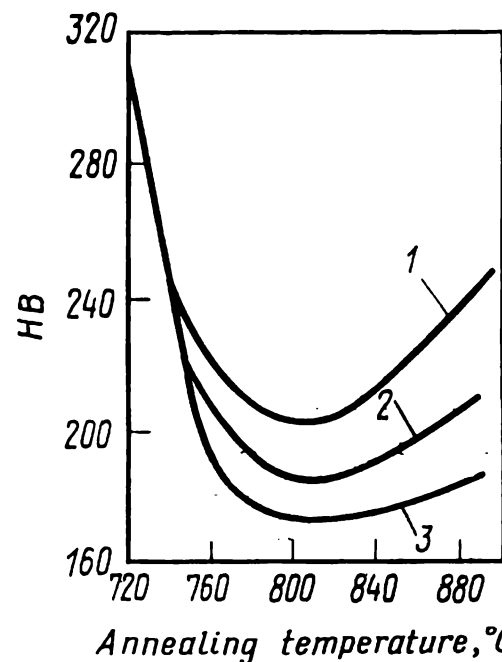


Fig. 103. Effect of annealing temperature on hardness of ball-bearing steel Grade IX15 at various cooling rates (after Ya. R. Rauzin)

1—100 °C/h; 2—30 °C/h; 3—5 °C/h

### Isothermal Annealing

Continuous cooling of steel in the furnace is not the sole method for obtaining a low degree of undercooling in austenite as needed for annealing. Another method is stepwise cooling with an isothermal holding within the range of pearlitic transformation (see Fig. 97). The method is called isothermal annealing. Upon

heating to a temperature above  $A_3$ , steel is cooled quickly to the temperature of isothermal holding, which is below the  $A_1$  point. Then follows quick cooling in air; small articles of plain shape can be cooled in hot water. The time of isothermal holding must be somewhat longer than the time required for full isothermal transformation of austenite, which is determined from the  $C$ -curve.

The closer is the temperature of isothermal holding to the  $A_1$  point, the greater is the interplate spacing in the pearlite and the softer is the steel, though the time required for the transformation becomes longer. Since isothermal annealing is mainly aimed at softening the steel, the temperature of isothermal holding is practically chosen so (30-100 degrees C below  $A_1$ ) as to soften the steel sufficiently in a relatively short interval of time.

Isothermal annealing is advantageous over common annealing in two respects. Firstly, it can save time, provided that the total time of quick cooling, isothermal holding and subsequent quick cooling is less than the time required for slow continuous cooling of articles in the furnace. The saved time can be especially considerable with alloy steels containing stable undercooled austenite.

Secondly, it can produce a more uniform structure in the metal, since the temperature is equalized over the cross-section of an article during the isothermal holding and the transformation occurs at the same degree of undercooling throughout the whole volume of metal.

Isothermal annealing can be carried out either in one furnace (which is blown with air and thus chilled to the specified temperature) or in two furnaces. Upon heating to a temperature above  $A_3$  in a box furnace, a batch of steel is transferred into another box furnace held at a temperature below  $A_1$ . The latter method is more efficient. It is also possible to use continuous conveyer furnaces with various temperatures zones. Isothermal annealing of alloy steels from temperatures of forging heating is economical. Since the time of decomposition of austenite increases appreciably as the temperature approaches  $A_1$ , isothermal annealing can compete successfully with common annealing only when the maximum softening effect is not required and the temperature of isothermal holding can be chosen at a sufficiently low level.

### Normalizing

In normalizing, steel is heated to a temperature 30-50 degrees C above the  $GSE$  line and cooled in air (see Fig. 98). Cooling proceeds more quickly than in common annealing, which gives a somewhat greater degree of undercooling of austenite (see Fig. 97). Because of this, normalizing produces a finer eutectoid structure (fine pearlite or sorbite) and finer eutectoid grain. Besides, the precipitation of an excess phase (ferrite or secondary cementite) is partially suppressed, and therefore, a quasi-eutectoid is formed (see Fig. 95b). Thus, normalized steel has a greater strength than the steel as annealed.

Normalizing is employed most often as an intermediate operation to soften the steel before machining, to eliminate structural defects, or to produce a general improvement in its structure before hardening. Thus, normalizing, as an intermediate operation serves the same purpose as annealing. Normalizing is more profitable than annealing and therefore should be preferred in all cases when both methods give similar results. However, it is not always a preferable substitute for annealing if the steel must be softened, which may be explained in the following way. Austenite becomes more prone to undercooling as the content of carbon and alloying elements in it increases. Thus, the composition of the steel determines the difference in the properties it will have upon annealing and upon normalizing. For instance, the hardness of steels with 0.2, 0.45 and 0.8 per cent C is respectively 120, 160 and 180 HB after annealing and 130, 190 and 240 HB after normalizing.

Normalizing is employed widely instead of softening annealing with low-carbon steels in which the austenite is only poorly liable to undercooling. However, it cannot replace softening annealing with high-carbon steels which can strengthen noticeably on air cooling owing to an appreciable degree of undercooling of austenite. As far as medium- and high-alloyed steels are concerned, they can form martensite on air cooling, i.e. are air-hardenable (see 3.2.8). Here, it is necessary to specify more accurately the term 'normalizing'. This is understood as a heat treatment operation in which air cooling causes the austenite to decompose within the temperature range of pearlitic transformation. Therefore, if an alloy steel, such as Grade 18X2H4BA, forms martensite on air cooling, the process bears no relation to normalizing.

Normalizing is widely employed instead of common annealing for eliminating steel defects formed through hot working or heat treatment. In many cases it gives better results. For instance, lineage structure in steel can be eliminated more easily by normalizing, since a greater degree of undercooling of the austenite causes ferrite to precipitate throughout the whole bulk of austenitic grains, rather than only at stretched slag and sulphide inclusions.

Normalizing can eliminate a coarse network of secondary cementite in hypereutectoid steels. On heating above the  $A_{cm}$  point (line *ES*), the secondary cementite dissolves and in the subsequent quick cooling in air has no time to form a coarse network that might impair the properties of the steel. For instance, a coarse cementite network in tool steels Y11-Y13 after hot rolling is eliminated before spheroidizing annealing by normalizing with heating to 850 °C, followed with quick cooling in air stream.



Normalizing is used very often for general refinement of the structure prior to hardening. If a steel before hardening contains coarse precipitates of excess ferrite, then the austenite has no time for homogenizing when being heated for hardening. The portions of the austenite which correspond to sites of coarse ferrite inclusions will be depleted in carbon and have an insufficient hardness upon hardening. Normalizing prior to hardening can refine excess ferrite precipitates, the eutectoid becomes more disperse and thus facilitates quick formation of homogeneous austenite on heating before hardening.

Normalizing is also used as a final operation for medium- and high-carbon steels, if requirements to resultant properties are moderate and high-tempering is not necessary.

It should be noted in conclusion that the rate of air cooling depends on the mass of an article and its surface area-to-volume ratio, so that these factors can also affect the structure and properties of normalized steel.

### Patenting

Patenting has been known from 1870's as an isothermal heat treatment operation for producing high-strength rope, spring and piano wire. Carbon-steel wire (0.45 to 0.85 per cent C) is heated in a continuous furnace to a temperature 150-200 degrees C above  $A_{c3}$ , passed through a lead or salt bath at a temperature of 450-550 °C and wound onto a driven drum. Austenitic decomposition takes place near the bend of the C-curve at the lower temperature limit of pearlitic transformation (see Fig. 97). Upon passing the quench bath, the wire has ferrite-cementite structure with a very small interplate spacing, which is usually called patented sorbite or troostite. Excess ferrite and secondary cementite have no time to form and the whole structure is of the quasi-eutectoid type.

Patented wire is repeatedly cold-drawn with a high total deformation ratio. The ultimate strength of patented wire is usually 150-200 kgf/mm<sup>2</sup>. A record tensile strength of 500 kgf/mm<sup>2</sup> was obtained in steel wire (Grade Y9A) produced by vacuum-arc melting (to eliminate the harmful effect of non-metallic inclusions and impurities), which was patented and cold drawn with a total reduction of 99 per cent.

The role of patenting in producing a high-strength state in the metal is two-fold. Firstly, it makes a wire more capable of withstanding large reductions in cold drawing without fracture. This is ensured by the structure of fine-lamellar pearlite and the absence of excess ferrite grains that might cause fracture of excessively tensioned wire. Secondly, the interplate spacing in the ferrite-cementite mixture upon cold plastic working becomes even



smaller than upon patenting, with a combination of a high strength and a high toughness in twisting and bending. The boundaries between ferrite and cementite platelets are impermeable barriers for dislocations and the ultimate strength of patented wire obeys the Petch-Hall relation (13) in which  $d$  is the inter-plate spacing in the case considered.

Patenting requires a high temperature of heating (usually 870-920 °C) in order to homogenize the austenite properly. The speed of wire motion should be such that the time of quenching in the bath be somewhat greater than the time of pearlitic transformation, because otherwise the austenite in the wire removed from the bath might transform into lower bainite or martensite which largely impair the plastic properties of the wire.

When patenting thick wire, the thermal effect of the transformation can cause overheating and coarsening of the wire structure. This is prevented by maintaining the bath temperature near the lower limit of the prescribed interval of 450-550 °C.

Though it is a specific process, patenting can be related to second-order annealing as regards the main classification feature, i.e. the type of phase transformations taking place in it, and therefore, is a variety of isothermal heat treatment.

#### LITERATURE

Gulyaev A. P., Heat Treatment of Steel (*Termicheskaya obrabotka stali*), Chs. II, III and VIII, Moscow, Mashgiz, 1960, 496 pp., ill.

Entin R. I., Austenitic Transformations in Steel (*Prevrashcheniya austenita v stali*). Moscow, Metallurgizdat, 1960, 252 pp., ill.

Sadovsky V. D., Structural Inheritance in Steel (*Struklurnaya nasledstvennost' v stali*). Moscow, Metallurgiya, 1973, 208 pp., ill.

Physical Metallurgy and Heat Treatment of Steels (*Metallovedenie i termicheskaya obrabotka stali*). A reference book, volume I, Moscow, Metallurgizdat, 1961, 1656 pp., ill.

## 2.3. ANNEALING OF CAST IRONS

The principal components in cast irons are iron, carbon and silicon. Common cast irons may additionally contain manganese, phosphorus and other elements. Though the composition of cast iron is rather complex, the principal structural changes upon annealing can be analysed qualitatively by using the constitutional diagram of Fe-C binary system. As is well known, austenite and ferrite in this system can be in a stable equilibrium with graphite (dotted lines in Fig. 85) and in a metastable equilibrium with cementite (solid lines).

Graphite can nucleate and grow in the metallic matrix less readily than cementite. An appreciably higher fluctuation of concentration is needed for nucleation of graphite, which is virtually

100 per cent carbon (and the solubility of iron in it is negligible), whereas cementite contains only 6.67 per cent C. For a graphite crystal to grow, iron atoms must be removed almost fully from the front of its boundary in the metallic matrix. For that reason the formation of metastable cementite under definite conditions, for instance, with quick cooling, is kinetically more favourable than the formation of stable graphite. However, the metastable equilibrium of austenite or ferrite with cementite corresponds to a relative minimum of free energy, whereas the stable equilibrium with graphite corresponds to the absolute minimum of free energy. Because of this, holding of cast iron at an elevated temperature must eventually result in cementite being replaced with graphite.

Silicon, nickel, aluminium and some other elements promote graphitization, while manganese, chromium, vanadium, magnesium, cerium, sulphur and some others, inhibit it.

The phase transformations taking place on heat treatment of cast irons are principally the same as in steels, but are additionally complicated by the processes related to the behaviour of the graphite phase.

An outstanding contribution to the study of phase transformations in cast irons, in particular of graphitization, has been made by the works of the school headed by K. P. Bunin. The analysis of the processes of annealing in cast irons is mainly based on the results and conclusions of that school.

The principal varieties of second-order annealing in cast irons are graphitizing annealing and normalizing.

### 2.3.1. GRAPHITIZING ANNEALING

Graphitizing annealing is employed with white, grey and high-strength (modified) cast irons.

#### White-to-Malleable Iron Annealing

White cast iron is hard and very brittle owing to the presence of considerable amount of much eutectic cementite in its structure. The present-day method for obtaining malleable cast iron by graphitizing annealing of white cast iron was developed at the beginning of the last century. At present, malleable cast iron is a material that is widely used in machine-building, since it combines high mechanical properties with the ease with which intricate castings can be made at low cost.

The manufacture of malleable cast iron uses castings of hypoeutectoid white cast iron containing 2.2-3.1 per cent C, 0.7-1.5 per cent Si, 0.3-1.0 per cent Mn, and up to 0.08 per cent Cr. The content of silicon, which facilitates graphitization, and that of

manganese and chromium, which inhibit graphitization, are controlled in the charge in such a way as to suppress the crystallization of graphite from the melt and induce as fast graphitization during annealing as practical. Note that when grey iron crystallizes, its graphite grows from the melt in the form of branched crab-like rosettes which are seen in microsections as bent platelets; this form of graphite is unfavourable for the mechanical properties of the metal. During annealing of white iron (Fig. 104), graphite, which is then called *temper carbon*, crystallizes in a much more compact form, which is favourable for the mechanical properties (Fig. 105). Though malleable iron is not actually

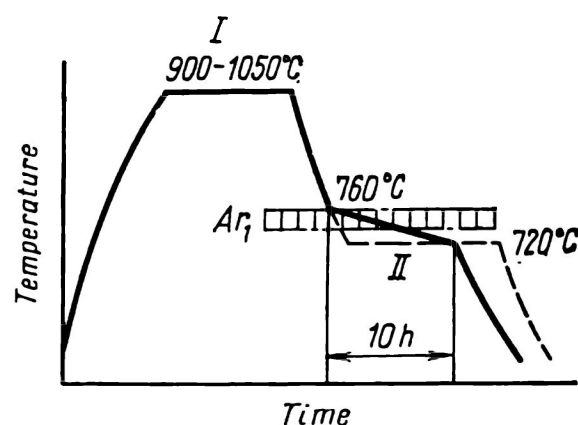


Fig. 104. Diagram of annealing of white cast iron to malleable iron  
I and II—graphitization stages

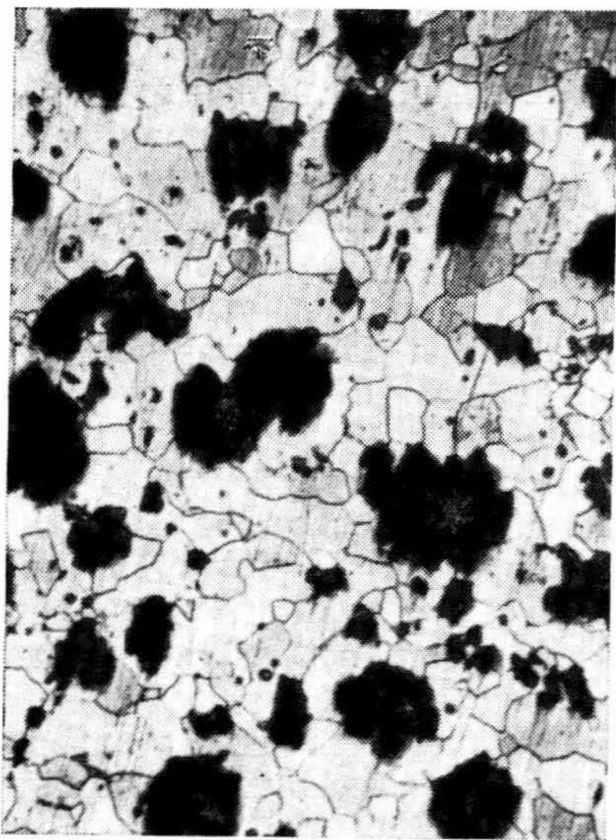


Fig. 105. Microstructure of ferritic malleable cast iron,  $\times 120$

(Fig. 104), after which all the cementite of eutectic origin and the remnants of the secondary cementite are replaced by graphite and the structure changes from austenite plus cementite to austenite plus graphite.

Forged, its relative elongation is within a range of 2 to 20 per cent (depending on the structure), whereas that of white cast iron does not exceed 0.2 per cent and that of grey cast iron, 1.2 per cent.

The initial phase composition of white cast iron is ferrite plus cementite, i.e. the same as that of steel, so that the mechanism of austenitization is analogous to that discussed in 2.2.1. Heating first causes the pearlite-to-austenite transformation and then dissolution of the secondary cementite and homogeneous distribution of C and Si in the austenite.

#### First Stage of Graphitization

During holding at 900-1050°C, the first stage of graphitization takes place

The assumption that cementite decomposes with graphite precipitating directly from it by the reaction  $\text{Fe}_3\text{C} \rightarrow 3\text{Fe} + \text{C}$  is in disagreement with many actual facts. In particular, the shape of temper carbon in malleable iron does not correspond to the shape of the initial cementite crystals.

It has been established that graphitization of white iron consists essentially in nucleation of graphite at austenite-cementite boundaries and in sites far from cementite crystals and in the growth of graphite crystals with simultaneous dissolution of cementite in austenite through the transfer of carbon atoms from austenite-cementite boundaries via austenite to austenite-graphite boundaries.

The specific volume of graphite is several times that of austenite, so that homogeneous nucleation of graphite in the dense metallic matrix is unlikely to occur, since the elastic component  $\Delta F_{el}$  in formula (25) is too large. For the same reason, dislocations, subboundaries and high-angle boundaries are not effective as sites for heterogeneous nucleation of graphite.

As is well known, grey tin, whose specific volume is 25 per cent greater than that of white tin, nucleates preferably at the open surface of a specimen of white tin. Naturally, when graphitization takes place, in which the specific volume of the new phase differs even more from that of the initial phase, graphite nuclei appear preferably at the free surface of austenite.

In the bulk of a casting, sites of heterogeneous nucleation of graphite are discontinuities, vacancy clusters, shrinkage voids, gas blowholes, microfissures, and fractures at boundaries between austenite and non-metallic inclusions caused by thermal expansion. Probable sites of graphite nucleation are diffusion pores formed on homogenization of austenite. For instance, when silicon atoms are removed from silicon-rich places and the composition of austenite is equalized, there remains an excess of vacancies which form pores. This is a probable explanation why silicon can accelerate graphitization, notwithstanding the fact that it has a retarding effect on carbon diffusion in austenite.

Upon the formation of graphitization nuclei there is a carbon concentration gradient in the austenite, since the ultimate solubility of cementite in austenite is higher than that of graphite (line  $ES$  in the constitutional diagram of Fig. 85 passes to the right of line  $E'S'$ ). For instance, if the first stage of graphitization takes place at a temperature  $t^*$  (Fig. 106), the composition of austenite at a boundary with cementite is determined by point  $b$  and that at a boundary with graphite, by point  $a$ . As the concentration of carbon in the austenite is equalized, the austenite becomes unsaturated relative to cementite (the composition of austenite at austenite-cementite boundary shifts to the left of point  $b$ ) and supersatu-

rated relative to graphite (its composition at an austenite-graphite boundary shifts to the right of point *a*). This results in a continuous dissolution of cementite, until it disappears fully, and in growth of graphite.

Apart from the transfer of carbon atoms through the solid solution, another process is required for graphitization: the evacuation of iron atoms from the surface of growing graphite to provide 'living space' for the latter. K. P. Bunin emphasizes, that this very diffusion process, but not the inflow of carbon atoms, controls the rate of growth of graphite inclusions in austenite, because the diffusion mobility of iron atoms is much lower than that of carbon.

The shape of graphite particles depends on the temperature of annealing and the composition of cast iron. Temper carbon can grow more quickly along high-angle boundaries and subboundaries, since these can remove carbon atoms more quickly. This undesirable branching of graphite is enhanced with increasing temperature, so that annealing at temperatures above 1050-1070 °C can largely impair the mechanical properties of cast iron. This fact determines the upper temperature limit of the first graphitization stage.

Additions and impurities can have a complicated effect on the growth of temper carbon by varying the diffusion rates of iron and carbon and other parameters. For instance, small additions of magnesium (around 0.1 per cent) ensure the growth of temper carbon in the form of compact inclusions. By controlling the temperature of annealing and composition of white cast iron, it is possible to produce malleable cast iron with very compact inclusions of temper carbon.

During cooling of cast iron after the first graphitization stage, the composition of the austenite varies along  $E'S'$  line with secondary graphite precipitating from it. This stage of graphitization is called *intermediate*. Secondary graphite precipitates at inclusions of temper carbon and usually does not form a separate structural component.

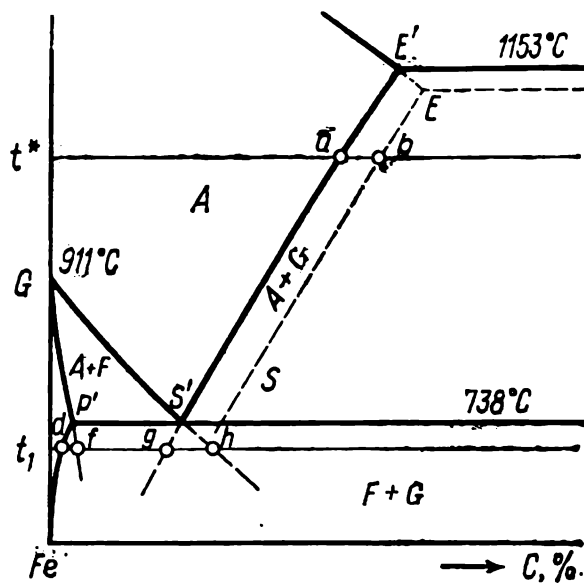


Fig. 106. Portion of Fe-C constitutional diagram. Solid lines refer to stable equilibrium, dotted, to metastable (schematically)

### Second Stage of Graphitization

The metallic matrix of malleable cast iron forms during the eutectoid decomposition of austenite.

To obtain purely ferritic matrix, the metal should be cooled slowly within the temperature range of eutectoid decomposition (see Fig. 104). The second stage of graphitization then takes place, i.e. austenite decomposes into ferrite plus graphite.

The sequence of structural changes taking place during the second graphitization stage can be conveniently retraced on the diagram of isothermal transformation of austenite in cast iron. In Fig. 107, line  $OE$  is the beginning of formation of eutectoid ferrite, line  $DH$  — the beginning of formation of eutectoid cementite, line  $NL$  — the end of eutectoid transformation, and line  $BK$  — the end of graphitization of pearlitic cementite.

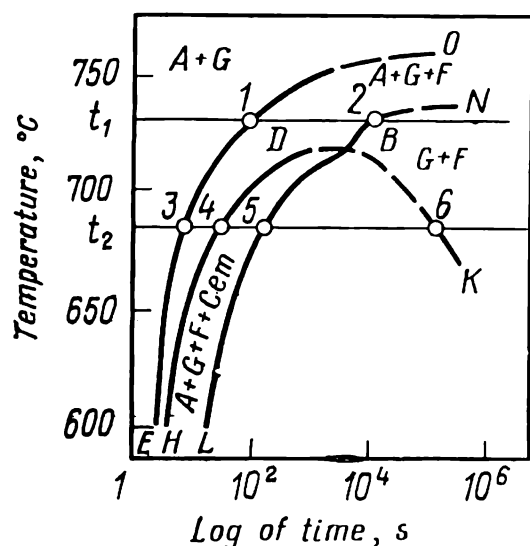


Fig. 107. TTT-diagrams for austenite in malleable cast iron with 2.9% C, 0.88% Si, 0.36% Mn and 0.09% S (after K. P. Bunin et al)

Consider the transformations in austenite on undercooling to a temperature  $t_1$ . Initially, graphite forms (without any induction period) at the surface of the existing inclusions of temper carbon. Beginning from a moment corresponding to point 1 (line  $OE$ ), eutectoid ferrite begins to form along with graphite, i.e. the eutectoid decomposition of austenite into

ferrite and graphite takes place. It ends at point 2, where austenite fully disappears.

In eutectoid decomposition, graphite precipitates at particles of temper carbon formed during the first and intermediate stages of graphitization, so that ferrite-graphite eutectoid in the form of disperse mixture of alternating phases does not appear as an independent structural component in the metal.

The eutectoid decomposition of austenite into ferrite and graphite can proceed either normally or abnormally. With normal decomposition, austenite is always in contact with the ferrite and graphite that have formed from it. Its concentration at a boundary with graphite corresponds to point  $g$  and that at a boundary with ferrite, to point  $h$  (see Fig. 106). As the composition of austenite is being equalized, it becomes supersaturated with carbon at austenite-graphite boundaries, where graphite precipitates, and is depleted of carbon at austenite-ferrite boundaries, where the  $\gamma \rightarrow \alpha$ -rearrangement, i.e. the formation of ferrite, takes place.

The *abnormal eutectoid transformation* can only take place when ferrite fully encloses graphite particles and thus disturbs the contact between austenite and graphite. Ferrite has a composition of point *d* at its boundary with graphite and that of point *f*, at its boundary with austenite. Though the carbon concentration gradient is not high, diffusion of an interstitial element in the b.c.c. lattice of ferrite proceeds quite rapidly. The carbon is transferred from ferrite-austenite to ferrite-graphite boundaries, where the ferrite becomes supersaturated with carbon, liberates graphite and thus restores the concentration to the value of point *d*. At a ferrite-austenite boundary, the concentration of carbon in ferrite lowers (the composition is shifted to the left of point *f*) and the ferrite becomes undersaturated relative to austenite; this causes  $\gamma \rightarrow \alpha$ -transformation with the resultant ferrite having the composition of point *f*. Therefore, in abnormal eutectoid transformation graphite precipitates from ferrite, rather than from austenite.

At temperatures above point *D* in Fig. 107, i.e. at relatively low degree of undercooling of austenite (or on a slow continuous cooling), the full ferritization of the matrix occurs directly during the eutectoid decomposition by the reaction: austenite  $\rightarrow$  ferrite + + graphite. At a deep undercooling (below the temperature of point *D* in Fig. 107), the formation of pearlite is possible (line *DH*). For instance, at temperature  $t_2$ , after graphite has precipitated without any induction period, the eutectoid decomposition of austenite into ferrite and graphite takes place during the period 3-4 and, beginning from the moment corresponding to point 4, pearlitic transformation (austenite  $\rightarrow$  ferrite + cementite) occurs. At a moment of point 5, the two eutectoid processes ( $A \rightarrow F + G$  and  $A \rightarrow F + \text{Cem}$ ) result in full disappearance of the austenite, producing the cast iron structure composed of temper carbon, ferrite and pearlite. The higher the degree of undercooling (or the greater the rate of cooling with continuously lowering temperature), the greater proportion of the austenite decomposes by the reaction  $A \rightarrow F + \text{Cem}$ . If the cooling of a casting is not slowed down within the range of eutectoid transformation, the structure will contain only pearlitic matrix and temper carbon, purely pearlitic malleable cast iron will be formed.

Pearlite is roughly 2.5 times stronger and harder than ferrite, but has a lower ductility. Because of this, increasing the proportion of pearlite in the structure of malleable cast iron enhances the strength properties, but lowers the ductility. For instance, ferritic malleable cast iron Grade K437-12 has  $\sigma_t = 37 \text{ kgf/mm}^2$  and  $\delta = 12$  per cent, while pearlitic cast iron Grade K463-2 has  $\sigma_t = 63 \text{ kgf/mm}^2$  and  $\delta = 2$  per cent.

The development of the second graphitization stage can be ensured not only by slower cooling in the eutectoid temperature

range, but also by an isothermal holding after a common (not slowed down) cooling (see the hatched rectangle in Fig. 104). During the continuous cooling, pearlitic transformation of the austenite takes place, while the subsequent long holding causes graphitization of pearlitic cementite. The mechanism of graphitization is here principally the same as in the first stage, but the graphitization proceeds by the transfer of carbon atoms not through austenite, but through ferrite from F/cem to F/G boundaries. The critical link of the process is the evacuation of iron atoms in the ferrite from the surface of growing graphite particles. At temperature  $t_2$  (see Fig. 107), pearlitic cementite disappears at a moment corresponding to point 6. A lower temperature of isothermal holding requires a greater time to attain this moment (note the slope of curve *BK*).

During the isothermal holding, the division of cementite platelets (at places where subboundaries in cementite and ferrite pass out onto Cem/F boundaries) and spheroidization of cementite occur along with the graphitization of pearlitic cementite. The mechanisms of these processes are similar to the mechanisms of formation of spheroidite discussed in 2.2.3.

By maintaining an increased content of manganese in the charge (up to 1 per cent), it is possible to slow down sharply the graphitization of pearlitic cementite, so as to retain pearlite in the metal and, by means of spheroidization, to produce malleable cast iron with the matrix of spheroidite.

Granular pearlite cast iron combines a high strength and an increased ductility and also has a good machinability and high antifriction properties. The relative elongation of such cast iron attains 10 per cent at  $\sigma_t = 60 \text{ kgf/mm}^2$ , so that it can replace cast or forged steel in many applications. Malleable cast iron with granular pearlite matrix is used for making some critical parts, such as crankshafts and camshafts.

The process of annealing of white cast iron to malleable iron requires much time, sometimes a few tens of hours. It is the most expensive operation in the manufacture of malleable cast iron, which affects appreciably the cost of castings. This is why various methods for accelerating the annealing process have been developed.

A rather effective method is to hold the metal preliminarily at a temperature around  $400^\circ\text{C}$  for approximately 6 hours; it increases the number of graphitization nuclei at the first stage.

Small additions of modifiers (0.02 per cent Al or 0.003 per cent B) are also effective in accelerating graphitization.

Graphitization can be accelerated sharply by preliminarily quenching of white-iron parts in oil, probably owing to the formation of numerous hardening submicrocracks which are then



filled with temper carbon in the first graphitization stage. This method is applicable, however, only to small parts of a simple shape.

### **Chill-eliminating Annealing**

Rapid chilling of thin sections in castings made of grey cast iron or high-strength spheroidal-graphite iron can cause crystallization of ledeburite, i.e. white cast iron is formed in such places. In die-cast articles, the whole surface may sometimes be chilled. The machinability and ductility of such articles can be improved by graphitizing annealing which eliminates the chilling effect.

Since grey iron and high-strength iron contain more silicon (up to 3.3 per cent) than malleable cast iron, graphitization proceeds quicker in them. Accordingly, the temperature and time of annealing to eliminate chill are lower than those required for white-to-malleable cast iron annealing. To eliminate chill, castings are heated at 850-950 °C for 0.5-5 hours and then cooled in air. The matrix in chilled places becomes pearlitic or ferrite-pearlitic, depending on the rate of cooling and the composition of cast iron.

### **Low-temperature Softening**

This method is used to lower the hardness and improve the machinability and cyclic toughness in castings made of grey cast iron with pearlitic or pearlite-ferritic matrix. Castings are annealed at 670-750 °C for 1-4 hours so as to graphitize partially pearlitic cementite, partial spheroidization of the cementite takes place simultaneously. The mechanisms of these processes are similar to those taking place during isothermal holding at the second stage of graphitization of malleable cast iron.

#### **2.3.2. NORMALIZING OF CAST IRONS**

Heat treatment of grey cast iron to increase its strength is not used as widely as heat treatment of steels. An explanation is that lamellar graphite can strongly lower the strength and ductility of the metallic matrix by affecting internal notches. Because of this a change in the structure of the metal caused by heat treatment gives no desirable strengthening effect and is often too expensive. More effective is heat treatment of grey cast irons with a more favourable form of graphite, in particular of high-strength cast irons with spheroidal graphite. A variety of this heat treatment is normalizing, which increases the strength, hardness and wear resistance of the metal.

Normalizing is commonly used with castings having ferritic or ferrite-pearlitic matrix, and less frequently, pearlitic matrix. Cas-

tings are heated at 850-950 °C for 0.5-3 hours and cooled in quiet air or by air jets. Intricate-shape castings are advised to be furnace-cooled beginning from a temperature of about 500 °C in order to diminish residual stresses.

The heating first causes austenitization of the metal, which includes  $\alpha \rightarrow \gamma$ -transformation, and dissolution of graphite and pearlitic cementite (if the matrix contains pearlite) in the austenite. The structure of cast iron upon austenitization is austenite plus graphite. With further heating, graphite dissolves partially in the austenite according to the  $S'E'$  line and the amount of bonded carbon increases.

With rapid cooling in air, pearlitic decomposition of the austenite takes place and the whole matrix becomes pearlitic or sorbitic. The strengthening effect on normalizing is due to two factors as follows: elimination of structurally free ferrite (i.e. an increase in the concentration of carbon that is bonded in cementite) and an increased dispersity of pearlite. The hardness of cast iron increases from 150 HB to 200-250 HB. The strengthening effect depends on the initial structure, being the highest for ferritic cast iron, since the soft ferritic matrix in it is replaced with harder pearlitic matrix. Normalizing of pearlitic cast iron only increases the dispersity of the eutectoid, but even in that case the wear resistance can increase by a factor of 1.5.

Normalizing can also be employed with malleable cast iron to increase hardness. Ferritic malleable cast iron transforms in one having a pearlitic or sorbitic matrix through normalizing. One should, however, keep in mind that such a matrix can also be formed during the process of white-to-malleable cast iron transformation, by quick cooling after the first graphitization stage.

#### LITERATURE

Bunin K. P., Taran Yu. N. The Structure of Cast Iron (*Stroenie chuguna*). Moscow, Metallurgiya, 1972, 160 pp., ill.

Machine-building Materials (*Materialy v mashinostroenii*). Volume 4, Moscow, Mashinostroenie, 1969, 248 pp., ill.

## 2.4. ANNEALING OF NON-FERROUS METALS AND ALLOYS

With non-ferrous metals and alloys, second-order annealing is used less frequently than with steels and cast irons.

Many commercial non-ferrous metals and alloys, such as single-phase brasses, bronzes and electrical nickel alloys, undergo no phase transformations in the solid state, so that second-order annealing is principally unfit for them. With other alloys, which show phase transformations in the solid state, second-order an-

nealing is also inapplicable since it can cause undesirable changes in their properties.

Depending on the type of phase transformation, two kinds of second-order annealing are distinguished, namely *heterogenizing annealing* and *annealing with phase transformation*.

### 2.4.1. HETEROGENIZING ANNEALING

Heterogenizing annealing is used with alloys in which one or more phases can precipitate from the matrix phase owing to a change in the equilibrium concentration with lowering temperature. In most alloys, the solid solution of the main metal is the matrix phase and a compound is an excess phase. These materials include all heat-hardenable alloys based on aluminium, magnesium, copper, nickel, etc., such as duralumins, elektron, beryllium bronze, nimonic. This is the largest group among non-ferrous alloys. In binary systems, the behaviour of alloys of this type during heterogenizing annealing is closely associated with the form of the solvus line (see, for instance, Fig. 68e).

The relative amount of a phase that can fully pass to the solid solution on heating and precipitate on slow cooling usually does not exceed 10-15 per cent of the whole volume of alloy. Under such conditions, the phase transformation causes no radical changes in the whole structure of the metal, as distinct from annealing of carbon steels at temperatures above  $A_3$ . The type of crystal lattice of the matrix phase is not changed when another phase dissolves in or precipitates from it. The annealing process, which includes only dissolution and precipitation, merely causes changes in the concentrations of components in the matrix phase and in the size and shape of particles of precipitating phase. These changes underlie the principle of heterogenizing annealing.

### Heterogenizing Softening

In many alloys the heterogenization of the structure upon precipitation of excess phases from the matrix solution, which takes place on slow cooling from the annealing temperature, causes the softening effect which can be used for various purposes.

*Full softening* is applicable with all heat-hardenable aluminium alloys (duralumins, Avial, etc.). Its purpose is to soften the metal and improve its ductility before stamping, bending, flanging or other operations of cold plastic working. For instance, hot-rolled coils, say, of duralumin, may harden partially owing to an accelerated cooling in air. They can be subjected to heterogenizing annealing, which enables a greater reduction to be used in subsequent cold rolling without intermediate annealing operations.

Heterogenizing annealing can be carried out by heating the alloy until its excess phase is completely dissolved (i.e. by heating above  $t_0$  in Fig. 68e), followed by very slow cooling, which is needed to lower the concentration of the solid solution as much as possible and to prevent precipitation of the phase in an excessively disperse form with very small distances between particles. A lower concentration of the matrix solution and a higher distance between

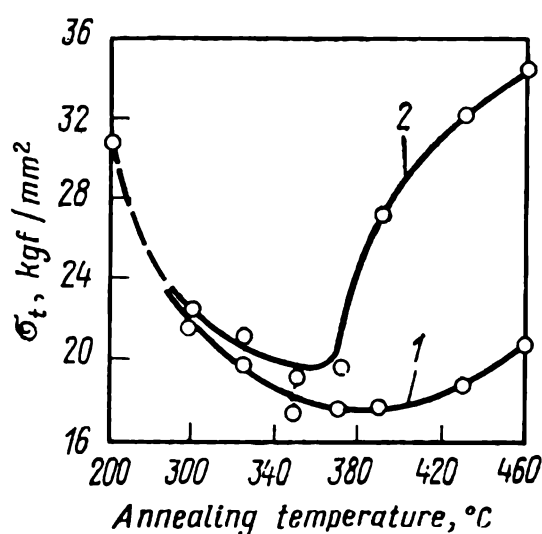


Fig. 108. Effect of annealing temperature on ultimate strength of cold-rolled duralumin Д16 at two different cooling rates (after V. A. Livanov and S. M. Voronov)  
1—furnace cooling to 200 °C; 2—air cooling

precipitated particles ensure a greater softening effect upon annealing.

In order to save time, it is advisable to heat the metal slightly below  $t_0$ . The heating temperature is so chosen as to attain an almost equilibrium concentration of the matrix phase in a relatively short time and also to cause the second phase to coagulate. It is followed by slow cooling.

Most of heat-hardenable aluminium alloys are fully softened by heating at 380-420°C for 10-60 minutes, followed by cooling at a rate not over 30 °C/h.

In full annealing, the principal heterogenizing process may be accompanied with recrystallization

which also contributes to the softening effect. This may occur, for instance, if a sheet of metal has been work-hardened owing to an excessively low temperature at the end of hot rolling. The annealing conditions for full softening are however selected from the requirements of structure heterogenization, for which slow cooling is needed, whereas in purely recrystallization annealing of single-phase alloys the rate of cooling is of no importance.

*Partial softening* of heat-hardenable aluminium alloys is done at a lower temperature than that required for full annealing. In this process, the concentration of the matrix solution lowers during heating to such an extent that quick cooling in air or even in water becomes possible. Owing to the lower temperature, the time of holding at that temperature in partial annealing must be greater than in full annealing, but the total time of heat treatment shortens owing to a quicker subsequent cooling.

As shown in Fig. 108, the annealing temperature for the maximum softening of duralumin Grade Д16 must be around 380-400 °C for furnace cooling or 350-370 °C for air cooling. At higher temperatures, the S-phase and  $\text{CuAl}_2$  can quickly pass to the alu-

minium solution, causing partial hardening and an increase in strength on subsequent cooling.

Partial softening of most aluminium alloys is carried out at 350-370 °C for 2-4 hours, followed with cooling in air or water.

Heterogenizing softening is applicable not only with aluminium alloys, but also with alloys of other metals. If, for instance,

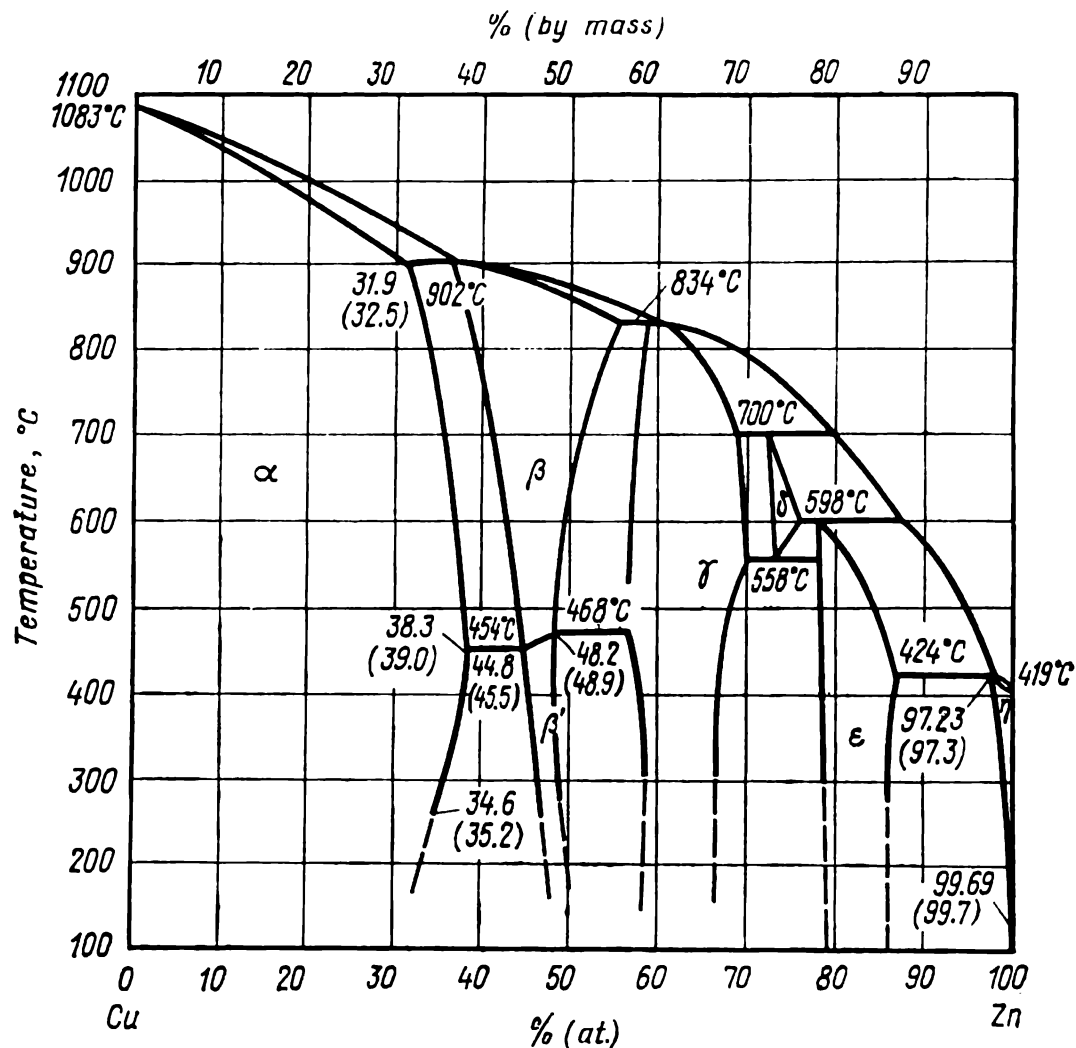


Fig. 109. Cu-Zn constitutional diagram (numbers in brackets are mass percentages)

( $\alpha + \beta$ )-brass has been cooled excessively quickly from the  $\beta$ -region after hot plastic working and thus has a reduced ductility (owing to a large amount of brittle  $\beta'$ -phase), this defect can be eliminated by annealing and slow cooling during which the lamellar  $\alpha$ -phase has enough time to precipitate from the  $\beta$ -phase (see the constitutional diagram in Fig. 109).

### Heterogenizing Annealing to Increase Corrosion Resistance

A two-phase structure with a definite degree of dispersity and with an optimum distribution of excess phase particles may ensure an increased corrosion resistance. Such a structure can be ob-

tained by heterogenizing annealing. For instance, the maximum resistance to stress corrosion in magnalium Grade AMr6 is ensured by a two-phase structure in which the  $\beta$ -phase ( $\text{Al}_3\text{Mg}_2$ ) is evenly distributed in grains of the aluminium solution. The effect is achieved by heterogenizing annealing of magnalium at  $320^\circ\text{C}$  prior to the final cold working operation.

### Phenomenon of Overheating in Cast Alloys

Grain boundaries in commercial cast alloys are quite stable. Single-phase cast alloys show virtually no grain coarsening on being heated.

The effect of structural strain hardening, which occurs on dissolution of one phase in another, can in principle destroy the stability of boundaries and cause grain coarsening in the matrix phase.

In heat-hardenable aluminium, magnesium and copper alloys, the content of secondary phases is relatively small, so that volume changes on dissolution of these phases cause no appreciable structural strain hardening. For that reason, heating of these alloys (as cast) with passage over the solubility limit into the single-phase region causes no appreciable grain coarsening in the main solid solution; exceptions are very rare.

A special case is  $(\alpha + \beta)$ -brass. Upon heating to a temperature above that needed for full passage from  $(\alpha + \beta)$  to  $\beta$ -state (Fig. 109), strong overheating (and grain coarsening) becomes possible, with  $\beta$ -grains sometimes growing to a few centimeters in diameter (Fig. 110). The conditions for grain coarsening in heated cast  $(\alpha + \beta)$ -brass are ensured by the phase transition from  $(\alpha + \beta)$  to  $\beta$ -state. In two-phase cast brasses the relative amount of  $\alpha$ -phase may be appreciable, and in any case much greater than the relative amount of secondary phases in heat-hardenable aluminium and magnesium alloys and in many bronzes. This follows from the pattern of the Cu-Zn constitutional diagram. The phase that dissolves on heating is  $\alpha$ -phase, whose relative weight amount at room temperature may vary from 0 to 100 per cent depending on zinc content. On heating a two-phase brass having a high proportion of  $\alpha$ -phase, the dissolution of the latter in the  $\beta$ -phase evidently produces structural strain hardening effect that provokes grain coarsening.

Overheating of  $(\alpha + \beta)$ -brass is often linked with burning, with zinc being preferably oxidized at grain boundaries. In the ingot shown in Fig. 110, the surface of grains had been found to be coated with thin white layer of zinc oxide.

In cast single-phase  $\alpha$ -brass, which undergoes no phase transformations in the solid state, overheating is not observed, and only burning is dangerous.

In some cases small additions in a cast alloy can cause strong grain coarsening of the main solid solution, though the alloy may

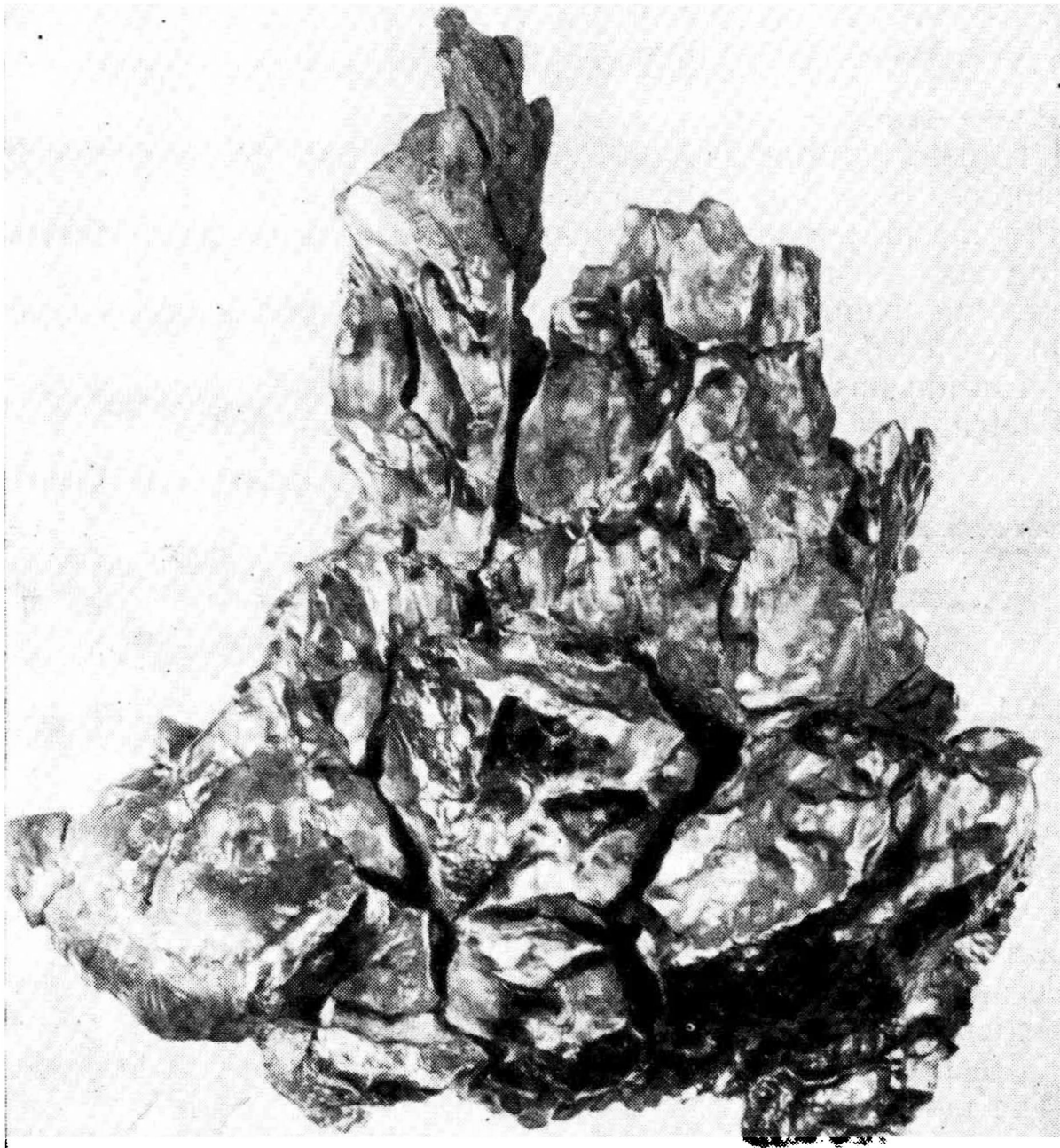


Fig. 110. Gigantic grains formed in overheated ingot of  $(\alpha + \beta)$ -brass,  $\frac{1}{2}$  full size

contain a relatively low amount of excess phases. For instance, when heating Grade MJ5 magnesium alloy castings, the dissolution of the excess  $\text{Mg}_{17}\text{Al}_{12}$  phase, whose content is quite small, causes no grain coarsening. If however, only a few thousandths of a per cent of zirconium ( $>0.002$  per cent) have passed into the



metal occasionally, then the cast metal will have an appreciably coarser grain on heating to 415 °C. The nature of this interesting effect is not yet established.

#### 2.4.2. ANNEALING WITH PHASE TRANSFORMATION

Phase transformation, which involves polymorphic or eutectoid transformation, causes a radical change in the structure throughout the whole volume of alloy (Fig. 68a-c).

Polymorphic transformations in metals can be used for eliminating an unwanted texture and changing the size of grains. An interesting example in this respect is the heat treatment of uranium (called  $\beta$ -heat treatment).

Uranium has a rhombic  $\alpha$ -lattice at temperatures below 668 °C and tetragonal  $\beta$ -lattice, at temperatures from 668 to 774 °C. At



Fig. 111. 'Growth' of uranium rod rolled at 300 °C. Above: before thermocycling; below: after 3000 thermal cycles within the range of 50 to 550 °C

the early stage of development of nuclear engineering it has been established that articles made of polycrystalline uranium change their dimensions when subjected to multiple heating and cooling within the temperature range of the  $\alpha$ -phase. A rough surface appears in cast coarse-grained articles. When being plastic worked, an article (rod, wire or plate) appreciably elongates ('grows') in one direction and contracts in another (Fig. 111).

The most decisive factor determining the 'growth' of uranium is the texture formed on plastic working in the  $\alpha$ -region. The preferable orientation of crystals in a piece of uranium results in a strong anisotropy of the thermal expansion, owing to which thermal cycles cause stresses and oriented changes in the dimensions of the article. The harmful effect of 'growth' of uranium can be avoided by eliminating the texture formed on plastic working in the  $\alpha$ -region.

If a uranium rod with a distinct texture is heated to a temperature within the  $\beta$ -range (above 668 °C) and then cooled, this causes phase recrystallization, with the  $\alpha$ -crystals formed by the polymorphic  $\beta \rightarrow \alpha$ -transformation losing their preferable orientation. Therefore, phase transformation can eliminate the oriented texture and make the coefficient of thermal expansion equal in



all directions. After such treatment, the rate of 'growth' of a uranium rod in thermal cycling diminishes appreciably.

The greater the size of grains, the more pronounced is the roughness of surface of uranium articles appearing after multiple thermal cycles. Grain refinement in uranium can be obtained by phase recrystallization. The size of  $\alpha$ -grains diminishes more and more as the rate of cooling from the  $\beta$ -state increases.

By analogy with uranium, polymorphic transformations in other non-ferrous metals and alloys and in solid solutions can be used for eliminating unwanted textures and for grain refinement.

Eutectoid transformations in non-ferrous metals are yet seldom used as the basis for second-order annealing.

It should be noted in conclusion that heating above the critical point during a polymorphic transformation can result in a strong grain growth in deformed and cast metals and alloys.

#### LITERATURE

Bochvar A. A., Fundamentals of Heat Treatment of Alloys (*Osnovy termicheskoi obrabotki splavov*). Moscow, Metallurgizdat 1940, 298 pp., ill.

Kolachev B. A., Livanov V. A., Elagin V. I., Physical Metallurgy and Heat Treatment of Non-Ferrous Metals and Alloys. (*Metallovedenie i termicheskaya obrabotka tsvetnykh metallov i splavov*). Moscow, Metallurgiya, 1972, 480 pp., ill.

## QUENCHING

Like second-order annealing, quenching is only applicable to those metals and alloys which can undergo phase transformations in the solid state. The principal parameters of quenching are the temperature of heating, the time of holding at that temperature, and the rate of cooling.

The temperature of heating and the time of holding should be such as to produce the required structural changes, for instance, the formation of a high-temperature phase through polymorphic transformation (see Fig. 68*a, b, d*), dissolution of an excess phase in the matrix (see Fig. 68*e*), etc. In that respect quenching is similar to second-order annealing.

The rate of quench cooling should be sufficiently high to preclude reverse phase transformations (eutectoid decomposition, precipitation of an excess phase from the matrix solution, etc.) which might be linked with diffusion or self-diffusion at a reduction of temperature. In that respect, quenching differs radically from second-order annealing.

There are two principal types of quenching which differ drastically from one another, i.e. *quenching without polymorphic change and that with polymorphic change*.

### 3.1. QUENCHING WITHOUT POLYMORPHIC CHANGE

Quenching without polymorphic change is applicable to all alloys in which one of the phases is fully or partially soluble in another. For instance, when a  $C_0$  alloy (Fig. 112) is being heated to  $T_h$ , its  $\beta$ -phase dissolves in the matrix  $\alpha$ -phase. With reverse slow cooling, the  $\beta$ -phase precipitates from the  $\alpha$ -phase and the concentration of  $B$  component in the latter diminishes following the solvus line  $nb$ .

Since the compositions of  $\alpha$ - and  $\beta$ -phase are different, precipitation of the  $\beta$ -phase involves diffusion redistribution of the components. If, however, cooling is done with a sufficiently high rate, diffusion redistribution, which is needed for nucleation and growth of  $\beta$ -phase crystals, has no time to proceed and  $\beta$ -phase cannot precipitate from  $\alpha$ -solution. Such type of heat treatment (quench-

ing) will yield an alloy containing the  $\alpha$ -phase only, i.e. having the same composition as at the temperature of heating for quenching.

Consequently, *quenching without polymorphic change consists essentially in that the state an alloy has been in at a higher temperature is artificially fixed at a lower temperature.*

When the  $C_0$  alloy is heated for quenching at  $T_h$ , its solid solution is unsaturated. Upon quenching, the  $\alpha$ -solution will have the same composition at room temperature as at the temperature of quenching, but the solution will be supersaturated, since the composition of saturated solution corresponds to point  $b$ .

Thus, *quenching without polymorphic change results in the formation of supersaturated solution.* This type of quenching is positively inapplicable to pure metals. It is widely used with alloys of aluminium, magnesium, nickel, copper and other metals and also with some types of alloy steel.

Quenching is not always linked with fixation of a single-phase state in alloys. For instance, the  $C_2$  alloy (Fig. 112) will contain some  $\beta$ -phase at any temperature, up to the eutectic temperature. When heated to  $T_h$ , this alloy contains the saturated solid solution, whose composition corresponds to point  $m$ , and an excess of  $\beta$ -phase. With sufficiently slow cooling, the composition of this alloy should vary along the line  $mb$  owing to the precipitation of  $\beta$ -phase from  $\alpha$ -solution. With fast cooling, however, the  $\beta$ -phase has no time to precipitate from  $\alpha$ -solution and the alloy will be quenched, i.e. its composition at room temperature will be determined by point  $m$ , as at the temperature of quenching. Therefore, the  $C_2$  alloy, as quenched, will contain the  $\alpha$ -solution of the composition defined by point  $m$  and excess  $\beta$ -phase which has remained undissolved on heating for hardening, i.e. the quenching fixes in the alloy the state which has been stable during the heating for quenching.

The beginners in the course of heat treatment sometimes arrive at an erroneous conclusion that quenching is only applicable to such alloys whose ordinate intersects the line of phase equilibrium in the solid state, such as the  $C_0$  alloy in Fig. 112. Actually, as we have shown for  $C_2$  alloy, it is not at all necessary. Quenching without polymorphic change is principally feasible always when an alloy has different compositions of its phases in the equilibrium state at different temperatures.

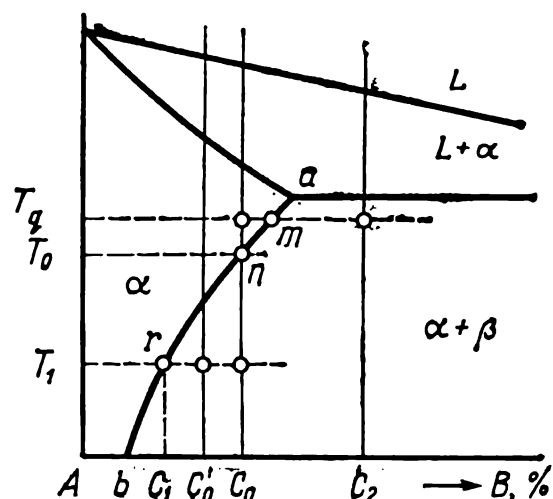


Fig. 112. A diagram to explain quenching without polymorphic change

### 3.1.1. VARIATIONS OF PROPERTIES DURING QUENCHING WITHOUT POLYMORPHIC CHANGE

Variations of the properties of an alloy on quenching depend on the phase composition and structure of that alloy in the initial and quenched state, quench conditions, preliminary heat treatment, and some other factors. The properties of various alloys may vary quite differently as far as the degree and direction of this change are concerned.

There exists an erroneous assertion that quenching is always linked with hardening of the metal, with the terms 'quenching' and 'hardening' being even considered synonymic. Actually, quenching can either harden or soften an alloy. In some alloys, quenching can increase the strength, but lower the ductility; in others, on the contrary, it can lower the strength parameters but increase the ductility, while in still other alloys it can increase both the strength and ductility. Finally, very many alloys that are principally hardenable do not practically change their properties on being quenched.

A large hardening effect with simultaneous sharp reduction in ductility is not observed in industrial alloys upon quenching without polymorphic change.

Deformable alloys, when quenched without polymorphic change, most often increase their strength and at the same time retain a high ductility, which differs only slightly from that of as-annealed alloy. A typical example is Д16 duralumin (Table 7).

**TABLE 7. Mechanical Properties of Selected Alloys  
(as cast, annealed, and quenched)**

Alloy	$\sigma_t$ , kgf/mm <sup>2</sup>		$\delta$ , %		Alloy	$\sigma_t$ , kgf/mm <sup>2</sup>		$\delta$ , %	
	as annealed	as quenched	as annealed	as quenched		as cast	as quenched	as cast	as quenched
Д16	20	30	25	23	АЛ8	15	30	1	12
Бр.Б2	55	51	22	46	АЛ9	16	20	2	6
					МЛ5	16	25	3	9

Less frequently, quenching of an alloy can lower the strength and increase appreciably the ductility, as compared with that in as-annealed state. A typical example is beryllium bronze Бр.Б2 (Table 7). Chrome-nickel stainless steel Grade X18H9, when quenched after hot rolling, exhibits an increase in the relative elongation from 20 to 45 per cent. Semiproducts made of such alloys as beryllium bronze or steel Grade X18H9 are therefore quenched before cold forming, instead of being annealed.

The following discussion will explain whether the strength of an alloy will increase or lower on quenching. The strength of a solid solution will increase with increasing the concentration of an alloying element in it. For that reason, the supersaturated solution in a quenched alloy has a higher strength than the less alloyed solution in the alloy as annealed. The strength of an annealed alloy is determined by the strength of the matrix solution and also by the size and structure of particles of an excess phase and the distances between these particles. If the hindering of dislocation by an excess phase does not contribute much to the strength of a two-phase mixture (for instance, owing to large distances between particles of that phase), then the hardening of the solution through increasing the degree of alloying on quenching will overcompensate the softening due to the dissolution of the excess phase, and the strength of the alloy will increase. If, however, the dissolution of an excess phase causes an appreciable softening, which outweighs the gain in strength resulted from an increase in the concentration of the matrix solution, then the alloy will soften on quenching. The total effect depends on how much the solubility changes on heating for quenching and also on the increase in the strength of the matrix solution per each per cent of the element being dissolved.

Quenching of casting alloys usually increases their strength and ductility compared with as-cast state (see alloys АЛ8, АЛ9 and МЛ5 in Table 7). In industrial casting alloys, excess phases are usually present in the structure as relatively large particles with large distances between them. Upon their dissolution, the strength of an alloy increases owing to a larger degree of alloying of the matrix solution.

Cast alloys can fracture and break along coarse and brittle inclusions of an excess phase, for instance of an intermetallic phase. In such alloys, quenching results in an increase of their ductility, the effect being especially high if the excess phase has dissolved fully, such as in aluminium alloy Grade АЛ8 ( $\text{Al}_3\text{Mg}_2$  dissolved) or magnesium alloy Grade МЛ5 ( $\text{Mg}_{17}\text{Al}_{12}$  dissolved), which are virtually single-phase alloys when quenched (see Table 7). In АЛ9 silumin, the ductility increases on quenching owing to partial dissolution and coagulation of the silicon and full dissolution of  $\text{Mg}_2\text{Si}$  silicide.

The main purpose of quenching without polymorphic change is to prepare an alloy for ageing. With some alloys (Бр.Б2, Х18Н9) it is used as an intermediate softening operation (instead of annealing) before cold forming. And it also, may be the final heat-treatment procedure aimed at imparting the required complex of properties to products. A quenched single-phase alloy may have

an appreciably higher ductility and a higher corrosion resistance than upon being aged. For these reasons, the aluminium alloy Grade A18 is employed only as-quenched.

### 3.1.2. HEATING AND COOLING DURING QUENCHING WITHOUT POLYMORPHIC CHANGE

#### Heating

The principal initial requirement for selecting the temperature of quenching is to make the excess phases to dissolve as fully as possible in the matrix phase.

If an alloy is so located in the constitutional diagram that it is capable of transforming fully into a single-phase state on heating (such as  $C_0$  alloy in Fig. 112), then its temperature of hardening should be above the solvus line of the binary system. Otherwise, i.e. if the  $C_0$  alloy is quenched from a temperature below  $T_0$ , a certain amount of  $\beta$ -phase may remain undissolved and the matrix  $\alpha$ -solution will be alloyed less than on quenching from a temperature above  $T_0$ .

The upper limit of the interval of quenching temperatures is selected somewhat lower than the solidus point of an alloy in order to prevent burning (see p. 36), taking into account probable temperature changes in a batch and the accuracy of temperature control. Should burning take place, grain boundaries will melt and thus destroy the bondage between grains, so that hardening stresses may cause intercrystalline cracks. Fine cracks, though being undetectable, can lower appreciably the strength and ductility. Burning may also occur through the formation of layers of a brittle phase on quenching, owing to non-equilibrium crystallization of melted portions which are enriched in alloying elements. Another cause of burning may be quick penetration of some components of the gas atmosphere into molten portions, where they may form oxides and gas blowholes. A slight burning is seen on a microsection as thickenings at grain boundaries. Burning is unrepairable and is therefore most dangerous kind of defect.

The feasible width of the interval of quenching temperatures for a binary system is determined by the distance between the points of solidus and solvus. As will be seen from Fig. 112, the range of probable quenching temperatures for  $C'_0$  alloy is wider than that for  $C_0$  alloy.

When quenching cast alloys which, unlike deformable grades, are not preliminarily homogenized nor heated prior to hot forming it is necessary to consider melting of the non-equilibrium eutectic (see the dotted line  $ka$  in Fig. 5). If a casting alloy is to be heated to a temperature above the non-equilibrium solidus point

(for instance, above point  $n$  for  $X_2$  alloy in Fig. 5a), in order to dissolve as fully as possible the excess phases, then stepwise heating can be resorted to; at the first stage of heating, which must be done at a temperature below the non-equilibrium solidus point, the fusible component is dissolved and then the temperature can be raised to the final value without any risk of burning. For instance, massive castings of alloy МЛ5 must be held for 3 hours at 375°C before being heated to 415°C for quenching.

If the content of an alloying element is in excess of the solubility limit and the alloy cannot be transformed into a single-phase state (for instance,  $C_2$  alloy in Fig. 112), then the temperature of heating for quenching is chosen as close as possible to the eutectic (peritectic) temperature, with a certain safety margin left to prevent burning.

The range of quenching temperatures may be a few degrees or tens of degrees (seldom above 100 degrees C), depending on the type of alloying, the contents of alloying elements, and on how much the properties of that alloy may be affected by incomplete dissolution of excess phases. For instance, with duralumins, the temperature range may vary from 5 to 15 degrees C, being from 495°C to 510°C for Grade Д1, from 495° to 505°C for Grade Д16, and from 503° to 508°C for high-magnesium duralumin Grade Д19П. With duralumins, the upper temperature limit may differ only by a few degrees from the solidus point. With such a narrow temperature range, reliable heating is only possible in either saltpetre baths or furnaces with forced air circulation.

A different example are deformable and casting aluminium alloys based on Al-Zn-Mg system, with which the possible range of quenching temperatures may be as large as 150 degrees C, i.e. an order of magnitude (!) wider than that of duralumins. These alloys can be quenched from temperatures of from 350° to 500°C. Naturally, such alloys can be heated for quenching much more easily without any risk of burning or overheating.

With a sufficiently wide range of quenching temperatures, the temperature within it should be selected as high as possible in order to shorten the time of dissolution of excess phases. The upper limit of quenching temperatures, however, depends more on grain coarsening in a deformed alloy, rather than on the solidus point. In addition, some semiproducts must retain non-recrystallized structure upon hot forming and then the temperature of heating for quenching must not exceed that of the beginning of recrystallization (see 5.2.1).

The time of holding at the selected temperature during quenching is so chosen as to let the processes of dissolution of excess phases to proceed to completion. It may depend on the composition of alloy, the temperature of heating for quenching, and the

original structure of the metal. Disperse excess phases can dissolve quicker. Forged semiproducts can often (but not always) be held at the quenching temperature for a shorter time than is needed for castings, since coarse particles of excess phases have been dissolved in them during homogenizing, while the forging proper has had a refining effect on their structure. For example, aluminium alloy sheets can be held at the temperature of quenching for 10-40 minutes, whereas castings of the same alloy require as much as 2-6 hours (and sometimes more than 10 hours).

The time for dissolution of excess phases in casting alloys during heating for quenching and the size of particles of these phases are connected by the relationship (3). Sand-mould castings should be heated for longer time for quenching than die castings, because of the fact that they usually have a coarser structure. The larger is the cross-section of a casting and respectively the lower is the rate of its cooling on casting, the greater will be the particles of excess phases and the longer the time needed for heating before quenching. For that reason the time of heating of castings may range from a fraction of an hour to 10-20 hours.

### Cooling

The concept of 'quenching' is commonly associated with quick cooling. Indeed, many articles are quenched in water. In the general sense, however, quenching does not necessarily require fast cooling. The only thing of importance is that the cooling time be short enough to preclude the decomposition of the matrix solution. Thus, the decisive factor is the rate of this decomposition and the cooling rate may be varied accordingly. For some alloys quenching in cold water is indispensable, while for others, in which the matrix solution decomposes only slowly, air cooling may suffice. Many industrial alloys based on iron, nickel, aluminium and magnesium are air-hardenable (see Table 8).

### *Kinetics of Decomposition of Undercooled Solution*

Let a thin specimen of  $C_0$  alloy (Fig. 112), heated up to a temperature  $T_h$ , i.e. in the state of supersaturated solid solution, be transferred quickly into a thermostatic apparatus held at a temperature  $T_1$ , with  $T_1 < T_0$ . The  $\alpha$ -solution in the specimen then turns to be supersaturated, as the saturated solution for the temperature  $T_1$  is that whose composition corresponds to point  $r$ . The degree of supersaturation may be characterized by the ratio  $C_0/C_1$ .

The supersaturated  $\alpha$ -solution of the composition  $C_0$  at temperature  $T_1$  is at the same time undercooled relative to the tempe-



Table 8. Conditions of Quenching without Polymorphic Change for Various Alloys

Base metal	Alloy grade	Article	Heating temperature, °C	Holding time, h	Quench medium
Fe	X12H20T3P (ЭИ696А)	Rods, forgings	1100-1150	2	Air or water
	X12H22T3MP (ЭИ696М)	Rods	1100-1130	2	Air or oil
Ni	XH77TЮP (ЭИ437Б) ЖС6К	Turbine blades and discs	1070-1090	8	Air
		Cast blades and rotors	1180-1220	4	Air
Ti	BT22	Rods	800	1	Water
Cu	Бр.Б2 Бр.Х0.8	Spring members	760-780	8-15 min	Water
		Rods	980-1000	1-1.5 min	Water
Al	Д16	2-4 mm sheets	495-505	10 min *	Water 10-40 °C
	В95	Ditto	465-475	10 min *	Ditto
	АК4-1	Shaped forgings and die-forgings 50-75 mm thick	525-535	2.5-3.5	Water
	АД31	Rolled stock 5-10 mm thick	515-530	0.5-1	Air or water
	1915	Rolled stock 5-10 mm thick	440-460	0.5-1	Air or water
	АЛ9	Castings	530-540	2-6	Water 20-100 °C
	АЛ19	Castings	1st stage: 525-535 2nd stage: 535-545	5-9 5-9	
	АЛ27-1	Castings	430-440	20	Water 80-100 °C Water 95-100 °C
Mg	МА5	Forgings and die-forgings	410-420	2-6	Air
	МЛ5	Castings	410-420	8-16	Air

\* Saltpetre-bath heating.

perature  $T_0$ , above which only the single  $\alpha$ -phase is stable, and below it, only the two-phase mixture  $\alpha + \beta$ . The degree of undercooling is  $\Delta T = T_0 - T_1$ . A lower temperature of the thermostatic apparatus into which a specimen heated to  $T_h$  is placed will cause a higher degree of undercooling and a higher degree of supersaturation of the solid solution.

The thermodynamic stimulus for decomposition of an undercooled solution is the difference  $\Delta F_{vol}$  between the free energy  $F_1$  of that solution and the free energy  $F_2$  of the two-phase mixture (Fig. 113).

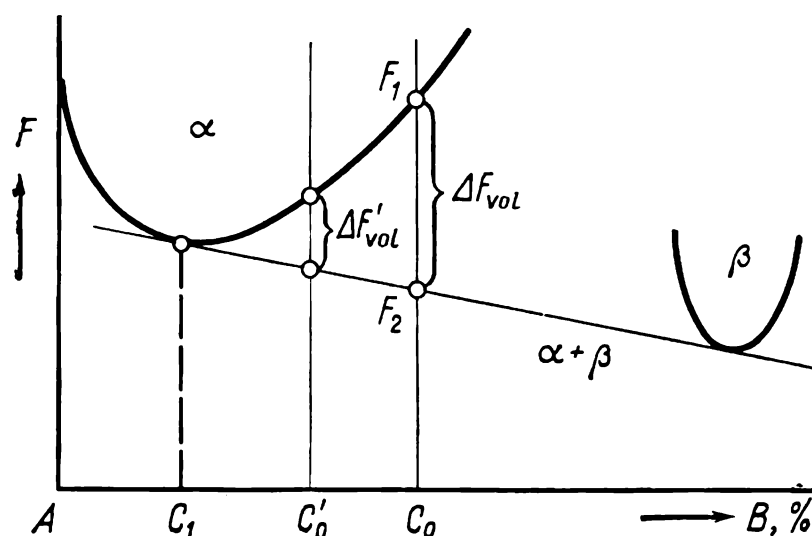


Fig. 113. Dependence of free energy of  $\alpha$ -phase and  $\beta$ -phase and two-phase ( $\alpha + \beta$ ) mixture on the composition of binary system at temperature  $T_1$  (see Fig. 112)

The rate of nucleation of a new phase in an undercooled solution, as in the case of a phase transformation in pure metal, is determined by expression (24). For a pure metal, however,  $Q$  is the activation energy of the passage of atoms through an interface, which is equal to the activation energy of self-diffusion, while in the case of decomposition of a solid solution  $Q$  is the activation energy of the diffusion of the element that diffuses most slowly. This diffusion is required for the nucleation of a new phase whose composition differs from that of the matrix solution.

In accordance with formula (24) the rate of formation of an excess phase in  $C_0$  alloy in Fig. 112, on increasing the degree of undercooling below  $T_0$ , should first increase owing to an increase in  $\Delta F_{vol}$  and the corresponding decrease in the work of formation of a critical nucleus,  $\Delta F_{cr}$ , and then diminish, since the diffusion mobility of atoms decreases. Consequently, the induction period, i.e. the time to the experimentally fixed start of the decomposition of the solution, first shortens with increasing degree of undercooling and then increases following the C-curve (Fig. 114).

The beginning of decomposition of an undercooled solution is determined by a change in one of the properties, such as ultimate strength or electric resistivity. Since these properties usually change gradually during isothermal holding, the starting point is taken conditionally as the one at which a property changes, for instance, by 2 or 5 per cent. Various properties begin to vary noticeably at different stages of decomposition of a solution. Duralumins, for example, may become sensitive to intercrystalline corrosion (which is linked with precipitation of excess phases at grain boundaries) much earlier before than their ultimate strength will change noticeably (see Fig. 114).

When plotting *C*-curves, it is practicable to measure the property which is one of the most important and which is sensitive to the earliest stages of decomposition of the solution. Since the experimentally fixed "start" of decomposition is a conditional moment, *C*-curves for various alloys can be compared only if they have been plotted by the same method.

### Critical Cooling Rate in Quenching

Quantitatively, the criterion of stability of an undercooled solid solution is the critical cooling rate ( $v_{cr}$ ), i.e. the lowest rate of continuous cooling which can prevent decomposition of the solution or, more strictly, to preclude a specified variation in the property selected. If the rate of cooling in the core of an article is faster than  $v_{cr}$ , the article will be hardened through. The critical cooling rate is found by drawing a tangent to a *C*-curve of conditional start of decomposition of undercooled solution from the point corresponding to the temperature of heating for quenching.

The magnitude of  $v_{cr}$  depends on the sensitivity of the method used for plotting the *C*-curve of the beginning of decomposition. For instance, for the same duralumin Grade Д16 the critical rate can be found as  $v_{cr} = 550^\circ\text{C/s}$ , if we use the *C*-curve plotted considering the sensitivity to intercrystalline corrosion in the metal, or as  $v_{cr} = 90^\circ\text{C/s}$ , if we use another *C*-curve corresponding to a 2-per cent change in the ultimate strength. If, however, the start of decomposition is taken as the moment when the ultimate strength changes by 5 per cent, then  $v_{cr} = 20^\circ\text{C/s}$ .

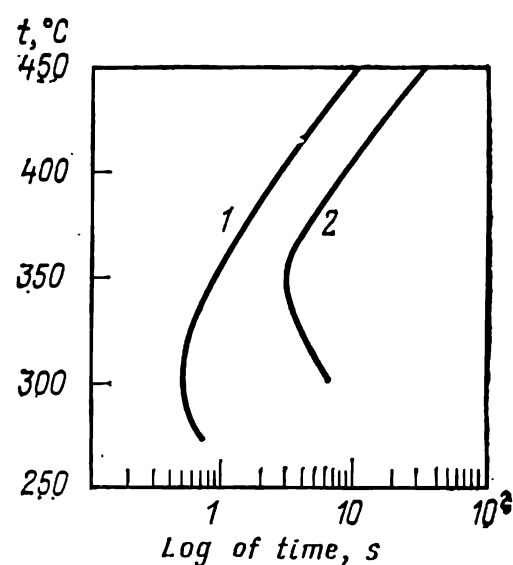


Fig. 114. *C*-curves of the beginning of breakdown of undercooled aluminium solution in Д16 alloy (after V. G. Davydov, I. I. Novikov, and E. D. Zakharov):

1—appearance of sensitivity to intercrystalline corrosion; 2—a 2-% change of ultimate strength

As has been shown in 2.1.5, quantitative estimations for continuous cooling should be done by using CCT-diagrams, rather than isothermal  $C$ -curves. Unfortunately, such diagrams for alloys hardenable without polymorphic transformations are still very few in number, so that the use of  $C$ -curves continues perforce.

Since the curve of the start of decomposition of the original phase in a CCT-diagram is shifted to the right and downwards relative to the corresponding  $C$ -curve plotted for isothermal conditions (see Fig. 84), the critical rate found by drawing a tangent to this  $C$ -curve will be somewhat higher than the actual value of  $v_{cr}$ . In some cases the difference is not large. For instance, the critical rate of cooling of duralumins found by means of an isothermal  $C$ -curve is only 1.1-1.2 times larger than the critical rate of isothermal cooling.

The lower  $v_{cr}$  is, i.e. the more the  $C$ -curve is shifted to the right, the larger will be the depth of hardening for the given cooling rate. Qualitatively, the hardenability of various alloys can be compared without calculating the critical cooling rate, simply by comparing the positions of their  $C$ -curves.

#### *Factors Affecting the Stability of Undercooled Solution*

The stability of undercooled solid solution may depend on the nature of the matrix, the type of alloying, the contents of alloying elements, and the structure of the alloy before quenching.

The diffusion mobility of atoms in alloys based on different elements cannot be the same as in alloys having the same base but different alloying elements [ $Q$  in formula (24)]. The work of formation of a critical nucleus depends on the surface energy at the interfaces between the matrix and precipitates and on the elastic strain energy which is due to the difference in specific volumes of the phases. For that reason the rate of nucleation of a precipitating phase [see formula (24)] is different in various systems. For instance, alloys based on the Al-Cu-Mg system (duralumins) are distinguished among aluminium alloys in having a rather low stability of undercooled solid solution, while alloys of the Al-Zn-Mg system (types 1915 and 1925), on the contrary, have a very high stability (Fig. 115). The difference in the stability of undercooled solution in the alloys of these two systems predetermines different methods of their heat treatment: the former should be quenched in water while the latter can be air-hardened. Pressed semiproducts of alloys 1915 and 1925 require no special quenching procedure, since they are self-hardened during air cooling from the temperature of pressing.

Quenching with air cooling is widely employed with heat-resistant austenitic age-hardenable steels with intermetallic strengthen-

ing, refractory nickel alloys of the Nimonic type, magnesium alloys of the Elektron type, etc. (see Table 8).

Increasing the concentration of alloying elements in a given system increases the degree of supersaturation, and therefore, decreases the stability of the solid solution. For instance, considering the alloys  $C_0$  and  $C'_0$  in Fig. 112, with the former being more

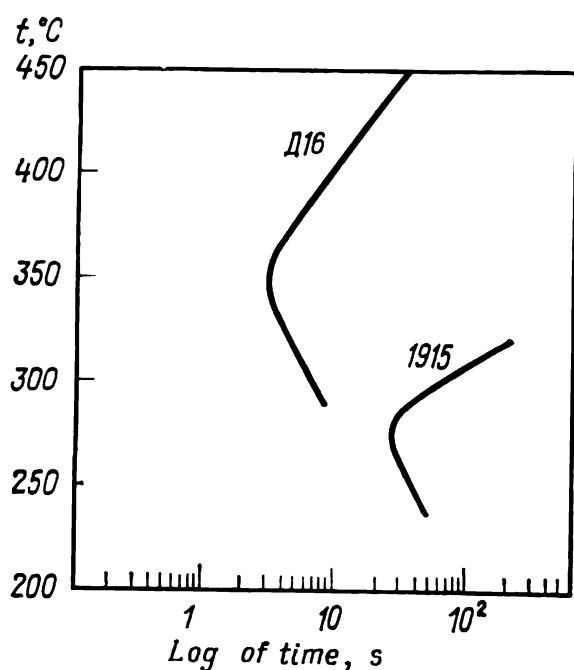


Fig. 115. C-curves of the beginning of breakdown of undercooled aluminium solution in alloys Д16 and 1915 at a corresponding 2-% change of ultimate strength (after V. G. Davydov, V. V. Zakharov, E. D. Zakharov, and I. I. Novikov)

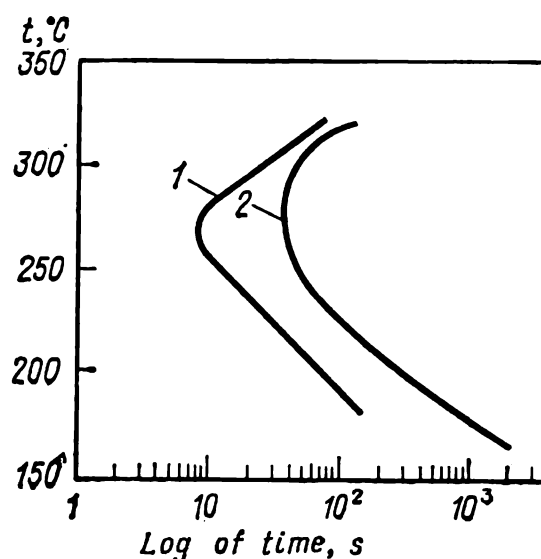


Fig. 116. C-curves of the beginning of breakdown of undercooled aluminium solution at corresponding 2-% change of ultimate strength in sheets of Al + 4.3% Zn + 1.9% Mg + 0.6% Mn + 2% Zr alloy with (1) unrecrystallized and (2) recrystallized structure (after V. V. Zakharov, I. I. Novikov, and V. I. Elagin)

heavily alloyed than the latter, we can find for their degrees of supersaturation at  $T_1$  that  $\frac{C_0}{C_1} > \frac{C'_0}{C_1}$  and for their thermodynamic stimuli of transformation that  $\Delta F_{vol} > \Delta F'_{vol}$  (see Fig. 113). Accordingly, the C-curve for  $C'_0$  alloy should be shifted rightwards relative to that for  $C_0$  alloy.

Disperse inclusions of intermetallics and other phases, if present in an alloy at the temperature of quenching, can lower the stability of undercooled solution and initiate decomposition. This can explain, for instance, the effect of small additions of transition metals (Mn, Cr, Ti) in aluminium alloys. When ingots are being homogenized or heated before plastic working or quenching, the solid solution is supersaturated with these elements during

crystallization of the melt, with disperse aluminides of these metals being precipitated. These serve as nucleators for precipitation of the main phases from the solution on cooling and the critical rate of cooling increases (i.e. the hardenability of the alloy diminishes).

The temperature of quenching may turn to be lower than the point of beginning of recrystallization. Alloys with unrecrystallized polygonized structure have a reduced stability of undercooled solid solution (Fig. 116) owing to easier nucleation of excess phases at dislocations and sub-boundaries.

Water quenching ensures high rates of cooling which for most articles (except for very large ones) made of alloys based on aluminium, magnesium, copper, nickel, iron and other metals are higher than  $v_{cr}$ . It can, however, produce large residual stresses and deformation of articles. For that reason the rate of cooling is lowered, where feasible, by using warm or boiling water. Softer quenchers, such as liquid nitrogen and special emulsions, have come into use recently for quenching of aluminium alloys. Some grades of heat-resistant austenitic steels are quenched in oil.

Quenching conditions for selected alloys are given in Table 8.

Stepwise and isothermal quenching without polymorphic change, as methods for reducing residual stresses and preventing warping of articles (see 3.2.9), have not found any wide application.

#### LITERATURE

Kolachev B. A., Livanov V. A., Elagin V. I., Physical Metallurgy and Heat Treatment of Non-ferrous Metals and Alloys. (*Metallovedenie i termicheskaya obrabotka tsvetnykh metallov i splavov*). Moscow, Metallurgiya, 1972, 480 pp., ill.

Diagrams of Isothermal Decomposition of Solution in Aluminium Alloys (*Diagrammy izotermicheskogo raspada rastvora v alyuminievykh splavakh*). Moscow, Metallurgiya, 1973, 152 pp., ill. Authors: V. G. Davydov, V. V. Zakharov, E. D. Zakharov, and I. I. Novikov.

### 3.2. QUENCHING WITH POLYMORPHIC CHANGE

Quenching with polymorphic change is principally applicable to all metals and alloys in which the crystal lattice is rearranged on cooling. Quick cooling by quenching causes martensitic transformation and produces a new phase which is called martensite. In recognition of this, quenching with polymorphic change is usually referred to as *martensitic quenching*, or *hardening to martensite*.

### 3.2.1. MARTENSITIC TRANSFORMATION IN CARBON STEELS

Martensitic transformation has been discovered in studies of steel hardening. The most typical features of martensitic transformation in carbon steels as compared with pearlitic transformation, are discussed below.

1. Martensitic transformation can occur in carbon steel heated to a temperature above  $A_1$  if the steel is quickly quenched, for instance, in water, i.e. under the conditions which suppress the breakdown of the austenite into a mixture of two phases (ferrite and carbide) whose composition differs largely from that of the original austenite. The concentration of carbon in martensite is the same as in the original austenite. Therefore, in contrast to pearlitic transformation *martensitic transformation is diffusionless*.

2. For each steel grade, the austenite-to-martensite transformation begins at a definite temperature  $M_s$  (where  $s$  stands for 'start'). *The  $M_s$  temperature is independent of cooling rate within a very wide range of cooling rates*, while the temperature of the beginning of pearlitic transformation lowers with increasing the cooling rate (see Sec. 2.2.2). Unlike the case with pearlitic transformation, *martensitic transformation cannot be suppressed even at the highest quenching rates attained*. The formation of martensite takes place within a definite temperature range between the upper martensitic point  $M_s$  and the lower point  $M_f$  (where  $f$  stands for 'finish'). The  $C$ -curve of transformations of undercooled austenite has two horizontal lines with the ordinates  $M_s$  and  $M_f$  (see Fig. 117) which define the beginning and end of the martensitic transformation. The effect of the carbon content in steel on the  $M_s$  and  $M_f$  points is shown in Fig. 118.

3. At  $M_s$ , the metal just begins to transform with first crystals of martensite being formed. *For the transformation to proceed, the steel must be cooled continuously within the martensitic temperature interval  $M_s$ - $M_f$* . If the cooling process is stopped and the steel is kept at a constant temperature within this interval, the formation of martensite ceases almost instantly. This is the most typical feature of the kinetics of martensitic transformation as distinct from pearlitic transformation which, as can be seen from its  $C$ -curve, always proceeds to the end at a constant temperature below  $A_1$ , i.e. results in full disappearance of the austenite, provided that the time of isothermal holding is long enough. In martensitic transformation, however, a definite amount of *retained austenite* remains in the steel even upon cooling to  $M_f$ .

4. As distinct from pearlitic transformation, *martensitic transformation in carbon steel has no induction period*. The  $M_s$  horizontal line in Fig. 117 simply defines the temperature below which

a certain amount of martensite can form in steel extremely quickly (virtually instantaneously), and its length does not bear the physical sense of a time interval during which the martensitic transformation proceeds.

5. In medium- and high-carbon steels, martensite is formed as platelets growing with a tremendous speed (of an order of 1 km/s) at any temperature, even at sub-zero temperatures. Upon having

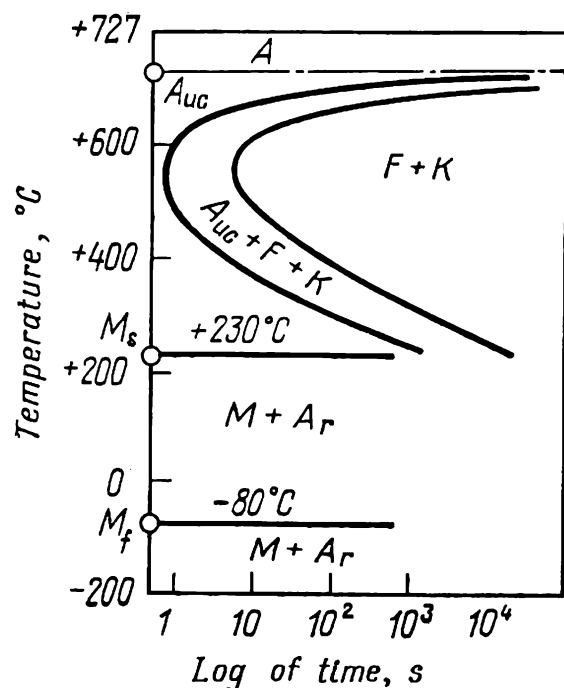


Fig. 117. C-curve with martensitic points for steel with 0.8% C  
A—stable austenite;  $A_{uc}$ —undercooled austenite;  $A_r$ —retained austenite; M—martensite; F—ferrite; K—carbide

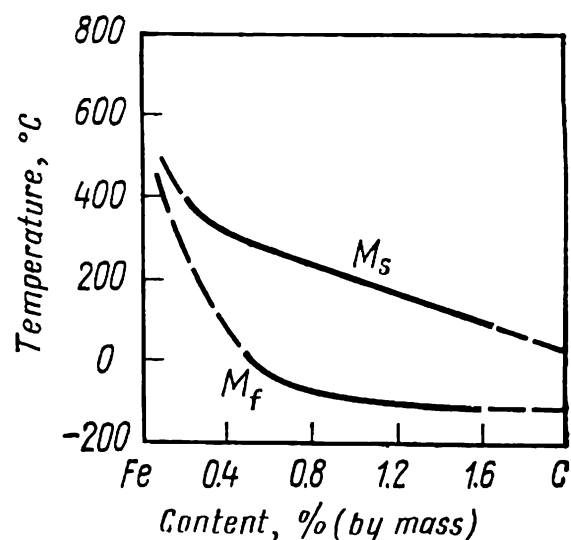


Fig. 118. Dependence of temperature points of the beginning ( $M_s$ ) and end ( $M_f$ ) of martensitic transformation on carbon content in Fe-C system

been formed 'instantaneously', a martensitic platelet does not grow further. Consequently, in a steel being cooled below  $M_s$ , the amount of martensite increases owing to 'instantaneous' formation of new platelets, rather than to the growth of those already formed. In this respect, martensitic transformation differs radically from pearlitic, in which the earlier formed nodules can grow along with the formation of new ones (see Figs. 89 and 90).

6. In martensitic transformation, the crystal lattice of martensite has a definite orientation relative to the lattice of original austenite, whereas in pearlitic transformation the lattices of the phases of the eutectoid mixture may have an arbitrary orientation relative to the lattices of original austenitic grains.

7. With martensitic transformation in carbon steels, the plane polished surface of a microsection has a typical relief indicative of shape changes in the transformed volume of austenite. With pearlitic transformation, no such relief is formed. This relief may serve as the main indication of martensitic transformation.



Martensitic transformation, which was originally discovered when studying the hardening of carbon and alloy steels, was later found to be inherent in very diverse crystal substances: pure metals, carbonless iron-base alloys, alloys of non-ferrous metals, semiconductor compounds, etc. It is one of the fundamental methods for rearrangement of crystal lattice.

For the theory of metal heat treatment, of the greatest importance are studies of martensitic transformations in the Fe-C (Fig. 85) and Fe-Ni (see Fig. 123) systems. In both systems the structural changes in the solid state are linked with polymorphism of the base component — iron ( $\gamma_{f.c.c.} \rightarrow \alpha_{b.c.c.}$ ). Carbon dissolves in the  $\gamma$ - and  $\alpha$ -modifications of iron by interstition and nickel, by substitution. At room temperature, the high-temperature modification of the solid solution (austenite) in the Fe-C system is unstable in any concentration, whereas the high-temperature modification of the solution in the Fe-Ni system is absolutely stable, provided that the content of nickel is sufficiently high (see the analogous systems in Fig. 68*a* and *b*). The two systems are of especial practical interest: the Fe-C system as the matrix in steels and the Fe-Ni system, as the matrix in the relatively novel group of high-strength maraging alloys (see Sec. 4.2.1).

These and other systems are used below as examples for discussing the laws and mechanism of martensitic transformation and the structure and properties of martensite-hardened alloys.

### 3.2.2. THERMODYNAMICS OF MARTENSITIC TRANSFORMATIONS

#### Diffusionless Transformation

Let us begin the thermodynamic analysis with the simplest case (Fig. 119): a system characterized by polymorphism of the solid solution and the absence of three-phase (eutectoid, peritectoid) equilibria. With sufficiently slow cooling within a temperature range from point 1 to point 2, an alloy  $C_0$  (Fig. 119*a*) undergoes a polymorphic transformation  $\beta_{1-2'} \rightarrow \alpha_{1'-2}$ . The ultimate solubility of component  $B$ , at the same temperature, is lower in the low-temperature modification of component  $A$  than that in the high-temperature modification, and therefore, the polymorphic  $\beta \rightarrow \alpha$  transformation will be attended by diffusion redistribution of the components between the initial and the new phase. As the temperature lowers during the transformation period, the composition of the initial  $\beta$ -phase varies along line 1-2' and that of the new  $\alpha$ -phase being formed, along line 1'-2. At the end of the transformation, the new  $\alpha$ -phase at equilibrium should have the same composition as the initial  $\beta$ -phase.

At any temperature, the  $\alpha$ - and  $\beta$ -solutions based on the modifications of the  $A$  component are characterized by their respective free energy-versus-composition curves (Fig. 119b). At a temperature  $T_0$ , the free energy curve of the  $\beta$ -phase passes below the

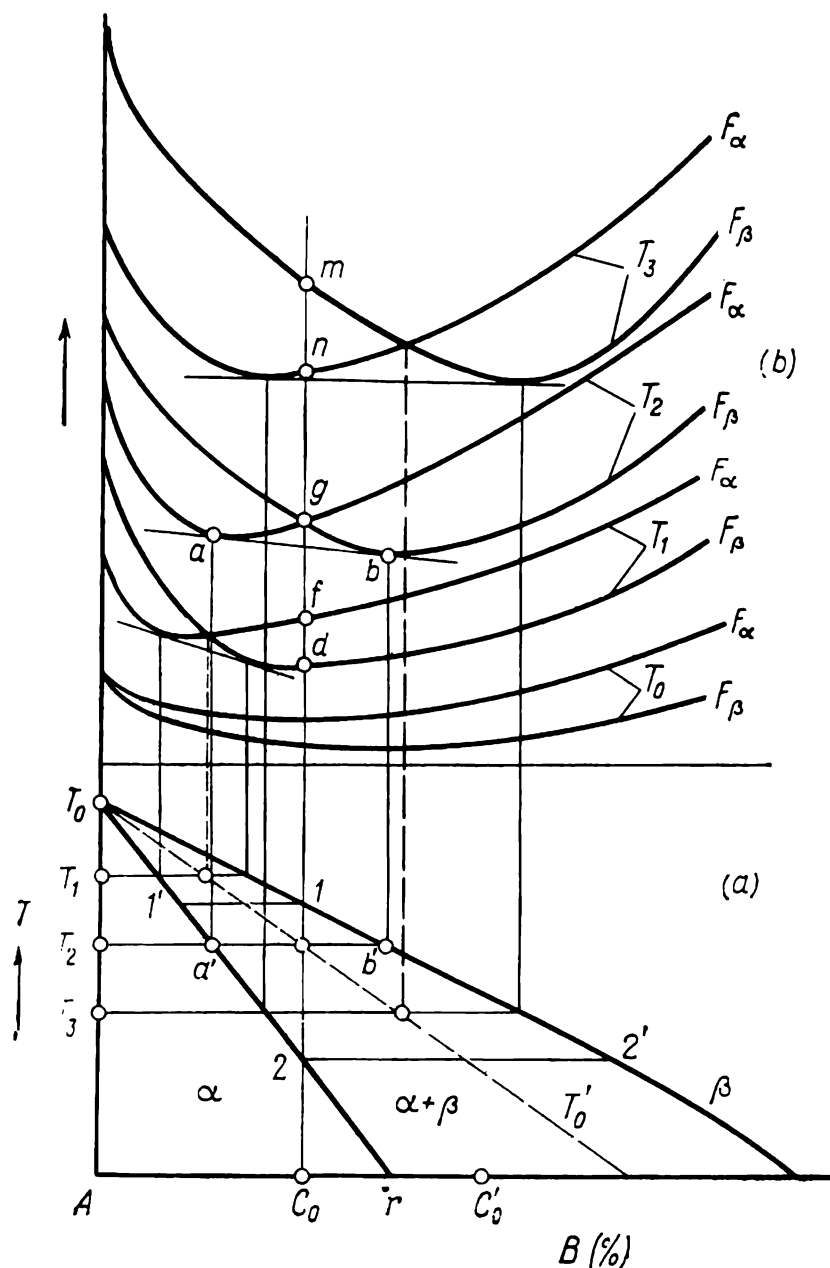


Fig. 119. A portion of constitutional diagram of a system with polymorphism of solid solution (a) and free-energy-composition curves for  $\alpha$ -phase and  $\beta$ -phase at different temperatures (b)

$T_0 T'_0$  — temperature: line of equal free energies of  $\alpha$ -phase and  $\beta$ -phase of the same composition

corresponding curve of the  $\alpha$ -phase, i.e. the  $\beta$ -solution is more stable than the  $\alpha$ -solution in any concentration ( $F_\beta < F_\alpha$ ). The  $F_\alpha$  and  $F_\beta$  curves converge at the point of equilibrium of the two modifications of pure component  $A$  (see the corresponding temperature point  $T_0$  in Fig. 69).

With the temperature being lowered to  $T_1$ ,  $T_2$  or  $T_3$ , the free energy of the  $\alpha$ - and  $\beta$ -phases increases so that the  $F_\alpha$  and  $F_\beta$  curves intersect each other. A tangent common to the two curves of free energy determines the concentrations of the phases that can be in equilibrium at the given temperature (see Sec. 2.1.4). For instance, the tangent  $ab$  in Fig. 119b determines the equilibrium of the  $\alpha$ -phase of composition  $a'$  and of the  $\beta$ -phase of composition  $b'$  at temperature  $T_2$  (Fig. 119a).

At a temperature  $T_2$ , it is the  $\alpha$ -solution that is stable to the left of point  $a'$  in the constitutional diagram (Fig. 119a), since  $F_\alpha < F_\beta$  (Fig. 119b), and the  $\beta$ -solution is stable in the region to the right of point  $b'$ , since  $F_\beta < F_\alpha$ , with a mixture of phases  $\alpha_{a'} + \beta_{b'}$  being stable between points  $a'$  and  $b'$ , since any point of the tangent section  $ab$  defining the free energy of the two-phase mixture is below the  $F_\alpha$  and  $F_\beta$  curves.

The  $\alpha_{a'} + \beta_{b'}$  mixture can be brought to stable equilibrium through very slow cooling in which the polymorphic transformation may be accompanied by diffusion redistribution of the components between the initial and the new phase. With quick cooling of the alloy from the  $\beta$ -region, this redistribution of the components is inhibited.

Let us compare the free energies of the  $\alpha$ - and  $\beta$ -phases of the similar composition corresponding to the composition of  $C_0$  alloy in Fig. 119 at various temperatures.

At  $T_1$ ,  $F_\beta < F_\alpha$  (points  $d$  and  $f$  in Fig. 119b); at  $T_2$ ,  $F_\beta = F_\alpha$  (point  $g$ ); and at  $T_3$ ,  $F_\beta > F_\alpha$  (points  $m$  and  $n$ ). Therefore, the free energy of the initial  $\beta$ -phase increases with cooling more intensively than that of the  $\alpha$ -phase of the same composition while below a definite temperature ( $T_2$  for  $C_0$  alloy) the picture is inverse, i.e. the initial phase has a higher free energy than the new phase. Thus, the temperature curves of free energies for two modifications of a solid solution of the same composition intersect each other, similar to the corresponding curves for two modifications of a pure component (see Fig. 69). The principal difference between the two cases consists in that the point of intersection of free energy curves corresponds in the latter case (pure metal) to the temperature of stable equilibrium of two modifications of that metal and in the former case (alloy), to the temperature of metastable equilibrium of the undercooled  $\beta$ -solution with the metastable  $\alpha$ -solution of the same composition. If diffusion redistribution of the components had time to proceed, then an equilibrium mixture of phases of differing composition,  $\alpha_{a'} + \beta_{b'}$ , would form in  $C_0$  alloy at the temperature of metastable equilibrium  $T_2$ .

For any alloy of the system considered, this method enables us to find a temperature point on the constitutional diagram at

which the free energies of the metastable  $\alpha$ - and  $\beta$ -phases of the same composition will be equal. The locus of these temperature points is line  $T_0T'_0$  in Fig. 119a.

For any alloy, with the initial  $\beta$ -phase being undercooled to a temperature below  $T_0T'_0$  line, the free energy of that phase becomes greater than that of the  $\alpha$ -phase of the same composition, i.e. there appears a thermodynamic stimulus  $\Delta F = F_\beta - F_\alpha$  of polymorphic  $\beta \rightarrow \alpha$  transformation without variation of the composition. For instance, for  $C_0$  alloy with its  $\beta$ -phase of composition  $C_0$  being transformed into  $\alpha$ -phase of the same composition, this stimulus ('driving force' of transformation) at temperature  $T_3$  is equal to the section  $mn$ .

The transformations being discussed relate to the class of diffusionless transformations. This type of transformation is feasible during crystallization of liquid solutions, but in metallic melts it is usually difficult to attain a degree of undercooling sufficient to provoke diffusionless crystallization of the liquid melt. On the contrary, in solid solutions, where the diffusion mobility of atoms is substantially lower, undercooling below the  $T_0T'_0$  line is very likely to occur, so that diffusionless polymorphic transformation of the solid solution becomes thermodynamically feasible. Kinetically, this transformation is feasible at a low mobility of atoms, since it takes place through a special martensitic mechanism of lattice rearrangement, which differs substantially from the 'normal' mechanism of diffusion transformation (see Sec. 3.2.3). The phase that is formed through this transformation is called martensite.

In the  $C_0$  alloy, the martensitic  $\alpha$ -phase formed through diffusionless transformation does not differ in its composition at room temperature from the  $\alpha$ -phase formed through the 'normal' diffusion transformation by the scheme  $\beta_{1-2} \rightarrow \alpha_{1'-2}$ , the composition of the  $\alpha$ -phase at room temperature corresponding to the composition of  $C_0$  alloy in both cases. In both the diffusionless martensitic transformation and the 'normal' diffusion transformation, the phase that is formed in  $C_0$  alloy is at room temperature an unsaturated solid solution of component  $B$  in the low-temperature modification of component  $A$  ( $\alpha$ -solution is saturated at point  $r$ ). Note that crystals of the  $\alpha$ -phase of composition  $C_0$  formed through the martensitic mechanism of transformation differ in their microstructure and substructure (see Sec. 3.2.4) from crystals formed through the 'normal' transformation mechanism. The martensitic  $\alpha$ -phase is sometimes denoted as  $\alpha'$  or  $M$  to distinguish it from the normal  $\alpha$ -phase.

With a higher degree of alloying, say, in an alloy of composition  $C'_0$  (Fig. 119a), diffusionless transformation results in the

formation of a martensitic  $\alpha$ -phase which at room temperature is a supersaturated solid solution of component  $B$  in the low-temperature modification of component  $A$ , since martensite ( $C'_0$ ) in such an alloy is to the right of the saturation point of the  $\alpha$ -phase in equilibrium ( $r$ ). Consequently, *the martensite that is formed through diffusionless polymorphic transformation in alloys may be either supersaturated or unsaturated solid solution of the alloying element in the low-temperature modification of the base component.*

Let us now consider the transformations in a system of the eutectoid type, using as an example the Fe-C system.

Decomposition of austenite into a ferrite-carbide mixture is a diffusion process linked with redistribution of carbon and with diffusion displacement of atoms over distances largely exceeding the lattice spacing.

With rapid cooling of carbon steel (water quenching at a rate of a few hundreds  $^{\circ}\text{C/s}$ ), the austenite can be undercooled appreciably without decomposing by diffusion into a two-phase mixture. Whatever the rate of cooling, the austenite cannot be retained fully in steel at room temperature, since its free energy in carbon steel, beginning from a certain temperature  $T_0$ , turns out to be higher than the free energy of supersaturated solid solution of carbon in  $\alpha$ -iron (martensite), which has the composition similar to that of the initial austenite and differs from the latter in the type of crystal lattice.

Martensite is a metastable phase; it is absent in the Fe-C constitutional diagram (Fig. 85), since in equilibrium conditions, when the system possesses the absolute minimum of free energy, the structure of steels below point  $A_1$  ( $727^{\circ}\text{C}$ ) is a mixture of two stable phases: ferrite and cementite. At any temperature, martensite has a higher free energy than this mixture, but at temperatures below  $T_0$  its free energy is lower than that of undercooled austenite. When, under conditions of deep undercooling, austenite cannot undergo diffusion decomposition into ferrite-carbide mixture, which might bring the system to the absolute minimum of free energy, it transforms by diffusionless process into martensite, thus bringing the system to a relative minimum of free energy. Austenite has a face-centred cubic lattice of  $\gamma$ -iron, while martensite has a tetragonal lattice similar to the body-centred cubic lattice of  $\alpha$ -iron. Below point  $A_1$ , stable existence of  $\gamma$ -iron lattice is unfeasible. With deep undercooling and low mobility of atoms, the polymorphic  $\gamma \rightarrow \alpha$ -transformation does occur, but the carbon has no time to precipitate as a carbide phase from the solution.

At room temperature, the equilibrium solubility of carbon in  $\alpha$ -iron is negligibly low (see Fig. 85). For that reason the martensite that has formed through diffusionless polymorphic trans-

formation of the austenite in carbon steel is always a supersaturated interstitial solution of carbon in  $\alpha$ -iron. A higher content of carbon in the initial austenite gives a higher carbon concentration in martensite. Increasing the carbon supersaturation of the martensite increases the tetragonal distortion of the martensite lattice by the formula  $c/a = 1 + 0.046 p$ , where  $c/a$  = axial ratio and  $p$  = carbon concentration, per cent (by mass). In pure  $\alpha$ -iron,

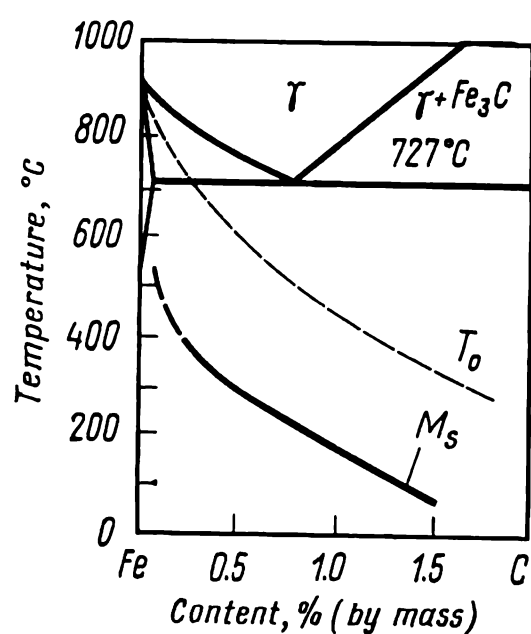


Fig. 120. Effect of carbon content in Fe-C system on the temperature of equal free energies of austenite and martensite of the same composition ( $T_0$ ) and  $M_s$  point

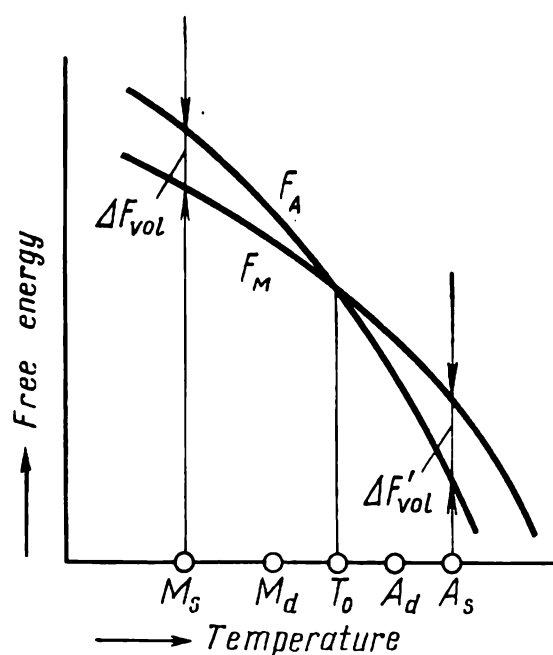


Fig. 121. Effect of temperature on free energy of austenite ( $F_A$ ) and martensite ( $F_M$ )

$c/a = 1$  (cubic lattice), while in martensite with 2 per cent carbon,  $c/a = 1.09$  (the nature of tetragonal distortion of martensite lattice is explained in Sec. 3.2.3).

For a system with eutectoid transformation, a temperature line of equal free energies of the two modifications of the solid solution can be drawn on its constitutional diagram (such as in Fig. 119), using the method of geometrical thermodynamics. For the Fe-C system, the position of this line was also found by calculation. Line  $T_0$  in Fig. 120 gives the temperatures of metastable equilibrium of undercooled austenite and martensite with the same concentration of carbon. For a steel of a given composition, each point of line  $T_0$  corresponds to the intersection of temperature curves of free energies of austenite and martensite (Fig. 121). Since the two solid solutions have the same composition, the two-component Fe-C system should behave as a single-component one (compare Figs. 121 and 69).

### Temperature of the Beginning of Martensitic Transformation

An arbitrarily small undercooling below  $T_0$  is still insufficient to initiate martensitic transformation. Here, an analogy exists with the polymorphic transformation in a single-component system (see Sec. 2.1.1). The formation of a martensitic crystal is linked not only with a reduction in the volumetric free energy ( $\Delta F_{vol}$  in Fig. 121), but also with the appearance of the surface energy ( $\Delta F_s$ ) and, what is most important, of the energy of elastic deformation ( $\Delta F_{el}$ ), which both hinder the transformation. The energy of elastic deformation is due, firstly, to a change in the unit volume during phase transformation (on  $\gamma \rightarrow \alpha$ -transformation in iron-base alloys the unit volume increases roughly by 4 per cent) and, secondly, to the coherence of the lattices of the martensite and initial phase (for more detail see Sec. 3.2.3).

The resultant drop in the free energy of the system is  $\Delta F = -\Delta F_{vol} + \Delta F_s + \Delta F_{el}$ . To initiate martensitic transformation, the austenite must be undercooled well below the point of its metastable equilibrium with the martensite so as to have a sufficiently high thermodynamic transformation stimulus ( $\Delta F_{vol}$ ). For that reason, the temperature of the beginning of martensitic transformation (martensitic point  $M_s$ ) is always below point  $T_0$  (see Figs. 120 and 121). For the Fe-C system, the difference between the free energies of austenite and martensite that would initiate martensitic transformation is 300-350 cal/mol, and the corresponding temperature difference is:  $T_0 - M_s \approx 200$ -250 degrees C (see Fig. 120).

The  $M_s$  point can characterize an alloy of a given composition (for the given conditions of preliminary heat treatment). The horizontal  $M_s$  line in Fig. 117 indicates that martensitic transformation in a given steel always begins at one and the same temperature, irrespective of the cooling rate.

Later studies have shown that the  $M_s$  point changes somewhat at very high cooling rates. More specifically, it then increases (Fig. 122), unlike the temperature point of normal transformation, which reduces with increasing cooling rate. For instance, the  $M_s$  point of steel with 0.5 per cent C at cooling rates below 6600 °C/s is virtually stable at 370 °C. With the cooling rate being raised from 6600 °C/s to 16,500 °C/s, the  $M_s$  point rises from 370° to 460 °C and remains at that level with the cooling rate being increased further. An explanation to this may be as follows.

At cooling rates of hundreds or thousands degrees C per second, the austenite may be in the undercooled state above the  $M_s$  point for a time interval of an order of a few tenths of a second or a few seconds. This time interval is sufficient for carbon atoms,

which are very mobile, to segregate quickly and form an equilibrium concentration of carbon at the lattice defects of the austenite, thus providing for the maximum strengthening of the latter. In such austenite, martensitic transformation is ultimately difficult to be accomplished and the  $M_s$  temperature is at its minimum and independent of the cooling rate within a certain range of cooling speeds, including those commonly employed in hardening (see the left-hand horizontal portion of the curves in Fig. 122). Beginning from a definite cooling rate, however, this segregation of carbon

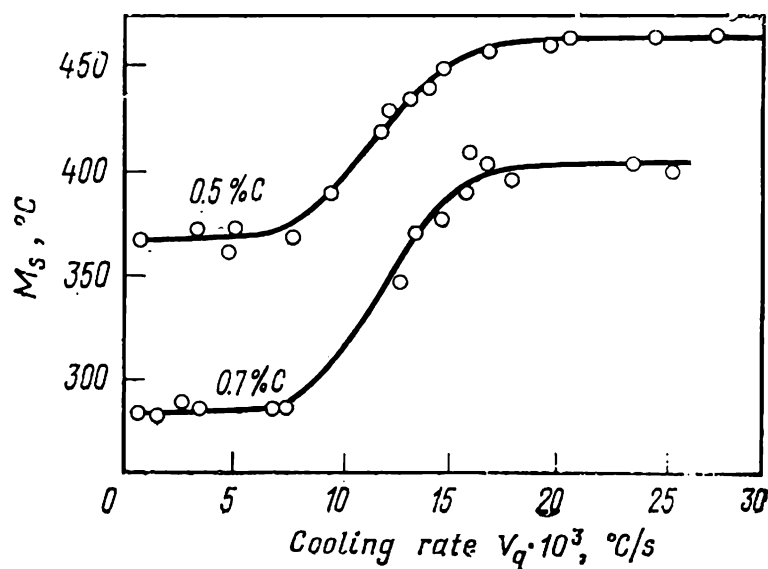


Fig. 122. Effect of quenching rate ( $V_q$ ) on temperature of beginning of martensitic transformation ( $M_s$ ) in iron alloys with 0.5% and 0.7% C (after G. S. Ansell and S. J. Donachie)

in austenite has no time to proceed fully and the  $M_s$  point rises. Finally, with very high cooling rates, the time when the steel is in austenitic state above point  $M_s$  becomes so small (of an order of a few hundredths of a second) that carbon segregation at lattice defects of austenite is inhibited almost fully and has no effect on the martensitic transformation—the  $M_s$  point is stable (see the right-hand portion of the curves in Fig. 122).

The temperature of the beginning of martensitic transformation usually is strongly dependent on the composition of alloy. Thus, increasing the nickel content in the Fe-Ni system by a few per cent may shift the  $M_s$  point into the region of sub-zero temperatures, as will be seen from the following:

Ni, %	18	22.5	29	31	32
$M_s$ , $^{\circ}\text{C}$	+280	+163	−10	−63	−97

The  $M_s$  point can be lowered appreciably by increasing the carbon content of steel: in steels with less than 1 per cent carbon it is above  $200^{\circ}\text{C}$  and in those with around 2 per cent C, close to the room temperature (see Fig. 118).



The content of carbon in the austenite is not always the same as that in the steel, since the carbon may be present in carbides. These carbides, which exist in the metal along with austenite, cannot by themselves affect the  $M_s$  point, but can produce an indirect effect. For instance, on increasing the hardening temperature, the carbides dissolve in the austenite, the latter becomes higher in carbon, and thus the  $M_s$  point is lowered.

The  $M_s$  point may be changed through variations in the steel composition, since this affects the  $T_0$  point and the degree of undercooling  $T_0 - M_s$ . In particular, alloying additions which increase the elastic modulus of the matrix (austenite) can hinder the martensitic transformation, since  $\Delta F_{el}$  increases and the undercooling degree  $T_0 - M_s$  also increases.

### Reversibility of Martensitic Transformation

As follows from Fig. 121, a martensite-hardened alloy may undergo a reverse diffusionless martensite-to-austenite transformation on being heated to a temperature above  $T_0$ , provided that a definite degree of superheating and a definite driving force of transformation  $\Delta F$  are attained. The point of the beginning of the process is denoted as  $A_s$ , by analogy with the  $M_s$  point.

Austenite can be formed by martensitic transformation only if diffusion redistribution of the components in the initial martensite is suppressed. For this, the  $T_0$  temperature should be sufficiently low and the heating should be done quickly.

Reverse martensitic transformation is not found in carbon steels, which may be explained by the high mobility of carbon atoms in the interstitial solution: on heating, the diffusionless breakdown of the martensite (tempering) takes place before the  $A_s$  temperature is attained.

Reverse martensitic transformation has been discovered in alloys of the Fe-Ni system (with a high nickel content, i.e. when the  $T_0$  point is sufficiently low), in copper alloys (such as aluminium bronzes), and in titanium alloys (Ti-Cr, Ti-Fe, Ti-Sn, Ti-Zr). In these alloys the reverse martensitic transformation has all the features typical of the direct transformation. The rate of heating can hardly affect the  $A_s$  point. The transformation starts at one temperature ( $A_s$ ) and terminates at a higher temperature ( $A_f$ ). For instance, for an alloy of Fe + 32.5 per cent Ni,  $A_s = 300-310^\circ\text{C}$  and  $A_f = 400-410^\circ\text{C}$ . The reverse martensitic transformation produces a characteristic relief on the polished surface of microsections, this relief sometimes reproducing the relief of the direct transformation. In both direct and reverse transformation, crystals are formed extremely quickly.

The difference between  $A_s$  and  $M_s$  (the temperature hysteresis) may be from a few degrees to a few hundreds of degrees C. A larger difference is due to the high energy of elastic deformation of the matrix ( $\Delta F_{el}$ ), which inhibits the formation of crystals of the new phase in the matrix.

Temperature hysteresis can be diminished by subjecting the austenite to plastic deformation at a temperature above the  $M_s$

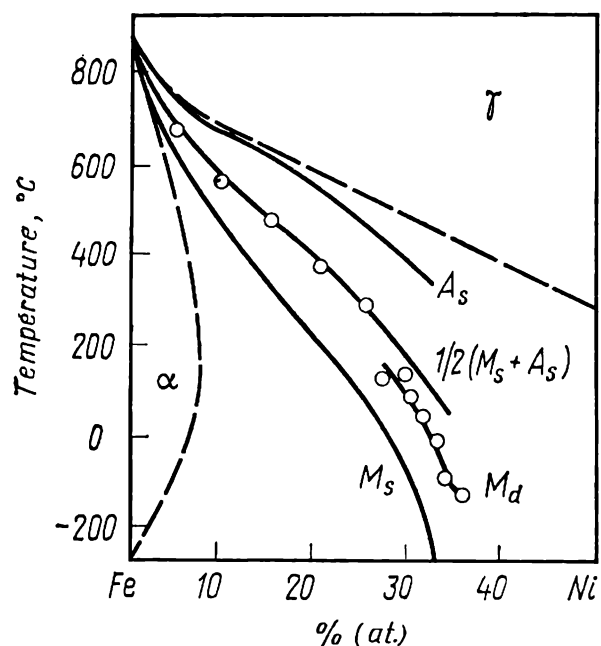


Fig. 123. Effect of nickel in Fe-Ni system on temperatures of beginning of martensitic transformation on cooling ( $M_s$ ), reverse martensitic transformation on heating ( $A_s$ ) and calculated temperature of equality of free energies of austenite and martensite  $T_0 = (M_s + A_s)/2$  (after D. F. Kaufman and M. Cohen)

$M_d$ —beginning of martensitic transformation in deformed austenite; dotted lines—boundaries of  $\alpha$ -region and  $\gamma$ -region in a diagram of stable equilibria

point (see also Sec. 3.2.5). Plastic deformation causes the martensitic transformation between the  $M_s$  point and a certain temperature  $M_d$  (where  $d$  stands for 'deformation'), which is somewhere below  $T_0$ , sometimes very close to the latter (see Fig. 123). Above the  $M_d$  point, no plastic deformation is capable of causing martensitic transformation. Similarly, plastic deformation of the martensite may cause the reverse martensitic transformation in the temperature region below the  $A_s$  point to a certain temperature  $A_d$ , which is somewhat higher than the  $T_0$  point (see the corresponding points in Fig. 121). Plastic deformation brings the starting points of the direct and reverse transformation closer to each other and thus enables an experimental estimation of the temperature of metastable equilibrium of the two phases having the same composition.

If the temperature hysteresis still remains large, we may assume that  $T_0 = 1/2(M_d + A_d)$ .

### 3.2.3. MECHANISM OF MARTENSITIC TRANSFORMATION

#### Cooperative Nature of Atom Displacements on Lattice Rearrangement

Some peculiar facts about martensitic transformation, in particular those that martensitic plates form 'instantaneously' even at low temperatures; their growth stops quickly; the martensitic

lattice has a definite strict orientation relative to the austenitic lattice; that the transformation stops on stopping the cooling, etc. — led in the beginning of 1930's to a wide-spread opinion that the martensitic transformation had nothing to do with common phase transformations, and therefore, with the formation and growth of martensitic nuclei. But already in 1932 A. A. Bochvar indicated that all phenomena of phase transformations, including martensitic transformation, should be explained by using the concept of transformation centres and the speed of their growth and that the specific features of martensitic transformations should be related to the conditions of their development. Later studies have confirmed this view. As has been very aptly noticed by G. V. Kurdjumov, metallurgists at the first stage studied the particulars in which the martensitic transformation differed from other transformations, but at the second stage had to examine what is common between this and other transformations.

The mechanism of lattice rearrangement in the martensitic transformation was described in Kurdjumov's classical works: "The martensitic transformation consists in regular rearrangement of the lattice in which atoms do not change places, but merely displace relative to one another over distances not exceeding the interatomic distances". Since atoms do not change places, the austenite-to-martensite transformation is diffusionless, there is no diffusion redistribution of the components in the austenite, and the concentration of carbon remains constant in the course of transformation. The absence of diffusion redistribution of unlike atoms cannot in itself be a specific feature of the martensitic mechanism of transformation. With polymorphic transformation in a pure metal, such as iron, which consists of like atoms, such redistribution of atoms is utterly out of the question. But even in a pure metal the mechanism of polymorphic transformation can be of the martensitic type under definite conditions and then differ from the 'normal' transformation.

With a normal polymorphic transformation in a pure metal, the crystals of a new modification grow owing to random displacements of atoms that are not mutually interrelated. When detached due to thermal activation from the lattice of the initial modification, say, of  $\gamma$ -iron, atoms are attached to the lattice of a new modification, for instance,  $\alpha$ -iron; as a result, the boundary of a crystal of  $\alpha$ -iron migrates relatively slowly towards  $\gamma$ -iron; the new phase 'devours', as it were, the mother phase. Such a disordered displacement of atoms, in which they move independently of one another, may be likened to self-diffusion, and the process called self-diffusion, or disordered phase transformation. On that account it is similar to the self-diffusion process of crystal growth in recrystallization after heat treatment, the only difference being

in the nature of the thermodynamic stimulus. In the case of recrystallization after heat treatment the difference between the free energies of initial and new grains is due to a greater distortion in the structure of the initial (deformed) grains of the same phase, whereas in the polymorphic transformation the thermodynamic stimulus is the difference between the free 'chemical' energies of the two phases having different crystal lattices. Like recrystallization, self-diffusion polymorphic transformation can only proceed at a sufficiently high temperature.

*The martensitic mechanism of lattice rearrangement can be characterized by a cooperative interrelated nature of atom displacements over distances less than interatomic distances (without changing places, which is typical of self-diffusion), with the neighbours of an atom in the initial phase remaining its neighbours in the new martensitic phase.* In cases when the initial phase is a solid solution, as in austenite, the martensitic mechanism predetermines the absence of diffusion redistribution of unlike atoms at the moment of transformation.

### Coherent Growth of Martensitic Crystal

A consequence of the main specific feature of martensitic transformation discussed above is the coherence at the boundary between the martensite and the initial phase during the growth of a martensitic crystal. Indeed, since the neighbours of an atom in the initial phase remain its neighbours in the new phase, an atom at the interface will have the same neighbours, i.e. the boundary will be coherent (see Fig. 75).

The coherence, or elastic conjugation, of two lattices at the interface between the martensite and the initial phase ensures the possibility of extremely quick motion of the boundary towards the matrix even at very low temperatures, since for this 'gliding' motion diffusion with migrations of atoms over distances exceeding the interatomic distances is not necessary. Only cooperative displacement of atoms over distances less than the interatomic distance occurs at the boundary, resulting in the displacement of the boundary proper towards the initial phase, i.e. in the growth of the martensitic crystal.

As the martensitic crystal grows, the coherent boundary accumulates elastic deformation until the yield limit is reached, after which the elastic stresses are released owing to disruption of the coherence. Now, with disorderly positioned atoms at the boundary between the martensitic crystal and mother phase, the 'gliding' motion of the boundary is no more possible, and the quick growth of the crystal by the martensitic mechanism ceases. Further growth of the martensitic crystal is only possible through self-diffusion, but since the martensitic transformation takes place in the tem-

perature range where self-diffusion can proceed only extremely slowly, no further growth of the martensitic crystal upon disruption of the coherence can be practically observed.

The fully coherent interface between martensite and initial phase is only known for the case of transformation of face-centred cubic lattice of  $\beta$ -cobalt into hexagonal closely spaced lattice of  $\alpha$ -cobalt. Both modifications have closely packed  $\{111\}_\beta$  and  $\{1000\}_\alpha$  planes of the same structure in the form of a hexagonal network (with six nearest neighbours around each atom). Such a plane of closest packing, as being common for crystals of both phases, ensures full coherence at the interface and makes this interface capable of gliding at any low temperature.

With martensitic transformations in steels and other alloys, coherence is partially disturbed owing to the appearance of dislocations at the interface. If these dislocations can glide along with the interface, then the martensitic crystal will grow as quickly as in the case of fully coherent interface. If however, dislocations can only climb with the advancement of the transformation front, then the quick growth of the crystal by the martensitic transformation may cease and further growth will only be possible through diffusion, which is not practically observed at low temperatures.

The mechanism of lattice rearrangement just discussed explains well the two important peculiarities of martensitic transformation: the tremendous speed of growth of martensitic crystals under conditions of a low mobility of atoms (up to temperatures near the absolute zero) and the quick stoppage of their growth.

By using the concept of coherent growth, G. V. Kurdjumov was able to predict *the phenomenon of 'thermoelastic equilibrium' of crystals of martensite and initial phase*, which was later discovered in aluminium bronzes and some other alloys. The phenomenon is essentially as follows.

With a coherent growth of a martensitic crystal, the accumulation of elastic strain energy may result in that the growth of the crystal stops even before the breakdown of coherence. A thermoelastic equilibrium then may establish between the martensite and the matrix. This equilibrium may shift in one or other direction with a change in temperature: with a reduction in temperature,  $\Delta F_{vol}$  increases and the crystal grows further until a new equilibrium is established (or until coherence is disturbed), while at an increase of temperature,  $\Delta F_{vol}$  decreases and the crystal will diminish. The discovery of 'thermoelastic' crystals of martensite may be considered as a brilliant confirmation of the concept of coherence at the boundary between the martensite and the initial phase and of the leading role of  $\Delta F_{vol}$ -to- $\Delta F_{el}$  ratio in the thermodynamics of martensitic transformations.

### Conditions for Realization of 'Normal' and Martensitic Transformations

As has been indicated earlier, the polymorphic transformation in pure metals and solid solutions on their basis may proceed through either disordered rearrangement of the lattice or the mechanism of martensitic transformation. The main prerequisites for the development of some or other mechanism of the transformation of a high-temperature modification into a low-temperature one have been analysed by G. V. Kurdjumov.

If the temperature of stable equilibrium of two modifications of a pure metal is sufficiently high (for instance, it is 911 °C for iron, 882.5 °C for titanium, 865 °C for zirconium, and 660 °C for uranium), then both mechanisms of lattice rearrangement can be realized. With a relatively low degree of undercooling, i.e. when the atom mobility is still sufficiently high, a 'normal' polymorphic transformation with disordered rearrangement of the lattice by self-diffusion will take place. With a low degree of undercooling, the martensitic transformation cannot proceed and thus cannot compete with the 'normal' transformation. This may be explained by the fact that, with a disordered rearrangement of the lattice, the elastic deformation of crystals of the initial phase is only due to a change in unit volume, whereas with the martensitic transformation it is also due to the lattice coherence of the initial phase and the martensitic crystal. The large magnitude of  $\Delta F_{el}$  in martensitic transformation requires high thermodynamic stimulus ( $\Delta F_{vol}$ ) for initiation of transformation, and therefore, a greater degree of undercooling of the high-temperature modification than that required for development of the 'normal' transformation.

With increasing the degree of undercooling, the rate of disordered rearrangement of the lattice first increases, attains maximum and then diminishes in accordance with the C-curve (see Fig. 82). At relatively high degrees of undercooling, i.e. when the difference between the free energies of the two modifications becomes high enough for the martensitic transformation to proceed, this transformation occurs much earlier than the 'normal' transformation starts, which is very sluggish at low temperatures. For instance, the  $M_s$  point of pure iron (with 0.0015 per cent C) is 750 °C, which corresponds to a degree of undercooling of around 160 degrees C. With  $\gamma$ -iron undercooled to a temperature within the range of 911-750 °C, the 'normal'  $\gamma \rightarrow \alpha$ -transformation takes place, while at a temperature below 750 °C, the martensitic  $\gamma \rightarrow \alpha$ -transformation occurs.

With metals having a high temperature of equilibrium of their modifications, it is not always easy to attain the high degree of undercooling required for martensitic transformation. For in-

stance, in order to realize the martensitic mechanism of polymorphic transformation in iron, iron specimens should be considerably overheated in the  $\gamma$ -region and then cooled very quickly so as to suppress the development of the 'normal' transformation at lower degrees of undercooling.

In pure metals having a relatively low temperature of equilibrium of their modifications ( $400^\circ\text{C}$  for cobalt and  $-196^\circ\text{C}$  for lithium), the mobility of atoms is low and therefore only the martensitic transformation is realized, with disordered lattice rearrangement being not at all observed.

In solid solutions based on polymorphic metals, the realization of one or the other transformation mechanism depends on how the alloying element present in the solution affects the equilibrium temperature of the two modifications. For instance, alloying additions of nickel and manganese to iron can lower the equilibrium temperature of the two phases so that the 'normal'  $\gamma \rightarrow \alpha$ -transformation becomes impossible and only martensitic rearrangement of the iron lattice takes place.

An opposite case is alloying of cobalt with some elements which can increase the equilibrium temperature of the two modifications to such an extent that along with the martensitic transformation, which can proceed at a sufficiently great undercooling, the 'normal' transformation also becomes possible (at low degrees of undercooling).

### Crystal Geometry of Austenite-to-martensite Transformation

In order to understand the structure of martensite in steels, one has to know the crystal geometry of rearrangement of the face-centred cubic lattice of austenite into the body-centred tetragonal lattice of martensite, which is similar to the body-centred cubic lattice of  $\alpha$ -iron. A simple transformation of the shape of an elementary cell of austenite, known in the specialist literature as the *Bain transformation* (Fig. 124), may help in understanding the crystal geometry of martensitic transformation in steel.

Figure 124a shows two neighbouring elementary cubic cells of the face-centred cubic lattice of austenite. Iron atoms, which are marked by circles, are disposed at cube corners and in centres of cube faces. Atoms of carbon, which is dissolved interstitially in  $\gamma$ -iron, occupy statistically uniformly a part of the octahedral voids in the face-centred lattice<sup>1</sup>. The octahedral voids, which are marked by crosses, are positioned at the middle of cube edges and

---

<sup>1</sup> For simplification, not all positions of iron and carbon atoms are shown in the figure.

in the centre of volumes of cubic cells (Fig. 124a). All these voids are structurally equivalent and indistinguishable from each other.

A tetragonal elementary cell (shown by solid lines in Fig. 124a), as well as a cubic cell, can be mentally separated in the face-centred lattice of austenite. In this tetragonal cell of austenite, the axial ratio is  $c/a = \sqrt{2}$ , whereas the experimentally found axial ratio (degree of tetragonality) for martensitic lattice is  $c/a < 1.09$ . The Bain transformation, which changes the austenitic lattice (Fig. 124a) in the simplest way into the martensitic

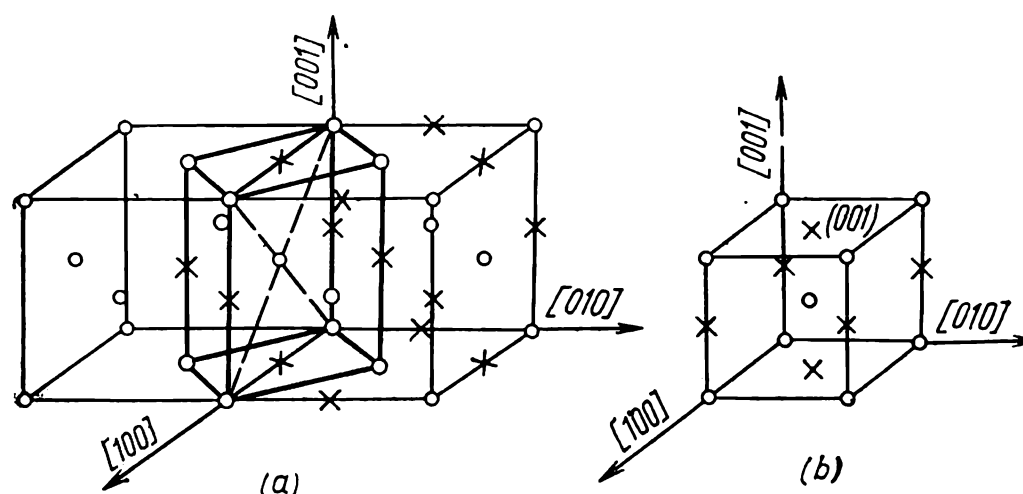


Fig. 124. Bain transformation of austenitic lattice (a) into martensitic lattice (b)

lattice (Fig. 124b), essentially consists in compressing the tetragonal cell of austenite along the  $c$  axis with the simultaneous expansion of its dimensions along the  $a$  axis.

Carbon atoms in the face-centred lattice of austenite are distributed statistically uniformly throughout the octahedral voids along the directions of the three edges of the cube,  $[100]$ ,  $[010]$  and  $[001]$  (see the crosses in Fig. 124a). In the same austenitic lattice, however, the carbon atoms are disposed selectively relative to the directions of the edges of the tetragonal cell: they are located only at the middle of edges along the  $[001]$  axis and in the centres of horizontal faces of the cell, i.e. again along the  $[001]$  direction. After the transformation, the interstitial carbon atoms occupy, as before, the octahedral voids in the martensite lattice along the  $[001]$  direction, but do not occupy the voids in the  $[100]$  and  $[010]$  directions (Fig. 124b). Since carbon atoms are positioned between iron atoms in rows parallel to the  $[001]$  axis, they prevent the Bain transformation from changing the face-centred lattice into a body-centred one with the axial ratio of unity. The degree of tetragonal distortion of martensitic lattice,  $c/a$ , increases proportionally with the carbon concentration in it.



The mobility of carbon atoms even at room temperature is sufficient for them to rearrange upon the transformation and occupy the nearest free octahedral voids along the  $[100]$  and  $[010]$  axes with simultaneous disappearance of tetragonality. Diffusion displacements over very small distances — within a single elementary cell — may be sufficient for this. Actually, however, the martensitic lattice retains its tetragonality at room temperature. A. G. Khachaturyan has shown by a theoretical analysis that between carbon atoms in the martensite of steel there exists such a deformational interaction that makes their ordered arrangement thermodynamically favourable, with the preferable orientation along one of the crystal axes. Thus, the tetragonal distortion of the martensitic lattice corresponds to the minimum of free energy because of the minimization of the elastic deformation of the lattice, which is linked with an ordered arrangement of interstitial carbon atoms.

With increasing temperature, the long-range order in the arrangement of carbon atoms should be expected to disappear. But this is prevented by the elastically stressed state of the martensitic crystal in the matrix of retained austenite. Owing to this, the long-range order of supersaturated solid solution of carbon in  $\alpha$ -iron (martensite) is retained at all temperatures at which the martensite still does not decompose.

The development of the concept of mechanism of martensitic transformation was bolstered by the discovery of the orientational relationships between the lattices of the initial and martensitic phases that have been found by X-ray analysis. For iron alloys, three main orientational relationships are known: Kurdjumov-Sachs', Nishiyami's, and Greninger-Troiano's.

*Kurdjumov-Sachs' orientational relationship* (an example are carbon steels with 0.5-1.4 per cent C) can be written as follows

$$(111)_A \parallel (101)_M \text{ and } [\bar{1}\bar{1}0]_A \parallel [11\bar{1}]_M$$

Such kind of mutual orientation of lattices can be readily explained: the plane of closest packing  $\{111\}$  in a face-centred lattice is most similar in its atomic structure to the plane of closest packing  $\{110\}$  in a body-centred lattice, with the direction of the closest packing  $\langle 110 \rangle$  in the former being most similar in the atomic structure to the direction of closest packing  $\langle 111 \rangle$  in the latter. This mutual orientation of lattices satisfies most fully the principle of structural correspondence. Since the face-centred lattice of austenite has four crystallographically equivalent planes of the  $\{111\}$  type, namely  $(111)$ ,  $(\bar{1}11)$ ,  $(1\bar{1}1)$ , and  $(11\bar{1})$ , and six crystallographically equivalent directions of the  $\langle 110 \rangle$  type, there may be 24 orientations of martensitic crystals obeying

Kurdjumov-Sachs' relationship for a single position of an austenitic crystal.

*Nishiyami's orientational relationship* (an example are iron alloys with 27-34 per cent Ni) is written as

$$(111)_A \parallel (101)_M \text{ and } [\bar{1}\bar{2}1]_A \parallel [10\bar{1}]_M$$

The *Greninger-Troiano relationship* (an example is an alloy of Fe with 22 per cent Ni and 0.8 per cent C) is an intermediate case between the two relationships discussed above.

The Bain transformation, which explains clearly how the face-centred lattice of austenite can by means of shortest atomic displacements be changed into the body-centred tetragonal lattice of martensite, cannot alone give, for instance, 24 Kurdjumov-Sachs' orientations, since the edges of an elementary cell of martensite remain parallel with the edges of the initial tetragonal cell of austenite (see Fig. 124). To obtain Kurdjumov-Sachs' relationship, more complex paths of atomic displacements are necessary than those envisaged by the Bain transformation. The actual paths of atomic displacements in martensitic transformation are not known. Formally, all the orientational relationships for austenite and martensite lattices that have been found experimentally can be obtained if the Bain transformation is complemented with rotation of the martensitic lattice so that the respective planes and directions in the initial and martensitic phases become parallel to one another.

### **Invariance of Habit Plane of Martensite and Additional Deformation in Martensitic Transformation**

Along with the orientational relationships discussed in the preceding section, the quantitative studies of the relief on plane polished surfaces of specimens have played an extremely important part for understanding the crystal geometry of martensitic transformations and internal structure of martensitic phase. All martensitic transformations are always followed by the appearance of such a relief.

In Figure 125, the plane area  $FGHE$  relates to the initial austenitic state of a specimen. As a martensitic plate  $ABCDLMNO$  is formed, the surface of the specimen on section  $ABCD$  tilts relative to the initial plane. As has been shown experimentally, the line  $AB$  remains unrotated and the lines of the  $STT'S'$  type, which were rectilinear before the transformation, remain such in the inclined portion of the surface  $ABCD$  and are continuous along their whole length. Since this is true of any arbitrarily chosen initial surface of the specimen, a conclusion may be made that the habit plane

$ABML$  of a martensitic crystal (i.e. the boundary plane between the martensitic and austenitic phases) is macroscopically approximately invariant in the course of martensitic transformation, i.e. it is neither distorted nor rotated (any sections on that plane remain invariant in both length and direction).

The invariance of habit plane ensures that the elastic deformations on the transformation are at their minimum. This can be conceived especially easily for the case of transformation with a single boundary plane between the initial and martensitic crystal: the invariance of that surface prevents the formation of elastic macrodeformations in the initial and martensitic phases.

A problem then arises: how the invariance of the boundary plane between the phases can be realized if an elementary cell changes in the martensitic transformation, i.e. the crystal lattice proper is deformed.

The answer can be found by referring to Fig. 126.

Figure 126a shows a portion of the initial phase before the transformation, and Fig. 126b, the same portion after the transformation which resulted in a change of the type of lattice. The figure shows clearly how a change in the shape and dimensions of elementary

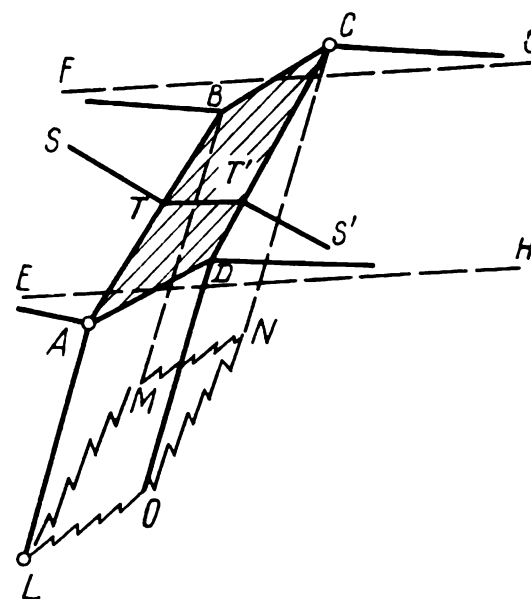


Fig. 125. Relief on initially flat surface  $FGEH$  of specimen due to formation of a martensitic platelet  $ABCDLMNO$  (after B. A. Bilby and J. W. Christian)

$STT'S'$  — broken line which was straight before transformation

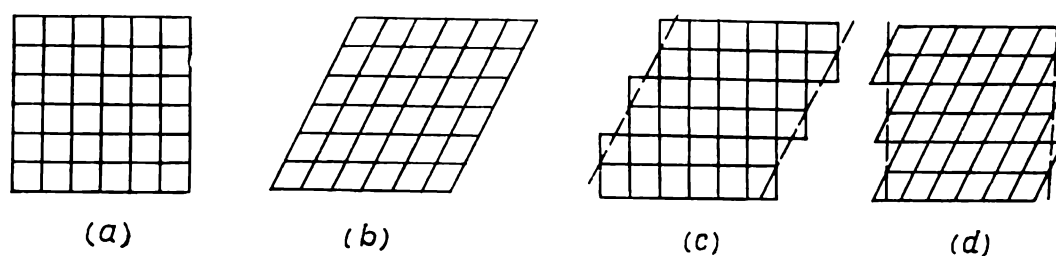


Fig. 126. Types of deformation in martensitic transformation (after B. A. Bilby and J. W. Christian)

cells, i.e. a uniform deformation of the lattice, can cause a macrochange in the shape of transformed portion.

A macroscopic change in the shape of a portion of the initial phase may be obtained in a principally different way, without changing the elementary cells, namely, through plastic deformation by glide (Fig. 126c) or else through twinning.

A combination of a lattice deformation (a change of the elementary cell) and a plastic deformation, say, a glide deformation (Fig. 126d), may leave unchanged the initial shape of a macroscopic portion, notwithstanding the phase transformation that occurs (the type of lattice in Fig. 126d differs from the initial type in Fig. 126a). Naturally, the side habit plane of the crystal of the new phase in Fig. 126d is invariant only on a macroscopic scale, since the process of glide has formed microscopic tilts in it.

Thus, the experimentally established fact of invariance of the habit plane in a martensitic crystal has a corollary of extreme importance, i.e. the formation of a crystal should consist not only in a change of the type of crystal lattice, but also in a simultaneous plastic deformation due to glide or twinning. Such an *additional deformation*, which is inherent in the mechanism of martensitic transformation, ensures that the energy of elastic distortions is at its minimum in an invariant boundary plane. This consequence is of especial importance for understanding the mechanism of martensitic substructure (see Sec. 3.2.4).

Various habit planes of martensitic crystals have been established experimentally. For iron-base alloys, the most typical habit planes are  $\{225\}_A$ ,  $\{259\}_A$ ,  $\{3, 10, 15\}_A$ , and  $\{111\}_A$ , where  $A$  implies that the subscripts of boundary planes between two phases are given in crystallographic axes of austenite lattice.

The type of habit plane depends on the composition of an alloy and the temperature of martensite formation. For instance, a  $\{111\}_A$  habit plane has been found in low-carbon steels,  $\{225\}_A$  in iron alloys with 0.5-1.4 per cent C, and  $\{259\}_A$  in iron alloys with 1.5-1.8 per cent C. The  $\{3, 10, 15\}_A$  habit plane has been found in alloys of the Fe-Ni system with 33-35 per cent Ni and in alloys of Fe with 22 per cent Ni and 0.8 per cent C or with 28 per cent Ni and 0.4 per cent C. The transition from one type of habit plane to another is not jumplike; with a change in the metal composition the habit plane changes smoothly from one type to another, for instance, from  $\{259\}_A$  to  $\{225\}_A$  in the Fe-C system. In alloys of the Fe-Ni system, the habit plane tilts from the  $\{3, 10, 15\}_A$  plane through approximately 10 degrees as the content of nickel is changed from 35 per cent to 29 per cent.

The type of habit plane is related to the type of additional deformation of the lattice in the martensitic transformation. For example, it can be predicted analytically that if such a deformation proceeds through twinning along the  $\{112\}_M$  plane, then the habit plane in the martensite will be  $\{3, 10, 15\}_A$ . The formation of martensite with the  $\{225\}_A$  habit plane occurs owing to an appreciably more complex additional deformation whose nature is still not clear.

### Martensitic Nuclei

The nature of martensitic nuclei is the most difficult to comprehend in the whole problem of martensitic transformations. The hypothesis of homogeneous nucleation, which is based on fluctuational formation of a nucleus of a critical size, is now rejected by the majority of researchers, since, owing to the high energy of

elastic distortions, the work of homogeneous formation of a critical nucleus is so great that the probability of fluctuational appearance of a nucleus is negligible.

Most hypotheses assume heterogeneous nucleation of martensite, with the transformation centres being attributed to special submicroscopic portions in the initial phase. The nature and structure of such portions may differ in various metals and alloys. Boundaries and sub-boundaries are excluded from consideration, since, as has been shown experimentally, they are not the preferable places for the formation of martensitic crystals.

The results of experiments with martensitic transformation in disperse particles of an alloy of Fe with 30.2 per cent Ni are considered a direct proof of heterogeneous nucleation. In the experiments, around  $1/20$  of the total number of particles up to 40  $\mu\text{m}$  in diameter remained in the austenitic state, without undergoing martensitic transformation, on cooling down to a temperature of  $-196^\circ\text{C}$ , whereas for a common massive specimen  $M_s = -20^\circ\text{C}$ . An explanation to this may be that martensite cannot be formed homogeneously and that the probability of existence of portions of heterogeneous nucleation in an austenitic particle diminishes with a reduction in the particle size.

The nature of heterogeneous nucleation of martensite can be elucidated most simply for cases where a phase having a face-centred cubic lattice transforms into martensite with close-packed hexagonal lattice. Stacking faults in the f.c.c. phase, which could appear, for instance, by extension of dislocations, are thin interlayers in the closely packed hexagonal lattice and are therefore, as it were, ready two-dimensional nuclei of hexagonal martensite. This situation is found in cobalt during its  $\beta_{f.c.c} \rightarrow \alpha_{h.c.p}$ -transformation.

It is known that what is called  $\epsilon$ -martensite can form in steels and iron-manganese alloys rich in manganese (over 10 per cent), as also in chrome-nickel stainless steels.  $\epsilon$ -martensite has a h.c.p lattice and can transform into common  $\alpha$ -martensite with body-centred cubic or tetragonal lattice. It is assumed that stacking faults in the austenite are ready nuclei of  $\epsilon$ -martensite. The mechanism of the  $\epsilon \rightarrow \alpha$ -transformation still has not been studied thoroughly. It is assumed, without experimental proof, that hexagonal martensite first forms at stacking faults in the austenite of carbon and other steels, and this is an intermediate phase which then transforms into common  $\alpha$ -martensite. The low stacking fault energy of austenite, i.e. strong extension of dislocations, should promote the nucleation of hexagonal martensite.

Another hypothesis relates the formation of martensite in carbon steels to the existence of portions of austenite depleted of carbon. Such portions of fluctuational origin, which are almost

free from carbon, can undergo a  $\gamma \rightarrow \alpha$ -transformation at temperatures below the  $M_s$  point, owing to considerable difference in the free energies of  $\gamma$ - and  $\alpha$ -phases. It is further assumed that at temperatures near  $M_s$  only the largest portions depleted of carbon can serve as transformation nuclei, whereas at lower temperatures smaller low-carbon portions may become such nuclei, which fact explains why the temperature of transformation should be lowered continuously.

The most actively developing hypotheses are those which relate the formation of martensite with the existence in the initial phase of some portions with a particular arrangement of dislocations. According to one of such assumptions, a martensitic nucleus forms owing to certain dislocational reactions or dislocation rearrangement within the martensitic temperature range. By another assumption, the largest portions of the initial phase with a certain arrangement of dislocations (embryons), which have formed at higher temperatures, become active sites of the transformation at lower temperatures (below  $M_s$ ). It is also assumed highly probable that the process of nucleation is promoted by the field of high internal stresses created by particularly located dislocations: the field performs, as it were, the work of creation of a nucleus.

Direct electron-microscopic observations on sites of heterogeneous nucleation of martensite in the initial phase are still absent. According to some estimations, the number of such sites in 1 cm<sup>3</sup> of austenite should be of an order of 10<sup>7</sup>.

#### 3.2.4. MICROSTRUCTURE AND SUBSTRUCTURE OF MARTENSITE-HARDENED ALLOYS

##### Microstructure

Structural studies of hardened carbon steels and carbonless iron-base alloys have revealed two principal morphological types of martensite: *lamellar martensite* and *lath martensite*.

These two types differ from each other in the shape and mutual disposition of crystals and also in substructure and habit planes.

**Lamellar martensite** (which is also called *acicular*, *low-temperature*, or *twinned martensite*) is the well-known classical type of martensite, which is most typical for hardened high-carbon steels and carbonless iron-base alloys with a high concentration of the second component, for instance, in Fe-Ni alloys with more than 28 per cent Ni (Figs. 127 and 128). Martensitic crystals have the form of thin lenticular plates. This shape of martensitic platelets corresponds to the minimum of energy of elastic distortions on their formation in the austenitic matrix and is similar to the shape of mechanical twins. Cases where the largest plane of a marten-

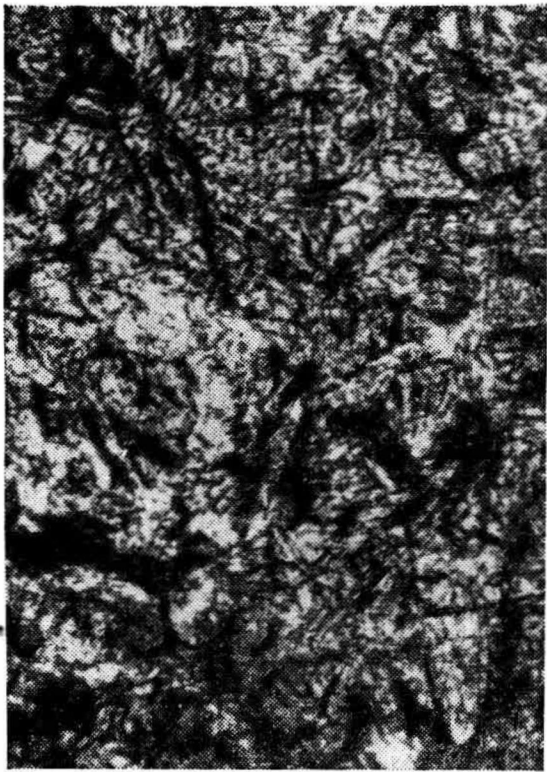


Fig. 127. Acicular martensite in hardened steel Y8,  $\times 300$

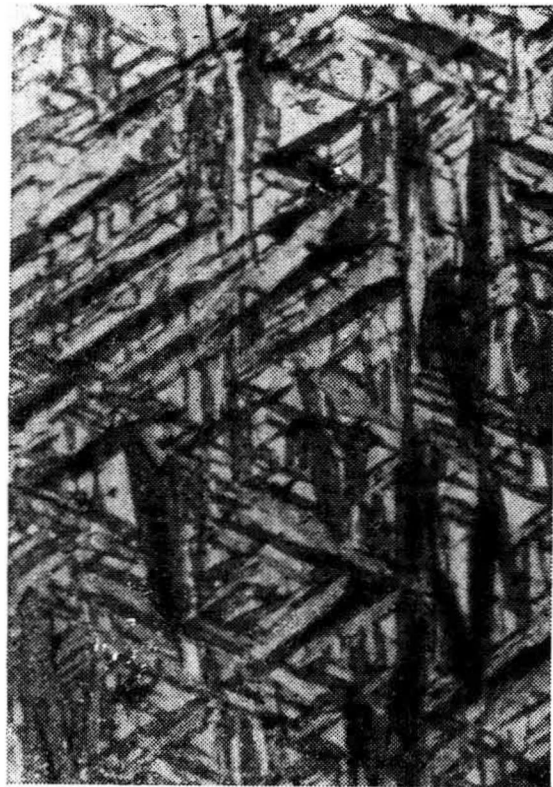


Fig. 128. Martensite platelets and retained austenite in hardened Fe-13.9% Mn alloy,  $\times 1000$  (after G. Krauss and A. R. Marder)

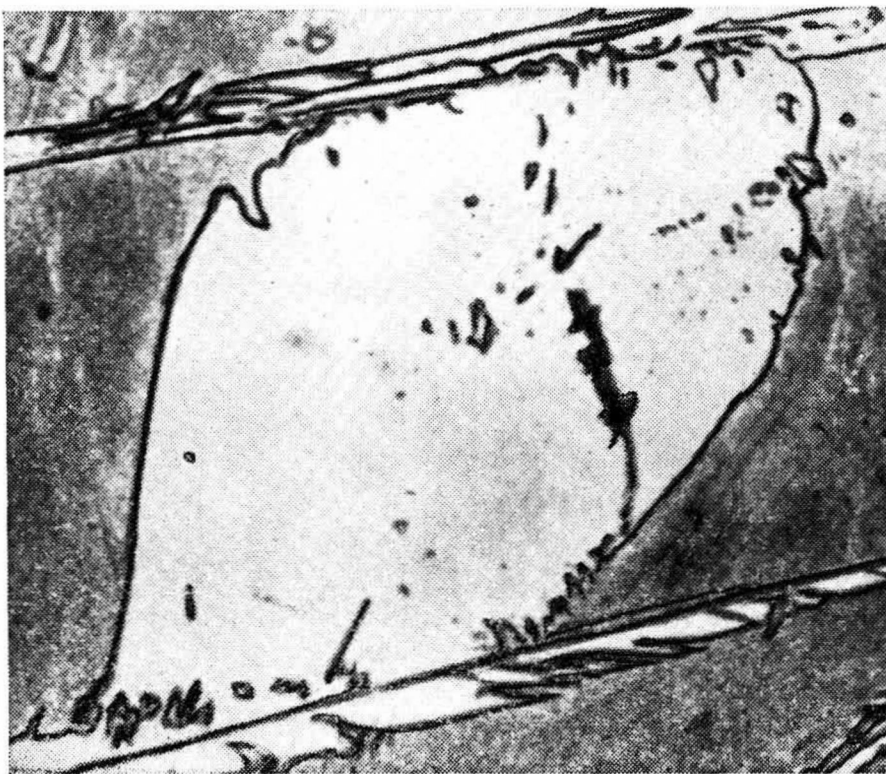


Fig. 129. A rare case of martensite platelet parallel with microsection plane,  $\times 750$  (after A. P. Gulyaev and E. V. Petunina)



site platelet coincides with the plane of a microsection are extremely rare (Fig. 129). At low magnifications of the microscope, arbitrary sections of martensitic platelets by the surface of a microsection form a false picture of needle-like shape of the crystals. Nevertheless, the historically established terms 'coarse-acicular' and 'fine-acicular' martensite are used widely in the specialist literature.

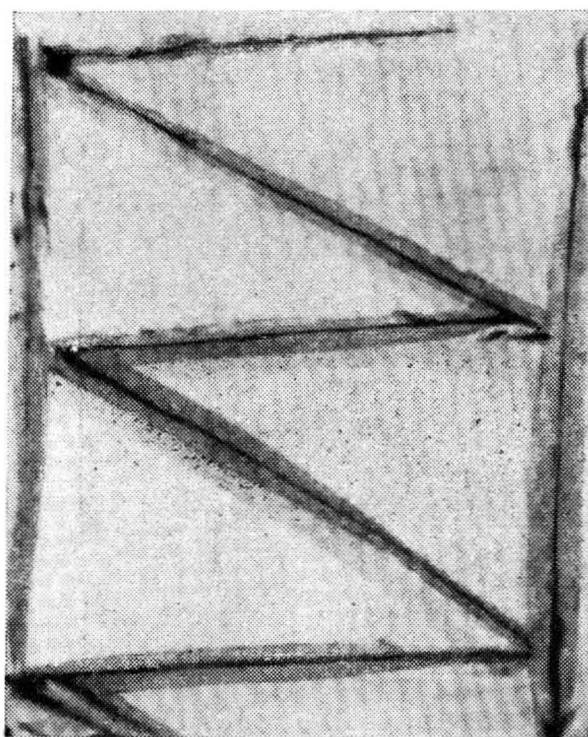


Fig. 130. Truss-shaped martensite platelets and retained austenite in hardened steel with 1.86% C. Mid-ribs are seen on platelets,  $\times 550$  (after G. Krauss and A. R. Marder)

Depending on the composition of an alloy, the habit plane of lamellar martensite may be the  $\{225\}_A$  or  $\{259\}_A$  plane in the Fe-C system and the  $\{3, 10, 15\}_A$  plane in the Fe-Ni system (see Sec. 3.2.3).

Adjacent platelets are not parallel to one another and often form truss-shaped ensembles (Fig. 130). Owing to the interference of long-range fields of elastic stresses from each platelet, this regular position of platelets in the matrix phase ensures that the elastic energy of the total field of a whole ensemble is at its minimum.

The earlier platelets (those formed near  $M_s$ ) penetrate the whole austenitic grain and separate it into portions. As follows from the mechanism of martensitic transformation, a platelet cannot pass beyond the boundary of a grain of the matrix phase and

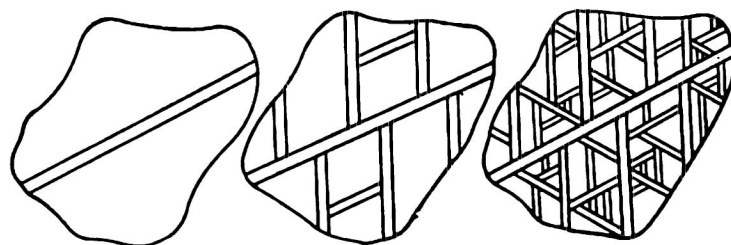


Fig. 131. Formation of martensite platelets of different length in an austenitic grain

that is why the maximum size of martensitic platelets is determined by the size of austenitic grains.

Upon lowering the temperature, new martensitic platelets form within austenitic portions, the size of these platelets being limited by the size of the portions of the matrix (see Figs. 130 and 131).



As the transformation proceeds, an austenitic grain breaks down into ever smaller portions with ever smaller platelets being formed in them. With a fine austenitic grain, for instance, if the steel has been only slightly overheated above  $A_{c3}$ , martensitic platelets are so small that microsections reveal no 'needle-like' structure. Such martensite is called 'structureless' and is the most desirable type in steel.



Fig. 132. Microcracks in martensite platelets in hardened steel with 1.39% C,  $\times 500$  (after G. Krauss and A. R. Marder)

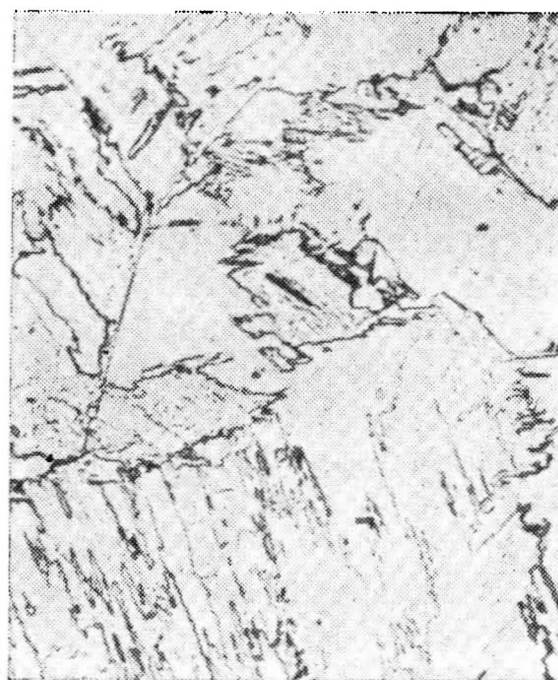


Fig. 133. Lath (massive) martensite in hardened Fe — 1.94% Mo alloy,  $\times 200$  (after G. Krauss and A. R. Marder)

Upon hardening, residual austenite may remain between martensitic platelets in the steel at room temperature. This may be clearly seen in high-alloyed iron alloys (see bright portions in Figs. 128 and 130).

Mechanical (deformation) twins and microfissures may form in places where two martensitic platelets oriented at different angles interfere with each other during their growth (Fig. 132).

**Lath martensite** (also called *massive*, *packet*, *high-temperature*, or *untwinned martensite*) is the most common morphological type in hardened low- and medium-carbon steels, many structural alloy steels and low-alloyed carbonless iron alloys, such as Fe-Ni alloys with less than 28 per cent Ni. Its crystals have the form of thin columns extending in one direction. Crystals of lath martensite pass parallel to one another and form a dense packet in which adjacent crystals are separated by low- or high-angle boundaries.

The habit plane of lath martensite crystals in iron alloys is close to the  $\{111\}_A$  crystallographic plane.

The width of all crystals in a packet is roughly the same, ranging from a few  $\mu\text{m}$  to fractions of a micrometer (usually 0.1-0.2  $\mu\text{m}$ ), i.e. may be at the limit of resolution of the optical microscope or even beyond that limit. For that reason lath martensite crystals are hardly seen, or even indiscernible, in the optical microscope, or else may be revealed as a fine structure of packets. Because of this, the main structural element in microsections is a packet of crystals (Fig. 133), rather than individual very fine crystals. In that connection, this type of martensite has been termed *massive*, or *packet-type*, as distinct from acicular martensite. A number of crystal packets may form in a single austenitic grain. As distinct from ferritic grains which form upon a 'normal' transformation, packets of lath martensite have a different internal structure, composed of laths, which is not always visible in the optical microscope, and also jagged extended outlines.

The formation of lath (massive) martensite has all the typical characteristic features of martensitic transformation, including the appearance of a relief on polished surface of microsections, which reproduces the internal lath structure.

### Substructure

Transmission electron microscopy reveals in many alloys a rather intricate fine structure of martensitic crystals with a large number of dislocations and twins. Such a substructure may form in two principally different ways: firstly, owing to an additional plastic deformation (through slip or twinning) which, as shown in Sec. 3.2.3, is an inseparable part of the mechanism of martensitic rearrangement of the lattice, and secondly, owing to the plastic deformation that a martensitic crystal already formed is subjected to from the surrounding elastic medium. In the former case we may speak of the initial substructure of transformation, and in the latter, of the secondary substructure of deformation. Accordingly, a distinction is made between transformation twins and deformation (mechanical) twins. It is not always possible to determine experimentally what is the origin of a substructure. In the discussion below we assume that all the substructures considered are of the transformation origin.

**The substructure of lamellar martensite**, as seen in the optical microscope, shows a characteristic *midline*, or more strictly, *midregion*, which is called *midrib* (see Fig. 130).

As has been revealed by electron microscopy, the midrib is a region with densely packed thin parallel twin interlayers (see the

wide band in Fig. 134). In the martensite of iron-base alloys, the twinning plane is most often  $\{112\}_M$ . The thickness of twinning interlayers may range from a few angstroms to a few hundred angstroms, depending on the composition of alloys and the conditions of formation of martensite. Twin interlayers of a thickness of only three atomic layers can be regarded as extended dislocations.

On both sides of a midrib there are peripheral regions of martensitic platelets in which dislocations of a relatively low density ( $10^9$  to  $10^{10}$  cm $^{-2}$ ) may be seen.

The width of a twinned zone in a martensitic platelet depends on the composition of alloy. For instance, in alloys of the Fe-Ni system, the width of this zone increases with the content of nickel until all the section of a martensitic platelet will be occupied by transformation twins.

Since the substructure and habit of a crystal are determined by the nature of additional deformation during the martensitic transformation (see Sec. 3.2.3), it is natural that the habit plane and substructure of crystals are interrelated with their shape. Thus, in Fe-Ni alloys, a deviation of the habit plane from the  $\{3, 10, 15\}_A$  plane, which is observed on reducing the content of nickel from 33 per cent to 30 per cent, is accompanied by a reduction in the density of transformation twins  $\{112\}_M$  in martensitic platelets and in the width of the zone of these twins, whereas the shape of platelets changes from lenticular to jagged. The more intricate substructure formed on deviation of the habit plane from the  $\{3, 10, 15\}_A$  plane is an indication that the martensitic transformation has taken place with a more complicated additional deformation.

Since a martensitic platelet in the general case consists of a twinning midzone and peripheral slip zones, a hypothesis has been suggested that the formation of a platelet proceeds in two stages. Initially, the additional twinning deformation plays the



Fig. 134. Parallel twin interlayers in midrib of martensite platelet of hardened Fe-32% Ni alloy (after G. Krauss and A. R. Marder)

principal part in the formation of a platelet (the future midrib). Because of the tremendous speed of platelet growth, the heat of transformation is not removed properly and the temperature of platelet surface increases appreciably, which results in a change in the mechanism of additional deformation, i.e. transition from twinning to dislocation slip. (As is well known, with a rapid plastic deformation in b.c.c. metals, a drop in temperature results in glide being changed to twinning.)

A. L. Roitburd suggested a different explanation for the change of the mechanism of additional deformation in the formation of martensitic platelets. As has been noted in Sec. 3.2.3, an additional deformation results in the appearance of tilts in the habit plane of a martensitic crystal (see Fig. 126d). These tilts increase the surface energy of the platelet. It is possible to lower the surface energy by reducing the height of tilts, which may be achieved by replacing perfect dislocations with partial twinning dislocations with a lower Burgers' vector. But as a twinning dislocation passes through the depth of a platelet, a stacking fault is formed, which increases the volume energy of the martensitic crystal. Calculations show that twinning is energetically more favourable than slip until the platelet is sufficiently thin, since the gain in the surface energy of the platelet outweighs the loss in the volume energy. With an increase in the thickness of the platelet, the extent of stacking faults from twinning dislocations increases and, beginning from a certain critical thickness, the additional slip deformation of perfect dislocations becomes more favourable than additional twinning deformation and the former replaces the latter.

**The substructure of lath martensite** differs from that of lamellar martensite in that it has no midzone of thin twinned interlayers. The substructure of lath martensite has a complicated dislocation structure characterized by dislocation tangles and high dislocation density, of an order of  $10^{11}$ - $10^{12}$  cm<sup>-2</sup>, i.e. the same as in the metal after heavy cold deformation. Martensitic laths are often composed of slightly disoriented stretched subgrains. Twin interlayers may form in lath martensite, but their density is incomparably lower than that in midribs of lamellar martensite, with many lath crystals having no twins at all.

**The substructure of retained austenite** differs from that of the original austenite by a higher density of imperfections which appear through local plastic deformation of the austenite by martensitic crystals. Near martensitic crystals, the austenite may show flat accumulations of dislocations, dislocation tangles, and stacking faults.

### **Transition from One Morphological Type of Martensite to Another**

The two principal types of martensite differ from each other in their micro- and substructure and the habit plane. It is then quite logical to conclude that the leading role in the formation of lamellar martensite, at least at the initial stage, is taken by the

additional twinning deformation, whereas additional slip deformation is mainly responsible for the formation of lath martensite.

**Table 9. Concentration Limits for the Formation of Lath or Lamellar Martensite (Krauss and Marder)**

System	Martensite	
	lath, % (not above)	lamellar, %
Fe-C	1.0 C	0.6-2.0 C
Fe-N	0.7 N	0.7-2.5 N
Fe-Ni	29 Ni	29-34 Ni
Fe-Cr	10 Cr	—
Fe-Mo	2 Mo	—
Fe-W	0.3 W	—
Fe-V	0.5 V	—

Which type of martensite will be formed depends on the ratio of critical shear stresses in the austenite that initiate glide and twinning. If glide requires a higher shear stress than twinning, then lamellar martensite is formed; otherwise it will be lath martensite. Using this assumption it is quite easy to explain many regularities of the transition from one type of martensite to the other, and in the first place the effect of alloy composition on the morphology of martensite (Table 9).

With a reduction in temperature, the resistance to slip increases rapidly and beginning from a definite temperature, becomes greater than the resistance to twinning (Fig. 135). For that reason, lamellar martensite is more probable to form at lower temperatures of martensitic transformation, and lath martensite, at higher temperatures. Hence, it is clear why in Fe-C, Fe-N and Fe-Ni alloys lath martensite forms at low concentrations of the second component and lamellar martensite, at high concentrations (Table 9). This transition may be logically linked with a reduction in the  $M_s$  temperature (see Fig. 118). For instance, with a higher content of carbon, the resistance to slip in a relatively low-temperature martensitic range is higher than that to twinning, and it is lamellar martensite that forms. The transition from one

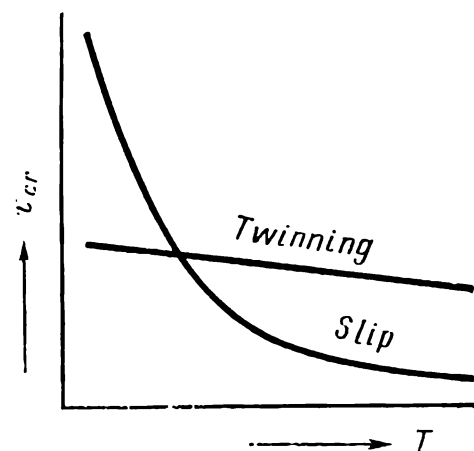


**Fig. 135. Effect of temperature on critical stress ( $\tau_{cr}$ ) of slip and twinning**

morphological type of martensite to the other occurs within an interval of compositions. It is then also clear why some crystals in lath martensite contain twin interlayers: these are crystals that have formed in the lower portion of the martensitic range and since they have been the last to appear, their morphological type is lath as before.

In some systems, such as Fe-Cr, Fe-Mo, Fe-W or Fe-V, which have a closed  $\gamma$ -region in the constitutional diagram, the  $M_s$  point at any concentrations of the alloying element is so high that lamellar martensite does not form at all (Table 9).

Any method of austenite strengthening, i.e. increasing the critical stress that can cause glide, should promote the formation of lamellar martensite, even at a constant temperature  $M_s$ . Carbon is one of the most active strengtheners of austenite, because of which an increase in its concentration is especially effective for twinning in the martensitic transformation.

It should be emphasized in conclusion that the structure of a metal or alloy after martensitic transformation differs in the whole from the structure of the same metal after a disordered rearrangement of the lattice in having a much larger number of imperfections: more developed boundaries and sub-boundaries and higher density of dislocations and twin interlayers.

### 3.2.5. KINETICS OF MARTENSITIC TRANSFORMATIONS

#### Types of Kinetics

According to their kinetics, martensitic transformations may be conditionally separated into three types: athermal, burst-type, and fully isothermal (Fig. 136).

Athermal transformation can be observed in carbon and alloy steels with the martensitic point  $M_s$  above 100°C, burst-type transformation in Fe-Ni and Fe-Ni-C alloys with  $M_s$  point below the room temperature, and fully isothermal transformation in Fe-Ni-Mn and Fe-Ni-Cr alloys with  $M_s$  point also below the room temperature.

The proportion of martensite and austenite, which may be characterized by the curves in Fig. 136, is determined magnetometrically (by deviation of the needle of a magnetometer), using the fact that austenite is paramagnetic and martensite is ferromagnetic; electroresistive and dilatometric methods can also be used for the purpose.

**Athermal transformation** (Fig. 136a and curve 1 in Fig. 137) is characterized by a smooth increase in the amount of martensite, with the temperature reducing continuously within the martensitic range  $M_s - M_f$ . An arrest of cooling results practically

in full stoppage of the transformation. When an austenitic specimen is placed in a quench bath at a temperature below  $M_s$ , the transformation proceeds at a very high speed during a few se-

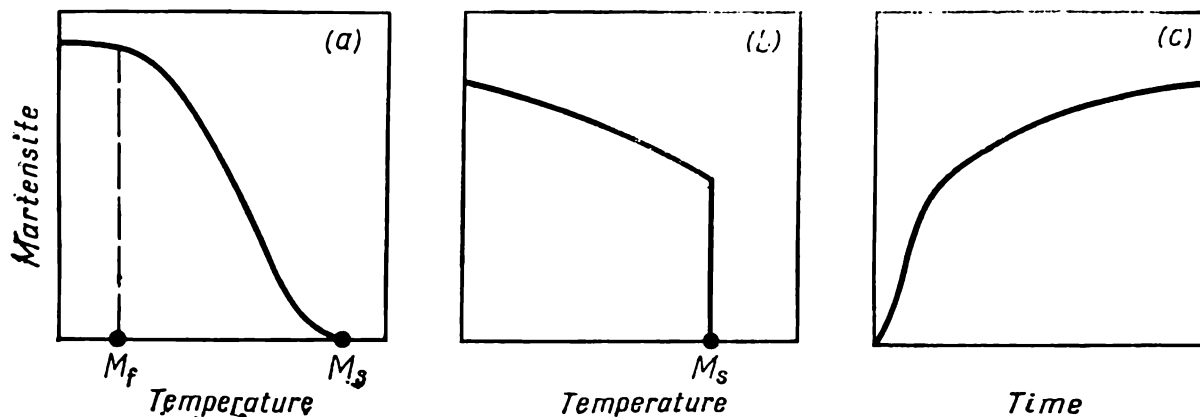


Fig. 136. (a) athermal, (b) burst-type and (c) fully isothermal type of martensitic transformation

conds until the temperature of the specimen is equalized with that of the bath. During the subsequent isothermal holding, no martensite is formed, notwithstanding the high amount of the initial phase (austenite) in the specimen, or more strictly, the speed of isothermal transformation of austenite is negligible (hence the name: 'athermal' transformation).

The rate with which the amount of martensite increases with lowering temperature depends only slightly on steel composition. In many low-alloy steels within the range of transformation degrees from 10 per cent to 50 per cent this rate is 0.75-1.4 per cent martensite per a degree C.

The amount of retained austenite upon hardening with cooling to room temperature depends on the composition of the initial austenite and is actually linked with the position of the upper martensitic point. With increasing the carbon content, the  $M_s$  point lowers (see Fig. 118) and the amount of retained austenite at room temperature increases. For instance, in steels with 0.6 per cent and 1.2 per cent C hardened from the austenitic state, the

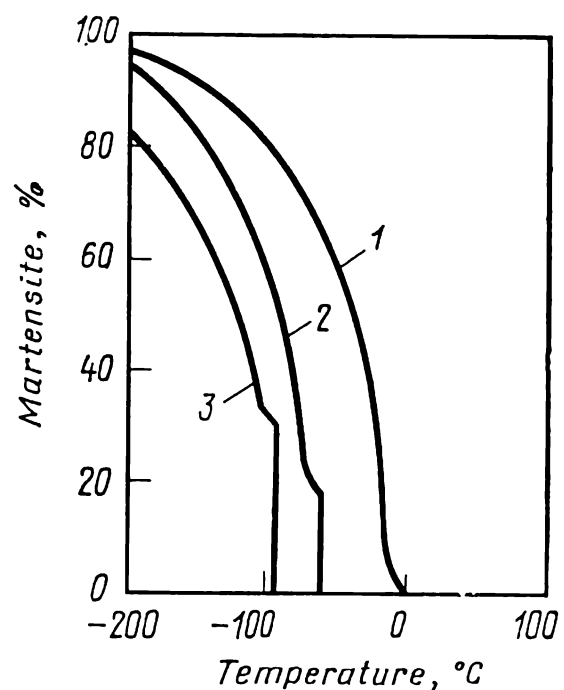


Fig. 137. Curves of martensitic  $\gamma \rightarrow \alpha$  transformation on continuous cooling of Fe-Ni alloys (after M. D. Perkas and V. M. Kardansky)

1—29% Ni,  $M_s = -10^\circ\text{C}$ ; 2—31% Ni,  $M_s = -63^\circ\text{C}$ ; 3—32% Ni,  $M_s = -97^\circ\text{C}$

amount of retained austenite is respectively 2 per cent and 20 per cent.

Retained austenite can also remain in the metal at temperatures below the lower martensitic point  $M_f$ . On passing this point, the martensitic curve is horizontal, which corresponds to a certain virtually invariable proportion of martensite and retained austenite (see Fig. 136a).

Athermal transformation is of the highest practical interest, since, as distinct from burst-type and isothermal transformations,

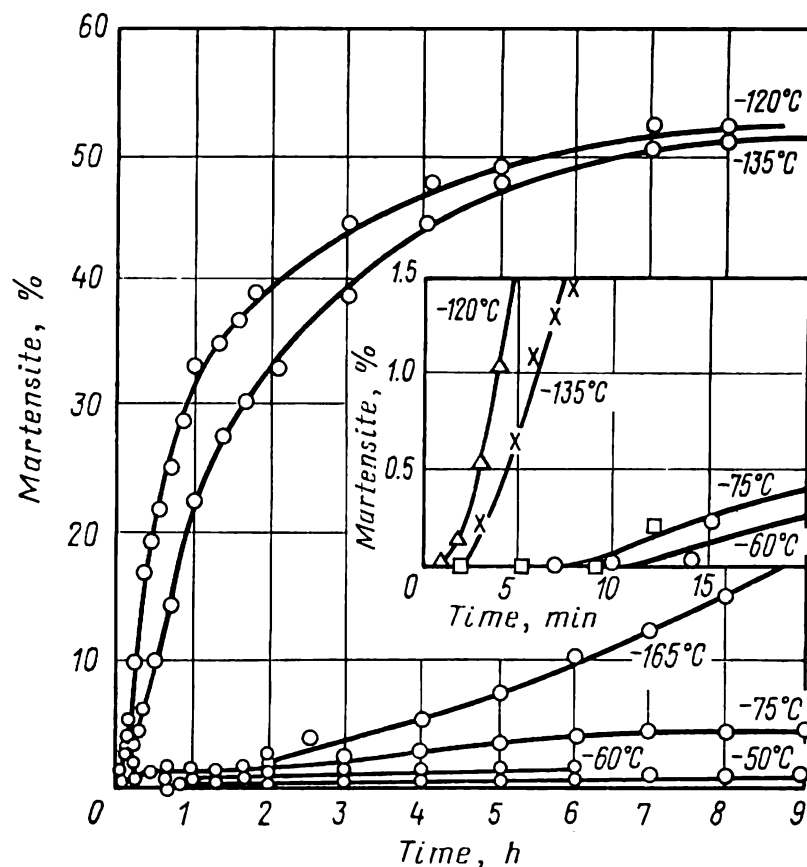


Fig. 138. Isothermal austenite-to-martensite transformation in Fe + 23.4% Ni + 3.3% Mn alloy at different temperatures (after O. P. Maksimova and A. I. Nikonorova)

which are mainly typical for sub-zero temperatures, it proceeds at temperatures above the room temperature, i.e. under common conditions of hardening of industrial alloys.

**Burst-type transformation** is characterized by a jump-like (burst) formation of a definite amount of martensite at a temperature near or slightly below  $M_s$  (Fig. 136b and curves 2 and 3 in Fig. 137). The amount of martensite thus formed depends on alloy composition and position of the  $M_s$  point, varying from a few per cent to approximately 70 per cent. The burst is accompanied with an acoustic effect (a clear audible click) and a temporary increase of temperature, sometimes by 30 degrees C, owing to rapid evolution of the latent heat of transformation.



**Fully isothermal transformation** (Figs. 136c and 138) in its kinetics bears some resemblance to a normal phase transformation (see Fig. 79). With isothermal holding after a certain induction period, the martensitic transformation proceeds with acceleration and then with a constant attenuation in time. As in ordinary phase transformation, the speed and induction period of isothermal martensitic transformation depend on temperature. For instance, in an iron alloy with 23.4 per cent Ni, 3.3 per cent Mn and 0.06 per cent C the martensitic transformation is accelerated on lowering the temperature from  $-50^{\circ}$  to  $-120^{\circ}\text{C}$  and decelerated with a further drop in temperature (Fig. 138). The induction period shortens on lowering the temperature down to  $-120^{\circ}\text{C}$  and increases with still lower temperatures. This makes it possible to plot C-curves of isothermal martensitic transformation (Fig. 139) similar to common C-curves of disordered phase transformations.

Since there is an induction period, the isothermal martensitic transformation can be fully prevented by cooling the austenite rapidly to a very low temperature. For instance, in some iron alloys characterized by isothermal martensitic transformation, the latter can be suppressed by quick cooling of specimens to the temperature of liquid nitrogen ( $-196^{\circ}\text{C}$ ). On subsequent heating, the austenite undergoes isothermal martensitic transformation with the rate depending on temperature.

Kinetically, isothermal martensitic transformation differs principally from a disordered phase transformation in that it does not proceed to full disappearance of the initial phase, i.e. a certain amount of austenite is always retained in the metal. The amount of isothermally formed martensite may range from a few fractions of a per cent to a few tens of per cent, depending on alloy composition, preceding heat treatment, and the temperature of isothermal holding. As is shown in Fig. 138, for instance, a 9-h holding time at  $-50^{\circ}\text{C}$  gives around 1 per cent martensite, and the same time at  $-120^{\circ}\text{C}$ , more than 50 per cent.

As has been shown experimentally, a strict delimitation between athermal or burst transformation and isothermal transfor-

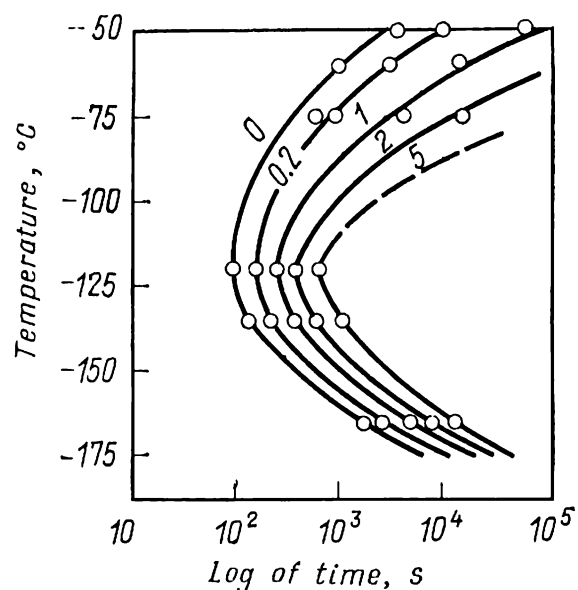


Fig. 139. C-curve of isothermal martensitic transformation in Fe + 23.4% Ni + 3.3% Mn alloy. Numerals at curves are percentages of martensite formed (after O. P. Maksimova and A. I. Nikonorova)

mation is impossible. In some alloys, for which athermal kinetics is typical and where a definite portion of martensite quickly forms athermally, an additional amount of martensite may form isothermally through the subsequent cooling to a given temperature. In other cases, after some burst martensite has formed an appreciable amount of 'isothermal' martensite may form at temperatures below the temperature of burst. A small amount of martensite may even form isothermally at temperatures slightly above the burst temperature.

Irrespective of the type of transformation kinetics, martensitic crystals grow with tremendous speeds at any temperature, including deep-freezing ones. Experiments were made on determining the speed and time of formation of martensitic platelets by the accompanying variations in their electric resistivity. The speed of growth of martensitic platelets (in the platelet plane) was found to be of an order of 1 km/s irrespective of the transformation temperature. In Fe-Ni alloys, midribs of martensitic platelets form within a time interval of an order of  $10^{-7}$  s and the whole platelet (after slower thickening), roughly within  $10^{-6}$  s. Note for comparison that the time of burst is as long as  $10^{-4}$  to  $10^{-3}$  s.

After being formed extremely quickly, a martensitic crystal does not grow further. A larger amount of martensite that can form at a lower temperature in athermal or burst-type transformation or on increasing the time of holding in isothermal transformation is due to the formation of new crystals, rather than to the growth of those already formed. This important peculiarity of martensitic transformation has been clearly demonstrated by high-speed photography.

A typical feature of the kinetics of all martensitic transformations is their autocatalytic nature, i.e. the formation of initial platelets involves the appearance of new platelets nearby, which promote the formation of ever greater number of new platelets, and so on, owing to which the process develops for some time as a chain reaction. It is this fact that explains well why martensite forms with acceleration at the initial stages of isothermal transformation (see Figs. 136c and 138). If some martensite, let a small quantity, has already formed in the volume or at the surface of a specimen by the beginning of isothermal holding, it stimulates the progress of isothermal transformation, which starts straight away at the maximum rate. In that case the curve of martensitic transformation has no initial portion of accelerated transformation.

The autocatalytic nature of the process can be seen most clearly in the burst-type transformation. A martensitic burst results from the fact that the formation of a single platelet immediately causes chain reaction of formation of a series of platelets. This autocata-

lytic nature is assumed to be due to the field of elastic stresses at the edge of a growing platelet of martensite, this field promoting the formation of new platelets.

A marked burst effect occurs if the plates have the {259} habit plane. As has been shown, this very habit plane of martensitic platelets provides the appearance of high stresses in the austenite, which stimulate the formation of new platelets. With the formation of martensitic platelets with the {225} habit plane, no burst takes place. For that reason, martensite with the {259} habit plane and typical twinned midrib is sometimes called *burst martensite*.

There is no sharp delimitation between the burst and common athermal transformation. If the composition of an alloy varies, for instance, the content of nickel in Fe-Ni-C alloys increases, the habit plane gradually changes from {225} to {259} and simultaneously the force of burst, i.e. the amount of martensite formed through the burst mode, also increases. Thus, with varying the composition of an alloy there occurs a gradual transition from athermal to markedly burst mode of transformation. For instance, in the Fe-Ni system with 29 per cent Ni the transformation has typically athermal kinetics, whereas at 31 or 32 per cent Ni it is of burst type, the force of burst in the alloy with 32 per cent Ni being greater than that in the alloy with 31 per cent Ni (see Fig. 137).

Burst-type transformation can be regarded as a variant of athermal transformation with especially marked autocatalytic nature of the process. Athermal transformation in turn does not differ principally from the isothermal mode. The two types of kinetics of martensitic transformations, as has been shown by G. V. Kurdjumov, should be considered on the basis of a single concept that the rate of formation of transformation centres is temperature-dependent.

Since the rate of growth of martensitic crystals is tremendous irrespective of temperature, the fact that a reduction in temperature causes first an increase and then a decrease in the rate of isothermal transformation (Figs. 138 and 139) should be explained by the temperature dependence of the rate of nucleation of martensitic crystals.

As in any phase transformation, the rate of nucleation of martensite is

$$J = Ae^{-\Delta F_{cr}/kT}e^{-Q/kT}$$

[see formula (24)]. At a temperature  $T_0$  of metastable equilibrium between the initial phase and martensite, the difference of free energies of these phases ( $\Delta F_{vol}$  in Fig. 121) is zero and the transformation does not proceed. With a reduction of temperature this difference, which is the thermodynamic stimulus of transforma-

tion, increases and the work of formation of a martensitic nucleus ( $\Delta F_{cr}$ ) decreases, which results in acceleration of the transformation and reduction of the induction period. With a further decrease of temperature the mobility of atoms becomes so small that formation of nuclei is retarded notwithstanding the high value of  $\Delta F_{vol}$  and respectively the low work of nucleation.

In a certain intermediate region where the temperatures are not excessively low, a reduction in the work of nucleation may result in such a rapid transformation that neither the induction period nor the isothermicity of transformation (i.e. its development in time) can be measured experimentally.

Various cases may be observed in experiments, depending on alloy composition and the absolute value of  $T_0$ . If, for instance,  $T_0$  is low, then the transformation will be isothermal at any temperature (Figs. 138 and 139), since at any temperature within the martensitic range the rate of transformation is relatively low. If, however,  $T_0$  is appreciably above room temperature, then isothermal transformation will be observed only at temperatures near  $M_s$  and at relatively low temperatures (usually at sub-zero temperatures and, less frequently, at room temperature). Between these temperature intervals, within which isothermal transformation is observed, there is a temperature interval in which the isothermal transformation proceeds at a tremendous speed, so that it produces an impression as if there is no isothermicity. From this standpoint, one may suppose that the athermal transformation proper is non-existent, since it is an ordinary isothermal transformation which proceeds with a tremendous speed at each temperature during quenching. This is precisely why isothermal transformation of martensite is often observed at the arrest of cooling in some alloys for which the 'athermal' kinetics is typical in the whole.

The phenomenon of fully isothermal martensitic transformation, which has been discovered by G. V. Kurdjumov and O. P. Maksimova, can serve as the direct proof that the nucleation of martensitic crystals is a temperature-dependent thermally activated process, like any other process of nucleation of crystals of a new phase (see 2.1.1). In that connection, the term 'athermal transformation' contradicts in its essence the thermal nature of formation of nuclei. A more appropriate, though less frequently used term is 'non-isothermal transformation', which only implies that martensite is formed at different temperatures during cooling, rather than at one and the same temperature.

The most important feature of the kinetics of martensitic transformations is that the formation of martensite stops when much of the initial phase (austenite) is still present in the metal, so that the temperature must be lowered in order to re-start the transformation. Since martensitic transformation proceeds owing to the

formation of new crystals, rather than to the growth of those already formed, the arrest of transformation implies a stop in the formation of martensitic nuclei. In view of the fact that the mechanism of formation of martensite has not been established reliably, this feature of the kinetics of martensitic transformations is only hypothetical.

Modern views on the problem are based on the hypothesis of heterogeneous nucleation of martensite in prepared portions of austenite having a different composition than the matrix as a whole or, what is more probable, a specific structure (see 3.2.3). These special portions in austenite (embryons) differ from one another in their size, composition and structure. When the thermodynamic stimulus of transformation, i.e. the difference of free energies of austenite and martensite, attains a definite value upon cooling, these special portions in the austenite are transformed into active martensitic nuclei capable of growing. At temperatures near  $M_s$ , only the portions of austenite in which the work of nucleation is at its minimum are realized into nucleation centres. With exhaustion of these portions, the transformation stops. To re-start it, we have to lower the temperature so as to increase the difference of free energies between austenite and martensite.

Attenuation of martensitic transformation with isothermal holding (see Fig. 138) is also favoured by the progressive breakdown of austenitic grains into ever smaller portions (see Fig. 131). With reduction in the size of these portions, the size of new martensitic crystals also decreases, so that the volumetric proportion of the martensite formed per each nucleus becomes respectively lower.

### Thermal Stabilization of Austenite

Stabilization of the initial phase should be understood as making the martensite less transformable, which may be realized through thermal, mechanical or some other effects. Accordingly, the stabilization will be termed *thermal*, *mechanical*, etc.

Thermal stabilization of austenite, which is usually called simply stabilization, can be observed upon a temporary arrest of the cooling process in an iron alloy within the martensitic range of athermal transformation. If the cooling process is interrupted at a temperature  $T_{ar} < M_s$  (but above  $M_f$ ) and a holding time is allowed, then the austenite will be stabilized. Its stabilization manifests itself in that, upon re-starting the cooling process, the transformation begins not immediately at temperature  $T_{ar}$ , but only after the austenite will be undercooled to a certain temperature  $M'_s$  (hysteresis effect), see Fig. 140. The amount of martensite thus formed may often be less than that obtained through uninterrupted cooling (the martensitic curve 2 in Fig. 140 passes

below curve 1) and the amount of retained austenite is accordingly larger. The martensitic transformation, on being re-started at temperature  $M'_s$ , may further proceed by burst (for instance, in Fe-Ni-C alloys).

The simplest case of heat treatment with stabilization of austenite is the one in which  $M_s$  is above room temperature and  $M_f$  below, with  $T_{ar} = 20^\circ\text{C}$ . For instance, holding a carbon steel at room temperature upon ordinary water quenching stabilizes the austenite, i.e. impedes the martensitic transformation of the steel

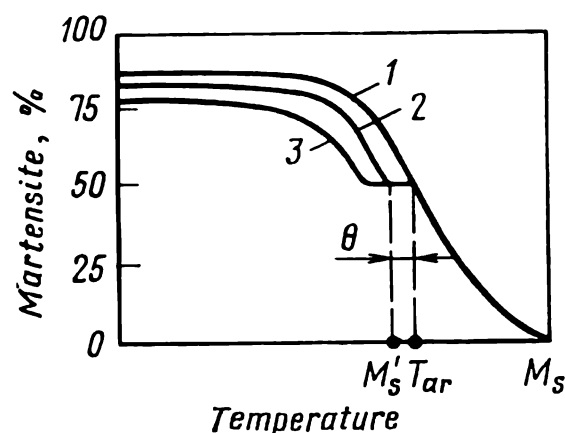


Fig. 140. Martensitic curves for various degrees of austenite stabilization

$T_{ar}$ —temperature at which cooling is arrested and a holding time is allowed; 1—continuous cooling; 2 and 3—curves at different holding time ( $\tau$ ) at  $T_{ar}$ , with  $\tau_3 > \tau_2$

on subsequent cooling to sub-zero temperatures, and increases the amount of retained austenite. In that connection, a study into the regularities of thermal stabilization of austenite is of interest for sub-zero treatment of steels (see Sec. 3.2.9).

The effect of stabilization is often determined in terms of the temperature hysteresis  $\theta = T_{ar} - M'_s$  (Fig. 140).

The degree of stabilization of austenite depends on the temperature at which the cooling process is interrupted,  $T_{ar}$ , and the time of holding at that temperature. If, upon interrupting the

cooling process, an alloy is heated to a temperature  $T_{st} > T_{ar}$ , then the degree of stabilization  $\theta$  will be dependent on  $T_{st}$  and the time of holding at that temperature.

With lowering the temperature  $T_{ar}$ , i.e. with an increase of the amount of martensite present in the metal during the stabilizing holding, the degree of stabilization increases. The time of holding may have a more complicated effect. With increasing the time of holding at  $T_{ar}$  or  $T_{st}$ , the degree of stabilization can increase continuously (curves 2 and 3 in Fig. 140). At sufficiently high temperatures, an extension of the holding time may first increase and then decrease the degree of stabilization. The higher  $T_{st}$  is, the more quickly  $\theta$  attains its maximum.

It was found for steel with 1.4 per cent C and 5 per cent Ni that, with increasing the time of holding at  $T_{st}$ ,  $\theta$  passed through its maximum and then diminished again and became even negative. This means that a large time of holding upon interrupted cooling may cause not stabilization ( $M'_s < T_{ar}$ ), but an opposite effect, i.e. activation of martensitic transformation ( $M'_s > T_{ar}$ ).

Thermal stabilization of austenite is a complicated process. It is quite probable that various stabilization mechanisms are active in different cases, for instance, in different temperature intervals.

A certain contribution to the thermal stabilization at temperatures below the  $M_s$  point may be brought by relaxation of elastic stresses in the austenitic matrix that surrounds martensitic platelets. As has been noted earlier, these stresses produce the autocatalytic effect, inherent in all martensitic transformations. The effect of reduction of elastic stresses around martensitic crystals may explain well why the degree of stabilization increases with the holding time, but fails to explain why  $\theta$  lowers as the time of holding increases.

Quite important for understanding the nature of austenitic stabilization is the fact that thermal stabilization is observed only in such iron-base alloys which contain interstitial elements — carbon and nitrogen, if only in small quantities. For that reason almost all modern hypotheses concerning the mechanism of thermal stabilization of austenite proceed from the assumption that segregation of carbon and nitrogen atoms is decisive for the process.

During a stabilizing holding, atoms of interstitial elements can segregate in potential portions of nucleation in the austenite, thus preventing these portions from becoming martensitic nuclei. They can also segregate at the interface between the matrix and a nucleus, thus impeding the growth of the latter.

The hypothesis that relates thermal stabilization to deformation ageing, i.e. formation of segregations of interstitial atoms at dislocations in the austenite, seems very convincing. Since the formation of a martensitic crystal causes plastic deformation of the austenitic matrix, the strengthening of this matrix through deformation ageing should impede martensitic transformation. The fact that deformation ageing of austenite develops with increasing holding time at  $T_{st}$  may explain well why  $\theta$  also increases. The effect of reduced stabilization obtained on longer holding may be easily attributed to overageing (see Sec. 4.1.4), which results in a lower yield limit of the austenite. Negative values of  $\theta$  may be linked with progressive overageing which, on one hand, weakens the austenite appreciably and, on the other, may deplete the austenite of carbon near carbide segregates. These low-carbon portions have a higher  $M_s$  point. Deformation ageing accelerates with increasing temperature and accordingly,  $\theta$  attains more quickly its maximum.

The reduction of  $M_s$  on changing from extremely high rates of cooling above that temperature to ordinary rates of water quenching, as discussed in Sec. 3.2.2, can also be attributed to the stabilization of austenite through the supposed pinning of dislocations produced by segregated carbon atoms.

Thermal stabilization during martensitic transformation can occur not only in iron-base alloys, but in other alloys as well. For instance, liquid-nitrogen cooling can induce athermal transformation in water-quenched alloys of copper with 15 per cent (at.) Sn. If a holding time is allowed at room temperature after water quenching of the alloy, then, upon subsequent cooling, the  $M_s$  point and the amount of martensite formed will be lower, the effect being greater with a longer holding time. A four-day holding time can fully suppress martensitic transformation. One of probable causes of this thermal stabilization may be the segregation of tin atoms in the initial phase, which proceeds gradually at room temperature and hampers the formation and growth of martensitic nuclei.

### Effect of Deformation of Initial Phase on Kinetics of Martensitic Transformation

Plastic deformation of the initial phase may have a complicated effect on martensitic transformation. As has been noted in Sec. 3.2.2, deformation at temperatures above  $M_s$ , either plastic or elastic, causes martensitic transformation. Above  $M_s$ , the thermodynamic stimulus of transformation  $\Delta F_{vol}$  ('chemical' driving force) cannot cause the transformation. Within a definite temperature range  $M_s$ - $M_s^\sigma$  above  $M_s$ , elastic stresses facilitate the nucleation of martensite crystals in the sites of the initial phase where crystals would appear at temperatures below  $M_s$  without any stresses being applied. The energy of the stresses applied is added, as it were, to the thermodynamic stimulus of transformation  $\Delta F_{vol}$  and the martensitic transformation becomes feasible at lower degrees of undercooling relative to  $T_0$ , i.e. at higher temperatures. The more the temperature differs from  $M_s$  (towards  $T_0$ ), the lower is  $\Delta F_{vol}$ , and therefore, the higher should be the elastic stress to induce martensitic transformation. As the temperature of deformation is being increased, it can attain the point  $M_s^\sigma$  at which the stress applied reaches the yield limit. Above  $M_s^\sigma$ , plastic deformation introduces a different mechanism for stimulating the martensitic transformation, namely, the formation of new sites of martensitic nucleation under the action of the strain applied. The higher is the temperature, and correspondingly, the lower is  $\Delta F_{vol}$ , the higher must be the deformation to cause martensitic transformation. Above the  $M_d$  point, no plastic deformation is capable of transforming austenite into martensite during straining.

In iron alloys having a relatively high stacking fault energy, martensite forms from austenite during plastic deformation by the scheme  $\gamma \rightarrow \alpha$ , while in those with a low stacking fault energy, it forms by the scheme  $\gamma \rightarrow \epsilon \rightarrow \alpha$  (on  $\epsilon$ -martensite see Sec. 3.2.3).



In view of what has been said above, three types of martensite should be distinguished, namely: (a) *common martensite*, which forms without any deformation, either plastic or elastic, being applied, merely through lowering the temperature below  $M_s$ ; (b) *stress-assisted martensite*, which forms under the action of a stress (elastic straining); and (c) *strain-induced martensite*, which forms on plastic straining of the initial phase. Stress-assisted martensite can nucleate in the same sites of the initial phase as the common martensite, the stresses only promoting its nucleation in these sites. Strain-induced martensite nucleates in sites which have been prepared by plastic deformation.

Plastic deformation, though causing no martensitic transformation directly during application, may affect the kinetics of martensitic transformation on subsequent cooling. Such a preliminary deformation may have a dual effect. On one hand, it can intensify the subsequent martensitic transformation by raising the starting point of transformation ( $M_s$ ), increasing the speed of transformation, and reducing the amount of retained austenite. On the other hand, it sometimes may produce a retarding effect by lowering the starting point, decelerating the transformation itself, and increasing the amount of retained austenite (mechanical stabilization). The total effect depends on the degree and temperature of deformation and the properties of the initial phase, i.e. on the composition of alloy.

A slight preliminary deformation usually activates the martensitic transformation on subsequent cooling, whereas a heavy deformation may have an inhibiting effect (Fig. 141). This may be explained as follows. With slight deformations, the structural distortions in the initial phase and the local stress fields that are formed are such that nucleation of martensite in respective portions of the metal becomes energetically favourable. With heavy deformations, however, the regular structure of the initial phase is distorted very strongly, these distortions (for instance, developed subgrain boundaries) being such that the coherent growth of martensitic nuclei is inhibited at the very early stages. A higher

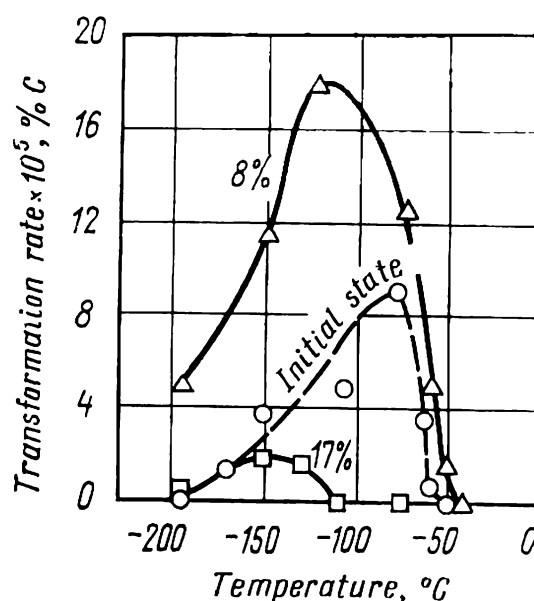


Fig. 141. Effect of temperature on initial rate of isothermal martensitic transformation in Fe + 17.2% Cr + 9.1% Ni alloy upon 8%- and 17%-deformation of austenite at 100 °C (after G. V. Kurdjumov, O. P. Maksimova and A. I. Nikonorova)

temperature of deformation and a lower elastic limit of the initial phase require a lower degree of deformation to cause mechanical stabilization.

### 3.2.6. VARIATIONS OF PROPERTIES OF ALLOYS ON MARTENSITIC HARDENING

#### Strengthening on Hardening

The most striking effect produced by martensitic hardening is the hardening of the metal, i.e. an increase in its hardness. Exactly this effect led to the discovery of steel hardening in the ancient times and extensive use of that method later on.

The nature of this hardening effect encountered in hardened steel remained a mystery for many centuries. In the medieval times, the hardening of a steel sword upon immersing it in hissing water was explained by supernatural forces. Even quite recently, at the verge of the XX century, attempts were made to attribute the high hardness of hardened steel to the conversion of its carbon into diamond. All these 'hypotheses' are extremely naive from the modern standpoint.

Studies into the nature of the martensitic transformation proper and the structure of martensite have played the decisive part in understanding the mechanism of hardening on quenching. This mechanism has been understood quite well in the whole, though some of its details still require explanation.

Attempts to explain the high hardness of hardened steel by some or other single reason have found no experimental verification. It can now be taken for certain that the hardening effect in martensite-hardened steel is due to the action of several mechanisms of dislocation trapping.

In all hypotheses of steel hardening, carbon is rightly assumed to play the most decisive part. It should be considered, however, that even in pure iron and carbonless iron alloys the martensitic transformation can increase the strength properties three to four times compared with the metal as annealed. For instance, martensitic transformation of the common ferritic structure of pure iron results in that the hardness of the metal increases from 60 to 200 HV and its ultimate strength, from 20 to 90 kgf/mm<sup>2</sup>. An alloy of iron with 8 per cent Cr and 0.45 per cent Ni has a yield limit of 22 kgf/mm<sup>2</sup> in annealed state and as high as 80 kgf/mm<sup>2</sup> upon hardening from 1000 °C.

As distinct from the phase of the same composition but formed on slow cooling owing to disordered rearrangement of the lattice, martensite can be characterized by a higher density of defects: twin interlayers and dislocations (see Sec. 3.2.4). The density of

dislocations in martensite can reach  $10^{10}$ - $10^{12}$   $\text{cm}^{-2}$ , i.e. the same order of magnitude as in cold-deformed metal. Twin boundaries and dislocation tangles serve as barriers for glide dislocations, i.e. provide a strengthening effect. The effect of structural strain hardening which appears on martensitic transformation contributes to some or other extent to strengthening of all metals and alloys upon martensitic hardening.

Consider the role of carbon in the strengthening of martensite in steels. In hardened steels, this effect is appreciably higher than in carbonless iron alloys, the hardening effect being greater at higher concentrations of carbon in the austenite (Fig. 142).

The ability of steel to increase its hardness on hardening is called the *hardening capacity*. It can be characterized by the maximum hardness that can be formed in the surface of a specimen of a given grade of steel upon hardening.

When austenite undergoes diffusionless transformation, a supersaturated solution of carbon in  $\alpha$ -iron is formed, the degree of supersaturation being higher with a higher content of carbon in the austenite. It is of interest to note that as the carbon content in the martensite increases, the interatomic forces in the martensite do not increase but, on the contrary, diminish somewhat, since the distances between iron atoms are increased through interstition of carbon atoms. At room temperature, the root-mean-square deviation of atoms caused by thermal oscillations is 0.115 Å in ferrite and respectively 0.126 Å and 0.136 Å in hardened steels with 0.35 per cent and 1 per cent C. This increase is indicative of weakening of interatomic bonds. Despite this fact, carbon is known to increase the hardness of martensite, which should be explained, in the first place, by that the carbon atoms, when being intersticed into the lattice of  $\alpha$ -iron, impede the glide of dislocations in the martensite (this is what is called the solid-solution mechanism of strengthening).

Other mechanisms of strengthening effect of carbon can be attributed to the interaction of carbon atoms with lattice defects. During hardening or holding of steel after hardening, carbon atoms in martensitic crystals form atmospheres (clouds) at dis-

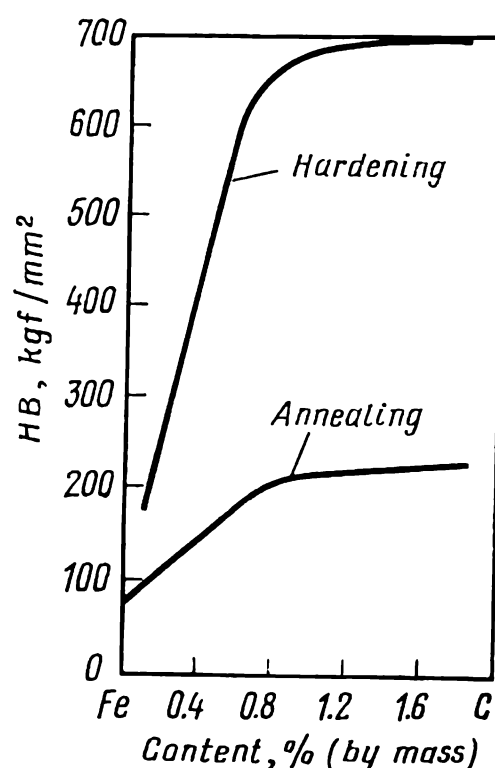


Fig. 142. Effect of carbon on hardening capacity of steel

locations and thus pin the latter. As has been shown by measurements of internal friction, heat evolution, hardness and yield limit in carbon-containing iron-nickel alloys, the diffusion processes of pinning of dislocations by carbon atoms and the corresponding strengthening effect can take place not only at room temperature, but even at lower temperatures (down to  $-60^{\circ}\text{C}$ ).

Diffusion redistribution of carbon during quenching or after hardening can proceed to a stage where disperse carbide particles precipitate from the martensite, thus contributing more to steel strengthening. In steels with a high  $M_s$  point, such as carbon steels with less than 0.5 per cent C ( $M_s$  above  $300^{\circ}\text{C}$ , see Fig. 118), quenching within the martensitic range can form the most favourable conditions for partial breakdown of martensite and precipitation of disperse carbide particles, i.e. for self-tempering of steel (see Sec. 4.2.2). In addition, at common quenching rates the carbon in any steel has enough time to form segregations at defects of the austenitic lattice during the period of cooling of the steel above  $M_s$  point. Carbon segregations in austenite are inherited by martensite, and since the latter has been supersaturated with carbon, they become sites of nucleation of carbide particles. As indicated in Sec. 3.2.2, accelerated quenching raises the  $M_s$  point (see Fig. 122), because carbon atoms have no time to form segregations at lattice defects of austenite. This agrees well with the fact that at very large rates of quenching the hardness of martensitic crystals turns to be almost by 33 per cent lower than that on common hardening.

Because of all the strengthening mechanisms mentioned, the strengthening effect of carbon on martensite is so large that the hardness of hardened steel is practically independent of the content of the alloying elements that are dissolved substitutionally in martensite, but is determined solely by the concentration of carbon.

To sum up, we may conclude that the large *strengthening effect in martensite-hardened steels is due to: supersaturation of  $\alpha$ -solution with carbon; appearance of a large number of twin interlayers and growth of dislocation density on martensitic transformation; formation of clouds of carbon atoms at dislocations; and precipitation of disperse carbide particles from  $\alpha$ -solution*. The contributions of each of these factors to the strengthening effect on hardening have not yet been established properly.

Beginners in the studies of metal heat treatment are often inclined to consider the strengthening in hardened steels as an exclusive phenomenon in its effect, i.e. in increasing the hardness of the metal. Let us refer to some facts. The hardness of eutectoid steel is 180 HB in annealed state and 650 HB as hardened, i.e. the hardening increases its hardness by a factor of 3.5.

Strengthening effect in metals and alloys can also be achieved by other methods. Cold plastic deformation of a metal can easily increase the hardness two or even three times (see 1.2.2). Increasing the concentration of the solid solution in alloying, especially of an interstitial solution, can increase the hardness several times. For instance, the hardness of a titanium solution with 0.7 per cent O is three times that of pure titanium (oxygen atoms are intersticed in the lattice of  $\alpha$ -titanium). Precipitation hardening in age-hardenable alloys can provide a high strengthening effect. For instance, ageing of beryllium bronze at 350 °C increases the hardness four times (!) against the as-quenched state. When compared with the examples given above, the strengthening effect in hardened steels ceases to be an exclusive phenomenon, especially if we consider that several strengthening mechanisms are simultaneously in action.

In alloys of other systems (not iron-based), the strengthening effect on martensitic hardening can be caused by the action of the same mechanisms as in hardening of steels and carbonless iron-base alloys. The most common among these is structural strain hardening, which is inherent in all martensitic transformations in metals and alloys and consists essentially in increasing the density of crystal lattice defects. In many martensite-hardenable alloys the strengthening occurs through the formation of supersaturated solid solution. This factor, however, cannot act in alloys in which the martensite is a supersaturated solution (see 3.2.2). In some alloys, such as aluminium bronzes, the process of ordering can play a substantial part in martensite strengthening.

### Change of Ductility on Hardening

Hardening of carbon steels results in a sharp reduction of all indices of ductility. The relative elongation and reduction of hardening high-carbon steels are almost zero. At the time when martensitic transformation was thought to take place in steels only, it was commonly emphasized that martensite is hard and brittle. When later martensitic transformations in carbon-free iron alloys and non-ferrous alloys have been discovered, it has turned out that brittleness is not a general property inherent in any martensite. It is now an established fact that the low resistance of martensite to brittle fracture in iron alloys is connected with the presence of interstitial elements — carbon and nitrogen — in the b.c.c. lattice of iron.

The main cause of strong embrittlement of carbon steels on hardening is a low mobility of dislocations in carbon-containing martensite. This is linked, firstly, with that the lattice of an in-

terstitial solution offers an increased resistance to dislocation glide and secondly, with that dislocations are trapped by atmospheres of carbon atoms. Because of the low mobility of dislocations, no stress relaxation through microplastic deformation can occur at the end of a brittle crack, which explains why martensite has a poor resistance to crack propagation.

Initiation of brittle cracks is promoted by local concentration of microstresses near dislocation tangles in martensite. Consequently, the martensite in carbon steels has a low resistance to initiation and especially to propagation of brittle cracks. In high-carbon steels, microcracks may sometimes be seen immediately after hardening, before any external load is applied (see Fig. 132).

The picture changes radically when carbon is eliminated from an alloy. Maraging steels, which are carbonless alloys of iron with nickel, cobalt, molybdenum and titanium (see Sec. 4.2.1), show high values of ductility ( $\delta = 14\text{--}20$  per cent,  $\psi = 70\text{--}80$  per cent) and impact toughness ( $\alpha_n = 27\text{--}30$  kgf·m/cm<sup>2</sup>) upon martensitic hardening. These steels can be plastic-worked at room temperature with high reduction ratios, whereas a hardened high-carbon steel is altogether impossible to be plastic-worked at room temperature, since its brittleness is very high.

The high ductility of carbonless iron-base alloys upon martensitic hardening can be explained as follows. With the density of dislocations in martensite being as high as up to  $10^{12}$  cm<sup>-2</sup>, the concentration of carbon for pinning all dislocations should be roughly 0.2 per cent. For that reason maraging steels with less than 0.03 per cent C may have unpinned dislocations. Nickel and cobalt, which are contained in large amounts in these steels (for instance, steel with 18 per cent Ni and 8 per cent Co), increase the mobility of dislocations in martensite by reducing the resistance of the martensitic lattice to dislocation glide (the Peierls-Nabarro force) and thus diminish the degree of dislocation pinning by impurity atoms of carbon and nitrogen. The high mobility of dislocations in iron-nickel martensite ensures stress release at the end of cracks, i.e. increases the resistance to brittle fracture.

Putting aside the problem of brittleness of b.c.c. solid solutions with interstitial elements, we should note that martensite-hardened metals and alloys may in the general have rather high ductility indices, though owing to an increased density of lattice defects on martensitic transformation these indices should be lower than those obtained through a polymorphic transformation with disordered rearrangement of the lattice.

### 3.2.7. BAINITIC TRANSFORMATION

#### The Structure of Bainite

Bainitic transformation can take place in carbon steels below the bend of the *C*-curve, i.e. within the temperature range of roughly 500-250 °C. It is also called *intermediate transformation* to emphasize the fact that it occurs somewhere between the pearlitic and martensitic transformation. The kinetics of this transformation and the structures formed have some features common to the diffusional pearlitic and diffusionless martensitic transformations.

Bainitic transformation results in the formation of a mixture of  $\alpha$ -phase (ferrite) and carbide, which is called bainite. Unlike pearlitic carbide, which has a lamellar structure, the carbide in bainite is in the form of very disperse particles detectable by electron microscopy only.

A distinction is usually made between '*upper*' and '*lower*' *bainite* to show that the bainitic transformation has taken place in either the upper or the lower region of the intermediate temperature range. Upper bainite has a feather-like structure, whereas lower bainite has a martensite-like acicular structure. The microstructure of lower bainite may sometimes be hardly distinguishable from that of temper martensite. These microstructural specifics of bainite, which should be linked with the shape of ferritic crystals, may be absent in some steels. For instance, the shape of ferrite in bainite may be other than acicular. Granular and columnar forms of bainite are sometimes possible. A stricter distinction between upper and lower bainite can be made by the pattern of distribution of the carbide phase. As has been shown by electron-microscopic examination, carbide particles in upper bainite may be present between ferritic platelets or at grain boundaries and inside platelets, whereas in lower bainite the carbide inclusions are always present inside platelets of  $\alpha$ -phase.

The products of isothermal transformation of undercooled austenite in the intermediate (bainitic) temperature range are very similar in their physical properties, composition and structure of phases to the products of tempering of martensite in hardened steel, provided that the temperature of bainitic transformation is the same as that of the tempering. The ferritic phase in bainite is a supersaturated solution of carbon in  $\alpha$ -iron. In the Fe-C constitutional diagram (see Fig. 85), the composition of ferrite occupies the region between *PQ* line and metastable extension of *GP* line, i.e. between the line of stable equilibrium  $\alpha/(\alpha + \text{Fe}_3\text{C})$  and that of metastable equilibrium  $\alpha/(\alpha + \gamma)$ . The carbide phase is an ordinary cementite  $\text{Fe}_3\text{C}$  having a rhombic lattice. In addi-

tion, hexagonal  $\epsilon$ -carbide may sometimes be found in lower bainite (which is similar to the process of steel tempering, see 4.2.1).

A probable explanation for the presence of  $\epsilon$ -carbide in lower bainite is the existence of metastable three-phase equilibrium  $\gamma \rightleftharpoons \alpha + \epsilon$  at a temperature around 350 °C (Fig. 143). As follows from the diagram in that figure, metastable  $\epsilon$ -carbide can only be formed on undercooling the austenite to a temperature below 350 °C. The rate of its nucleation is higher than that of cementite,

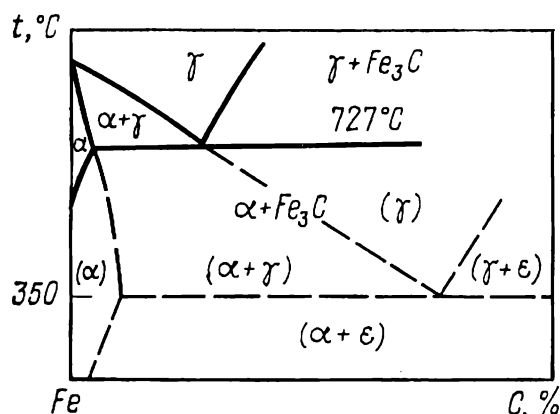


Fig. 143. Portion on Fe-C constitutional diagram with supposed metastable equilibrium between austenite, ferrite and  $\epsilon$ -carbide. Letters in brackets are phase regions in the metastable system (after R. F. Hehemann, K. R. Kissman, and H. J. Aaronson)

since  $\epsilon$ -carbide has more structural similarity with austenite and should be characterized by a lower work of formation of critical nuclei (see 2.1.4).

On heating a steel having the structure of lower bainite to a temperature above 350 °C, the metastable  $\epsilon$ -carbide dissolves and is replaced by cementite.

### Kinetics of Bainitic Transformation

In the bainitic temperature range, like in the pearlitic range, decomposition of undercooled austenite begins only after a certain induction period. In diagrams of isothermal decomposition of carbon steels, the bainitic transformation is not distinguished from pearlitic transformation: the temperature dependence of induction period is expressed by a single C-curve. The minimum of the induction period (the bend of the C-curve) for carbon steels lies in the pearlitic region. Below that bend, a reduction in the temperature of isothermal transformation gives a gradual transition from pearlitic to bainitic region, with bainitic transformation taking place first, and pearlitic transformation, only upon increasing the time of isothermal holding. The resulting structure of steel is upper bainite plus fine-lamellar pearlite. With lowering temperature, the amount of pearlite diminishes and, beginning from a definite temperature below the bend of C-curve, only bainite can form.

The difference between the bainitic and pearlitic transformation can be seen very clearly in diagrams of isothermal breakdown of austenite in alloy steels. With steels alloyed with carbide-forming elements (Cr, W, Mo, etc.), C-curves of the beginning and end of bainitic transformation pass below the C-curve of pearlitic breakdown (Fig. 144). The regions of pearlitic and bainitic trans-



formation in these steels may partially overlap. For instance, as follows from Fig. 144b, at a temperature of 500°C bainitic transformation begins in 100 s, but after approximately 60 min from the beginning of isothermal holding it turns into pearlitic transformation.

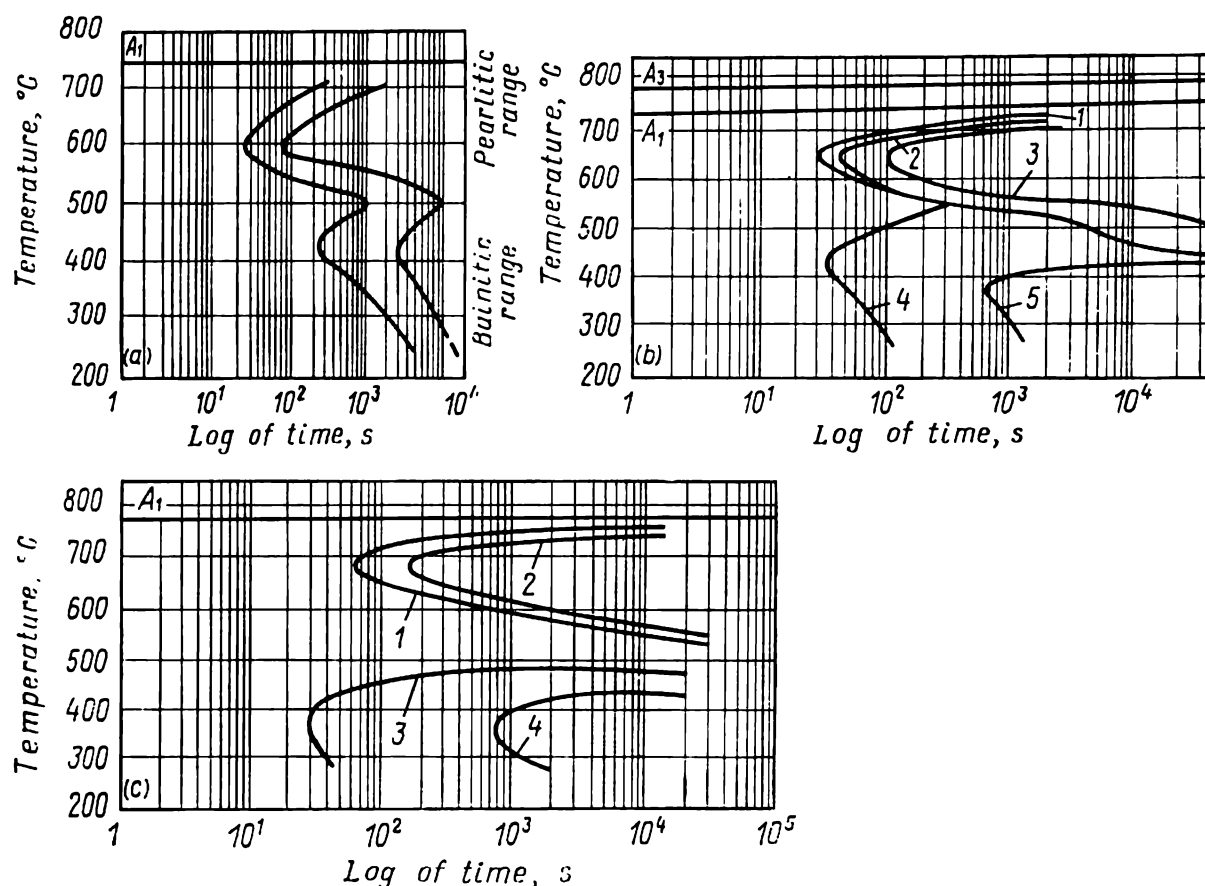


Fig. 144. Diagrams of isothermal decomposition of austenite in alloy steels with separate C-curves for pearlitic and bainitic transformations

*a*—steel IIIХ15 and 1.07% C and 1.52% Cr (*I. L. Mirkin and A. N. Rozanov*); *b*—steel with 0.43% C, 1.22% Cr, 0.82% Mn and 0.11% V (*A. Rose and W. Peter*); 1—beginning of ferrite formation; 2—beginning of pearlite formation; 3—end of pearlite formation; 4—beginning of bainite formation; 5—end of bainite formation; *c*—steel with 0.43% C and 3.52% Cr (*A. Rose and W. Peter*); 1—beginning of pearlite formation; 2—end of pearlite formation; 3—beginning of bainite formation; 4—end of bainite formation

With high-alloyed steels, the C-curves of pearlitic and bainitic transformation may be separated by a temperature interval of high stability of undercooled austenite, within which pearlitic breakdown does not start for many hours, and bainitic transformation does not start since the degree of undercooling is insufficient (Fig. 144c).

The maximum temperature of the beginning of bainitic transformation on a C-curve is denoted as  $B_s$ . Above that point, austenite transformation is impossible.

The kinetics of bainitic transformation bears some resemblance with that of pearlitic transformation not only in that it has an induction period, but also in the nature of volume change during

isothermal holding: the proportion of transformed volume of austenite increases first with acceleration and then with deceleration (see the kinetic curve in Fig. 79). On the other hand, in many alloy steels the bainitic transformation has a feature very typical of martensitic transformation, i.e. it does not proceed to full disappearance of austenite. Each point of a C-curve of the end of bainitic transformation (for instance, of curve 4 in Fig. 144c) corresponds to a definite amount of retained austenite. As the transformation temperature departs from  $B_s$ , the amount of bainite

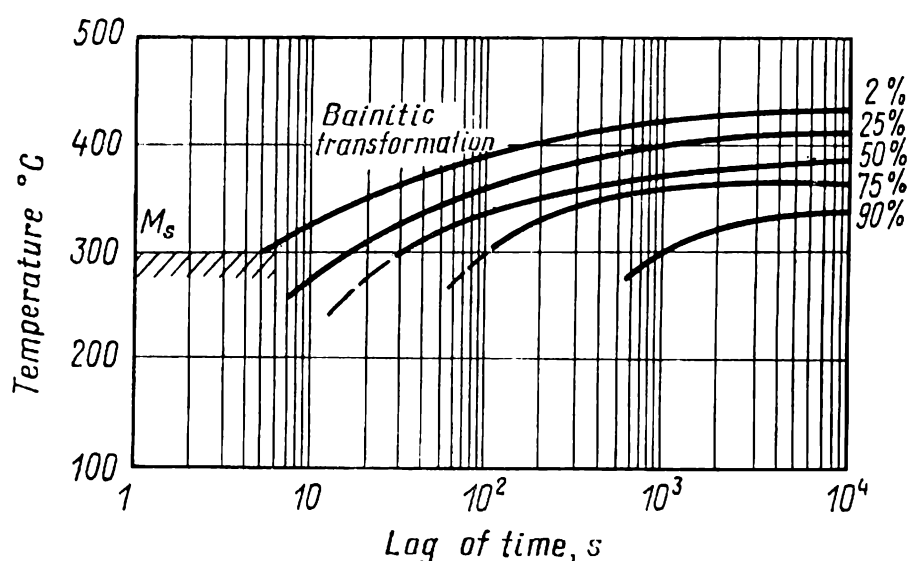


Fig. 145. TTT-diagram for austenite in steel 18X2H4BA (after A. A. Popov)

increases (from zero at  $B_s$ ), while the amount of retained austenite decreases (a direct analogy with the reduction of the amount of retained austenite on lowering the temperature of martensitic transformation, see 3.2.5).

Part of the retained austenite may transform into martensite on cooling the steel from the point of bainitic transformation down to room temperature.

Alloying elements may have a different effect on the speed of breakdown of austenite in the pearlitic and bainitic regions. With some steels, the C-curve of the beginning of pearlitic transformation, and with others, that of bainitic transformation may be shifted considerably to the right (see Fig. 144). In high-alloy steels having a low content of carbon, the pearlitic transformation may proceed so slowly that it cannot be depicted in the diagram of isothermal decomposition (Fig. 145), and the diagram then shows only the bainitic transformation. An opposite case is also probable, i.e. the bainitic transformation is very slow and the diagram of isothermal decomposition of austenite then shows the pearlitic transformation only.

### Mechanism of Bainitic Transformation

Bainitic transformation comprises the following principal processes:  $\gamma \rightarrow \alpha$ -rearrangement of the lattice, carbon redistribution, and carbide precipitation. Though the bainitic transformation was discovered some fifty years ago, its mechanism still remains an object of discussion.

The disputable questions of importance are as follows: (a) in what sequence of processes of  $\gamma \rightarrow \alpha$ -rearrangement, do carbon redistribution and carbide precipitation occur during the transformation; (b) what is the mechanism of formation of ferrite; and (c) from which phase (either austenite or ferrite) does carbide preferably precipitate.

Most researchers believe that the formation of ferrite from austenite follows the martensitic mechanism within the whole temperature range of bainitic transformation. Some facts in favour of this are as follows: appearance of a relief pattern in polished specimens (no relief appears on pearlitic transformation); the presence of retained austenite in alloy steels after bainitic transformation (pearlitic transformation is known to proceed always to full disappearance of austenite); close similarity between the microstructures of lower bainite and temper martensite; crystallographic similarity between bainitic ferrite and martensite; and similarity of substructures of upper bainite and low-carbon martensite.

The mechanism of bainitic transformation, the peculiarity of its kinetics, and its similarity with both pearlitic and martensitic transformation may be explained as follows. Bainitic transformation occurs at temperatures below 500-450 °C, i.e. below the recrystallization limit of iron. This means that diffusion displacement of atoms of the main component — iron — is virtually fully suppressed in the bainitic interval. For that reason the formation of ferrite through disordered  $\gamma \rightarrow \alpha$ -rearrangement becomes unfeasible, i.e. pearlitic transformation is inhibited. But at temperatures above 200-250 °C the diffusion of carbon still proceeds sufficiently actively to enable precipitation of carbides from austenite and ferrite. R. I. Entin holds that when austenite is undercooled to temperatures of the intermediate range, i.e. below 500-450 °C but above 200-250 °C, its carbon is redistributed, with some portions being enriched in carbon and others, depleted. The carbon-depleted portions then undergo martensitic  $\gamma \rightarrow \alpha$ -transformation.

Within the intermediate temperature range, crystals of  $\alpha$ -phase are formed through their coherent growth, retaining the elastic bondage with the initial  $\gamma$ -phase, i.e. exactly in the same way as martensitic platelets form during transformation below the mar-

tensitic point  $M_s$ . As distinct, however, from the martensitic transformation for which 'instantaneous' formation of martensitic platelets is typical, platelets of  $\alpha$ -phase in bainitic transformation grow relatively slowly. This may be explained by the fact that within the intermediate temperature range the  $\alpha$ -phase forms from the  $\gamma$ -phase that has been depleted in carbon, and therefore, the rate of growth of crystals of  $\alpha$ -phase is controlled by the rate of diffusion removal of carbon atoms.

The martensitic mechanism of the formation of  $\alpha$ -phase in bainitic transformation provides for the appearance of relief in specimens, acicular type of the microstructure of bainite, formation of crystallogometrical linkage between the lattices of  $\alpha$ - and  $\gamma$ -phase, and the presence of retained austenite.

At the moment of martensitic transformation, the concentration of carbon is not changed, but only the lattice changes with the formation of supersaturated  $\alpha$ -solution. Because of this, precipitation of carbide (either cementite or  $\epsilon$ -carbide) from  $\alpha$ -solution begins immediately after the  $\gamma \rightarrow \alpha$ -transformation, i.e. the metal is actually tempered (see 4.2.1).

In portions of the austenite which have been enriched in carbon before the  $\gamma \rightarrow \alpha$ -transformation, precipitation of carbide is possible. This results in the appearance of carbon-depleted portions of the austenite, which undergo martensitic  $\gamma \rightarrow \alpha$ -transformation. The sequence of the processes occurring in bainitic transformation according to P. I. Entin is shown in Fig. 146.

According to other views, carbon redistribution occurs immediately after the  $\gamma \rightarrow \alpha$ -rearrangement of the lattice, rather than before it; the neighbouring zones of austenite are then enriched in carbon, so that carbide precipitates from austenite at  $\alpha/\gamma$  boundaries.

Substitutional alloying elements have no time for redistribution during bainitic transformation and their content in ferrite is the same as that in austenite.

The difference between the structures of upper and lower bainite is usually related to a different mobility of carbon in the upper and lower portions of the bainitic temperature range. When carbon is less mobile, the martensitic  $\gamma \rightarrow \alpha$ -rearrangement of the lattice is the primary process, while the secondary process is tempering, i.e. carbide precipitation from the supersaturated  $\alpha$ -solution. This forms the structure of lower bainite. At higher temperatures, carbide is supposed to nucleate directly in austenite, like ferrite, with the structure of upper bainite being thus formed.

The term 'bainitic transformation', originally proposed in studies of isothermal transformations in steels, was later given a broader meaning to include some non-ferrous alloys, such as  $\beta$ -brasses, aluminium and tin bronzes, titanium alloys, etc.

In brasses,  $\alpha$ -phase may precipitate from  $\beta$ -phase on cooling (see Fig. 109). On slight undercooling,  $\alpha$ -phase precipitates in the regular way, i.e. by diffusion. On deep undercooling, for instance, at temperatures below 350 °C in an alloy of copper and 41 per cent Zn,  $\alpha$ -phase forms thin platelets revealing a relief pattern on polished specimens. Platelets of  $\alpha$ -phase are composed of regular rows of stacking faults, i.e. have a structure similar to martensite,

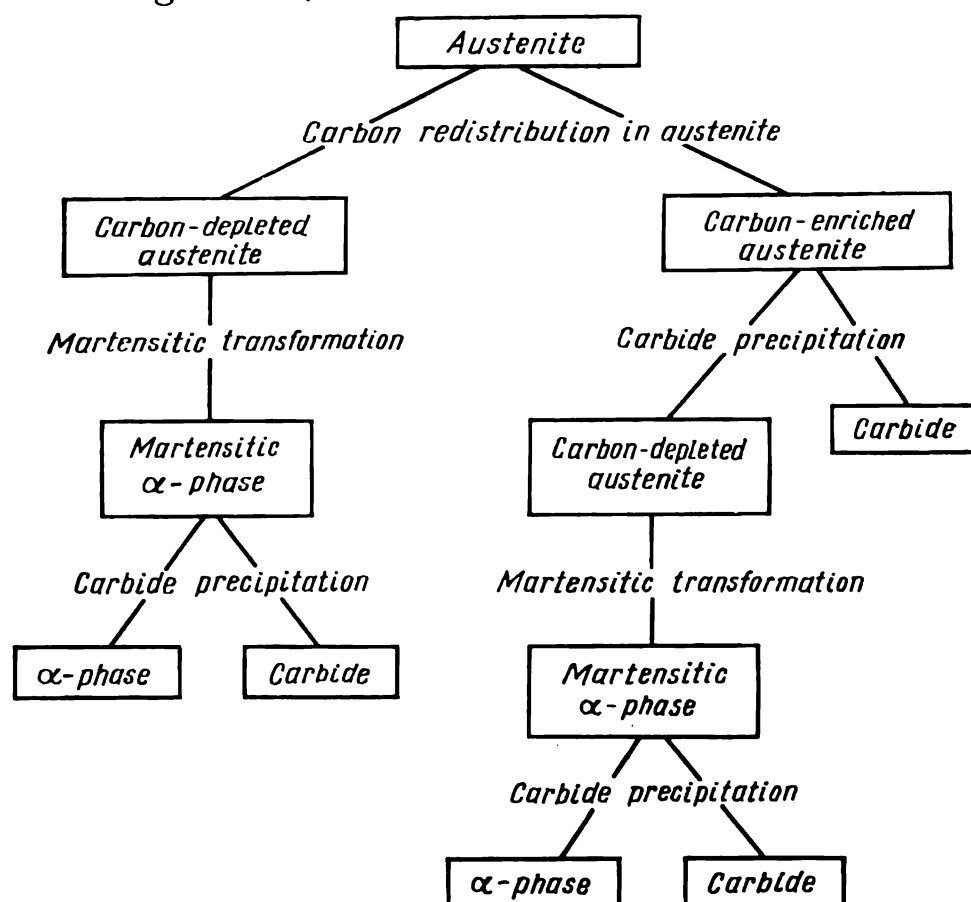


Fig. 146. A probable scheme of bainitic transformation

which may form in  $\beta$ -brasses at temperatures below 0 °C. The axial ratio in the lattices of  $\alpha$ - and  $\beta$ -phase is similar to that in the brass upon martensitic transformation. On the other hand, this formation of  $\alpha$ -phase platelets differs qualitatively from purely martensitic transformation in that it is accompanied with zinc redistribution: the  $\alpha$ -phase contains less zinc than the original  $\beta$ -phase. These peculiarities of the formation of lamellar  $\alpha$ -phase in undercooled  $\beta$ -brass make it possible to regard it as bainitic transformation.

According to an assumption, bainitic transformation in  $\beta$ -brass begins with diffusionless martensitic  $\beta \rightarrow \alpha$ -rearrangement of the lattice and then changes to diffusion redistribution of the components between  $\alpha$ - and  $\beta$ -phase, which follows the slowly moving  $\alpha/\beta$  front. By another view, the primary process is redistribution of zinc in the  $\beta$ -phase, which is followed with martensitic  $\beta \rightarrow \alpha$ -rearrangement of the lattice in zinc-depleted portions.

The martensitic rearrangement of the lattice has been considered above as an indispensable and most important process of bainitic transformation in steels and brasses, the differences between various views being mainly related to the sequence of the processes of martensitic rearrangement and diffusion redistribution of the components.

A principally different explanation of bainitic transformation has however been proposed, according to which the transformation is considered eutectoid decomposition of austenite which differs from the pearlitic transformation in that the shape of ferrite-carbide mixture is other than lamellar. According to that view, precipitation of platelets of  $\alpha$ -phase from  $\beta$ -phase in brasses should not be related to bainitic transformations, since no eutectoid transformation occurs in  $\beta$ -brass (see Fig. 109). It is noted that no martensitic shear rearrangement takes place in the formation of bainitic ferrite. It is also emphasized that surface relief in polished specimens is typical not only of martensitic transformations. It has been found, for instance, on purely diffusional precipitation of h. c. p.  $\gamma$ -phase in f. c. c. solution of silver in aluminium.

It is also assumed that the content of carbon in the ferrite of lower and upper bainite is between the  $PQ$  lines and metastable extension of  $GP$  line in the Fe-C constitutional diagram, i. e. the degree of supersaturation of  $\alpha$ -phase with carbon is not high. It then follows that carbide precipitates from austenite mainly at the  $\alpha/\gamma$  boundary. This conclusion by no means contradicts the fact that carbide is found inside ferritic grains. Moreover, it helps in understanding why carbide particles inside  $\alpha$ -phase are often stretched parallel to the  $\alpha/\gamma$  boundary.

When chains of carbide particles are formed on the  $\alpha/\gamma$  boundary, the austenite is depleted in carbon, the thermodynamic stimulus of transformation increases, and the ferrite front moves further into the austenite, leaving behind a chain of carbides. Carbon accumulates in the austenite before the advancing ferrite front, a new chain of carbide particles forms, and the process is repeated. As a result, stretched rows of carbide particles parallel to the  $\alpha/\gamma$  boundary, turn to be embedded inside the ferrite, though the carbides have precipitated from austenite, rather than from ferrite (this does not preclude precipitation of a certain amount of carbides from ferrite itself).

### Mechanical Properties of Bainitic Steel

Bainite is stronger than pearlite, its strength properties improving at lower temperatures of isothermal transformation (Fig. 147).

The high strength of bainite is due to small size of ferrite crystals, disperse carbide precipitates, a high density of dislocations pinned by carbon atoms, and distortion of the lattice of ferrite owing to the supersaturation with carbon and alloying elements.

The yield limit of bainite is related with the size of ferrite crystals by the Petch-Hall formula (13), since the boundaries of  $\alpha$ -crystals serve effectively as barriers to dislocations. With lowering the temperature of isothermal transformation within the bainitic range, ferrite crystals become smaller owing to a slower removal of carbon atoms from the  $\alpha/\gamma$  boundary into austenite;

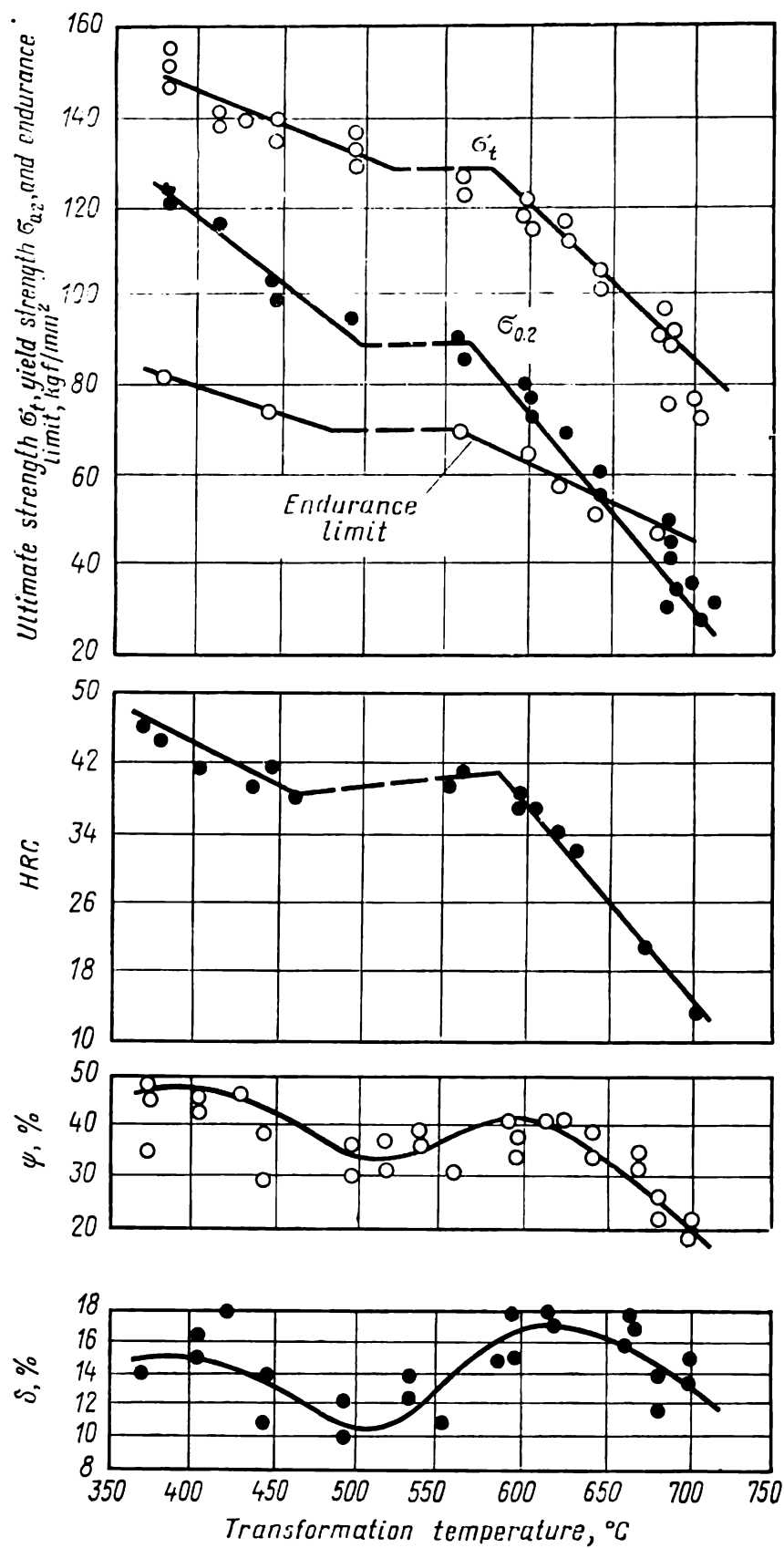


Fig. 147. Effect of transformation temperature of austenite on mechanical properties of eutectoid steel (after M. Gensamer, E. B. Pearsell, W. S. Pellini, and J. R. Low)

this is one of the main reasons why bainite acquires a high strength.

Carbide particles inside the  $\alpha$ -phase impede the movement of dislocations, the effect being stronger when a large number of particles is uniformly distributed in unit volume of metal. In upper bainite, carbide particles are located mainly on boundaries of ferrite crystals and therefore cannot contribute substantially to the strengthening effect. With a lower temperature of transformation, carbides become more disperse and locate mainly inside ferrite grains, thus increasing the strength of bainite.

The ferrite in bainite has a larger density of dislocations than the excess ferrite in hypoeutectoid steel. Probably, this may result from martensitic  $\gamma \rightarrow \alpha$ -rearrangement. Dislocations in bainitic ferrite are pinned by Cottrell atmospheres composed of carbon atoms and thus contribute appreciably to the strengthening effect. The solid-solution mechanism of strengthening, especially with elements dissolved substitutionally, probably contributes more to the strength of bainite.

As shown in Fig. 147, the ductility of the metal drops on passage from the pearlitic into bainitic region, but then again increases with a reduction in temperature. The loss of ductility can be attributed to the relatively coarse structure of upper bainite, with carbide particles being located on boundaries of ferritic crystals. In lower bainite, carbide particles are inside grains of  $\alpha$ -phase, because of which lower bainite has a higher ductility.

A steel having the structure of lower bainite can be characterized by a high strength combined with a high toughness.

The formation of bainitic structure underlies the method of hardening to bainite (see 3.2.9). In addition, bainitic structure in what is called *bainitic steel* can be formed through air cooling from the temperature of hot rolling or by ordinary heat treatment with heating to the austenitic state and subsequent cooling in air. The C-curve of bainitic transformation in such steels should be shifted appreciably towards the axis of ordinates, and the precipitation of excess ferrite should, on the contrary, be decelerated, otherwise ferrite will precipitate during continuous cooling before the start of bainitic transformation. These requirements are met, for instance, by a low-carbon steel alloyed with 0.5 per cent molybdenum and boron.

### 3.2.8. HARDENABILITY OF STEELS

#### Hardenability and Critical Cooling Rate

In martensitic hardening, steel should be cooled from the hardening temperature in such a way as to undercool its austenite below  $M_s$  point without allowing it to decompose into ferrite-car-



bide mixture. For this, the rate of cooling of steel articles should be higher than a definite critical value. Thus, the *critical cooling rate (critical quenching rate) is the minimum rate at which austenite still does not decompose into ferrite-carbide mixture.*

As a first approximation, the critical quenching rate is determined by the slope of a tangent to the C-curve of the beginning of austenitic decomposition ( $v_{cr}$  in Fig. 148). When determined in this manner, its magnitude is roughly 1.5 times the actual critical rate. As has been indicated in 2.1.5, superposition of cooling curves onto a C-curve of isothermal transformations cannot be used for accurate calculation of the temperatures of the start and finish of the transformation of the initial phase in continuous cooling. Above the point of tangency of  $v_{cr}$ -curve and C-curve (Fig. 148), the transformation proceeds more feebly than at the temperature corresponding to that tangency point. Therefore, the austenite, which is being cooled continuously, still will not start to decompose during the time equal to the induction period at the temperature of the tangency point. The actual critical rate should therefore be less than that determined by the slope of the tangent to the C-curve of the beginning of isothermal decomposition. The actual critical rate  $v_{cr}$  can be found by using CCT-diagrams (see 2.1.5 and 3.1.2).

An article is always cooled more quickly at its surface than in the core. The rate of cooling at the surface may be greater than the critical rate, while that in the core may be lower. In that case the austenite in the surface layers will transform into martensite, whereas the core of the article will undergo pearlitic transformation, i.e. the article will not be hardened through. The *hardenability* is one of the most important characteristics of steels. It is understood as the depth to which the hardened zone extends in the metal.

Hardenability depends in the first place on the critical cooling rate. Figure 149 shows a curve of distribution of cooling rates across the diameter of a cylindrical steel specimen, with the critical cooling rate given for comparison. The annular volume at the surface of the article is cooled at a higher rate than the critical value, and thus will be hardened to martensite. The core of the

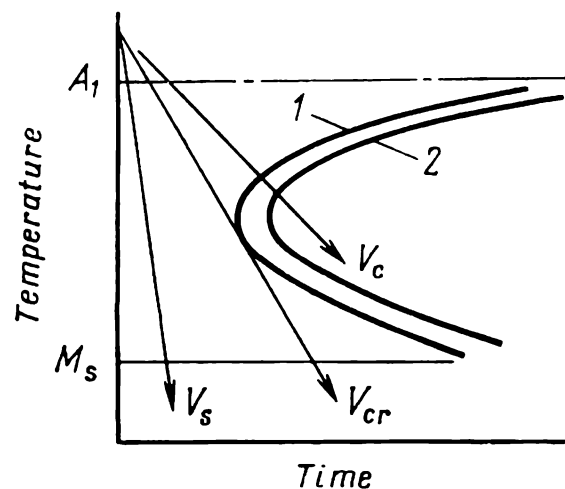


Fig. 148. Determination of critical hardening rate on C-curve

$v_c$  and  $v_s$ —cooling rates in the core and at the surface; 1—beginning of austenitic decomposition; 2—end of austenitic decomposition

cylinder is cooled at a lower rate than the critical cooling rate and thus cannot be hardened to martensite. In massive articles of large cross-section, the whole spectrum of structures may be found, with smooth transition from martensite at the surface via troostite, troostite and sorbite to pearlite in the core.

If the core of an article is cooled at a rate greater than the critical value, the article will be hardened through to martensite (Fig. 149*b*). As can be seen from that figure, the hardenability of an article of a given cross-sectional size may be increased by

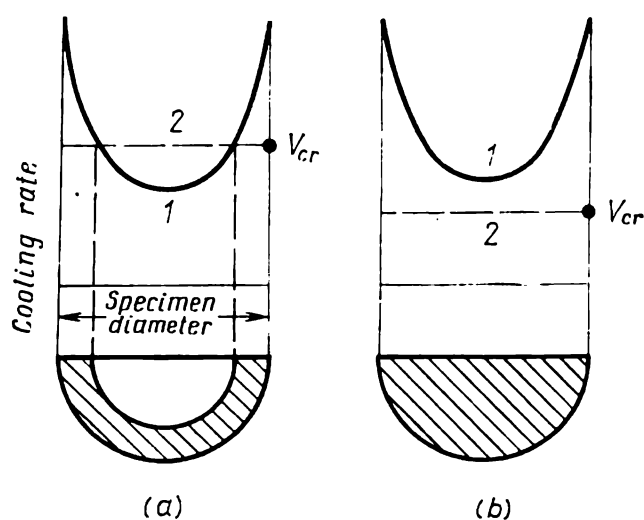


Fig. 149. Hardenability of a cylinder  
*a*—shallow hardening; *b*—through hardening; 1—distribution of cooling rate across cylinder diameter; 2—critical cooling rate (hatched area—martensitic hardening)

either increasing the cooling rate (curve 1 then shifts upwards) or lowering the critical quenching rate; in either case the hardened zone (hatched area) will increase.

The critical cooling rate depends on all the factors which affect the rate of decomposition of austenite. The factors which increase the stability of undercooled austenite against decomposition, i.e. shift the *C*-curve rightwards, also increase the hardenability (on shifting the *C*-curve to the right, its tangent will form a smaller angle with the axis of abscissae).

The stability of undercooled austenite against eutectoid decomposition depends on the homogeneity of the austenite, the actual size of its grains, composition, and the presence of undissolved carbides and other inclusions in the steel, as also on slight amounts of impurities, including those which are uncontrollable.

Since the  $\gamma$ -solution should be locally enriched and depleted in carbon in order to initiate eutectoid nucleation, austenite with a more homogeneous structure is more stable against eutectoid breakdown and exhibits a higher hardenability.

Increasing the actual size of austenitic grains reduces the total intergranular surface at which the decomposition preferably begins, and thus increases the hardenability.

Increasing the temperature of heating and the time of holding before hardening results in an equalization of the concentration of  $\gamma$ -solution and in coarsening of austenitic grain, i.e. increases the stability of undercooled austenite. For that reason, a higher temperature of heating or a longer time of holding before hardening can increase the hardenability of steel, the first factor being more effective. But it is altogether unnecessary to quench a steel

from an elevated temperature in order to have a higher hardenability. Equalization of the concentration of  $\gamma$ -solution and coarsening of its grain are irreversible processes. If a steel has been heated to a high temperature and then cooled slowly within the austenitic range to the normal temperature of hardening, its hardenability will also increase.

The hardenability of steel depends strongly on the composition of the austenite. With a higher content of carbon, austenite becomes more stable and the critical quenching rate decreases. Steels having nearly eutectoid composition have the least critical rate, i.e. the best hardenability (Fig. 150). A higher critical rate in hypereutectoid steels may be explained by the fact that they are hardened not from the austenitic temperature range, but from a temperature higher than  $A_1$  but lower than  $A_{cm}$  (see Fig. 156 below). With a higher carbon content in hypereutectoid steels, the concentration of carbon in austenite at a normal hardening temperature ( $A_1 + 35\text{--}60$  degrees C) does not increase, but the concentration of cementite increases. Cementite particles serve as initiators for pearlitic transformation and thus lower the stability of undercooled austenite. Therefore, the critical quenching rate of hypereutectoid steels increases with increasing the carbon content. If hypereutectoid steel is hardened from a temperature above  $A_{cm}$  (from the austenitic range), the critical cooling rate will diminish continuously with increasing content of carbon in the steel, since this increases the concentration of carbon in the austenite.

Even slight additions of boron (hundredths or thousandths of a per cent) can increase appreciably the hardenability of carbon steels. A probable explanation may be that boron, being a surface-active element in  $\gamma$ -solution, concentrates at boundaries of austenitic grains, lowers the surface energy of grains and thus impedes the preferable formation of decomposition nuclei at grain boundaries. That boron quickly concentrates at boundaries of austenitic grains during cooling of a steel is now an experimentally established fact. However, the mechanism of the inhibiting effect of boron on austenitic decomposition in such places is still unclear. It has been found quite recently that in a steel containing a few thousandths of a per cent of boron, disperse particles of  $\text{Fe}_{23}(\text{B}, \text{C})_6$  precipitate at grain boundaries before the formation of excess fer-

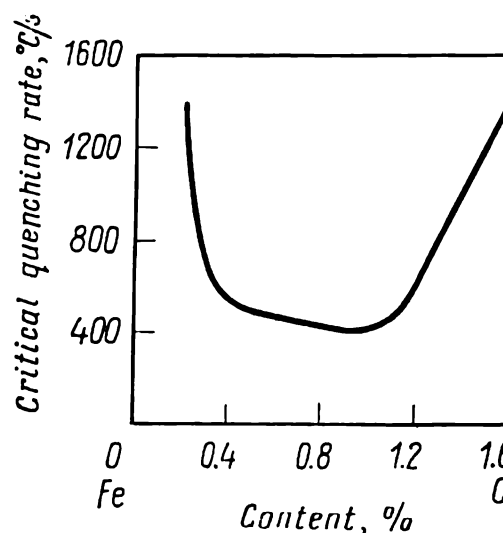


Fig. 150. Effect of carbon on critical cooling rate in hardening (after H Esser)

rite. Thus, it still remains unclear whether these particles or, as has been supposed formerly, boron atoms in the solid solution in boundary regions (in the region of boron segregation) are responsible for impeding the formation of excess ferrite, and consequently for increasing the hardenability of steel.

The hardenability of a steel of one and the same grade may be different in various melts, which may be explained by differences

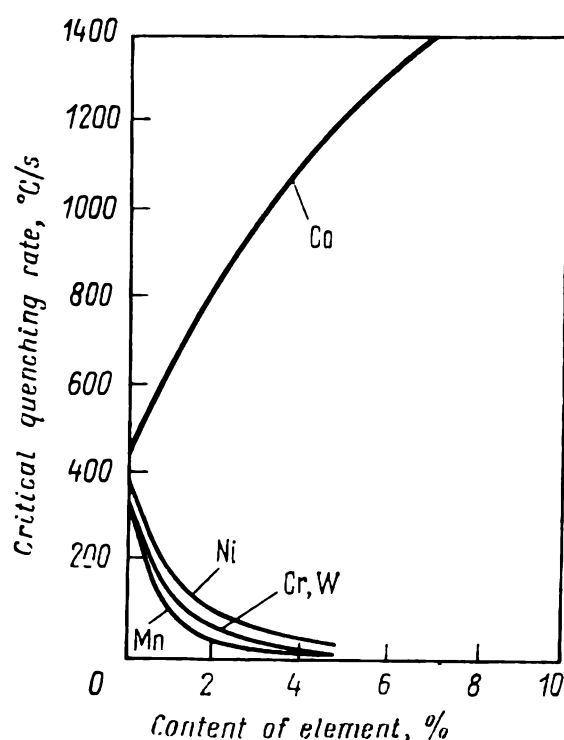


Fig. 151. Effect of alloying elements on critical cooling rate in steel with 0.9-1% C (*H. Esser*)

in the size of austenitic grains and by the effects of some uncontrollable amounts of impurities and inclusions in steel, such as oxides, nitrides, sulphides, etc.

All alloying elements, except for cobalt, provide an inhibiting effect on decomposition of austenite when being dissolved in the latter, and thus diminish the critical quenching rate and improve the hardenability (Fig. 151). The nature of the retarding effect of alloying elements on decomposition of austenite has been discussed in 2.2.2. Additions of manganese, nickel, chromium and molybdenum are widely used in practice for improving the hardenability of steels. In this respect, complex alloying is especially effective, in which the useful effects

of individual elements are mutually enhanced. For instance, the critical quenching rate of a steel with 0.4 per cent C and 3.5 per cent Ni is 150 °C/s, but it can be lowered to approximately 4 °C/s by alloying the steel with 0.75 per cent Mo.

Carbide-forming elements can increase the hardenability only when they are in dissolved state in the austenite at the temperature of hardening. If the temperature of hardening is not high enough, undissolved carbides may serve as centres of decomposition of austenite and thus impair the hardenability.

Enhancing hardenability through alloying is utilized for two different purposes. Firstly, articles of a large cross-section may be made through-hardenable by using an alloy steel instead of plain carbon steel. For instance, the critical diameter for steel Grade 45 is only 20 mm even for water quenching (see p. 284), whereas alloy steel Grade 40XHMA can be hardened through in articles up to 120 mm in diameter by oil quenching.

Secondly, the use of alloy steels in place of carbon steel in articles of a small cross-section enables a softer quenching mode to be employed. For instance, small-size articles made of carbon steel may be hardened through by water quenching, but this can form excessive residual stresses and cause warping and hardening cracks, especially in articles of an intricate shape. The use of an alloy steel instead of carbon steel then makes it possible to use a softer mode of quenching (in emulsions, oil or even in air) instead of water quenching.

### Characteristics of Hardenability

The simplest characteristic of hardenability is the *depth of hardened layer* upon quenching in a specified coolant. The depth of hardening can be determined by the *quench test method* with examining a fracture, macrosection or the distribution of hardness over the cross-section of a specimen. Martensite-hardened steel is brittle; the hardened zone of a specimen has a smooth, fine-grained, dull-grey, often porcelain-like fracture. The unhardened core is tougher and has an uneven, rough, slightly fibrous fracture. The boundary between these two zones is usually seen quite clearly in a fractured specimen (Fig. 152).

In macrosections, the hardened and unhardened zones can be made quite discernible through etching.

Figure 153 shows the distribution of hardness over the cross-section of a hardened cylindrical specimen. A very typical feature is that hardness changes abruptly at a certain distance from the surface of an article, this distance (depth) corresponding to the boundary between the hardened and unhardened zones, as may be seen in fractures or macrosections.

The depth of hardening is taken conditionally as the distance from the quenched surface to a layer having semimartensitic structure (i.e. 50 per cent troostite and 50 per cent martensite). The hardness of the metal within that layer is largely dependent on the distance from the surface. For that reason the hardening depth as defined above can be determined quite accurately by measuring the hardness. The hardness of semimartensitic steels, including those alloyed, depends on their content in carbon (see Table 10).

Using the table and a curve of hardness distribution (such as that shown in Fig. 153), we may find, for instance, that a rod 38 mm in diameter made of steel Grade 60 will have the hardening depth of 7 mm on water quenching from 815°C and only 0.4 mm on oil quenching.

Another characteristic of hardenability is the *critical diameter*, i.e. the diameter of a maximum cross-section that can be hardened through in a given quencher.

The hardenability of carbon and alloy steels, except for air-hardenable steels, is determined by the standard *end-quench test*



Fig. 152. Fracture of water-quenched rod of steel Y8,  $\times 2$  (brighter area is unhardened core)

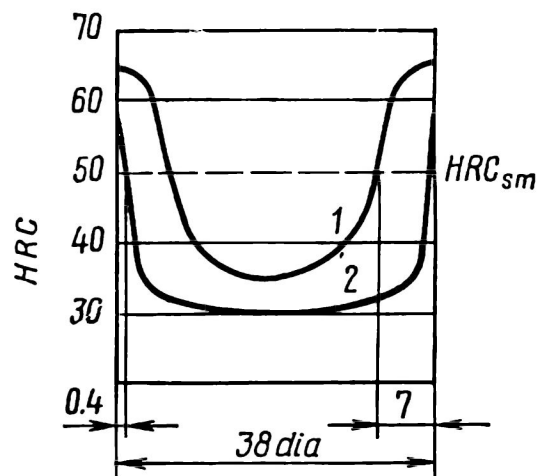


Fig. 153. Hardness distribution across the diameter of a specimen of steel Grade 60 quenched from 815 °C

1—water quenched; 2—oil quenched;  
HRC<sub>sm</sub>—hardness of semimartensitic steel structure

(Jominy test), which is widely used in practice. A standard specimen is heated in a furnace and quickly transferred into a test setup where it is cooled by a water jet directed against the end face (Fig. 154). Upon complete cooling, the specimen is ground longitudinally at two opposite sides to a depth of 0.5 mm. Care should be exercised during grinding so as not to overheat the

Table 10. Hardness of Semimartensitic Steel, HRC

Carbon, %	Steel type		Carbon, %	Steel type	
	carbon	alloy		carbon	alloy
0.08-0.17	—	25	0.33-0.42	40	45
0.18-0.22	25	30	0.43-0.52	45	50
0.23-0.27	30	35	0.53-0.62	50	55
0.28-0.32	35	40			

metal. The hardness of the flat sides is measured by the Rockwell C scale in intervals of 1.5-3 mm and the hardenability curve is plotted in the coordinates hardness-distance from end face. The

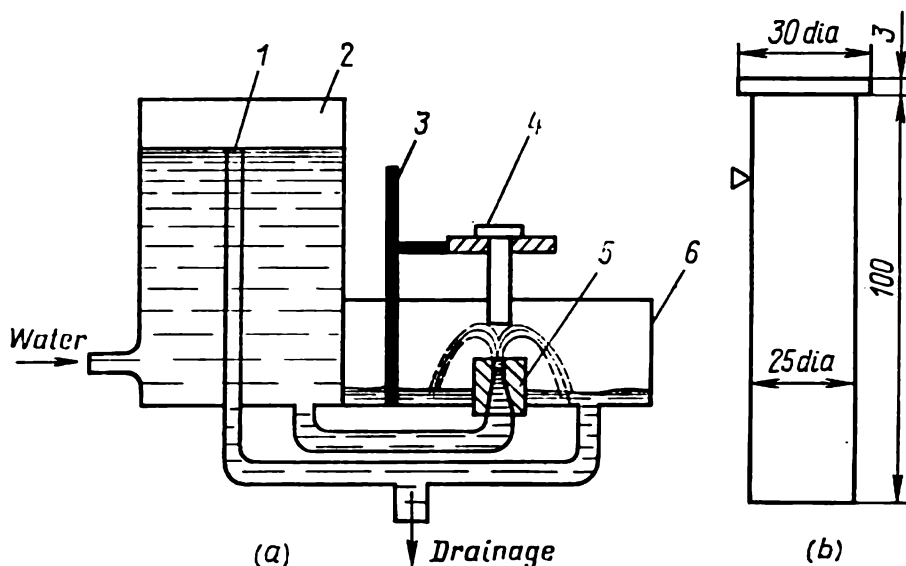


Fig. 154. Setup (a) and specimen (b) for end-quench test  
1—constant-head pipe; 2—head tank; 3—holder; 4—specimen; 5—nozzle; 6—drainage box

lower is the hardenability of a steel, the quicker its hardness diminishes with the distance from the end face (i.e. the steeper is the hardenability curve). Since the hardenability of a steel grade may vary in different melts, their tests will give a set of hardenability curves. For that reason a steel grade is usually characterized by a *hardenability band* (Fig. 155). Numerical indices of the hardenability of a steel grade may be the maximum and the minimum hardness at a definite distance from the quenched end, the maximum and the minimum distance from the end face to points of a specified hardness (for instance, to points of 'semimartensitic structure'), etc. The end-quench test gives quite reproducible results. It can be used for solving many problems of practical interest, for instance, to determine (by means of nomograms) the size of articles which can be hardened through in a given quencher.

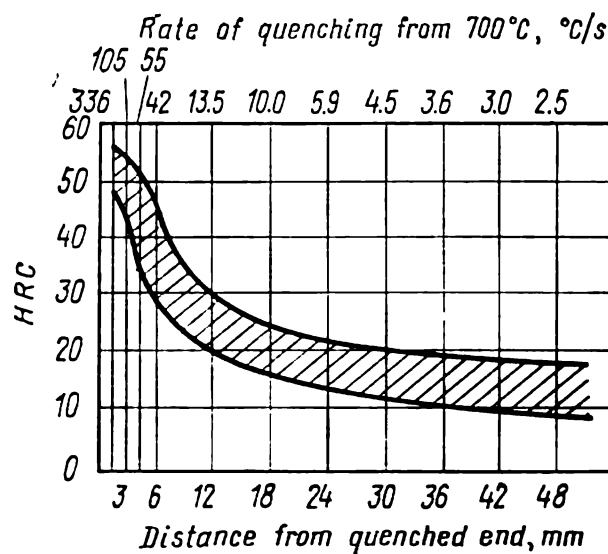


Fig. 155. Hardenability band of steel Grade 40

### 3.2.9. HEATING AND COOLING IN STEEL HARDENING

#### Through Heating for Hardening

The transformations in steel on heating have been discussed in 2.2.1. The temperature of heating for hardening of carbon steel may be determined by reference to the constitutional diagram (Fig. 156). Hypoeutectoid steels are hardened from a temperature 30-50 degrees C above the  $A_3$  point. Steels possessing inherited fine-grain structure can be hardened from a higher temperature. Overheating of a coarse-grained steel usually gives a structure of coarse acicular martensite. Hardening from temperatures within

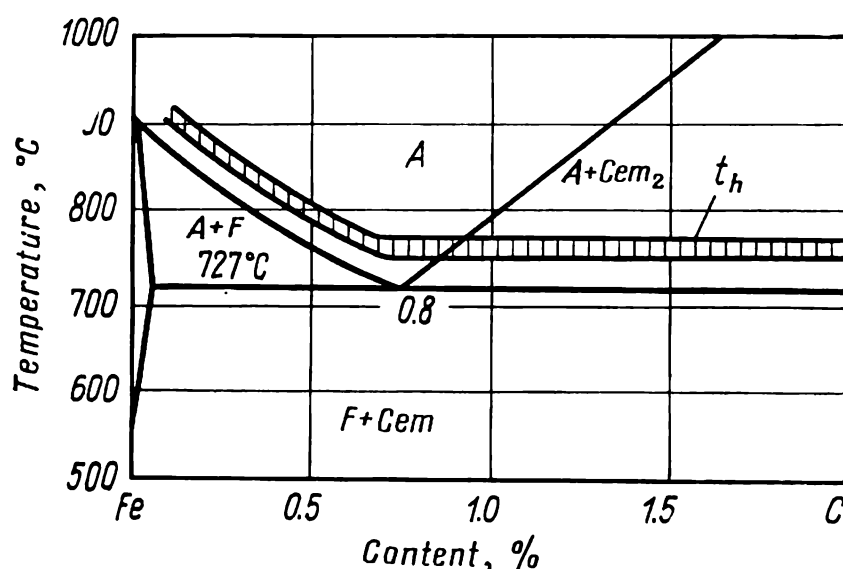


Fig. 156. Temperature range for hardening carbon steels

the  $A_1$ - $A_3$  range (*incomplete hardening*) forms a structure of martensite and excess ferrite, which largely lowers the hardness of the hardened steel and impairs the mechanical properties upon tempering.

Hypereutectoid steels are hardened from temperatures 35-60 degrees C above the  $A_1$  point. When hardened from a temperature within the  $A_1$ - $A_{cm}$  range, they form a structure of martensite and secondary cementite, which increases the wear resistance of the steel in tools. Hardening from temperatures above  $A_{cm}$  may be unfavourable: it does not increase the hardness, but coarsens the austenitic grains, increases surface decarbonization, and enhances hardening stresses. The hardness of a steel hardened from a temperature above  $A_{cm}$  may even drop somewhat owing to the dissolution of hard cementite particles and to an increased amount of retained austenite.

For the majority of structural and alloy tool steels the temperature of heating for hardening is within the range of 800-



880 °C (a narrow range is experimentally determined for each grade). Steels with a high content of carbide-forming elements (W, V, Cr) are hardened from higher temperatures, sometimes close to the solidus line, so as to transform a large amount of hard-soluble carbides into austenite. For instance, high-speed steels of types P9 and P18 are hardened from 1250-1300 °C, die steels of type 3X2B8Φ, from 1050-1100 °C.

The time of holding at the heating temperature should be such as to allow full homogenization of the austenite. The rate of heating should be as high as practicable from the standpoint of productivity. Some grades of high-alloy steels, such as high-speed steels, which require a high temperature of hardening, are heated by a stepwise schedule in order to diminish thermal stresses.

### Surface Heating for Hardening

Many steel articles should combine a high hardness and strength in the surface layer with a tough core. Such a combination of properties can be achieved by surface hardening.

For surface hardening of a steel article, only its surface layer of a specified depth should be heated above  $A_{c3}$ . This heating must be done quickly and intensively so as not to heat up the core to the hardening temperature through heat conduction. The various kinds of surface hardening differ from one another in the methods of heating.

Two principal methods of surface heating are widely used industrially: (a) induction heating and (b) heating by a torch flame.

**Induction heating** has certain unquestionable advantages over all other methods of surface hardening and is used most widely.

As is well known, increasing the frequency of alternating current increases the non-uniformity of current distribution over the cross-section of a conductor. At high frequencies, the current virtually passes through a thin surface layer only. This *surface effect* (or *skin effect*) underlies the method of induction heating proposed by V. P. Vologdin in 1935. An article is placed into a high-frequency current inductor. It is practically assumed that the current induced in the article is concentrated in the surface layer of a depth:

$$\delta = 500 \sqrt{\frac{\rho}{\mu f}} \text{ mm} \quad (31)$$

where  $\rho$  = resistivity, ohm·cm  
 $\mu$  = magnetic permeability  
 $f$  = current frequency, Hz

Thus, the depth of current penetration, and therefore, the depth of hardened layer, decreases with increasing current frequency; this relationship may be illustrated by the following data:

Current frequency, Hz . . . . .	0.5-10 <sup>2</sup>	2 × 10 <sup>3</sup>	10 <sup>4</sup>	10 <sup>5</sup>	10 <sup>6</sup>
Depth of current penetration in steel					
Grade 45 at 800 °C, mm . . . . .	91.4	14.5	6.5	2.1	0.65

A single- or multi-turn copper inductor is so made as to match the shape of the surface of an article to be heated. The hollow inductor is cooled inside with water. The clearance between the surfaces of article and inductor should be of a strictly definite width, since it determines the depth of hardening, which is principally due to the *proximity effect* consisting in that the density of induced current is dependent on the distance between current conductors. With the current flowing in opposite directions in two conductors, the current density will be at its maximum in places where the distance between conductor surfaces is the smallest. Articles of circular cross-section may be rotated during heating in the inductor for obtaining a uniform depth of hardened layer.

An important advantage of high-frequency induction hardening is that the rate of heating of the whole hardened layer is extremely high. In other heating methods, based on the use of external heat sources, such as torch flame, the heating rate is limited by the heat conductivity of the metal, so that a high rate of heating, which is required for surface hardening, is inevitably linked with an appreciable overheating of the metal surface. With induction heating, on the contrary, heat is generated in the metal proper and the whole layer to be hardened can be rapidly heated up to the required temperature. With the same depth of hardened layer, induction heating differs advantageously from other heating methods in a lower degree of overheating of the surface and a much more uniform temperature distribution in the layer being hardened.

The high rate of induction heating (a few hundred °C/s) has an important effect on phase transformation in the metal. As can be seen in Fig. 87, phase transformations are shifted into the region of higher temperatures as the heating rate is increased. In addition, it should be noted that in hypoeutectoid steels the rise of temperature in induction heating outruns, as it were, the diffusion of carbon, the result being that the excess ferrite transforms into low-carbon austenite.

Consequently, the temperature of high-frequency hardening should be higher than that specified for conventional furnace heating, especially at high heating rates and with coarse precipitates of excess ferrite. For instance, steel Grade 40 is usually hardened from temperatures within 840-860 °C in furnace heating, 880-920 °C

for induction hardening with a heating rate of 250 °C/s, and from 930-980 °C for a heating rate of 400 °C/s.

Steel to be hardened by induction heating should preferably have a fine original structure, which can be achieved by normalizing or, in some cases, by improving heat treatment, i.e. conventional through-hardening with high-temperature sorbitic tempering.

The principal parameters of induction heating are the temperature of hardening and the rate of heating within the region of phase transformations. The optimum temperature of hardening for a given melt of steel and its original structure is determined depending on the heating rate selected.

With increasing the degree of overheating, the rate of nucleation of austenite increases quicker than the linear speed of growth of austenitic grains. This is why high-frequency heating, which may be distinguished by an extensive overheating above  $A_1$  and  $A_3$  points and by no holding time allowed at the maximum temperature, results in the formation of a very fine grain of austenite. The optimum temperature of hardening ensures that the typical non-acicular ('structureless') martensite forms in high-carbon steels and fine-acicular martensite, in hypoeutectoid steels. With rising the hardening temperature above the optimum value the structure becomes more coarse with inclusions of large needles of martensite.

If heating has been done to a temperature below the optimum value, the steel has a reduced hardness owing to incomplete austenitization; the same effect, but owing to an increased amount and coarser grain of retained austenite, is produced on overheating above the optimum temperature (Fig. 157).

Induction hardening increases the surface hardness and wear resistance of steel products. In this respect it can successfully replace less productive cementation.

The use of induction surface hardening is also essential for increasing the fatigue resistance. Many machine elements, such as shafts and pins, are subjected to bending and torsion with the highest stresses developing in the surface layers. With sign-alternating loads, fracture of metal usually begins at the surface of an article. High-frequency hardening strengthens the surface layer and forms residual compressive stresses in it, thus increasing the endurance limit appreciably (1.5 to 2 times).

The depth of hardened layer in induction surface hardening is usually not greater than the depth of hardening (hardenability). Owing to this, induction hardening is widely used with carbon steels having a low hardenability, such as Grades 40 and 45.

Alloy steels can in some cases be successfully replaced with less expensive carbon or low-alloy steels, which are strengthened through induction hardening.

Thus, the advantages offered by induction hardening are as follows: a high productivity, higher indices of wear resistance and fatigue resistance, no decarbonization, insignificant oxidation, the possibility of controlling accurately the depth of hardened layer, wide possibilities for automation and mechanization of the process and organization of automatic flow lines.

Among the drawbacks worth mentioning are a high cost of equipment and inefficiency of induction hardening for single ar-

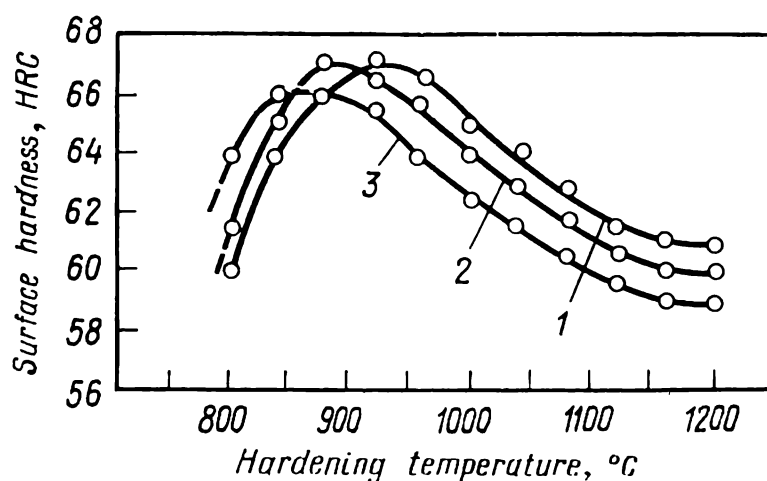


Fig. 157. Effect of heating temperature on surface hardness of steel Grade Y10 at different heating rates (after I. N. Kidin)

1—700 °C/s; 2—400 °C/s; 3—200 °C/s

ticles, since each article requires a special inductor and properly selected heating conditions. With series production, these drawbacks are eliminated and the method of induction hardening becomes profitable. The induction method has found application for hardening such articles as crankshafts, distributor shafts, pinions, brake shoes, crank pins, cold-rolling rollers, rails (their ends being induction hardened), mill cutters, screw taps and dies, chisels, files, etc.

**Surface hardening with flame heating** is carried out in the following way.

A combustible gas (such as acetylene) and oxygen are mixed in a burner, their mixture flowing out from a hardening nozzle. The mixture burns with the formation of a high-temperature flame (2400-3000 °C). The flame is directed onto a section of an article to be hardened, where it heats up quickly a layer 2-4 mm thick to a temperature above the  $A_{c3}$  point. The heated portion is then sprinkled with water supplied at a pressure through holes provided in the nozzle.

The principal advantage of this method as compared with the induction hardening is that the equipment used is more simpler in design.

Flame hardening is advantageous in individual production and repairs, i.e. when induction hardening is unprofitable, or for hardening large articles (such as rolling mill rolls), for operation in field conditions (hardening without disassembling). Its drawbacks are the probability of strong overheating and less accurate control of the depth of hardened layer.

### Quenching

The quenching conditions in hardening should in the first place ensure the specified depth of hardened layer. On the other hand, they should be such as to prevent large hardening stresses, which might cause warpage of articles and formation of hardening cracks.

*Hardening stresses* may be of either *thermal* or *structural origin*. Hardening is always linked with the appearance of a temperature gradient across the cross-section of an article. The differences in thermal compression of outer and deeper layers during quenching are responsible for the appearance of thermal stresses.

Martensitic transformation causes an increase of the metal volume by a few per cent. Surface layers are heated to the martensitic point more quickly than the core of the metal. Thus, martensitic transformation and the accompanying growth of volume occur at different instants in various points across the cross-section of an article, resulting in the appearance of structural stresses.

The total hardening stresses become higher on increasing the heating temperature and the rate of quenching, since in both cases the temperature gradient across the cross-section increases. A greater temperature gradient results in an increase of both thermal and structural stresses.

In steels, hardening stresses are most probable to appear within a temperature range below the martensitic point, i.e. when structural stresses and the brittle phase — martensite — are formed. Above the martensitic point only thermal stresses can appear, the steel being in the tough austenitic state.

As may be seen from a *C*-curve, quick quenching is necessary within the region of the least stability of undercooled austenite. For most steels this is the region within the temperature range from 650 to 400 °C. Above or below that temperature interval, austenite is much more stable against decomposition than near the inflexion of the *C*-curve and the articles can be cooled comparatively slowly. Slow cooling is especially important beginning

from 300-400 °C, since in most steels martensite forms below these temperatures. A slow cooling above the inflexion of the C-curve reduces only thermal stresses, whereas a slow cooling in the martensitic range can lower both thermal and structural stresses.

The quenching media that are used most widely are cold water, 10-per cent aqueous solutions of NaOH or NaCl, and mineral oils.

Table 11 gives quenching rates for small steel specimens in two temperature ranges for various quenchers. Quenchers that might cool quickly in the pearlitic region and slowly in the martensitic are not yet found.

**Table 11. Cooling Rates for Hardening Steel in Various Quenchers**

Quencher	Cooling rate, °C/s, in temperature range of	
	650-550 °C	300-200 °C
Water at 18 °C	600	270
Water at 74 °C	30	200
10-% NaOH in water at 18 °C	1200	300
Mineral oil	100-150	20-50

Cold water is the cheapest and quite powerful quencher. It cools quickly in both pearlitic and martensitic temperature ranges. The high cooling capacity of water may be attributed to its low temperature and tremendous latent heat of boiling, low viscosity and comparatively high heat capacity. Additions of salts or alkalis increase the cooling capacity of water in the pearlitic range. The main disadvantage of water is the high cooling rate in the martensitic range.

Mineral oil cools slowly in the martensitic range (which is its principal merit), but it cools equally slowly in the pearlitic range (which is its main drawback). For that reason mineral oils are used for hardening steel grades possessing a high hardenability.

Hot water cannot be a substitute for mineral oil, since the heating of water largely reduces the cooling rate in the pearlitic range, but has almost no effect on that in the martensitic range.

### Hardening Methods

Since quenching media that might cool quickly in the temperature range of 650-400 °C and slowly above and especially below that range are unavailable, the required cooling conditions are ensured in practice by using various methods of hardening and quenching.

*Quenching in two media* is resorted to when it is needed to lower the cooling rate in the martensitic range (Fig. 158). An article is first immersed into water and, after a short holding time, transferred into oil. The process is accordingly called *water-to-oil quenching*. The quick cooling in water inhibits pearlitic transformation, whereas the subsequent slower cooling in oil diminishes the hardening stresses in the martensitic range. The most critical moment is the holding in water, whose duration should be selected properly in each particular case. Both underquenching and overquenching in water can spoil the hardened articles. With underquenching, the austenite undergoes full or partial decomposition,

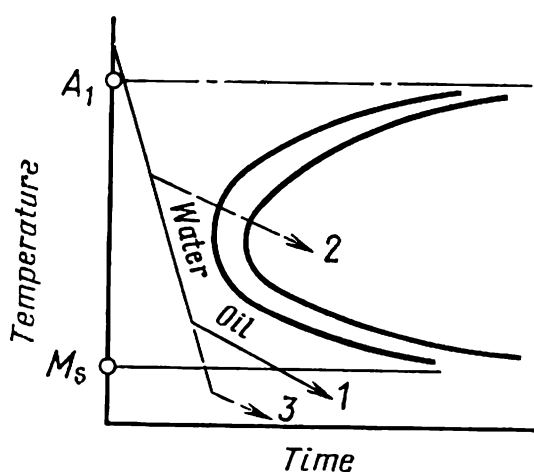


Fig. 158. Water-to-oil quenching (in two quenchers)  
1—normal conditions; 2—underquenching in water; 3—overquenching in water

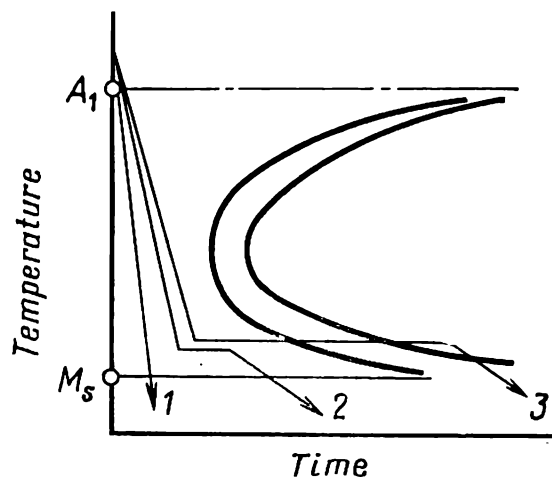


Fig. 159. Hardening in water and hot quenchers  
1—water quenching; 2—stepwise hardening; 3—isothermal hardening

thus lowering the final hardness of the steel, and overquenching can form excessive hardening stresses resulting in warpage and cracking of articles. But even though with these drawbacks, water-to-oil quenching is used widely for cutting tools made of carbon steels (which has a low hardenability, so that oil quenching only gives poor results).

Another method for reducing the cooling rate in the martensitic range is *stepwise hardening* (Fig. 159). An article, after being heated to the hardening temperature, is quickly placed into a hot bath and, upon a short holding time, cooled in air or cold oil. The hardening in hot media has been described for the first time by D. K. Chernov in 1885 in his famous paper 'On the Manufacture of Armour-piercing Steel Shells', where he wrote that shell steel, when hardened in a lead-tin melt, acquired the same hardness as on quenching in cold water.

The conditions of stepwise hardening can be selected properly by using the *C-curve*. The temperature of the hot medium (the temperature of 'hardening step') is chosen near the martensitic

point (usually 20-30 degrees C above it), i.e. within the range where undercooled austenite is quite stable. The time of holding in the hot melt (the length of the 'step') should be less than the induction period for the corresponding temperature. Stepwise quenching is less complicated in practice than water-to-oil quenching and yields more reliable results. Another advantage of importance is that the temperature is equalized over the cross-section of an article on holding in the hot bath. Upon that holding, the martensitic transformation takes place uniformly over the whole volume, resulting in lower hardening stresses. Finally, a merit of no less importance is that at the 'step' temperature the steel is in the austenitic state. Upon removal from the hot bath, the article remains ductile for a while and can be straightened to eliminate warpage. This is especially important for thin and long articles which warp inevitably even in hot baths. Manual straightening is often employed, but the best results are provided by press straightening. The straightening process can continue on cooling below the  $M_s$  point, since directly at the moment of martensitic transformation (but not upon it) the metal has an increased ductility.

The principal drawback of stepwise hardening is a low cooling rate in the hot bath (compare curves 1 and 2 in Fig. 159). For that reason, stepwise hardening of carbon steel has only a limited application to articles of small cross-section (up to 8-10 mm thick). Large articles are cooled too slowly in the hot bath and the austenite has enough time to decompose eutectoidally. Articles made of alloy steels, which have a lower critical cooling rate, are more suitable for stepwise hardening. For instance, stepwise hardening is widely used for tools and machine elements made of chromium steels (ШХ15, ХВГ, and 9ХС).

A variety of stepwise hardening is *martempering*, a method of hardening in a hot bath whose temperature is somewhat below the martensitic point. The lower temperature of the 'step' ensures a higher hardenability, but the method retains the principal advantages of stepwise hardening, since the amount of martensite formed is still not large. A drawback is that quenched articles cannot be straightened.

Three different groups of hot media: mineral oils, saltpetre melts, and alkali melts — are used in stepwise hardening.

If the length of the 'step', which is within the temperature range of bainitic transformation, is greater than the time of isothermal decomposition of austenite, the process of heat treatment is called *isothermal* or *bainitic hardening*, or *austempering* (Fig. 159). Bainitic transformation is an intermediate one between pearlitic and martensitic transformation (see 3.2.7). A steel having the structure of lower bainite is closer in its mechanical properties to martensite-hardened steel than to pearlitic steel. Bainitic trans-



formation involves martensitic  $\gamma \rightarrow \alpha$ -rearrangement of the lattice. In its practical realization, the process considered differs only slightly from stepwise hardening and is therefore regarded as hardening with polymorphic change.

Isothermal hardening uses the same quenchers as stepwise hardening. The time of holding in the hot bath should be longer than the time of isothermal transformation of austenite and can be roughly selected by reference to the *C*-curve. Isothermal hardening can be used for articles of a small cross-section, since the hot bath is a slow quencher.

The time of holding in the hot bath is sufficient for the temperature to equalize across the cross-section even to a greater extent than in stepwise hardening. An important merit of isothermal hardening is that it reduces appreciably hardening stresses and warpage.

Its another advantage consists in the following. For the same value of hardness, the toughness of lower bainite is higher than of the steel upon martensite hardening and tempering, a probable cause for this being assumed that carbide particles distribute more uniformly in bainite. In some grades of alloy steel, bainitic transformation results in the retention of a large amount of austenite, which cannot transform into martensite during cooling after isothermal holding. Isothermal hardening ensures a high impact toughness in such steels and reduces appreciably the notch and skew sensitivity as compared with the steel after martensite hardening and tempering. Therefore, isothermal hardening increases the structural strength of steels. The properties of steel Grade 30XГC upon conventional hardening and tempering and isothermal hardening compare as follows:

	$\sigma_t$ , kgf/mm <sup>2</sup>	$\sigma_{0.2}$ , kgf/mm <sup>2</sup>	$a_n$ , kgf · m/cm <sup>2</sup>
Water quenching from 880 °C + tempering at 520 °C . . . . .	110	85	4.5
Isothermal hardening from 880 °C in molten saltpetre (300 °C) . . . . .	165	130	6

### Hardening with Sub-zero Treatment

In many steels the martensitic range ( $M_s$ - $M_f$ ) extends to sub-zero temperatures (see Fig. 118). In that case the hardened steel contains retained austenite which can be transformed into martensite by cooling the metal to a sub-zero temperature. Such freezing treatment (the method was proposed by A. P. Gulyaev in 1937) essentially continues the hardening quenching that has been interrupted at room temperature (which is not the critical point for the given steel).

Sub-zero treatment is always possible when the  $M_f$  point is below zero. Its effect depends on the amount of retained austenite present in the steel at room temperature. With an increase in the carbon content of a steel, the martensitic range shifts towards lower temperatures, thus increasing the amount of retained austenite that can transform into martensite on cooling the hardened steel to a temperature below its lower martensitic point  $M_f$  (Fig. 160). Further cooling of the steel below  $M_f$  is of no use, since it can cause no additional martensitic transformation.

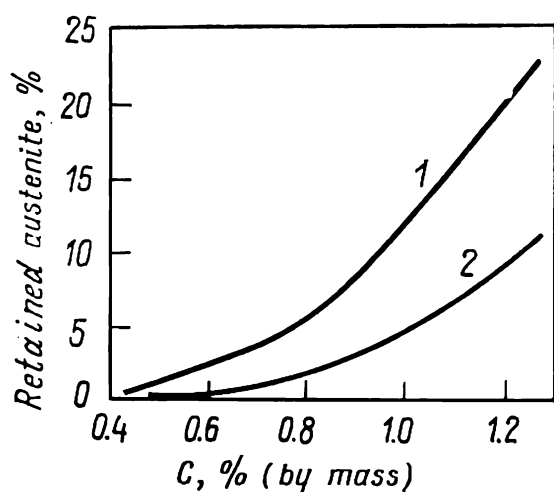


Fig. 160. Effect of carbon on retained austenite in steel hardened from austenitic state (after V. G. Vorobyev)

1—at 20 °C; 2—upon cooling down to  $M_f$

The main purpose of sub-zero treatment is to stabilize the size of articles. The structure of hardened steel with a large amount of retained austenite is unstable. Retained austenite gradually transforms into martensite already at room temperature, and the more so at a lower temperature, this transformation being linked with an increase in the volume and size of articles. But the size of such articles as ball and roller bearings or gauges and other measuring tools should remain stable with an accuracy of a

micron or fractions of a micron. For this, the articles are subjected to sub-zero treatment. In many cases deep freezing (below zero) is needless, with cooling hardened articles in water at a temperature of room +5 to +10 °C being quite sufficient.

Another aim of freezing treatment is to increase the hardness and wear resistance of cutting tools, dies and measuring instruments. High-speed steel may contain a large percentage of austenite (up to 25-40 per cent) upon hardening. Naturally, freezing treatment of such steel is especially effective.

Sub-zero treatment can increase the hardness and wear resistance and eliminate grinding cracks in cemented articles made of structural alloy steels. The high-carbon cemented layer formed on hardening contains a large amount of austenite, which lowers the hardness of steel and, additionally, can decompose during grinding and thus cause cracking.

Finally, sub-zero treatment can improve magnetic properties of permanent magnets owing to the additional transformation of paramagnetic austenite into ferromagnetic martensite.

In sub-zero treatment, the effect of stabilization of austenite should be taken into consideration (see 3.2.5). The time lag be-

tween the hardening and sub-zero treatment may cause strong stabilization of the austenite at room temperature in some steels, which lessens the effect of freezing. The maximum admissible time lag is therefore specified. For instance, it should not exceed 30 minutes for measuring gauges made of steel Grade X.

Temperatures not below  $-80^{\circ}\text{C}$  are usually sufficient for sub-zero treatment.

#### LITERATURE

Kurdjumov G. V., Utevsky L. M., Entin R. I., Transformations in Iron and Steel (*Prevrashcheniya v zheleze i stali*). Moscow, Nauka, 1977, 238 pp., ill.

Gulyaev A. P., Heat Treatment of Steel (*Termicheskaya obrabotka stali*), Chapters IV, VII and IX. Moscow, Mashgiz, 1960, 496 pp., ill.

Bockstein S. Z., Structure and Properties of Metal Alloys (*Struktura i svoistva metallicheskih splavov*), Chapters 7 and 8. Moscow, Metallurgiya, 1971, 496 pp., ill.

Entin R. I., Transformations of Austenite in Steel (*Prevrashcheniya austenita v stali*), Chapter VI. Moscow, Metallurgizdat, 1960, 252 pp., ill.

Imperfections of Crystal Structure and Martensitic Transformations (*Nesovershenstva kristallicheskogo stroeniya i martensitnye prevrashcheniya*). A collection of papers. Moscow, Nauka, 1972, 238 pp., ill.

Kidin I. N., Physical Principles of Electrochemical Treatment of Metals and Alloys (*Fizicheskie osnovy elektrotermicheskoi obrabotki metallov i splavov*). Moscow, Metallurgiya, 1969, 375 pp., ill.

Shepelyakovsky K. Z., Strengthening of Machine Elements by Surface Hardening with Induction Heating (*Uprochnenie detalei mashin poverkhnostnoi zakalkoi pri induktsionnom nagreve*) Moscow, Mashinostroenie, 1972, 287 pp., ill.

Shewmon P. G., Transformations in Metals. New York. McGraw-Hill, 1969. Quenching and Martempering New York, ASM, 1964.

Warlimont H., Delay L., Martensitic Transformations in Copper-silver- and Gold-based Alloys. Progress in Materials Science, vol. 18. Oxford, Pergamon Press, 1974.

## AGEING AND TEMPERING

A quenched alloy is in a metastable state and possesses an increased free energy. The process of quenching, either without or (in most cases) with polymorphic transformation, forms a supersaturated solid solution and the hardened alloy tends to lower its free energy with consecutive solid solution decomposition. Some precipitates can separate from the supersaturated solution even at room temperature, but in most alloys the diffusion mobility of atoms at room temperature is insufficient for precipitation from the solution to occur during an acceptable time. Therefore, heating is required in order to change the structure and properties of a quenched alloy, i.e. the latter should be aged or tempered.

By historical tradition, the term “ageing” has been used preferably with some non-ferrous, in particular, aluminium alloys and “tempering”, with steels, while with some other alloys, such as bronzes and titanium alloys, both terms have been equally applicable. It has been suggested quite recently to use “tempering” for alloys which are quenched with polymorphic transformation and “ageing” for those quenched without polymorphic transformation. This classification is adhered to in the book.

The principal process in ageing or tempering of a quenched alloy is the precipitation from the metastable solid solution, the alloy passing to a stable state, though far from the real equilibrium which can be characterized by the absolute minimum of free energy. The processes of precipitation from a supersaturated solution in a quenched alloy, like the processes of recovery and recrystallization, occur spontaneously with heat liberation.

Though heating is required for ageing or tempering, this fact does not contradict the concept of spontaneous nature of these processes, since the heating is only needed to accelerate diffusion, which is the basis of all structural changes during precipitation from supersaturated solutions.

The main characteristics of ageing and tempering are the temperature and time of holding, the rates of heating and cooling being of secondary importance. An exception is the specific phenomenon of temper embrittlement in alloy steels which appears on slow cooling from the temperature of tempering (see 4.2.2).

## 4.1. AGEING

In 1906, Alfred Wilm, a German engineer, discovered the phenomenon of natural ageing. He found that a quenched alloy of aluminium with copper and magnesium (duralumin) increased its hardness when stored for a while at room temperature.

Wilm patented a method for improving duralumins, which consisted in quenching of duralumin alloys, followed with natural ageing which increased the hardness, ultimate strength and yield limit.

Merica, Waltenberg and Scott of the USA were first to analyse the nature of ageing of duralumins in their famous article published in 1919. Merica proposed a hypothesis which related the ageing of duralumin to a variable solubility of  $\text{CuAl}_2$  compound in aluminium. Upon heating the alloy, this compound passes to the solid solution and has no time for reverse precipitation during the short time of quenching, but gradually precipitates from the supersaturated solution during subsequent storage at room temperature in the form of very disperse and therefore microscopically invisible particles which cause the hardening effect. This hypothesis explained quite simply and convincingly the experimental data available at the time.

The absence of the hardening effect upon holding a quenched specimen at  $-180^\circ\text{C}$  was explained by a low rate of formation of precipitates, while the appearance of hardening effect during storage at room temperature and at  $100^\circ\text{C}$  was attributed to the atom mobility becoming sufficiently high for precipitation of  $\text{CuAl}_2$  in disperse form. The facts that the hardness during storage at  $200^\circ\text{C}$  first increased, attained the maximum and then decreased were explained by the formation of  $\text{CuAl}_2$  particles having a definite degree of dispersity corresponding to the maximum hardness, and by subsequent coagulation of these particles.

An increased age-hardening effect on increasing the temperature of heating for quenching could be easily attributed to a deeper dissolution of  $\text{CuAl}_2$  on heating, the formation of a more supersaturated solution on quenching and accordingly the appearance of a greater number of disperse precipitates from the solution on ageing.

In 1921, Z. Jeffries and A. R. S. Archer developed further Merica's hypothesis of *precipitation hardening* and proposed a general theory of strengthening of alloys by disperse particles of any origin. According to that theory, hard disperse particles act as 'pins' and 'wedge' the slip planes, thus producing hardening effect in an alloy. Upon coagulation of particles, in which only their total number, but not the total volume, is changed, many slip planes are freed of 'pins' and thus produce softening. The maxima of hardness and strength have a corresponding critical degree of dispersity of hard particles. This critical dispersity can be easily attained during precipitation from the supersaturated solid solutions.

The original theory, which explained hardening of duralumins at room temperature by precipitation of  $\text{CuAl}_2$  particles from the supersaturated solid solution, ran into some conflicting facts already in 1920's. The precipitation of  $\text{CuAl}_2$  and respective depletion of the solid solution in copper should have been expected to lower the electric resistivity, though the latter actually increased on natural ageing. Further, precipitation of  $\text{CuAl}_2$  from the solid solution should have increased the lattice period owing to a lower (than in aluminium) atomic diameter of copper which dissolved interstitially in aluminium. X-ray studies, however, revealed no changes in the lattice period as the hardness of the alloy attained its maximum, and only after overageing at elevated temperatures, when softening took place, did the lattice period increase, which was a direct indication that  $\text{CuAl}_2$  precipitated from supersaturated solution.

Considering these controversial facts and abundance of novel experimental data, Merica in 1932 proposed the following explanation of hardening effect on ageing as a further development of his original hypothesis. According to him, strengthening at any temperature of ageing proceeds with time. A holding time is needed for the development of diffusion processes which are basic for precipitation from the supersaturated solid solution. At elevated temperatures, the diffusion of copper atoms ensures precipitation of  $\text{CuAl}_2$  particles proper, which 'wedge' the slip planes. At room temperature, the diffusion processes only prepare the solid solution to the formation of  $\text{CuAl}_2$  crystals, without causing  $\text{CuAl}_2$  to precipitate. By Merica's assumption, diffusion in a supersaturated solid solution results in the formation of nodules or segregates of copper atoms which however are not separated by interfaces from the matrix lattice. The structure of these regions in a solid solution of aluminium is such as needed for subsequent formation of particles of  $\text{CuAl}_2$  or a certain intermediate metastable compound. Copper atom nodules should cause local compression of the lattice, so that these strongly distorted portions in the solid solution hamper slip on plastic deformation and thus cause hardening.

Merica's predictions have found a brilliant confirmation. In 1935, G. Wassermann and Weerts of Germany established by X-ray studies of Al-Cu alloys that an intermediate phase (which is now denoted  $\theta'$  to distinguish it from the equilibrium  $\theta$ - $\text{CuAl}_2$  phase) formed in the supersaturated solution at the stage of maximum hardening. In 1938, A. Guinier of France and G. D. Preston of Great Britain explained (independently) the effects of diffusion scattering in Laue photographs of naturally aged Al-Cu single crystals as a result of formation of small copper-rich zones in the supersaturated solution, which were later called *Guinier-Preston zones*.

Thus, Merica's basic concept that ageing of alloys is linked with a variable solubility of an excess phase and that hardening on ageing occurs through the formation of disperse precipitates in the solid solution turned to be principally correct and exceptionally fruitful, though it has been later corrected more than once and supplemented with concepts on the role of *pre-precipitates* and intermediate phases.

The whole history of the development of modern concepts on ageing of alloys is quite instructive. Wilm's discovery of ageing in duralumins can hardly be overestimated, but it could not in itself be the basis for development of novel age-hardening alloys, since it was utterly unclear what was the nature of that mysterious (at that time) phenomenon and in what alloys it could be expected.

Development of the theoretical principles of ageing is a bright example of how a scientific hypothesis which correctly reflected, in the general outline, the nature of a new important phenomenon, has served as a basis for subsequent amazingly fast progress in theoretical and applied metallurgy. No age-hardening alloys were discovered in the period from Wilm's discovery of ageing in duralumins to the year when Merica forwarded his theory, but since then, in 1920's, ageing was predicted and found in many alloys of aluminium, iron, copper, nickel and other metals and new age-hardening alloys were developed. Beginning from 1930's, the information on structural changes caused by ageing in various groups of alloys grew progressively. In the last two or three decades, important results were obtained by using electron microscopy which has enabled disperse precipitates to be 'seen' directly.

Development of novel age-hardening alloys possessing high mechanical and special physical properties and of optimum conditions for their heat treatment, as also continued vast studies into the mechanism and laws of ageing in various groups of alloys constitute one of the central trends in modern physical metallurgy, with all theoretical and applied work in the field being based, as before, on the general initial concepts of Merica's theory of ageing.

### 4.1.1. THERMODYNAMICS OF PRECIPITATION FROM SOLID SOLUTION

In the general case, a phase precipitated from a supersaturated solid solution differs from the matrix in both the composition and the structure. To begin with, let us consider a simpler case where the precipitated phase differs from the matrix in composition only.

Figure 161a shows the constitutional diagram of a system which forms a continuous series of solid solutions at high temperatures. The line  $MKN$ , which is often called stratification curve (by analogy with the corresponding curve for liquid solutions) is the solubility boundary in the solid state. If an alloy is cooled to a temperature below this line, another solid solution precipitates from the original one, which has the same crystal lattice but a different composition.

Above the critical point  $K$ , for instance at temperature  $T_1$ , one of the phases is stable with any concentration, so that a curve relating the free energy of the solid solution to the composition is concave upwards in all its portions (Fig. 161b). As the temperature is lowered down, the free energy of the components and solid solutions increases (see the free energy curve for temperature  $T_2$ ). At still lower temperatures (such as  $T_3$ ) and a sufficiently large positive heat of intermixing of concentrated solid solutions, the free energy curve becomes convex upwards in its middle portion. This means that a mixture of two solutions of different composition, rather than a single solid solution, is stable in a certain region of the system. Their compositions can be determined by drawing a tangent to the free energy curve (see 2.1.4). The  $as_1s_2b$  portion of the curve is above the  $ab$  tangent line, and therefore, relates to solid solutions which are unstable at  $T_3$ , since the free energy of a single phase is always greater in this region than that of a mixture of phases of the same average composition (for instance,  $F_1 > F_2$ ).

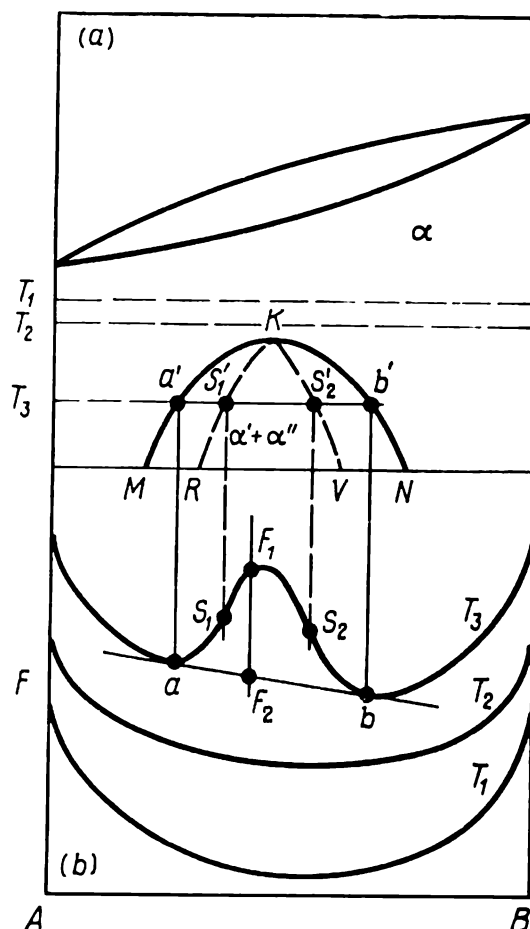


Fig. 161. Constitutional diagram with stratification curve  $MKN$  and spinodal line  $RKV$  (a) and composition free-energy curves for three different temperatures (b)

If an unstable solid solution has been formed, by some or other method, at the temperature  $T_3$ , it must decompose by precipitation into a mixture of two solid solutions having a lower free energy. This precipitation can occur in two principally different ways.

### Spinodal Precipitation

Consider the isothermal precipitation of a thermodynamically unstable solid solution of free energy  $F_1$  in an alloy of composition  $C_0$  (Fig. 162). The final equilibrium state with a free energy  $F_2 < F_1$  cannot appear at once, since it is very unlikely that fluctuations in the solid solution of composition  $C_0$  can form many re-

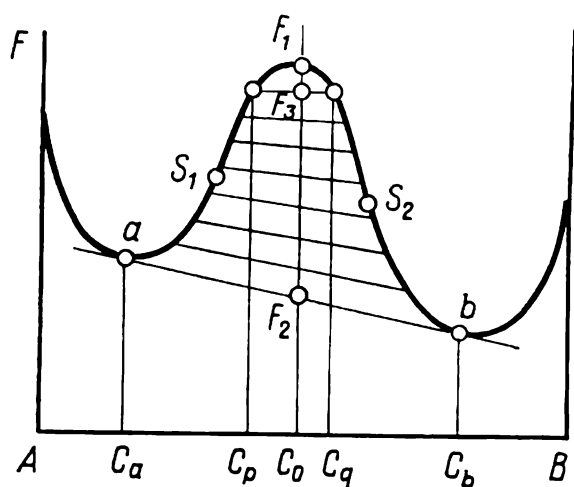


Fig. 162. A diagram to explain spinodal precipitation in  $C_0$  alloy in a system forming a continuous series of solid solutions

gions of equilibrium compositions  $C_a$  or  $C_b$  differing largely from  $C_0$ . It is more probable that fluctuations will initially result in the appearance of regions with compositions not differing much from the original composition  $C_0$ , for example  $C_p$  and  $C_q$ . The free energy will then decrease to  $F_3 < F_1$ . In the alloy considered, any arbitrarily small stratification in the compositions of unstable solid solution will result in decreasing free energy and, therefore, no critical nuclei will be needed to initiate precipitation. This type of precipitation, which is called spi-

nodal, propagates immediately throughout the whole volume of the original phase. An increase in concentration stratification must continuously decrease the free energy (see the series of straight lines in Fig. 162) until an equilibrium concentration difference  $C_a - C_b$  is established.

At a given temperature, spinodal precipitation is possible in all alloys whose composition is within the concave-down portion of the free energy curve, i.e. where  $\frac{\partial^2 F}{\partial C^2} < 0$ . This portion is limited by inflexion points  $S_1$  and  $S_2$  at which  $\frac{\partial^2 F}{\partial C^2} = 0$  (Fig. 161b). Such points are called spinodal. With increasing temperature, the *spinodal inflexion points*  $S_1$  and  $S_2$  gradually approach one another and disappear when temperature reaches the critical value ( $K$  in Fig. 161a), i.e. the free energy curve becomes concave upwards in all its portions ( $\frac{\partial^2 F}{\partial C^2} > 0$ ). By fixing the compositions at spinodal



points (such as  $S'_1$  and  $S'_2$  in Fig. 161a) at different temperatures on a constitutional diagram, we can obtain what is called the *spinodal line* (curve  $RKV$  in the figure). A solid solution can undergo spinodal precipitation when cooled to a temperature below the spinodal line.

In the system considered, there is no energy barrier in all stages of spinodal precipitation. Actually, however, such a barrier can appear owing to elastic strain energy of the lattice. Portions of the solid solution with different concentrations, though being similar in structure, can differ from each other in their specific volumes. Since the boundary between these portions is coherent, its appearance causes elastic deformation of matching portions with different lattice periods.

The elastic energy appearing on spinodal precipitation contributes positively to free energy; this has been neglected in the system of Fig. 161b. Because of this fact, additional undercooling of the initial solid solution by tens or hundreds of degrees C against the position of the 'chemical' spinodal line  $RKV$  in Fig. 161a may be needed in order to initiate spinodal precipitation. By calculating the temperatures of the beginning of spinodal precipitation with due regard of elastic deformation at coherent phase boundaries, we can find what is called the *coherent spinodal line*, which passes below the 'chemical' spinodal line. A high elastic energy can even fully inhibit spinodal precipitation.

The hypothesis of spinodal precipitation, proposed initially for liquid solutions by Gibbs in the last century, was for a long time studied in all classical courses of thermodynamics. Later, when the hypothesis of crystallization through nucleation and growth of new phases was widely accepted in mid-twenties, spinodal precipitation was almost fully forgotten. In the last two decades or so, it again has attracted much interest, particularly in connection with the possibility of obtaining evenly distributed disperse precipitates in alloys by means of heat treatment (see 4.1.2).

### Precipitation by the Mechanism of Nucleation and Growth of Nuclei

Let us analyse the isothermal precipitation of a solid solution whose composition  $C_0$  is beyond the spinodal region (Fig. 163). The free energy  $F_1$  of the solution is larger than the free energy  $F_2$  of an equilibrium two-phase mixture. If fluctuations at early stages of precipitation cause the formation of two phases with compositions  $C_f$  and  $C_g$ , which are close to  $C_0$ , then the free energy of this two-phase mixture is higher than that of the initial solution  $C_0$  ( $F_3 > F_1$ ). This follows inevitably from the fact that the free energy curve beyond the spinodal region  $S_1S_2$  is concave



The above discussion has neglected the role of surface energy and elastic strain energy in the formation of a new phase through nucleation. The difference  $F_1 - F_2$  in Figs. 163 and 164 is the

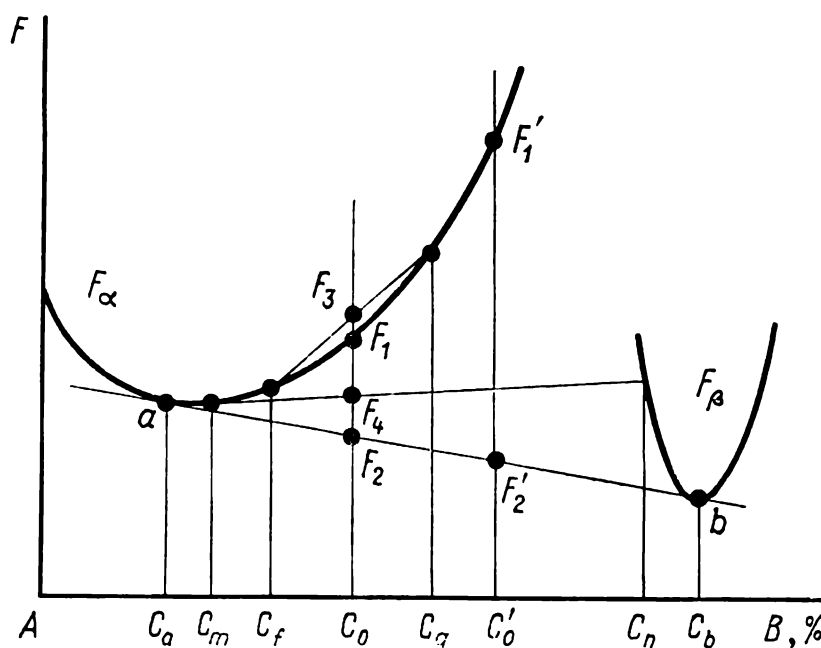


Fig. 164. A diagram to explain precipitation of  $\beta$ -phase from  $\alpha$ -solution by the mechanism of nucleation and growth in  $C_0$  and  $C'_0$  alloys

thermodynamic stimulus of transformation. Its role is similar to that of  $\Delta f$  in Fig. 69, which relates to a phase transformation without a change in the composition. The difference  $\Delta F_v = F_1 - F_2$  is the loss of free energy per unit volume in the precipitating solution ( $F_1$  and  $F_2$  are respectively the specific free energies of the initial phase and the equilibrium mixture of phases). But two more components also contribute to the general change in the free energy on precipitation from the solid solution  $\Delta f$ ; these are the increment of surface energy  $\Delta F_s$  and the rise in free energy due to the appearance of elastic deformation of matrix and new phase,  $\Delta F_{el}$ , upon formation of crystals in an elastic medium  $\Delta F = -\Delta F_v + \Delta F_s + \Delta F_{el}$ . The formation of new surfaces and the appearance of elastic deformations prevent precipitation from the solution.

In the analysis of phase transformations without compositional changes (2.1.1) it has been proved that increasing degree of un-

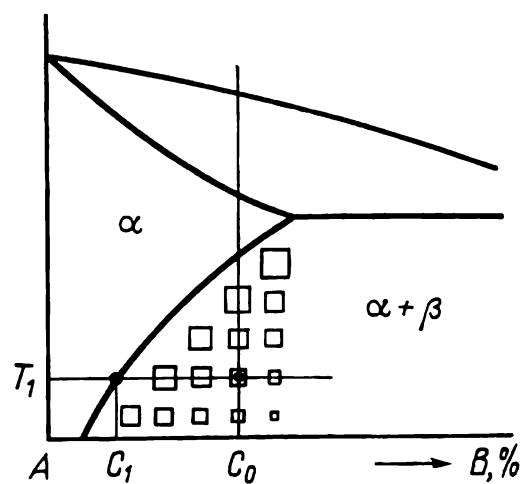


Fig. 165. Size of precipitates at various degrees of supersaturation of solid solution (schematically)

dercooling increases  $\Delta F_v$  and thus diminishes the size of critical nucleus  $a_{cr}$  and the work for its formation,  $\Delta F_{cr}$ . It can be shown that in the case of precipitation from solid solution with a change in composition the critical size of nucleus and the work for its formation also diminish with increasing  $\Delta F_v$ . For instance, the  $C'_0$  alloy in Fig. 164 is more alloyed than  $C_0$  and its driving force of precipitation is also greater ( $F'_1 - F'_2 > F_1 - F_2$ ). Therefore, with a constant temperature of ageing  $T_1$ , the size of critical nucleus of a new phase diminishes with increasing concentration of the initial solid solution, i.e. with increasing degree of supersaturation  $C_0/C_1$  (Fig. 165). With a constant concentration of the initial solid solution, say, in  $C_0$  alloy (Fig. 165), the size of critical nucleus increases with increasing temperature of ageing, since the degree of supersaturation of the solution decreases.

#### 4.1.2. STRUCTURAL CHANGES ON AGEING

The principal structural changes occurring on ageing may be reduced to various stages of precipitation from the supersaturated solid solution that has been formed through quenching of an alloy. Since precipitation from a supersaturated solution is a diffusional process, the extent of precipitation, the type, dispersity and shape of precipitates, and other structural characteristics depend on temperature and time of ageing, nature of the alloy, and its composition in main components. Besides, the structure of an age-hardened alloy may be influenced by impurities, temperature of heating and rate of cooling in quenching, plastic deformation before and after quenching (before ageing), the time of storage of the quenched alloy at room temperature before artificial ageing, and many other factors.

Studies of structural changes in ageing are rather complicated, since the structure of age-hardened alloys is influenced by many factors and since precipitation from the supersaturated solid solution runs through many stages; this is aggravated by high dispersity of precipitates, especially at the initial stages of precipitation. The main methods employed for the purpose are electron microscopy and X-ray structural analysis.

Some useful data can also be obtained by studying the variations in mechanical and physical properties, especially one of electric resistivity, on ageing. Such studies make it possible to draw some suppositions or sometimes conclusions on the nature and sequence of structural changes, first of all at the early stages of precipitation, when direct structural methods are only limitedly applicable.

## Types of Precipitates

According to the structure of interfaces between precipitates and matrix, a distinction is made between *fully coherent*, *partially coherent* and *incoherent precipitates* (Fig. 166).

With a coherent precipitate, its whole interface with the matrix is coherent and the matrix lattice around the precipitate is elastically distorted (Fig. 166a). With a partially coherent precipitate, one of its boundaries with the matrix is coherent, while others may

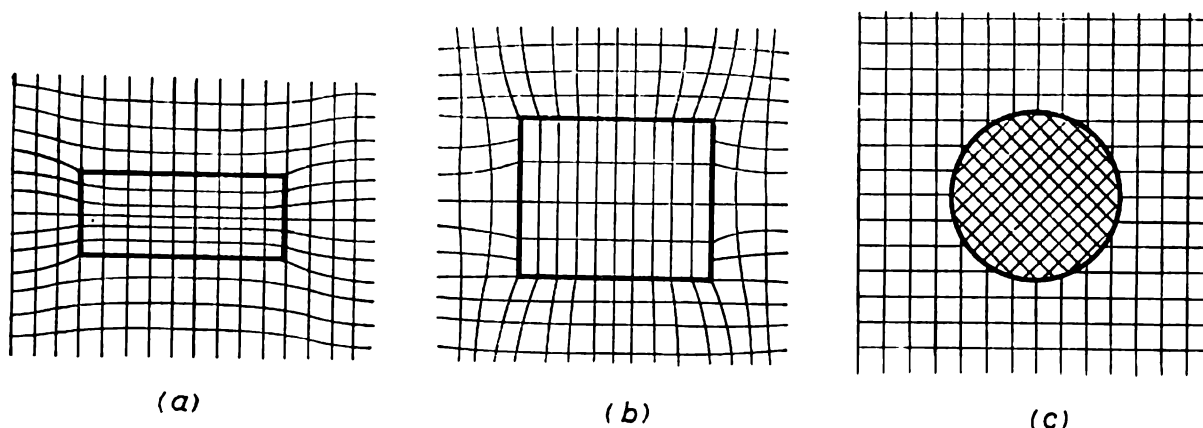


Fig. 166. Schematic structure of matrices with (a) coherent, (b) partially coherent, and (c) incoherent precipitates

be either semicoherent (Fig. 166b) or even incoherent. An incoherent precipitate has no coherent boundaries with the matrix (Fig. 166c). In Al-Cu alloys, for instance, examples of fully coherent precipitates are G. P. zones and  $\theta''$ -phase, while  $\theta'$ -phase is partially coherent and  $\text{CuAl}_2$  precipitates are incoherent (their structure will be discussed later, see Fig. 177).

## Shape and Spatial Distribution of Precipitates

### Shape of Precipitates

The main shapes of precipitates from the solid solution in age hardening alloys are fine-lamellar (usually disc-shaped), equiaxed (usually spherical or cubic) and acicular.

The shape of precipitate is determined by two rivalling factors, i.e. the surface energy and elastic strain energy, both tending to reach a minimum. Since the surface energy tends to its minimum, there is a tendency of formation of equiaxed precipitates and of appearance of faceted forms with the least surface tension at all the faces. The elastic strain energy is the lowest with fine lamellar precipitates. Thus, the shape of precipitates will tend to be either equiaxed or fine-lamellar depending on which of these two factors prevails.

In fully and partially coherent precipitates, the elastic strain, which ensures a smooth matching between the lattices at a coherent boundary, propagates from that boundary into the depth of both matrix and precipitate (Fig. 166*a*, and *b*). The elastic strain energy of the lattices of matrix and precipitates is greater at higher structural difference between these lattices. When the difference of atomic diameters of the components in a solid solution does not exceed 3 per cent, the shape of coherent precipitates is determined by the minimum of surface energy and is close to spherical, while with a difference  $\geq 5$  per cent the decisive factor is the increased energy of elastic distortions, so that fine-lamellar (most often disc-shaped) precipitates predominantly form. Coherent precipitates may sometimes be of acicular shape, which corresponds to an elastic strain energy which is higher than that of the disc-shaped precipitates but lower than that of the equiaxed precipitates. Examples of various shapes of Guinier—Preston zones (for coherent precipitates) are given in Table 12.

**Table 12. Shape of Guinier—Preston Zones in Various Systems**

Shape of G. P. zones	System	Atomic diameter difference, %	Shape of G. P. zones	System	Atomic diameter difference, %
Spherical	Al-Ag	+0.7	Lamellar	Al-Cu	-11.8
	Al-Zn	-1.9		Cu-Be	-8.8
	Al-Zn-Mg	+2.6	Acicular	Al-Mg-Si	+2.5
	Cu-Co	-2.8		Al-Cu-Mg	-6.5

In f.c.c. solid solutions, coherent lamellar precipitates are often located along  $\{100\}$  planes of the matrix. This may be explained by an anisotropic modulus of elasticity of such a matrix; the normal elasticity modulus is at its minimum along  $\langle 100 \rangle$  directions, i.e. the deformation along these directions is at its maximum, which ensures the lowest strain energy.

When an incoherent precipitate forms, tangential stresses are absent, but normal stresses appear always, since different specific volumes of the matrix and the precipitate inevitably cause hydrostatic (tridimensional) compression or tension (not shown in Fig. 166*c*). This can be easily imagined by mentally placing an oversized rigid inclusion into a yieldable elastic matrix; a region of tridimensional compression must then appear in the matrix around that inclusion.

A calculation for an incoherent spheroidal inclusion with semi-axes  $a$ ,  $a$ , and  $c$ , under an assumption that the elastic deformation is concentrated entirely in the matrix, has given the following results (Fig. 167). The elastic strain energy is at its maximum for a spherical precipitate ( $c/a = 1$ ), at its minimum for a thin disc ( $c/a \ll 1$ ), and has an intermediate value for an acicular particle ( $c/a \gg 1$ ).

### Modulated Structures

As the energy of elastic distortions tends to the minimum, it can influence the mutual disposition of precipitates, as well as their shape. Upon the precipitation from the solid solution, this tendency of the elastic energy is conducive in some alloys to the formation of the so-called *modulated* (or *periodic*) structures, which can be characterized by a regular spatial disposition of coherent precipitates spaced at definite distance from each other, this distance being called the *modulation period of a structure*,  $\lambda$  (Fig. 168a and b and Fig. 169b).

Since the modulation period usually is not more than a few hundreds of interatomic distances, modulated structures are invisible in the optical microscope. The best method for their study is thin-foil electron microscopy.

In some alloys modulated structures can appear at the earliest stages of precipitation, for instance, during spinodal precipitation, while in others they may appear a certain time after the precipitation has started. As the ageing time is increased, a modulated structure may first become even more pronounced and then gradually transform into a combination of chaotically located precipitates, which usually occurs owing to coagulation of particles and the loss of coherence.

The morphology of modulated structures in various alloys can be different depending on the conditions of heat treatment. In some cases there may be thin lamellar precipitates spaced at equal distances and parallel to a definite crystal plane; in others there may be periodically disposed rod-like precipitates forming a tridimensional network of overlapping rods which are parallel to a definite direction in the matrix, for instance, the 'elastically soft'  $\langle 100 \rangle$  direction in cubic-lattice crystals. Such a network of preci-

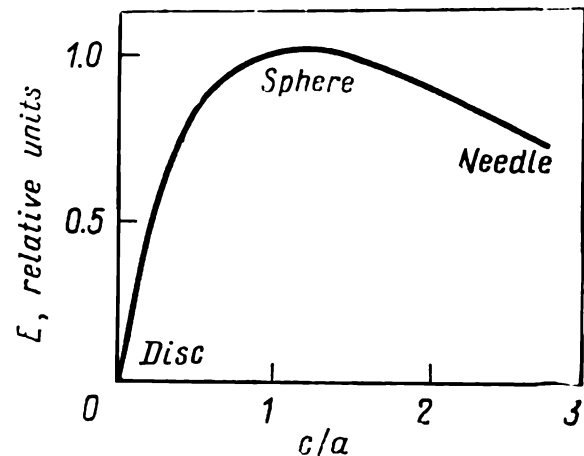


Fig. 167. Dependence of elastic strain energy  $E$  of matrix on the axial ratio  $c/a$  of an incoherent spheroidal precipitate (after F. R. N. Nabarro)



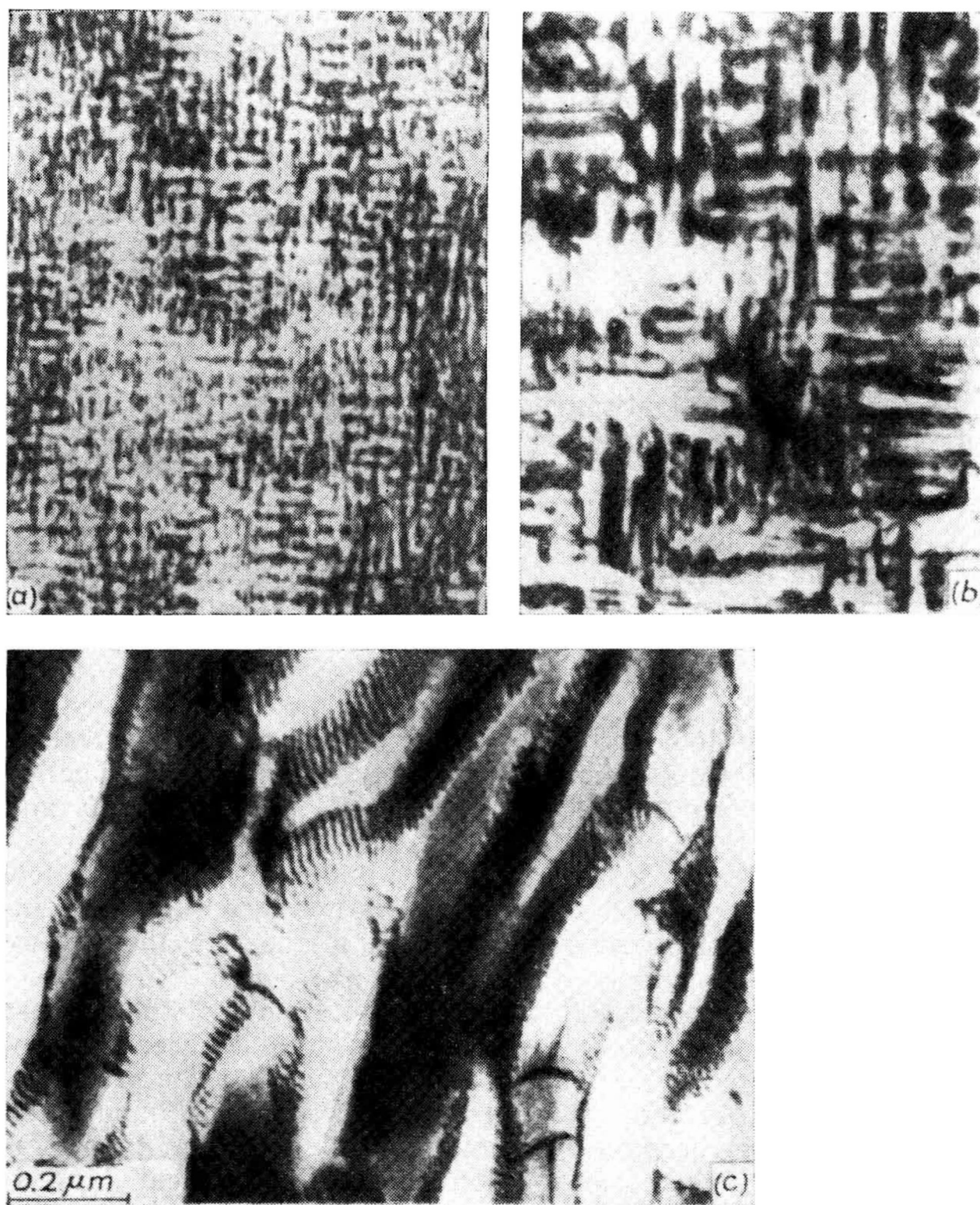


Fig. 168. The structure of Cu + 33.5% Ni + 15% Fe alloy upon ageing for different time at 775 °C; thin-foil electron micrograph (after *E. P. Butler* and *G. Thomas*)

*a* — 15 min, modulated structure with  $\lambda = 254 \text{ \AA}$ ; *b* — 5 h, modulated structure with  $\lambda = 635 \text{ \AA}$ ; *c* — 200 h



precipitates is usually seen as a typical 'basket-interlacing' pattern (Fig. 168*a* and *b*). Most typical variety of modulated structure is the one formed by rows of cubic precipitates parallel to the  $\langle 100 \rangle$  directions of the cubic-lattice matrix (Fig. 169*b*).

Modulated structures can appear in such alloys, in which coherent precipitates form relatively strong elastic stress field around them, for instance, owing to a large difference in the specific volumes of the initial and new phase. A classical example are precipitation-hardening alloys for permanent magnets based

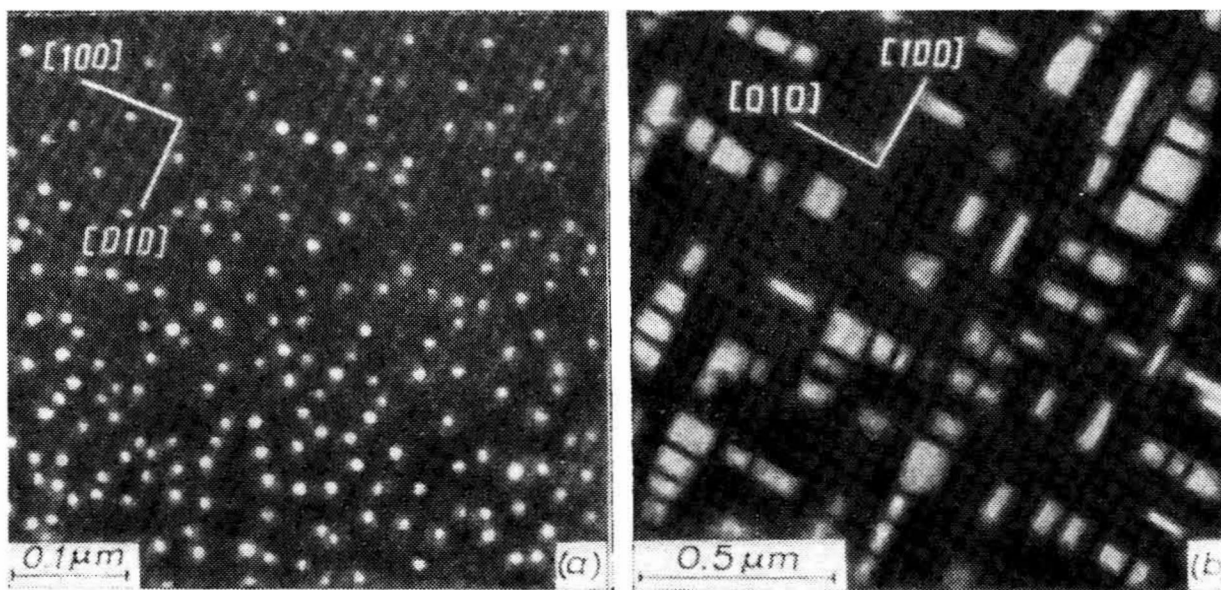


Fig. 169.  $\gamma'$  ( $\text{Ni}_3\text{Al}$ ) precipitates in  $\text{Ni} + 6.7\% \text{ Al}$  alloy aged at  $750^\circ\text{C}$  for (a) 15 min and (b) 96 h; thin-foil electron micrograph (after A. J. Ardell and R. B. Nicholson)

*a*—chaotically distributed precipitates; *b*—cubic precipitates oriented along  $\langle 100 \rangle$  directions (modulated structure)

on the Cu-Ni-Fe and Cu-Ni-Co systems. In such alloys, quenching stabilizes a supersaturated f.c.c. solid solution, while ageing causes this solution to decompose into two solutions, each of them having an f.c.c. lattice in equilibrium but differing from one another and from the matrix in the composition, and therefore, in the lattice period and specific volume (the appropriate binary system is described by the constitutional diagram in Fig. 161*a*).

Another example of alloys with a thoroughly studied modulated structure are age-hardening nickel alloys, in particular, those of the Nimonic type, in which a coherent f.c.c.  $\gamma'$ -phase precipitates from the supersaturated solid solution, which also has an f.c.c. lattice. Studies of Ni-Al binary alloys have shown that ageing begins with the formation of chaotically disposed cubic  $\gamma'$ -precipitates, which then arrange themselves into rows parallel to the  $\langle 100 \rangle$  directions of the matrix as the ageing time is increased (Fig. 169). This regular arrangement is due not to the precipita-

tion from the supersaturated solution proper, but to a slow coagulation in which some particles grow larger and others dissolve. A specific feature of this coagulation is that, owing to elastic interaction of  $\gamma'$ -phase precipitates, favourably positioned particles grow selectively, while those positioned unfavourably are dissolved, the process resulting in the formation of a modulated structure.

### Structural Changes During Spinodal Precipitation

At the initial stage of spinodal precipitation there forms a highly disperse mixture of the phases whose lattices are coherent, i.e. pass smoothly one into the other, and whose interfaces are not sharp but strongly diffuse. What is the difference between this mixture of phases and compositional fluctuations always observed

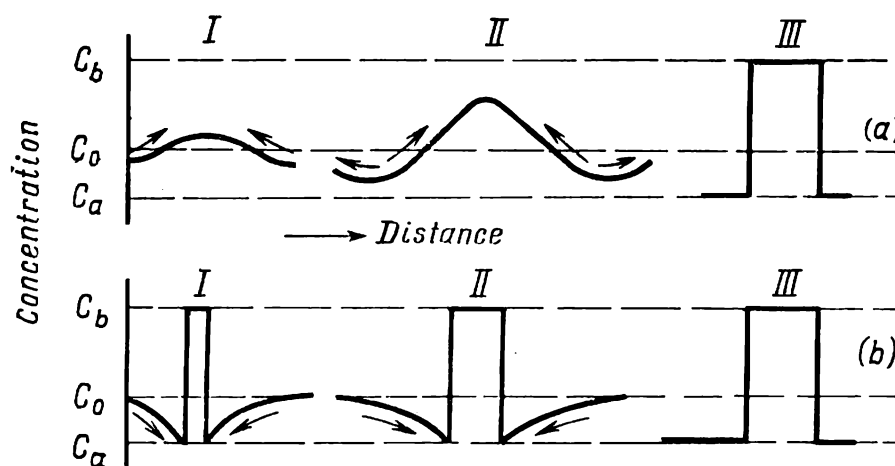


Fig. 170. Evolution of distribution of an alloying element in supersaturated solid solution at various stages (I-III) of spinodal precipitation (a) and precipitation by the mechanism of nucleation and growth (b) (after J. Cahn)  
For concentrations  $C_0$ ,  $C_a$  and  $C_b$  see Figs 162 and 164

in solid solutions, even above the spinodal curve  $RKV$  in Fig. 161a? With fluctuations of the composition, adjacent portions of a solid solution can also be characterized by different concentrations, and therefore, by different lattice periods. As has been noted in 2.1.1, compositional fluctuations continuously appear and disappear. In contrast to this, portions of the solid solution having a reduced or increased concentration of fluctuational origin become stable during spinodal precipitation, i.e. they do not disappear, but on the contrary grow more and more.

Figure 170a shows schematically the sequence of changes in a random fluctuation of the composition in the course of spinodal precipitation. At the initial moment (I in Fig. 170a), a *cluster* forms in the solid solution, i.e. a stable portion having an increased concentration of the dissolved element (above the average con-

centration  $C_0$ ), which is enclosed by a region of reduced concentration. At subsequent moments (for instance,  $II$  in Fig. 170a), the preferable mutual attraction of like atoms causes a further increase in the concentration in the cluster, while the surrounding region is being depleted in the corresponding element. This process is ensured by the uphill diffusion (shown by arrows in Fig. 170a), which corresponds to a negative coefficient of diffusion. This is due to the fact that a second derivative of free energy with respect to concentration enters the formula for diffusion coefficient  $D$  and, since for the range of spinodal precipitation  $\frac{\partial^2 F}{\partial C^2} < 0$  (see 4.1.1),  $D < 0$ . This is the most important feature that distinguishes the spinodal precipitation from the common precipitation by nucleation, which will be discussed later in the book.

Like atoms at the outer edge of the depleted region in the initial matrix are also susceptible to preferable mutual attraction. Since these attraction forces are of the short-range order, the atoms are 'insensitive' of the existence of a cluster, but are only under the effect of the adjacent depleted region. Because of this they move further from the depleted region and form a new cluster, which is also surrounded by a depleted region. Thus, the formation of a cluster then causes a new cluster to form nearby and so on, i.e. the process propagates rapidly as a concentration wave along the matrix lattice. Thus, ever new clusters form spaced an equal distance apart, which is called the *concentration wavelength*.

Structural changes in spinodal precipitation have been studied most thoroughly for Cu-Ni-Fe alloys whose composition is somewhere in the middle of the stratification region in the constitutional diagram. In corresponding thin-foil electron micrographs, bright portions are copper-rich regions, while dark ones are those enriched in iron and nickel (Fig. 168). In the Cu-Ni-Fe solid solution which, as many other cubic-lattice crystals, is characterized by an appreciably anisotropic modulus of elasticity, spinodal precipitation proceeds along each of the three 'elastically soft'  $\langle 100 \rangle$  directions. This is why spinodal precipitation in Cu-Ni-Fe alloys first forms a modulated structure composed of rod-like regions separated by diffuse boundaries ('basket interlacing' in Fig. 168a). As the time of ageing is increased, the concentration amplitude and concentration wavelength ( $\lambda$ ) increase, i.e. the modulated structure becomes coarser (see Fig. 168b) and the boundaries between coherent precipitates become sharper. Elastic deformations cause a change from the f.c.c. lattice of clusters to tetragonally distorted lattices of two intermediate phases. Compositional stratification gradually attains its maximum which corresponds to an

equilibrium of the two phases with the f.c.c. lattice (the tetragonality disappears). The coherence also disappears (owing to increasing elastic stresses), with structural dislocations (readily seen in Fig. 168c<sup>1</sup>) being formed at the interfaces. The loss of coherence is accompanied with the disappearance of the modulated structure and strong coarsening of the precipitates owing to their coagulation.

This sequence of structural changes, though being quite typical of spinodal precipitation, is found not in all alloys. For instance, an alloy of the same Cu-Ni-Fe system, but with the composition at the edge of the spinodal region rather than in the centre, shows no basket interlacing structure upon ageing. Furthermore, no modulated structure at all has been found in the alloy at the early stage of ageing and it appears only later due to the arrangement of cubic precipitates in rows along the  $\langle 100 \rangle$  direction. This is very similar to the formation of a modulated structure in a Ni-Al alloy caused by selective growth of cubic precipitates of the  $\gamma'$ -phase during coagulation, rather than through spinodal precipitation.

There are no specific morphological features typical only of structures obtained through spinodal precipitation. Spinodal precipitation not always produces a modulated structure and the latter is not necessarily linked with the former, as was thought earlier. On the other hand, elastically anisotropic crystals are very likely to form basket-interlaced modulated structures on spinodal precipitation.

The thermodynamics and mechanism of spinodal precipitation predetermine that the process is homogeneous: no preferable precipitation at grain boundaries or dislocations is observed. It is important for practice that spinodal precipitation produces a typical highly disperse structure which is uniform throughout the whole volume of the initial phase grains.

Since there are no specific structural features, it is not always easy to determine whether the precipitation in a given alloy is of the spinodal type. Industrial alloys actually undergoing spinodal precipitation during ageing include magnetic-hard alloys of the Cu-Ni-Fe and Cu-Ni-Co type.

## Continuous and Discontinuous Precipitation

### *Continuous Precipitation*

With continuous precipitation, individual precipitates of an excess phase form and grow in the initial supersaturated solution. Since these precipitates are enriched in one of the components, the matrix phase is respectively depleted of that component and a concentration gradient is present in it.

---

<sup>1</sup> The transformation of a coherent boundary into an incoherent one upon appearance of structural dislocations is discussed in 2.1.2 (see Fig. 75).

Crystals of the excess phase grow owing to common downhill diffusion: the flow of atoms (see arrows in Fig. 170b) is directed towards decreasing concentration and the diffusion coefficient  $D$  is positive. This is due to the fact that beyond the region of spinodal precipitation the second derivative of free energy with respect to concentration is positive, i.e.  $\partial^2 F / \partial C^2 > 0$  (compare with spinodal precipitation owing to uphill diffusion at negative values of  $D$ ).

During continuous precipitation, the growing precipitates gradually 'suck out' the alloying element from the matrix phase and the latter is depleted of that element throughout the whole volume down to an equilibrium concentration  $C_a$  (see Figs. 164 and 170b).

As the time of ageing  $\tau$  with continuous precipitation increases, the size  $r$  of precipitates increases approximately by a parabolic law:

$$r = (D\tau)^{1/2} \quad (32)$$

The rate of growth of precipitates is controlled by the volume diffusion coefficient  $D$  in the matrix lattice.

A feature characteristic of the process discussed is that the concentration of an alloying element diminishes continuously throughout the whole volume of the initial grains, whence follows the name 'continuous precipitation'. The crystal orientation of the initial phase remains unchanged.

According to microstructural features, continuous precipitation of a solution during ageing may be classed into *general* and *localized*.

With general precipitation, the precipitates are uniformly distributed over the volume of grains. The nucleation in the general precipitation may be either homogeneous or heterogeneous (see 2.1.3). In the latter case the sites of preferable nucleation (dislocations, vacancy nodules, etc.) are distributed uniformly throughout the bulk of grains.

With localized precipitation, the distribution of precipitates throughout the bulk of grains is non-uniform. Precipitation products can be detected at boundaries of grains and subgrains, in slip bands and other places. The nucleation in localized precipitation is always heterogeneous.

### *Discontinuous (Cellular) Precipitation*

With discontinuous precipitation, *cells* (or *nodules*) of a two-phase mixture  $\alpha_1 + \beta$  nucleate and grow inside grains of the initial supersaturated solution  $\alpha_s$ , these cells often having a pearlite-like structure (Fig. 171). The  $\alpha_1$ -phase inside the cells has the same lattice as the initial  $\alpha_s$ -phase, but its composition is an

equilibrium one at a given temperature of precipitation or is intermediate between the initial and equilibrium composition. The transformation being discussed can be written as follows:



The average composition of the two-phase  $\alpha_1 + \beta$  mixture in a cell is the same as that of the initial solution  $\alpha_s$ .

The process develops as the cell front moves into the initial solution owing to the cooperative growth of  $\alpha_1$ - and  $\beta$ -phase which is similar to the growth of a pearlitic nodule.



Fig. 171. Nodules in Ni + 20% Cr + 9% Nb alloy formed through discontinuous precipitation; ageing at 850 °C for 2 h after quenching from 1180 °C;  $\times 1350$  (after A. G. Rachstadt, O. M. Khovova, and N. N. Geveling)

During the transformation, the concentration of the initial solution remains all the time unchanged until the solution disappears fully. In a narrow zone between a cell and initial solution there occurs an abrupt jump of the concentration: from the initial concentration in  $\alpha_s$  solution to the concentration of  $\alpha_1$  solution inside the cell. This is why this type of precipitation is called discontinuous in contrast to continuous precipitation during which the concentration of an alloying element in the initial solution decreases smoothly, since the element is gradually sucked out owing to the growth of the excess  $\beta$ -phase.

Discontinuous precipitation was first detected radiographically by N. V. Ageev, M. Hansen and G. Sachs in 1930 in a silver-copper alloy. With continuous precipitation, the lattice period of the

matrix solution changes smoothly, since the concentration of the element gradually decreases throughout the whole volume, and the lines on the radiograph are correspondingly shifted and become blurred. In discontinuous precipitation, two systems of lines are seen on the radiograph, one of them corresponding to the initial  $\alpha_s$ -solution with a definite lattice period and the other, to the  $\alpha_1$ -solution with the final concentration and its own lattice period. As discontinuous precipitation proceeds, the lines on the radiograph are not shifted, i.e. the lattice periods of the  $\alpha$ -solution of two different compositions are not changed.

Discontinuous precipitation is always localized and starts most often at grain boundaries. With a small interplate distance in cells or an appreciable etchability of the transformed region, it may be seen in the optical microscope as dark portions usually contrasting sharply against bright background of the initial supersaturated solution. At early stages it is seen in the form of thickened grain boundaries of the initial phase.

The crystal orientation of  $\alpha_1$ -phase in a cell differs from the initial orientation of  $\alpha_s$ -phase in the grain inside which the cell is growing. On the other hand, the orientation of  $\alpha_1$ -phase in the cell is the same as in a neighbouring grain at the other side of the boundary, where discontinuous precipitation has started. Thus, the motion of the front of a cell in discontinuous precipitation towards a grain is accompanied with a re-orientation of the crystal lattice of the matrix phase and can be regarded as the motion of an intergranular boundary towards the grain that is being consumed. The process thus has an external similarity with the formation of protrusions ('tongues') in primary recrystallization, where individual portions of a high-angle boundary bend and move towards one of the grains (see Fig. 21).

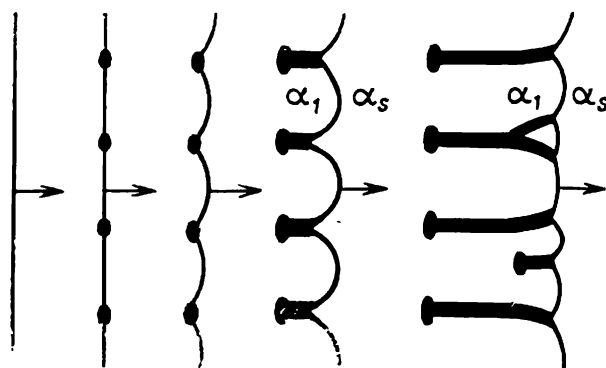


Fig. 172. Diagram of a cell formation through discontinuous precipitation at a migrating boundary (after R. A. Fournelle and J. B. Clark)

With discontinuous precipitation, the excess phase precipitates from the matrix behind the intergranular boundary which moves towards a neighbouring grain. The thermodynamic stimulus for this motion is the difference between the volume free energy of the initial supersaturated solution and that of the two-phase mixture inside the cell ( $F_1 - F_2$  in Fig. 164). Even when the composition of the phases in a cell does not reach equilibrium, the formation of the mixture lowers the volume free energy, though not to the virtual minimum.

The mechanism of formation of a cell in discontinuous precipitation is still not clear enough. By one of assumptions, which is based on the structure of the transformation front, it may be reduced to the following. As a grain boundary migrates, a dissolved element precipitates near it in the form of particles which locally pin the boundary. When migrating further, the boundary bends between precipitates and the latter are stretched during their growth and follow the moving boundary (Fig. 172). The process forms alternate portions of  $\alpha_1$ - and  $\beta$ -phase, i.e. a pearlite-like cell nuclea-



tes behind the migrating intergranular boundary. Other hypotheses have also been proposed to explain the nucleation of cells.

The mechanism of growth of a formed cell is more comprehensible. The concentration of an element  $B$  at the end faces of plates or rods of the  $\alpha_1$ - and  $\beta$ -phase is respectively increased or reduced (since the  $\beta$ -phase is enriched in  $B$  and  $\alpha_1$ -phase, depleted). As in the growth of a pearlitic nodule in austenite, the cooperative growth of a two-phase cell in discontinuous precipitation causes the components to redistribute diffusionally along the interface between the matrix and the cell. With continuous precipitation, however, the growth of a precipitate is controlled by volume diffusion normally to the surface of the precipitate. The rate of diffusion along the interface between the matrix and the cell is appreciably higher than that of volume diffusion, but the diffusion paths are very short owing to the small interplate distance in the cell. Because of this, discontinuous precipitation can proceed rapidly at relatively low temperatures, even at such temperatures when the growth of isolated precipitates of  $\beta$ -phase by continuous precipitation occurs only very slowly or is fully inhibited. The interplate distance in cells decreases with lowering temperature of ageing.

Discontinuous and continuous precipitation may be considered as competing processes. Discontinuous precipitation is favoured by a high probability of heterogeneous nucleation at grain boundaries compared with that inside grains, high coefficient of diffusion at grain boundaries and high mobility of the grain boundary. Discontinuous precipitation is impeded by additions which slow the diffusion at grain boundaries. It can also be slowed by precipitations at grain boundaries of particles of excess phases which hamper the migration of grain boundaries.

Plastic deformation of a quenched alloy may have a strong and diverse effect on the development of discontinuous precipitation. Upon a strong deformation during heating, redistribution of dislocations in deformation bands promotes the formation of new boundaries which serve as additional sites for nucleation of cells on discontinuous precipitation inside grains of the initial phase.

In a work-hardened alloy, the advancing front of cellular precipitation 'sweeps out' dislocations in the supersaturated solution and, consequently, the thermodynamic stimulus of discontinuous precipitation, i.e. the difference in free energies of the initial  $\alpha_s$ -phase and the phase mixture  $\alpha_1 + \beta$ , has a new component due to the lower density of dislocations. On the other hand, work-hardening favours continuous precipitation in the whole bulk of the initial grains. The particles that form on continuous precipitation retard the motion of a cell boundary on discontinuous precipitation. Which of these opposing factors will prevail depends on the deformation and the temperature of ageing, because of which plastic deformation on quenching can either facilitate or impede discontinuous precipitation in subsequent ageing. In beryllium bronze, preliminary cold rolling with 20-50 per cent reduction can accelerate discontinuous precipitation, while the process is retarded on increasing the deformation from 50 to 90 per cent and can be fully inhibited at deformation above 90 per cent.

Commercial alloys in which discontinuous precipitation is industrially feasible include beryllium bronzes (such as Grade



Бр.Б2), magnesium alloys based on the Mg-Al-Zn system (such as Grade МЛ5), and austenitic ferrous alloy Grade 36HXTЮ.

In ageing, discontinuous precipitation is usually avoided where possible, since the two-phase structure with incoherent precipitates that forms on it is coarser and respectively less strong than that obtained through common precipitation hardening which forms coherent or semicoherent disperse precipitates. Besides, incoherent lamellar precipitates of an excess phase at grain boundaries may have an embrittling effect on alloys.

With beryllium bronzes, the harmful discontinuous precipitation can be fully avoided by using a high deformation (above 90 per cent) in the cold state or by introducing small additions, for instance 0.2 per cent Co or 0.1 per cent Mg. The volume that can undergo discontinuous precipitation in beryllium bronze is decided by the conditions of heat treatment. For instance, the volume proportion of boundary zones of discontinuous precipitation in age-hardened bronze Grade Бр.Б2 upon quenching from 760, 780 and 800 °C is respectively 30, 20 and 12 per cent. A lower temperature of ageing favours discontinuous precipitation and impedes continuous precipitation. Uniform precipitation over the whole volume of grains is especially important for obtaining high elastic properties in beryllium bronzes.

In magnesium alloys, a slower cooling on quenching can increase the volume that undergoes discontinuous precipitation on ageing. In air-hardened castings, grain boundaries on a micro-section can be etched appreciably, which is an indication that discontinuous precipitation has had enough time to proceed there owing to the slow cooling on quenching.

Discontinuous precipitation can sometimes produce a useful effect. If it forms a phase coherent with the matrix, such as the  $\gamma'$ -phase (of the  $\text{Ni}_3\text{Al}$  type) in alloy Grade 36HXTЮ, ageing results in the formation of a disperse structure and improved mechanical properties of the metal.

If we manage to cause controlled growth of strictly oriented fibrous precipitates on discontinuous precipitation, the process could be used for making composite materials in which monocrystalline fibres of a compound will be uniformly distributed in and firmly bonded with the metallic matrix.

## Stages of Solution Decomposition in Precipitation Hardening

### *Formation of Guinier-Preston Zones*

Precipitation-hardening aluminium alloys and beryllium bronzes have an increased electric resistivity at room temperature just after being quenched (Fig. 173). This is explained by aggregates

(clusters) of alloying elements which form in the supersaturated solid solution and can dissipate electronic waves. Probably, part of the clusters can form already during quenching. The size of clusters is initially very small and they cannot be detected by

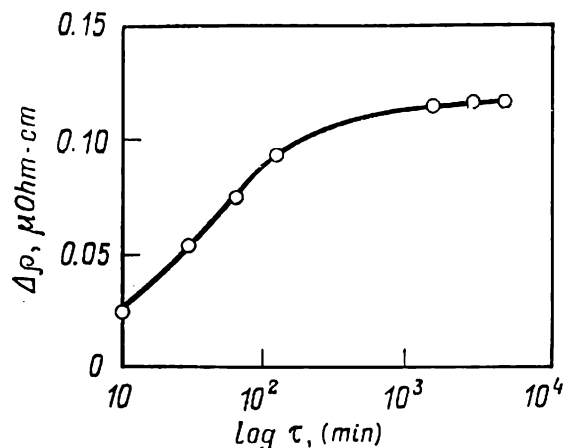


Fig. 173. Effect of ageing time ( $\tau$ ) on the rise of electric resistivity  $\Delta\rho$  in Al + 1.2% (at.)  $\text{Mg}_2\text{Si}$  alloy aged at  $30^\circ\text{C}$  after quenching from  $520^\circ\text{C}$  (after Y. Baba and A. Takashima)

Copper atoms occupy one of the  $\{100\}$  planes, with the parallel planes at both sides of that plane composed of aluminium atoms only. Since the atomic diameter of copper is less than that of aluminium, the planes that are filled with aluminium atoms are displaced towards the plane composed of copper atoms only. The displacement of atomic layers from their regular positions decreases from the centre of a G. P. zone and, according to the model discussed, the fourteenth atomic layers at both sides of the central plane remain intact. Owing to the high difference in the atomic diameters of copper and aluminium, which causes an appreciable elastic deformation of the lattice, G. P. zones in aluminium-copper alloys have a fine lamellar or discshaped form (see 4.1.2).

In Al-Ag and Al-Zn alloys, the difference between the size of atoms of aluminium and an addition is small, so that the elastic deformation of the lattice is not large and the G. P. zones are spherical (see Table 12). Silver and zinc atoms form spherical

structural methods. After a certain period, they grow to such an extent that can cause diffraction effects in radiographs of single crystals and thin-foil transmission electron micrographs. Clusters detectable by structural methods are called the Guinier-Preston zones (G. P. zones). They have the same crystal lattice as the matrix solution, but the difference in atomic diameters between the matrix metal and alloying element causes local changes in interplane distances.

Figure 174 shows a model of a G. P. zone in aluminium-copper alloy as proposed by V. Gerold.

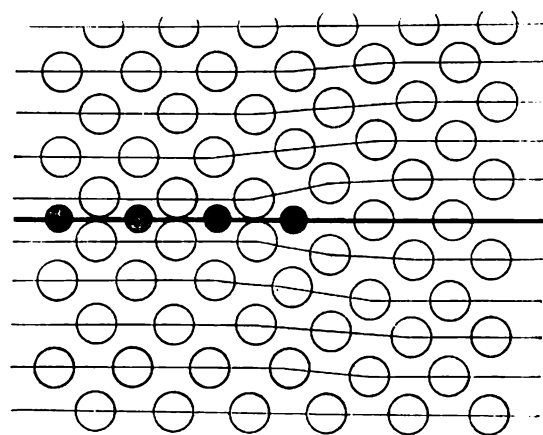


Fig. 174. A model of structure of solid solution of copper in aluminium with G. P. zone (after V. Gerold)

clusters around which the solution is depleted of the alloying element.

The size of G. P. zones depends on alloy composition and the temperature and time of ageing and may be of an order of  $10^1$ - $10^2$  Å. For instance, disc-shaped G. P. zones in Al-Cu alloys have a diameter of an order of 100 Å.

Cluster formation is a diffusion process linked with the displacement of atoms of an alloying element in the lattice of solid solution. The most essential feature of the formation of clusters is an unusually high diffusion mobility of atoms of dissolved elements. Clusters can form even at sub-zero temperatures (at  $-100^\circ\text{C}$  in Al-Zn alloys).

The coefficient of diffusion of alloying elements in an aluminium solution at room and lower temperatures can be found by a known rate of cluster growth using, for instance, formula (32). These calculated data turned to be many orders of magnitude greater than the diffusion coefficients obtained by extrapolation of values determined experimentally at high temperatures in common diffusion tests. For a solution of copper in aluminium, the discrepancy at room temperature is  $10^8$  (!).

An anomalously high diffusion rate in the formation of clusters during ageing is attributed to the supersaturation of the solid solution with vacancies during quenching. The equilibrium concentration of vacancies at the quenching temperature is many orders of magnitude greater than that at the temperature of ageing. During quenching, an appreciable part of vacancies have no time to annihilate in sinks and the solid solution turns to be supersaturated with vacancies, as well as with the alloying element. Since diffusion in substitutional solutions proceeds by the vacancy mechanism, quenching vacancies can sharply accelerate the migration of atoms of an alloying element owing to which the rate of cluster formation is very high even at relatively low temperatures.

With increasing temperature of heating for quenching, the solid solution becomes more supersaturated with vacancies, which accelerate the formation of clusters. An opposite effect can be obtained by a slower cooling on quenching, since more vacancies have then time to flow to sinks (dislocations, grain boundaries and the free surface of a specimen) during quenching.

The electric resistivity, upon having risen rapidly during a few tens of minutes of the initial period of ageing (*'quick reaction'*), then continues to grow slowly for an appreciable time (see Fig. 173). During this slow growth (*'slow reaction'*), the rate of diffusion which ensures the formation of G. P. zones still remains anomalously high. The main theoretical difficulty is how to explain why an appreciable surplus of quenching vacancies remains

in the metal for a long time (many hours or even days), even at the presence of large number of sinks (dislocations and grain boundaries) available for them.

A hypothesis proposed to overcome this difficulty can be reduced to the following.

Vacancies are combined in complexes with atoms of a dissolved element and the growth of G. P. zones is promoted through migration of these complexes. Upon approaching a zone, a complex dissociates into a vacancy and an atom of alloying element and the latter is attached to the zone. An increased concentration of free vacancies at a boundary of the zone causes these vacancies to migrate directionally into the matrix where they meet atoms of dissolved element and form new complexes. Since the concentration of complexes near the boundary is higher than further from it, the complexes migrate to the zone, dissociate by giving to it an atom of alloying element, and so on. The zone acts as a pump, as it were, i.e. pumps atoms of dissolved element from the matrix and sends vacancies into the matrix. Part of free vacancies annihilate in sinks, because of which the rate of diffusion to promote the formation and growth of G. P. zones drops down.

When discussing the nature of G. P. zones, these are usually compared with metastable intermediate phases. It is often emphasized that a G. P. zone is a portion of the initial solid solution that is enriched in a dissolved element, rather than a new phase. In contrast to intermediate phases, which are characterized by their own lattice, a G. P. zone has the same lattice as the matrix solution, but deformed owing to the difference of atomic diameters of the solute and solvent. There is no distinct interface between a G. P. zone and the surrounding solution. In some alloys, G. P. zones (clusters) form without any induction period, i.e. immediately after or even during quenching, whereas intermediate and stable phases appear only after a certain induction period. All these facts show clearly that G. P. zones differ from intermediate and stable phases. In that respect G. P. zones are often called preprecipitates, to distinguish them from 'real' precipitates of intermediate and stable phases which have a qualitatively different structure.

In contradistinction to this structural approach which considers G. P. zones as preprecipitates, they may be regarded thermodynamically as an independent metastable phases which are intermediate between the matrix solution and a stable phase. This interpretation follows from many important specifics of the behaviour of G. P. zones. As distinct from concentration fluctuations which appear and disappear continuously owing to thermal motion, G. P. zones remain stable for a long time (indefinitely long

at low temperatures). As has been established experimentally, the size of G. P. zones increases with the time of ageing (Fig. 175), with larger zones growing at the expense of smaller ones which are dissolved, i.e. exactly in the same way as is the case with coagulation of phase particles. The composition of G. P. zones at a given temperature of ageing is independent of the composition of alloy. Finally, what is most important, G. P. zones in a binary system have their own solvus line (Fig. 176): they can form only on undercooling of the matrix solution below that line. If G. P. zones are present in an alloy, they dissolve in the matrix upon heating to a temperature above their solvus line, i.e. in full analogy with the precipitation and dissolution of a stable phase.

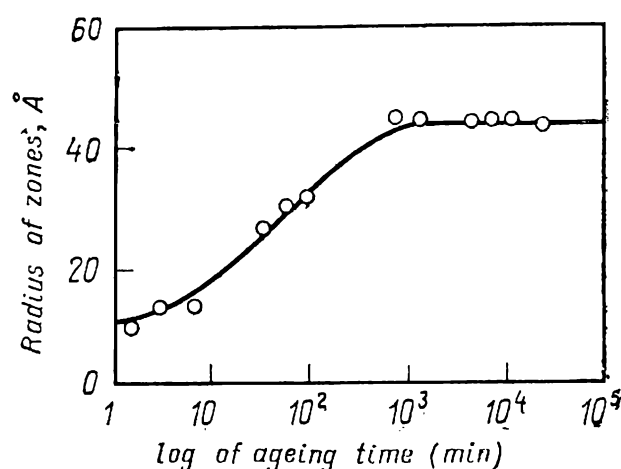


Fig. 175. Size of G. P. zones in Al + 6.8% (at.) Zn alloy versus time of ageing at room temperature (after M. Murakami and O. Kawano)

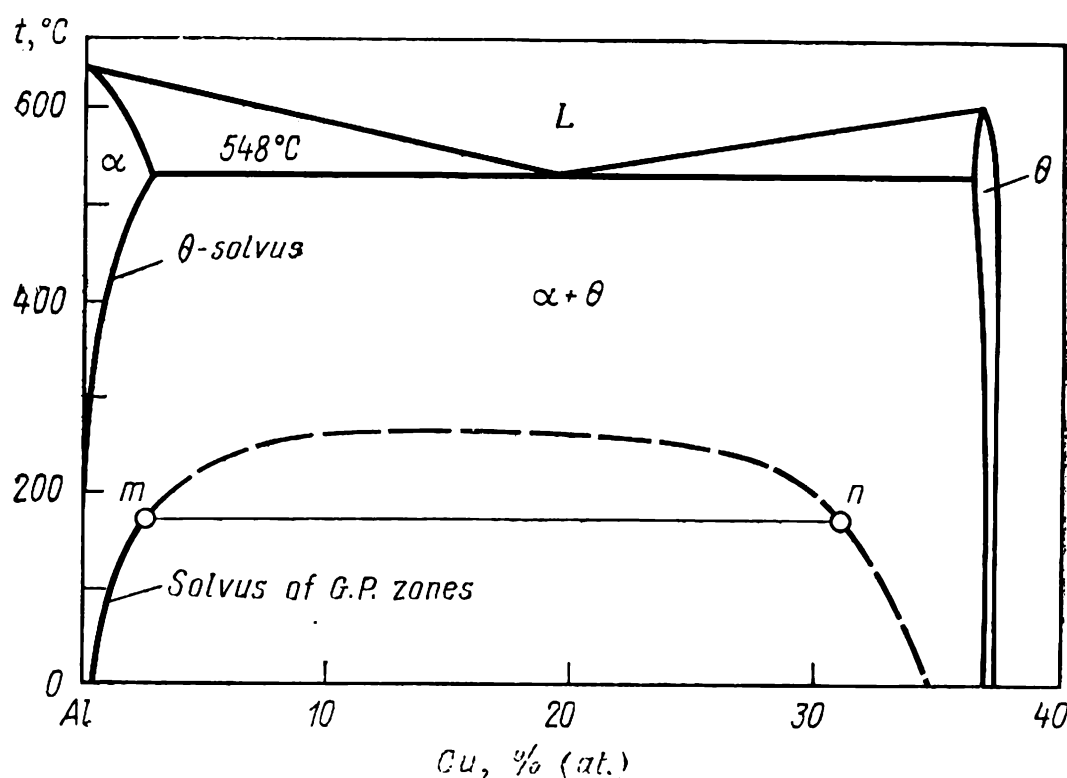


Fig. 176. Al-Cu constitutional diagram with solvus line of G. P. zones (after R. H. Belton and E. C. Rollason) and  $mn$  conode

Thus, G. P. zones may be considered as a second phase which is in metastable equilibrium with the matrix solution. This concept does not contradict the fact that G. P. zones have the same type of lattice as the matrix, since, for instance, in a system form-

ing a continuous series of solid solutions (see Fig. 161a), the stable phase that precipitates under the stratification dome has the same lattice as the matrix. By analogy with the stratification curve relating to a stable equilibrium of two phases with the same lattice (Fig. 161a), a dome-shaped curve of metastable equilibrium of the matrix solution and G. P. zones can be drawn on the constitutional diagram (see the dotted line in Fig. 176). At any temperature, a conode, say  $mn$ , must connect the composition points of G. P. zones (in the right-hand branch of dome-shaped curve) with those of the depleted matrix solution (in the left-hand branch). The depleted matrix solution and G. P. zones are regarded here as metastable phases formed from the initial homogeneous solid solution.

G. P. zones differ from other intermediate phases in the structure of their boundary with the matrix. G. P. zones are fully coherent precipitates, because of which their boundaries are diffuse.

It is clear from the above that the term 'pre-precipitate' as applied to G. P. zones is rather conditional, since they can be considered as coherent precipitates.

The mechanism of formation of G. P. zones has been studied only slightly. The dislocation density in a recrystallized quenched alloy is  $10^7$ - $10^8$   $\text{cm}^{-2}$  and, in the case of heterogeneous nucleation at dislocations, the number of G. P. zones per unit cross-sectional area should be described by a comparable number. Actually, the density of precipitated G. P. zones (the number of zones per unit volume) is of an order of  $10^{18}$   $\text{cm}^{-3}$ , or of an order of  $10^{12}$   $\text{cm}^{-2}$  per unit cross-sectional area. It is assumed that homogeneous nucleation at concentration fluctuations is mainly typical of clusters.

If a G. P. zone is regarded as a phase, then the free energy of an alloy should change on its nucleation as  $\Delta F = -\Delta F_v + \Delta F_s + \Delta F_{el}$  [see formula (25)]. Since the zone and the matrix are coherent, the term  $\Delta F_s$  can be neglected. Then, with a sufficiently high supersaturation, the energy barrier for the nucleation of a G. P. zone must be very low, which explains well why clusters appear immediately after or even during quenching.

Of high practical value is the fact that G. P. zones nucleate easily throughout the whole volume of the matrix solid solution and produce the structure of uniform precipitation with a high density of precipitates (see 4.1.3).

### *Precipitation of Intermediate and Stable Phases*

In most age-hardening industrial alloys a metastable phase can precipitate from the supersaturated solution, the structure of that phase being an intermediate one between the matrix solution

and stable phase (see Table 13). In some systems two intermediate metastable phases can precipitate.

With the formation of a nucleus of any precipitate the total change in the free energy is a sum of three components:

$$\Delta F = -\Delta F_v + \Delta F_s + \Delta F_{el}$$

The free energy of a metastable phase is higher than that of a stable one, so that the formation of a nucleus of the metastable phase in the matrix causes a smaller drop in the volume ('chemical') free energy  $\Delta F_v$ . Precipitation of an intermediate phase instead of a stable one is due to the fact that the former has an appreciably lower surface energy at a boundary with the matrix and, respectively, a smaller increase in  $\Delta F_s$  is required to form

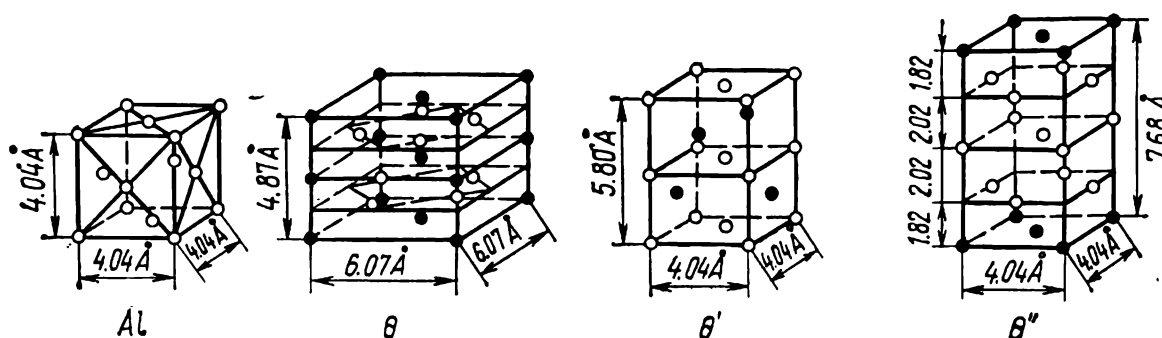


Fig. 177. Elementary cells of stable ( $\theta$ ) and metastable intermediate phases ( $\theta'$  and  $\theta''$ ) that can precipitate from aluminium solution upon ageing of Al-Cu alloys (after E. Hornbogen)

a nucleus (see 2.1.4). Thus, the most important general feature of the structure of all intermediate phases in age-hardening alloys is that this structure ensures at least one coherent boundary between the matrix and precipitate. Intermediate phase precipitates are usually partially or sometimes fully coherent.

Fully and partially coherent precipitates of intermediate phases have been studied in detail in age-hardening Al-Cu alloys. Figure 177 shows an elementary cell of a stable  $\theta$  phase ( $\text{CuAl}_2$ ) and metastable intermediate phases  $\theta'$  and  $\theta''$ . It also shows an elementary cell in aluminium which approximately characterizes the structure of the matrix (neglecting copper atoms in the matrix  $\alpha$ -solution which lower somewhat the lattice period).

The stable  $\theta$ -phase has a tetragonal lattice with periods  $a = 6.07 \text{ \AA}$  and  $c = 4.87 \text{ \AA}$ . The structure of the  $\theta$ -phase in the (001), (010) and (100) planes (and any other planes) differs appreciably from the structure of the matrix, because of which  $\theta$ -phase precipitates are fully incoherent.

The lattice of the intermediate  $\theta''$ -phase is tetragonal, with the phase composition corresponding to  $\text{CuAl}_2$ . In this structure,

part of the planes are occupied by aluminium atoms only, and another part, by copper atoms only. Precipitates of  $\theta''$ -phase are fully coherent, with the (001) plane matching ideally the aluminium matrix (the lattice period of  $\theta''$ -phase  $a = 4.04$  Å, i.e. the same as that of aluminium). Along the (010) and (100) planes, coherence is ensured by a high elastic deformation, since the inter-plane distance is reduced near the layers occupied by copper atoms (1.82 instead of 2.02 Å). The elastic stress field around  $\theta''$ -precipitates plays an important part in strengthening of age-hardening alloy (see 4.1.3).

The maximum thickness of  $\theta''$ -precipitates is 100 Å and their diameter is up to 1500 Å. They are also called G. P.2 zones, in contrast to G. P.1 zones, which have the lattice of the matrix and are designated above simply as G. P. zones. The designation  $\theta''$  is coming into wider use instead of G. P.2, since the lattice of these precipitates differs from that of the matrix.

The lattice of the intermediate  $\theta'$ -phase is tetragonal with the periods  $a = 4.04$  Å and  $c = 5.80$  Å and its composition corresponds to  $\text{CuAl}_2$ . Disc-shaped  $\theta'$ -precipitates have a coherent boundary with the matrix along the (001) plane and the two lattices match ideally. The structural misfit between  $\theta'$  and matrix along the (010) and (100) planes is appreciable and the interface is semicoherent: thin-foil electron microscopy reveals misfit dislocations. Thus,  $\theta'$ -phase precipitates are partially coherent and the elastic stress field around them is smaller than around coherent precipitates of  $\theta''$ -phase and G. P. zones.

Unlike G. P. zones of which homogeneous nucleation is typical, intermediate and stable phases nucleate heterogeneously. The general relationships of heterogeneous nucleation have been discussed in 2.1.3.

Sites of preferable nucleation of intermediate phases (in ageing) are individual dislocations, low-angle boundaries (dislocation arrays), stacking faults and, probably, vacancy clusters. An intermediate phase can also nucleate in G. P. zones.

Stable-phase precipitates preferably form at high-angle boundaries and vacancy clusters. Besides, stable phases can nucleate at intermediate-phase precipitates which have formed earlier.

Nucleation of intermediate-phase precipitates at dislocations is facilitated mainly owing to the fact that the structural misfit between the nucleus and matrix solution is compensated partially or fully due to compression or dilatation near the edge of the extra-plane. Platelets of an intermediate phase nucleate at edge dislocations with such an orientation that the stress fields from these platelets and from dislocations partially subdue one another. With precipitation of a semicoherent particle at a dislocation, the nucleation-inhibiting component  $F_{el}$  in formula (25) is small or



even may be negative, i.e. the elastic energy of dislocation favours the nucleation.

In the case of the nucleation of an incoherent precipitate of a stable phase with a high surface energy, the component  $\Delta F_s$ , but not  $\Delta F_{el}$ , is decisive in formula (25). On the formation of an incoherent precipitate at an intergranular boundary, which is a ready interface, the component  $\Delta F_s$ , which inhibits nucleation, turns to be reduced, i.e. the nucleation of an incoherent precipitate at a high-angle boundary is facilitated.

The surface energy of coherent and semicoherent precipitates is appreciably lower than that of fully incoherent ones and in this case the component  $\Delta F_{el}$ , but not  $\Delta F_s$ , is decisive in formula (25) for their nucleation.

Dislocations and grain boundaries are sites of preferable nucleation also because segregations of atoms of the dissolved element (Cottrell atmospheres) can form at dislocations and equilibrium segregations, at high-angle boundaries. Since intermediate and stable phases are characterized by an increased concentration of an alloying element, they can be more easily formed in matrix portions already enriched in that element.

At grain boundaries, stable-phase precipitates can even appear during quenching. This occurs, in particular, in quenching of some aluminium alloys in boiling water.

If intermediate and stable phases have a higher specific volume than the matrix, it is quite natural that their nucleation is facilitated at vacancy clusters, which can rapidly form in the matrix when the latter is supersaturated with quenching vacancies.

Stacking faults can be sites of heterogeneous nucleation only when the structure of the precipitate is identical to that of the stacking fault. For instance, the intermediate  $\gamma'$ -phase in Al-Ag alloys has a h.c.p. lattice, while a stacking fault in a f.c.c. lattice is known to be a thin interlayer of a h.c.p. lattice. Therefore, the stacking fault band between partial dislocations in the solid solution of silver in aluminium, which is enriched in silver atoms (Suzuki atmosphere), is a ready nucleus of the  $\gamma'$ -phase.

As has been established in 2.1.4, the solubility of metastable phases is always greater than that of stable phases. Let us consider a hypothetical system in which G. P. zones, intermediate  $\beta'$ -phase and stable  $\beta$ -phase can form in the  $\alpha$ -solution.

In Figure 178, curve  $F_\alpha$  gives the free energy versus the composition of the  $\alpha$ -phase which can stratify and form G. P. zones (by analogy with the free energy curve at temperature  $T_3$  in Fig. 161b). A common tangent to the branches of the free energy curve gives the composition of the matrix ( $C_{\alpha-G.P.}$ ) which is in metastable equilibrium with G. P. zones, the latter being regarded

here as a metastable phase having the same lattice as the matrix.

The intermediate  $\beta'$ -phase and stable  $\beta$ -phase have their own crystal lattice which differs from that of the matrix, because of which the free energy curves  $F_{\beta'}$  and  $F_{\beta}$  are not extensions of  $F_{\alpha}$  curve. A common tangent to  $F_{\alpha}$  and  $F_{\beta'}$  curves determines the composition of the matrix ( $C_{\alpha-\beta'}$ ) in metastable equilibrium with the intermediate  $\beta'$ -phase. In a similar manner, we can find the composition of the matrix ( $C_{\alpha-\beta}$ ) in equilibrium with the stable phase. As may be seen  $C_{\alpha-G.P.} > C_{\alpha-\beta'} > C_{\alpha-\beta}$ .

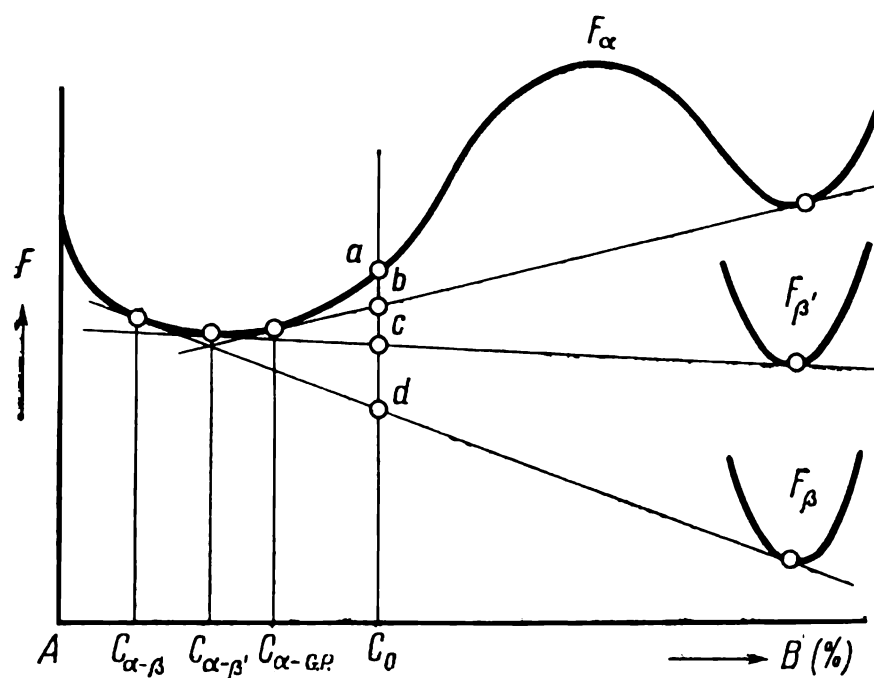


Fig. 178. Dependence of free energy on composition of supersaturated  $\alpha$ -solution which stratifies with the formation of G. P. zones, metastable  $\beta'$ -phase and stable  $\beta$ -phase

Figure 178 corresponding to a definite temperature, will not change qualitatively at other temperatures: the solubility of G. P. zones is always higher than that of the  $\beta'$ -phase, and the latter should be higher than that of the  $\beta$ -phase. In the constitutional diagram, the solvus (solubility) lines of the intermediate  $\beta'$ -phase and G. P. zones must pass below the solubility line of the stable  $\beta$ -phase (Fig. 179). Experimentally determined solvus lines of intermediate  $\theta'$ - and  $\theta''$ -phases and G. P. zones in the Al-Cu system are shown in Fig. 180.

### *Kinetics and Sequence of Precipitation on Ageing*

As may be seen from Fig. 178, the free energy in an alloy of composition  $C_0$  reduces more appreciably on the precipitation of the stable  $\beta$ -phase than on the formation of intermediate  $\beta'$ -phase and G. P. zones, i.e.  $ad > ac > ab$ . This, however, by no means

implies that the probability of formation of a stable phase in ageing is always greater. The axis of ordinates in Fig. 178 gives the values of volume ('chemical') free energy. As has been shown in 2.1.4, the sequence of phase formation is controlled by the energy barrier on nucleation of a new phase, rather than by the attainable level of volume free energy.

The energy barrier of nucleation, i.e. the work of formation of a critical nucleus ( $\Delta F_{cr}$ ) without elastic component, is equal to one-third of the surface energy [see formula (23)]. The surface

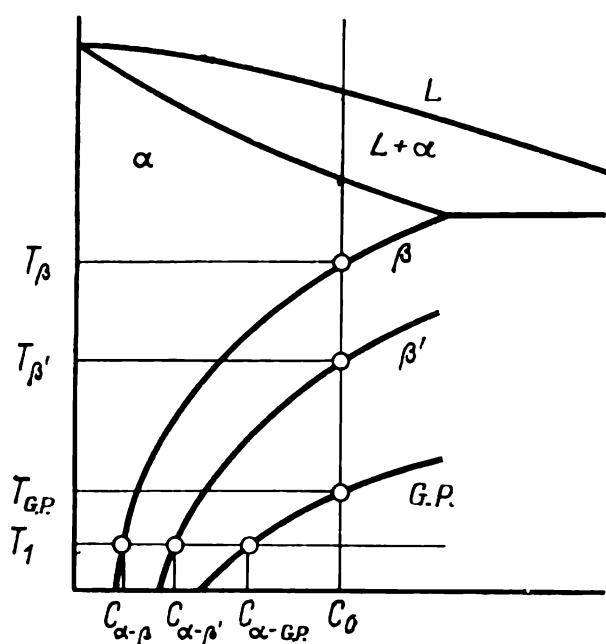


Fig. 179. Constitutional diagram with solvus lines of stable  $\beta$ -phase, meta-stable  $\beta'$ -phase and G. P. zones (schematically)

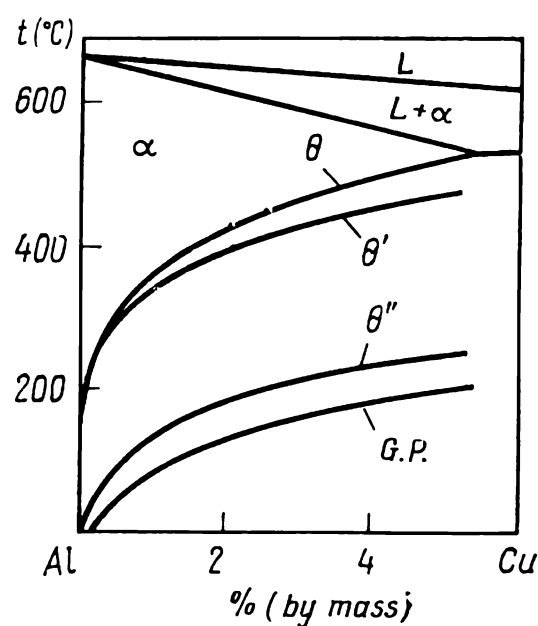


Fig. 180. Solvus lines of G. P. zones and intermediate  $\theta'$ -phase and  $\theta''$ -phase, in Al-Cu system (G. P. zones and  $\theta'$ -phase according to R. H. Beton and E. C. Rollason,  $\theta'$ -phase according to E. Hornbogen)

energy is at its minimum in G. P. zones and at the maximum with incoherent precipitates of a stable phase. Therefore,  $\Delta F_{cr}^{G.P.} < \Delta F_{cr}^{\beta'} < \Delta F_{cr}^{\beta}$ . In ageing, the energy barrier to nucleation of precipitates is formed due to elastic deformation of the lattice, as well as to the formation of an interface. The elastic deformation on nucleation of semicoherent precipitates of  $\beta'$ -phase can be greater than that on nucleation of incoherent precipitates of  $\beta$ -phase. Then, inequality  $\Delta F_{cr}^{\beta'} < \Delta F_{cr}^{\beta}$  can only be satisfied if the gain in surface energy outweighs the possible loss in the elastic strain energy.

The rate of precipitates nucleation in an ageing alloy is determined by a formula similar to formula (24), in which Q is the activation energy of diffusion of the element having the lowest diffusion rate.

A higher rate of nucleation shortens the induction period, i.e. the time before precipitation starts as detected by a given method. With increasing temperature of ageing, the induction period first shortens owing to a higher diffusion mobility of atoms, and then increases due to lower supersaturation of the solid solution relative to a given phase.

G. P. zones, intermediate and stable phases can be characterized by their own C-curves (Fig. 181). The upper branches of

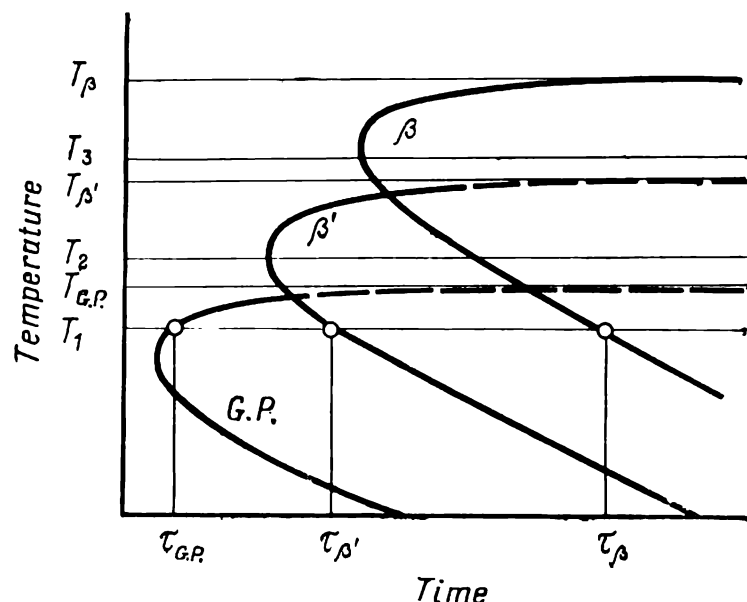


Fig. 181. C-curve for formation of G. P. zones, intermediate  $\beta'$ -phase and stable  $\beta$ -phase on precipitation of supersaturated solution in an aged alloy (schematically)

$T_{G. P.}$ ,  $T_{\beta'}$  and  $T_{\beta}$ —solvus temperatures of precipitates in  $C_0$  alloy in Fig. 179

C-curves approach asymptotically the respective solvus temperatures  $T_{G. P.}$ ,  $T_{\beta'}$  and  $T_{\beta}$ .

For a given temperature of ageing, i.e. at a constant diffusion mobility of atoms, the rate of precipitates nucleation according to formula (24) is only determined by  $\Delta F_{cr}$ . The precipitates having the least work of formation of critical nucleus are first to appear, after which a phase with a larger  $\Delta F_{cr}$  can precipitate. For instance, at ageing temperature  $T_1$ , G. P. zones appear in a period of  $\tau_{G. P.}$ , after which the intermediate  $\beta'$ -phase forms by moment  $\tau_{\beta'}$ , and finally, after a holding time of  $\tau_{\beta}$ , the stable  $\beta$ -phase precipitates. This sequence of formation of precipitates is often written as  $\alpha \rightarrow G. P. \rightarrow \beta' \rightarrow \beta$ .

At ageing temperature  $T_2$ , which is higher than the solvus temperature of G. P. zones, the  $\beta'$ -phase is first to precipitate from the supersaturated solution followed by the precipitation of the  $\beta$ -phase, i.e. by the  $\alpha \rightarrow \beta' \rightarrow \beta$  sequence of precipitates formation. At temperature  $T_3$ , exceeding the solvus temperature of the  $\beta'$ -phase, only the stable  $\beta$ -phase can precipitate from the super-

saturated solution. This obeys the general rule stating that the *lower the degree of supersaturation of the solid solution relative to a stable phase, the smaller is the number of intermediate transformations*. In the above discussion, this rule has been demonstrated by an example of an alloy: the degree of supersaturation of the solution diminished with increasing temperature of ageing. The rule is true for alloys of various composition at a constant temperature of ageing. For instance, if we take a relatively low-alloyed alloy of the composition to the left of point  $C_{\alpha\text{-G.P.}}$  in Fig. 179, then no G. P. zones can form in it at an ageing temperature  $T_1$ .

**Table 13. Precipitation Stages in Supersaturated Solutions of Some Industrial Alloys**

System	Example of alloy	Precipitation stages
Al-Cu	АЛ7	G. P. zones $\rightarrow \theta'' \rightarrow \theta' \rightarrow \theta$ ( $\text{CuAl}_2$ )
Al-Mg	АЛ8	G. P. zones $\rightarrow \beta' \rightarrow \beta$ ( $\text{Al}_3\text{Mg}$ )
Al-Cu-Mg	Д16	G. P. zones $\rightarrow S' \rightarrow S$ ( $\text{Al}_2\text{Cu}_2\text{Mg}$ )
Al-Cu-Mg-Fe-Ni	AK4-1	G. P. zones $\rightarrow S' \rightarrow S$ ( $\text{Al}_2\text{CuMg}$ )
Al-Mg-Si	АД31	G. P. zones $\rightarrow \beta' \rightarrow \beta$ ( $\text{Mg}_2\text{Si}$ )
Al-Zn-Mg	1915	G. P. zones $\rightarrow \eta' \rightarrow \eta$ ( $\text{MgZn}_2$ ) $\rightarrow T(\text{Al}_2\text{Mg}_3\text{Zn}_3)$
Al-Zn-Mg-Cu	B95	G. P. zones $\rightarrow \eta' \rightarrow \eta$ ( $\text{MgZn}_2$ )
Cu-Be	Бр.Б2	G. P. zones $\rightarrow \gamma' \rightarrow \gamma$ ( $\text{CuBe}$ )

Table 13 gives the sequences of precipitation in various alloys as the time of ageing is increased or the temperature of ageing is increased at a constant holding time. The table actually gives not the sequence of precipitation in industrial ageing, but the probable number of precipitation stages within a wide range of temperatures and holding times on ageing, including the conditions not used industrially. For instance, the ageing conditions for most alloys are so chosen as to avoid precipitation of the stable phase (see 4.1.3 and 4.1.4).

For the theory and practice of ageing (see 4.1.5), it is essential to know in what way more stable precipitates nucleate and grow if less stable precipitates formed earlier are already present in the metal. The statement of the process of supersaturated solution precipitation  $\alpha \rightarrow \text{G. P.} \rightarrow \beta' \rightarrow \beta$  only indicates the time (at constant temperature) or temperature (at constant holding time) sequence of the appearance of various precipitates. This formula should not be understood as if G.P. zones always transform due to lattice rearrangement into  $\beta'$ -phase and the latter, into  $\beta$ -phase.

There are three possible ways for the formation of more stable precipitates. The first is the above-discussed direct transforma-

tion of less stable precipitates into stabler ones, i.e. a change in the type of lattice, allotropic transformation within the volume of a precipitate without the participation of the matrix. This method is only feasible at a low difference in the structures of precipitates and is, therefore, used only rarely. Experimental data obtained for ageing Al-Cu alloys can be treated as the case of direct rearrangement of G. P. zones into  $\theta''$ -phase precipitates, which correspondingly have been called G. P.2 zones.



Fig. 182. Structure of Al + 15% Ag alloy quenched from 520 °C and aged at 160 °C for 10 days; thin-foil electron micrograph,  $\times 22\,500$  (after J. B. Clark)

The second method is the nucleation of a  $\beta'$ -phase at G. P. zones and the growth of  $\beta'$ -precipitates in the matrix, and similarly, the nucleation of  $\beta$ -phase at  $\beta'$ -precipitates and the growth of  $\beta$ -particles in the matrix.

The third method is an independent nucleation of a stabler phase in the matrix far from the precipitates of a less stable phase and far from G. P. zones.

Above the solvus temperature of the intermediate phase, the stable  $\beta$ -phase can precipitate only from the matrix. It is still unpredictable what will be the sites of its preferable nucleation at lower temperatures of ageing, when the intermediate phase has already precipitated. For instance, the  $\theta$ -phase ( $\text{CuAl}_2$ ) in Al-Cu al-

loys at early stages of precipitation forms at grain boundaries of the matrix and at later stages at interfaces between the  $\theta'$ -phase and aluminium solution. The  $\theta'$ -phase in the same alloys precipitates at dislocations at earlier stages and at the  $\theta''$ -phase precipitates, at later stages. There is some experimental evidence that the  $\theta''$ -phase forms not through rearrangement and development of G. P. zones, but precipitates directly from the matrix.

Numerous data show that  $\eta'$ -phase precipitates in Al-Zn-Mg alloys nucleate during artificial ageing at the G. P. zones which have formed on natural ageing. This phenomenon is used for the designing of ageing conditions (see 4.1.5).

As has been established in 2.1.4, the formation of a stabler phase must cause dissolution of a less stable phase. This relationship is most essential for ageing of alloys. The concentration

of the matrix solution near G. P. zones is  $C_{\alpha-G.P.}$  (see Figs. 178 and 179). Upon the formation of the intermediate  $\beta'$ -phase a concentration  $C_{\alpha-\beta'}$  of the solution establishes at its boundary. Therefore, a concentration gradient  $C_{\alpha-G.P.} = C_{\alpha-\beta'}$  forms in the matrix. The equalizing diffusion in the matrix, which proceeds in the direction of this gradient, makes the solution supersaturated relative to the  $\beta'$ -phase and undersaturated relative to G. P. zones. The  $\beta'$ -phase precipitates will therefore grow owing to the simultaneous dissolution of G. P. zones.

Similarly, upon the formation of a stable  $\beta$ -phase, the concentration of the solution at the boundary with that phase will be  $C_{\alpha-\beta} < C_{\alpha-\beta'}$  and  $\beta$ -precipitates will grow due to the simultaneous dissolution of the  $\beta'$ -phase.

In Figure 182, grey regions are spherical G. P. zones that have formed earlier; dark lines are needles of the  $\gamma'$ -phase that have precipitated later; bright fields near them are portions of the matrix in which the G. P. zones were dissolved during growth of the  $\gamma'$ -needles.

### *Precipitate-free Zones*

During ageing of some alloys (aluminium, titanium, iron, nickel, etc.), no precipitation takes place near grain boundaries of the matrix solution, so that precipitate-free zones are seen clearly (Figs. 183 and 184). In aluminium alloys the width of these zones is usually a fraction of a micron and the zones can only be detected by electron microscopy. In titanium  $\beta$ -alloys, precipitate-free zones formed on ageing are of a width of a few microns and can be seen in the optical microscope.

The existence of boundary zones which are free of precipitation products does not contradict the concept that grain boundaries facilitate the nucleation of precipitates of a new phase. The point is that we consider a zone near a boundary rather than the boundary proper. In many cases, as, for instance, the one shown in Fig. 183, precipitates form directly at a grain boundary, while a precipitate-free zone forms near that boundary.

There are two causes that can explain the formation of precipitate-free boundary zones. If the precipitation starts at grain boundaries and there nucleates a new phase that is enriched in one of the components of the alloy, this growing phase 'sucks' that component from the boundary zone. The later precipitation in the bulk of the grain cannot occur in a certain zone adjacent with the precipitate, since the matrix solution turns to be less supersaturated in that zone (see the widened portion of the zone near the precipitate in Fig. 183). This explanation is unsuitable for zones of non-precipitated solution at boundaries at which there

are no precipitates (see the narrow zone extending along the 'clean' boundary in Fig. 183).

A more common cause for the appearance of precipitate-free zones is the depletion of boundary zones in vacancies, owing to the sink to the boundary. The equilibrium concentration of thermal vacancies diminishes sharply (by an exponential law) with reducing temperature. In quenching, this process has no time to de-

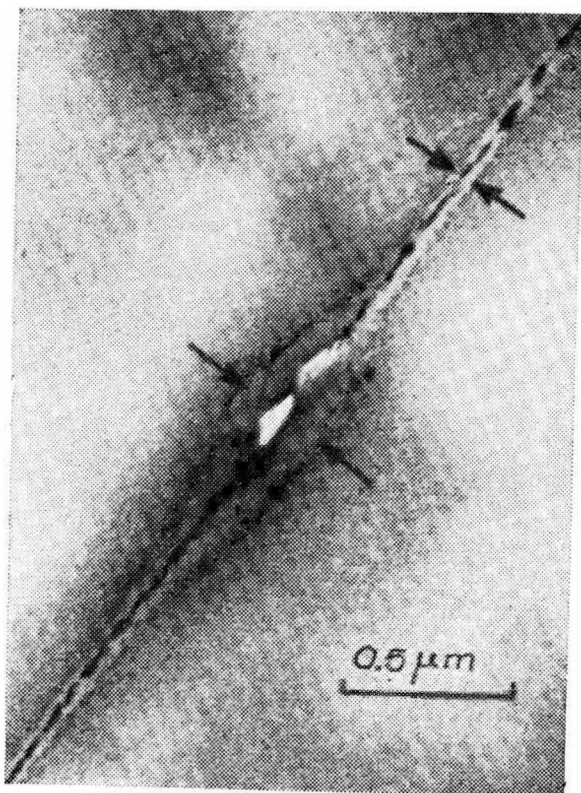


Fig. 183. Precipitate-free boundary zone (bright) in Al + 5.9% Zn + 2.9% Mg alloy aged at 180 °C for 3 h (after P. N. T. Unwin, G. W. Lorimer and R. B. Nicholson)

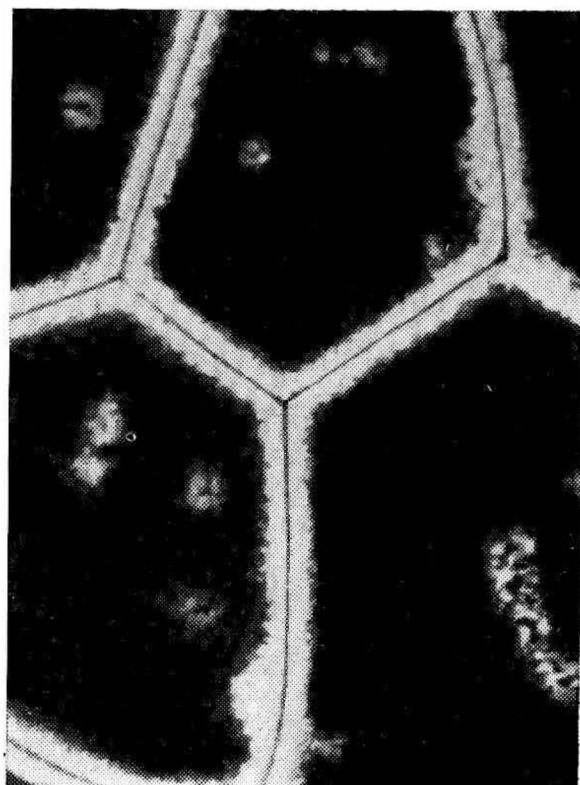


Fig. 184. Precipitate-free boundary zones (bright) in titanium alloy BT15 quenched to β-phase from 900 °C and aged at 450 °C for 15 h. The dark background is strongly etchable β-phase from which disperse α-phase has precipitated,  $\times 200$  (after I. I. Novikov, O. V. Kasparova and I. S. Pol'kin)

velop to a sufficient extent and the lattice becomes largely supersaturated with vacancies. At the initial stage of quenching, when the temperature is still high and the vacancies are quite mobile, they move to grain boundaries which serve as sinks for vacancies. As a result, the concentration of vacancies in a certain zone near grain boundaries decreases relative to the remaining portion of the grain where the concentration of excess vacancies remains at a high level (Fig. 185).

As has been noted earlier, vacancy clusters facilitate the nucleation of precipitates, especially when the specific volume of the



solution increases on precipitation. Quenching vacancies also promote the diffusion growth of nuclei of a new phase. It may be assumed that, for a certain degree of supersaturation of the solution with an alloying element, i.e. for a certain ageing temperature  $T_1$ , the process of precipitation in a given time takes place only in that portion of the grain where the concentration of vacancies is not less than a certain critical value  $C_1$ .

If curve 1 in Fig. 185 describes distribution of the vacancy concentration over the cross-section of a grain of the matrix solution in a quenched alloy, then, for a given temperature of ageing  $T_1$ , no precipitation will take place in the boundary zone of a width of  $ob_1$ , since the concentration of vacancies there is lower than  $C_1$ . At a lower temperature of ageing, say  $T_2$ , the solution is more supersaturated with the alloying element than at  $T_1$ , so that precipitation can proceed at a lower concentration of vacancies (critical concentration of vacancies  $C_2 < C_1$ ). Accordingly, as the temperature of ageing lowers, the precipitation-free zone must get narrower:  $ob_2 < ob_1$ .

At higher temperatures of heating for quenching, the equilibrium concentration of vacancies increases and the concentration gradient near a sink (grain boundary) becomes more pronounced (curve 2 in Fig. 185). Thus, for the same temperature of ageing and respectively the same critical concentration of vacancies, the zone of unprecipitated solution becomes narrower with increasing temperature of quenching ( $ob_4 < ob_1$ ).

If quenching is slowed down, then a greater number of vacancies have time to move to a grain boundary (compare curves 2 and 3), so that the precipitate-free zone becomes wider ( $ob_3 > ob_4$ ).

Thus, precipitate-free boundary zones can be narrowed by increasing the temperature of quenching, accelerating the quenching rate or decreasing the temperature of ageing. Plastic deformation of a quenched alloy before ageing, which favours precipitation in the supersaturated solution, can fully preclude the formation of these zones.

The aforementioned regularities governing the effect of various factors on the width of precipitate-free zones were verified more than once in experimental studies of aluminium and titanium al-

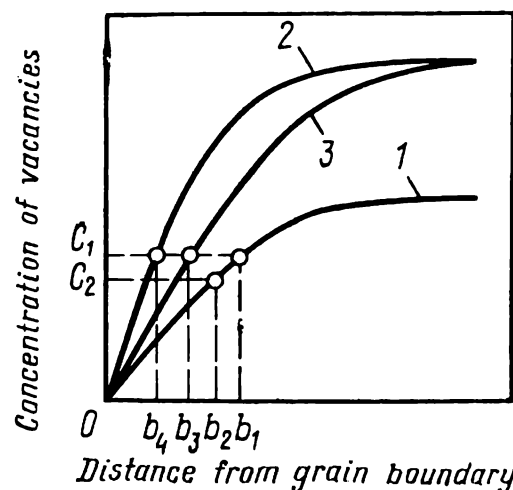


Fig. 185. Distribution of vacancy concentration near a grain boundary at various conditions of quenching

1—quenching from  $T_1$ ; 2—quenching from  $T_2 > T_1$ ; 3—quenching from  $T_2$  followed with slow cooling

loys. The effect of these zones on behaviour of age-hardened alloys in many cases still remains unclear. For instance, there have been some conflicting views on the role of these zones in high-strength alloys of the Al-Zn-Mg system. At one time, it was emphasized persistently that precipitate-free zones are harmful. Firstly, owing to their lower strength, they should have localized plastic deformation and served as sources of premature fracture. Secondly, localized dissolution of plastically deformed zones serving as the anode relative to the remaining grain, could have accelerated intergranular cracking in stress corrosion. Later experimental results have shown, however, that widening of precipitate-free boundary zones increases both the ductility (on lowering the temperature of heating for quenching) and the resistance to stress corrosion (with slower quenching). The gain in ductility can be explained by the fact that the softer boundary zone can more fully relieve the stresses that concentrate in places where a slip band is stopped by a grain boundary. The wider this softer zone is, the more fully it can relieve the stresses and, therefore, impede the formation and propagation of cracks.

We are still unable to draw final conclusions on the role of precipitate-free boundary zones, since a change in their width, which may be caused by varying the conditions of heat treatment, can also affect other structural characteristics and thus influence the properties of an alloy.

### *Particle Coarsening in Ageing*

In the course of continuous precipitation from the solid solution, the total volume of precipitates increases, while the concentration of the alloying element decreases. When the composition of the matrix solution approaches the equilibrium at a given temperature of ageing, the total volume of precipitates stops changing, but the structure of the age-hardened alloy is unstable, i.e. the disperse precipitates are liable to coarsening, or Ostwald ripening.

Precipitates in an age-hardened alloy are separated from each other by the matrix lattice and thus cannot coarsen in the same way as, for instance, coalesce mercury droplets under the action of surface tension forces. The driving force of particle coarsening in ageing is the difference of free energies between finer and coarser particles. The size of precipitates in an age-hardened alloy is different owing to different local conditions of particle growth. Finer precipitates have a greater proportion of atoms at the surface (relative to all the atoms in a particle), and therefore, a higher mean free energy per 1 g-atom of a precipitate.

In Figure 186, the free energy curve for finer particles of the  $\beta$ -phase ( $F_{\beta}^{sm}$ ) passes below the free energy curve of coarser particles of the same phase ( $F_{\beta}^l$ ). As may be seen from the figure, the concentration of the  $\alpha$ -solution in equilibrium with finer precipitates of the  $\beta$ -phase ( $C_f$ ) must be higher than that in equilibrium with coarser precipitates ( $C_c$ ). This follows from equation (30).

Thus, there exists a concentration gradient of an alloying element in the matrix solution between precipitates of different size

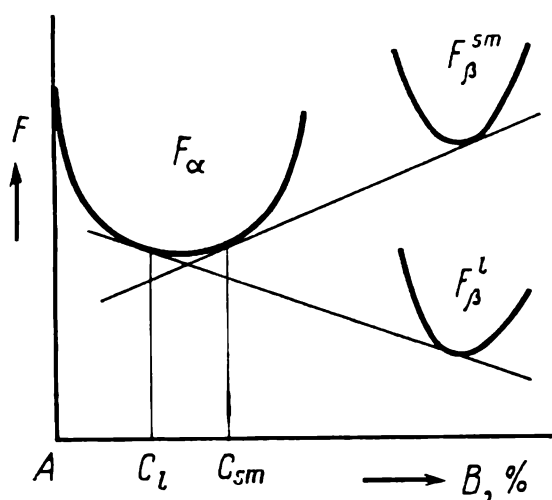


Fig. 186. Effect of composition on free energy of  $\alpha$ -solution ( $F_{\alpha}$ ) and free energy of large ( $F_{\beta}^l$ ) and small ( $F_{\beta}^{sm}$ ) precipitates of  $\beta$ -phase

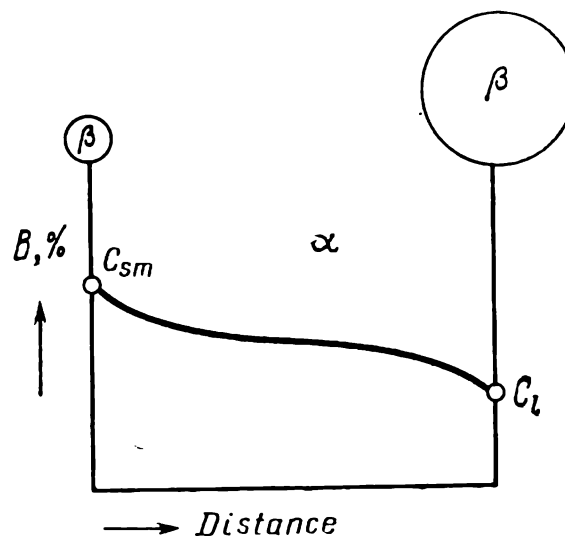


Fig. 187. Concentration gradient of an alloying element in  $\alpha$ -solution between small and large precipitates of  $\beta$ -phase ( $C_l$  and  $C_{sm}$  see in Fig. 186)

(Fig. 187). This gradient is directly responsible for particle coarsening. The equalizing diffusion lowers the concentration of the solution at a boundary with a fine precipitate, the latter is dissolved and thus the equilibrium concentration of the solution is maintained at this boundary. The same diffusion increases the concentration of the solution at a boundary with a large precipitate, the solution becomes supersaturated and causes the  $\beta$ -phase to precipitate and thus the equilibrium concentration  $C_c$  is maintained. The  $\beta$ -phase precipitates at the ready surface of a coarse particle, i.e. the latter grows while a fine particle is being dissolved up to the full disappearance. Consequently, *particle coarsening in ageing takes place owing to the transfer of matter through the matrix solution (due to the concentration gradient) with dissolution of finer and growth of coarser precipitates.*

As the time of ageing  $\tau$  increases, the average radius  $\bar{r}$  of particles in particle coarsening varies according to the Lifshits-Slezov equation:

$$\bar{r}^3 = \bar{r}_0^3 + B\tau \quad (34)$$

where  $\bar{r}_0$  is the average initial radius of precipitates prior to particle coarsening and  $B$  can be expressed by the formula

$$B = \frac{8D\gamma C_\infty V^2}{9kT} \quad (35)$$

where  $D$  = diffusion coefficient

$\gamma$  = surface energy at the boundary between precipitate and matrix

$C_\infty$  = equilibrium concentration of the matrix solution at the plane interface with the excess phase

$V$  = volume of precipitate per one atom of the dissolved element

The rate of particle coarsening increases with  $D$  and  $\gamma$ . The diffusion coefficient increases exponentially with temperature, because of which the rate of particle coarsening can increase appreciably with increasing temperature of ageing. This is also favoured by the fact that  $C_\infty$  increases with temperature. Surface-active additions, which lower  $\gamma$  at the boundary between the matrix and precipitate, can decrease the rate of particle coarsening.

Particle coarsening is the sole structural change in an age-hardened alloy after the formation of stable-phase precipitates. This by no means implies that only stable-phase precipitates are capable of coarsening. Intermediate-phase precipitates and Guinier-Preston zones can equally coarsen in a similar manner, since the concentration of the solution that is in metastable equilibrium with them depends on the size of respective precipitates (including G. P. zones). This is why particle coarsening can be observed at various stages of precipitation in a solution, though the final stage of precipitation is of especially high practical interest.

#### 4.1.3. VARIATIONS OF ALLOY PROPERTIES ON AGEING

##### The Nature of Hardening on Ageing

The hardening effect of ageing is due to impediment of dislocations by precipitates formed in the supersaturated solid solution. The mechanisms of this hardening may be as follows: (a) impediment of dislocations by the elastic stress field around precipitates in the matrix; (b) 'chemical' hardening owing to precipitates being sheared by dislocations; and (c) hardening through dislocations circumventing precipitated particles.

An elastic stress field inevitably appears in the matrix upon formation of coherent or semicoherent precipitates, since the coherence of the lattices is ensured by elastic deformation of precipi-

tates at the interface (see Fig. 166a and b). The elastic stresses are greater at a larger size misfit between the structures of the matrix and a precipitate, a higher elastic modulus of the matrix or a greater surface of the coherent boundary. To move a dislo-

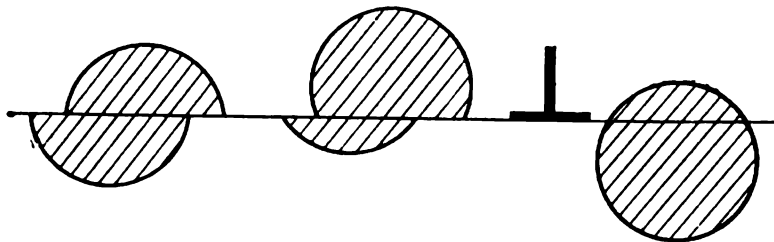


Fig. 188. Shear of precipitates by a gliding edge dislocation (schematically)

cation through the elastically deformed matrix, a stress must be applied which is greater than the mean stress of the elastic strain field around the precipitates. The corresponding hardening is a result of long-range effect of precipitates on dislocations.

'Chemical' hardening is a result of short-range interaction between dislocations and precipitates. When passing through precipitates, dislocations shear them, as it were (Fig. 188), and the latter are deformed together with the matrix.

The lattice of a precipitate is not identical with that of the matrix, even with fully coherent precipitates. When a dislocation enters with its Burgers vector into a precipitate, it disturbs the arrangement of atoms along the slip plane. The greater is the difference between the structure of the precipitate in the shear plane and that of the matrix in the same plane, the more disturbed will be the arrangement of atoms in the precipitate and the higher will be the stress required to shear the precipitate by dislocation. With a coherent precipitate (G. P. zone), the surface energy in the 'shear' plane is of an order of  $10^2$  erg/cm<sup>2</sup>, while that for an incoherent precipitate is of an order of  $10^3$  erg/cm<sup>2</sup> (i.e. as with a high-angle boundary).

The shear modulus of a precipitate is usually higher than that of the matrix. The more hard is a precipitated particle, the more difficult it is for a dislocation to cut it.

Another cause of dislocation impediment is the formation of edges in a sheared precipitate (Fig. 188) and a respective increase in its surface, which is linked with an excess of energy.

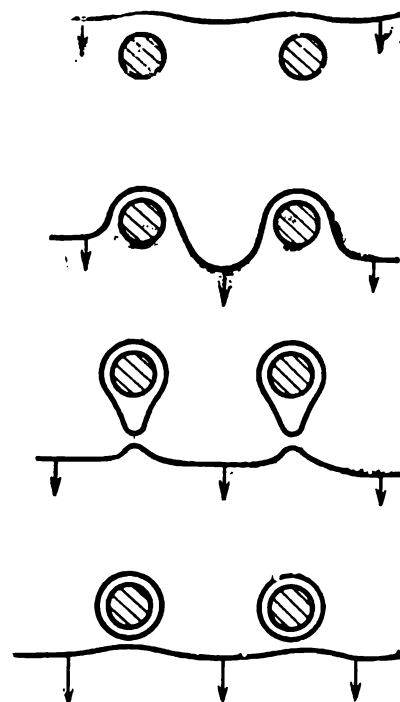


Fig. 189. Squeezing of a dislocation between precipitates with the formation of dislocation rings (schematically)

**Hardening through circumvention of precipitated particles by dislocations** appears when dislocations cannot shear the precipitates. One of the ways is 'squeezing' of a dislocation between two precipitated particles (Fig. 189). For this to occur, the stress applied must be increased so as to bend the dislocation between the particles. The portions of the dislocation at both sides of the precipitate become bent, join and form a dislocation ring around the particle (Fig. 189). Upon detaching from a ring, a dislocation continues to glide in the matrix.

The critical stress required for 'squeezing' is inversely proportional to the distance  $l$  between precipitated particles:

$$\tau_{cr} = \frac{Gb}{l} \quad (36)$$

where  $G$  = shear modulus of the matrix

$b$  = Burgers vector of the dislocation

Dislocations can also circumvent precipitates by cross-slip. The stress needed to overcome an obstacle in this way decreases with increasing temperature. Dislocation climb at elevated temperatures also helps dislocations to circumvent precipitated particles.

### **Hardening Effect on the Formation of Various Types of Precipitate**

The magnitude of hardening effect in ageing depends on the type of precipitates, their structure, size, shape, pattern and density of distribution, the degree of misfit between the lattices of matrix and precipitate, and temperature of testing.

Since G. P. zones nucleate homogeneously, their distribution density is rather high, and the spacing between them is usually so small (of an order of  $10^2$  Å) that the stress required for dislocation to circumvent them is appreciably higher than that needed for shear. Therefore, G. P. zones can cause 'chemical' hardening. If the difference in atomic diameters between the solute and the solvent is not large, the elastic strain energy of the matrix is small and 'chemical' hardening is the sole factor responsible for age-hardening (an example are Al-Ag and Al-Zn alloys). With a large difference in atomic diameters, as for instance, in Al-Cu and Cu-Be alloys, a field of appreciable elastic stresses forms around G. P. zones, which also contributes to dislocation hindering by G. P. zones and age-hardening.

Semicoherent precipitates of an intermediate phase can produce a strong hardening effect if the spacing between them is small. All other things being equal, the stress field around semicoherent precipitates is weaker than that around coherent ones, and therefore, the corresponding hardening component in ageing

must be lower. Intermediate-phase precipitates, however, differ more appreciably in their structure from the matrix than G.P. zones, so that their atom arrangement is disturbed more by shearing dislocations. Consequently, an intermediate-phase precipitate is capable of causing a stronger 'chemical' hardening than a G.P. zone, which with a sufficiently high density of precipitates can give a higher strength in an age-hardened alloy compared with the zone stage of precipitation. If, however, the density of intermediate-phase precipitates is substantially lower than that of G.P.

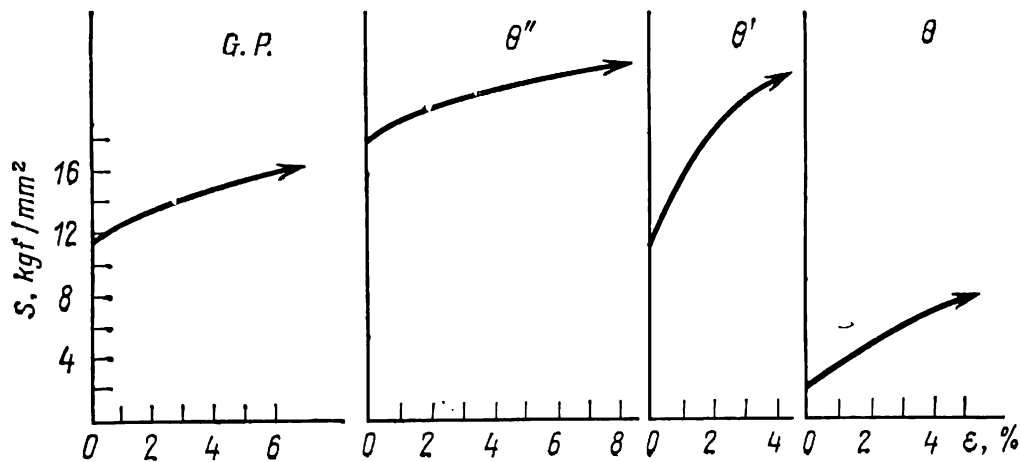


Fig. 190. Actual stress-elongation curves for Al-4% Cu alloy with monocrystalline matrix and various types of precipitate (after M. E. Fine, J. G. Byrne and A. Kelly)

zones, the stress required to squeeze a dislocation between precipitates may be less than that needed for shearing G.P. zones. In that case the strength of the alloy at the stage of intermediate-phase precipitation will be lower than that of the zone stage.

Stable phase precipitates are usually incoherent with the matrix and have no elastic stress fields, whereas the spacings between them are quite large, so that relatively low stresses are required for dislocations to circumvent them. This is why stable-phase precipitates usually give an appreciably lower hardening effect on ageing than G.P. zones of metastable-phase precipitates.

Let us use Al-Cu alloys as an example for discussing the role of the type of precipitate. Figure 190 shows curves of actual creep stresses during deformation of crystals of the supersaturated solid solution of Al + 4% Cu in which various types of precipitate, i.e. G.P. zones,  $\theta''$ -,  $\theta'$ - and  $\theta$ -phases, have been formed by ageing. The figure enables us to compare the initial (critical) creep stresses and the capability of the alloy of being strain-hardened by the growth of creep stresses with the degree of deformation (determined by the slopes of the curves).

An alloy with G.P. zones and coherent  $\theta''$ -phase precipitates can be characterized by a high initial creep stress and a low

strain-hardening. The actual stress curves for this alloy are not steep.

In single crystals, for which test results are shown in Fig. 190, the spacing between centres of G.P. zones and that between  $\theta''$ -phase precipitates are respectively 150 and 250 Å. Substitution of the latter in formula (36) reveals that the critical stress required to squeeze a dislocation turns to be several times the experimentally found initial creep stress. Electron-microscopic studies of Al + 4% Cu alloy have shown that dislocations do not squeeze between G.P. zones and  $\theta''$ -phase precipitate, but shear them.

Precipitates of  $\theta''$ -phase can more strongly than G.P. zones increase the level of creep stresses in Al-Cu alloy, since the elastic stresses in the matrix around them are higher [compare the structural misfit of the lattices of matrix and  $\theta''$ -phase along (010) and (100) planes in Fig. 177].  $\theta''$ -phase precipitates, which differ more appreciably in the structure from the matrix, must cause a higher 'chemical' hardening, since their atom arrangement is disturbed by shearing dislocations more than that of G.P. zones.

The initial creep stress in an alloy with  $\theta'$ -phase precipitates is lower than that in one with  $\theta''$ -phase, and the strain-hardening is respectively greater (the actual stress curve in Fig. 190 is more steep). An explanation to this may be that the spacings between  $\theta'$ -phase precipitates have been sufficiently large, so that dislocations could squeeze between them at a lower stress than that required for shear. As the deformation ratio increases, the number of dislocation rings left behind by a gliding dislocation also increases. These rings impede the squeezing of next dislocations, which explains well why the resistance to deformation increases intensively with an increase in the deformation ratio.

A similar picture is found in alloy with stable  $\theta$ -phase precipitates. Since these precipitates are fully incoherent with the matrix (see Fig. 177) and the spacing between them is also greater (of an order of 1  $\mu\text{m}$ ), the initial creep stress in a alloy with the stable  $\theta$ -phase ( $\text{CuAl}_2$ ) is substantially lower than that in an alloy with G.P. zones of  $\theta''$ - and  $\theta'$ -phase precipitates (Fig. 190). The coefficient of strain-hardening (the slope of curves) for the  $\theta$ -phase alloy is higher than for those with G.P. zones or  $\theta''$ -phase, owing to accumulation of dislocation rings around precipitates.

### Effect of Time and Temperature of Ageing on Mechanical Properties of Alloys

Considering the role of various types of precipitate in hardening and the sequence of precipitation stages in a supersaturated solution (see 4.1.2), we can analyse the effect of ageing time at various temperatures on the mechanical properties of an alloy.



In the most general case the ultimate strength, yield strength and hardness of an alloy increase with ageing time, reach a maximum, and then diminish (see curves  $T_2$  and  $T_3$  in Fig. 191).

The process before attaining the maximum of strength properties (in the ascending branch of curves) is called *hardening ageing* and that to the right of the maximum (in the descending branch), *softening ageing*, or *overageing*; the latter term implies that the metal is softened relative to the state on ageing for a shorter time. However, when compared with the initial quenched alloy (the starting point at the axis of ordinates), an overaged alloy can be appreciably stronger.

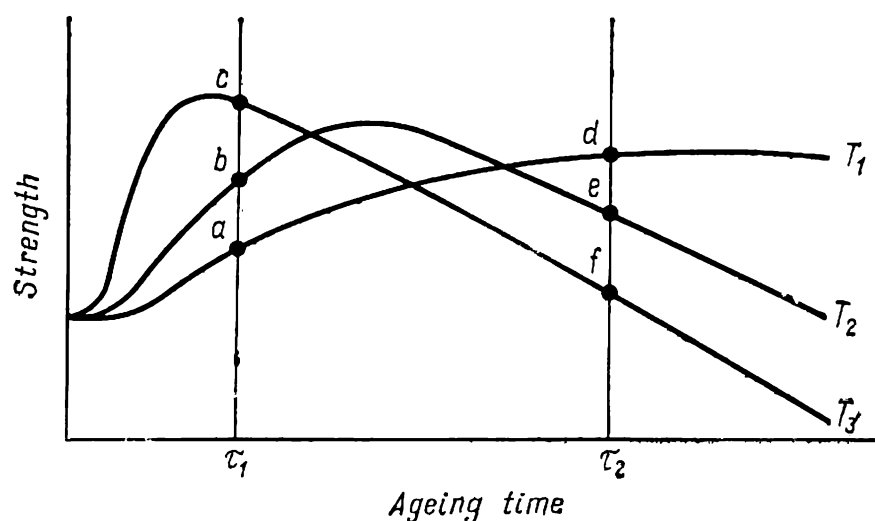


Fig. 191. Effect of ageing time at various temperatures ( $T_1 < T_2 < T_3$ ) on strength properties

The hardening along the ascending branch of curve on increasing the ageing time can be due to various causes. Firstly, cases are possible where the density of precipitates at the stage of hardening ageing is so large that dislocations cannot circumvent precipitates and shear them (provided that the stress applied is sufficiently high). In such cases an increase in the strength properties with the increasing time of ageing is due to a higher 'chemical' hardening and impediment of dislocations by elastic stress field owing to coarsening of precipitate particles (in particular, of G. P. zones, see Fig. 175), an increased density of distribution of the precipitates in the matrix, and the appearance of hard-to-shear particles of a stabler phase (for instance,  $\theta'$ -phase in addition to  $\theta''$ -phase in Al-Cu alloys).

Secondly, cases are possible where dislocations are squeezed between precipitates at the stage of hardening ageing. Then the rise in strength properties at longer time of ageing is due to increasing density of precipitates as the precipitation is being developed, and, correspondingly, to an increase in the critical stress for dislocation squeezing [see formula (36)].

In an overaged alloy, dislocations do not shear precipitates, but only circumvent them at lower stresses than those needed for shear. The loss in strength properties as hardening ageing changes to overageing may be due to various causes. One of them is an increased spacing between earlier formed precipitates, which is due to particle coarsening. Another probable cause is replacement of less stable precipitates with stabler ones, which may be characterized by a lower number of particles per unit volume of the matrix. A third cause of overageing is lessening or disappearance of the elastic stress field in the matrix when coherent precipitates are replaced first with semicoherent and then with incoherent ones.

The maximum of hardening in various alloys or at different temperatures of ageing in the same alloy can correspond to different structural states. It is impossible to predict, without experimental tests, what will be the particular structure of maximum hardening in a given alloy. The answer depends on what stages of precipitation are likely to occur in the alloy at a given ageing temperature, what is the structure of the precipitates and the density of each type of particles, and on some other factors. One can only state that the maximum hardening is obtained in an alloy in which G. P. zones and precipitates of an intermediate metastable phase, or only the latter (with a high density of their distribution), have formed inside grains of the supersaturated solution.

Stable phases usually precipitate at the stage of overageing. Their formation is undesirable if the alloy should be used in the maximum hardened state. It may be noted in that connection that the term '*hardening phase*' is conditional. For instance, the S-phase ( $\text{Al}_2\text{CuMg}$ ) in duralumins,  $\eta$ -phase ( $\text{MgZn}_2$ ) in Al-Zn-Mg alloys, type 1915, and  $\gamma$ -phase ( $\text{CuBe}$ ) in beryllium bronzes are considered hardening phases. But the formation of these stable phases in the alloys indicated can cause overageing and softening, and therefore, be harmful. An appreciably higher strength is obtained through the formation of G. P. zones and intermediate  $S'$ -,  $\eta'$ -, and  $\gamma'$ -phase precipitates. Since, however, we cannot say without making structural studies, which of the precipitates will give the maximum hardening effect, whereas the stable phase is known from the constitutional diagram, this phase is conditionally termed hardening phase, though actually the ageing can be done under the conditions where the stable phase proper does not altogether precipitate.

In alloys of aluminium with 2 and 3 per cent Cu, a structure with only  $\theta'$ -phase precipitates corresponds to the maximum of hardness upon ageing at  $190^\circ\text{C}$  (Fig. 192). The rise in hardness on increasing the ageing time of these alloys at  $190^\circ\text{C}$  is evi-

dently due to an increase in the density and size of the precipitates, while overageing is due to a strong particle coarsening which increases the spacing between precipitated particles.

In alloys of aluminium with 4 or 4.5 per cent Cu aged at the same temperature, the maximum of hardening corresponds to a structure with  $\theta''$ - and  $\theta'$ -phase precipitates (Fig. 192). Coherent  $\theta''$ -precipitates form stronger elastic strain in the matrix than do semicoherent  $\theta'$ -phase precipitates. But  $\theta'$ -phase precipitates are

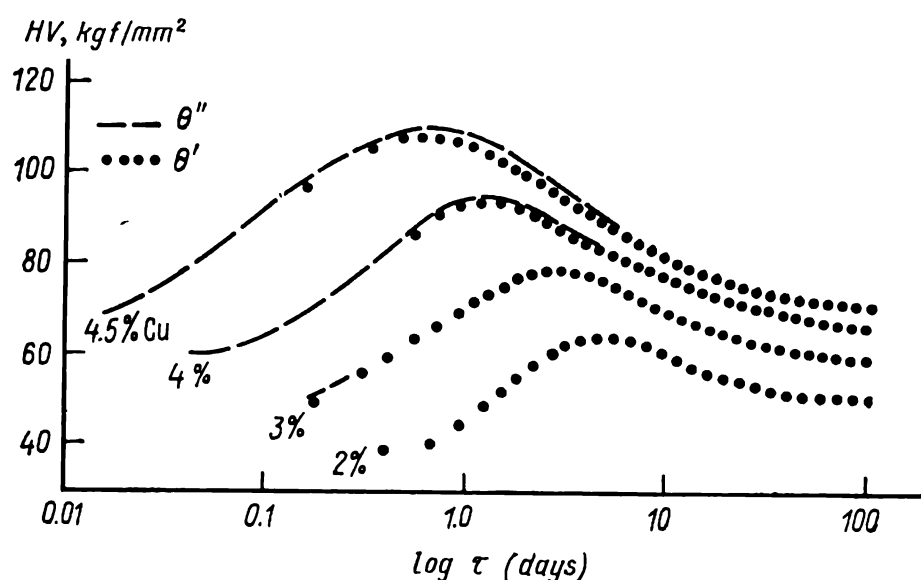


Fig. 192. Effect of time of ageing at 190 °C on hardness in aluminium alloys with 2, 3, 4 and 4.5% Cu at 20 °C (after J. M. Silcock, T. J. Heal and H. K. Hardy)

appreciably more difficult to be sheared by dislocations. Because of this, a certain combination of  $\theta''$ - and  $\theta'$ -phase precipitates can ensure the maximum strength of an age-hardened alloy. By a rough estimate, the maximum of hardness is attained when ageing results in the formation of 70 per cent of  $\theta''$ -precipitates and 30 per cent of  $\theta'$ -precipitates. Overageing of alloys of aluminium with 4-4.5 per cent Cu at 190 °C may be attributed, firstly, to a reduced density of  $\theta''$ -precipitates, which are gradually replaced with  $\theta'$ -precipitates, which weakens the elastic stress field in the matrix and increases the mean spacing between particles, and secondly, to particle coarsening of  $\theta'$ -precipitates.

With a sufficiently low temperature of ageing, the overageing stage is not reached and the alloy is hardened due to an increased density of coherent precipitates, and to their coarsening, the two processes and the corresponding hardening proceeding attenuatedly (see curve  $T_1$  in Fig. 191). Such, in particular, is the behaviour of duralumin in ageing at room temperature (see the curves for 18 °C in Fig. 193a and b).

As the temperature of ageing is increased, the process can attain the overageing stage and does so the sooner, the higher is the temperature (see Figs. 191 and 193a and b). This is quite explainable, since all the processes of precipitation in the solution are diffusional.

In practice, when choosing the temperature conditions of ageing, use is often made of strength-ageing temperature curves (Fig. 194). Such a curve always has portions in which the strength increases or decreases with increasing temperature of ageing. When analysing such curves, one should keep in mind that adjacent points on the ascending (or descending) branch of the curve can relate to different stages of ageing at different temperatures. For instance, with ageing time  $\tau_1$  and the temperature being increased from  $T_1$  to  $T_3$ , the strength increases continuously (see Fig. 191). On the other hand, points *a* and *b* relate to

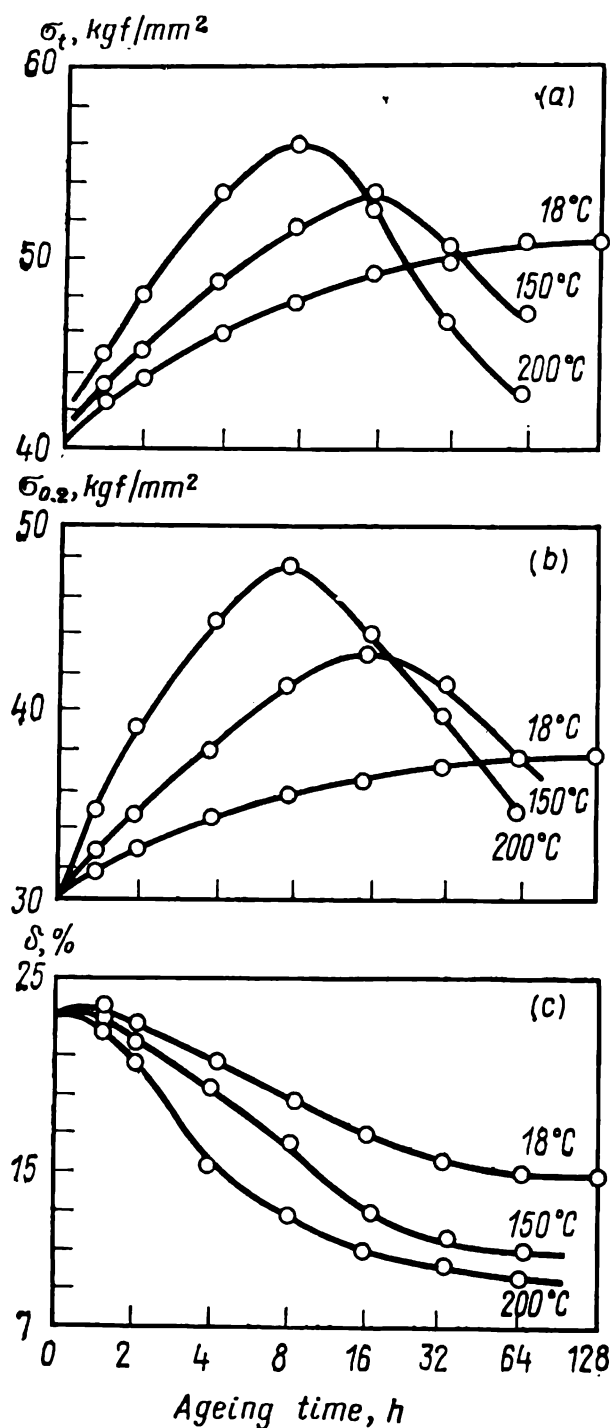


Fig. 193. Effect of time of ageing at 18, 150 and 200 °C on mechanical properties of duralumin D16 shaped sections

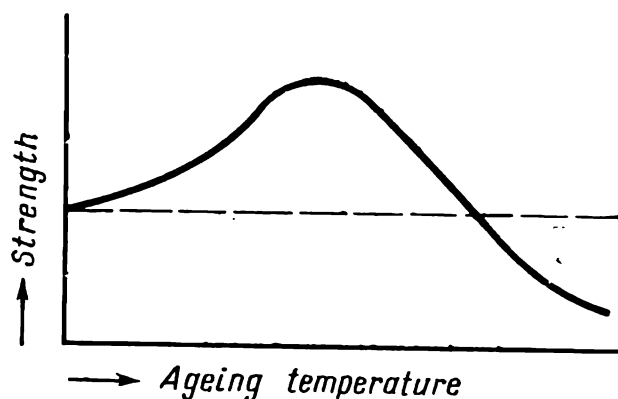


Fig. 194. Effect of ageing temperature at a constant holding time on ultimate strength

the stage of hardening ageing at temperatures  $T_1$  and  $T_2$ , while point *c*, to the stage of overageing at temperature  $T_3$ . If the holding time is  $\tau_2$ , then increasing the temperature of ageing from  $T_1$  to  $T_3$  will lower the strength (points *d*, *e*, and *f*), with the alloy

being at the stage of hardening ageing at temperature  $T_1$  and at the stage of overageing, at temperatures  $T_2$  and  $T_3$ .

Having summarized the results for various alloys, M. V. Zakharov has established that the ageing temperature required to age an alloy to the maximum strength and hardness is a constant fraction of the solidus temperature (on the absolute scale):

$$T_{ag} = (0.5-0.6) T_{m.p} \quad (37)$$

This empirical relationship should not be considered as the one enabling exact calculation of the temperature of ageing to the maximum strength by the melting point. It only allows us to estimate roughly the level of these temperatures when comparing alloys with sharply differing solidus points, and therefore, with sharply different diffusion mobility of the components at the same temperature (for instance, alloys based on different metals).

As the temperature of ageing is increased, the strength of an alloy may turn to be lower than in the initial quenched state (Fig. 194). Such a strong overageing may be caused by progressive particle coarsening and a strong decrease in the degree of alloying of the matrix. The corresponding heat treatment is sometimes incorrectly called annealing, though the processes that take place here are essentially the same as in common ageing, i.e. precipitation from the solution and coarsening of precipitated particles.

The relative elongation of the metal can decrease substantially on hardening ageing (Fig. 193c); in overageing, however, it most often changes insignificantly and either continues to diminish weakly or slightly increases.

#### 4.1.4. EFFECT OF ALLOY COMPOSITION ON AGEING

##### Effect of Composition in Binary Systems

In Figure 195, line  $Amnp$  shows schematically how the content of an alloying element in a binary alloy can influence the rise in hardness in ageing to the maximum strength<sup>1</sup>. Such a curve can characterize the effect of composition on the ultimate strength and yield strength in ageing.

In alloys with the concentration of the  $B$  component below  $C_1$ , ageing is impossible since it is impossible to form a supersaturated solid solution (i.e. hardening is also impossible). In all alloys with the alloying element concentration above  $C_1$ , hardening stabilizes the supersaturated solid solution, so that ageing becomes

<sup>1</sup> The effect of temperature and time of ageing to the maximum strength may differ substantially with various alloys of the same system.

feasible. If these alloys are aged under the conditions which are optimal for each of them (to ensure the maximum hardening), we may expect that with an increasing concentration of the second component the hardness during ageing will first increase (section  $mn$ ) to a maximum and then gradually decrease (section  $np$ ).

In the  $C_3$  alloy, all other things being equal, a higher density of precipitates can be formed than in the  $C_2$  alloy, owing to a greater supersaturation of the solid solution. Therefore, the  $C_3$

alloy can be strengthened to a greater degree than the  $C_2$  one.

Theoretically, the age-hardening effect should be at its maximum in the  $C_5$  alloy, whose composition corresponds to the point of maximum solubility at the eutectic temperature. Practically, however, it is impossible to obtain the  $\alpha$ -solution of a composition  $C_5$ , since this would require that the alloy be quenched exactly from the melting point of the eutectic. Since quenching temperature is usually taken somewhat below the solidus point (in order to avoid burning), the maximum supersaturation of the solution and the maximum hardening on ageing are attained at the

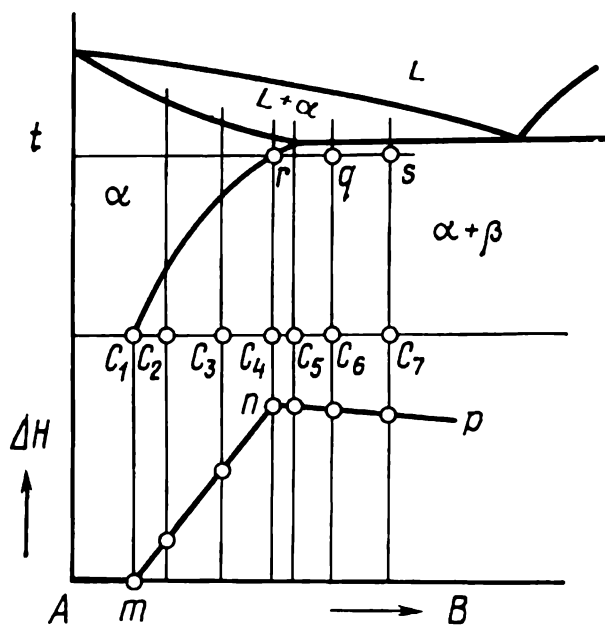


Fig. 195. Effect of composition of a binary alloy on the maximum attainable gain in hardness upon ageing  $\Delta H$ —difference between hardness values of as-aged and as-quenched alloy

concentration of alloying element somewhere to the left of the point of ultimate solubility, for instance, in an alloy of composition  $C_4$ .

Decreasing hardening along the section  $np$  may be explained as follows. In alloys  $C_6$  and  $C_7$ , when quenched from the same temperature, the composition of the  $\alpha$ -solution is the same (point  $r$ ). Therefore, the density of precipitates in the  $\alpha$ -phase of these alloys upon ageing must be the same at the same temperature, i.e. the hardness of the  $\alpha$ -solution in both alloys must increase identically. But the  $C_6$  and  $C_7$  alloys, as quenched, contain an excess  $\beta$ -phase from the eutectic, as well as primary  $\alpha$ -crystals. The  $C_7$  alloy contains more of  $\beta$ -phase and less of  $\alpha$ -phase than does the  $C_6$  alloy ( $rs > rq$ ). Since age-hardening occurs owing to precipitation from the  $\alpha$ -solution and since the content of  $\alpha$ -phase is lower in the  $C_7$  alloy, the rise in hardness must be lower in the latter. In other words, with the same increase in the microhard-

ness of primary  $\alpha$ -crystals, the hardness of the whole alloy  $C_7$  in ageing increases less appreciably, owing to the higher percentage of the 'ballast'  $\beta$ -phase which does not participate in the ageing.

The strength of an aged alloy depends on the initial level of strength in the alloy as quenched. Since the strength of the  $\alpha$ -solution increases with increasing concentration of the alloying element, alloys whose composition is close to the ultimate solubility point at the eutectic temperature have a high strength as quenched and can be strengthened appreciably by ageing. It then follows that the compositions of the most strong ageing alloys are near the ultimate solubility points in constitutional diagrams.

The role of supersaturation of the solid solution is illustrated in Fig. 192. On changing the content of copper in aluminium alloys from 2 per cent to 4.5 per cent, the hardness at the maximum points on the curves of ageing at 190 °C increases. This may be attributed, in the first place, to the rise of hardness of the initial alloy (as quenched) and, in the second, to a higher increase in hardness on ageing.

Owing to the higher supersaturation, precipitation from the solution takes place faster and, therefore, the maximum of strengthening is attained in a shorter ageing time, after which overageing begins (see in Fig. 192 how the maximum shifts along the time axis on transfer from the alloy with 2 per cent Cu to that with 4.5 per cent Cu).

### Effect of Composition in Ternary Systems

The laws by which the composition of ternary alloys affects ageing are essentially the same as for binary systems. Knowing the isothermal sections at the temperature of hardening (solid lines in Fig. 196) and at a lower, say room, temperature (dotted lines) one can predict whether ageing is possible in any alloy that is of interest, and, for alloys belonging to the same phase region, where the highest hardening should be expected. For instance, alloy 1 in the figure is incapable of ageing, since it belongs to the single-phase region at room temperature. Alloys 2, 3, 6 and 7, whose compositions are on the same conode, are analogous with alloys  $C_2$ ,  $C_3$ ,  $C_6$  and  $C_7$  in the binary system of Fig. 195 as regards the hardening effect.

Alloys 2 and 3 are located in the single-phase  $\alpha$ -region at the temperature of quenching and in the two-phase  $\alpha + \beta$ -region at room temperature. Therefore, they can be quenched to form supersaturated  $\alpha$ -solution and then subjected to ageing. Alloy 3 has a more supersaturated solution than alloy 2 and therefore must give a greater hardening effect on ageing (in full analogy with binary alloys  $C_2$  and  $C_3$  in Fig. 195). Alloys 6 and 7 are also

capable of being hardened in ageing. Since they are located on the same conode, they have the same composition of the  $\alpha$ -solution (point  $r$ ) at the quenching temperature. The hardening effect in alloy 7 must however be lower owing to the greater amount of the 'ballast'  $\beta$ -phase which has not passed into the  $\alpha$ -solution on heating (in full analogy with alloys  $C_6$  and  $C_7$  in Fig. 195).

Alloys 4, 5 and 8 also can be age-hardened. They differ from alloys 2, 3, 6, and 7 in the phases that precipitate: it is the  $\gamma$ -phase in alloy 4 and the  $\beta$ - and  $\gamma$ -phases in alloys 5 and 8.

The phase region that includes the strongest ageing alloys is usually unpredictable, since even with the known composition

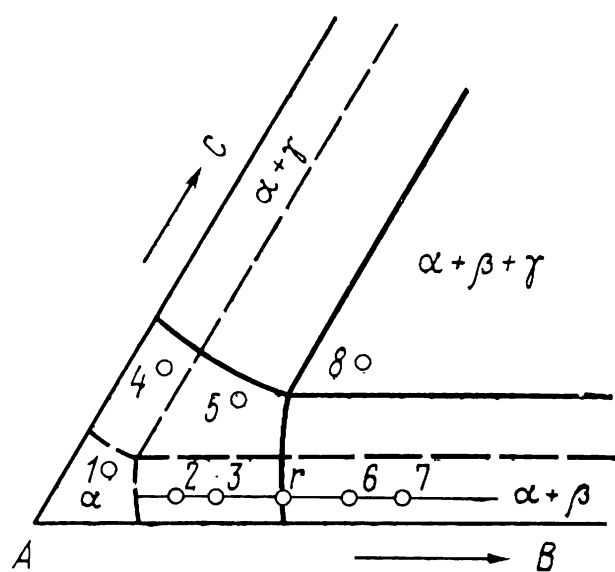


Fig. 196. Isothermal sections through a ternary system at quenching temperature (solid lines) and room temperature (dotted lines)

and structure of the stable phases we most often know nothing in advance on the type and structure of intermediate metastable precipitates. These very precipitates, as a rule, are responsible for the maximum hardening on ageing. An obvious case are industrial alloys of the Al-Zn-Mg system (type 1915). According to the constitutional diagram, a ternary  $T$  compound ( $\text{Al}_2\text{Mg}_3\text{Zn}_3$ ) is in stable equilibrium with the  $\alpha$ -solution of aluminium in these alloys, whereas ageing to the maximum strength results in the precipitation of the  $\eta'$ -phase, which is intermediate between

the  $\alpha$ -solution and the  $\eta$ -phase ( $\text{MgZn}_2$ ). Such cases still remain unpredictable.

Notwithstanding certain limitations, the constitutional diagram is nevertheless of an extreme value for the selection of composition and conditions of heat treatment of ageing alloys. It can show in what compositional region ageing alloys are to be looked for, enables an appropriate selection of the range of quenching temperatures (see 3.1.2), the temperature level of ageing to the maximum strength [see formula (37)], and selection of the compositions of alloys near the solubility limit at quenching temperature for subsequent experimental testing. The greater is the difference between the ultimate solubility at the eutectic (peritectic) point and that at room temperature ( $C_5 - C_1$  in Fig. 195), the greater hardening effect can be expected on quenching and ageing, since quenching can produce a larger supersaturation of the solid solution.



If it is already known that alloys from the two-phase  $\alpha + \beta$ -region in a ternary A-B-C system can harden appreciably on ageing, then *thermally hardenable alloys* in another ternary system, say A-B-D, must be sought in the first place in the composition range where the  $\beta$ -phase can precipitate from the  $\alpha$ -solution. This approach largely facilitates the search for new high-strength ageing alloys by narrowing it to some particular phase regions in the constitutional diagram.

### Effect of Trace Additions and Impurities

Special additions or occasional impurities contained in alloys from thousandths to tenths of a per cent can sometimes strongly affect the kinetics of precipitation and the structure and properties of age-hardened alloys.

The effect of additions that is directly linked with the formation of a new phase will not be discussed here, since such an addition acts as a common component in an alloy. The mechanisms of the effect of trace additions, which cause no qualitative changes in the phase composition, may be diverse. An addition may be characterized by a high energy of its bond with vacancies, in which case its atoms in the solid solution act as traps for vacancies. Such is the effect of additions of Cd, In, Sn and Be in aluminium-copper solution.

Pinning of vacancies by impurity atoms lowers the contribution of vacancies to the transfer of atoms of the main alloying element (such as copper in Al-Cu) to G. P. zones. Trace additions of Cd, In, Sn and Be retard the formation and growth of G. P. zones in Al-Cu alloys and thus retard hardening on ageing.

An addition may turn to be *homophile* and segregate to the interface between the matrix and precipitate, where it can lower the interfacial energy. For instance,  $\gamma = 1530 \text{ erg/cm}^2$  at the boundary between  $\theta'$ -phase and aluminium solution in an Al-4% Cu alloy, but lowers to  $250 \text{ erg/cm}^2$  when 0.1% Cd is added to the same alloy. With decreasing interfacial energy, the size of critical nucleus of a precipitate diminishes according to formula (20), i.e. the density of precipitates increases. In accordance with formulae (34) and (35), a decrease in interfacial energy can retard coarsening of precipitated particles. For instance, a trace addition of cadmium can diminish the rate of particle coarsening of  $\theta'$ -phase in Al-Cu alloy by a factor of five. Retarded particle coarsening is of especial value for age-hardening refractory alloys as an effective tool for impeding softening of these alloys in operation at elevated temperatures.

An addition can produce a different effect on ageing at various temperatures. For instance, a trace addition of cadmium impedes

the formation of G. P. zones in Al-Cu alloys by retarding hardening in natural ageing, but the same addition can also increase the density of  $\theta'$ -phase precipitates and thus enhance hardening in artificial ageing.

Another mechanism of the effect of trace additions may be attributed to the fact that an addition enters the composition of G. P. zones and thus stabilizes the latter. An addition of 0.25 per cent Si in AK4-1 alloy (Al-Cu-Mg-Fe-Ni system) increases the density of the  $S'$ -phase precipitates and refines these precipitates at 190 °C, thus increasing the strength of the alloy. It is assumed that silicon atoms enter the composition of G. P. zones and stabilize these at higher temperatures, so that the precipitation of the  $S'$ -phase at 190 °C takes place at these zones, rather than at dislocations. Since the density of distribution of G. P. zones, which nucleate homogeneously, is very high, the density of the  $S'$ -phase precipitates also turns to be increased.

The concentration of atoms of a trace addition in a precipitating phase can lower the volume free energy of that phase to such an extent that the work for the formation of critical nucleus will diminish and the density of precipitates increase (on shifting the  $F_\beta$  curve in Fig. 164 downwards, the difference of volume free energies  $F_1 - F_2$ , which is the thermodynamic stimulus of the precipitation, increases). Such may probably be the effect of small additions of silver in Al-Zn-Mg alloys: it causes refining of the precipitated  $\eta'$ -phase particles.

Apart from increasing the density of precipitates, an important role of trace additions is to inhibit discontinuous precipitation (see 4.1.2).

The use of trace additions and control of the content of impurities are effective means for controlling ageing processes.

#### 4.1.5. SELECTION OF AGEING CONDITIONS

##### Selection of Temperature and Time of Ageing

Upon preliminary rough estimation of the temperature level of ageing by formula (37) or by analogy with other alloys based on the same metal, the conditions of ageing are worked out experimentally by plotting curves similar to those shown in Figs. 191 and 194.

As is known, ageing is classed into *natural*, i.e. occurring at room temperature, and *artificial*, which requires heating to a specified temperature.

In most age-hardening alloys, holding at room temperature after hardening causes no changes in the properties that might be of practical use. The mechanical properties of hardened copper,

nickel and many other alloys do not change at all at room temperature, as this is too low to initiate diffusion processes.

In aluminium alloys (duralumins and the like) the formation of G. P. zones in natural ageing results in a strong hardening, which is widely used industrially.

The terms 'natural' and 'artificial' only define the conditions of ageing, but do not determine definitely the nature of structural changes in the supersaturated solid solution. Neglecting low-melting alloys in which natural ageing occurs at a high homological temperature (around  $0.5T_{m.p}$  for lead alloys) and results in progressive precipitation, it may be stated that only clusters form during natural ageing in most alloys. On the other hand, precipitation in the solution during artificial ageing stops, depending on the temperature and time, either at the zone stage or at the stage of precipitation of intermediate phases, or else, proceeds to precipitation of a stable phase.

I. N. Fridlander proposed the terms *zone* and *phase ageing* to be used in parallel with natural and artificial ageing. Zone ageing of aluminium alloys can be either natural or artificial and stops at the stage of formation of G. P. zones. Phase ageing of aluminium alloys can be only artificial, as a rule. Exception is many-years holding of Al-Zn-Mg alloys at room temperature. It is important practically that the complex of properties of an alloy after zone ageing differs from that obtained on phase ageing.

Typical of zone-aged aluminium alloys are a high relative elongation ( $\delta > 10-15$  per cent), an appreciable difference between the ultimate strength and the yield strength ( $\sigma_{0.2}/\sigma_t = 0.7-0.8$ ), a high impact strength and a high resistance to stress corrosion. Zone ageing can be only hardening.

Phase ageing can be either hardening or softening (overageing)<sup>1</sup>. The former can be characterized by a reduced relative elongation, a low difference between the ultimate strength and the yield strength ( $\sigma_{0.2}/\sigma_t = 0.8-0.95$ ), a reduced impact strength, and a reduced resistance to stress corrosion.

Division into zone and phase ageing is rather conditional. Firstly, the division of precipitates proper into G. P. zones and intermediate phases (see 4.1.2) is also conditional, which is reflected in the double designation: G.P.2 zones or  $\theta''$ -phase, which is used arbitrarily. Secondly, during precipitation in the solution, G. P. zones are gradually replaced by intermediate-phase precipitates and can co-exist with the latter for a long time (see the ageing curves for aluminium alloys with 4 and 4.5 per cent Cu in Fig. 192). Thirdly, the curves of property variations may fail

<sup>1</sup> Overageing at the stage of precipitates coarsening can be termed as *coarsening ageing*.

to fix the moments when an intermediate phase appears or G. P. zones fully vanish.

Without direct structural studies, by only measuring the properties, one cannot say definitely what is the structural state he has to deal with. The division into zone and phase ageing, though being conditional, can be of use, since it helps in selecting ageing conditions to obtain a specified combination of properties.

The optimum conditions of ageing are often assigned in view to attain the maximum strength. For many products, the appropriate criterium of optimal ageing conditions may however be a combination of other properties, rather than the maximum strength.

Depending on the conditions, structural changes and the complex of properties it produces, artificial ageing can be classed into full, partial ageing, overageing and stabilizing ageing (the corresponding conditions and properties for a casting aluminium alloy Grade AJ19 are given in Table 14).

*Full artificial ageing* is carried out at a temperature and time providing the maximum strength.

*Partial artificial ageing* differs from the former in a shorter holding time at a lower temperature, so as to increase the strength with simultaneously retaining a sufficient ductility. The conditions for partial ageing correspond to the ascending branches of the curves in Figs. 191 and 194. A certain loss in the strength (compared with full ageing) is compensated for by a lower loss in ductility.

*Overageing* is done at a higher temperature or with a longer holding time than full ageing, in order to form a suitable combination of elevated strength, ductility, corrosion resistance, electric conductivity and other properties. Overageing conditions correspond to the descending branches of the curves in Figs. 191 and 194. As compared with partial ageing, overageing gives a greater degree of precipitation of the solid solution at the same strength, which often provides the desired complex of various properties.

*Stabilizing ageing* is a variety of overageing aimed at stabilization of the properties and dimensions of products.

Refractory alloys for long operation at high temperatures are usually age-hardened at a temperature above the operating level, otherwise some structural changes might take place in the metal during operation and cause softening and instability of properties. Heat treatment of refractory alloys is often done under the conditions of overageing.

Ageing conditions must be chosen with due regard to the conditions of quenching. Upon raising the temperature of heating for quenching from the single-phase region (above  $T_0$  for  $C_0$  alloy in Fig. 112), the ageing is accelerated owing to an increased con-

centration of quenching vacancies [this concentration enters the pre-exponential factor  $A$  in expression (24) for the rate of nucleation of a new phase]. Thus,  $C$ -curves in Fig. 181 are shifted to the left on increasing the temperature of quenching, this shift being larger in the low-temperature region where the role of quenching vacancies is especially meaningful.

Some alloys are *age-hardened without being specially heated for quenching*. In such cases the solution is made supersaturated by accelerated cooling from the temperature of the end of solidification in a casting or from that of the end of hot plastic working. The hardening effect in the alloy then does not attain its maximum, owing to the lower supersaturation of the solid solution, but the economic effectiveness (exclusion of quenching procedure) makes this method favourable for the manufacture of selected products. For some alloys, such as MJ12 alloy of the Mg-Zn-Zr system, ageing of castings without special heating for quenching is the main method of heat treatment.

The rate of cooling upon ageing has no effect on the properties of alloys. Cooling from the ageing temperature is usually done in air.

### Step Ageing

Step ageing is carried out with holding the metal first at one and then at another temperature, the temperature of the first stage being usually selected lower than that of the second stage. *Two-step*, or *duplex*, *ageing* is aimed at forming a large number of precipitation nuclei at the low-temperature stage when the solid solution is appreciably supersaturated (in Fig. 165, the degree of supersaturation  $C_0/C_1$  increases with lowering temperature  $T_1$ ) and causing the solution to precipitate at the second stage to a required degree so as to form precipitates of the optimum size. This provides a higher density and greater uniformity of distribution of precipitates than is possible in one-step ageing at an elevated temperature.

Assume that operating conditions of an alloy dictate that it be aged artificially to form precipitates of an intermediate phase. If this phase can nucleate heterogeneously at dislocations and grain and subgrain boundaries at the optimum temperature of ageing, the density of precipitates will be relatively low. If the phase is additionally capable of nucleating at G. P. zones, preliminary low-temperature ageing, even natural, can sharply increase the density of intermediate phase precipitates and refine them at the high-temperature stage of ageing. Examples are Al-Zn-Mg alloys (type 1915) which increase their corrosion resistance upon ageing at 150-175 °C. G. P. zones which form in these alloys at the low-temperature ageing stage (at 100 °C) in-

crease the density of the  $\eta'$ -phase precipitates (see Table 13) at the high-temperature ageing stage (at 175 °C), so that the duplex ageing gives an increased strength combined with a high resistance to stress corrosion. The low-temperature stage may be either natural ageing for a month or, more effectively, artificial ageing at 100 °C for 10-20 hours.

Under industrial conditions, it is not always possible to put products into ageing furnaces immediately after quenching, i.e. there always is a time interval, sometimes rather long, between quenching and artificial ageing. Therefore, natural ageing, even when not planned specially, usually precedes artificial ageing, the latter actually being the second (high-temperature) stage of duplex ageing (unplanned natural ageing is called storage upon quenching). For this reason, the laws of step ageing are of a broader interest than may seem on the face of it. These laws may be quite complicated and often depart from the above-mentioned scheme of the favourable effect of pre-ageing.

Consider a practically important case of a complicated role of natural ageing, using as an example Al-Mg-Si alloys (of the Avial type) which are located in or near the quasibinary Al-Mg<sub>2</sub>Si section. Natural ageing in these alloys forms acicular G. P. zones rich in magnesium and silicon, while artificial ageing (at 170 °C) forms a metastable  $\beta'$ -phase (see Table 13). The maximum hardening effect is obtained on artificial ageing.

It has been known for a long time that Avial alloys lose in strength on artificial ageing if a time interval has been allowed between quenching and this operation. Electron-microscopic studies show this effect being due to coarsening of the structure. A probable explanation of the detrimental effect of natural ageing may be as follows. As G. P. zones are being formed during natural ageing, the matrix solution around them is depleted of alloying elements. On heating to the temperature of artificial ageing, the degree of supersaturation of the solution decreases even more, since the equilibrium solubility ( $C_1$  in Fig. 165) becomes higher. Each degree of supersaturation has a corresponding minimal size of precipitates (including that of G. P. zones) that can be obtained on ageing, this size decreasing with increasing degree of supersaturation. When a naturally aged alloy is heated to the temperature of artificial ageing, small G. P. zones dissolve and only larger ones remain in the metal and serve as the  $\beta'$ -phase nuclei, i.e. a coarse structure is formed. If the alloy is however aged artificially immediately after quenching, it will have a high degree of supersaturation at the initial period, resulting in a large number of fine  $\beta'$ -phase precipitates nucleating homogeneously.

Several methods have been proposed to prevent impairment of properties in artificially aged alloys owing to a long storage on

quenching. The simplest one, which unfortunately is not universally applicable, is to restrict the time of storage or to keep quenched products at a reduced temperature (in a refrigerator). By another method, products made of Avial alloys are heated for a short time (1-3 minutes) at approximately 250 °C before being aged finally at 160-170 °C. This heating causes the G. P. zones formed through natural ageing to dissolve fully, the state of the alloy thus becoming similar to that immediately after quenching (see reversion heat treatment in 4.1.6). The most effective method however uses trace additions which can inhibit natural ageing.

Impairment of properties through storage after quenching is typical not only of Al-Mg-Si alloys, but of ageing alloys of some other systems as well. In the Al-Mg-Si system, the detrimental effect of storage time is characteristic of alloys containing not less than 1 per cent Mg<sub>2</sub>Si. In an alloy with, say, 0.8 per cent Mg<sub>2</sub>Si pre-ageing at room temperature, on the contrary, increases the strength of the metal as aged artificially. This may be explained by the fact that, since the metal is less alloyed with magnesium and silicon, and therefore, the solid solution is less supersaturated, the  $\beta'$ -phase in a freshly quenched alloy with 0.8 per cent Mg<sub>2</sub>Si can nucleate at 170 °C only heterogeneously, at dislocations, and the structure that is formed is coarse. Pre-ageing at room temperature forms G. P. zones serving as nuclei for the  $\beta'$ -phase and thus refines the structure of artificially aged alloy with 0.8 per cent Mg<sub>2</sub>Si and produces a more uniform distribution of  $\beta'$ -phase precipitates.

Thus, two-step ageing may produce either useful or detrimental effect depending on the composition of an alloy and the temperature of ageing stages.

The issue of pre-ageing is closely associated with the role of heating rate in one-step ageing. The rate with which the metal is heated up to the ageing temperature is commonly neglected. However, initial stages of precipitation with a slow heating may have some effect on the properties of aged alloys. For instance, a slower heating of some aluminium alloys to the ageing temperature can increase somewhat their strength.

Table 14 gives typical ageing conditions and mechanical properties of selected alloys.

Table 15 can give notion on how the strength properties of selected industrial alloys increase on ageing. The difference in properties between as-aged and as-quenched states of an alloy is related to the property of the initial alloy as quenched, all tabulated data being given for ageing to the maximum strength.

The yield limit increases on ageing more strongly than does the ultimate strength, so that the  $\sigma_{0.2}/\sigma_t$  ratio increases, which is very typical of full artificial ageing.

Table 14. Ageing Conditions \* and Mechanical Properties of Selected Alloys

Base metal	Alloy grade	Products	Heating temperature, °C	Holding time, h	$\sigma_t$ , kgf/mm <sup>2</sup>	$\sigma_{0.2}$ , kgf/mm <sup>2</sup>	$\delta$ , %
Ni	XH77TIOP (ЭИ437Б)	Turbine blades	690-710	16	100	65	20
Ti	BT22	Rods	550	1	155	152	4
Cu	Бр.Б2	Springs	310-330	2	135	128	2
Al	Д16	Sheets	20	4, days	44	29	19
			188-193	11-13	45	40	6
	B95	Ditto	120-125	23-25	55	48	10
	AK4-1	Plates	190-200	24	43	34	8
	АД31	Rolled sections	160-170	10-12	24	20	10
	1915	Ditto	1st stage: 100	10-24			
			2nd stage: 175	3-5	38	30	10
	АЛ9 **	Castings	T1 170-180	5-17	17	14	2
			T5 145-155	1-3	23	17	4
			T6 195-205	2-5	24	21	2
			T7 215-235	3-5	19	14	4.5
	АЛ19	Ditto	170-180	3-5	37	26	5
Mg	МЛ5	Ditto	170-180	16	25.5	12	4

\* For quenching conditions see Table 8.

\*\* T1—ageing without preliminary quenching, T5—partial ageing; T6—full ageing; T7—stabilizing ageing.

Table 15. Relative Increase ( $\Delta$ ) of Ultimate and Yield Strength in Selected Industrial Alloys on Full Ageing

Base metal	Alloy grade	$\Delta\sigma_t$ , %	$\Delta\sigma_{0.2}$ , %	$\sigma_{0.2}/\sigma_t$	
				as-quenched	as-aged
Ti	BT22	72	80	0.93	0.98
Cu	Бр.Б2	160	—	—	0.94
Al	Д16	50	80	0.73	0.88
	1915	70	170	0.50	0.78
	АЛ9	20	90	0.55	0.87
Mg	МЛ5	2	40	0.34	0.47



Beryllium bronzes and aluminium alloy Grade 1915 of the Al-Zn-Mg system can harden appreciably on ageing, while magnesium alloy MJ15 hardens only weakly (because of which it is more often used as quenched).

Alloys which undergo hardening on ageing are called *age-hardening* or *thermally hardening*. Development of new age-hardening alloys is one of the principal objects of physical metallurgy.

#### 4.1.6. REVERSION IN AGE-HARDENED ALLOYS

The phenomenon of reversion after ageing was first discovered in duralumins. If naturally aged duralumin is heated to approximately 250 °C, held at that temperature for 20-60 s and cooled quickly, its properties return to the values existed in as-quenched state.

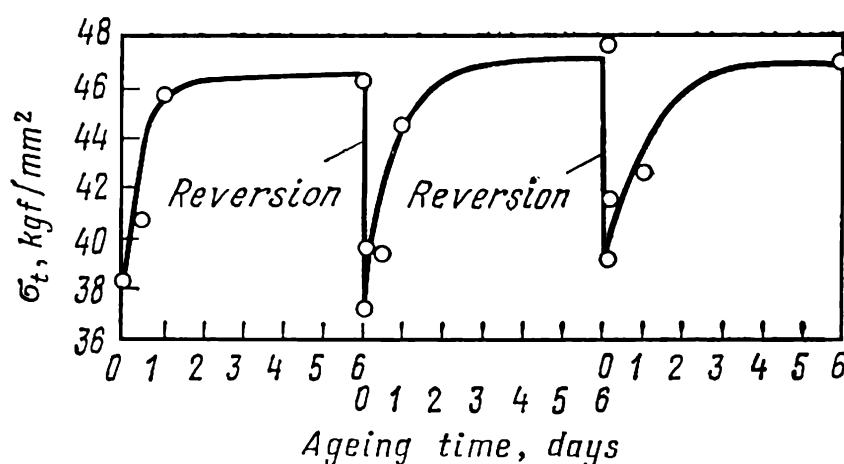


Fig. 197. Variations of ultimate strength of duralumin on natural ageing and double reversion treatment after ageing (after D. A. Petrov)

Reversion consists essentially in that the G. P. zones formed on natural ageing are dissolved when the alloy is heated to a temperature above their solvus line<sup>1</sup>, but the short holding time is insufficient for the formation of metastable and stable phases, so that quick cooling that follows fixes the supersaturated solid solution. The temperature of reversion heat treatment of duralumin (roughly 250 °C) is well below the temperature of heating for quenching (near 500 °C) which is required to dissolve the stable phases.

Upon reversion heat treatment, as upon common requeenching, duralumin is capable of hardening in natural ageing. A new procedure of reversion heat treatment again softens it, and so on (Fig. 197). Since each procedure of heating to the reversion temperature allows an irreversible structural age-hardening to proceed

<sup>1</sup> That is, above  $T_{G.P.}$  but below  $T_{\beta'}$  for  $C_0$  alloy in Fig. 179.

to a small extent (especially at grain boundaries), the properties of the metal gradually depart somewhat from those of the freshly quenched alloy. In particular, duralumin becomes more prone to intercrystalline corrosion.

Reversion heat treatment is used when the plasticity of duralumin must be restored before bending, flanging, etc., but re-quenching is undesirable because of the risk of warpage. The main technological disadvantage of reversion heat treatment is that the time of holding in a saltpetre bath must be controlled quite accurately (within 10 s). With a shorter holding time, not all G. P. zones have time to dissolve and softening will be incomplete, whereas a more prolonged time can cause hardening owing to the onset of structural age-hardening. For that reason, and also in view of the possible loss in corrosion resistance, reversion heat treatment of duralumins has found only a limited application.

The phenomenon of reversion plays an important part in the theory of ageing. It allows us to estimate the stability of G. P. zones formed under different ageing conditions and determine the temperature for their dissolution.

The temperature of heating for full reversion of properties (i.e. the temperature of dissolution of G. P. zones) in the general case is not a constant for a given alloy. It depends on the stability of zones, and therefore, on the temperature and time of their formation. A longer time of low-temperature ageing produces larger and stabler G. P. zones, which require a higher temperature of heating for full dissolution. Beginning from a certain holding time in ageing, the temperature of full reversion becomes independent of ageing time. This critical temperature of reversion is characteristic of an alloy aged at a definite temperature and it increases with increasing temperature of ageing owing to a higher stability of G. P. zones. The maximum temperature at which stable G. P. zones can still exist in an alloy corresponds to a point on the solvus line of G. P. zones in the diagram of metastable equilibria (see Fig. 179).

It follows from the above that the solvus temperature of G. P. zones cannot be found by heating, say, a naturally aged alloy. The corresponding tests determine not the maximum temperature for existence of G. P. zones in a given alloy, but a lower temperature of dissolution of the zones formed in a given time at room temperature. The solvus line of G. P. zones shown in Fig. 180 is not actually a solvus line, since it gives temperatures of dissolution of zones formed in 10 days of ageing at room temperature. The actual solvus line of G. P. zones in the Al-Cu system should pass higher than is shown in Fig. 180. For instance, the maximum temperature of existence of G. P. zones in Al + 4% Cu alloy is not 180 °C but around 275 °C.

Reversion can be observed not only after ageing with the formation of G. P. zones and not only in aluminium alloys.

Reversion heat treatment can principally dissolve G. P. zones and metastable-phase precipitates in alloys of other bases. The temperature ( $t_{rev}$ ) and time ( $\tau_{rev}$ ) of reversion heat treatment must be selected individually for each alloy and particular conditions of ageing. For instance, the following conditions may be recommended for naturally aged duralumins:

	Д1	Д16	Д19
$t_{rev}, ^\circ\text{C}$ . . . . .	240-250	265-275	270-280
$\tau_{rev}, \text{s}$ . . . . .	20-45	15-30	10-15

#### LITERATURE

Kelly A., Nicholson R. B., Precipitation Hardening. Oxford, Pergamon Press, 1963.

Physical Metallurgy of Aluminium and Aluminium Alloys (Metallovedenie alyuminiya i ego splavov). Ed. by I. N. Fridlander. Moscow, Metallurgiya, 1971, Part III, 352 pp., ill.

Martin J. W., Precipitation Hardening. Oxford, Pergamon Press, 1968.

Shewmon P. G., Transformation in Metals. New York, McGraw-Hill Book Co., 1969, Ch. 7.

## 4.2. TEMPERING

Tempering as an operation of heat treatment has been well known from the Middle Ages. It is used with martensite-quenched alloys. The processes of tempering will be considered here for steels only, since steels constitute an overwhelming majority of all martensite-hardenable alloys. Despite the numerous research studies into the process of tempering by means of X-ray structural analysis, electron microscopy and measurements of various physical properties, some important processes inherent in tempering are still being debated, which is mainly due to the large diversity of structural changes simultaneously taking place in the process, a high dispersity of precipitates at earlier stages of tempering and some difficulties encountered when attempting to explain unambiguously the structure of these precipitates.

### 4.2.1. STRUCTURAL CHANGES IN TEMPERED STEEL

The structure of hardened steel is metastable. Heating of hardened steel increases the mobility of atoms and thus forms conditions favourable for the processes which can change the structure of the steel towards greater equilibrium. The nature of these

processes is determined by the three most important features in the structure of hardened steel: (a) a strong supersaturation of the solid solution — martensite; (b) an increased density of crystal lattice defects — dislocations, low- and high-angle boundaries, twin interlayers; and (c) the presence of an appreciable amount of retained austenite in many steels.

The principal process that takes place during tempering of steel is decomposition of the martensite with precipitation of carbides. The laws by which martensite decomposes are in many respects similar to the laws of precipitation from the supersaturated solution during ageing of alloys after quenching without polymorphic change. Depending on the temperature and time of tempering, decomposition of martensite can pass through stages of pre-precipitation, precipitation of metastable carbides, precipitation of cementite, and coagulation.

An increased dislocation density due to an additional strain during the martensitic rearrangement of the lattice makes the structure of martensite similar to that of a strain-hardened metal (see 3.2.3 and 3.2.4). As a result, tempering produces a stimulus for polygonization and recrystallization.

In the discussion below, we agree to refer to tempering not only precipitation from supersaturated solution, but also any combination of structural changes occurring in heating after martensitic quenching. Taking this in view, heating of polymorphic pure metals upon quenching, in which martensitic transformation has taken place, as also heating of alloys in which the martensite is not a supersaturated solution (such as quenched  $C_0$  alloy in Fig. 119) should also be referred to tempering. In all such materials, martensitic transformation produces an increased dislocation density, so that it is possible to perform tempering in which the structural changes are only due to polygonization and recrystallization. In that respect, tempering differs principally from ageing which is only applicable to alloys containing supersaturated solid solution<sup>1</sup>.

The high density of lattice defects in hardened steels not only predetermines the development of recovery and recrystallization processes, but also affects strongly the decomposition of martensite on tempering.

Finally, the structural changes in tempering may be complicated by decomposition of retained austenite.

---

<sup>1</sup> This approach to the concept of tempering of pure metals and unsaturated solid solution having martensitic structure is conditional. The corresponding heat treatment may be also regarded as annealing (pre-recrystallizational), but since preliminary quenching is necessary and in view of the specific substructure of martensite, the term 'tempering' seems more appropriate.

### Tempering of Carbon Steels

The nature of structural changes in tempering of carbon steels depends on the temperature and time of tempering and the content of carbon in the metal. At higher concentrations of carbon in austenite, the supersaturation of the  $\alpha$ -solution increases, the  $M_s$  point lowers down, lath martensite changes to plate (twinned) type, and the amount of retained austenite increases. All this affects the processes of tempering.

**Segregation of carbon** in martensitic crystals is the first structural change taking place in tempering of carbon steels. Experimental studies have established two processes of carbon segregation which differ in their nature, namely, the formation of impurity atmospheres at defects of martensitic lattice and the formation of clusters.

Crystal lattice defects are energetically more favourable sites for carbon atoms than are the normal positions of these atoms in the martensitic lattice. Carbon atoms are elastically attracted to dislocations and dislocation arrays. Carbon segregates can form at structural imperfections at room temperature immediately after hardening or even during quenching from  $M_s$  to room temperature. Consequently, self-tempering can take place during quenching within the martensitic range, especially in steels having high  $M_s$  points (such as low-carbon steels). Approximately 0.2 per cent C is sufficient to saturate atmospheres at dislocations in martensite.

Another process of carbon segregation is not linked with the attraction of carbon atoms to structural imperfections. At room temperature, carbon atoms in martensite form clusters along  $\{100\}$  planes and in plate martensite — along  $\{112\}$  twinning planes. These clusters can grow larger in size on increasing the temperature of tempering up to 100°C.

The formation of carbon clusters may be treated as a zone stage of decomposition of the solution, which is analogous with the concentration stratification in ageing of substitutional solid solutions.

Yu. A. Skakov emphasizes that the formation of carbon-rich zones should be considered not as a preparatory stage of carbide precipitation. Since the solid solution at this zonal stage is more stable than a uniform supersaturated solution, the concentration stratification in itself (i.e. the formation of carbon-rich zones) may have no accelerating effect on precipitation of the carbide phase.

**Precipitation of intermediate carbides** from martensite is the structural change that follows carbon segregation in tempering. Beginning from about 100°C, metastable  $\epsilon$ -carbide can be detected

experimentally in the metal. This carbide differs from cementite in the type of lattice (which is hexagonal with  $\epsilon$ -carbide and rhombic with cementite) and a reduced carbon content (a probable formula of  $\epsilon$ -carbide is  $\text{Fe}_{2.4}\text{C}$ ).

In steels with less than 0.2 per cent C, precipitation of  $\epsilon$ -carbide in tempering is inhibited, since most carbon atoms are locked by dislocations.

The orientation of  $\epsilon$ -carbide relative to the matrix is  $(0001)_\epsilon \parallel (011)_m$ , which provides coherence of the interface. At low temperatures,  $\epsilon$ -carbide precipitates as very fine disperse platelets or needles. With increasing temperature or time of tempering,  $\epsilon$ -carbide particles coarsen and elastic deformations accumulate at the boundaries with martensite, so that a coherent boundary may change to semicoherent (see 2.1.2).

The preferable formation of intermediate  $\epsilon$ -carbide in place of more stable  $\text{Fe}_3\text{C}$  cementite may be explained by the fact that lattice matching at boundaries between martensite and  $\epsilon$ -carbide is better, and therefore, the surface energy is lower than at boundaries between matrix and cementite.

Within a temperature range of 100-200 °C, a small amount of 'low-temperature' cementite forms together with  $\epsilon$ -carbide. This cementite differs from that in annealed steel by the parameters of the rhombic lattice. It precipitates from twinned martensite, whereas  $\epsilon$ -carbide forms in untwinned martensite.

Recent studies of the structure of low-temper carbide (120 °C) by means of electron microdiffraction have shown that the first phase that precipitates from high-carbon martensite is rhombic lattice  $\eta$ -carbide (probably of the formula  $\text{Fe}_2\text{C}$ ), but not hexagonal  $\epsilon$ -carbide, as has been widely assumed formerly. The two metastable carbides are very similar in their structure. In particular, there is no marked difference in the spacings between close-packed layers of iron atoms. The lattice of metastable  $\eta$ -carbide, as also that of  $\epsilon$ -carbide, can match well the lattice of martensite. This similarity in the structure of  $\eta$ - and  $\epsilon$ -carbide makes it difficult to identify the actual structure of the first precipitating phase.

An intermediate  $\chi$ -carbide having a monoclinic lattice (probable formula  $\text{Fe}_5\text{C}_2$ ) precipitates in high-carbon steels on tempering at 250-350 °C. Its lattice matches well the lattice of martensite along the  $\{112\}_m$  twinning planes. Because of this  $\chi$ -carbide forms in twinned martensite, which is typical of high-carbon steels.

**The formation of  $\text{Fe}_3\text{C}$  cementite** with the same, or nearly the same, structure as that of cementite in annealed steel, takes place at temperatures above 250 °C, and especially actively, within 300-400 °C.

$\text{Fe}_3\text{C}$  cementite is a stabler phase which possesses a lower volume ('chemical') free energy than any of intermediate carbides.

Besides, the reduction in carbon concentration in the decomposing  $\alpha$ -solution caused by an increased temperature of tempering changes the interplane distances so that the lattice of the  $\alpha$ -phase matches more the lattice of cementite, rather than that of  $\varepsilon$ -carbide (or  $\eta$ -carbide). Thus, the gain in volume and surface energy at higher temperatures of tempering makes the nucleation and growth of  $\text{Fe}_3\text{C}$  cementite more preferable than the nucleation and growth of intermediate carbides.

Two different mechanisms of cementite nucleation have been established. Firstly, cementite can precipitate directly from the supersaturated  $\alpha$ -solution, the growth of its particles being accompanied with the dissolution of the precipitates of a less stable carbide that have formed earlier (see 2.1.4).

Secondly, cementite can form through rearrangement of the lattice of an intermediate carbide into the  $\text{Fe}_3\text{C}$  lattice (within the volume of particles of that carbide). There are experimental data which can be treated as a proof of allotropic transformation of  $\varepsilon$ -carbide, 'low-temperature' cementite and  $\chi$ -carbide into 'high-temperature'  $\text{Fe}_3\text{C}$  cementite.

**Cementite particle coarsening and spheroidization** is the final stage of the processes of carbide formation on tempering. At relatively low temperatures, cementite grows as disperse platelets which are semicoherent with the matrix, the size of platelets being very diverse. The concentration of carbon in the  $\alpha$ -solution around finer particles is greater than near larger ones [see formula (30)]. This concentration gradient causes carbon diffusion in the  $\alpha$ -solution from finer to coarser cementite particles, resulting in the  $\alpha$ -solution becoming undersaturated near finer particles and supersaturated near larger ones, so that finer particles dissolve and coarser ones grow at their expense. This fact can be verified by frequency curves of the size distribution of cementite particles on isothermal tempering (Fig. 198): as particle coarsening proceeds, the number of fine particles diminishes. Cementite precipitates from the  $\alpha$ -solution on large particles in sites far from their edges and corners, so that the shape of particles gradually approaches the spherical. Thus, the transfer of matter through the solution effects particle coarsening and spheroidization of cementite on

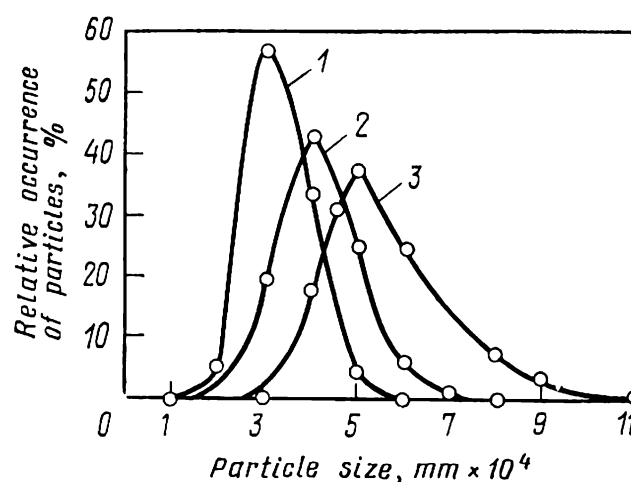


Fig. 198. Size distribution of cementite particles in steel with 0.4% C upon tempering at 630°C (after S. Z. Bockstein)

Holding time: 1—10 min; 2—1 h; 3—25 h

steel tempering. Below 350 °C, these processes develop very weakly and proceed intensively only beginning from 350-400 °C. Above 550 °C, cementite particles become perfectly spherical. With isothermal holding, coarsening of cementite particles develops intensively in a short time (one hour) and then attenuates. The average size of cementite particles increases with increasing temperature of tempering.

**Decomposition of retained austenite** plays an important part in tempering of high-carbon steels where it can present in an appreciable amount (see Fig. 160). Austenite decomposes actively within a temperature range of from 200 to 300 °C. Retained austenite transforms on tempering into lower bainite, which is a mixture of  $\alpha$ -solution and platelets of cementite (or  $\epsilon$ -carbide). In the above discussion, we have concentrated on the formation of carbides in tempering. Of no less importance are the changes in the state of the matrix phase, including the reduction of carbon concentration in the  $\alpha$ -solution and changes in the substructure and microstructure of the  $\alpha$ -phase.

**The concentration of carbon** in the  $\alpha$ -solution diminishes within the whole temperature range of precipitation of carbide phase from it.

By analysing the diffraction patterns on X-ray photographs, G. V. Kurdjumov has separated two stages in decomposition of martensite.

The first stage may be called 'two-phase' decomposition, which takes place at temperatures below 150 °C.

The mobility of carbon atoms at temperatures below 150 °C is still too low. It is quite sufficient to ensure the formation of carbide platelets at the expense of the carbon from the nearest martensitic surrounding, but insufficient for the growth of precipitated carbide particles through the diffusion of carbon from martensitic regions still not involved in decomposition and having a high initial concentration of carbon. As a result of this decomposition, martensite becomes inhomogeneous, with the carbon content varying in its various portions. The concentration of carbon in portions where carbide has precipitated is lower, and, therefore, the tetragonality is also lower than in portions yet not subjected to decomposition. Owing to a low rate of diffusion, the two solid solutions of different carbon concentration co-exist for a long time, because of which this type of decomposition is called 'two-phase'. The 'two-phase' decomposition of martensite develops through precipitation of new carbide particles in portions having the initial concentration of carbon, rather than owing to the growth of carbide particles from carbon-depleted portions of the solution.

Since carbide particles precipitated at low temperatures are extremely fine, they are in a metastable colloidal equilibrium with



the surrounding solution which has an excess of carbon [see formula (30)]. For further depletion in carbon of the portions of the solution which surround carbide particles, coarsening of the latter is essential.

The second stage of decomposition of martensite is the removal of carbon from the  $\alpha$ -solution with simultaneous growth of carbide particles (150–300 °C). The rate of carbon diffusion at temperatures above 150 °C is sufficient to ensure the growth of carbide particles by the transfer of atoms through the  $\alpha$ -solution. Because of this, common diffusion growth of carbide particles occurs

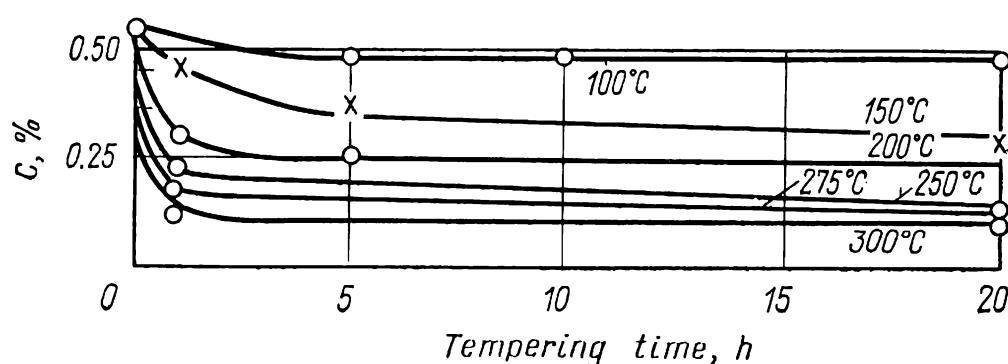


Fig. 199. Variation of carbon content in  $\alpha$ -solution upon martensite tempering of steel with 0.56% C (after E. Z. Kaminsky and T. I. Stelletsckaya)

at temperatures above 150 °C along with the 'two-phase' decomposition. However, carbide crystals grow only slowly at temperatures up to 300 °C and remain extremely fine. Typical of the kinetics of this decomposition is that the  $\alpha$ -solution is quickly depleted of carbon in a relatively short time, which depends on temperature, after which the process of depletion quickly attenuates (Fig. 199). Each tempering temperature has a corresponding carbon concentration in the supersaturated  $\alpha$ -solution. At 300 °C, nearly 0.1 per cent C remains in the  $\alpha$ -solution. Above that temperature, common X-ray structural analysis fails to detect any difference between the lattice of  $\alpha$ -solution and that of  $\alpha$ -iron. Below 300 °C, the degree of tetragonality ( $c/a > 1$ ) still can be measured. At 400 °C or a somewhat higher temperature, the  $\alpha$ -solution is fully spared of surplus carbon and the martensite-to-ferrite transformation comes to the end.

**Recovery and recrystallization** in the  $\alpha$ -phase can take place within a wide range of tempering temperatures. The development of these processes is retarded by precipitated carbide particles which lock individual dislocations, dislocation arrays and high-angle boundaries. The locking effect is less pronounced in low-carbon steels, where the corresponding processes have been studied in more detail.

The lower temperature limit of recovery on tempering cannot be specified definitely. The changes in the dislocation structure of

the  $\alpha$ -phase which can be revealed by electron microscopy, start at temperatures near 400 °C. The extension of low-angle boundaries in lath martensite at tempering temperatures above 400 °C can drop sharply in a few fractions of a second. A probable mechanism of this process is 'unraveling' of dislocation arrays, which has been mentioned when discussing the coalescence of subgrains during annealing of cold-deformed metal (see 1.2.3). At the initial moments of tempering, carbide precipitates are still scarce and thus cannot be effective barriers for low-angle boundaries and individual dislocations. Then, upon precipitation of a large number of carbide particles, the structure of the matrix stabilizes. The extension of the laths of  $\alpha$ -phase in low-carbon steels is retained at relatively high temperatures of tempering.

At certain stages of high-temperature tempering, polygonization rearrangement of the dislocation structure causes the formation of low-angle boundaries. Unlike the case with primary recrystallization in cold-deformed metal, the formation of recrystallization nuclei of the  $\alpha$ -phase and their development into recrystallized grains are not observed in tempered steel, notwithstanding the high dislocation density in martensite.

After a sufficiently long time of tempering at high temperatures, when boundary locking weakens owing to coagulation of cementite particles, grains coarsen through migration of the initial high-angle boundaries. The microstructure of the metal then loses the typical morphological features of lath martensite.

In high-carbon steels, the recrystallization growth of  $\alpha$ -phase grains is even more impeded owing to a strong retarding effect of cementite particles on boundary migration, so that an acicular structure is retained up to a tempering temperature of nearly 650 °C.

It follows from what has been said above that tempering of hardened carbon steel involved various processes which overlap one another in the time and temperature interval of their development.

All the above-mentioned temperature ranges of various structural changes are rather conditional. They diminish on increasing the time of tempering and can shift upwards or downwards on changing the carbon content in steel.

It has been agreed to separate three temperature ranges and the corresponding three 'transformations' in tempering of carbon steels. This division, which is based on an analysis of volume changes in tempering, though being rather conditional, may be taken as a first approximation.

*The first 'transformation' in tempering* is related to a temperature range of 100-200 °C. At these temperatures, a hardened specimen becomes shorter. Since martensite has the greatest specific

volume among all structural components in steel, this first 'transformation' is explained by martensite decomposition.

*The second 'transformation' in tempering* is related to a temperature range from 200 to 300 °C. The length of hardened specimens of medium- and high-carbon steels increases within this temperature range proportionally with the content of carbon. Since austenite has the lowest specific volume and the amount of retained austenite increases with increasing carbon content in the steel, the second 'transformation' is explained by decomposition of austenite. Naturally, one should keep in mind that martensite continues to decompose within the temperature range of the second 'transformation'.

*The third 'transformation' in tempering* is related to a temperature range of 300-400 °C, within which the length of specimens diminishes. Calculations show that this shortening effect can be attributed to the replacement of an intermediate carbide by cementite.

The structure formed in steel upon tempering at temperatures below 300 °C is called *temper martensite*. Microscopically, it differs from the martensite in hardened steel by a greater etchability owing to carbide precipitates. Tempering at 300-450 °C produces especially strongly etchable acicular structure called *temper troostite*. Tempering at temperatures within the range of 450-650 °C gives *temper sorbite*, a two-phase structure clearly visible at large magnifications of the optical microscope. At high temperatures of tempering, the structure of sorbite changes from acicular to clearly spheroidal type.

### Effect of Alloying Elements

The diffusion mobility of atoms of alloying elements dissolved substitutionally in  $\alpha$ -iron is many orders of magnitude lower than that of atoms of carbon, which dissolves interstitially in iron. At tempering temperatures below 450 °C, no diffusion redistribution of alloying elements takes place in the matrix: the iron carbides precipitating from the  $\alpha$ -solution have the same concentration of alloying elements as that in the martensite. Atoms of alloying elements in the lattice of intermediate carbides and cementite, which form at temperatures below approximately 450 °C, partially substitute iron atoms:  $(\text{Fe}, \text{Cr})_3\text{C}$ ,  $(\text{Fe}, \text{V})_3\text{C}$ , etc.

Alloying elements have no effect of substantial practical importance on the first stage of martensite decomposition, i.e. on the 'two-phase' decomposition at temperatures below 150 °C. This agrees well with the fact that the main process in this first stage, i.e. the nucleation of carbide particles, depends mainly on the degree of supersaturation of the  $\alpha$ -solution with carbon, while diffu-

sion growth of carbide precipitates is only weakly developed in carbon steels.

Many alloying elements can have an appreciable effect on the second stage of martensite decomposition, by retarding the growth of carbide particles and retaining the supersaturation of the  $\alpha$ -solution with carbon, i.e. maintaining the state of temper martensite up to temperatures of 450-500 °C. Additions of Cr, W, Mo, V, Co, and Si can act in this manner.

The retarded decomposition of martensite may be explained in two ways.

Firstly, some alloying elements, such as vanadium, molybdenum or chromium, can lower the rate of carbon diffusion in the  $\alpha$ -solution. This cause, however, fails to explain why cobalt and silicon also produce a retarding effect, though they do not lower the diffusion of carbon in iron. Another cause is an increase in the strength of interatomic bonds in the lattice of  $\alpha$ -solution under the effect of some elements, such as Co, Si, Cr, Mo, or W, which inhibits the transition of atoms through boundaries between carbides and  $\alpha$ -solution, and therefore, inhibits the decomposition of martensite.

Alloying elements can strongly affect carbide transformations at temperatures above 450 °C, i.e. when their diffusion redistribution becomes possible. This effect results in the formation of special carbides, their appearance being probably due to two mechanisms. Firstly, the concentration of a carbide-forming alloying element in cementite may increase (owing to its diffusion redistribution between the  $\alpha$ -solution and cementite) to such an extent that it transforms into a special carbide. For instance, alloyed cementite  $(\text{Fe}, \text{Cr})_3\text{C}$  may transform into a chromium carbide  $(\text{Cr}, \text{Fe})_7\text{C}_3$ . Secondly, a special carbide may nucleate directly in the  $\alpha$ -solution when the latter is supersaturated with an alloying element. Initially, partially coherent precipitates of an intermediate special carbide may form, their precipitation being accompanied with the dissolution of cementite, which is the least stable phase in alloy steel. Special carbide particles usually nucleate preferably at dislocations in the martensite. At higher temperatures of tempering, an intermediate special carbide is replaced with a stable special carbide.

It is highly important for the practice (see 4.2.2) that precipitated particles of some carbides, such as  $\text{TiC}$ ,  $\text{V}_4\text{C}_3$ ,  $\text{Mo}_2\text{C}$  or  $\text{W}_2\text{C}$ , are much smaller than dissolvable cementite particles, one of the probable reasons for this being that atoms of alloying elements have a low diffusion mobility.

Alloying elements can affect the rate of coarsening of carbide particles. Nickel accelerates particle coarsening, while chromium, molybdenum, vanadium and some other elements produce an in-

hibiting effect. The elements which can strengthen the interatomic bonds in the lattices of  $\alpha$ -solution and carbides (in the latter case they are strong carbide-formers) and decrease the rate of carbon diffusion in the  $\alpha$ -solution, can impede the passage of atoms through the carbide  $\alpha$ -solution and  $\alpha$ -solution-carbide boundaries and the transfer of carbon through the solution. These elements can inhibit the dissolution of fine and growth of coarser particles.

Alloying additions can retard polygonization and recrystallization processes in tempering, firstly, by retarding the diffusion processes of dislocation climb and, secondly, owing to the fact that dislocations, low-angle and high-angle boundaries are locked by disperse particles of special carbides having a small interparticle spacing.

Most alloying elements raise the temperature range of decomposition of retained austenite. In tempering of carbon steel, retained austenite decomposes within the range of 200-300 °C, but can remain up to temperatures of 500-600 °C in alloy steel. Hardened high-alloy high-carbon steels, such as free-cutting grades, usually contain a large amount of retained austenite. If such a steel is tempered at 500-600 °C, its retained austenite becomes capable of martensitic transformation when cooled from the temperature of tempering, since carbides precipitate from the retained austenite and the latter is depleted of carbon and alloying elements in high-temperature tempering. As a result, the martensitic point  $M_s$  increases and the retained austenite becomes capable of martensitic transformation when cooled from the temperature of tempering.

### Tempering of Maraging Steels

Maraging steels are carbonless Fe-Ni alloys additionally alloyed with cobalt, molybdenum, titanium and some other elements. A typical example is an iron alloy with 17-19 per cent Ni, 7-9 per cent Co, 4.5-5 per cent Mo and 0.6-0.9 per cent Ti (Grade H18K9M5T). Alloys of this type are hardened to martensite and then tempered at 480-500 °C, the tempering resulting in strong precipitation hardening owing to the precipitation of intermetallics from the martensite, which is supersaturated with the alloying elements. By analogy with the precipitation hardening in aluminium, copper and other non-ferrous alloys, this process has been termed ageing, and since the initial structure is martensite, the steels have been called maraging.

We have agreed earlier (see p. 298) to use the term 'ageing' only to alloys which are quenched without polymorphic transformation and the term 'tempering', to all alloys which are hardened to martensite. So as not to disturb the

adopted classification and terminology, let us agree to relate the process of martensite decomposition in maraging steels to tempering, though the combination 'tempering of maraging steels' is not the best choice.

The structure of commercial maraging steels at the stage of maximum hardening can contain partially coherent precipitates of intermediate metastable phases  $\text{Ni}_3\text{Mo}$  and  $\text{Ni}_3\text{Ti}$  or  $\text{Ni}_3(\text{Mo}, \text{Ti})$ . The h.c.p.  $\text{Ni}_3\text{Ti}$  phase is similar to hexagonal  $\epsilon$ -carbide in carbon steels. Like  $\epsilon$ -carbide particles in carbon steels,  $\text{Ni}_3\text{Ti}$  precipitates in maraging steels are so oriented relative to martensite that  $(0001)_{\text{Ni}_3\text{Ti}} \parallel (011)_m$ .

Of special practical value is the fact that particles of intermediate intermetallics in maraging steels are extremely disperse, which is mainly due to their precipitation at dislocations.

The structure of maraging steels has a high density of dislocations, which appear on martensitic rearrangement of the lattice. In lath (untwinned) martensite, the density of dislocations is of an order of  $10^{11}$ - $10^{12} \text{ cm}^{-2}$ , i.e. the same as in a strongly strain-hardened metal. In that respect the substructure of maraging steel (as hardened) differs appreciably from that of aluminium, copper and other alloys which can be quenched without polymorphic change.

It is assumed that the precipitation of intermediate phases on tempering of maraging steels is preceded with segregation of atoms of alloying elements at dislocations. The atmospheres formed at dislocations serve as centres for the subsequent concentration stratification of the martensite, which is supersaturated with alloying elements.

In maraging steels the dislocation structure, that forms in the course of martensitic transformation, is very stable during the subsequent heating and practically remains unchanged at the optimum temperatures of tempering (480-500 °C). Such a high density of dislocations during the whole course of tempering may be due, to an appreciable extent, to dislocation pinning by disperse precipitates.

A long holding in tempering at a higher temperature (550 °C or more) may coarsen the precipitates and increase the interparticle spacing, with the dislocation density being simultaneously reduced. With a long holding time, semicoherent precipitates of intermediate intermetallics are replaced with coarser incoherent precipitates of stable Laves phases of the type  $\text{Fe}_2\text{Ni}$  or  $\text{Fe}_2\text{Mo}$ .

At increased temperatures of tempering (above 500 °C), maraging steels may undergo the reverse  $\alpha \rightarrow \gamma$  martensitic transformation, since the  $A_s$  point is very close to the optimum temperatures of tempering (see Fig. 123). The formation of austenite is then accompanied with the dissolution of the intermetallics that have precipitated from the  $\alpha$ -phase.

#### 4.2.2. VARIATIONS OF MECHANICAL PROPERTIES IN TEMPERED STEELS AND SELECTION OF TEMPERING CONDITIONS

##### Variations of Properties in Carbon Steels

A hardened carbon steel has a high hardness and is very liable to brittle fracture. Besides, hardening can cause appreciable residual stresses. For that reason, hardening is not commonly used as a final procedure with carbon steels, though it can impart a high strength ( $\sigma_t = 130\text{--}200 \text{ kgf/mm}^2$ ) to the metal. Hardening is usually followed with tempering in order to increase the ductility and lower residual stresses.

The decomposition of martensite should have caused, on the face of it, precipitation hardening and, in the general case, the dependence of the strength properties of a steel on the temperature of tempering should have been the same as in ageing of non-ferrous alloys. But, as may be seen in Fig. 200, up to a tempering temperature of about  $100^\circ\text{C}$ , the hardness of hardened steel either remains unchanged or changes only weakly (by 1-2 HRC numbers). With further increase of temperature, the hardness lowers smoothly.

Why the decomposition of martensite with precipitation of fine carbide particles in low-temperature tempering of hardened steel does not cause a strong precipitation hardening, as is the case with aluminium and other age-hardenable alloys? An explanation may be that carbon atoms have a high mobility and thus have enough time to form segregates at dislocations already during quenching. Thus, the process of self-tempering takes place during quenching, during which the precipitation hardening can proceed to the stage of maximum hardening. Since the carbon that is dissolved in  $\alpha$ -iron contributes much to the hardening of the martensite (see 3.2.6), the depletion of the solution in carbon upon precipitation of intermediate carbides (for instance,  $\epsilon$ -carbide) already at low temperatures of tempering produces the softening effect.

As the temperature of tempering is increased, the softening effect is enhanced due to the following reasons:

- (1) a lower concentration of carbon in the  $\alpha$ -solution;

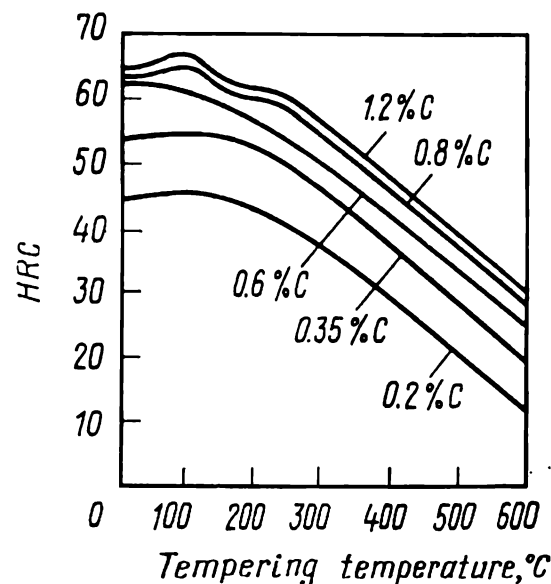


Fig. 200. Effect of tempering temperature on hardness of carbon steels of various composition (after G. V. Kurdjumov)

(2) disturbance of coherence at carbide-matrix boundaries and relief of elastic microstresses;

(3) coarsening of carbide particles and an increase of inter-particle spacing;

(4) development of recovery and recrystallization. Various softening factors may act in various temperature intervals, in accordance with the intensity of development of some or other structural changes (see 4.2.1). In high-carbon steels, which contain an appreciable amount of retained austenite, the latter decomposes with the precipitation of carbide and thus retards the drop

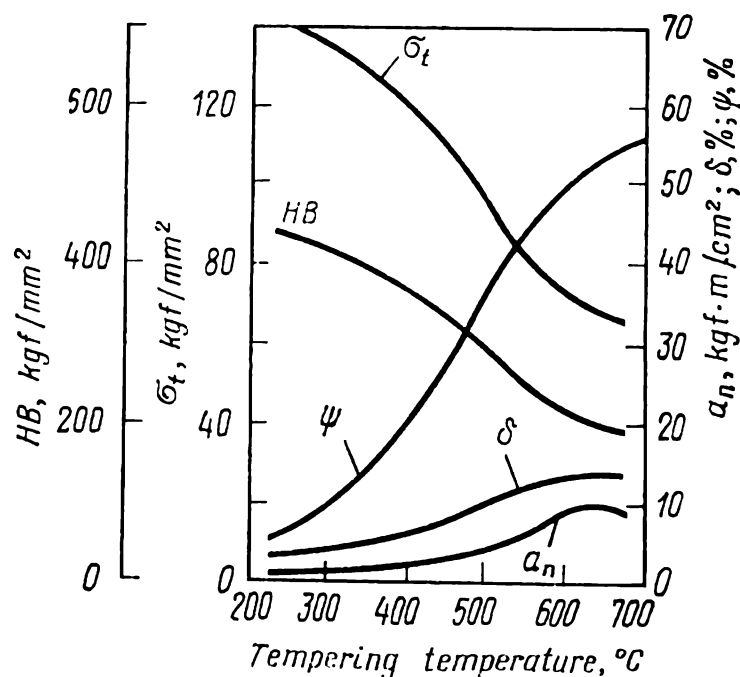


Fig. 201. Effect of tempering temperature on mechanical properties of steel Grade 45

in hardness and even can increase the hardness within a temperature range of 200-250 °C (see Fig. 200).

Since the hardening tempering of hardened carbon steel has no practical significance, it is often assumed that tempering of any steel inevitably results in softening of the metal, though the concept is erroneous, as will be shown below.

The strength characteristics (ultimate strength, yield limit and hardness) of carbon steel decrease continuously as the temperature of tempering is raised above 300 °C, while the ductility indices (relative elongation and relative reduction) continuously increase (Fig. 201). The impact toughness, a characteristic of high importance in structural steel, begins to increase intensively on tempering above 300 °C. The maximum impact toughness is found in sorbitic steel tempered at 600 °C. A certain drop in impact toughness at tempering temperatures above 600 °C can be explained by the fact that cementite particles, which grow at boun-



daries of ferritic grains owing to the dissolution of particles in the  $\alpha$ -phase, become excessively coarse.

According to the temperature of heating, a distinction is made between low-, medium- and high-temperature tempering.

*Low-temperature tempering* to martensite (at 120-250 °C) is widely used after hardening of tools, cemented and cyanided products and after case hardening. The low-temperature tempering serves to reduce the residual hardening stresses; the temperature is selected at a level that causes no or almost no loss in hardness and wear resistance. The holding time at the temperature of low tempering is usually not more than 1-3 hours; a further increase in the holding time has almost no effect on residual stresses.

A variety of low-temperature tempering is *stabilizing tempering*. Slow processes (for many years) of decomposition of martensite, transformation of retained austenite into martensite, and relief of residual stresses can occur in hardened steel at room temperature and the more so, as a result of climatic temperature changes. All these phenomena cause a gradual change in the dimensions of products. In some types of tools, such as high-precision measuring instruments or precision ball bearings, dimensional variations by even a few  $\mu\text{m}$  are inadmissible. The dimensions of such products must therefore be stabilized. The harmful effect of retained austenite is eliminated by diminishing its amount by sub-zero treatment (see 3.2.9). The stabilization of the martensite and of the stressed state is obtained by a low-temperature (stabilizing) tempering at 100-180 °C with a holding time of up to 30 hours, or, sometimes, up to 150 hours.

*Medium-temperature tempering* to troostite (at 350-450 °C) is a procedure that is employed relatively seldom, only when it is required to combine a high strength and high elasticity with a sufficient toughness in some products, such as springs.

*High-temperature tempering* to sorbite (450-650 °C) is employed in machine-building for structural steel parts which must possess a sufficient strength combined with a high impact resistance. The holding time in high-temperature tempering (usually a few hours) is chosen experimentally to provide the desired complex of properties.

Quasi-eutectoid sorbitic structure can be obtained by normalizing directly from austenite on cooling a steel; this method gives the same hardness as high-temperature tempering. For the same hardness, however, the values of relative reduction and impact toughness are appreciably higher in tempered steel. This can be explained by the fact that hardness depends mainly on the dispersity of ferrite-cementite mixture, while relative reduction and impact toughness may be affected strongly by the shape of cementite particles. The sorbite formed on decomposition of auste-

nite contains cementite in the form of elongated platelets, whereas the cementite in temper sorbite is in the form of short rounded-off platelets or even in spheroidal form, which imparts greater toughness to the metal.

In medium-carbon steels (0.35 to 0.6 per cent C), sorbite is formed by a duplex operation: i.e. hardening followed with high-temperature tempering. The hardening forms greater residual stresses than does normalizing. Despite this, the method is preferred for critical machine elements, since the gain in impact toughness is quite appreciable. In addition, quenching stresses are relieved almost fully by the high-temperature tempering.

The quality of hardening procedure may have an appreciable effect on the properties of steel after high-temperature tempering. Through-hardening of parts is essential, otherwise the inner layers will have a lower impact toughness than the external ones (for the same hardness), since the former will contain lamellar cementite and the latter, spheroidized cementite. If the precipitation of excess ferrite has not been suppressed during quenching, this can lower not only the impact toughness, but also the ultimate strength, hardness and especially fatigue strength.

Suppose, for example, that a blank of steel Grade 45, 15 mm in diameter, is quenched through in water. High-temperature tempering then forms a structure of spheroidized sorbite in its core, which may be characterized by the properties as follows:  $\sigma_t = 80$  kgf/mm<sup>2</sup>,  $\sigma_{0.2} = 65$  kgf/mm<sup>2</sup>,  $\delta = 16$  per cent, and  $a_n = 10$  kgf·m/cm<sup>2</sup>. In a blank 100 mm in diameter, the central layers are cooled at a rate appreciably lower than the critical rate of quenching. This results in the central layers having the structure of lamellar sorbite and excess ferrite, which has reduced values of strength and ductility compared with that of spheroidized sorbite:  $\sigma_t = 70$  kgf/mm<sup>2</sup>,  $\sigma_{0.2} = 45$  kgf/mm<sup>2</sup>,  $\delta = 13$  per cent, and  $a_n = 5$  kgf·m/cm<sup>2</sup>.

The rate of cooling from the temperature of tempering has no effect on mechanical properties of carbon steels, so that accelerated cooling is possible, provided that the thermal stresses are not critical.

Quenching and tempering can sometimes be combined in a single operation, which is then called *quenching with self-tempering*. A heated part is immersed for a short time in water or sprinkled with water. The surface layer is thus quenched to martensite and then tempered owing to the heat supplied from the core. This method is employed for sorbitizing the surface layer of rail tops, which should possess an appropriate resistance to crushing and wear and at the same time have a sufficient impact toughness and a high endurance limit, which are ensured by the formation of temper sorbite structure.

### Variations of Properties in Alloy Steels

The alloying elements that can inhibit decomposition of martensite and coarsening of carbide particles (see 4.2.1), shift the temperature limit of the beginning of intensive softening from 200-300 °C upwards to 450-550 °C. Increasing the *red hardness* of hardened steel, i.e. the capability of resistance to softening on heating, is one of the main aims of alloying in tool manufacture.

For structural alloy steels it is very important that special carbides precipitate on high-temperature tempering in a more disperse form than that of cementite. This ensures an increased toughness, since microvoids (possible centres of fracture) nucleate near fine particles of special carbides less easily than near larger particles of cementite.

#### Secondary Hardening

In steels with additions of Ti, Mo, V or W at increased temperature of tempering after the common softening, which has been caused by decomposition of martensite and coarsening of cementite particles, the hardness increases again (Fig. 202). This phenomenon, which takes place upon tempering at 500-600 °C, is called secondary hardening.

The cause of secondary hardening is the replacement of relatively coarse particles of cementite, which are being dissolved with appreciably more disperse precipitates of a special carbide ( $\text{TiC}$ ,  $\text{V}_4\text{C}_3$ ,  $\text{Mo}_2\text{C}$  or  $\text{W}_2\text{C}$ ). These carbide particles, which precipitate preferably at dislocations, are responsible for the hardening effect in tempered steel.

An addition of chromium, which retards softening on tempering, may have only a slight or even no secondary hardening effect. This may be explained by the fact that  $\text{Cr}_7\text{C}_3$  carbide precipitates rapidly coarsen at 550 °C, unlike other carbides, such as  $\text{Mo}_2\text{C}$ .

Additions of cobalt, which forms no carbide of its own, can intensify secondary hardening, which may be probably linked with inhibited polygonization (retention of a high density of dislocations at which carbides of other elements can precipitate), as also with a higher supersaturation in carbon of the  $\alpha$ -solution.

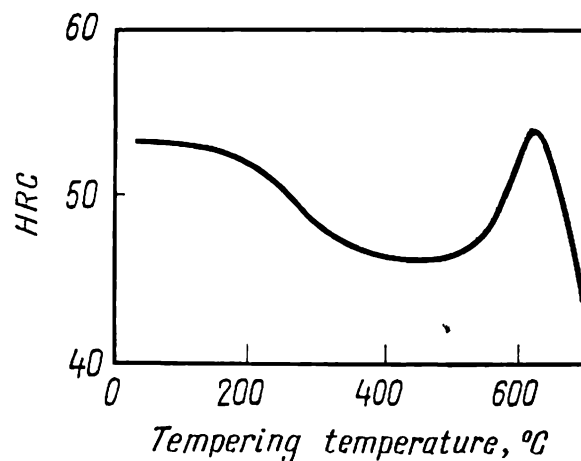


Fig. 202. Secondary hardening on tempering of steel with 0.32% C and 1.36% V

It is quite interesting that the rise in the yield limit on secondary hardening is accompanied with an increase in toughness, owing to dissolution of relatively coarse cementite particles. With an increase in the time of tempering, the yield limit usually decreases and the toughness increases, owing to partial coarsening of special carbides. Therefore, it is possible to choose the optimum time of tempering to obtain a high toughness and a high yield limit on secondary hardening.

### Temper Embrittlement

Temper embrittlement is inherent in many steels and can be characterized by a reduced impact toughness. The state of temper embrittlement has practically no effect on other mechanical properties at room temperature.

Figure 203 shows schematically the effect of temperature on impact toughness of an alloy steel which is strongly liable to temper

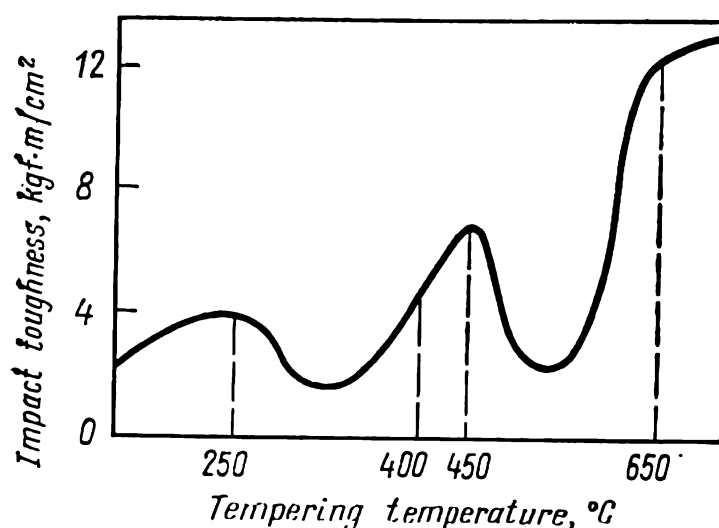


Fig. 203. Effect of tempering temperature on impact toughness of steel having a high susceptibility to temper embrittlement (schematically)

per embrittlement. Many alloy steels have two temperature intervals of temper embrittlement. For instance, *irreversible temper brittleness* may appear within the interval of 250-400°C and *reversible temper brittleness*, within 450-650°C.

The impact toughness of quenched steel after tempering at 250-400°C is lower than that obtained on tempering at temperatures below 250°C. If a brittle steel tempered at 250-400°C is heated above 400°C and transferred into a tough state, a second tempering at 250-400°C cannot return it to the brittle state. The rate of cooling from the tempering temperature within 250-400°C has no effect on impact toughness. A steel in the state of irreversible temper embrittlement has a bright intercrystalline frac-

ture at boundaries of former austenitic grains. This type of brittleness is inherent to some extent in all steels, including carbon grades. For that reason medium-temperature tempering is, as a rule, not employed in practice, though it can ensure a high yield limit.

Irreversible temper embrittlement is thought to be due to the formation of carbides on decomposition of martensite, in particular, precipitation of carbides in the form of films at grain boundaries. At higher temperatures of tempering, this film disappears and cannot be restored on repeated heating at 250-400 °C. Silicon in low-alloy steels can prevent irreversible temper embrittlement by retarding the decomposition of martensite.

The embrittlement on high-temperature tempering may manifest itself in two different ways: (a) as a result of heating at 450-600 °C (irrespective of the rate of subsequent cooling) and (b) as a result of tempering at temperatures above 600 °C with subsequent slow cooling within the range of 600-450 °C. A high-rate cooling from a tempering temperature above 600 °C, for instance, water cooling, can prevent the appearance of temper embrittlement. On the other hand, a quick cooling on tempering at 450-600 °C, cannot prevent temper embrittlement. Thus, entering the dangerous temperature interval from either 'below' (on heating and holding at that temperature) or from 'above' (on slow cooling) can produce the same result.

The most important feature of embrittlement on high-temperature tempering is that the process is reversible. If a steel embrittled through tempering at a temperature above 600 °C with subsequent slow cooling or through tempering at 450-600 °C (with any rate of cooling) is again heated above 600 °C and cooled quickly, its impact toughness will restore to the initial value. If the steel then again enters the dangerous interval of tempering temperatures, it is again embrittled. A new heating at a temperature above 600 °C, followed with quick cooling, can eliminate the embrittling effect, and so on. This is why the phenomenon discussed is called reversible embrittlement.

Carbon steels with less than 0.5 per cent Mn are not prone to reversible temper embrittlement. The phenomenon can only appear in alloy steels. Alloying elements may have different effects on the steel proneness to temper embrittlement. Unfortunately, the most widely used alloying elements, such as chromium, nickel, and manganese, promote temper embrittlement. When taken separately, they produce a weaker effect than in the case of combined alloying. The highest embrittling effect is observed in chrome-nickel and chrome-manganese steels. Small additions of molybdenum (0.2-0.3 per cent) can diminish temper embrittlement, while greater additions enhance the effect.

A fundamental fact is that alloy steels of very high purity are utterly unsusceptible to temper embrittlement which is caused by the presence of various impurities, in the first place of phosphorus, tin, antimony and arsenic, in commercial steels.

The rate and degree of development of temper embrittlement depend on the temperature and time of holding a steel within the dangerous temperature interval (450-600 °C). With a certain temperature of tempering within this interval, the initial stages of embrittlement appear appreciably sooner than at a higher or a lower temperature.

Many scientists adhered for a long time to the 'solution precipitation' hypothesis, according to which the loss in impact toughness was caused by precipitation of some phases, such as phosphides, at grain boundaries. These phases were thought to pass into the  $\alpha$ -solution on heating up to approximately 650 °C and to precipitate from the solution and embrittle the steel on slow cooling; quick cooling should prevent the precipitation of embrittling phases. As has been found by electron-microscopic analysis, however, there are no special precipitates at grain boundaries in embrittled steel, so that the 'solution precipitation' hypothesis turned to be inconsistent.

Another hypothesis explained temper embrittlement by an increased concentration of impurities in boundary layers of the solid solution. This was proved by an increased etchability of grain boundaries in embrittled steel by picric acid. The hypothesis on the leading role of impurity segregates has been fully confirmed in the recent years by a brilliant series of research work using Auger spectroscopy, a method enabling determination of concentrations of elements in monatomic surface layers. Using this method makes it possible to detect segregations of phosphorus and other impurity elements at the fracture surface in embrittled steel and measure their concentrations (as also the concentrations of alloying elements) at the fracture surface. It has also been shown that the development of temper embrittlement is directly linked with the rise of impurity concentration near the prior austenite boundaries.

Owing to equilibrium segregation (see 2.1.3), the concentration of harmful impurities at the surface of a fracture may exceed tens or hundreds times their average concentration in the steel. The concentration of impurities in commercial purity steels is usually a few thousandths or hundredths of a per cent, but amounts to a few per cent at the surface of fracture.

As the temperature increases, the diffusion process of grain-boundary segregation is accelerated, with the absolute value of equilibrium segregation being simultaneously decreased owing to thermal motion.

At temperatures above 600-650 °C, the segregation of impurities either disappears fully (Sb) or drops to a very low level (P). On subsequent cooling of the steel in water, the segregates have no time to restore.

The role of alloying elements in the development of temper embrittlement is not less than that of impurities. The segregation of harmful impurities in iron-carbon alloys is so small that causes no temper embrittlement. In the presence of alloying elements (Ni, Cr or Mn), the segregation of impurities increases appreciably. In this process, the alloying elements themselves, which cause no equilibrium segregation in high-purity steels, segregate at grain boundaries in the presence of harmful impurities. Therefore, we can assume that an alloying element and impurity interact with each other in the  $\alpha$ -solution and thus mutually promote their segregation. It can be also assumed that if atoms of an impurity and alloying element attract one another stronger than atoms of that impurity and iron, the segregation of the impurity and alloying element will be mutually enhanced. Namely in this way behave P and Ni, P and Cr, Sb and Ni, Sb and Mn and other 'impurity-alloying element' pairs. A second alloying element can additionally enhance segregation of an impurity. For instance, nickel and chromium, when present together in steel, can cause a greater segregation of antimony than might be expected from simple summation of their separate effects.

An increased concentration of harmful impurities in boundary layers of the solid solution which may be caused by the effect of alloying additions, weakens the intergranular bondage and is one of the main causes why alloy steels containing Ni, Cr or Mn are highly susceptible to temper embrittlement. The main measures to prevent temper embrittlement are as follows: (a) reduction of the content of harmful impurities in steel; (b) accelerated cooling from the temperature of high-temperature tempering (above 600 °C); (c) alloying of steel with small additions of molybdenum (0.2-0.3 per cent); and (d) subjecting the metal to high-temperature thermomechanical treatment (see 5.2.2. below).

### Variations of Properties in Maraging Steels

The dependence of mechanical properties of maraging steels on the temperature of tempering (Fig. 204) is of the same pattern as that for all precipitation-hardenable alloys, i.e. the strength properties increase to a maximum, after which softening takes place. By analogy with ageing, the stages of *hardening* and *softening tempering* may be separated in the process.

The hardening effect is caused by the formation of segregates at dislocations and, what is most important, by the formation of

partially coherent precipitates of intermediate phases of the type  $\text{Ni}_3\text{Ti}$  or  $\text{Ni}_3\text{Mo}$ . The softening is due, in the first place, to replacement of disperse precipitates of these phases with coarser stable precipitates having greater interparticle spacings and, in the second place, to the reverse  $\alpha \rightarrow \gamma$  martensitic transformation which is accompanied by the dissolution of intermetallics in the austenite.

The ultimate strength of maraging steels increases on tempering roughly by 80 per cent and the yield limit, by 140 per cent

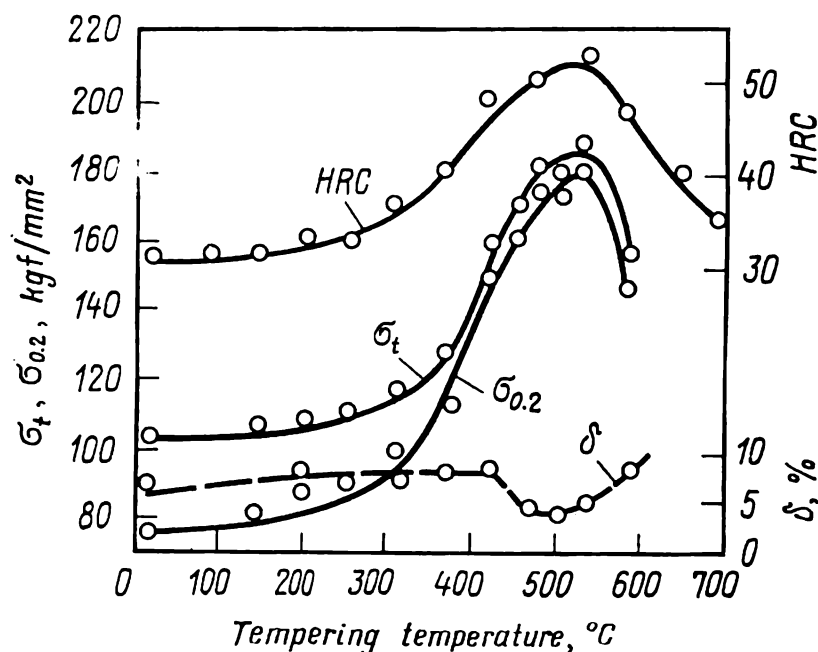


Fig. 204. Effect of tempering temperature on mechanical properties of maraging steel with 18% Ni, 7% Co, 4.5% Mo and 0.3% Ti (after *Banerjee, Capenos and Hansen*)

(Fig. 204), i.e. the relative gain in strength properties is not greater than in typical age-hardening alloys, such as beryllium bronze or aluminium alloy Grade 1915 (see Table 15), but the absolute values of ultimate and yield strength on tempering of maraging steels reach record figures among all precipitation-hardening alloys. This is mainly due to the fact that maraging steels have a very high strength ( $\sigma_t = 110 \text{ kgf/mm}^2$ ) in the initial (as-hardened) state.

The high strength of maraging steels on tempering at 480-500 °C for 1-3 hours may be explained by the precipitation of very disperse semicoherent particles of the size and interparticle spacing of an order of  $10^2 \text{ \AA}$  in the strong matrix, these intermetallic precipitates also possessing a high strength. Thus, with the same dispersity of precipitates as that of G. P. zones in precipitation-hardening non-ferrous alloys, maraging steels possess an appreciably higher ultimate strength ( $\sigma_t = 180\text{-}200 \text{ kgf/mm}^2$ ).



As compared with martensite-hardenable carbon-containing steels, carbonless maraging steels show, for the same strength, a substantially greater resistance to brittle fracture, which is their most remarkable merit. The causes why they have a high resistance to brittle fracture in as-hardened state were discussed in 3.2.6. On tempering to the maximum strength, the ductility indices and impact toughness, though diminish somewhat, still remain rather high. The high ductility of the carbonless matrix and the high dispersity of uniformly distributed intermetallic precipitates are responsible for a very high resistance to cracking, which is the most valuable property of modern high-strength structural materials.

#### LITERATURE

Kurdjumov G. V., Utevsky L. M., Entin R. I., Transformations in Iron and Steel (*Prevrashcheniya v zheleze i stali*). Moscow, Nauka, 1977, 238 pp., ill.

Starodubov K. F. in: Physical Metallurgy and Heat Treatment of Metals (*Metallovedenie i termicheskaya obrabotka*), vol. 1 pp. 691—709. Moscow, Metallurgizdat, 1961, 747 pp., ill.

Belous M. V., Cherepin V. T., Vasilyev M. A., Transformations in Tempered Steel (*Prevrashcheniya pri otpuske stali*). Moscow, Metallurgiya, 1973, 231 pp., ill.

Perkas M. D., Kardonsky V. M., High-strength Maraging Steels (*Vysokoprochnye martensitno-stareyushchie stali*). Moscow, Metallurgiya, 1970, 224 pp., ill.

## CHEMICAL HEAT TREATMENT AND THERMO-MECHANICAL TREATMENT

As distinct from heat treatment proper, the thermal effect in chemical heat treatment and thermo-mechanical treatment is assisted by respectively chemical or mechanical (deformation) action on the metal. This complicates the general picture of the changes in structure and properties occurring on heat treatment.

The equipment for chemical heat treatment and thermo-mechanical treatment also is, as a rule, more complicated and may, in addition to common heat-treatment arrangements, comprise, for instance, installations for controlling furnace atmosphere, equipment for plastic forming of metal, etc.

In view of the specifics of the structural changes, the equipment and processing employed, chemical heat treatment and thermo-mechanical treatment should be considered independent scientific and technological methods. But since the thermal action on the metal plays the most important part in them, they are usually regarded as varieties of heat treatment of metals (see Fig. 1).

The general laws of variations in the structure and properties of metals on chemical heat treatment and thermo-mechanical treatment and some varieties of these methods will be discussed below.

### 5.1. CHEMICAL HEAT TREATMENT

#### 5.1.1. CHANGES IN COMPOSITION AND STRUCTURE OF METAL ON CHEMICAL HEAT TREATMENT

*Chemical heat treatment, which combines thermal and chemical action on the metal, changes the composition and structure in the surface layers and, sometimes, in the bulk of the metal.*

To change the composition, a metal part is heated in an active medium. During the holding time, the metal is diffusionally enriched with some or other elements from the external medium. Besides, chemical heat treatment can be used to remove, by diffusion, some impurities and in individual cases, even some main elements from the metal.

The overwhelming majority of industrial processes of chemical heat treatment includes diffusion enrichment of surface layers of

products with metals or non-metals from an external active medium, which may be gaseous, liquid or solid. The most common among these processes is cementation, i.e. carburization of steel products in charcoal at a high temperature. The method has been known from the ancient time, long before the Common Era.

Three simultaneous processes can be distinguished, which ensure that the metal is enriched with elements from the external medium.

The first process is the formation of an element in an activated atomic state (*in statu nascendi*) as a result of various chemical reactions (see 5.1.2) or owing to vaporization. In some cases, for instance, if metal atoms are supplied directly from the melt, this stage may be absent.

The second process is the adsorption of atoms at the metal surface. The adsorption process may include simple physical adsorption, in which mono- or polyatomic adsorption layer is formed at the whole surface of an article or in its most active portions owing to the effect of van der Waals attraction forces. Chemical adsorption (chemisorption) may simultaneously take place and form strong chemical bonds between the atoms being adsorbed and atoms of the metallic surface. Adsorption is always an exothermal process, i.e. it lowers the free energy.

The third process possible in chemical heat treatment is the diffusion of adsorbed atoms from the surface into the depth of metal. Adsorption occurs quickly, whereas diffusion is a slow process. Since the depth of the zone having the changed composition (*diffusion zone*) and the concentration distribution in that zone depend primarily on the course of diffusion, the analysis of chemical heat treatment pays the principal attention to the laws of diffusion.

### Formation of a Single-phase Diffusion Zone

Consider the process of diffusion penetration of an element from the surface into the depth of a metal article. In any point of the diffusion zone at a depth  $x$  from the surface, the concentration  $C$  of the solid solution varies in time  $\tau$  by Fick's second law:

$$\frac{\partial C}{\partial \tau} = D \frac{\partial^2 C}{\partial x^2} \quad (38)$$

For simplicity, it is assumed henceforth that the diffusion coefficient  $D$  is independent of concentration.

The diffusion equation (38) can be solved for definite boundary conditions. In the case considered, use can be made of the solution for diffusion into a semi-infinite space with a constant concentration at the surface. (Fig. 205). In a point at a depth  $x$

from the surface, the concentration  $C(x, \tau)$  depends on the concentration at the surface,  $C_s$ , the initial concentration in the bulk,  $C_0$ , the diffusion coefficient  $D$ , and the time  $\tau$  elapsed from the beginning of the process:

$$C(x, \tau) = C_s - (C_s - C_0) \operatorname{erf} \left( \frac{x}{2\sqrt{D\tau}} \right) \quad (39)$$

For the case of diffusion into a pure metal,  $C_0 = 0$  and

$$C(x, \tau) = C_s \left[ 1 - \operatorname{erf} \left( \frac{x}{2\sqrt{D\tau}} \right) \right] \quad (40)$$

The error function  $\operatorname{erf}(z)$ <sup>1</sup> can be found in tables, such as Table 16 below.

Table 16. Selected Values of Error Function  $\operatorname{erf}(z)$

$z$	$\operatorname{erf}(z)$	$z$	$\operatorname{erf}(z)$	$z$	$\operatorname{erf}(z)$	$z$	$\operatorname{erf}(z)$
0	0	0.4	0.4284	0.8	0.7421	2.0	0.9953
0.1	0.1125	0.5	0.5205	1.0	0.8427	2.5	0.9996
0.2	0.2227	0.6	0.6039	1.2	0.9103	2.8	0.9999
0.3	0.3286			1.5	0.9661		

The error function is zero at  $z = 0$  and tends to unity at higher values of  $z$ . For any holding time at  $x = 0$  (the surface

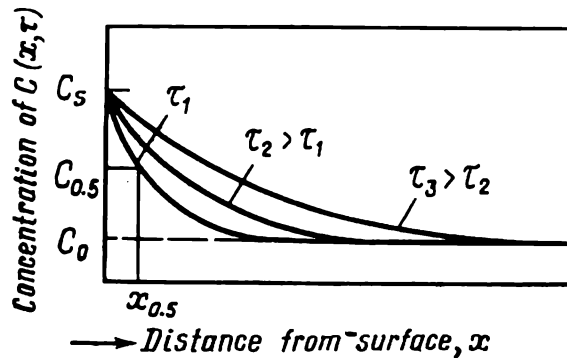


Fig 205. Distribution of concentration in a single-phase zone of diffusion saturation with constant surface concentration  $C_s$  at various moments of time

The area under the curve of distribution of the concentration of the element over the cross-section of the article determines the total content of the element in the diffusion zone for a given holding time.

of article),  $(x/2\sqrt{D\tau}) = 0$  and  $C(0, \tau) = C_s$ , while with departure from the surface and with higher values of  $x$ ,  $\operatorname{erf} \left( \frac{x}{2\sqrt{D\tau}} \right)$  tends to unity and  $C(x, \tau)$  tends to  $C_0$  [see formula (39)]. Thus, the boundary conditions, we have chosen for solving the diffusion equation, are satisfied.

With increasing holding time, the diffusion zone expands and the content of the diffusing element in it increases (see Fig. 205).

<sup>1</sup> In formulae (39) and (40)  $z = \frac{x}{2\sqrt{D\tau}}$

Let us analyse how the depth of diffusion zone can vary with increasing holding time and increasing temperature.

Let us initially characterize the depth of penetration of the diffusing element by the distance  $x_{0.5}$  from the surface at which the concentration gradient is half of the maximum, i.e.  $(C_s - C_{0.5})/(C_s - C_0) = 0.5$  (see Fig. 205). If  $C(x, \tau) = C_{0.5}$ , then  $\text{erf}(x_{0.5}/2\sqrt{D\tau}) = 0.5$ . According to Table 16, with  $z = 0.5$ ,  $\text{erf}(z) = 0.5205$ , and therefore,  $x_{0.5}/2\sqrt{D\tau} \approx 1/2$ . Hence  $x_{0.5} = \sqrt{D\tau}$ .

Taking  $x$  as the depth of penetration of the element from the surface to any point of a given concentration, we can find that

$$x = K \sqrt{D\tau} \quad (41)$$

where  $K$  is a constant.

Thus, the depth of the diffusion zone varies proportionally to the square root of holding time at constant temperature. In order

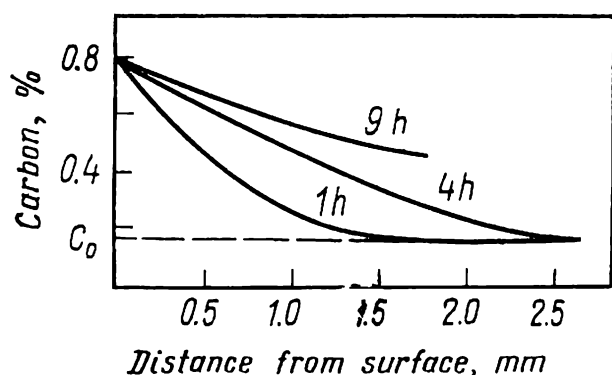


Fig. 206. Distribution of carbon concentration in diffusion zone after 1, 4 and 9 hours of carburizing at 920 °C with constant surface concentration (after P. G. Shewmon)

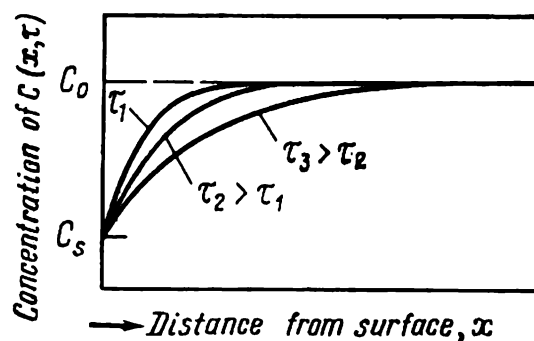


Fig. 207. Distribution of concentration in a single-phase diffusion depletion zone at various moments of time with constant surface concentration  $C_s$

to increase the depth of diffusion zone, say, three times, the holding time must be increased by a factor of nine.

Figure 206 shows calculated curves of carbon distribution in the diffusion zone in a steel article for three different holding times at constant temperature. As will be seen, as the time of carburization is increased, the concentration of carbon in any point of the diffusion zone increases attenuatedly.

In actual processes of chemical heat treatment, the parabolic pattern of the growth of diffusion zone, which is described by formula (41), may be violated owing to a varying concentration at the surface (for instance, with a high activity of the surrounding medium, the concentration  $C_s$  may increase).

Experiments show that the dependence of the depth of a single-phase diffusion zone on temperature is exponential or nearly ex-

ponential. This should have been expected, noting that the diffusion coefficient in formula (41) increases exponentially with temperature [see formula (2)].

Removal of an impurity or a main component by diffusion from the bulk of metal into the external medium with a constant concentration of the element at the surface (Fig. 207) can be expressed by the equation

$$C(x, \tau) = C_s + (C_0 - C_s) \operatorname{erf} \left( \frac{x}{2\sqrt{D\tau}} \right) \quad (42)$$

If the diffusing element is removed quickly from the surface and the concentration  $C_s$  is practically zero, then

$$C(x, \tau) = C_0 \operatorname{erf} \left( \frac{x}{2\sqrt{D\tau}} \right) \quad (43)$$

If the diffusion zone is being depleted of an element, its depth is also proportional to  $\sqrt{D\tau}$ , i.e. changes with holding time by a parabolic law.

### Formation of a Multiphase Diffusion Zone

When an article is cooled from the temperature of chemical heat treatment, certain phase transformations can occur in a single-phase diffusion zone, such as polymorphic transformation of the solid solution, eutectoid transformation, precipitation of an excess phase, etc.

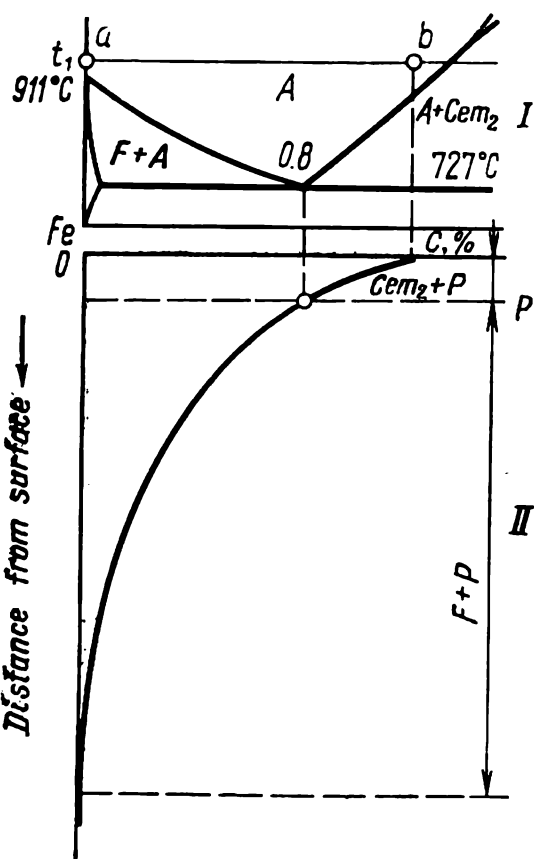


Fig. 208. A portion of Fe-C constitutional diagram (I) and curve of carbon distribution across the diffusion zone (II) upon carburization of iron at temperature  $t_1$  (schematically)

Suppose that during carburization of iron at a temperature  $t_1$  (above  $911^\circ\text{C}$ ) the concentration of carbon at the surface increases from point  $a$  (pure iron) to point  $b$ , without reaching the boundary of the austenitic region (Fig. 208, I). At the

temperature of chemical heat treatment, the diffusion zone at any instant has an austenitic structure with a variable carbon concentration which diminishes on moving from the surface into the depth of metal (see the curve in Fig. 208, II).

With slow cooling from the carburization temperature, austenite undergoes certain phase transformations in accordance with the Fe-C constitutional diagram. In the portion of the diffusion

zone which is near the surface and has the carbon concentration above 0.8 per cent, the structure at room temperature is secondary cementite plus pearlite and in the portion with less than 0.8 per cent carbon, it is excess ferrite plus pearlite. With moving from the surface deeper into the metal, the network of secondary cementite gradually disappears owing to continuously decreasing carbon concentration and the structure becomes purely pearlitic, after which the amount of pearlite gradually decreases and the structure becomes ferritic (Fig. 209).

Thus, in the case considered the diffusion zone is single-phase during the chemical heat treatment, but becomes two-phase (ferrite + cementite) throughout its whole bulk owing to the transformations taking place on cooling.

New phases can appear directly in the process of diffusion changes of the composition at the temperature of chemical heat treatment. The diffusion process which is accompanied with the appearance of new phases is called *reaction* diffusion.

The principal probability of occurrence of reaction diffusion is determined on the constitutional diagram. Reaction diffusion is impossible in systems forming continuous series of solid solutions, but can take place in any system with a limited solubility of the components in the solid state.

Two different mechanisms have been proposed to explain the appearance of new phases on reaction diffusion,

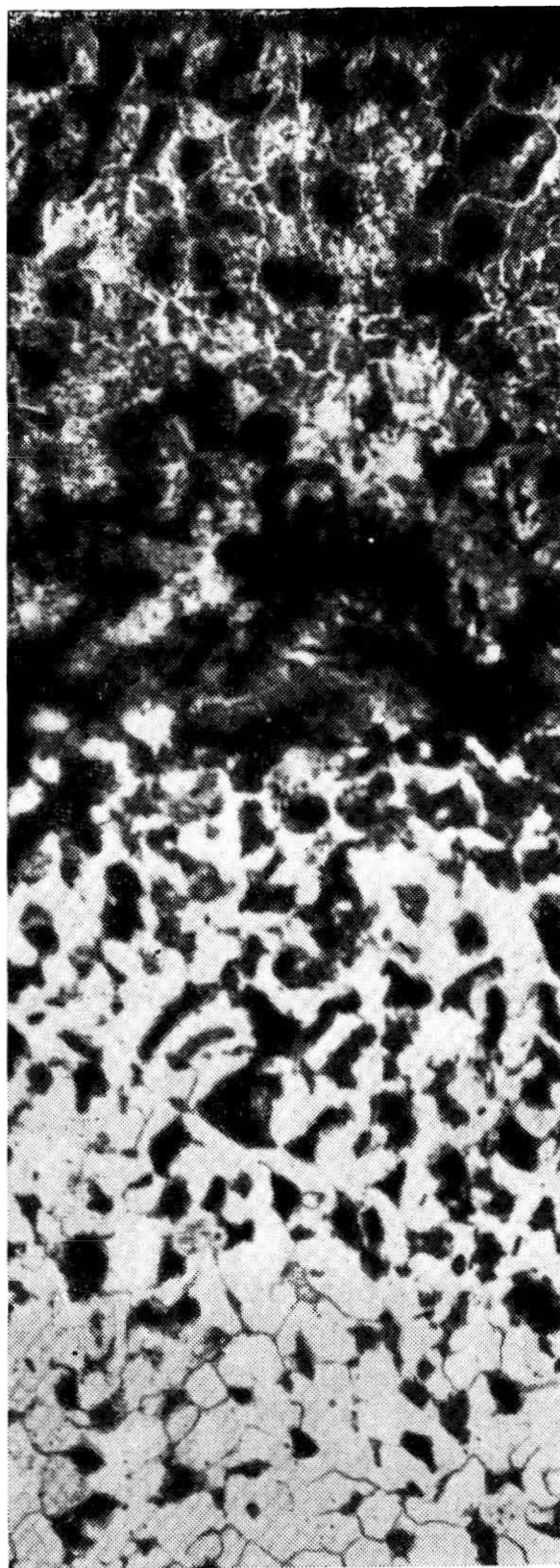


Fig. 209. Microstructure of diffusion zone after slow cooling from the carburization temperature of iron,  $\times 200$

By one of them, a chemical reaction takes place directly at the interface between the metal and the surrounding medium. This reaction is regarded as the initial stage of reaction diffusion, which determines the essence of the diffusion process (V. Z. Bugakov). A new phase forms owing to forces of chemical interaction between the reacting elements. This mechanism can produce only a very thin (of an order of atomic size) layer of a compound, since, once formed, it isolates atoms of the reacting elements. Further growth of the new phase is ensured by the diffusion of one or both elements through the layer formed.

By another mechanism of reaction diffusion, the ultimate solubility must necessarily be reached as the diffusing element is being supplied from an external medium, after which conditions are formed that ensure the formation of the phase which, in accordance with the constitutional diagram, should be in equilibrium with the saturated solid solution (D. A. Prokoshkin). This diffusion is also commonly called reaction diffusion, but the process is essentially decided by the saturation (more exactly, supersaturation) of the initial solution with the diffusing element, rather than by the chemical reaction at the surface. Therefore, a more appropriate term is diffusion with phase transformations. The analysis that follows is based exactly on this concept of the appearance of new phases in chemical heat treatment.

Consider the diffusion of element  $B$  into an article made from element  $A$  at temperature  $t_1$  (Fig. 210). As the holding time is increased, the concentration of element  $B$  in the  $\alpha$ -solution increases smoothly in the surface layer (Fig. 211) until the solubility limit is reached at a sufficiently high activity of the external medium (point  $a$  in Fig. 210). Upon reaching this moment ( $\tau_2$  in Fig. 211), further supply of element  $B$  from the external medium supersaturates the  $\alpha$ -phase in this element, so that the  $\beta$ -phase of composition of point  $b$  (see Fig. 210) precipitates from the  $\alpha$ -phase in the surface layer. As a result, the concentration of element  $B$  in the surface layer increases jumplike by  $ab$ .

As element  $B$  continues to be supplied from the external medium, its concentration increases smoothly in the whole layer of the  $\beta$ -phase. Atoms of element  $B$  diffuse continuously from the surface of the article to the boundary between  $\beta$ - and  $\alpha$ -phase, enter the  $\alpha$ -phase and maintain a supersaturated state in the latter near the  $\beta/\alpha$  boundary. Because of this, the  $\beta$ -phase precipitates continuously at the  $\beta/\alpha$  boundary and this moves into the depth of the article (see the positions of layer boundaries at moments  $\tau_3$  and  $\tau_4$  in Fig. 211).

When the concentration of element  $B$  in the  $\beta$ -phase of the surface layer has reached the limit for the given temperature (point  $c$  in Fig. 210), after which the  $\beta$ -phase becomes supersaturated, the



$\gamma$ -phase of the composition of point  $d$  forms in that layer. With further supply of component  $B$ , its concentration in the  $\gamma$ -phase increases smoothly, causing the  $\gamma/\beta$  boundary to move into the depth of the article.

The following typical features of the formation of a multiphase diffusion zone may be noted.

*The sequence in which the phases are formed in diffusional variation of the composition of metal corresponds to their positions*

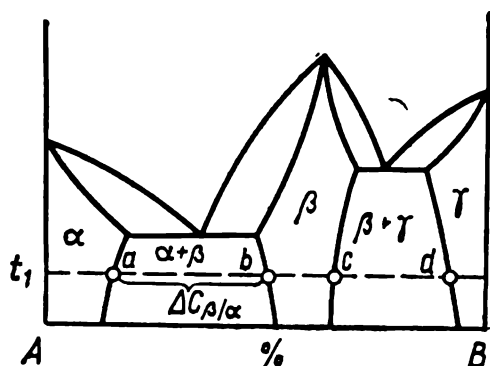


Fig. 210. Constitutional diagram of a binary A-B system

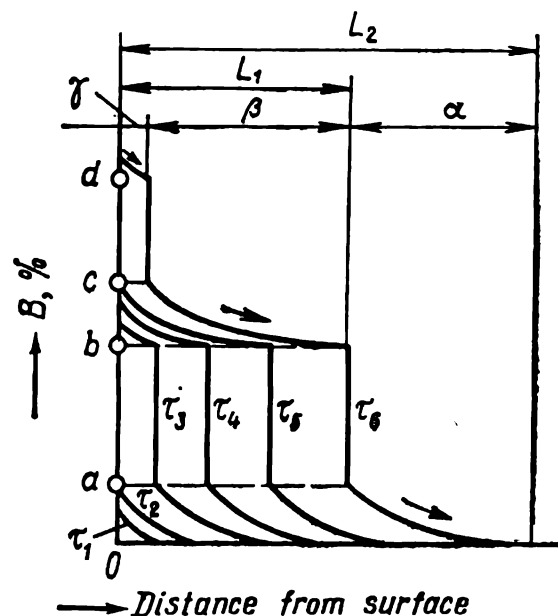


Fig. 211. Distribution of concentration of element  $B$  in diffusion zone upon saturation of metal  $A$  at temperature  $t_1$  at various moments of time  $\tau_1$ - $\tau_6$  (for A-B constitutional diagram see Fig. 210)

in the constitutional diagram ( $\alpha \rightarrow \beta \rightarrow \gamma$  in Fig. 210). The phases appear in this order as the concentration of the diffusing element in the surface layer increases with holding time and are distributed in the same order in the diffusion zone from the core towards the surface (see the instant  $\tau_6$  in Fig. 211). If a phase is not detected experimentally (by optical microscopy or X-ray analysis) in the diffusion zone, this by no means implies that the phase has been 'missed' during the formation of the zone. Owing to a low rate of diffusion growth, the thickness of the zone may be such that the phase cannot be revealed experimentally for a given time of chemical heat treatment. A 'missing' phase is usually detected with a longer holding time.

*There is a concentration gradient across each growing layer of a phase.* Without such a gradient, diffusion penetration of an element into the depth of an article, i.e. the formation of a diffusion zone would be impossible.

The compositions of phases at a boundary between neighbouring layers in a diffusion zone are determined by the compositions of the phases that are in equilibrium in the constitutional diagram (see, for instance, points *a* and *b* or *c* and *d* in Fig. 210). This follows from the fact that a new phase can only form after the saturation limit of the initial phase has been reached.

When one element is being diffusively saturated with another, there are no two-phase regions in a diffusion zone, i.e. only single-phase layers can verge with one another (see Fig. 211). An

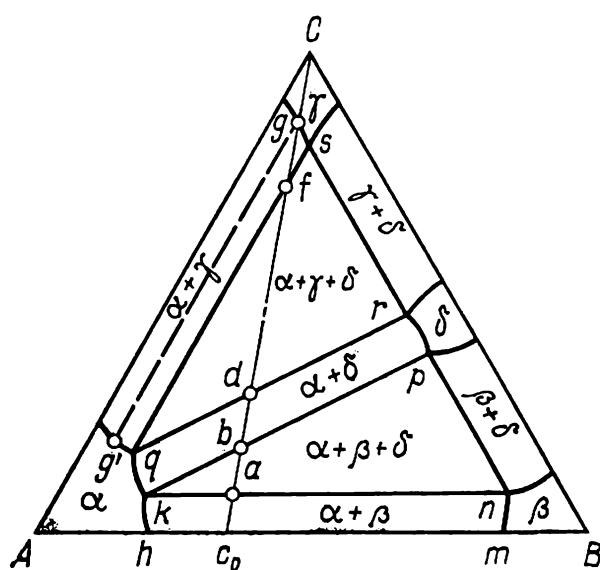


Fig. 212. Isothermal section through a ternary *A-B-C* system to explain the sequence of layer formation during diffusion of element *C* into  $c_0$  alloy (after A. P. Gulyaev)

explanation is that the compositions of each of the phases in a two-phase mixture are invariable at any ratio between them and are determined by the corresponding points in the constitutional diagram (for instance, points *a* and *b* in Fig. 210). On the other hand, a concentration gradient in a variable-composition phase is required for diffusion growth of a layer. This is why, the growth of a two-phase layer across which the compositions of each of the phases are constant is impossible, as also is impossible in the general the transfer of an element from the surface into the depth of an article across such a layer.

Two-phase layers can grow in chemical heat treatment of alloys (but not of pure metals) or in diffusion saturation of a metal with two elements at once. In such cases the diffusion zone is a ternary system in which the compositions of equilibrium phases in the two-phase region are variable.

Suppose that element *C* diffuses into a two-component alloy of composition  $c_0$  (Fig. 212). With a constant ratio of components *A* and *B* in the diffusion zone, its composition varies along line  $c_0C$ . Element *C* is dissolved in the phases  $\alpha$  and  $\beta$  and, while the average composition of the two-phase  $\alpha + \beta$  layer varies along  $c_0a$  line, the composition of the  $\alpha$ -phase varies along  $hk$  line and that of the  $\beta$ -phase, along  $mn$  line. A three-phase layer cannot form in this system, since, according to the isothermal section, the compositions of the three phases  $\alpha_k$ ,  $\beta_n$  and  $\delta_p$  that are in equilibrium are constant and diffusion across the three-phase layer into the depth of article is impossible. Thus, as the average com-

position of the two-phase  $\alpha + \beta$  layer reaches point  $a$ , it changes jumpwise to point  $b$ ; a two-phase  $\alpha_k + \delta_p$  layer then forms owing to the replacement of  $\beta_n$  phase with  $\delta_p$  phase.

When the average composition of the  $\alpha + \delta$  layer varies along  $bd$  line, the compositions of the  $\alpha$ -phase and  $\delta$ -phase vary respectively along  $kq$  and  $pr$  lines. With a further supply of component  $C$  into the diffusion zone, the average composition of the zone at the surface varies jumpwise from point  $d$  to point  $f$ , since the  $\delta_r$ -phase is replaced with  $\gamma_s$ -phase.

The average composition of the two-phase layer then changes along  $fg$  line, and those of the  $\alpha$ -phase and  $\gamma$ -phase, along  $qg'$  and  $sg$  lines (the dotted line  $gg'$  in Fig. 212 is a conode which determines the compositions of equilibrium phases  $\alpha$  and  $\gamma$ ). In this process, the  $\alpha$ -phase transforms into  $\gamma$ -phase and finally, only the  $\gamma$ -phase remains in the surface layer, the composition of that phase varying along the ray towards  $C$  component.

Thus, upon chemical heat treatment a  $\gamma$ -layer is at the surface and two-phase  $\alpha + \gamma$ ,  $\alpha + \delta$ , and  $\alpha + \beta$  layers, below it (Fig. 213).

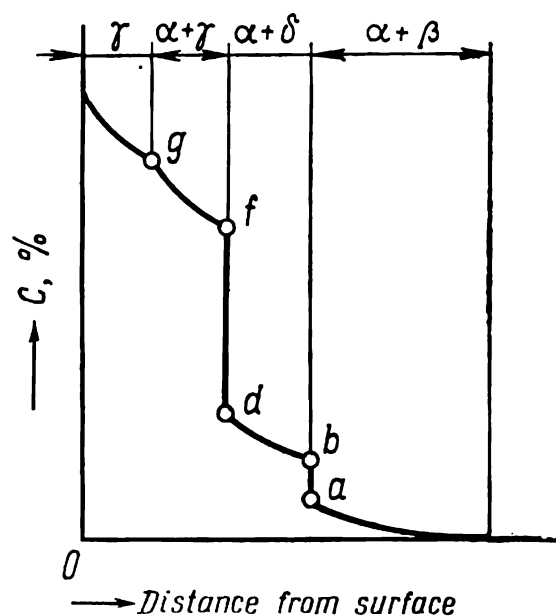


Fig. 213. Distribution of average concentration of element  $C$  in diffusion zone of  $c_0$  alloy (see Fig. 212)

The above analysis based on the use of an isothermal section through a ternary system is only valid if the concentration ratio between  $A$  and  $B$  components is invariable at any point of the diffusion zone and if the phases in the two-phase layers are always in equilibrium.

Consider the kinetics of growth of single-phase layers during chemical heat treatment by using the analysis of diffusion processes made by A. A. Popov.

When element  $B$  diffuses into metal  $A$ , the boundary of the  $\beta$ -phase moves towards the  $\alpha$ -phase by  $dL$  during time  $d\tau$  (see the corresponding constitutional diagram in Fig. 210 and the distribution of the element in the diffusion zone in Fig. 214). The increment of the volume of  $\beta$ -phase layer is  $dV = SdL$ , where  $S$  is the area of the interface between  $\alpha$ -phase and  $\beta$ -phase.

The  $\beta$ -phase contains more of component  $B$  than the  $\alpha$ -phase. The concentration jump at their interface is  $\Delta C_{\beta/\alpha}$  (see Fig. 210). As the volume of the  $\beta$ -phase increases by  $dV$ , the amount of element  $B$  in the layer of that phase increases by  $dV \Delta C_{\beta/\alpha}$ .

Let us reduce our calculations to a unit surface area of the interface ( $S = 1$ ). Then  $dV \Delta C_{\beta/\alpha} = dL \Delta C_{\beta/\alpha}$  (see the hatched portion in Fig. 214).

The diffusion in the  $\beta$ -phase brings  $B$  atoms to the  $\beta/\alpha$  interface, while the diffusion in the  $\alpha$ -phase removes  $B$  atoms from that interface. The amount of  $B$  element supplied to the  $\beta/\alpha$  interface through the  $\beta$ -phase may be denoted by  $dm_\beta$  and that removed from the interface through the  $\alpha$ -phase, by  $dm_\alpha$ . The difference

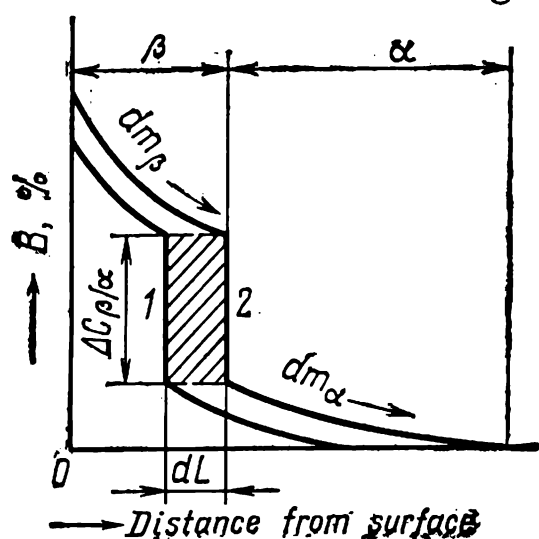


Fig. 214. Distribution of element  $B$  in diffusion zone at moments  $\tau_1$  (1) and  $\tau + d\tau$  (2)

$dm_\beta - dm_\alpha$  is equal to the gain in the total content of  $B$  element in the  $\beta$ -phase layer as the interface has moved through  $dL$ .

Consequently

$$dL \Delta C_{\beta/\alpha} = dm_\beta - dm_\alpha$$

In accordance with Fick's first law [see formula (1)], we can write for unit surface area of the interface that

$$dL \Delta C_{\beta/\alpha} = D_\beta \left( \frac{\partial C_\beta}{\partial x} \right) d\tau - D_\alpha \left( \frac{\partial C_\alpha}{\partial x} \right) d\tau$$

Hence, the rate of motion of the boundary of the  $\beta$ -layer towards  $\alpha$ -phase is

$$\frac{dL}{d\tau} = \frac{D_\beta \left( \frac{\partial C_\beta}{\partial x} \right) - D_\alpha \left( \frac{\partial C_\alpha}{\partial x} \right)}{\Delta C_{\beta/\alpha}} \quad (44)$$

The solution of this equation for a constant concentration at the surface of the article shows that the thickness of the layer of a new phase ( $L$ ) increases parabolically with the holding time ( $\tau$ ):

$$L = K \sqrt{\tau} \quad (45)$$

This formula is analogous with equation (41) for the growth of diffusion zone in chemical heat treatment without the formation of new phases, but the proportionality factor  $K$  depends here on an appreciably greater number of factors.

It follows from equation (44) that the *thickness of the layer of a new phase is the greater, the more intensive is the diffusion in that layer, the slower the diffusion in the layer of an adjacent phase, and the smaller is the concentration jump at the boundary between these phases.*

If the diffusion zone is composed of layers of different phases, the thickness of an intermediate layer ( $\beta$  in Fig. 211) depends on the ratio of velocities of motion of the layer boundaries, and therefore, on the development of diffusion processes in each of the phases.

The directions of diffusion flows in layers of a diffusion zone are shown by arrows in Fig. 211. The diffusion inflow of element  $B$  in the  $\beta$ -layer towards the  $\beta/\alpha$  interface maintains the  $\alpha$ -phase supersaturated near that interface and tends to shift that interface to the right and thus to increase the thickness of the  $\beta$ -layer. The diffusion outflow of element  $B$  in the  $\alpha$ -layer from the  $\beta/\alpha$  interface decreases the supersaturation of the  $\alpha$ -phase near that interface and tends to shift the latter to the left. Similarly, the diffusion inflow of element  $B$  in the  $\gamma$ -layer towards the  $\gamma/\beta$  interface tends to shift this interface to the right and diminish the depth of the  $\beta$ -layer. This is counteracted by the diffusion outflow of element  $B$  inside the  $\beta$ -layer from the  $\gamma/\beta$  interface.

In accordance with Fick's first law, the diffusion flow through a phase layer is more intense with a higher diffusion coefficient in the phase and a higher concentration gradient across the layer. In turn, the concentration gradient is greater at greater difference in the composition of the phase at the two boundaries and a smaller depth of the layer. As has been noted earlier, the compositions at the boundaries of a layer are determined by the corresponding points in the constitutional diagram, such as points  $b$  and  $c$  for  $\beta$ -phase layer (see Figs. 210 and 211). Therefore, *with a constant diffusion coefficient, the flow of a diffusing element through a layer of a given depth increases with widening of the homogeneous region of the phase in the constitutional diagram* (see line  $bc$  in Fig. 210).

It follows from the above that the depth of the layer of a new phase in the diffusion zone cannot, in the general case, increase exponentially with increasing temperature, since it depends not only on the diffusion coefficient in the phase considered.

The depth of phase layers may vary in different ways with increasing temperature of chemical heat treatment. It depends on the ratio of diffusion flows in the layer in question and in adjacent layers. For example, if the width of the homogeneous region of a phase in the constitutional diagram changes only slightly with increasing temperature, only the layer of a phase whose diffusion coefficient increases more will grow in thickness. If, however, the diffusion coefficients in adjacent layers increase almost similarly with increasing temperature of chemical heat treatment, the layer of the phase whose homogeneous region widens more in the constitutional diagram will grow in thickness. The growth of phases having very narrow homogeneous regions may

be so slow that their layers in the diffusion zone will not be revealed experimentally.

Owing to simultaneous and different variations of diffusion coefficients, concentration gradients within phases and concentration jumps at their interfaces, the rate of growth of the layers of these phases, which is determined by equation (44), may vary in a complicated manner with increasing temperature of chemical

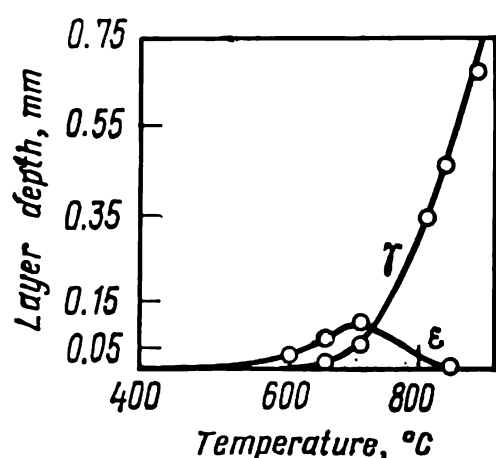


Fig. 215. Effect of temperature on the depth of layers of  $\epsilon$ -phase and  $\gamma$ -phase in nitriding of iron for 6 h (after Yu. M. Lakhtin)

heat treatment. For instance, the depth of  $\epsilon$ -phase layer in nitriding (see 5.1.2) increases with increasing temperature of the process up to approximately 700 °C and then decreases (Fig. 215). In other (not seldom) cases, the depth of a phase layer may depend almost exponentially on temperature (see the curve for  $\gamma$ -phase in Fig. 215).

### The Structure of Diffusion Zone

The diffusion zone can be revealed in microsections by etching, since the surface layer has a different composition. In a single-phase zone, the concentration changes smoothly from the surface into the depth of metal (see Fig. 205), because of which the boundary of such a zone is very diffuse or even (more often) invisible in the microscope.

If diffusion is accompanied with phase transformations, the structure of the diffusion zone differs sharply from that of the deeper layers of the metal. The difference in the type of lattice and the concentration jump at the boundary between the new and initial phase are responsible for a sharp difference in etchability at both sides of the boundary and promote etching of the boundary proper in the form of a *diffusion line* (Fig. 216).

The distance from the surface of metal to the boundary with the initial solution ( $L_1$  in Fig. 211) is usually taken conditionally as the depth of diffusion zone (the actual depth  $L_2$  is greater by the depth of the layer of the initial solid solution in which the composition has changed).

Crystals of a new phase that form in the diffusion zone have columnar form (Fig. 216). This may be explained by the fact that they grow only at an interface between different phases, where the diffusion inflow of the element maintains the initial phase supersaturated. As the boundary between the layers moves into the depth of metal, crystals of the new phase grow in that direction.

If a polymorphic transformation takes place upon cooling from the temperature of chemical heat treatment, columnar crystals of the phase formed through diffusion saturation can change to equiaxed crystals of a phase that forms on cooling.

Diffusion at grain boundaries proceeds quicker than in the body of grains, because of which chemical heat treatment can sometimes result in that the diffusing element penetrates more deeply at grain boundaries of the initial phase and precipitates

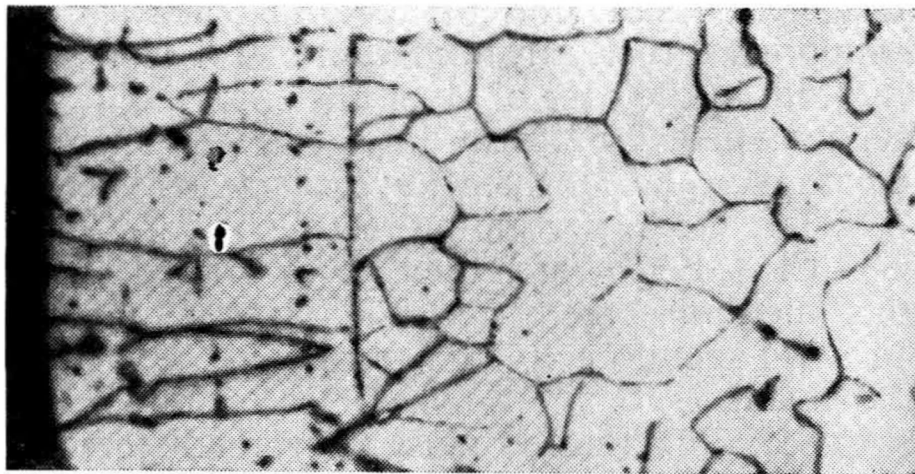


Fig. 216. Microstructure of diffusion zone after saturation of iron with molybdenum at 1200 °C for 12 h,  $\times 200$  (after G. N. Dubinin)

there as a network of crystals of the new phase. At relatively high temperatures, however, which are common for chemical heat treatment, the difference in diffusion rates at grain boundaries and in the body of grains is levelled off.

### 5.1.2. KINDS OF CHEMICAL HEAT TREATMENT

Methods of chemical heat treatment employed industrially are very diverse and differ in the diffusing elements, type and composition of the external medium, chemical processes occurring in the latter, techniques of realization, and other features.

Depending on the state of aggregation of the external medium in which articles to be treated are placed, a distinction is made between *chemical heat treatment in solid, liquid and gaseous media*.

Atoms of the diffusing element can pass from the solid medium into the surface of an article only in places of direct contact. This process is ineffective and is used only seldom. A solid medium is usually employed to form an active gaseous or vapour phase from which atoms can pass into the metal. For instance, in cementation in a solid carburizer (charcoal), carbon atoms which

diffuse into steel are formed from carbon monoxide by the reaction  $2\text{CO} \rightarrow \text{C} + \text{CO}_2$ , and charcoal is only needed to form the gaseous phase. Another example is chromizing in a 'solid' medium, when articles are packed into chromium or ferro-chrome powder. On heating, chromium evaporates and its atoms pass into the metal mainly from the vapour phase, rather than in places of direct contact of the powder with the surface of metal.

With chemical heat treatment in a liquid medium, atoms of an element to diffuse into the metal are formed by chemical reactions in a molten salt (for instance, in NaCN in steel cyaniding) or are supplied directly from molten metal (for instance, from molten aluminium in the case of steel alitizing).

With chemical heat treatment in a gaseous medium, the diffusing element may be formed by reactions of dissociation ( $\text{CH}_4 \rightarrow \text{C} + 2\text{H}_2$ ), disproportioning ( $2\text{CO} \rightarrow \text{C} + \text{CO}_2$ ), exchange ( $\text{CrCl}_2 + \text{Fe} \rightarrow \text{Cr} + \text{FeCl}_2$ ) or reduction ( $\text{VCl}_2 + \text{H}_2 \rightarrow \text{V} + 2\text{HCl}$ ).

A gaseous medium and an active gaseous phase formed on heating in a solid medium are the most widely used suppliers of atoms for the surface saturation of articles in industrial processes.

A purely gaseous medium is most convenient for chemical heat treatment; its composition can be easily controlled, it can be heated quickly to the specified temperature, enables mechanization and automation of chemical heat treatment, and allows quenching to be made immediately (without reheating).

The examples given above show that the classification of methods of chemical heat treatment according to the state of aggregation of the medium in which articles are being placed is not always in good agreement with the physico-chemical essence of the process.

G. N. Dubinin has proposed the following classification of the methods of chemical heat treatment, which is based on the physico-chemical characteristics of the active phase which supplies the diffusing element: *saturation from a solid phase, saturation from a vapour phase, saturation from a gaseous phase, and saturation from a liquid phase*. According to this classification, cementation of steel in a solid carburizer should be related to the saturation from the gaseous phase and chromizing in powdered chromium, to the saturation from the vapour phase.

As regards changes in the composition of articles, all methods of chemical heat treatment may be divided into three groups as follows: *diffusion saturation with non-metals, diffusion saturation with metals, and diffusion removal of elements*. These groups include numerous industrial processes of chemical heat treatment (see Table 17).

Each process of chemical heat treatment may be effected by various methods (saturation from gaseous, vapour, liquid or solid



Table 17. Types of Chemical Heat Treatment

Diffusion saturation with non-metals	Diffusion saturation with metals	Diffusion removal of elements
Carburizing (cementation) Nitriding Cyaniding Nitrocementation Boriding Silicification Sulphidizing Sulpho-cyaniding Oxygenizing	Alitizing Chromizing Chrome-alitizing Zincing Copperizing Titanizing Berrylizing Vanadizing	Dehydrogenation Deoxygenation Decarbonization Complex removal of impurities

phase) and in very diverse forms of engineering realization (for instance, with the active gaseous phase being produced in a furnace, or in an individual gas producer, etc.). Some typical types of chemical heat treatment are briefly discussed, by way of examples, hereinafter. These examples mainly relate to steels, since chemical heat treatment is industrially employed predominantly with steels and incomparably less often, with cast irons and non-ferrous metals and alloys.

### Diffusion Saturation with Non-metals

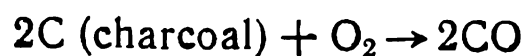
The most widely used processes of chemical heat treatment are those in which steel is surface saturated with carbon and/or nitrogen.

Carbon and nitrogen dissolve interstitially in iron and, therefore, can diffuse quickly to an appreciable depth. The active media containing these elements are inexpensive and the formed through carbon and/or nitrogen saturation or in subsequent heat treatment change sharply the mechanical and physico-chemical properties of the steel.

#### *Carburizing (Cementation)*

Cementation is employed with articles made of low-carbon steels (usually up to 0.25 per cent C).

With solid-carburizer cementation, steel parts are placed in boxes filled with a compacted mixture of charcoal and 20-25 per cent  $\text{BaCO}_3$ . On heating, the carbon of charcoal combines with atmospheric oxygen of the air which fills voids between carburizer particles in the box, to form carbon monoxide:



In contact with iron, carbon monoxide dissociates with the liberation of atomic carbon

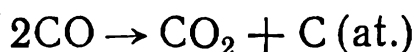


This active (*in statu nascendi*) carbon is absorbed by austenite and diffuses into the depth of metal.

The addition of  $\text{BaCO}_3$  has a strong intensifying effect on cementation, since it supplies more carbon monoxide and active carbon:

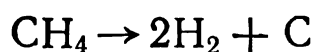


and



In gaseous cementation, the carburizer may be natural gas (composed mainly of  $\text{CH}_4$ ), controllable atmospheres produced in special gas producers, or liquid hydrocarbons (kerosene, benzene, etc.) supplied dropwise into the furnace, where they form an active gaseous phase.

The main supplier of carbon in gaseous carburizers is methane:



In artificial controllable atmospheres, the carbon supplier is usually carbon monoxide.

Gaseous cementation is the principal process in mass production, while solid-carburizer cementation is employed in small-scale production.

The depth of cemented layer is usually 0.5 to 2.0 mm, depending on steel composition and application of cemented parts.

Cementation is carried out at 910-930 °C or sometimes at 1000-1050 °C, for greater speed. The time upon which a specified cementation depth can be obtained decreases with increasing temperature. For instance, gaseous cementation can produce a cemented layer of a depth of 1.0-1.3 mm on heating for 15 h at 920 °C or for 8 h at 1000 °C. High-temperature cementation is only used with intrinsically fine-grained steels; otherwise, strong overheating (and growth of austenitic grains) is very probable.

The concentration of carbon in the surface layer of cemented articles is usually 0.8-1.0 per cent and does not reach the solubility limit at the temperature of cementation. Therefore, no  $\text{Fe}_3\text{C}$  carbide network forms at the cementation temperature and both the surface layer and the core are in austenitic state. Upon slow cooling, a cemented layer of a variable carbon concentration consists of ferrite and cementite and can be characterized by a range of structures typical of hypereutectoid, eutectoid and hypoeutectoid steel (see Fig. 208).

Cementation is an intermediate procedure aimed at enriching the surface layer in carbon. The required hardening of the surface layer is attained by subsequent quenching, which must not only harden the surface layer but also amend the overheated structure that has appeared owing to holding the metal for many hours at the cementation temperature.

Critical parts upon solid-carburizer cementation are subjected to double quenching, since the content of carbon in the core differs from that at the surface, while the optimum temperature of heating for quenching depends on the carbon content in steel (see Fig. 156).

The first quenching procedure is done from 850-900 °C (i.e. above the  $A_3$  point of the core) in order to cause full phase transformation and refinement of austenitic grain in hypoeutectoid steel. In carbon steel, which has a low hardenability, the core after the first quenching consists of ferrite and pearlite. With carbon steels, the first quenching can be replaced by normalizing. In alloy steels, which can be readily hardened through, the core is composed of low-carbon martensite. This structure ensures an elevated ultimate strength and a sufficient toughness in the core.

After the first quenching procedure the cemented layer turns to be overheated and contains an increased amount of retained austenite. For this reason, a second quenching is done from 760-780 °C, which is the optimum temperature for hypereutectoid steels. Upon the second quenching, the surface layer consists of fine-acicular high-carbon martensite and globular inclusions of secondary carbide.

With gaseous cementation, only one quenching is done, the cemented articles being chilled from the cementation temperature down to 840-860 °C and immediately quenched from that temperature. Cemented articles are always heated after quenching to 160-180 °C in order to relieve quenching stresses.

Cementation is widely employed in machine-building to increase the hardness and wear resistance of articles with simultaneously retaining a high toughness in the core. The unit volume of a hardened carburized layer is greater than that of the soft core, and therefore, appreciable compressive stresses develop in the layer. Residual compressive stresses in the surface layer may reach 40-50 kgf/mm<sup>2</sup> and thus increase the endurance limit of articles.

A high toughness in the core is ensured by the low content of carbon (0.08-0.25 per cent). Cementation is employed with quality carbon steels, Grades 08, 10, 15 and 20 and alloy steels, Grades 12XH3A, 18XГT, etc. Here, the main purpose of alloying is to increase the hardenability and, therefore, the mechanical properties in the core of articles made of cementable steel,



At the nitriding temperature of 600 °C, the order of layers formed in the metal should be (from surface to core) as follows:  $\varepsilon \rightarrow \gamma' \rightarrow \gamma \rightarrow \alpha$ . With slow cooling, austenite decomposes at temperatures below 590 °C and forms a eutectoid  $\alpha + \gamma'$  mixture and secondary precipitates of the  $\gamma'$ -phase appear in  $\alpha$ -layer and  $\varepsilon$ -layer. Upon slow cooling, the order of layers (from surface to core) at room temperature should be as follows:  $\varepsilon \rightarrow \varepsilon + \gamma'_{ec} \rightarrow \gamma' \rightarrow \text{eutectoid } (\alpha + \gamma') \rightarrow \alpha + \gamma'_{sec} \rightarrow \alpha$ .

In alloy steels, nitrogen forms very disperse nitrides with aluminium, chromium, molybdenum and other elements, owing to which the nitrided layer has a hardness much higher than that of cemented steel.

The formation of a nitrided layer involves an increase in the specific volume, with residual compressive stresses (up to 60-80 kgf/mm<sup>2</sup>) developing at the surface, which increase the endurance limit of nitrided steel parts.

The thin layer of the  $\varepsilon$ -phase (0.01-0.03 mm) protects the steel well against corrosion in moist ambient and other media.

Thus, nitriding is employed to increase the hardness, wear resistance, endurance limit and corrosion resistance of steels.

Parts made of steel type 38XM10A are nitrided in order to increase the hardness and wear resistance. Before nitriding, parts are hardened and tempered from a high temperature so as to increase the strength and toughness of the core. The nitriding is done at 500-520 °C. Because of the relatively low temperature, and therefore, low mobility of nitrogen atoms, the process takes considerable time (24-90 hours). The depth of nitrided layer obtained is 0.3-0.6 mm. The time of nitriding can be reduced by increasing the temperature (Fig. 218), but this is linked with a sharp drop in hardness owing to coarsening of particles of nitrides of alloying elements. Because it is a time-consuming process, nitriding for increasing the hardness and wear resistance can only be recommended for critical parts.

Nitriding is used to increase the corrosion resistance in parts made of various grades of steel (mainly carbon grades). Since high hardness is not an aim here, the temperature of the process

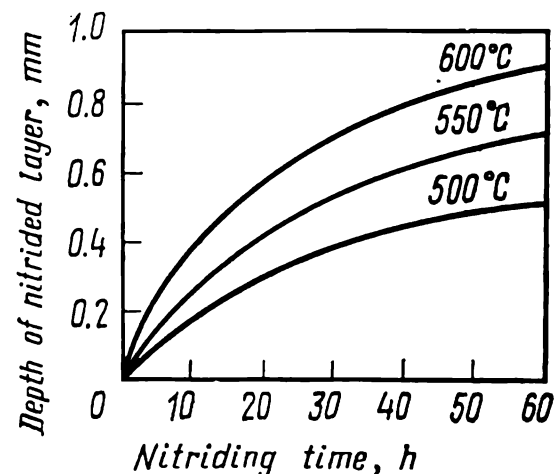


Fig. 218. Effect of time of nitriding at various temperatures on the depth of nitrided layer in steel 38XM10A (after Yu. M. Lakhtin)

is chosen at a higher level (600-700 °C); the time of nitriding may vary from 15 minutes to 10 hours.

Nitriding has also found some application with high-strength cast irons and titanium alloys.

**Nitriding of titanium alloys** is one of the rare examples of industrial application of chemical heat treatment to non-ferrous metals. Nitriding of titanium alloys is resorted to in order to increase the wear resistance and diminish the risk that parts may stick to each other when operating under conditions of friction.

Titanium-alloy parts are nitrided in a nitrogen medium at 850-950 °C for 10–50 h. The process forms a very thin hard nitride layer at the surface and a layer of solution of nitrogen in  $\alpha$ -titanium, below it. The depth of nitriding is 0.1-0.15 mm. A higher temperature of nitriding is inadmissible in view of the probable strong grain growth in deeper layers of the metal. The principal danger in nitriding of titanium alloys is embrittlement of the surface layer.

### *Cyaniding and Nitrocementation*

Surface saturation of parts simultaneously with carbon and nitrogen in molten cyan salts is called cyaniding and that in a gaseous medium, nitrocementation. The carbon to nitrogen ratio in the diffusion zone can be controlled by varying the composition of the medium and the temperature of the process.

**Cyaniding of steels** is carried out in a bath with NaCN at 820-960 °C for 30-90 minutes. Sodium cyanide oxidizes with the formation of atomic nitrogen and carbon monoxide.

The advantages of cyaniding over cementation are an appreciably shorter time of the process and higher values of wear resistance and corrosion resistance obtained (due to nitrogen presence in the surface layer). A disadvantage is that the cyan salts employed are toxic.

**Nitrocementation of steels**, which is also called gaseous cyaniding, is carried out at 850-870 °C for 2-10 hours in a medium containing ammonia and a carburizing gas. Nitrocementation excels gaseous cementation in that it is carried out at a lower temperature and, therefore, diminishes grain coarsening; it also gives a higher wear resistance and lowers the risk of warping of articles.

### **Diffusion Saturation with Metals**

Metals are dissolved in iron and other metals by substitution and, therefore, their diffusion is slower than that of non-metals. As a rule, diffusion saturation with metals is carried out at higher temperatures than saturation with non-metals. Typical examples are alitizing and chromizing.

**Alitizing** is employed to increase the scaling resistance of steels and less frequently, of cast irons. Another application relates to

gas-turbine cast blades made of refractory nickel alloys. Upon heating an alitized part in an oxidizing medium, a thin strong film of  $\text{Al}_2\text{O}_3$  oxide forms on its surface and prevents the part against further oxidation. The depth of alitizing may be 0.02 to 0.8 mm depending on the method and conditions used.

The most widely used method is alitizing of steel parts in powders with saturation from gaseous phase. A powder mixture is made of ferro-aluminium, ammonium chloride and alumina. In the presence of  $\text{NH}_4\text{Cl}$  there forms gaseous aluminium chloride  $\text{AlCl}_3$  which supplies active aluminium atoms. Alumina prevents sintering of ferro-aluminium particles. Alitizing is done at 950-1050 °C for 3-12 hours.

Another method is alitizing in a molten bath of aluminium and 8-12 per cent Fe at 700-800 °C for 1-1.5 h (iron is introduced into the melt to prevent strong dissolution of steel parts).

An example of a relatively rare process of chemical heat treatment with saturation from solid phase only is alitizing by metallization (spraying) of aluminium, followed with diffusion annealing at 900-1000 °C for 2-4 h.

**Chromizing** is employed to increase the corrosion resistance and also the scale resistance and wear resistance of steel parts. Also known are industrial processes of chromizing of molybdenum and niobium to increase their heat resistance.

The method that is used most widely is chromizing in powder mixtures of ferro-chrome (or chromium), ammonium chloride and alumina at 1000-1050 °C with a holding time of 6-12 h. The gaseous  $\text{CrCl}_2$  that is formed is a supplier of active chromium atoms. Another method is vacuum chromizing at 1000-1050 °C for a few hours with saturation from the vapour phase which is formed on vaporization of chromium powder.

For higher corrosion resistance and scale resistance, the surface layer must have the structure of plastic solid solution of chromium in  $\alpha$ -iron. If one of the purposes of chromizing is to increase hardness, the process must be carried out so as to form chromium carbides ( $\text{Cr}_{23}\text{C}_6$ ,  $\text{Cr}_7\text{C}_3$ ) in the surface layer. The steel for the purpose must contain more than 0.4 per cent C. The depth of chromized layer is usually not more than 0.2 mm.

### Diffusion Removal of Elements

The removal of impurities from the metal by heating in vacuum or other media is a variety of chemical heat treatment which is of high importance in the manufacture of some types of articles. It relies on the diffusion process of motion of atoms from the core to the surface of an article [see formula (42) and Fig. 207], which thus removes an unwanted element from the metal. As a rule, total removal of harmful impurities is usually needed (i.e. from the whole bulk of metal, rather than from the surface layers only). An example may be dehydrogenizing of titanium alloys by heating in vacuum, which prevents hydrogen em-

brittleness and increases the impact toughness. Dehydrogenizing is carried out at 670-700 °C for 2-6 h at a pressure not above  $10^{-4}$  mm Hg.

Refractory metals are heated in vacuum for complex removal of all interstitial impurities from them.

A method that has been long used industrially is dehydrogenizing of transformer steel by annealing steel sheets in a hydrogen atmosphere.

Partial removal of a main component from an alloy is sometimes carried out in order to change the properties of the surface layer in the desired direction.

Owing to the inexhaustible diversity of the chemically active media and vast possibilities of varying the properties of metal in the surface layers and in the body of articles, the processes of chemical heat treatment have found wide use in the industry. They are developing rapidly and winning ever new fields of application.

#### LITERATURE

Minkevich A. N., Chemical Heat Treatment of Metals and Alloys (*Khimiko-termicheskaya obrabotka metallov i splavov*). Moscow, Metallurgiya, 1965, 491 pp., ill.

Popov A. A., Theoretical Principles of Chemical Heat Treatment of Steel (*Teoreticheskie osnovy khimiko-termicheskoi obrabotki stali*). Sverdlovsk, Metallurgizdat, 1962, 120 pp., ill.

Lakhtin Yu. M., Physical Principles of Nitriding (*Fizicheskie osnovy protsessy azotirovaniya*). Moscow, Mashgiz, 1948, 143 pp., ill.

Dubinin G. N., Chromizing of Alloys (*Diffuzionnoe khromirovanie splavov*). Moscow, Mashinostroenie, 1964, 451 pp., ill.

## 5.2. THERMO-MECHANICAL TREATMENT

Plastic deformation can change the pattern of distribution and increase the density of imperfections, such as dislocations, vacancies, stacking faults, low- and high-angle boundaries in a crystal structure. Since crystal lattice defects produce a strong effect on the formation of structure in alloys during phase transformations, plastic deformation before or during phase transformations can be used to form the optimum structure in a heat-treated alloy.

*Thermo-mechanical treatment is a kind of heat treatment including plastic deformation which increases the density of defects and thus affects the formation of the structure in the phase transformations occurring during the thermal action.*

Consequently, not every combination of straining, heating and cooling can be called thermo-mechanical treatment. For example, if plastic deformation is carried out after all operations of heat treatment, we are dealing with common heat treatment followed



with plastic working, rather than with thermo-mechanical treatment. Such plastic deformation, for instance, cold rolling after ageing, may produce strain-hardening and increase strength properties, but has no effect on the structure formed through phase transformations, since these transformations have taken place before the plastic deformation was applied.

If plastic deformation was effected prior to heat treatment and produced no decisive effect on the final structure formed in an alloy during phase transformations, it should be regarded as a simple combination of plastic deformation and heat treatment, rather than thermo-mechanical treatment. For example, cold rolling followed by heating for quenching, during which recrystallization takes place, are not components of thermo-mechanical treatment, since the recrystallized structure has a low density of crystal imperfections.

The processes of plastic deformation and heat treatment in thermo-mechanical treatment may be either combined in a single technological operation (i.e. carried out simultaneously) or made with a time interval of up to a few days one after the other. It is only important that phase transformations take place under the conditions of increased density of the lattice defects formed through plastic deformation.

At present, various methods of thermo-mechanical treatment are being used or tested in the industry; all of them include plastic deformation which produces a decisive effect on the formation of the structure in alloys on ageing or during polymorphic, mainly martensitic, transformations.

### 5.2.1. THERMO-MECHANICAL TREATMENT OF AGEING ALLOYS

Figure 219 shows the principal schemes of thermo-mechanical treatment (THT) applicable with ageing alloys. The toothed lines denote plastic deformation.

#### Low-temperature Thermo-mechanical Treatment (LTHT)

Low-temperature thermo-mechanical treatment (LTHT) of ageing alloys is the oldest (introduced in 1930's) and most widely used method of thermo-mechanical treatment.

It is mainly used to enhance the strength properties of alloys.

With LTHT, an alloy is first quenched by a common technique and then subjected to cold deformation prior to ageing (Fig. 219).

As compared with ageing without preliminary deformation, LTHT yields higher values of ultimate strength and yield strength, but lowers ductility indices.

Figure 220 shows how the degree of cold deformation can affect the hardness of a quenched nickel alloy (curve 1) and of the same alloy after deformation and ageing (curve 2).

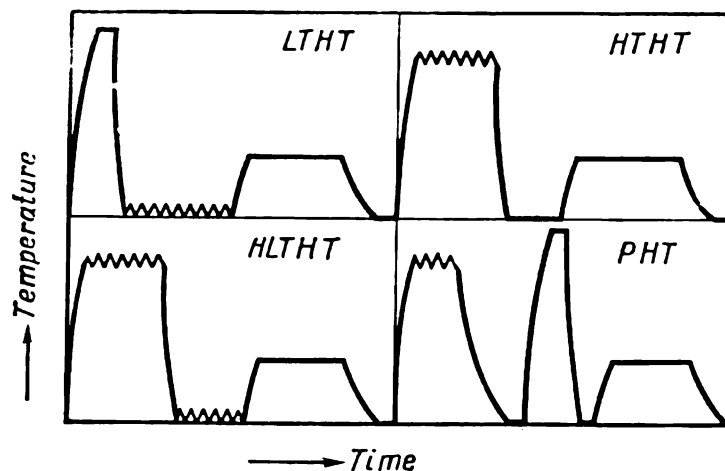


Fig. 219. Schemes of thermo-mechanical treatment of ageing alloys

The hardening effect produced by LTHT may be explained by two causes. Firstly, the cold deformation produces strain-hardening, so that the subsequent precipitation hardening begins from a higher initial hardness level of an alloy. Secondly and most important, cold deformation enhances the effect of precipitation hardening.

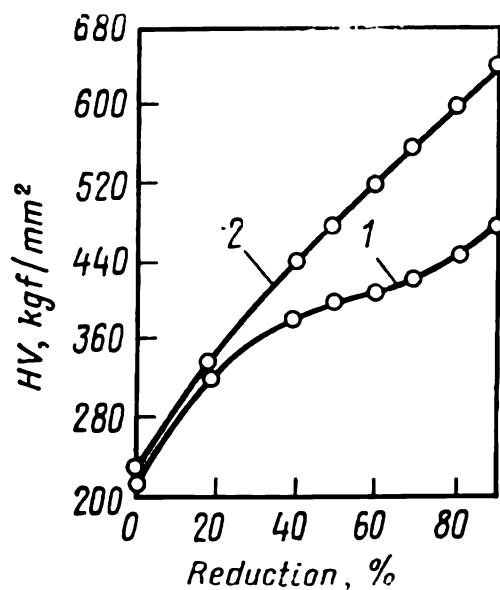


Fig. 220. Effect of reduction in drawing after quenching from 1000 °C on hardness of cold-drawn and aged 4-mm wire made of Ni-monic-9 alloy (after W. Bette-ridge)

1—cold-drawn; 2—deformed and aged at 450 °C for 16 h

For instance, the hardening effect produced in Nimonic-90 alloy through ageing at 450 °C without cold strain-hardening is very low — only 15 kgf/mm<sup>2</sup>. With increasing degree of cold deformation, the hardening effect on ageing increases continuously (see the diverging curves 1 and 2 in Fig. 220). With 90-per cent reduction, the gain in hardness produced by ageing has amounted to 175 kgf/mm<sup>2</sup>. Consequently, cold strain-hardening in the case considered has enhanced the hardening effect on ageing by one

order of magnitude (!). Such a strong hardening effect on LTHT, compared with hardening by a common technique (quenching followed with ageing) is a relatively rare phenomenon and may be explained by the fact that an ageing temperature of 450 °C is

too low for the Nimonic alloy, so that the precipitation from the supersaturated solid solution in the absence of cold strain-hardening can proceed only very feebly. If ageing upon quenching is done at a temperature that is optimal for the maximum hardening effect (around 700 °C), the effect produced by cold strain-hardening will be appreciably weaker.

In the first approximation it may be stated that cold strain-hardening by increasing the density of imperfections in crystals of a supersaturated solution makes the latter less stable thermodynamically and accelerates ageing. Experimental evidence and a more detailed analysis show, however, that the effect of strain-hardening on ageing may be quite complicated. The nature of this effect depends on the conditions of quenching, straining and ageing, the nature of alloy and, for the same alloy, on the type of precipitates in ageing.

Let us first consider the effect of cold deformation on zone ageing. It might seem that deformation should accelerate zone ageing, since it increases the density of dislocations and the concentration of vacancies. It should be noted, however, that, firstly, zones nucleate homogeneously, but not at dislocations, and secondly, dislocations are effective sinks for vacancies. A very strong plastic deformation can increase vacancy concentration (the ratio of the number of vacancies to that of atoms) only by  $10^{-6}$ , whereas quenching can produce an appreciably greater supersaturation of the lattice with vacancies: the concentration of quenching vacancies may reach  $10^{-4}$ .

The 'sweeping off' of a large number of quenching vacancies by gliding dislocations during plastic deformation of a quenched alloy can fully outweigh the relatively small supply of vacancies which are generated by jogs of gliding dislocations. As a result, plastic deformation of a quenched alloy slows down zone ageing, since excess vacancies play an important part in the diffusion transfer of atoms of the dissolved element to the growing zones (see 4.1.2).

In alloys having a low concentration of a dissolved element, cold strain-hardening can slow down the formation of zones on ageing, since atoms of that element are attracted to dislocations and thus the matrix is depleted of that element.

A slower growth of zones in a strain-hardened alloy manifests itself in decelerated hardening and a lower gain in strength on ageing. Such a result is obtained, for instance, on cold deformation of a freshly quenched duralumin. That is why zone ageing is not commonly used as the final operation in LTHT.

If the metal is cooled at a relatively moderate rate on quenching, for instance, in air, and the lattice is not supersaturated strongly with quenching vacancies, the strain-hardening may

cause no decelerating effect on zone ageing. Moreover, strain-hardening can then even accelerate zone ageing, since it increases the concentration of mobile vacancies owing to the fact that vacancy clusters that have had time to form during the slower quench cooling are being destroyed by dislocations. Besides, accelerated zone ageing under such conditions may also result from the generation of vacancies by jogs of gliding dislocations. In such cases LTHT with zone ageing can be employed for additional hardening of alloys.

Of incomparably greater interest is LTHT with phase ageing. Dislocations facilitate the nucleation of phase precipitates. Because of this, phase ageing proceeds quicker in a strain-hardened alloy having an increased dislocation density, and therefore, the density of precipitates and correspondingly, the hardening effect turns to be higher than on ageing of the alloy without strain-hardening. The higher the degree of cold deformation, the greater will be the dislocation density, and correspondingly, the higher will be the density of precipitates and the hardening effect on phase ageing (see Fig. 220).

The effectiveness of LTHT is decided by the strengthening phase that precipitates on ageing. For instance, the additional hardening effect produced by straining prior to artificial ageing is greater in Al-Cu-Mg alloys (where the strengthening phase is  $S'$ ) than in Al-Cu alloys (where the strengthening phase is  $\theta'$ ).

Usually, heating for ageing after cold deformation is not accompanied by recrystallization with only recovery and polygonization processes developing, which diminish somewhat the hardening effect provided by LTHT. It should be born in mind that these processes and those of precipitation from the solution can mutually influence each other: precipitates retard the polygonization, while the latter, if it has had time to proceed, varies the density and pattern of distribution of precipitates.

The effect of cold strain-hardening may be not only in accelerated precipitation from the solution and increased density of precipitates. It can also cause the formation of a phase that cannot precipitate under the same ageing conditions without strain-hardening. It even may be capable of altering the sequence in which the phases appear on ageing.

For instance, during ageing of Al + 4% Cu alloy at 150 °C without strain-hardening,  $\theta'$ -phase can be detected radiographically in 15 days, while  $\theta$ -phase ( $\text{CuAl}_2$ ) does not appear at all. In ageing at the same temperature after cold rolling with 90-per cent reduction,  $\theta$ -phase appears first (in 5 minutes) and soon after it,  $\theta'$ -phase (in 30 minutes). The appearance of the metastable phase after the precipitation of the stable one contradicts the common sequence of formation of phases on precipitation from solid

solution (see 2.1.4 and 4.1.2) and may be explained as follows. Cold deformation with a high reduction distorts the lattice of the solid solution in the whole bulk of crystals to such an extent that semicoherent  $\theta'$ -phase precipitates cannot nucleate. On the other hand, nucleation of  $\theta$ -phase precipitates is facilitated in portions which have been distorted especially strongly. After a certain while, the processes of recovery and polygonization which take place at the temperature of ageing make the lattice in some portions of crystals so perfect that nucleation of semicoherent  $\theta'$ -phase precipitates becomes possible there (provided that precipitation with the formation of  $\theta$ -phase still has had no time to proceed in those portions).

The formation of incoherent precipitates of a stable phase instead of semicoherent precipitates of the metastable phase during precipitation from a strongly strain-hardened solid solution can diminish the hardening effect on ageing. For this reason, the strength of aged alloy after a heavy deformation may turn to be lower than that of a less deformed alloy, notwithstanding the higher strength level of the former before ageing.

If the solid solution has undergone partial precipitation before cold deformation, this may have an effect on the kinetics of final ageing and on the properties of the alloy. As shown in Fig. 221, with cold deformation of freshly quenched Al + 4% Cu alloy, the maximum of hardness in ageing at 160 °C is obtained in 20-30 h (curve 1), but if the same deformation is applied upon natural ageing, the maximum hardening in ageing at 160 °C is attained in 8-10 h. This accelerating effect on artificial ageing may be explained by the fact that dislocations are stopped by G. P. zones during plastic deformation of a naturally aged alloy, so that on subsequent artificial ageing there are copper-enriched portions near the dislocations, which facilitate the nucleation of  $\theta'$ -phase. Consequently, in the case considered it is advantageous to deform alloy after natural ageing in order to accelerate the subsequent artificial ageing.

Pre-ageing (prior to plastic deformation) cannot only accelerate the final ageing, but also enhance the final hardening effect. One of the probable causes may be that plastic deformation of a

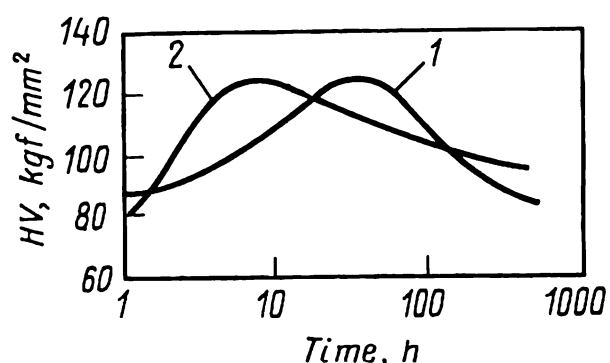


Fig. 221. Dependence of hardness of Al + 4% Cu alloy on time of ageing at 160 °C after LTHT by various methods (after J. Nutting)

1—quenching → cold deformation (10%) → ageing at 160 °C; 2—quenching → natural ageing (18 h) → cold deformation (10%) → ageing at 160 °C

preliminarily aged alloy forms a more favourable structure characterized by a high density of uniformly distributed dislocations.

In view of what has been said above, a time interval must be allowed between quenching and cold deformation in LTHT of naturally ageing alloys. For instance, in LTHT of sheets and tubes made of АД31 alloy, this interval must be at least 2 h in order to obtain the maximum hardening effect.

Pre-ageing can be either natural or artificial. It may be recommended to try on various alloys more complicated methods of LTHT of the type of quenching → ageing → cold deformation → ageing.

An increased strength can also be obtained by using common cold deformation after ageing (without LTHT). As compared with this common method, LTHT ensures a higher ductility for the same strength, as also lower residual stresses and a structure possessing a higher thermal stability.

At present, LTHT is widely used in the manufacture of semi-products and products from ageing copper, aluminium and austenitic alloys.

Cold rolling of beryllium bronze Бр.Б2 before ageing increases the yield limit of the metal additionally by 20 per cent. Electrode copper alloys of the type of chrome-zirconium bronzes can partially retain the hardening effect produced by LTHT at elevated temperatures at which contact-welding electrodes operate. The degree of cold deformation of ageing copper alloys in LTHT may be from 10 to 80 per cent.

With LTHT of austenitic spring alloys of the type 36ХХТЮ, with deformation of 50 per cent, their yield limit  $\sigma_{0.002}$  turns to be 20-30 per cent higher than in the case of quenching and ageing.

For some types of aluminium alloys, LTHT with large deformations is very promising. For instance, LTHT of sheets and tubes of АД31 alloy by the scheme: quenching → natural ageing for at least 2 h → 60-90 per cent cold deformation → ageing at 200 °C, can increase the ultimate strength by 25-30 per cent compared with that obtained on common heat treatment (quenching + ageing).

LTHT can be resorted to not only for increasing the ultimate strength. Aluminium alloys of the type АМг6 are recommended to be cold-deformed by 30-40 per cent, followed with ageing at 220 °C for a few hours. In this process, polygonization takes place in the first 20 minutes of heating after the deformation, after which  $\beta$ -phase ( $\text{Al}_3\text{Mg}_2$ ) precipitates uniformly at sub-boundaries. This structure possesses an increased resistance to stress corrosion.

Semiproducts (shaped sections, tubes, sheets, etc.) made of ageing aluminium alloys are always straightened by stretching or planishing after quenching. The degree of deformation in straightening is not high, usually not more than 3 per cent. However, even a low cold deformation, 1-3 per cent, can strongly enhance the hardening effect in subsequent artificial ageing. For instance, the yield limit of duralumin Д16 aged at 190 °C can be increased from 40 to 45.5 kgf/cm<sup>2</sup> by stretching by 1.5 per cent before ageing.

The process by the scheme: quenching → stretching → ageing is not usually called thermo-mechanical treatment, though it actually is a typical low-temperature thermo-mechanical treatment.

Owing to simple techniques and high effectiveness of the process, the number of various ageing alloys and the assortment of articles subjected to LTHT will widen in the future. However, when resorting to LTHT, one should always consider the possible adverse effects, such as a reduced ductility which is characteristic of most alloys, a lower creep resistance in some aluminium alloys, anisotropy of properties, etc.

### High-temperature Thermo-mechanical Treatment (HTHT)

High-temperature thermo-mechanical treatment includes hot deformation, quenching from deformation temperature, and ageing (see Fig. 219).

Hot deformation increases the density of dislocations and produces *hot strain-hardening effect*, which can be partially or fully removed owing to the development of *dynamic polygonization* and *dynamic recrystallization*.

The stress-strain curve of the process has an ascending section of creep stress, which corresponds to the stage of hot strain-hardening, and a descending stress section, which is due to the development first of polygonization and then of recrystallization.

With dynamic polygonization (as also with the common static polygonization which is observed in heating after cold deformation) the formation and migration of low-angle boundaries are controlled by dislocation climb. In contrast to static polygonization, however, dislocations are continuously 'pumped' into the body of subgrains under the action of the stresses applied in the course of hot straining. A similar difference exists between static and dynamic recrystallization. In the course of hot deformation, the processes of hardening (increasing the dislocation density) and softening (decreasing the dislocation density in polygonization and recrystallization) alternate continuously.

Depending on the nature of alloy, temperature, rate, degree and pattern of straining, the metal at the end of hot deformation may be either strain-hardened or have a polygonized, recrystallized or mixed-type (partially polygonized and partially recrystallized) structure.

A fully recrystallized structure with the minimum dislocation density corresponds to the most stable state. If the structure has been not recrystallized, or has been recrystallized only partially at the end of hot deformation, there forms a stimulus to static recrystallization. Upon straining with a high degree of deformation, a very quick recrystallization without any induction period

may be observed, since the nuclei of recrystallized grains have formed already in the course of hot deformation. This process is called metadynamic recrystallization.

*The aim of HTHT is to form a supersaturated solid solution with non-recrystallized structure upon hot deformation and quenching*, i.e. a structure having an increased density of imperfections (subgrain boundaries and free dislocations). An alloy of such a structure obtains better mechanical properties on subsequent ageing. In most cases the polygonized matrix of the quenched alloy is the best choice.

When using HTHT, at least three requirements must be fulfilled: (a) a non-recrystallized structure must form at the end of hot deformation; (b) probable recrystallization upon hot deformation must be prevented and (c) the degree of supersaturation of the solid solution must be sufficient for subsequent ageing.

If the first two requirements have not been fulfilled and the quenched alloy is fully recrystallized, the actual process is quenching from the temperature of deformation heating, rather than HTHT. Such a process, which combines hot deformation with heating for quenching, is profitable, but cannot improve the properties of the metal compared with a common heat treatment in which the metal is specially heated for quenching.

The formation of polygonized structure at the end of hot deformation is favoured by increased temperature, reduced rate and degree of deformation, and by the deformation pattern approaching uniform compression (as in pressing).

The use of HTHT is limited by the factors as follows.

An alloy may have a very narrow range of temperatures of heating for quenching, so that it is practically impossible to maintain the temperature of hot plastic working in the same narrow range (for instance within  $\pm 5^\circ\text{C}$  with Д16 duralumin).

The optimum temperature range of hot deformation may be substantially lower than the range of temperatures of heating for quenching. For instance, the rate of deformation in pressing of aluminium alloys can be the lower (without the appearance of surface cracks), the higher is the temperature. If it is required to increase substantially the temperature of hot deformation (to the temperature level of heating for quenching), the rate of deformation must be inevitably reduced, which lowers the productivity.

The precipitation from the undercooled solution in an alloy of non-recrystallized structure can proceed more quickly than in one fully recrystallized (see Fig. 116). If such alloy has a low hardenability, the latter turns to be even lower under the conditions of HTHT, so that through quenching will be impossible.

With an alloy having a high susceptibility to recrystallization, it may be difficult to form unrecrystallized structure to the end



of deformation and retain it in the period between the end of deformation and the moment when the temperature will drop down to  $t_r^s$  in cooling.

HTHT is used to improve the strength properties of alloys compared with the properties they have in recrystallized state. The strength increases on HTHT owing to the total increase in the density of imperfections already in as-quenched state and to a

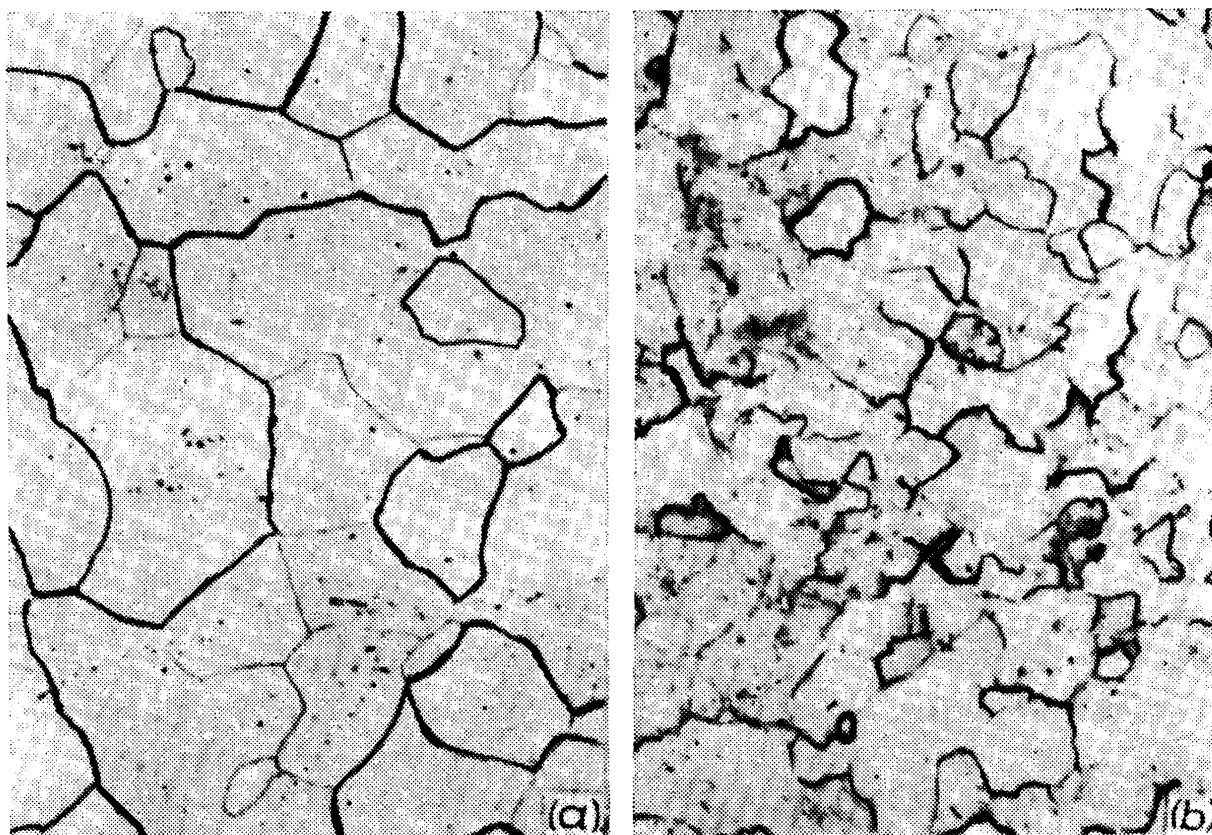


Fig. 222. Microstructure of titanium  $\beta$ -alloy (BT15) upon common quenching (a) and upon HTHT (b),  $\times 300$  (after S. G. Glazunov and I. S. Pol'kin)

more uniform precipitation from the supersaturated solution in the body of grains in ageing (the strengthening phase precipitates at subgrain boundaries and at individual dislocations inside subgrains).

A more uniform precipitation from the solution and very fine grains with curved boundaries, which are typical of many alloys (Fig. 222), ensure a high level of ductility upon HTHT. In contrast to LTHT, which noticeably lowers the ductility, the additional hardening effect produced by HTHT is obtained with the ductility being virtually unchanged. In aluminium alloys, the ductility and impact toughness can even increase upon HTHT.

The hardening effect produced by HTHT can be retained at higher temperatures than that obtained through LTHT. An increased heat resistance of alloys on HTHT may be attributed to

the toothed shape of grain boundaries, which inhibit intergranular fracture, and to the appearance of subgrain boundaries locked by precipitated particles.

HTHT has found some applications in the industry for increasing the heat resistance of parts made of precipitation-hardening austenitic steels or nickel and titanium alloys and intended for operation at relatively low temperatures. At high operating temperatures, HTHT may give poorer results than common heat treatment. For instance, Grade XH77TЮP (ЭИ437Б) Nimonic alloy has  $\sigma_{100} = 80$  kgf/mm<sup>2</sup> at 550 °C upon quenching and ageing and  $\sigma_{100} = 92$  kgf/mm<sup>2</sup> upon HTHT. At 750 °C, an inverse picture is obtained:  $\sigma_{100} = 30$  kgf/mm<sup>2</sup> on quenching and ageing and 27 kgf/mm<sup>2</sup> on HTHT.

HTHT of titanium alloy Grade BT8 by the scheme: deformation at 970 °C → water quenching → ageing at 570 °C for 2 hours, increases the ultimate strength at room temperature by 20-40 kgf/mm<sup>2</sup>, with the ductility and impact toughness remaining at the same level as upon quenching with ageing. At 450 °C, the additional hardening effect produced by HTHT still does not appear.

Among aluminium alloys, only Al-Mg-Si (АД31) and Al-Zn-Mg (Grades 1915 and 1925) alloys are often subjected to HTHT. Aluminium may be characterized by a high stacking fault energy, so that polygonization can occur in it quite easily. Pressing usually forms a very stable polygonized structure in aluminium alloys, so that special measures to form and retain this structure in HTHT are not needed.

The aluminium alloys indicated are characterized by a wide range of temperatures of heating for quenching (from 350 °C to 500 °C for Al-Zn-Mg alloys) and possess a very high hardenability (see Fig. 115). For these reasons, they can be subjected to HTHT without any difficulties. With pressing of thin-walled shaped sections (up to 12 mm thick), air cooling provides through-hardening of the metal. With a larger thickness of shaped sections made of АД31 or 1915 alloy, they are cooled by water directly in the press.

With ageing alloys, HTHT is used industrially substantially less frequently than LTHT, mainly because of the processing limitations mentioned above and the lower hardening effect.

A process has been recommended for industrial application, which is a combination of HTHT and LTHT and has been called high-low-temperature thermo-mechanical treatment (HLTHT). It comprises quenching from the deformation temperature, followed with cold deformation and ageing (see Fig. 219). The process gives a higher ultimate strength and a lower ductility than HTHT.

### **Preliminary Thermo-mechanical Treatment (PHT)**

In preliminary thermo-mechanical treatment (PHT), the processes are such that a semiproduct, which has an unrecrystallized structure upon hot deformation, retains this structure during heating for quenching. PHT differs from HTHT in that the operations

of hot deformation and heating for quenching are performed separately (see Fig. 219).

PHT is widely employed in the manufacture of semiproducts from aluminium alloys. It has been long known that pressed semiproducts of alloys of the type of duralumin, Avial, etc. have an appreciably higher strength than rolled or forged products. The phenomenon has been called *extrusion effect*. The difference in strength values is due to that pressed semiproducts have an unrecrystallized structure upon quenching, while the structure of rolled and forged products is recrystallized. As has been found later, hot-rolled sheets and stampings of some alloys may also be in unrecrystallized state upon quenching and thus have an increased strength.

V. I. Dobatkin has proposed to replace the term 'extrusion effect' and some other synonymous terms by the term '*structural strengthening*', which is understood as an increase in the strength of heat-treated semiproducts due to the retention of unrecrystallized structure upon quenching. The properties of an alloy in the state of structural strengthening are usually compared with those it has in recrystallized state. The gain in the ultimate strength and yield strength in ageing aluminium alloys due to the retention of unrecrystallized structure may be from 10 to 40 per cent. This gain may appear already in a freshly quenched state owing to an increased density of imperfections (dislocations locked in sub-boundaries and individual dislocations). Ageing of an unrecrystallized alloy produces a higher hardening effect by increasing the difference between the properties of recrystallized and unrecrystallized semiproducts. The ductility is, however, higher in alloys in recrystallized state. For that reason, semiproducts are produced either with a recrystallized structure and increased ductility or with polygonized structure and increased strength. For instance, duralumin rods type Д1Р (having a recrystallized structure) have  $\sigma_t \geq 38$  kgf/mm<sup>2</sup> and  $\delta \geq 14$  per cent, while rods type Д1РР (with elevated strength) have  $\sigma_t \geq 43$  kgf/mm<sup>2</sup> and  $\delta \geq 10$  per cent.

Both in PHT and HTHT, the formation of an unrecrystallized structure is favoured by higher temperature and lower rate of deformation, a lower degree of deformation and by the pattern of deformation approaching uniform compression. As has been noted earlier, polygonization can develop intensively in aluminium alloys and produce a stable network of sub-boundaries, because of which an unrecrystallized structure can be easily formed in them, especially by pressing.

Additions of manganese, zirconium and other antirecrystallizers, which form disperse aluminides (Al<sub>6</sub>Mn, Al<sub>3</sub>Zr, etc.), increase the temperature of the beginning of recrystallization and

promote the formation of unrecrystallized structure on hot deformation. What is most important is that these additions, which are contained in many aluminium alloys, favour the retention of unrecrystallized structure in subsequent heating for quenching.

Structural strengthening of aluminium alloys (or PHT) has found a wide application in large-tonnage mass production of semiproducts and is an example of effective industrial use of thermo-mechanical treatment.

### 5.2.2. THERMO-MECHANICAL TREATMENT OF MARTENSITE-HARDENABLE STEELS

Intensive studies into the processes of thermo-mechanical treatment of steels have been started in the middle of 1950's in connection with the search for new ways of increasing the structural strength.

#### Low-temperature Thermo-mechanical Treatment (LTHT)

With low-temperature thermo-mechanical treatment (LTHT), undercooled austenite is deformed in the temperature range where it has an elevated stability, but always below the point of the beginning of recrystallization, and then transforms into martensite (Fig. 223). After that, a low-temperature tempering is made (not shown in Fig. 223).

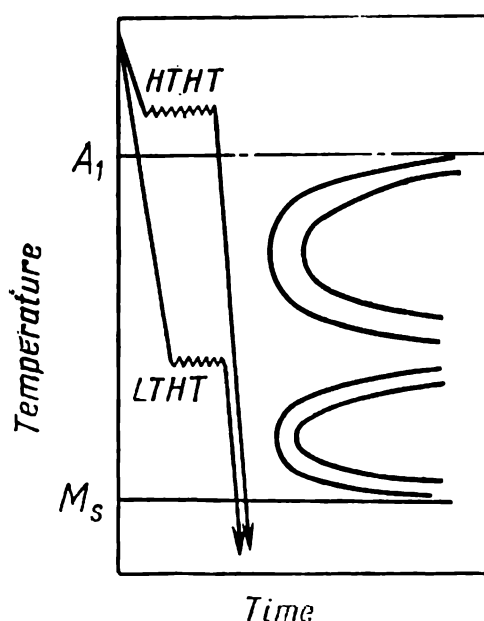


Fig. 223. Schemes of high-temperature (HTHT) and low-temperature (LTHT) thermo-mechanical treatment of martensite-hardened alloy steel

The effect of strong strengthening owing to plastic deformation of undercooled austenite followed with quenching from the temperature of straining was discovered by E. Lips and H. Van Zuilen of the USA in 1954. This process, called *ausforming*, allowed the ultimate strength of structural steels to be increased up to 280-330 kgf/mm<sup>2</sup> at  $\delta = 5-7$  per cent. The values of ductility and impact toughness were not lower, and in some cases even higher, than those obtained on a common heat

treatment which ensured  $\sigma_t = 180-220$  kgf/mm<sup>2</sup>. It is quite understandable that ausforming, which produced superstrong steels, attracted an enormous interest.

*The cause why steels are strengthened on LTHT lies in that the martensite inherits the dislocation structure of the deformed austenite.*

Cold deformation cannot produce a high strengthening in martensitic steel, since the martensite, which contains much carbon, is brittle and cannot be deformed with high reductions. On the contrary, austenite can be heavily deformed at temperatures below the point of beginning of recrystallization. Such a deformation can strongly increase the total density of dislocations in austenite, with the formation of dense dislocation tangles and a cellular structure.

With martensitic transformation, neighbours of any atom in the austenite remain such in the martensite. Therefore, dislocations do not disappear in the  $\gamma \rightarrow \alpha$ -transformation by the martensitic mechanism, but are 'passed over' from the initial phase to the new one, i.e. the martensite inherits the substructure of deformed austenite. A very high density of dislocations in martensite, which are locked by carbon atoms and carbon precipitates, is responsible for the record figures of ultimate strength on LTHT of steels.

The large refinement of martensite crystals explains why the steel in the high-strength state can have an acceptable level of ductility indices.

LTHT is practically applicable only to alloy steels possessing an appreciable stability of undercooled austenite.

To obtain record figures of ultimate strength (up to 330 kgf/mm<sup>2</sup>), alloy steels can be subjected to LTHT by the scheme: austenitization with heating above  $A_{c3}$   $\rightarrow$  undercooling of austenite down to 600-400 °C  $\rightarrow$  plastic working with deformation up to 90 per cent  $\rightarrow$  martensite hardening  $\rightarrow$  tempering at 100-200 °C.

The gain in strength properties on LTHT depends on the degree and temperature of straining, the temperature of tempering, the content of carbon, and other factors. The strengthening effect on LTHT increases continuously with increasing degree of deformation.

Figure 224 shows how the temperature of rolling in LTHT can affect the properties of Cr-Ni-Mo steel. The rise in the strength properties of steel on lowering the temperature of deformation is caused by increased strain hardening of the austenite. The loss in strength properties on rolling at 400 °C is due to bainitic transformation taking place during deformation. Since the non-martensitic products of the transformation which are formed in LTHT can lower the strength, the process must be carried out so as to prevent their appearance. It should be remembered that a common C-diagram cannot provide us with precise quantitative data for establishing the temperature-time conditions of deforming in LTHT, since deformation accelerates the decomposition of the

austenite. Deformation of undercooled austenite can shorten the induction period quite appreciably.

The optimum mechanical properties upon LTHT of structural steels are obtained after low-temperature tempering (at 100-200 °C). With increasing tem-

perature of tempering, the strengthening effect produced by LTHT is gradually lost.

The highest effect from LTHT is obtained in steels with 0.4-0.5 per cent C. With a higher carbon content, the relative elongation and ultimate strength can diminish owing to embrittlement.

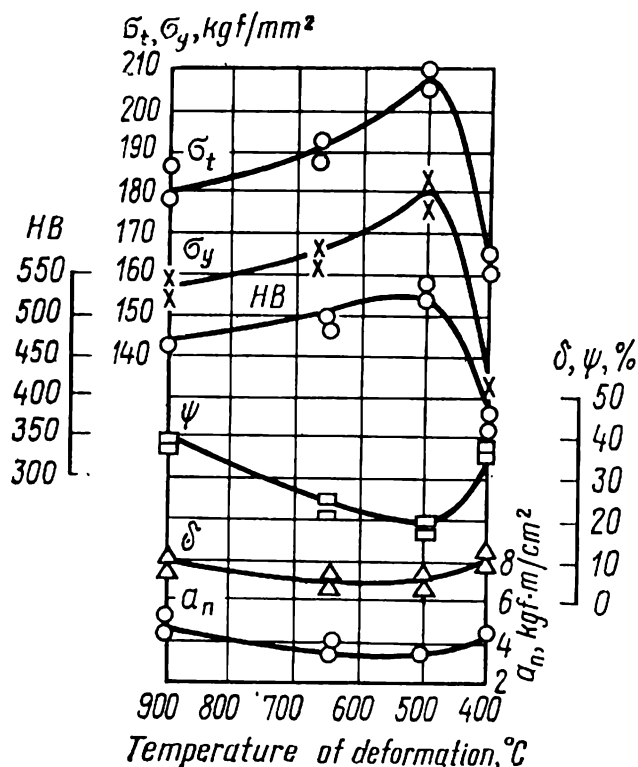


Fig. 224. Effect of rolling temperature on mechanical properties of steel 30XHMA upon LTHT. Conditions of LTHT: austenitization at 1150°C → chilling → rolling with 50-% reduction → oil quenching → tempering at 200 °C or 4 h (after S. I. Sakhin and O. G. Sokolov)

Industrial application of LTHT of steels encounters some difficulties linked with the necessity to use powerful equipment for plastic working, since the steel must be subjected to heavy deformations (not less than 50 per cent) at temperatures at which its strain resistance is still quite high.

Another essential drawback of LTHT is that a highly strengthened steel has a low resistance to brittle fracture. With an increase in the density of dislocations in martensite, which is needed to produce a high strengthening effect, the resistance of the metal to crack

propagation (which is the most important characteristic of structural materials) does not change or even lowers somewhat upon LTHT.

In view of the need to use powerful special equipment for deforming and also because the treated steel has a too low brittle fracture resistance, which is insufficient for modern structures, low-temperature thermo-mechanical treatment of steels is unlikely to find wide application in the industry.

### High-temperature Thermo-mechanical Treatment (HTHT)

With HTHT, austenite is deformed in the temperature range where it is thermodynamically stable, then quenched to martensite (Fig. 223), and finally subjected to low-temperature tempering.

The main aim of common heat treatment from deformation (rolling or forging) heating is to avoid special heating for har-

dening and owing to this, obtain a certain economic effect. The main purpose of HTHT is, however, to improve the mechanical properties of steel.

*In HTHT, martensite inherits the substructure of the unrecrystallized austenite that has been formed through hot deformation.*

The structural changes on hot deformation have been discussed in 5.2.1. As the degree of deformation is increased at a constant temperature, the density of dislocations in austenite increases, so that only strengthening (hot strain hardening), is initially produced in the metal, after which the processes of softening (dynamic polygonization and dynamic recrystallization) develop. Austenite may be characterized by a low stacking fault energy, and therefore, extended dislocations cannot easily leave their slip planes. Thus, austenite can be strongly strain-hardened and then can recrystallize quickly.

The best complex of mechanical properties is obtained in steel when martensite forms from austenite having a well developed polygonized structure. It has been revealed by diffraction electron microscopy that martensitic crystals fully inherit the dislocation sub-boundaries from hot-deformed austenite. Dislocation tangles can also be inherited by martensite.

As a result of fragmentation of martensitic crystals by subgrain boundaries, the ultimate strength and yield strength of a steel increase on HTHT. The substructure of the martensite obtained from hot-deformed austenite is such that HTHT can increase the strength without changing the ductility indices, such as relative reduction (Fig. 225). As compared with common hardening and tempering, however, HTHT of steel can give higher indices of ductility with the same ultimate strength.

HTHT of machine-building carbon, low-alloyed and medium-alloyed steels gives the following complex of mechanical properties:  $\sigma_t = 220\text{--}260$  kgf/mm<sup>2</sup>;  $\sigma_{0.2} = 190\text{--}220$  kgf/mm<sup>2</sup>;  $\delta = 7\text{--}8$  per cent, and  $\psi = 25\text{--}40$  per cent.

A steel upon HTHT has lower strength properties and higher ductility properties than upon LTHT.

HTHT of steel can be used to diminish drastically or, in some cases, even remove almost fully both reversible and irreversible temper embrittlement (Fig. 226). It causes a change from inter-

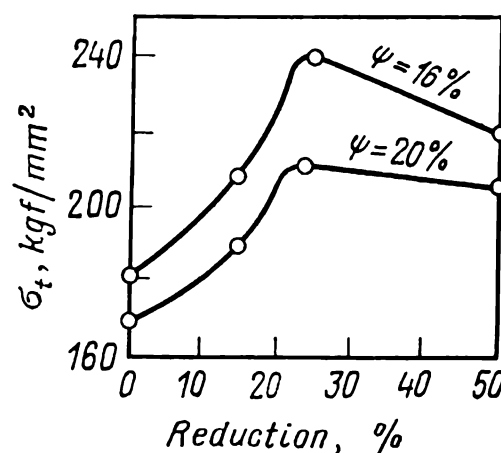


Fig. 225. Effect of deformation ratio in HTHT on the ultimate strength of steel at constant relative reduction (after M. L. Bernstein)

granular fracture, which is typical of the state of temper embrittlement, to intragranular fracture.

The ultimate strength can easily be raised up to 220 kgf/mm<sup>2</sup> without resorting to HTHT, simply by increasing the content of carbon in steel and carrying out common hardening and low-temperature tempering. But the steel upon the common heat treatment will be characterized by a very high susceptibility to brittle

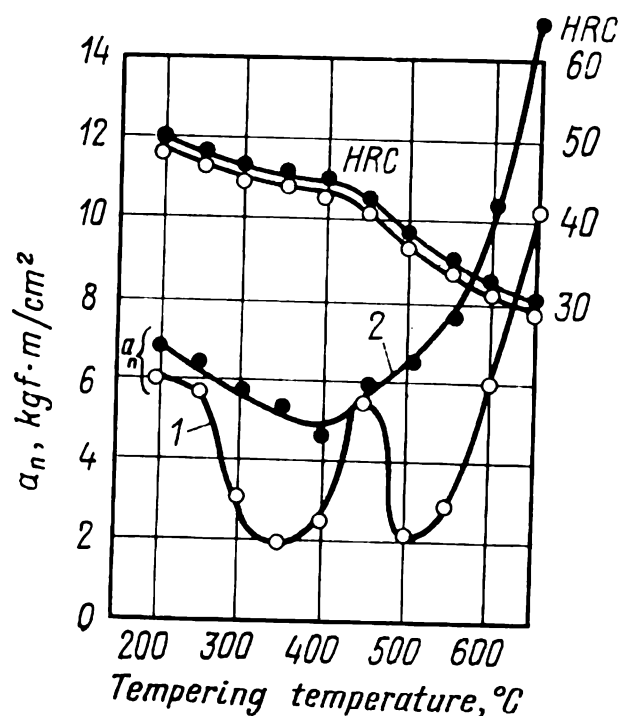


Fig. 226. Dependence of impact toughness on temperature of tempering after common hardening (1) and after HTHT (2) of steel 40XH1 (after L. V. Smirnov, E. N. Sokolov, and V. D. Sadovsky)

fracture and a high sensitivity to sharp notches at the surface of articles. Fatigue cracks in such a steel can propagate quickly owing to stress localization at the ends of cracks, thus causing sudden brittle fracture at stresses well below the yield limit. A steel having high values of ultimate strength and yield limit, but a low resistance to crack propagation cannot be used in heavily stressed structures.

The most essential merit of HTHT is its remarkable capability for increasing simultaneously both the strength indices and the resistance to crack propagation (fracture toughness).

In martensitic crystals fragmented by sub-boundaries, dislocation tangles that form on straining are smaller, i.e. the peaks of local stresses are

lower. Besides, with a developed subgranular structure, the stresses localized at the ends of cracks can relax easily. The lower level of peak stresses and their greater capacity of relaxing are responsible for a high resistance to crack propagation in steels subjected to HTHT.

The conditions for HTHT are so chosen that the austenite has a well developed polygonized structure at the beginning of martensitic transformation.

The degree of hot deformation in HTHT must not be excessively high, otherwise recrystallization might develop and lower the strengthening effect (Fig. 225). With increasing rate of deformation, hot strain-hardening is enhanced, which, combined with deformation heating, may cause recrystallization.



The use of multiple deformation with the total reduction equal to a heavy deformation in one pass, can facilitate the process of deforming and promote dynamic polygonization.

The temperature, degree and rate of deformation and the number of deformation stages should be selected at the optimum level for each grade of steel and each kind and size of product, in order to obtain a developed polygonized structure in the austenite.

Carbon and low-alloy steels should be quenched immediately after deforming, so as to prevent static recrystallization and retain the polygonized structure up to the beginning of martensitic transformation. In medium-alloyed and especially in high-alloyed steels, the climb of dislocations, and therefore, polygonization can proceed only slowly. Such steels upon deforming may be in a state of hot strain-hardening and have an unpolygonized structure, which, if inherited by martensite, will not ensure the required level of mechanical properties. For these reasons, a strictly specified holding interval between deformation and hardening stages is required for such steels, so as to allow sufficient time for the development of static polygonization.

Of large interest is the phenomenon discovered by M. L. Bernstein, consisting in that the *strengthening effect produced by HTHT is inherited upon repeated heat treatment*. It has turned out that the strengthening produced by HTHT is retained if the steel is re-hardened with a short holding at the temperature of heating for hardening or if the steel strengthened by HTHT is first subjected to high-temperature tempering and then re-hardened. For instance, the ultimate strength of steel Grade 37XH3A after HTHT (25-per cent deformation at 950 °C → hardening → tempering at 100 °C) is 250 kgf/mm<sup>2</sup>. If the steel is tempered at 500 °C for 30 minutes, hardened from 900 °C for 2 minutes, and tempered at 100 °C, its ultimate strength will again be around 250 kgf/mm<sup>2</sup>. Thus, the substructure formed on hot deforming of the austenite, has been inherited once on the  $\gamma \rightarrow \alpha$ -transformation during HTHT, retained to a certain extent during the high-temperature tempering, and again inherited twice during re-hardening on the  $\alpha \rightarrow \gamma$ - and  $\gamma \rightarrow \alpha$ -transformations. The mechanism of inheritance of substructure on  $\alpha \rightarrow \gamma$ -transformation still remains unclear. A short holding time of the second hardening operation prevents the development of recrystallization in the austenite, which otherwise might destroy the polygonized structure, and therefore, the strengthening effect provided by the preceding HTHT.

The phenomenon of inherited strengthening in repeated short-time heating can widen the range of application of HTHT. For instance, steel can be hardened at the steelmaking works directly

from the rolling temperature and then subjected to high-temperature tempering to improve its machinability. The final products are hardened with a short holding time and subjected to a low-temperature tempering and thus acquire the increased strength that has been imparted to the metal on HTHT.

Notwithstanding the lower strengthening effect produced, HTHT has undeniable advantages over LTHT. It simultaneously increases both the ultimate strength and fracture toughness, can be performed more easily (no special powerful equipment is required for deformation), can be applied to carbon and low-alloy steels, as well as to alloy steels having an increased stability of undercooled austenite.

The above discussion of the pattern of changes of the structure and properties of steels on HTHT shows that this kind of thermo-mechanical treatment is one of the most promising ways for improving the structural strength of steels.

### **Preliminary Thermo-mechanical Treatment (PHT)**

Preliminary thermo-mechanical treatment is carried out by the scheme: cold plastic deformation  $\rightarrow$  pre-recrystallizational heating  $\rightarrow$  hardening with accelerated heating and short holding time  $\rightarrow$  tempering.

The initial structure before deformation is ferrite-carbide mixture. Cold deformation increases the density of dislocations which rearrange in pre-recrystallization heating to form a polygonized structure of ferrite. In subsequent hardening with accelerated heating and short holding time, the substructure is inherited on the  $\alpha \rightarrow \gamma$ - and  $\gamma \rightarrow \alpha$ -transformation and martensitic crystals are fragmented. Therefore, the strengthening mechanism in PHT is the same as the mechanism that gives an increased strength on repeated hardening after HTHT.

The substructure formed by hot deforming of the austenite in HTHT is more stable than that obtained on pre-recrystallizational heating after cold deformation. For that reason, the polygonized structure and, therefore, the strengthening effect on repeated hardening after HTHT are inherited more fully than in the process of preliminary thermo-mechanical treatment.

PHT is attractive by the ease with which it can be performed. The time interval between cold deformation and heating may be of any length. Deformation requires no special equipment. PHT with short salt-bath or induction heating before hardening is an effective method for strengthening cold-rolled sheets and thin-walled tubes.

---

**LITERATURE**

Bernstein M. L., Thermo-mechanical Treatment of Metals and Alloys (*Termomekhanicheskaya obrabotka metallov i splavov*). Moscow, Metallurgiya, 1968, 1171 pp., ill.

Bernstein M. L., Technology of Thermo-mechanical Treatment of Steel (*Tekhnologiya termomekhanicheskoi obrabotki stali*). Moscow, Mashinostroenie, 1971, 30 pp., ill.

Dobatkin V. I., On Structural Strengthening of Aluminium Alloys; in: Physical Metallurgy of Light Alloys (*Metallovedenie legkikh splavov*). Moscow, Nauka, 1965, 116 pp., ill.

Rabinovich M. Kh. Thermo-mechanical Treatment of Aluminium Alloys (*Termomekhanicheskaya obrabotka alyuminievykh splavov*). Moscow, Mashinostroenie, 1972, 160 pp., ill.

McQueen H. J., Jones J. J., Recovery and Recrystallization During High-temperature Deformation: In: Treatise on Materials Science and Technology. V. 6. Plastic Deformation of Materials, 1975.

Compositions (mass percentage) of Steels and Non-ferrous Alloys Mentioned in the Book

Steels

Grade	C	Si	Mn	Cr	Ni	Other elements
08	0.05-0.12	0.17-0.37	0.35-0.65	≤ 0.10	≤ 0.25	—
10	0.07-0.14	0.17-0.37	0.35-0.65	≤ 0.15	≤ 0.25	—
15	0.12-0.19	0.17-0.37	0.35-0.65	≤ 0.25	≤ 0.25	—
20	0.17-0.24	0.17-0.37	0.35-0.65	≤ 0.25	≤ 0.25	—
40	0.37-0.45	0.17-0.37	0.70-1.00	≤ 0.25	≤ 0.25	—
60	0.57-0.65	0.17-0.37	0.70-1.00	≤ 0.25	≤ 0.25	—
Y8A	0.75-0.84	0.15-0.30	0.15-0.30	—	—	—
Y9A	0.85-0.94	0.15-0.30	0.15-0.30	—	—	—
Y10A	0.95-1.04	0.15-0.30	0.15-0.30	—	—	—
Y11A	1.05-1.14	0.15-0.30	0.15-0.30	—	—	—
Y12A	1.15-1.24	0.15-0.30	0.15-0.30	—	—	—
Y13A	1.25-1.35	0.15-0.30	0.15-0.30	—	—	—
X	0.95-1.10	0.15-0.35	0.15-0.40	1.30-1.65	—	—
9XC	0.85-0.95	1.2-1.6	0.30-0.60	0.95-1.25	—	—
XBГ	0.90-1.05	0.15-0.35	0.80-1.10	0.90-1.20	—	1.2-1.6 W 7.5-9.0 W 0.2-0.5 V
3X2B8Φ	0.30-0.40	0.15-0.40	0.15-0.40	2.2-2.7	—	—

P9	0.85-0.95	≤ 0.4	≤ 0.4	3.8-4.4	≤ 0.4	8.5-10.0 W 2.0-2.6 V
P18	0.70-0.80	≤ 0.4	≤ 0.4	3.8-4.4	≤ 0.4	17.5-19.0 W 1.0-1.4 V
ШХ15	0.95-1.05	0.17-0.34	0.2-0.4	1.3-1.65	—	—
18ХГТ	0.17-0.23	0.17-0.37	0.80-1.10	1.00-1.30	≤ 0.25	0.06-0.12 Ti
12ХН3А	0.09-0.16	0.17-0.37	0.30-0.60	0.60-0.90	2.75-3.15	—
38ХМЮА	0.36-0.42	0.17-0.37	0.30-0.60	1.35-1.65	≤ 0.25	0.15-0.25 Mo 0.70-1.10 Al
55ХГР	0.52-0.60	0.17-0.37	0.9-1.2	0.90-1.20	≤ 0.25	0.002-0.005 B
30ХГС	0.28-0.35	0.90-1.20	0.80-1.10	0.80-1.10	≤ 0.25	—
40ХНМА	0.37-0.44	0.17-0.37	0.50-0.80	0.60-0.90	1.25-1.65	0.15-0.25 Mo
18Х2Н4ВА	0.14-0.20	0.17-0.37	0.25-0.55	1.35-1.65	4.00-4.40	0.80-1.20 W
X18H9	≤ 0.12	≤ 0.8	1.0-2.0	17.0-19.0	8.0-10.0	—
X25H16Г7АР (ЭИ835)	≤ 0.12	≤ 1.0	5.0-7.0	23-26	15.0-18.0	0.3-0.45 N
X12H20ТЗР (ЭИ696А)	≤ 0.10	≤ 1.0	≤ 1.0	10.0-12.5	18.0-21.0	2.3-2.8 Ti 0.008 B
X12H22Т3МР (ЭИ696М)	≤ 0.10	≤ 0.6	≤ 0.6	10.0-12.5	21.0-25.0	2.6-3.2 Ti 1.0-1.6 Mo ≤ 0.02 B
36НХТЮ	≤ 0.05	≤ 0.5	0.8-1.2	11.5-13.5	34.5-36.5	2.8-3.2 Ti 0.9-1.2 Al
Э310 } Э320 }	—	2.8-3.5	—	—	—	—

Aluminium Alloys

Grade	Al	Cu	Mg	Zn	Mn	Si	Fe	Other elements
АД1	≥ 99.3	≤ 0.05	≤ 0.005	≤ 0.1	≤ 0.025	≤ 0.30	≤ 0.30	—
АД	≥ 98.80	≤ 0.1	≤ 0.1	≤ 0.1	≤ 0.1	≤ 0.50	≤ 0.50	—
АМц	Base	≤ 0.2	≤ 0.5	≤ 0.1	1.0-1.6	≤ 0.6	≤ 0.7	—
АМг1	Same	≤ 0.01	0.5-1.8	—	—	≤ 0.05	≤ 0.05	—
АМг2	Same	≤ 0.1	1.8-2.8	≤ 0.2	0.2-0.6	≤ 0.4	≤ 0.4	—
АМг6	Same	≤ 0.1	5.8-6.8	≤ 0.2	0.5-0.8	≤ 0.4	≤ 0.4	0.02-0.10 Ti 0.0002-0.005 Be
АД31	Same	≤ 0.1	0.4-0.9	≤ 0.2	≤ 0.15	0.3-0.7	≤ 0.5	—
АВ	Same	0.1-0.5	0.45-0.90	≤ 0.2	0.15-0.35	0.5-1.2	≤ 0.5	—
Д1	Same	3.8-4.8	0.4-0.8	≤ 0.3	0.4-0.8	≤ 0.7	≤ 0.7	—
Д16	Same	3.8-4.9	1.2-1.8	≤ 0.3	0.3-0.9	≤ 0.5	≤ 0.5	—
Д19	Same	3.8-4.3	1.7-2.3	≤ 0.1	0.5-1.0	≤ 0.5	≤ 0.5	0.0002-0.005 Be
Д19П	Same	3.2-3.7	2.1-2.6	0.1	0.5-0.8	0.3	0.3	0.0003-0.005 Be
АК4-1	Same	1.9-2.5	1.4-1.8	≤ 0.3	≤ 0.2	≤ 0.35	0.8-1.3	0.8-1.3 Ni
1915	Same	≤ 0.1	1.3-1.8	3.4-4.0	0.2-0.6	≤ 0.3	≤ 0.4	{ 0.15-0.22 Zr 0.08-0.2 Cr
1925	Same	≤ 0.8	1.3-1.8	3.4-4.0	0.3-0.7	≤ 0.7	≤ 0.7	0.1-0.2 Zr
В95	Same	1.4-2.0	1.8-2.8	5.0-7.0	0.2-0.6	≤ 0.5	≤ 0.5	0.1-0.25 Cr
В96	Same	2.2-2.8	2.5-3.2	7.6-8.6	0.2-0.5	≤ 0.5	≤ 0.5	0.1-0.25 Cr
АJ12	Same	≤ 0.6	≤ 0.1	≤ 0.3	≤ 0.5	10.0-13.0	≤ 0.8	—
АJ17	Same	4.0-5.0	≤ 0.3	≤ 0.2	≤ 0.1	≤ 1.2	≤ 1.0	—
АJ18	Same	≤ 0.3	9.5-11.5	≤ 0.1	≤ 0.1	≤ 0.3	≤ 0.3	—
АJ19	Same	≤ 0.2	0.2-0.4	≤ 0.3	≤ 0.5	6.0-8.0	≤ 0.6	0.15-0.35 Ti
АJ119	Same	4.5-5.3	≤ 0.05	≤ 0.2	0.6-1.0	≤ 0.3	≤ 0.2	0.05-0.15 Ti
АJ127-1	Same	≤ 0.05	9.5-11.5	≤ 0.05	≤ 0.1	≤ 0.05	≤ 0.05	0.05-0.15 Be 0.05-0.20 Zr

Appendix (continued)

*Magnesium Alloys*

Grade	Al	Zn	Mn
MA5 MJ5	7.8-9.2 7.5-9.0	0.2-0.8 0.2-0.8	0.15-0.5 0.15-0.5

*Titanium Alloys*

Grade	Al	Mo	Cr	Other elements
BT8 BT15 BT22	6.0-7.3 2.3-3.6 4.0-5.7	2.8-3.8 6.8-8.0 4.0-5.5	— 9.5-11.0 0.5-2.0	0.20-0.40 Si — 4.0-5.5 V 0.5-1.5 Fe

*Nickel Alloys*

Grade	Cr	Ti	Al	Other elements
XH77THOP (ЭИ437Б) ЖС6К Nimonic-90	19-22 10.5-12.5 18-21	2.4-2.8 2.5-3.0 1.8-3.0	0.60-1.0 5-6 0.8-2.0	— 4-5 Co, 3.5-5.4 Mo; 4.5-5.5 W, 0.02 B 15-21 Co

*Copper Alloys*

Grade	Content of elements
Л68 Л70 Бр.Б2 Бр.Х0.8	67.0-70.0 Cu, balance Zn 69.0-72.0 Cu, balance Zn 1.9-2.2 Be, 0.2-0.5 Ni 0.6-0.9 Cr

## NAME AND SUBJECT INDEX

- Aaronson H. J. 270  
Acicular martensite 244  
Ageev N. V. 316  
Ageing, 298  
    artificial 352  
    duplex 355  
    natural 352  
    phase 353  
    stabilizing 354  
    two-step 355  
    zone 353  
Alitizing 404  
Allen B. C. 101  
Allison H. 125  
Alloying elements,  
    effect of pearlitic transformation 177  
Anderson M. A. 58  
Anisotropy of properties 46, 108  
Annealing with phase transformation  
    201  
Ansell G. S. 230  
Archer A. R. S. 299  
Ardell A. J. 311  
Artificial ageing 352  
Assmus F. 83  
Asterism 50  
Athermal transformation 252  
Ausforming 418  
Aust K. T. 80  
Austempering 294  
Austenite, 160  
    intrinsic grain in 168  
    thermal stabilization of 259  
Austenitic transformation 175  
Austenitization 160  
Avial alloys 356
- Baba J. 320  
Baikov A. A. 13  
Bailey J. E. 60  
Bain E. C. 158  
Bain transformation 237  
Bainite 269  
Bainitic hardening 294  
Bainitic steel 278  
Bainitic transformation 269  
Bakhmetyev E. F. 50
- Baldwin W. M. 109  
Basket interlacing 313  
Batisse M. 99  
Beck P. A. 59  
Belous M. V. 383  
Belyaev N. I. 184  
Benson L. 125  
Berkovsky I. Ya. 46, 108  
Bernstein M. L. 421, 423, 425  
Beton R. H. 323, 329  
Betteridge W. 408  
Bilby B. A. 241  
Blanter M. E. 160  
Bochvar A. A. 8, 14, 16, 50, 65, 166,  
    175, 207, 233  
Bockstein S. Z. 297, 365  
Bozorth R. M. 112  
Brass-type texture 41  
Bugakov V. Z. 390  
Bunin K. P. 195, 200  
Burke J. E. 82  
Burning 36, 103, 212  
Burst martensite 257  
Burst-type transformation 254  
Butler E. P. 310  
Byrne J. G. 341
- Cahn R. W. 50, 117, 160, 312  
Carbide segregation 34  
Carbon segregation 363  
Carbon steels,  
    tempering of 363  
Carburizing 399  
CCT-diagrams 159  
C-curves 157  
Cellular precipitation 315  
Cellular structure 42  
Cementation 399  
Cementite 160  
Chemical hardening 339  
Chemical heat treatment, 15, 384  
    kinds of 397  
Chemical spinodal line 303  
Chemisorption 385  
Cherepin V. T. 383  
Chernov D. K. 12, 16, 131, 166, 293  
Chill-eliminating annealing 199



- Christian J. W. 160, 241  
Chromizing 405  
Churbakova T. N. 26  
Clark J. B. 317, 332  
Climb of dislocations 49  
Clusters 312, 320, 363  
Coalescence of subgrains 52  
Cohen M. 232  
Coherence 139  
Coherent interface 139  
Coherent precipitates 307  
Coherent spinodal line 303  
Coincidence-site boundary 80  
Common martensite 263  
Concentration fluctuation 138  
Concentration wavelength 313  
Continuous grain growth 82  
Continuous precipitation 314  
Copper-type texture 41  
Coring 20  
Cottrell atmospheres 56, 66, 106, 327  
Cross-slip of dislocations 41, 49  
Crystallization, non-equilibrium 17  
Cubic recrystallization texture 76  
Cyaniding 404  
Cyclic annealing 187
- Dankov P. D. 141  
Darken L. S. 171  
Davenport E. S. 158  
Davydov V. G. 217, 219, 220  
Deformation texture 40  
Degree of overheating 138  
Degree of undercooling 131  
Delay L. 297  
Dendritic segregation 17, 20  
Density of dislocations 42  
Depth of hardened layer 283  
Detert K. 83  
Diagram of isothermal transformation 156  
Diffusion coefficient 26  
Diffusion line 396  
Diffusion porosity 32  
Diffusion saturation,  
    with metals 404  
    with non-metals 399  
Diffusion zone, 385  
    structure of 396  
Discontinuous grain growth 82  
Discontinuous precipitation 314  
Dislocations,  
    nucleation at 147  
Dislocation cross-slip 41  
Dislocation tangles 42  
Dobatkina V. I. 417, 425
- Doherty R. D. 39, 117  
Donachie S. J. 230  
Double annealing 183  
Double texture 41  
Dubinin G. N. 397, 398, 406  
Dunn C. G. 83  
Duplex ageing 355  
Duralumin 13  
Dynamic polygonization 413  
Dynamic recrystallization 413
- Earing 108  
Elagin V. I. 39, 207, 219  
Electric resistivity 45, 107  
End-quench test 284  
Entin R. I. 191, 273, 297, 383  
Equalizing diffusion 18  
Equilibrium segregation 144  
Equilibrium solidus 19  
Error function 386  
Esser H. 281  
Eutectoid grains 174  
Eutectoid nodules 170  
Extrusion effect 31, 417
- Ferrite 160  
Ferrite network 176  
Fick's law of diffusion 26  
Fine M. E. 341  
Fire brittleness 114  
First-order annealing 15  
First-order recovery 48  
Fish-scale fracture 24  
Flemings M. C. 29  
Fournelle R. A. 317  
Free-cutting steels 35  
Fridlander I. N. 353, 361  
Full annealing 180  
Full softening 201
- Galvanic microcouples 24  
General precipitation 315  
Gensamer M. 277  
Gerold V. 320  
Geveling N. N. 316  
Glazunov S. 415  
Glide of dislocations 40, 49  
Globular pearlite 186  
Golikov I. N. 39  
Gorelik S. S. 60, 66, 90, 105, 117  
Goss texture 112  
Grain coarsening, 29  
    in primary recrystallization 70  
Grain growth 71, 82  
Grain refinement 29

- Graphitizing annealing 192  
 Greninger-Troiano relationship 240  
 Group coalescence 54  
 Guinier A. 300  
 Guinier-Preston zones, 300  
   formation of 319  
 Gulyaev A. P. 191, 245, 295, 297, 392
- Habit plane** 242  
 Hagel W. C. 170  
 Hansen M. 316  
 Hardenability of steels 278  
 Hardenability band 285  
 Hardening,  
   chemical 339  
   to martensite 220  
   secondary 377  
 Hardening ageing 343  
 Hardening capacity 265  
 Hardening phase 344  
 Hardening stresses 291  
 Hardening tempering 381  
 Hardy H. K. 345  
 Heal T. J. 345  
 Heat treatment, classification of types 14  
 Hehemann R. F. 270  
 Heterogeneous nucleation 142  
 Heterogenization 30  
 Heterogenizing annealing 201  
 Heterogenizing softening 201  
 High-temperature cementite 365  
 High-temperature homogenizing 39  
 High-temperature martensite 247  
 High-temperature tempering 375  
 Hirsch P. B. 60  
 Homogeneous nucleation 142  
 Homogenizing 17  
 Homological temperature 47  
 Honeycombe R. W. K. 117  
 Hornbogen E. 325, 329  
 Horophile elements 143  
 Horophobic elements 145  
 Hot strain-hardening effect 413  
 Hypereutectoid steels 175  
 Hypoeutectoid steels 175
- Ibe G. 83  
 Imgram A. G. 104  
 Impurity atmospheres 363  
 Inclusions, nucleation at 148  
 Incoherent interface 139  
 Incoherent precipitates 307  
 Induction heating 287  
 Induction period 58, 155  
 Inequigranular structures 96
- Inherited strengthening 423  
 In-situ recrystallization 55  
 Intercrystalline fracture 24  
 Intermediate transformation 269  
 Interplate spacing 172  
 Intrinsic grain, in austenite 168  
 Isothermal annealing 180, 187  
 Isothermal hardening 294  
 Istomin V. V. 31
- Jeffries Z. 299  
 Jones J. J. 425
- Kaminsky E. Z. 367  
 Kardonsky V. M. 253, 383  
 Kaufman D. F. 232  
 Kawano O. 323  
 Kelly A. 341, 361  
 Khachaturyan A. G. 239  
 Khenkin M. L. 124  
 Khovova O. M. 316  
 Kidin I. N. 164, 290, 297  
 Kinetic curve 153  
 Kinsman K. R. 270  
 Kirkendall effect 32  
 Kolachev B. A. 39, 207, 220  
 Kolmogorov A. N. 154  
 Kolokolova A. G. 46, 108  
 Konobeevsky S. T. 50, 141  
 Krauss G. 245, 246, 247, 249  
 Kronberg M. L. 78, 84  
 Kronberg-Wilson boundary 80  
 K-state 45  
 Kurbatova A. V. 38  
 Kurdjumov G. V. 233, 236, 257, 258, 263, 297, 366, 373, 383  
 Kurdjumov-Sachs orientational relationship 239
- Lainer D. I. 110  
 Lakhtin Yu. M. 396, 403, 406  
 Lamellar pearlite 173  
 Lath martensite 244  
 Laurent P. 99  
 Laves phases 372  
 Li J. C. M. 54  
 Lineage structure 24, 182  
 Lips E. 418  
 Livanov V. A. 39, 202, 207, 220  
 Lorimer G. W. 334  
 Low J. R. 277  
 Low-temperature cementite 364  
 Low-temperature martensite 244  
 Low-temperature tempering 375

- Maksimova O. P. 254, 255, 258, 263  
Maraging steels, 268  
    tempering of 371  
    variations in properties 381  
Marder A. R. 245, 249  
Martempering 294  
Martensite,  
    acicular 244  
    burst 257  
    common 263  
    high-temperature 247  
    lamellar 244  
    lath 244, 247  
    massive 247  
    packet 247  
    strain-induced 263  
    stress-assisted 263  
    structureless 247  
    temper 273, 369  
    twinned 244  
    untwinned 247  
Martin J. W. 39, 117, 361  
McQueen H. J. 425  
Mehl R. F. 58, 170  
Merica P. 14, 299, 300  
Metastable phases, formation of 149  
Microdiscontinuities, nucleation at 148  
Midrib 248  
Migration of sub-boundaries 52  
Minkevich A. N. 406  
Mirer I. I. 50  
Mirkin I. L. 132, 154, 271  
Misfit parameter 67  
Modulated structures 309  
Modulation period 309  
Murakami M. 323
- Nabarro F. R. N. 309  
Natural ageing 352  
Nicholson R. B. 311, 334, 361  
Nikonorova A. I. 254, 255, 263  
Nishiyami orientational relationship 240  
Nitriding 402  
Nitrocementation 404  
Nodules 315  
Non-equilibrium crystallization 17  
Non-equilibrium solidus 19  
Non-isothermal transformation 258  
Normalizing 16, 180, 188  
Novikov A. I. 42  
Novikov I. I. 22, 26, 38, 39, 88, 89, 91, 92, 94, 103, 217, 219, 220  
Nucleation 59, 143, 147  
Nutting J. 411
- Oberhoffer P. 95  
Obukhov P. M. 12  
Oertel W. 95  
Orange peel 116  
Oriented growth, hypothesis of 78  
Osmond F. 13  
Overageing 343, 354  
Overheating 103, 168
- Packet martensite 247  
Pairwise coalescence 54  
Partial annealing 183  
Partial softening 202  
Patenting 180, 190  
Pearlite 160, 173  
Pearlitic nodule 170  
Pearlitic transformation, 169  
    effect of alloying elements on 177  
Pearsell E. B. 277  
Pellini W. S. 277  
Periodic structures 309  
Perkas M. D. 253, 383  
Perryman E. C. W. 99  
Petch-Hall relation 101  
Peter W. 271  
Peti A. M. 29  
Petrov D. A. 359  
Petunina E. V. 245  
Phase ageing 353  
Phase transformations,  
    kinetics of 153  
    thermodynamics of 129  
Point defects 43  
Pol'kin I. S. 415  
Polygonization, 48, 50  
    dynamic 413  
Popov A. A. 272, 393, 406  
Porosity 32, 38  
Portevin A. 13  
Precipitate-free zones 333  
Precipitation,  
    continuous 314  
    discontinuous 315  
    of intermediate carbides 363  
    by nucleation 304  
    spinodal 302  
    thermodynamics of 301  
Precipitation hardening 299  
Pre-precipitates 300, 324  
Prerecrystallization annealing, 39  
    structural changes on 47  
Prerecrystallization softening 17, 113  
Prerecrystallization strengthening 17, 114  
Presston G. D. 300

- Primary recrystallization, 56, 58  
   grain coarsening in 70  
   textures of 76  
 Principle of structural correspondence 141  
 Prokoshkin D. A. 390  
 Proximity effect 288
- Quasi-eutectoid, 175  
   structure 375  
 Quenching,  
   with polymorphic change 220  
   without polymorphic change 208  
   with self-tempering 376  
 Quench test method 283
- Rabinovich M. Kh. 425  
 Rachstadt A. G. 105, 316  
 Radchenko K. M. 44  
 Rauzin Ya. R. 187  
 Reaction diffusion 389  
 Recovery 47  
 Recrystallization,  
   dynamic 413  
   induction period of 58  
   in-situ 55  
   primary 56, 58  
   secondary 82  
   temperature threshold of 64  
 Recrystallization annealing 10, 17, 39, 114  
 Recrystallization diagrams 94, 116  
 Recrystallization texture 108  
 Red hardness 377  
 Red shortness 35  
 Relative elongation 44  
 Removal of elements by diffusion 405  
 Residual stresses 118  
 Retained austenite,  
   decomposition of 366  
 Reversion in age-hardened alloys 359  
 Rib texture 87  
 Rogelberg I. L. 89, 91, 92, 94, 103, 106  
 Roitburd A. L. 250  
 Rollason E. C. 323, 329  
 Rose A. 271  
 Rosenberg V. M. 42  
 Rozanov A. N. 271  
 Rutter J. W. 80
- Sachs G. 316  
 Sadovsky V. D. 166, 191, 422  
 Sakhin S. I. 420  
 Sauveur A. 13
- Season cracking 126  
 Secondary hardening 377  
 Secondary porosity 32  
 Secondary recrystallization 82  
 Second-order annealing 15, 127  
 Second-order recovery 48  
 Segregation, dendritic 20  
 Self-tempering 363  
 Semicohherent interface 139  
 Shepelyakovsky K. Z. 297  
 Shewmon P. G. 61, 117, 297, 361, 387  
 Silcock J. M. 345  
 Skakov Yu. A. 363  
 Skin effect 287  
 Smirnov L. V. 422  
 Smiryagin A. P. 102  
 Softening ageing 343  
 Softening tempering 381  
 Sokolov E. N. 422  
 Sokolov O. G. 420  
 Solvus line 69  
 Sorbite, 173  
   temper 369  
 Spektor E. N. 105  
 Spheroidite 184  
 Spheroidization of cementite particles 365  
 Spheroidizing annealing 183  
 Spinodal line 303  
 Spinodal points 302  
 Spinodal precipitation 302  
 Stabilization of matrix 85  
 Stabilizing ageing 354  
 Stabilizing tempering 375  
 Stacking faults,  
   nucleation at 147  
 Starodubov K. F. 383  
 Stelletskaia T. I. 367  
 Step rule 152  
 Stepwise hardening 293  
 Strain hardening 10, 44  
 Strain-induced martensite 263  
 Stremel M. A. 164  
 Stress-assisted martensite 263  
 Stress-relief annealing 117, 124  
 Structural strain hardening 166  
 Structureless martensite 247  
 Sub-boundaries, migration of 52  
 Subgrain structure 43  
 Supersaturation of solid solution 349  
 Superstructure 45  
 Surface effect 287  
 Suzuki atmospheres 56, 106, 327
- Takashima A. 320  
 Tammann G. 131, 132

- Tammann curves 131  
Taran Yu. N. 200  
Temper carbon 193  
Temper embrittlement 298, 378  
Temper martensite 273, 369  
Temper sorbite 369  
Temper troostite 369  
Temperature threshold of recrystallization 64  
Tempering 298, 361, 375  
Ternary systems 349  
Textural retardation 85  
Textured transformer steel 111  
Texturizing annealing 117  
Thermal hysteresis of transformation 130  
Thermal stabilization of austenite 259  
Thermocycling 124  
Thermoelastic equilibrium 235  
Thermo-mechanical treatment 15, 406, 413, 418  
Thickness effect 75, 85  
Thomas G. 310  
Thompson-Friendlich equation 185  
Titanium alloys, nitriding of 404  
Tongues 59, 317  
Tretyakov A. V. 44  
Triple points, 53  
    boundaries of 72  
Troostite, 173  
    temper 369  
TTT-diagrams 158  
Turbulent creep 52  
Twinned martensite 244  
Twinning 40  
Two-step ageing 355  
Umansky Ya. S. 50  
Unravelling 53  
Untwinned martensite 247  
Unwin P. N. T. 334  
Utevsky L. M. 297, 383  
Vandermeer R. A. 79  
Van Zuilen H. 418  
Vasilyev M. A. 383  
Vologdin V. P. 287  
Vorobyev V. G. 296  
Voronov S. M. 202  
Walter J. L. 83  
Warlimont H. 297  
Warping 120  
Wassermann G. 300  
Water-to-oil quenching 293  
Widmanstätten A. 142  
Widmanstätten structure 142, 176  
Williams H. J. 111  
Wilm A. 13, 299  
Wilson H. F. 78  
Work hardening 44  
Zakharov E. D. 38, 217, 219, 220  
Zakharov V. V. 219, 220  
Zakharov V. Z. 92, 103  
Zhdanov G. S. 50  
Zolotarevskaya A. Yu. 103  
Zolotarevsky V. S. 22, 26, 31, 38, 39  
Zone ageing 353  
Zones, precipitate-free 333

## **TO THE READER**

Mir Publishers welcome your comments on the content, translation, and design of the book.

We would also be pleased to receive any suggestions you care to make about our future publications.

Our address is:

USSR, 129820,  
Moscow, I-110, GSP,  
Pervy Rizhsky Pereulok, 2,  
Mir Publishers

*Printed in the Union of Soviet Socialist Republics*

## ALSO FROM MIR PUBLISHERS

**Electrometallurgy of Steels and Ferro-Alloys, Vols. I-II** *F. Edneral, D. Sc.*

This textbook describes the modern equipment of steel-making and ferro-alloy-making shops. Much attention is given to problems of mechanization of the melting process, description of charging and fettling machines. Considers the advanced methods of intensified electric melting: application of fuel burners and powder materials, argon treatment of steel in the ladle, vacuum degassing of steel, stopperless teeming. Presents the newest data on manufacture of ferro-alloys.

The book is very popular in this country as a textbook on electrometallurgy of steels and ferro-alloys. Abundant materials, presented in a logical form, make it indispensable as a textbook for training electrometallurgical engineers and as a general course in electrometallurgy of steels and ferro-alloys to be read to students of other metallurgical specialities.

## **Engineering Physical Metallurgy and Heat-Treatment**

*Yu. Lakhtin, D. Sc.*

This textbook deals, among other aspects of physical metallurgy, with defects in the crystal lattices of metals, and with the thermodynamics of phase transformations. New sections have been added to the chapter on refractory metals. Comprehensively presented are topics on the mechanical properties of metals, with due consideration for the engineering strength and failure mechanism under conditions of static and cyclic loading. Devotes much space to the theory and techniques of heat-treatment and case hardening of steel, description of structural, tool, stainless and heat-resistant steels, alloys with special physical properties and to alloys based on aluminium, copper, titanium, magnesium, etc. Intended as a textbook for students majoring in metallurgy.



## **Metallurgical Furnaces**

*V. Krivandin, D. Sc. and B. Markov, D. Sc*

The book presents the theoretical principles of metallurgical heat engineering: motion of gases at subsonic and supersonic velocities; theory of similarity; heat transfer and heating of metals; principal characteristics of fuels and fuel combustion. Gives the required data on materials for furnace construction and describes the elements and structures of furnaces employed in non-ferrous metallurgy.

The book is a study aid for higher-school students of metallurgical specialities. It may also be of use for students of machine-building speciality and for those specializing in metallurgical heat engineering.